P. Thambidurai
Anil Kumar Dikshit *Editors*

Impacts of Urbanization on Hydrological Systems in India

Springer

Impacts of Urbanization on Hydrological Systems in India

P. Thambidurai • Anil Kumar Dikshit
Editors

Impacts of Urbanization on Hydrological Systems in India

Springer

Editors
P. Thambidurai
Department of Coastal Disaster Management, School of Physical, Chemical and Applied Sciences
Pondicherry University – Port Blair Campus Port Blair, Andaman and Nicobar Islands, India

Anil Kumar Dikshit
Environmental Science and Engineering Department
Indian Institute of Technology Bombay
Mumbai, Maharashtra, India

ISBN 978-3-031-21617-6 ISBN 978-3-031-21618-3 (eBook)
https://doi.org/10.1007/978-3-031-21618-3

This Springer imprint is published by the registered company Springer Nature Switzerland AG
The registered company address is: Gewerbestrasse 11, 6330 Cham, Switzerland

Preface

As urban spaces continue to expand to accommodate a growing population, there remains a real need to quantify and qualify the impacts of the urbanized areas on natural processes. Human growth and their livelihood demand large quantities of safe, fresh water all across the world, leading to shortage and even the severe condition of drying out surface water sources and depletion of groundwater reservoirs. Urbanization also causes frequent flooding of habitat areas as well as adds to loads of pollution. Not only do traditional sources of municipal and industrial nature cause pollution, fertilizers, and pesticides draining from agriculture, but improper solid and hazardous wastes also contribute to complex, recalcitrant, and toxic pollution. Rainfall and precipitation patterns change from evenly distributed events to a few events of high intensity-low duration or cloudburst, leading to heavy rains or flash floods. At this juncture, this book intends to introduce the various newer advanced techniques, modeling, and other programming applications applied to address the current scenario and the impact of urbanization on the surface water, the groundwater, and the entire hydrological system to provide possible options/solutions with respect to development and management of water environment.

Development towards urbanization is not an avoidable component in the present century, and hence, we need a new thought to plan, design, and develop water resources. Our philosophy should be arranging an adequate supply of water while providing safeguards against drought, floods, and pollution. The integration of many different pieces of multi-disciplinary research contributions shall make a complete guide for future prospective on the current situation of the hydrological system. The present book contains case studies on various aspects of urbanization and hydrological issues.

We hope that the book will be useful for a wide range of readers such as researchers, educators, municipal and city authorities, decision-makers, government officials, and NGOs.

Port Blair, India — P. Thambidurai
Mumbai, India — Anil Kumar Dikshit

Introduction

Hydrological systems are concerned with the water in the atmosphere: rainfall, snowfall, snow, and ice; streams, rivers, and lakes; and groundwater occurring below the Earth's surface in pores of soil and rocks. They encompass all processes such as evaporation from the ocean, precipitating raindrops, land, and water bodies, and evapotranspiration from crops, vegetation, trees, and forests, followed by the formation and movement of clouds, then occurrence of rainfall, snowfall, interception, infiltration, surface runoff, streamflow, deep percolation, and storage of groundwater. The natural occurrence, circulation, and distribution of water on the earth and the earth's atmosphere have plenty of opportunities coming in contact with various human activities such as water supply to villages, towns, cities, and industries; irrigation and drainage of cropland, generation of thermal, hydro and nuclear power; drought control, flood control, navigation, coastal works, recreation and pollution due to disposal from point and non-point sources. In this way, there are numerous pathways, such as urbanization, industrialization, and changes in climate, by which hydrological systems are getting impacted.

This book is a preliminary attempt to put together relevant research works on the impact of urbanization on the hydrological system, including conventional and modern approaches, in one place. It starts by putting forward the status of the hydrological system in the river basins and urban areas. The most pronounced hydrological problems in cities are the results of changes in precipitation and ensuing runoff from the urban regions. The urban runoff is entirely different from that of rural areas. However, the substantial increase in runoff causes floods in the urbanized area, and a significant decrease in runoff results in water scarcity and persistence in drought conditions. These are generally attributed to the reduction in infiltration due to the development of built-up areas, roads, and industries or to a reduction in retention time, resulting in groundwater decline and depletion. The most common opinion expressed by developmental authorities is that due to enhanced urbanization, more runoff is occurring now, and also, at the same time, less recharge is taking place. In recent times, rain events have become fewer but quite intense, sometimes leading to flash floods, cloud bursts, etc. Further, qualitative deterioration of streamflow has also become important where urban runoff carries pollutants, fertilizers,

and pesticides and contaminates different water supply sources. Water pollution levels are rising as more wastes are being generated and discharged with or without the due degree of treatment.

There are 17 chapters in this book. For the convenience of the reader, a brief overview is provided. The focus on urbanization and surface water starts with the status of the hydrological system in the urban area, i.e., the catchment characteristics and changes in rainfall dynamics. Chapters 1, 2, 3, 4, 5, 6, and 7 focus on the impact of urbanization on water resources. The potential sites for rainwater harvesting and artificial recharge for structures such as check dams, farm ponds, and percolation tanks were identified in a typical semi-arid river basin in Maharashtra, India, in Chap. 1. Chapter 2 discusses Pallikaranai swamp land, a freshwater ecosystem situated in the southern region of Chennai, India, which has been significantly damaged due to garbage dumping, sewage discharges, and unplanned urbanization activities. Various plans were evaluated for implementing management actions to improve the wetland and surrounding aquifer systems. Chapter 3 addresses the dynamics of land use and land cover (LULC) and its implications in hydrological modeling, irrigation management, urban planning, and land and water resource management for the Chittar catchment in Western Ghats situated on the border of Tamil Nadu and Kerala. Chapter 4 analyzes how unplanned rapid urbanization, deforestation, exploitation of flood plain, and lack of proper drainage networks aggravated the flooding in Patna. It also demonstrated how to work out appropriate mitigation strategies, which can be implemented to abate future urban floods in Patna. Chapter 5 focuses on flood susceptibility zonation of Chalakudy Taluk, Thrissur, Kerala, using a statistical Dempster-Shafer evidential belief function model to map the flood susceptibility of the region. Chapter 6 is on the Ganga River, a symbol of faith for hundreds of millions of Indians in its about one million square kilometer basin. Over the last 100 years, various urban projects have been introduced in the basin. Various multipurpose dams/barrages were constructed on the river's mainstream and on its tributaries for hydropower production, irrigation, and drinking water supply.

Similarly, forest cover changed into agricultural land, and barren land was developed for buildings to support housing and factories for an increasingly urban population of the basin. The effects of anthropogenic activities and anthropogenic activity–induced climate change have started to degrade surface-water bodies in terms of their quality and quantity, and in some cases, surface water bodies have been lost completely. A few suggestions from the sustainable development perspective have also been proposed. Chapter 7 shows how population explosion, hasty urbanization, economic and industrial developments, and climate change have led to growing pressure on water resources. Moreover, an increased number of cities are relying on remote water resources, inter-basin water transfers, domestic virtual water trade, and seawater desalination to cope with the rising demands for water. Strategies such as resilient building and nature-based solutions, including green infrastructures, aquifer recharge, storm-water management, reducing non-revenue water, grey water usage, and planning of smart cities, should be implemented for sustainable urban water management.

From Chap. 8 onwards, the impacts on groundwater systems have been discussed; Chap. 8, titled "Groundwater Scarcity in Urban Areas is a Major Issue: Case Studies from West Bengal," deals with the case studies on identifying water scarcity in the two hard rock cities of West Bengal, namely Purulia and Bankura. It is to be noted that water is becoming scarce at present, and in the near future, the sources may dry up. Also, some suggestive measures for overall balanced groundwater development in the short term and long term are discussed to preserve water. The impact of urbanization and river morphology on groundwater system in Patna Urban Area, Bihar, India, is discussed in Chap. 9. Here, a numerical groundwater flow model has analyzed the impact of increased groundwater demand due to vertical urban growth and a shift in the course of the river Ganges in the Patna Urban Area (PUA). The simulated results with the existing stress conditions on the aquifer system indicate that there is a 0.5 m/year decline in the hydraulic head of the deep aquifer in the central parts of PAU. Chapter 10 covers concentrates on key issues and feasibility of aquifer storage and recovery. This study aims to comprehend, identify, and improve the global understanding of groundwater remediation methods based on the dilution of contaminants. Chapter 11 is titled "Temporal Prediction of Groundwater Levels: A Gap in Generalization." This study tries to identify the performance of two well-known predictive algorithms, which have their footprints both in data-driven and data mining models, namely a) artificial neural network (ANN) and b) support vector machine (SVM). The results inferred that even though the study of groundwater wells is pertaining to the same basin (where climate and lithology are almost similar), the algorithms may not be generalized for the domain application. The above observation may be due to the draft and land use pattern variability. Chapter 12 discusses the suitability of groundwater for drinking and agricultural use in Patna district, Bihar, India. The chemical characteristics of groundwater samples in the Patna district were obtained from the Central Ground Water Board 2021 report for a total of 37 locations. Although most of the parameters were within the range, parameters such as coliform value and arsenic content are also equally important and need to be measured before declaring groundwater fit for drinking. Chapter 13 is titled "Groundwater Potential Assessment using GIS-based Weighted Linear Combination Technique: A Case Study of Hard Rock Terrain Around Bhopal City, India." An integrated knowledge-based weighted linear combination (WLC) method was applied for the assessment of groundwater potential and grouped as very good, good, moderate, and poor. Chapter 14, titled "The Effect of Urbanization on Groundwater Quality and Hydrochemical Characteristics," presents an effort made to understand the impacts of urban growth on groundwater quality and its variations vis-à-vis hydrochemical characteristics in the Ennore coastal aquifers, Chennai. Ninety-five groundwater samples comprising the surface bore wells and dug wells for dual seasons (pre-monsoon and post-monsoon) were collected between August 2019 and January 2020. In general, groundwater was found unsuitable for drinking and domestic utilities, with fewer exceptions irrespective of seasons in most locations. Chapter 15 discusses groundwater contamination in parts of northwestern Hyderabad from a hydrogeochemical and geospatial perspective. The groundwater of the area is polluted due to the existence of industries for decades

together. Spatiotemporal dynamics of groundwater recharge in Dras sub-basin of the Upper Indus River Basin, Western Himalayas, has been studied in Chap. 16. The spatiotemporal variance of isotopes $\delta^{18}O$ and $\delta^{2}H$ were studied to understand groundwater recharge dynamics in the study area. The results indicated meltwater derived from high altitudes dominates the groundwater recharge. The global climate warming observation suggests the dependence of recharge on meltwaters obtained from snow and glacier melt in the Dras sub-basin. The study further indicated that variation in precipitation pattern, form, and shift in regional glacier mass might negatively influence the local and regional groundwater resources and, eventually, the social and economic aspects of the region. Finally, Chap. 17 presents the impact of urbanization on groundwater in changing climatic scenario with a case study at two locations in the National Capital Region (NCR). Faridabad and Manesar have witnessed an intense increase in population and rapid urbanization due to industrialization and considerable migration. The average temperature of the area has increased by 2 degrees with a corresponding increase in rainfall intensity along with a reduction in rainy days while maintaining the overall average rainfall of the area; the groundwater level is depleting at 0.7 m/year, and average groundwater electrical conductivity (EC) has increased. There has been land subsidence in a few patches.

The reader is suggested to read through all chapters of the book or only the ones that might interest them.

P. Thambidurai
Anil Kumar Dikshit

Acknowledgments

The editors are thankful to all the authors for contributing their chapters to this book, and for their unfailing commitment and cooperation.

Contents

1 **GIS-Based Multi-criteria Decision Analysis for Identifying Rainwater Harvesting Structures Sites in a Semiarid River Basin** . . 1
Pawan S. Wable, Madan K. Jha, V. M. Chowdary, and Smaranika Mahapatra

2 **Hydrochemical Investigation and Water Quality Mapping in and Around Pallikaranai Marshland Area in Chennai, India** 25
S. Packialakshmi, K. Nagamani, and B. Anuradha

3 **Catchment Scale Modeling of Land Use and Land Cover Dynamics** 43
P. Dinagarapandi, K. Saravanan, and K. Mohan

4 **Urban Floods: A Case Study of Patna Floods 2019 – Natural or Anthropogenic?** 57
Ahmad Rashiq and Om Prakash

5 **Flood Susceptibility Zonation Using Dempster-Shafer Evidential Belief Function (EBF) Method in Chalakudy Taluk, Kerala, India** . . 79
Shweta Bhardwaj and Ramesh Veerappan

6 **Impact of Urbanization on Ganga River Basin: An Overview in the Context of Natural Surface Water Resources** 111
Ankit Modi, Chandrashekhar Bhagat, and Pranab Kumar Mohapatra

7 **Urban Water Scarcity: A Global Challenge and Impending Solutions** 129
Paulami Sahu and Chitrangada Debsarma

8 **Groundwater Scarcity in Urban Areas Is a Major Issue: Case Studies from West Bengal** 143
Mayank Sharma

9 **Impact of Urbanization and River Morphology on Groundwater System in Patna Urban Area, Bihar, India** 167
Ashok Kumar and P. Thambidurai

10 Aquifer Storage and Recovery: Key Issues and Feasibility 187
Gopal Krishan and Rahul Garg

11 Temporal Prediction of Groundwater Levels: A Gap in Generalization 203
N. Ramsundram, Mohammad Taghi Sattari, R. Kaviya, M. Kaarthic, and M. Niveditha

12 Suitability of Groundwater for Drinking and Agricultural Use in Patna District, Bihar, India 227
Yash Aryan, P. Thambidurai, and Anil Kumar Dikshit

13 Groundwater Potential Assessment Using GIS-Based Weighted Linear Combination Technique: A Case Study of Hard Rock Terrain Around Bhopal, India 255
Prafull Singh

14 The Effect of Urbanization on Groundwater Quality and Hydrochemical Characteristics in Ennore Coastal Aquifers of Chennai, South India 273
S. Senthilkumar, K. Srinivasamoorthy, and B. Gowtham

15 Groundwater Contamination in Parts of Northwestern Hyderabad: A Hydrogeochemical and Geospatial Approach 293
Pothuri Ramesh Chandra Phani and Kanchi Rajendra Prasad

16 Spatio-temporal Dynamics of Groundwater Recharge in Dras Sub-Basin of Upper Indus River Basin, Western Himalayas 313
Suhail A. Lone and Ghulam Jeelani

17 Impact of Urbanization on Groundwater in Changing Climatic Scenario: A Case Study 323
Alifia Ibkar, Arunangshu Mukherjee, Nidhi Didwania, and Sneha Rai

Index 345

About the Editors

P. Thambidurai is an assistant professor in the Department of Coastal Disaster Management at Pondicherry University – Off Campus, Port Blair, Andaman, India. He received his PhD in hydrogeology from the Department of Earth Sciences, Indian Institute of Technology Bombay, India, and *Gian Maria Zuppi* scholarship for high-achieving in research in the international student category, awarded by the University of Venice during his doctoral degree. He completed his graduate and postgraduate degrees from Periyar University, Salem, India. Dr. P Thambidurai joined Amrita Vishwa Vidyapeetham, Kerala, as a *research associate* after completing his PhD in 2015 and then served there as an *assistant professor* till 2018. He gained intensive field and consultancy experience at Geo Technical Mining Solution, Dharmapuri, Tamil Nadu, India.Dr. P Thambidurai has vast field experience in hydrogeology, where he contributed to building the national level policy called *Revitalization of Rivers in India Draft Recommendation – The Fundamentals* to improve the groundwater and surface water resources. This river policy has been adopted by the Government of India – Ministry of Environment, Forest & Climate Change and Jal Sakthi to rejuvenate 13 major rivers in India. He has published about 20 scientific articles in international journals, conference proceedings, and book chapters.

Anil Kumar Dikshit is higher administrative grade (HAG) professor in the Environmental Infrastructure & Clean Tech (EICT) Group and in-charge of GIS Laboratory for Environmental Management & Sustainability (GEMS) in the Environmental Science and Engineering (ESE) Department at Indian Institute of Technology Bombay, India.He did his graduation and master's in civil engineering in 1985 and 1987, respectively, and completed PhD in civil and environmental engineering from Cornell University, USA, in the year 1994.He has more than 30 years of experience in teaching, research, and consultancy at IIT Kanpur; Cornell University; IIT Kharagpur and IIT Bombay; Kigali Institute of Science & Technology, Rwanda; University of Kwazulu-Natal, South Africa; Nanyang Technological University and National University of Singapore, Singapore; Malardalen University, Sweden; and Asian Institute of Technology, Bangkok. He has guided 40 master's and 22 doctoral scholars while 6 research scholars are working on their PhDs. He has also worked on more than 150 national and international research and consultancy projects. The results of academic research work have provided 1 patent, 8 books, 11 chapters in edited books, 200 reports, 150 publications in international and national journals, and 140 in international and national conferences while many more papers are under review. In addition, more than 20 prototypes/equipment related to various environmental pollution management topics, academic versions of more than 10 environmental modeling and simulation software(s), and about 7 GIS applications on environmental management problems have been developed under his guidance.

Chapter 1
GIS-Based Multi-criteria Decision Analysis for Identifying Rainwater Harvesting Structures Sites in a Semiarid River Basin

Pawan S. Wable, Madan K. Jha, V. M. Chowdary, and Smaranika Mahapatra

Abstract The current study was accomplished in a drought-prone semiarid basin of Maharashtra with the objectives of assessing rainwater harvesting (RWH) in potential sites and identifying the most appropriate sites for RWH and artificial recharge structures. The analysis was performed using remote sensing, GIS, and multi-criteria decision analysis (MCDA). The thematic layers, i.e., land slope, drainage density, and runoff coefficient of the normal years, were used to develop the RWH potential map. Saaty's scale was used to assign suitable weights to the thematic layers and their respective features, and then they were normalized by utilizing the analytic hierarchy process-based MCDA technique. In addition, the suitable sites for the RWH and recharge structures were identified using desirable criteria and Boolean logic, and later sites were prioritized for their cost-effective implementation based on socio-hydrological conditions. The results revealed that 80% of the study area is dominated by zones with "moderate" RWH potential in "normal" years. Moreover, 35% of the study area is suitable for the farm ponds, whereas 2% each for check dam and percolation tanks. For the cost-effective implementation of

P. S. Wable (✉)
Department of Soil Science, Kerala Forest Research Institute, Thrissur, India

Agricultural and Food Engineering Department, Indian Institute of Technology Kharagpur, Kharagpur, India
e-mail: pawan.wable@kfri.res.in

M. K. Jha
Agricultural and Food Engineering Department, Indian Institute of Technology Kharagpur, Kharagpur, India

V. M. Chowdary
Regional Remote Sensing Centre – North, National Remote Sensing Centre, New Delhi, India

S. Mahapatra
Agricultural and Food Engineering Department, Indian Institute of Technology Kharagpur, Kharagpur, India

International Water Management Institute, South Asia, New Delhi, India

P. Thambidurai, A. K. Dikshit (eds.), *Impacts of Urbanization on Hydrological Systems in India*, https://doi.org/10.1007/978-3-031-21618-3_1

proposed RWH structures, 11% of the agricultural area is prioritized for the excavation of farm ponds, and 284 sites are prioritized for the construction of check dams.

Keywords Multi-criteria decision analysis · SCS curve number method · Geospatial techniques · Rainwater harvesting · Zone prioritization

1 Introduction

Development of any area primarily depends on water availability as it plays an important role in social, economic, and environmental dimensions. Agriculture, domestic, and industrial sectors are the major water-demanding sectors. Among them, economy-wise agriculture is the most responsive to water scarcity as it accounts for 70% of global freshwater use and not less than 90% of the consumptive use (FAO, 2012). By 2050, it is projected that 60% more food will be required to fulfill the demand of a concluding population of 9 billion. In many areas, currently, water scarcity has severely limited food production, thereby threatening food security. Rainfed agriculture is the prime source of food grains in the world. India with 60% total land area under rainfed area ranks first, and All India Report on Agriculture Census 2010–2011 (2015) highlights that India's 89% millet, 88% pulses, and 73% cotton production come from rainfed agriculture, and it supports 72% of total livestock. However, these areas are characterized by land degradation, poverty, malnutrition, water scarcity, climate variability, crop failure, and a lowest average productivity of less than 1 t/ha (Rockstrom et al., 2010). In addition, these regions also experienced droughts every 3-year cycle (DTE, 2015). On the other hand, the remaining 40% of India's total land area is irrigated land that helps to serve 55% food requirements of the country. However, it consumes 70% of the freshwater resources and provides less scope to extend it further (CWC, 2005). Even though with the implementation of the best scenario of irrigation development, Parthasarathy Committee (2006) estimated that about 40% more supply of food grains would be needed from rainfed agriculture to fulfill increased future demand. Hence, revolution is vital in rainfed agriculture for food security as well as mitigating poverty and malnutrition in India.

Nowadays, among the several solutions available for mitigating the impacts of droughts, rainwater harvesting (RWH) has emerged as the most effective solution for water conservation and groundwater augmentation. This is due to fact that rainwater is easy to collect and a reliable resource for domestic and agricultural use without any treatment. RWH is gaining popularity as they ensure the availability of fresh and safe water when the common source of water fails. Besides that, the conserved surplus monsoon runoff can be used for underlying aquifers, thereby artificially augmenting depleting groundwater resources. The RWH can be achieved by both in situ and ex situ interventions (Kahinda & Taigbenu, 2011; Wani et al., 2011). In situ interventions are performed in farmer's fields to conserve the rainwater in the form of soil moisture, e.g., field bunding, broad bed and furrow practices, etc. Ex situ interventions are structures constructed outside the fields, e.g., farm ponds, check dams, and percolation tanks with storage capacities ranging from 100 to

5000 m^3. Among them, the cost of ex situ interventions is much higher than in situ interventions. Furthermore, ample government funds are assigned to numerous rural development and employment schemes through which the construction and maintenance of different ex situ interventions are executed at a basin scale. Hence, the decision for the selection of the RWH sites for ex situ interventions is very important.

Successful implementation of RWH and artificial recharge structures in any area depends mainly on the runoff potential of the area and the identification of suitable sites for constructing these structures. According to FAO (2003), six main parameters should be studied for selecting RWH sites: rainfall, runoff, terrain slope, crop characteristics, physical properties of soil, and socio-economic conditions. The rapid progress in geospatial techniques has served as a valuable tool for effective decision-making planning and management of natural resources at a larger scale. It facilitates an effective and user-friendly analysis of the spatiotemporal data (FAO, 2003). Few of its applications are the evaluation of groundwater prospect, runoff potential, RWH potential, zoning of waterlogged/salt-affected areas, recharge-discharge areas, etc. The RWH has been practiced in semiarid/arid regions of India (Sahoo, 2004; Ramakrishnan et al., 2008; Jasrotia et al., 2009; Bamne et al., 2014), Jordan (Ziadat et al., 2012), Iran (Ghayoumian et al., 2007), West Asia and North Africa (Oweis et al., 1998), etc. In these studies, thematic layers derived mainly were slope, drainage, land use, and surface runoff. For the Indian regions, the suitability criteria for RWH sites in most studies were based on the guidelines of the Integrated Mission for Sustainable Development (Ramakrishnan et al., 2008; Jasrotia et al., 2009; Bamne et al., 2014). For RWH planning, the important component surface runoff was estimated using either Soil Conservation Service Curve Number (SCS-CN) method (Sahoo, 2004; Ramakrishnan et al., 2008; Kadam et al., 2012) or Thornthwaite-Mather method (Jasrotia et al., 2009) with former one being widely used. Ramakrishnan et al. (2008) conducted a field survey to validate recommended sites for RWH structures that indicated 80–100% accuracy. A different study by Ziadat et al. (2012) demonstrated a methodology to identify suitable RWH structures using a participatory GIS approach that combines social, economic, and biophysical criteria.

In the RWH planning for large areas, multiple factors were often conflicting, e.g., different soil types, slope classes and land use/land cover (LULC), drainage density, runoff classes, etc. GIS-based multi-criteria decision analysis (MCDA) and Boolean logic can deal with this problem, which constitutes a powerful framework (Voogd, 1983; Malczewski, 1999). Hence, in the recent past, the combination of multi-criteria decision analysis (MCDA) along with geospatial techniques has attracted several researchers for the evaluation and identification of potential RWH potential and artificial recharge sites (Chowdhury et al., 2010; Weerasinghe et al., 2011; Jha et al., 2014; Mahmoud et al., 2016; Singh et al., 2017). In most of these studies, the analytic hierarchy process (AHP)-based multi-criteria decision analysis technique was used to assign different weights to the thematic layers according to their importance. They were combined using the weighted linear combination method to

generate RWH potential maps. Weerasinghe et al. (2011) developed the Geographic Water Management Potential (GWAMP) model, which was tested and validated in Sao Francisco and Nile catchments with different geographic and climatic conditions. They concluded that in a given catchment, the GWAMP model could be used for identifying RWH potential sites. Mahmoud et al. (2016) presented a methodology for managing agricultural drought in arid and semiarid regions by RWH in El Beheira Governorate, Egypt. The agricultural drought was monitored using the NDVI differencing technique. For drought management, the developed RWP map was categorized into suitable and unsuitable classes. In another study, Singh et al. (2017), for the realistic implementation of the RWH and artificial structures in Damodar canal command of West Bengal, India, prioritized the identified zones by considering some key factors like groundwater level during the post-monsoon season, groundwater fluctuation, and spatial water demand. Recently, Toosi et al. (2020) presented a realistic method to identify probable RWH areas using the GIS-based MCDA technique and to consider socio-economic factors at a basin scale in northeast Iran. The study revealed that 52% of the study area was appropriate for various RWH structures.

A review of the above pertinent literature suggests that several studies have reported using RS- and GIS-based MCDA for the RWH potential zoning. However, prioritization of sites for RWH and artificial recharge structures for cost-effective implementation of the RWH plan by considering socio-hydrological factors is not common, although it is very helpful for water management decision-makers. With these facts and issues, this study was done in an agriculture-dominated drought-affected semiarid climate-characterized river basin of Western India (Wable et al., 2018). The objectives of this study are (i) to identify RWH potential zones using GIS-based MCDA, (ii) to identify suitable sites for the different RWH structures, and (iii) to prioritize the selected RWH structures for their cost-effective implementation. In this study, specific thematic layers like post-monsoon groundwater level, irrigation command area under major/medium projects, and proximity of rural settlements are considered for prioritizing zones/sites for the construction of RWH and artificial recharge structures. The study presents a one-of-a-kind practical approach for identifying the best suitable RWH sites and artificial recharge structures, which can be easily adopted by the policymakers and water managers of any area.

2 Material and Methods

2.1 Overview of Study Area

The present study was carried out in the semi-urban Sina River basin. The location of the study area is confined between 17° 28′ N and 19° 16′ N latitude and 74° 28′ E and 76° 7′ E longitude. The area covers 12,244 km^2 in Western India (Fig. 1.1). The basin falls into four districts, namely, Solapur, Osmanabad, Ahmednagar, and Beed, with the major portion (42%) of the basin coming under the Solapur district. The

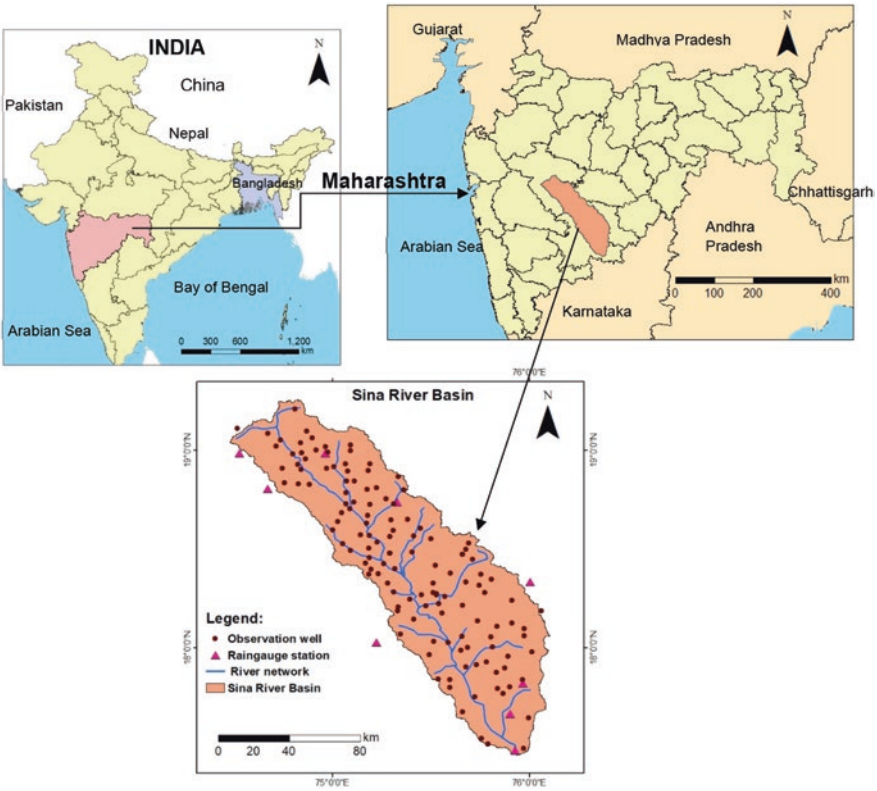

Fig. 1.1 Study area map showing the locations of hydrometeorological monitoring sites

elevation ranges between 420 and 964 m above MSL. The climate of the river basin is characterized as semiarid. The average annual rainfall of the study area is 644 mm, with most rainfall falling during the monsoon season (June–October). In the study area, the majority of the part (80%) is covered by agricultural use in which both type monsoon (*Kharif*) and non-monsoon (*Rabi*) season crops are grown. The main crops grown are fodder grass, groundnut, pearl millet, pulses, safflower, sorghum, sugarcane, wheat, and various other horticultural crops. Sugarcane is the major cash crop, which is mainly cultivated in the assured irrigated area of the region. Agriculture, hydropower, industries, and drinking demands are the main consumers, with agriculture sharing the largest among all. The main sources of irrigation in the study area are canals and/or groundwater. However, groundwater fulfills more than half of the irrigation water requirement in the catchment. Hard rock underlies the basin with an unconfined aquifer at shallow depth (up to 20 m), while semi-confined and confined aquifers prevail at deeper depths. The thickness of the unconfined aquifer over the area varies from 5 to 20 m (MoWR & CGWB, 2013). Groundwater is generally extracted from dug wells or dug-cum-bore wells, which tap water from the upper portions of weathered or fractured Deccan basalt. The

surface water source of irrigation in the study area is carried out with one major, 20 medium, and several minor irrigation projects.

2.2 Data Acquisition

Daily rainfall data for the period 1985–2009 were collected for nine rain gauge stations from the State Data Storage Center, Hydrology Project (HP), Nashik, India, and India Meteorology Department (IMD), Pune. The land use/land cover map (scale 1:50000) was collected from the National Remote Sensing Center (NRSC), Hyderabad, India. The soil map of the study area (scale 1:250000) and the related soil physical and hydraulic characteristics were acquired from the National Bureau of Soil Survey and Land Use Planning (NBSS & LUP), Nagpur, India. The SRTM digital elevation model of grid size 90 m was downloaded from the CGIAR Consortium for Spatial Information website (Jarvis et al., 2008). In addition, the post-monsoon groundwater level data of 132 wells (1985–2009) were procured from the Groundwater Survey and Development Agency (GSDA), Pune, India.

2.3 Extraction of Thematic Layers

Rainwater harvesting (RWH) mainly depends upon the threshold value of rainfall, a prime factor that generates runoff. Also, catchment types (with different soil conditions and land use/cover) and catchment characteristics like slope, drainage density, etc. play a crucial role in evaluating the potential of an area for harvesting rainwater and identifying the suitable sites of harvesting structures, which makes it as a complex multi-criteria problem. In this study, the RWH potential map was generated using the basic and derived thematic layers, e.g., runoff coefficient, slope, and drainage density, as recommended by Jha et al. (2014). Rainfall maps were generated using the daily rainfall data for 25 years. The standard "Thiessen polygon" method was employed for quantifying the mean areal rainfall, which was further used for creating the rainfall map of the studied catchment (Singh, 1992; Subramanya, 2008). The soil map was again classified into hydrologic groups based on soil properties such as its texture and infiltration characteristics to obtain the soil hydrologic group map. Maps depicting spatial "runoff potential" and "runoff coefficient" over the basin were developed by considering rainfall, soil, and land use/cover information, which is illustrated in the next sections. The slope map and drainage density of the study area was extracted from DEM by using in-built algorithms in ArcGIS 10.1 software. For the drainage density map, first, the sub-watershed map and drainage network maps of the study area were prepared. Further, the drainage network map and the sub-watershed map were combined, and a drainage density map was prepared as a composite layer. In addition, some more thematic layers such as drainage network map, settlement map, irrigation command map, and post-monsoon water

table map for the "normal" year were also prepared to identify the appropriate sites for RWH and artificial recharge structures.

2.3.1 Runoff Coefficient Map Preparation

The runoff coefficient is that part of total rainfall which directly contributes to the generation of runoff. Many previous studies used direct surface runoff estimation by the Soil Conservation Service Curve Number (SCS-CN) technique (SCS, 1985), a conceptual model developed by USDA, which has proven to provide accurate results in lack of runoff measurements areas (Al-Ghobari et al., 2020). Hence, this method was used in the current study to quantify direct surface runoff, i.e., runoff potential. For this, a distributed CN approach was applied in the GIS environment. Rainfall data, along with soil and LULC cover maps, were utilized for modeling runoff and generating runoff potential maps. The value of the initial abstraction ratio (λ) in the SCS-CN method, which generally ranges from 0.1 to 0.4 as found in different studies conducted in different geographic locations, was taken to be 0.3 in this study (Subramanya, 2008). Following standard guidelines, the antecedent moisture condition (AMC) was determined (Singh, 1992; Subramanya, 2008). The values of potential maximum retention (S) were calculated using the assigned distributed CN values for daily rainfall. Thiessen polygon method was used for computing the area coverage for each rain gauge station. After that, the estimated daily runoff values were converted to an annual scale, and the maps of runoff potential of the basin were prepared for three rainfall scenarios: wet, normal, and dry conditions for the years. It is to be noted that the wet year indicates that the year has higher rainfall than the average annual rainfall (AAR), while it is considered that the normal year was defined as a year when the total rainfall received was equal to the AAR. On the other hand, a year having annual rainfall less than or equal to 25% of the AAR was defined as a dry year (Subramanya, 2008). Further, runoff coefficient maps were created for the study area for all these three rainfall scenarios, i.e., wet, normal, and dry years, by dividing runoff by the corresponding rainfall year.

2.4 Multi-criteria Decision Analysis

The runoff coefficient map for the normal year and slope and drainage density maps were used for delineating RWH potential zones. Analytic hierarchy process (AHP), which is a multiple criteria decision-making tool (Saaty, 1980), was used for generating an RWH potential map for the study area. Based on the local experience and experts' notions, weights were allotted to the three thematic layers (i.e., runoff coefficient, drainage density, and land slope) and their features based on their relative effect on the RWH potential in the 1–9 scale (Saaty, 1980). Further, the eigenvector technique was applied for the normalization of these assigned weights. The

consistency ratio (CR) was calculated to evaluate the consistency of the normalized weights as follows:

$$\text{Consistency ratio } (\text{CR}) \frac{\lambda_{\max} - n}{n-1} \tag{1.1}$$

where $\lambda_{\max}$= principal eigenvector (obtained from eigenvector technique) and n = number of criteria or factors. To maintain consistency in the assigned weights, the CR should be less than 10% (Saaty, 1980); otherwise, assigned weights should be reassessed.

2.5 Development of Rainwater Harvesting Potential Map

The abovementioned thematic layers, viz., runoff coefficient, slope, and drainage density, along with their respective normalized weights, were combined by weighted linear combination (WLC) method using ArcGIS software, and thereafter, the Rainwater Harvesting Potential Index (RWHPI) was calculated to delineate RWH potential zones, as follows:

$$\text{RWHPI} = \left(\text{RC}_{\text{w}}\text{RC}_{\text{wi}} + \text{SL}_{\text{w}}\text{SL}_{\text{wi}} + \text{DD}_{\text{w}}\text{DD}_{\text{wi}}\right) \tag{1.2}$$

where RC = runoff coefficient; SL = slope; and DD = drainage density. The subscript "w" denotes the normalized weight of a theme, and "wi" represents the normalized weight of the individual features. The RWHPI is a unit less quantity that indicates the feasible RWH potential zones/sites in an area. Thus, the study area's RWH potential map was generated for the "normal" rainfall year using GIS. The entire procedure followed for this study is illustrated in the flowchart (Fig. 1.2).

2.6 Identification and Prioritization of Suitable Sites

After identifying RWH potential zones in the basin, suitable sites for constructing RWH structures (farm ponds) and artificial recharge structures (percolation tanks and check dams) were determined by overlaying the thematic layers of the slope, rainfall, soil, LULC, and stream network in the GIS environment. From the pertinent and critical review of past literature (Chowdary et al., 2009; Jha et al., 2014) and professional experience, the suitability criteria for each RWH structure used in this study were finalized and are summarized in Table 1.1. Agricultural lands are suitable for the construction of farm ponds, while percolation tanks (on the ground) in degraded forest and pasture lands. On the other hand, for the check dams and percolation tank (along the stream), a stream-order buffer map was developed by

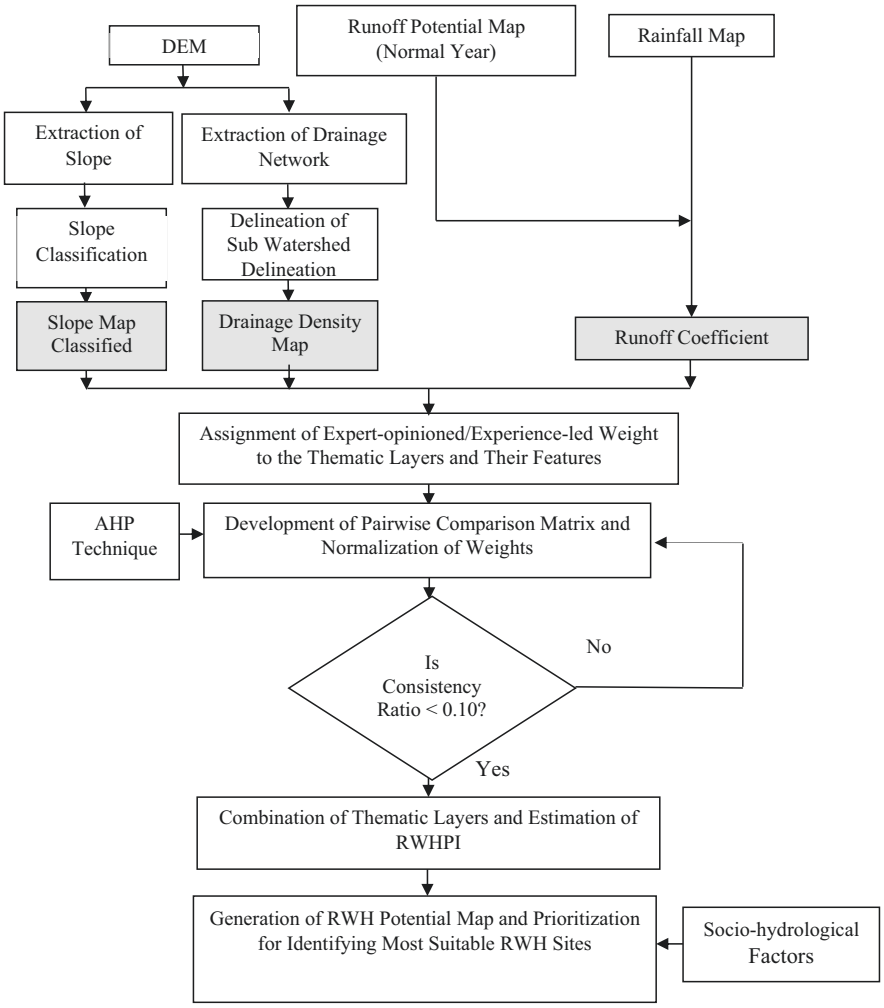

Fig. 1.2 Framework of the methodology adopted in the study

extracting all the 3rd order streams of 100 m buffer from the stream network map. The specified suitability criteria (Table 1.1) were applied to the integrated map using the GIS-based Boolean logic method, and suitable sites were identified for building the RWH and artificial recharge structures.

Additionally, the RWH and artificial recharge sites were prioritized considering socio-hydrologic factors for the cost-beneficial execution of RWH measures. For the prioritization of farm ponds, a settlement buffer of 500 m, an irrigation command area for major and medium dams, and a safe groundwater-level zone during the post-monsoon season were considered. On the other hand, priority sites for

Table 1.1 Suitability criteria used for RWH and artificial recharge structures identification

SI. no.	RWH/recharge structures	Land slope	Soil	Land use/land cover	Drainage order
1	Farm pond	<3%	Fine texture (dense clay at moderate depth)	Agriculture	–
2	Percolation tank (on the ground)	<3%	Loam (very shallow, shallow, and deep depth)	Degraded forest and pasture land	–
3	Percolation tank (along the stream)	<5%	Loam	–	3rd
4	Check dam	<15%	Fine texture (clay at shallow depth and dense clay at moderate depth)	–	3rd

check dams were selected considering minimum spacing of 5 km between two consecutive dams and a 500 m buffer for the proximity of these structures to the settlement. It should be noted that somewhat arbitrary spacing is considered between the two check dams, which can be altered when the RWH plan is implemented after essential field investigations.

3 Results and Discussion

3.1 Features of the Thematic Layers

3.1.1 Land Use/Land Cover

The study area has classified in twelve main land use/cover (LULC) classes, which are (a) agriculture, (b) wasteland, (c) dense forest, (d) fallow land, (e) mining area, (f) open forest, (g) plantation, (h) river/water bodies, (i) rural settlement, (j) degraded forest, (k) pastureland, and (l) urban settlement. The spatial distribution of LULC for the study area is depicted in Fig. 1.3. Most of the LULC is under agriculture (79%), succeeded by pastureland (9%) and fallow land (6%).

3.1.2 Soil

The study area has three types of soil, i.e., loam, clay, and dense clay (Fig. 1.4). Dense clay soil covers the majority of the area, around 45%, followed by clay, 30%, and loamy soil, 25%. The depth of soil is shallow for the clay soil, very shallow to deep for the loam type, and moderately deep to very deep for the dense clay soil, which was respectively classified on the basis of soil physical properties into hydrologic soil groups (HSG) B, C, and D.

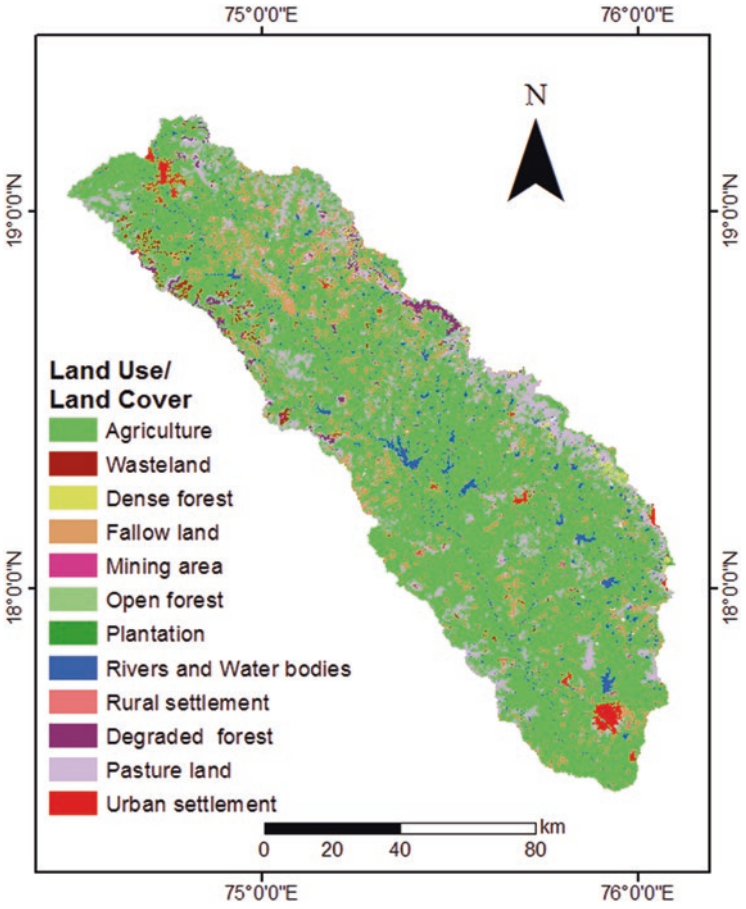

Fig. 1.3 Land use/land cover map of the study area

3.1.3 Slope

The topographic slope map (Fig. 1.5) reveals that the slope varies from zero (level) to 55% (very steep). The study area's land slopes were classified into six dominant classes (Jha et al., 2014): (a) nearly level (0–1%), (b) gentle (1–3%), (c) moderately gentle (3–5%), (d) steep (5–10%), (e) moderately steep (10–15%), and (f) very steep (15–55%). It is clear from Fig. 1.5 that 5820 km^2 (48% of the study area) has a nearly level slope and 4362.61 km^2 (36%) has a gentle slope. These two slope classes are suitable for designing rainwater harvesting (RWH) sites. Several small patches in the river basin are characterized as moderately gentle with a total area of 1236 km^2 (10%), and the zones having steep slopes (including moderately steep and very steep slopes) cover 823 km^2, i.e., only 7% which located in the northeast portion of the study area.

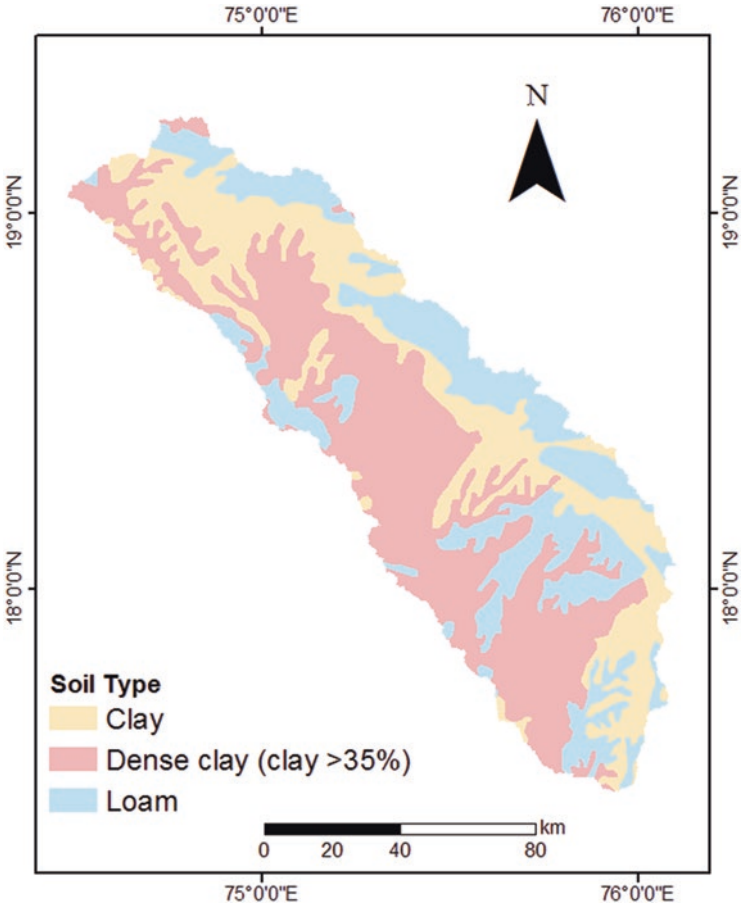

Fig. 1.4 Soil map of the study area

3.1.4 Drainage Network

The prepared drainage network map (Fig. 1.6) reveals that the channel in the river basin area has a maximum order of seven. It is evident from the figure that first-order streams have maximum drainage with a length of 6295 km (53% of the total length). The second-order streams have a drainage length of 2850 km (24%), whereas second-order streams have a drainage length of 1466 km (12%). The fourth- and fifth-order drainage networks have 681 and 357 km lengths, which constitute 6% and 3% of the total drainage lengths, respectively. The remaining part is only 1% of the total length and is covered by both sixth- and seventh order streams with 148 km and 139 km, respectively.

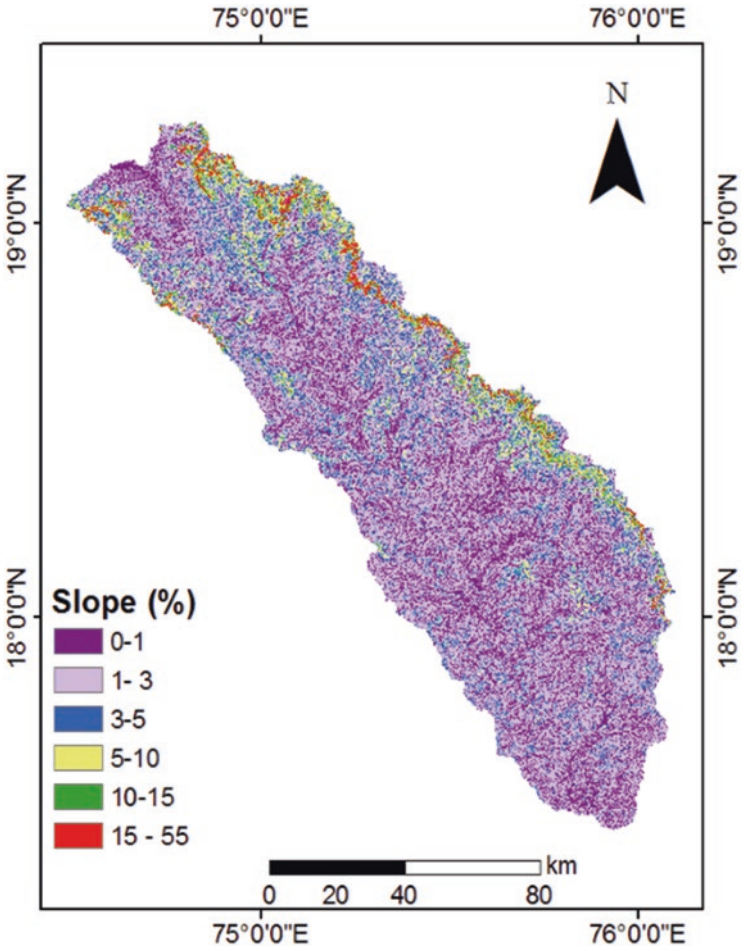

Fig. 1.5 Slope map of the study area

3.1.5 Drainage Density

The spatial drainage density values vary from 0.40 to 1.17 km/km^2 (Fig. 1.7). Based on the values of the drainage density, the sub-watersheds were classified into three categories: (a) low (<0.5 km per km^2), (b) moderate (0.5–1.0 km per km^2), and (c) high (>1.0 km per km^2). A substantial part of the study area falls under the high drainage density class, encircling an area of 8986 km^2 (73%). This class is dominantly occupied, except for the northern part of the study area. The moderate drainage density zone covers an area of 3178 km^2 (26%). On the other hand, only one micro-watershed comes under the low drainage density category having an area of 80 km^2 (1%), located in the northeast part of the study area. It is worth mentioning that the areas with high drainage density values are unsuitable for constructing

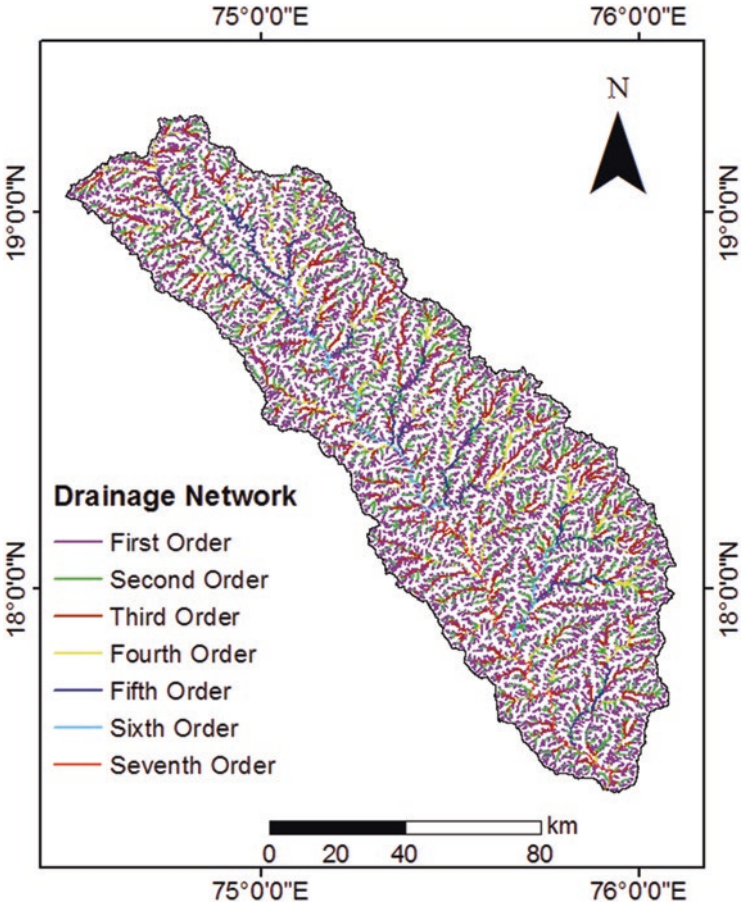

Fig. 1.6 Drainage network map of the study area

RWH structures as the water will drain faster, and therefore there will be less water to store. Hence, these areas were eliminated from the computation, and only the zones having low drainage density were preferred for selecting RWH structures in the construction sites.

3.2 Runoff Coefficient Maps

Runoff coefficient (RC) maps were developed for the wet year (1998), normal year (2000), and dry year (2003), which are presented in Figs. 1.8a–c. The study area is classified into four classes with respect to the spatial variation of RC values: (i) very high (>0.40), (ii) high (0.3–0.4), (iii) moderate (0.2–0.3), (iv) low (0.1–0.2), and (v)

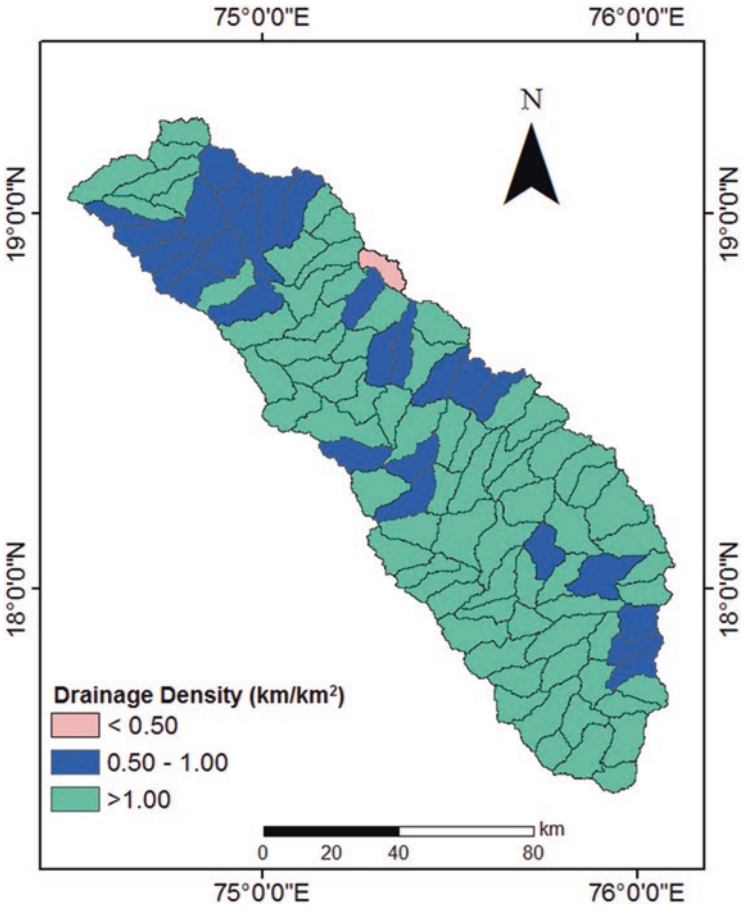

Fig. 1.7 Drainage density map of the study area

very low (<0.1). For the wet year, the RC map of the study area is shown in Fig. 1.8a. It is seen that a major part of the study area has a high RC which covers an area of 7499 km^2 (61%) and is spread in northeast/north and southeast/south parts of the study area. The area has moderate RC and is spread over the lower and northeastern parts, covering about 3303 km^2 (27%). The areas under very low, low, and very high RC categories are 249 km^2 (2%), 499 km^2 (4%), and 693 km^2 (6%), respectively. The RC map for the normal year (Fig. 1.8b) reveals that most of the study area is covered by low and moderate RC categories, covering an area of 5935 km^2 (48%) and 5146 km^2 (42%), respectively. The zones falling under moderate RC class are in the northeast/north and southeast/south portions of the study area, whereas low RC class falls in the northeast and southeast/south parts. The very low RC class covering an area of 749 km^2 (6%) is observed in a narrow strip in the northeast part of the study. The very high RC class incorporating an area of 414 km^2 (3%) is seen

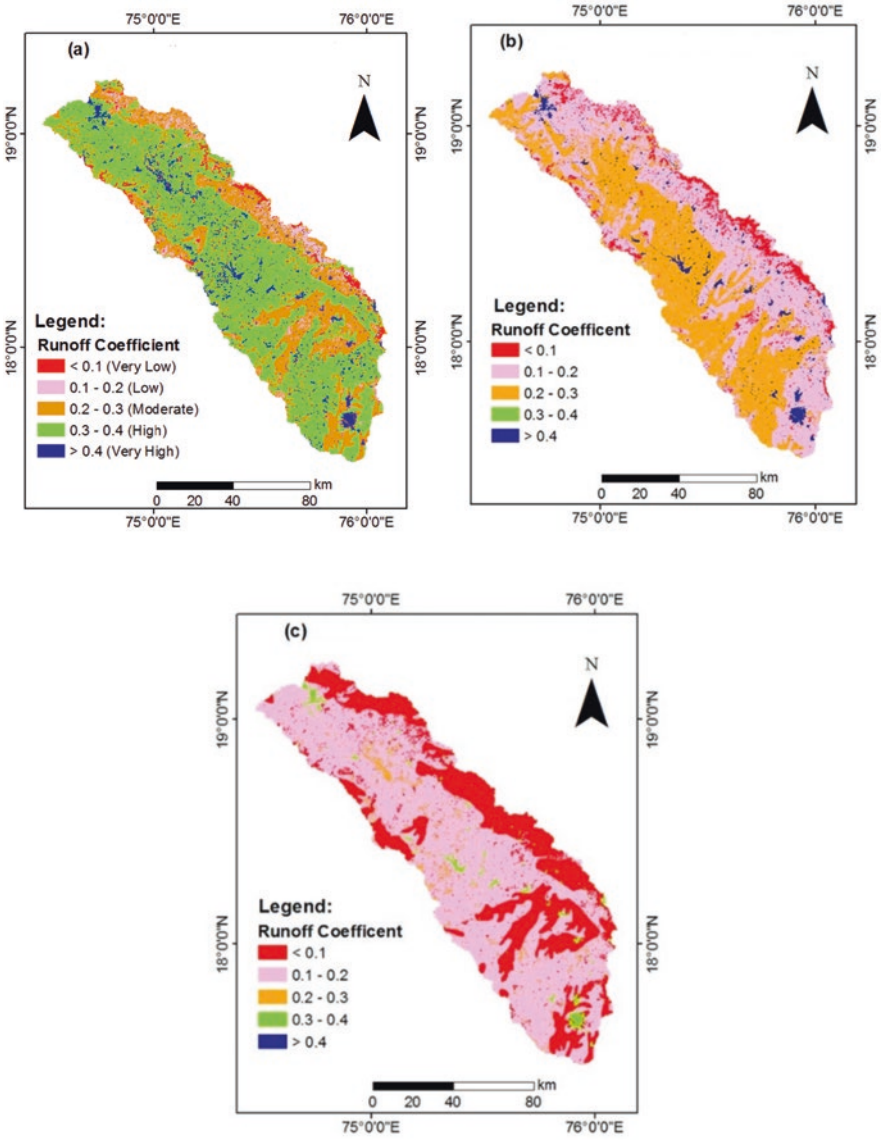

Fig. 1.8 Runoff coefficient map of the study area for (**a**) wet year (1998), (**b**) normal year (2000), and (**c**) dry year (2003)

in small patches over the area. The RC map of the study area for the dry year (Fig. 1.8c) shows that the low runoff coefficient class zone covers a major part of the study area (7890 km^2; 64%) on the northeast/north and southeast/south side. Also, the very low RC class encompasses 3661 km^2 (30%) area and is spread in the northeast and lower parts.

Table 1.2 Pairwise comparison matrix and normalized weights of the thematic layers

Thematic layer	Assigned weight	Thematic layer			Normalized weight
		Runoff coefficient	Slope	Drainage density	
Runoff coefficient	9	9/9	9/8	9/6	0.391
Slope	8	8/9	8/8	8/6	0.348
Drainage density	6	6/9	6/8	6/6	0.261
Total					1

Table 1.3 Weights assigned and the normalized weights of the thematic layers and their corresponding features

Thematic layer	Feature class	Weight assigned	Normalized weight
Runoff coefficient	Very high: >0.4	8	0.333
	High: 0.3–0.4	6	0.250
	Moderate: 0.2–0.3	5	0.208
	Low: 0.1–0.2	3	0.125
	Very low: <0.1	2	0.083
Slope	Nearly level: 0–1%	9	0.346
	Gentle: 1–3%	7	0.269
	Moderately gentle: 3–5%	5	0.192
	Steep: 5–10%	3	0.115
	Moderately steep: 10–15%	1	0.038
	Very steep: 15–55%	1	0.038
Drainage density	Low: <0.5	8	0.471
	Moderate: 0.5–1	6	0.353
	High: >1	3	0.176

3.3 Assignment of Weights to Thematic Layers

The weights allotted to the thematic layers were normalized by applying AHP and Eigenvector techniques. These are compiled in Table 1.2, along with the respective pairwise comparison matrix. The allotted weights associated with the respective thematic layers were found consistent as the consistency ratio is not more than 0.10 for all three thematic layers. Similarly, appropriate weights allocated to the features of each thematic layer were normalized (Table 1.3). In this case, the consistency ratios were also not more than 0.10 for all the features of the thematic layers, which indicates the consistency of the assigned weights.

3.4 Rainwater Harvesting Potential Map

The RWH potential map of the study area was developed (Fig. 1.9) by combining the concerned thematic layers and then calculating the rainwater harvesting potential index (RWHPI) in the GIS environment. On the basis of obtained RWHPI

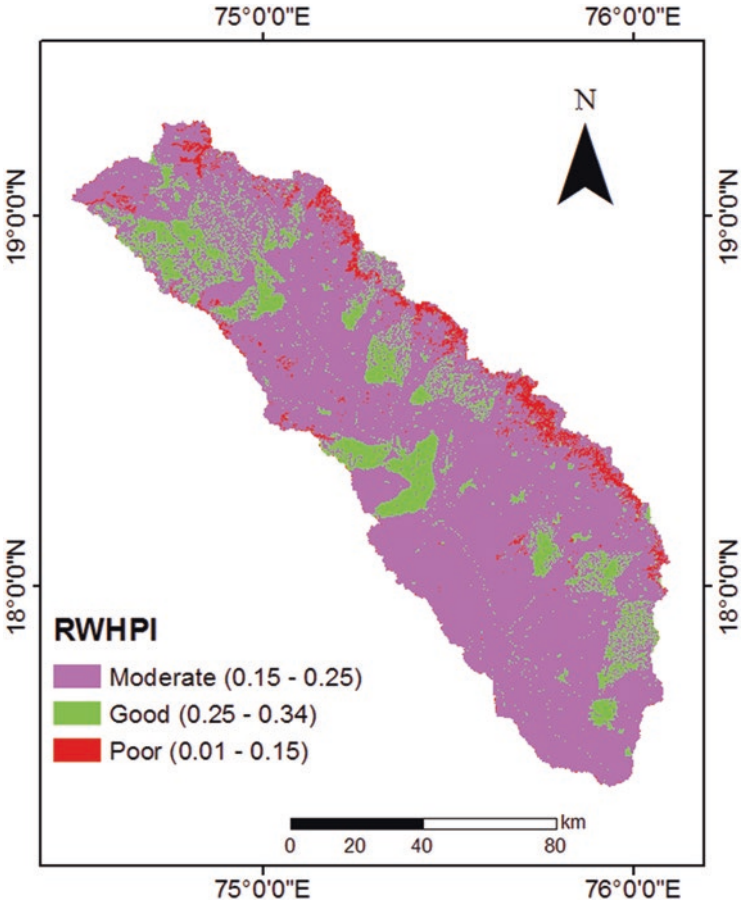

Fig. 1.9 Map showing RWH potential zone classes in the study area

values (0.01–0.34), the study area was classified into three zones indicating: (a) good (RWHPI = 0.25–0.34), (b) moderate (RWHPI = 0.15–0.25), and (c) poor (RWHPI = 0.01–0.15) RWH potential. The area having good RWH potential is 1930 km^2 (16%), which extends into the small patches in the study area. The moderate RWH potential zone is large in the study area covering 80% of the study area (9802 km^2). The area with poor RWH potential is about 513 km^2 (about 4%), extending in small strips in the eastern and northeastern parts. The main reason for this poor RWH potential zone is that moderately steep to very steep slope (10–55%) prevails in this zone. Based on the developed RWH potential map, suitable areas were identified for RWH measures to conserve rainwater and augment groundwater in the area.

3.5 Zones/Sites for RWH and Artificial Recharge Structure

For the construction of different RWH structures, suitable RWH sites are chosen based on land slope, LULC cover, drainage order, and soil type (Table 1.1). Agricultural land is most appropriate for excavating farm ponds (Table 1.1) as harvested water can be used for supplemental irrigation. Two types of fine textural soil are available in the study area, (i) dense clay and (ii) clay soil. The dense clay soil is available at moderate to very deep depths. Hence, considering the depth of farm ponds, the area having dense clay is considered for farm pond excavation. However, the depth of clay soil is shallow (25–50 cm); the zones having clay soil are not suitable for farm ponds. The zone appropriate for farm pond is 35% (4236 km^2), spread over southeast/south portions of the study area (Fig. 1.10). In contrast, suitable areas for percolation tanks (on the ground and along the stream) are only 1% each, which

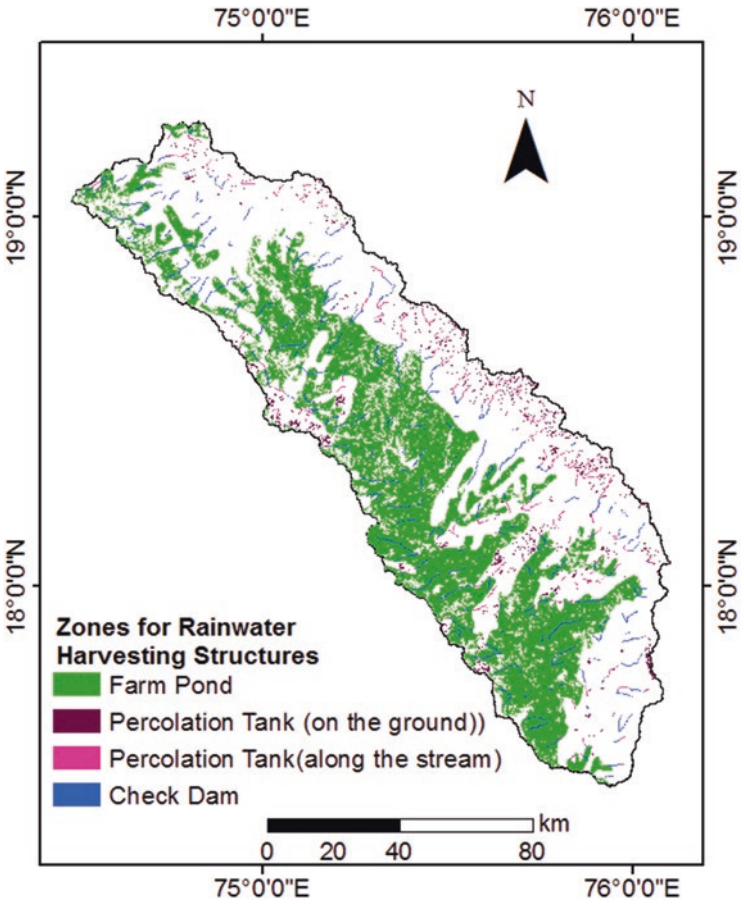

Fig. 1.10 Map of suitable zones for rainwater harvesting structures in the study area

cover scattered mostly northeastern parts of the study area. For the construction of check dams, an area of 270 km^2 (2% of the study area) is found applicable.

3.6 *Prioritized Sites/Zones for RWH and Artificial Recharge*

Based on the GIS analysis, 46,952 locations are found to be appropriate for farm ponds, which are practically infeasible. Hence, the sites for farm ponds are prioritized based on the proximity of rural settlements, irrigation commands under major/medium dams, and safe groundwater levels. However, the command area maps of each major and minor dam are not available, but the area of irrigation command is known. Hence, the buffer of 3000 m is estimated based on the average area of irrigation command (30 km^2) under major/medium projects. Further, this buffer is applied for the entire major/medium irrigation projects because farm pond construction within this buffer is unnecessary. In addition, the farm pond zone beyond the area having 3–6 m depth to post-monsoon water table during normal years is preferred since it is assumed that this zone of groundwater would be available for irrigation. Hence, out of the total area under farm pond, the area outside of rural settlement has a buffer of 500 and 3000 m buffer of major and minor irrigation projects, and the buffer of 3–6 m depth to post-monsoon water table is used to prioritize farm ponds as shown in Fig. 1.11a. The area of the prioritized zone of the farm pond is 1098 km^2, which is 11% area of the agriculture area (9616 km^2).

Furthermore, considering suitability criteria (Table 1.1), 8546 sites are found suitable for check dams, which are practically infeasible. For this prioritization of

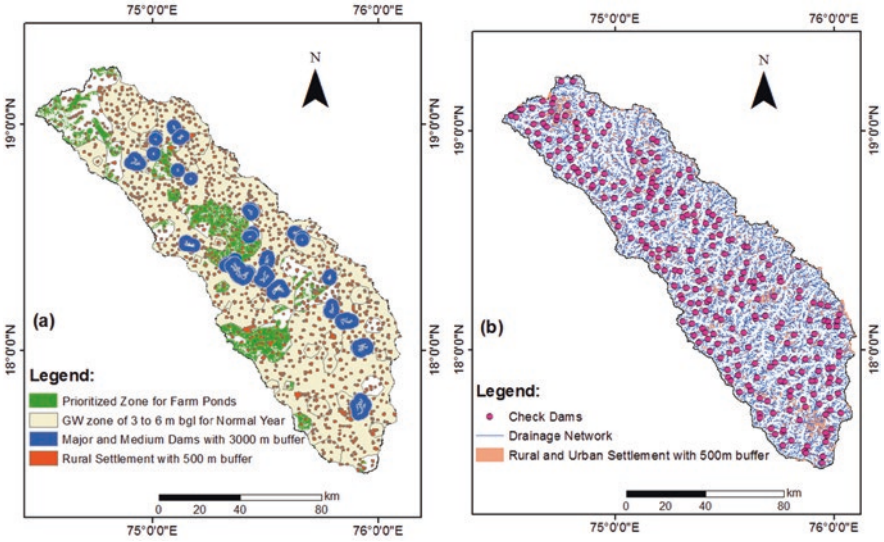

Figs. 1.11 Prioritized sites for RWH structures (**a**) farm pond and (**b**) check dam

check dams, based on the regional/local experience, the minimum distance between two conservative check dams is considered 5 km, and the proximity of this structure to the settlement is taken as a 500 m buffer. In this way, in the study area, 284 sites are prioritized for check dams, as shown in Fig. 1.11b. During field implementation of the proposed plan, the prioritized check dam sites can be further optimized depending upon the streamflow availability, amount of water harvested per structure, and local conditions. The prioritized sites for farm ponds and check dams can be used for the cost-effective implementation of the RWH plan.

4 Conclusions

In any area/region, rainwater harvesting (RWH) plays the main role in mitigating the impacts of droughts. The present study illustrates the capability of geospatial techniques and multi-criteria decision analysis (MCDA) methods for planning RWH measures in the study area. Further, appropriate sites/zones for RWH and artificial groundwater recharge have been identified for efficient water management. Prioritization of these sites/zones has also been carried out for the cost-effective implementation of water conservation strategies considering some socio-hydrological criteria. The major findings drawn from the analysis of the results are as follows:

- The runoff coefficient for most of the study area varies from moderate (0.2–0.3) to high (0.3–0.4) in the wet year, low (0.1–0.2) to moderate in the dry year, and very low (0.0–0.1) to low in the dry year. Approximately 14% of the total rainfall received over the basin is transformed into the runoff.
- The rainwater harvesting potential of the area varies from 0.01 to 0.34 in normal years. About 80% of the study area (9802 km^2) comes under the moderate RWH potential (0.15–0.25) zone, while about 16% (1930 km^2) of the total basin has good (0.25–0.34) RWH potential.
- A total of 8546 sites are found suitable for check dams covering an area of 270 km^2 (2% of the area), while 46,952 locations are found to be appropriate for farm ponds covering (4236 km^2) 35% of the study area. Suitable lands for percolation tanks (both “on the ground” and “along the stream”) cover an area of 260 km^2 (2% of the study area).
- For the economical implementation of RWH structures in the study area, 11% of the agricultural land is prioritized for the excavation of farm ponds, and 284 sites and construction of check dams in the study area are prioritized.

Overall, this study demonstrates the use of the GIS-MCDA integrated tool for assessing the RWH potential zones, identifying the most suitable locations for the RWH, and augmenting the groundwater from a socio-hydrologic aspect for cost-effective implementation. On the overlapping cadastral map on the RWH maps, this study can help water managers with effective planning for RWH and artificial groundwater recharge structures to combat the droughts in the study area,

particularly in the rainfed farming areas. The field survey for the validation of the suggested sites for RWH structures is recommended as a follow-up to this study.

Acknowledgment The first author is thankful to the Ministry of Human Resource Development (currently the Ministry of Education), New Delhi, India, for the financial support in terms of scholarship during his Ph.D. research. We are sincerely thanking of the data resource agencies, including National Remote Sensing Center (NRSC), Hyderabad; National Bureau of Soil Survey and Land Use Planning (NBSS LUP), Nagpur; Groundwater Survey and Development Agency (GSDA), Pune; State Data Storage Center, Hydrology Project (HP), Nashik; and India Meteorological Department (IMD), Pune for their support.

References

Al-Ghobari, H., Dewidar, A., & Alataway, A. (2020). Estimation of surface water runoff for a semi-arid area using RS and GIS-based SCS-CN method. *Water, 12*(7), 1924. https://doi.org/10.3390/w12071924

All India Report on Agriculture Census 2010–11. (2015). *Agriculture Census Division Department of Agriculture*. Cooperation & Farmers Welfare Ministry of Agriculture & Farmers Welfare, Government of India.

Bamne, Y., Patil, K. A., & Vikhe, S. D. (2014). Selection of appropriate sites for structures of water harvesting in a watershed using remote sensing and geographical information system. *International Journal of Emerging Technology and Advanced Engineering, 4*(11), 270–275.

Chowdary, V. M., Ramakrishnan, D., Srivastava, Y. K., Chandran, V. & Jeyaram, A. (2009). Integrated water resource development plan for sustainable management of Mayurakshi watershed, India using remote sensing and GIS. *Water resources management, 23*(8): 1581–1602.

Chowdhury, A., Jha, M. K., & Chowdary, V. M. (2010). Delineation of groundwater recharge zones and identification of artificial recharge sites in West Medinipur district, West Bengal using RS, GIS and MCDM techniques. *Environmental Earth Science, 58*(6), 1209–1222.

CWC. (2005). *Hand book of water resources statistics, Central Water Commission (CWC)*. Ministry of Water Resources, Government of India.

DTE. (2015). *India must focus on rainfed farming*. Down to Earth (DTE). https://www.downtoearth.org.in/coverage/india-must-focus-on-rainfed-farming6259#:~:text=It%20accounts%20for%2068%20per,86%20million%20ha%20is%20 rainfed. Accessed on 10 July 2020.

FAO. (2003). *Training Course on Water Harvesting* (Land and water digital media series: CD-ROM No. 26). Food and Agriculture Organization of the United Nations (FAO).

FAO. (2012). *Coping with water scarcity: An action framework for agriculture and food security*. Food and Agriculture Organization of the United Nations.

Ghayoumian, J., Saravi, M. M., Feiznia, S., Nouri, B., & Malekian, A. (2007). Application of GIS techniques to determine areas most suitable for artificial groundwater recharge in a coastal aquifer in southern Iran. *Journal of Asian Earth Sciences, 30*(2), 364–374.

Jarvis, A., Guevara, E., Reuter, H. I., & Nelson, A. D. (2008). *Hole-filled SRTM for the globe: Version 4: Data grid*. Web publication/site, CGIAR Consortium for Spatial Information. http://srtm.csi.cgiar.org/

Jasrotia, A. S., Majhi, A., & Singh, S. (2009). Water balance approach for rainwater harvesting using remote sensing and GIS techniques, Jammu Himalaya, India. *Water Resources Management, 23*(14), 3035–3055.

Jha, M. K., Chowdary, V. M., Kulkarni, Y., & Mal, B. C. (2014). Rainwater harvesting planning using geospatial techniques and multicriteria decision analysis. *Resources, Conservation and Recycling, 83*, 96–111.

Kadam, A. K., Kale, S. S., Pande, N. N., Pawar, N. J., & Sankhua, R. N. (2012). Identifying potential rainwater harvesting sites of a semi-arid, basaltic region of western India, using SCS-CN method. *Water Resources Management, 26*(9), 2537–2554.

Kahinda, J. M., & Taigbenu, A. E. (2011). Rainwater harvesting in South Africa: Challenges and opportunities. *Physics and Chemistry of the Earth, Parts A/B/C, 36*(14-15), 968–976.

Mahmoud, S. H., Adamowski, J., Alazba, A. A., & El-Gindy, A. M. (2016). Rainwater harvesting for the management of agricultural droughts in arid and semi-arid regions. *Paddy and Water Environment, 14*(1), 231–246.

Malczewski, J. (1999). *GIS and multicriteria decision analysis*. Wiley.

MoWR, & CGWB. (2013). *Ground Water Information Solapur District Maharashtra*. Ministry of Water Resources/Central Ground Water Board (CGWB), Central Region.

Oweis, T., Oberle, A., & Prinz, D. (1998). Determination of potential sites and methods for water harvesting in central Syria. *Advances in Geoecology, 31*, 83–88.

Parthasarathy Committee Report. (2006). *From Hariyali to Neeranchal: Report of the technical committee on watershed programmes in India*. Department of Land Resources, Ministry of Rural Development, Government of India.

Ramakrishnan, D., Durga Rao, K. H. V., & Tiwari, K. C. (2008). Delineation of potential sites for water harvesting structures through remote sensing and GIS techniques: A case study of Kali watershed, Gujarat, India. *Geocarto International, 23*(2), 95–108.

Rockstrom, J., Karlberg, L., Wani, S. P., Barron, J., Hatibu, N., Oweis, T., Bruggeman, A., Farahani, J., & Qiang, Z. (2010). Managing water in rainfed agriculture—The need for a paradigm shift. *Agricultural Water Management, 97*, 543–550.

Saaty, T. L. (1980). *The analytic hierarchy process*. McGraw-Hill.

Sahoo, P. K. (2004). *Selection of sites for water harvesting structures using GIS*. Unpublished M.Tech Thesis, Agricultural and Food Engineering Department, IIT Kharagpur, West Bengal, India.

SCS. (1985). *National engineering handbook, Section 4, hydrology. Soil Conservation Service (SCS)*. US Department of Agriculture (USDA).

Singh, V. P. (1992). *Elementary hydrology* (pp. 474–482). Prentice-Hall of India Private Limited.

Singh, L. K., Jha, M. K., & Chowdary, V. M. (2017). Multi-criteria analysis and GIS modeling for identifying prospective water harvesting and artificial recharge sites for sustainable water supply. *Journal of Cleaner Production, 142*, 1436–1456.

Subramanya, K. (2008). *Engineering hydrology* (pp. 155–160). Tata McGraw-Hill Publishing Company Limited.

Toosi, A. S., Tousi, E. G., Ghassemi, S. A., Cheshomi, A., & Alaghmand, S. (2020). A multi-criteria decision analysis approach towards efficient rainwater harvesting. *Journal of Hydrology, 582*, 124501.

Voogd, H. (1983). *Multicriteria evaluation for Urban and Regional Planning*. Pion Limited, 361 pp.

Wable, P. S., Jha, M. K., & Shekhar, A. (2018). Comparison of drought indices in a semi-Arid River Basin of India. *Water Resources Management, 33*(1), 75–102.

Wani, S. P., Venkateswarlu, B., & Sharda, V. N. (2011). Watershed development for rainfed areas: Concept, principles, and approaches. In Wani et al. (Eds.), *Integrated watershed management in rainfed agriculture* (pp. 53–86). CRC Press/Taylor and Francis Group.

Weerasinghe, H., Schneider, U. A., & Loew, A. (2011). Water harvest-and storage-location assessment model using GIS and remote sensing. *Hydrology and Earth System Sciences Discussions, 8*(2), 3353–3381.

Ziadat, F., Bruggeman, A., Oweis, T., Haddad, N., Mazahreh, S., Sartawi, W., & Syuof, M. (2012). A participatory GIS approach for assessing land suitability for rainwater harvesting in an arid rangeland environment. *Arid Land Research and Management, 26*(4), 297–311.

Chapter 2
Hydrochemical Investigation and Water Quality Mapping in and Around Pallikaranai Marshland Area in Chennai, India

S. Packialakshmi, K. Nagamani, and B. Anuradha

Abstract Wetlands perform a wide range of ecological functions. It acts as a natural flood barrier that traps and deliberately releases surface water, groundwater, and flood waters. The groundwater system is among the integral components of the wetland/swamp and ecosystem. Pallikaranai swamp land is a freshwater ecosystem situated in the southern region of Chennai, India is supportive of recharging the surrounding aquifers and is the important flood regulator for southern part of the Chennai region. Human interventions such as garbage dumping, sewage discharges, and unplanned urbanization activities have substantially damaged the wetland ecosystem, and the nature of the wetland has been destroyed. The current study investigates the prevailing groundwater quality in and around the wetland and highlights the vulnerable status of the wetland. In addition, the study used geospatial tools and methodologies to understand the regional variation in groundwater quality, which served as a guide for implementing management actions to improve the wetland and surrounding aquifer system.

Keywords GIS mapping · Water quality · Spatial variation of groundwater · Pallikaranai · Chennai

S. Packialakshmi (✉)
Department of Civil Engineering, Sathyabama Institute of Science and Technology, Chennai, India
e-mail: packialakshmi.civil@sathyabama.ac.in

K. Nagamani
Center for Remote Sensing and Geo-Informatics, Sathyabama Institute of Science and Technology, Chennai, India

B. Anuradha
Department of Civil Engineering, Chennai Institute of Technology, Chennai, India

P. Thambidurai, A. K. Dikshit (eds.), *Impacts of Urbanization on Hydrological Systems in India*, https://doi.org/10.1007/978-3-031-21618-3_2

1 Introduction

Freshwater scarcity has become an environmental and social challenge that requires immediate attention at the local, regional, national, and global levels. Groundwater resources are in great demand for household, agricultural, and industrial applications since surface water resources are not equally distributed and sensitive to anthropogenic pollution (Paul et al., 2019; Packialakshmi et al., 2011; Sonkamble et al., 2014; Thambidurai et al., 2019; Thambidurai, 2017). On average, 65 percent of available groundwater is consumed for drinking and domestic purposes, while 15% and 20% of groundwater has been utilized for industrial and agricultural purposes correspondingly (Salehi et al., 2018; Adimalla et al., 2019). Groundwater appropriateness, particularly for domestic uses, is mostly governed by its quality, which has grown increasingly essential in recent years. In many places, groundwater resources are very sensitive as they have been exploited by various anthropogenic causes such as farming activities, land-use conversions, cultivation methods, and industrial activities. A significant role contributed to the freshwater environment by the wetlands ecosystem. Understanding how wetlands function and characterizing and measuring their buffer role would aid authorities in maintaining such ecosystems(Patnaik & Srihari, 2004; Sridevi & Ramachandran, 2012).

1.1 Reviews on Investigation of Water Quality

Water quality indexing is one of the most efficient methodologies for disseminating knowledge and awareness of the water quality of any potential region. Verma et al. (2020) have explored the importance of conducting water quality investigation using water quality indexing (WQI) and Geographic Information System (GIS) approaches for the Bokaro district, India. The GIS-based water quality index maps for the study area reveal that the area's alarming water quality was greater in the pre-monsoon season when compared to the post-monsoon season. In the pre- and post-monsoon seasons, water quality mapping revealed that 50.98% and 45.10% of the samples were found to be in a bad category, making them unfit for drinking. The high WQI readings in various groundwater samples from the Bokaro district suggest that the water is unfit for direct consumption and requires long-term treatment before being used for drinking. Further, the study found that rock weathering, ion exchange mechanisms, and anthropogenic activities all influenced groundwater chemistry. The research calls for proper water resource management plans to address groundwater resource issues. Piyathilake et al. (2022) conducted a study for developing the water quality indexing to establish a relation between the incidence of chronic kidney ailment of indefinite etiology and intake water quality in the Uva Province (UP), Sri Lanka. The WQI has a substantial positive association with the spatial variation of chronic kidney ailment patients in the study region, implying that the status of water quality had a major impact on the occurrence of chronic

kidney disorders, according to the statistical study. The authorities can use these spatial distribution water quality maps for groundwater quantity-quality assessment strategies in these regions. The method of water quality indexing is extensively utilized as one of the promising techniques to express the prevailing status of water quality in an area of concern to the common public and officials. Also, the method of indexing can be effectually utilized for assessing the suitability of water for its various uses.

Also, Chabuk et al. (2020) assessed the surface water quality of River Tigris by using the water quality indexing technique in the geospatial platform. Twelve parameters (TDS, EC, Ca, Na, Mg, Cl, HCO_3, K, SO_4, BOD, TH, and NO_3) were taken from fourteen stations in and around the river regions. The weighted arithmetic technique was employed to assess the overall water quality index. The method of interpolation (IDW) was adopted in ArcGIS to develop the probability or forecasting maps for the selected 12 parameters at the stations in and around the River Tigris during the year 2016 for dry and wet seasons. The methodology consists of three approaches: field dimensions, mapping processes using GIS, and calculations. The inverse distance weighted interpolation technique (IDW) was employed to create the interpolation maps for each parameter during the study of the river's dry and wet seasons. In this interpolation technique, the points closer to the likely spots will have a better outcome on the projected values than those placed farther away from those points. This process was adopted to deliver interpolation between the selected points within the values between lower and higher ranges for all the parameters. The prediction methodology was adopted for the seasons on the three stations within the study region among the observed and predicted values. The outcomes showed that prediction for all the selected parameters assumed the suitable values for the regression coefficient. Also, the status of prevailing water quality for the study region deteriorated especially in the downstream regions, during the dry and wet seasons, and evidently in the southern parts of Iraq.

The GIS and remote sensing technologies have essential roles to perform altogether with spatial and topographical features of the event and for monitoring the water resource. These techniques will offer influential and analytical gears for analyzing and demonstrating the habitual structure procedure and functions. Furthermore, testing with satellite imageries and checking with segment data will give an alternate and precise factor recognition technique. The selected water quality parameters were chosen to quantify temporal changes for the investigation period, and a replacement technique was suggested by Najme (2016). This replacement technique supported the parametric statistic model. The empirical equation predicted the variable's significance by considering the events' cause and effects. Generally, the parametric statistic is considered a constant when a curve is presumed as a linear function ($y = ax + b$). This constant parameter established the relation between the variable (i.e., rate of change in water quality) as a function of the time factor (x) and the slope of the equation (Webster, 1997). Henceforth, the values of every water quality variable for the study periods were plotted to obtain the best fit of the linear line. Then, the constant of parametric statistics was defined as a relentless value for every water quality variable, called the regression

coefficient. Values of negative sign for each and every water quality variable infers that variable over time will reduce trend and contrariwise. During this study, geo-based statistical analysis was executed in two stages, namely, (a) structural analysis, which targets in labeling and modeling of a spatial building of regression coefficient for the selected water quality variables, employing a structural implement of variogram, and (b) the employment of this construction for a chosen study problem (i.e., for mapping every water quality parameters).

Further, a few geostatistical algorithms were examined, including simple, ordinary, probability, and disjunctive natured kriging (ESRI, 2008). The simplest model (i.e., exponential, spherical, or Gaussian) and the related parameters were also tested through the semi-variogram analysis. From variography analysis, spatial and temporal changes in the groundwater quality were derived for each and every variable. A regression approach integrated with the kriging technique was applied to develop the mapping for spatial and temporal variation of water quality parameters. The outcome exposed that most soluble ions of Na and Cl ions are in the greatest ranges compared to other ions. Except for Ca ions, most of the soluble ions, including EC and TDS, were exceeded the most permissible ranges for domestic and drinking purposes. Then parameters such as EC, Na, and SO_4 showed no restriction for farming activities which supported the projected regression coefficient, and soluble ions such as Ca, Na, and Cl and total anions, cations, and EC have significantly increased during the study period. Comparing the most soluble ions indicated that during the study period, the ranges of HCO_3 are in an increasing trend, while the contrary trend was identified for Ca and SO_4 ions. The regression coefficient for SAR and EC has a greater correlation with Na and Cl. The results identified the spatial and temporal variations of groundwater sodicity and salinity for the study region which are greatly influenced by soluble ions such as Na and Cl. Juniet et al. (2016) have worked on the wetlands providing numerous invaluable amenities for society like attenuating floods, recycling nutrients, and recharging water to the subsurface and as natural environs supporting several species and their ecosystem. Because of unplanned urbanization activities, the sole available natural recharging system of Pallikaranai marshland, labeled as a reserved and protected area, is under threat and constricted to 1/10 of its authentic areal extent due to anthropogenic-related stresses. Further, the existence of a dump yard and wastewater treatment facilities that functioned within the ecologically preserved region of wetlands created a potential threat to the diversified species population of this wetland. Also, Kaaviya and Devadas (2021) established distinct water resilience regions in Chennai, India. The approach contained a total of 15 essential parameters. The AHP was used to disperse weight to every parameter by applying a multi-criteria analysis technique. A pairwise decision matrix was used to determine the factors comparative significance and the consistency ratio. Five important ranges in the water resilience strengths were represented by combining all maps using a weighted overlay analysis technique. This study is unique in that it takes a holistic approach to water resilience, incorporating food, famine, efficiency, and adequacy of required infrastructure facilities.

As a novel perception of successful management of water resources and climate change scenarios, scholars and policymakers can excellently apply the research outcomes to maintain resilience. This decision-making tool determines how the system is exposed to water-related concerns and implements flexibility measures. The mapping of water resilience provides a model for a researcher to evaluate in what different ways assumptions about future climate or other variables affect decision-making. The AHP-related planning method has been developed as a decision-making tool for using resilience processes. Water quality monitoring is widely acknowledged as the important phase for gaining a better indulgent of the features of water polluting phenomenon and developing effective alleviation strategies. The physical, chemical, and biological constituents of water regulate its quality. Substances such as heavy metals, insecticides, petroleum, and fertilizers are all part of the chemical composition. Turbidity, color, and temperature are part of the physical composition, while plankton and pigments are part of the biological constituent. Said and Hussain (2019) mapped and monitored pollution levels inside the study region that runs through the entire region using advanced GeoEye-2 data by examining the relationship between water quality variables and the value of the image's spectral reflectance. A total of hundred samples were collected at arbitrary spots in the river region and examined in the laboratory for 12 WQPs, which were then categorized as organic or inorganic. The lighter color shades on the WQP maps appear to represent the lowermost levels of pollution in all WQPs at the Wazirabad site, while the darker tones appear to show significant pollutant concentrations along the river segment. The research, on the other hand, demonstrates how GeoEye-2 photos may be used to regulate and reduce pollution levels in water bodies, which could be useful for long-term surface water resource planning and management. The study noted that pollution levels on the temporal scale during the study period in all different seasons might be addressed in future studies, which help devise appropriate solutions for reviving the polluted river region.

Investigating groundwater status and the various risk assessment factors are crucial for assessing measures for preventing probably dangerous ecological health complications in any part of the world. Due to extensive groundwater pumping in recent years, especially during the summer months, the setback of groundwater movement has resulted in seawater incursion, especially in the agricultural regions located in the coastal zones, rendering water of shallow and deep wells unhealthy for farming activities and consumption. The hydrogeochemical analysis combined with geospatial techniques identifies the regions where water quality is adequate for drinking, agriculture, and industry. Geospatial tools are used to geographically characterize data sets to generate maps and make spatial data comparisons. The Arc GIS spatial analyzer is an essential tool for creating maps that facilitate the interpretation of primary and other data sets. The water quality of the research area is depicted by spatially distributed maps and analytically interpreted hydrochemical variables (Gnanachandrasamy et al., 2015).The results indicated that during the pre-monsoon season, the values of TH were higher when compared with the post-monsoon season. The values of Na and Cl ions in both pre- and post-monsoon seasons disclose the ranges that are exceeded drinking water norms. This may be

due to the effect of saline water intrusion into the aquifers near to the coastal zone. The study argued that requirement of sustainable management practices is crucial in order to prevent these circumstances. It also requested that the new deep bore well be drilled regularly to ensure local supply. Henceforth, it is recommended to investigate the groundwater quality in a consistent manner and strategy to be controlled in a rigorous mode to avert a further worsening of water quality, specifically for the coastal cities.

One of the concerns of the twenty-first century is the degradation of water quality. An agent which causes contamination lowers the standards of water, making the water risky to drink and causing health problems. The measured water quality variables are interpolated using the inverse distance weighted method for predicting the water quality variables of surrounding points (Ram et al., 2021; Aouiti et al., 2021; Inson et al., 2021). A GIS-based best fit semi-variogram model integrated with the ordinary kriging method in the geospatial platform is used to prepare the thematic maps for the selected water quality variables (Bhunia et al., 2018). Khan et al. (2017) investigated groundwater quality by developing GIS-based quality indexing. Each parameter's geographically varying grids were changed by normalizing them to WHO standards before being merged into a GQI grid. A new GIS-based technique was used to compare the GQI grids to the land-use map. The findings show that the land-use pattern does not fully influence the geographical variability of groundwater quality in the region. This is most likely due to the heterogeneous nature of land-use classes, particularly communities and plantations. Mohan and Gandhimathi (2009) investigated the impact of Perungudi dumping site leachate on groundwater located on the Pallikaranai marshland. The Chennai Corporation delivers 1650 tonnes of municipal solid waste per day. The occurrence and availability of groundwater greatly depend on the changes in topography, subsurface geology, and the prevailing climate in the particular region. The position of the aquifer also determines its recharge rate and its susceptibility to pollution and overuse. Hydrogeological investigations require a thorough grasp of the physical structure of the aquifers in which groundwater resides and circulates (Kulkarni et al., 2000; Mohamed et al., 2018; Li et al., 2021; Malar et al., 2015). The availability of huge volumes of good-quality data is crucial for the reliability and validity of hydrogeological investigations. Also, Ghalib (2017) assessed the groundwater quality degradation in the aquifers of the shallow depth in the study region of Iraq's Wasit Governorate in the northeast. The appropriateness of groundwater for drinking purposes was assessed using physicochemical parameters such as important anion and cation concentrations, TDS, pH, and EC, which are compared with WHO and Iraqi criteria. Water availability and quality have always been essential factors in determining life quality. Water quality is inextricably tied to water use and economic development. With the swift increase of urban population and related developmental activities need for more freshwater, Chennai is among the worst affected in the aspect of water quality and quantity. The city's municipal solid waste (MSW)

generation rate has increased rapidly as a result of population growth and rising affluence. During the last decade, daily waste creation has doubled (Malleshappa & Jayanthi, 2013).

2 Description of the Study Area

Pallikaranai marshland is a freshwater environment situated in part Chennai, India (Fig. 2.1 & Table 2.1). It has an area of 80 km^2 and is located near the Bay of Bengal, about 20 km south in the direction of the city center. The Pallikaranai marsh is Chennai city's only remaining wetland habitat and one of South India's few and last natural wetlands. The wetland has reduced significantly due to the dumping of toxic solid waste along the road, sewage discharge, and the development of houses, railway stations, and a new road that connects Old Mahabalipuram Road and Pallavaram. Wetlands and river bodies in Chennai are chosen areas for solid waste disposal and as an unloading bowl for both industrial and domestic effluents (Aravindkumar et al., 2014).

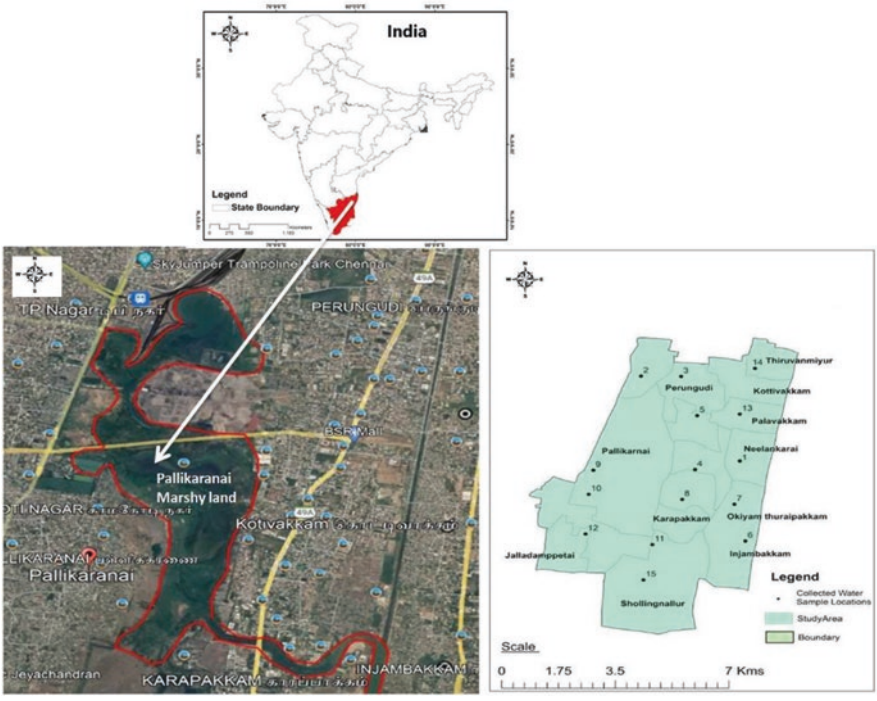

Fig. 2.1 Map of study area with its administrative boundaries

Table 2.1 Geographical characteristics of Pallikaranai marshland

Characteristics	Pallikaranai marshland
Geographical location	Located in between longitudes of 80.20° N and 80.23° N and latitudes of 12.92° E and 12.96° E
Areal extent	80 km^2
Catchment area	235 km^2
Surface elevation	3–7 m
Rainfall recharge	340 mm NE monsoon (November–January) and SW Monsoon (July–September)
Geology	Weathered rock – charnockite
Hydrology	Overflow from Velachery, tanks and hills in the western and south western direction find their way down channels, flooding the Pallikaranai marsh on a seasonal basis
Drainage	Surplus flow is released into Okkiyum Madavu and to Cooum, before finally reaching the Bay of Bengal via the Muttukkadu-Kovalam waterway

3 Material and Methods

The common method of garbage disposal in developing nations is to landfill municipal solid trash in an unlined dumping site. It pollutes natural and fragile land, air, and water resources, affecting the communities near the dumpsite. The major and most serious consequence for the residents was groundwater pollution. The people residing near the dumpsite for a longer period were unaware of the quality of water that had been poisoned owing to the dumping yard, which arose 20 years back because they had lived near the dumpsite for three to four generations.

Stream of solid waste generated by individuals, institutions, industries, and business centers is designated as municipal solid waste (MSW). When MSW is incorrectly disposed of, it harms the surrounding environment and human health. Groundwater contamination and related health hazards are among the most severe problems nowadays. Most Asian countries encounter municipal solid waste management challenges due to rapid expansion in solid waste creation and unscientific dumping practices. Water permeates through this solid waste, resulting in leachate, which is made up of rotting organic substances mixed with other harmful metals such as lead, iron, mercury, chromium, and zinc and is a principal source of groundwater contamination around the dumpsite. From the identified background understanding, sampling was conducted post-monsoon season (January 2021) to investigate prevailing groundwater quality. The parameters of pH, EC, TDS, salinity, Ca, Mg, Na, Cl, K, SO^4, HCO^3, and CO^3 were tested for analysis. These result values were compared with standard (BIS) limits. Spatial variation of hydrochemical parameters was plotted as thematic maps using Arc GIS 10.3 Software. The sampling locations were determined after a thorough field study and by discussing with stakeholders. Selecting sampling wells (shallow open wells) to undertake a water quality study is critical for mapping the groundwater quality. The sampling wells were chosen within an aerial coverage of approximately 3–5 km^2, and a

Table 2.2 List of sampling wells for analysis

Sl. no	Location	Latitude	Longitude	Water level below the ground level (ft)
1	Neelankarai	12.94556	80.25162	15
2	Taramani	12.97387	80.23537	40
3	Thoraipakkam	12.94269	80.23924	35
4	Perungudi	12.96073	80.23983	30
5	Akkarai	12.91878	80.25316	25
6	Injambakkam	12.93107	80.25015	20
7	Karapakkam	12.93269	80.23567	30
8	Narayanapuram	12.94246	80.21105	40
9	Pallikaranai	1293441	80.20978	35
10	Sholinganallur	12.91758	80.22743	40
11	Jalladianpettai	12.92113	80.20891	35
12	Palavakkam	12.96125	80.25163	40
13	Thiruvanmiyur	12.97656	80.25585	35

random sampling technique was used. Table 2.2 shows the list of sampling wells for conducting water quality investigation. Thirteen sampling points were selected and plotted using GPS for the accuracy of the location to conduct the investigation. The earlier finding (Packialakshmi et al., 2011; Packialakshmi & Ambujam, 2012; Parameswari & Mudgal, 2014, 2015; Ebong et al., 2017) suggested that concentration hydrochemical parameters such as Ca, Mg, Na, and Cl were exceeded during post-monsoon than in pre-monsoon season which may be due to dissolution rock minerals, dilution, and weathering effects.

4 Results and Discussions

Due to population increase, urbanization, and related industrial development, groundwater is being increasingly contaminated by the issues like alkalinity, acidity, heavy metals, and related noxiousness and microbes worldwide. Examining groundwater quality in the possible contamination zone and surrounding surface water is now critical to preparing for remedial procedures. The investigation of groundwater quality was carried out at Pallikaranai marsh area, Chennai, India, by examining its physicochemical features. The hydrochemical investigation was carried out in the Pallikaranai marshland area to identify the area affected by poor water quality and the source of salinity in this aquifer. The study area is completely surrounded by the charnockite hard rock aquifer on the western side and the coastal aquifer zone in the eastern direction. Residential and industrial developments, especially in the coastal zone, may have an impact of saline water ingression. The evaluation of hydrochemical values (Table 2.3) also suggests that samples taken near coastal zones are of very poor quality and groundwater in this sector is unfit for human consumption. It is apparent that the overextraction of groundwater sources

Table 2.3 hydrochemical parameters of selected sampling wells

S. no	pH	TDS	EC	Salinity	Ca	Mg	Na	K	Cl	CO_3	HCO_3	SO_4
1.	8.24	1358	1912.68	600	144.15	105.60	50	28	382.86	0	505	141.91
2.	8.30	1616	2276.06	702	134.14	161.43	56	17	485.67	0	625	136.76
3.	8.21	1092	1538.03	545	84.09	65.12	108	37	33.23	0	310	155.88
4.	8.20	2591	3649.30	1920	250.26	137.12	388	38	786.12	100	750	241.18
5.	8.40	1050	1478.87	416	140.15	103.17	30	6	304.87	0	365	100.74
6.	8.80	619	871.83	211	108.11	49.77	23	7	212.70	0	130	88.97
7.	8.00	1401	1985.92	927	106.11	131.09	100	28	545.23	0	315	184.56
8.	8.40	4172	5876.06	2800	384.12	174.23	645	124	1745	0	555.23	545.23
9.	8.01	1498	2109.86	685	224.23	122.59	144	9	726.73	0	145	126.47
10.	8.14	763	1074.65	614	90.09	44.91	66	11	243.23	0	245	62.50
11.	8.25	1118	1574.65	463	152.16	81.32	50	3	287.15	0	475	69.12
12.	8.10	1170	1647.89	660	150.16	65.54	64	34	402.12	0	325	129.41
13.	7.90	808	1138.03	620	150.16	10.23	56	20	305.12	0	234	32.35

has a severe impact on the coastal sector. The dump is in a sea-level low land area with poor drainage characteristics and comprises a large expanse of marshy terrain that is continually damp and seasonally flooded. The daily dumping rate is currently around 2000 tonnes. The liner on this dumpsite is insufficient to prevent leachate from accessing the underlying and nearby groundwater environment. The most prominent influencing element for assessing the current status of wetland and its future concerns is the possible implications of leachate formation from dumpsites on groundwater quality. The findings revealed that the wetland region and its surroundings are precarious. Figures 2.2, 2.3, and 2.4 depict the regional fluctuation of hydrochemical parameters, indicating a higher level of contamination throughout the research.

The collected water samples have pH in the range of 7.90–8.80 with an average of 8.20. Well no. 7 shows high level of pH, whereas location numbers 8, 10, 11, 13, and 14 are in permissible range. Humans are exposed when the pH is excessive acidic; their eyes, skin, and mucous membranes may get irritated. Main sources of TDS in receiving waterways include farm and residential overspill, soil contamination leaching, and point and nonpoint causes of water pollution. According to WHO guidelines, the TDS levels in drinking water should be between 500 and 1500 mg/l. The TDS levels in 50% of the samples collected exceeded the limits. High and protected quality deionized water is having a conductivity value of about 5.5 S/m, while regular water used for drinking purposes has a conductivity of 5–50 mS/m, and saline water has a conductivity of about 5 S/m (Table 2.4).

The regional variation of hydrochemical parameters in the research area is depicted in Figs. 2.2 and 2.3. Chloride increases both the electrical conductivity and the corrosive characteristics of water. Chloride concentrations above 250 mg/li can produce discernible taste in water; however, the related cations determine the threshold. Consumers, on the other hand, may acquire used to concentrations greater than 250 mg/l. Potassium is an electrolyte and a mineral. The K concentrations

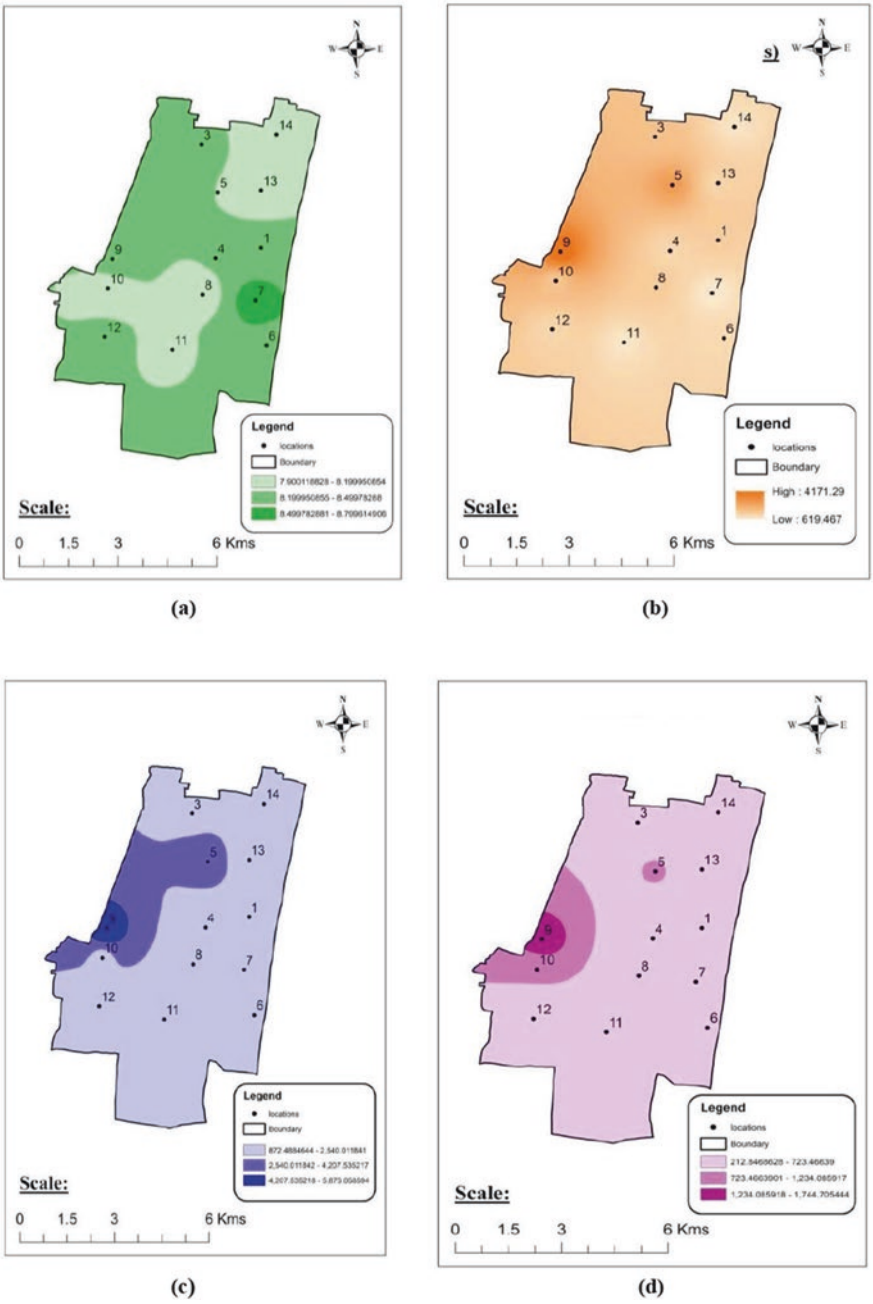

Fig. 2.2 Spatial variation of (**a**) pH, (**b**) TDS, (**c**) EC, and (**d**) Cl concentrations in the study area

Fig. 2.3 Spatial variation of (**a**) Na, (**b**) K, (**c**) Ca, and (**d**) Mg concentrations in the study area

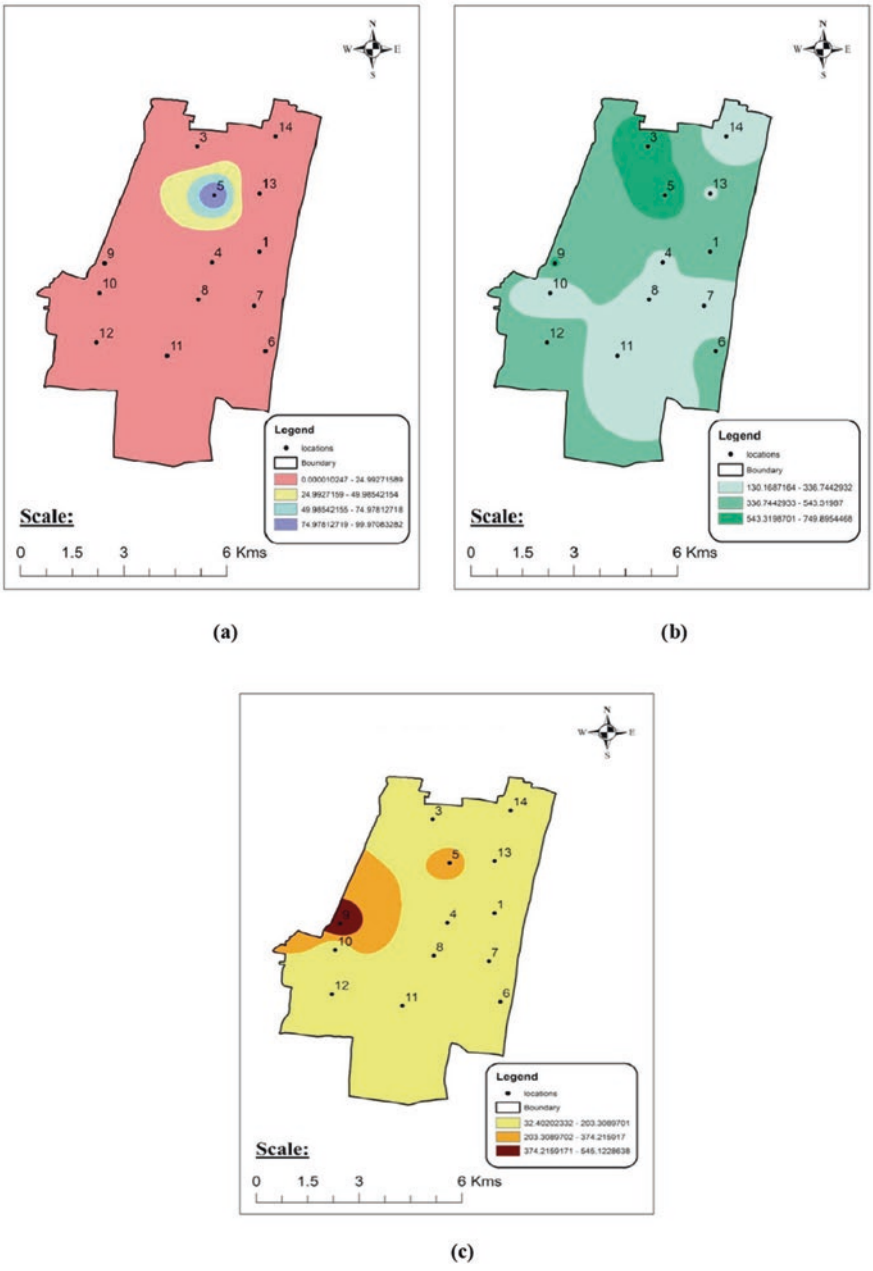

Fig. 2.4 Spatial variation of (**a**) CO_3, (**b**) HCO_3, and (**c**) SO_4 concentrations in the study area

Table 2.4 Standards of drinking water as per World Health Organization (WHO) guidelines

Parameters	Range
pH	6.5–8.5
EC	500–1500 µs/cm
TDS	500–1500 mg/l
Ca^2+	70–200 mg/l
Mg^2+	50–150 mg/l
Na+	≤200 mg/l
$_K$+	≤12 mg/l
NH4+	≤0.5 mg/l
NO3 −	≤50 mg/l
Cl−	≤250 mg/l
SO4	≤500 mg/l
HCO3	≤400 mg/l

measured ranges from 3 to 124 mg/l, with an average value of 27.14 mg/l. Carbonates are a function or relation of pH, temperature, dissolved carbon dioxide, cations, and other dissolved salts in the natural fluids. Concentrations of above 1000 mg/L have been reported in low-calcium, low-magnesium waters and notably where carbon dioxide-releasing activities, namely, sulfate reduction, are taking place in the groundwater storage formations. Calcium and magnesium are dissolved in most solids and rocks but particularly in gypsum, dolomite, and limestone.

Scale formation in boilers, water heaters, and pipes, as well as the unpleasant curd in the presence of soap, are mostly caused by calcium and magnesium. The sampling wells in the research area's western section have higher TDS, EC, Na, Ca, Cl, Mg, K, and SO_4 values than the other locations, implying that polluted water has accumulated and stagnated from nearby dumping activities in the marshy area. The parameters of EC, K, Cl, and HCO_3 exceeded more than WHO standards in 90% of the samples. The concentration of EC, K, Cl, and HCO_3 ranges from 871 to 5876, 3 to 124, 33 to 1745 and 130 to 750 mg/l, respectively. The majority of the parameters exceeded many fold higher than WHO standards in the sampling wells positioned in the western and central regions of the study location.

The leachate has created elevated pollutant concentrations in the majority of the water parameters. This high concentration is most likely owing to contamination from the disposal site's leachates, which have filtered into the groundwater (Eldho, 2001; Mor et al., 2006). The considerable volume of harmful inorganic minerals that have leached out from the dumpsite accounts for the greater total dissolved solids values. A high chemical oxygen demand indicates the presence of organic stuff. In most of the samples, the amount of chlorides is found to be higher than acceptable levels, irrespective of the seasons. The previous study conducted by Vasanthi et al. (2008) stated that in the majority of the areas in the Pallikaranai surroundings, total hardness is between 250 and 5800 mg/l, above the acceptable ranges. At some sites, it is noted that amount of nitrates and sulfates is higher than standards. The main dominating anions and cations in the groundwater in and around the dumping yard located in the wetland area were Na > Mg > Ca > K and

$Cl > HCO_3 > SO_4 > NO_3$. The Marshland's hydrogeological formations cause ions such as Na, HCO_3, Cl, and K to accumulate, potentially dominating groundwater chemistry and importing salinity and hardness, rendering the water unfit for potable use.

5 Conclusions

The present study investigated the prevailing status of hydrochemistry of groundwater aquifers in and around Pallikaranai marshland. This study aims to determine the likely concentrations of major and most dominating ions in the groundwater over time as a result of ions or contaminants being discharged from landfill leachate into the underlying groundwater. The leachate formed by indiscriminate dumping of solid and liquid waste on the eco-sensitive wetland region has a significant impact on groundwater quality in that location, according to the field survey and stakeholder debate. According to the hydrochemical investigation, the current groundwater quality is saline, and higher EC values reflect a greater ionic strength than WHO limits. The majority of the parameters exceeded WHO standards in the sampling wells located in the western and central portions of the study region. The Marshland's hydrogeological formations cause ions such as Na, HCO_3, Cl, and K to accumulate, potentially dominating groundwater chemistry and importing salinity and hardness, rendering the water unfit for potable consumption. According to the study, municipal solid waste disposal is a complicated element progressively disturbing natural and human ecosystems. Developing improved management approaches will pave the way to alleviate environmental and socioeconomic problems. The studies conducted by several researchers have also confirmed that identified groundwater quality parameters in the study area exceeded the acceptable level and showed that groundwater available in that study region is not protected and safe for the usage of any purposes such as drinking, domestic, agricultural, aquatic life, and industrial uses. Further, the results suggested that regions affected due to the anthropogenic sources of contamination need to be protected. It urges the need for innovative treatment options to revamp the system for the sustenance of the vulnerable wetland ecosystem. Hence the study recommends continual research on heavy metal accumulation, which threatens human health and livelihoods and affects the entire wetland ecosystem. The present investigation strongly advised that further study should be carried out on cost-effective, bio-based options to restore the functions and services offered by this vulnerable urban wetland system.

Acknowledgments The authors would like to thank the Sathyabama Institute of Science and Technology for providing the necessary support and laboratory facilities for conducting filed work and utilizing g GIS facilities to carry out this research. The authors are grateful to the editors and anonymous reviewers for their valuable suggestions and inputs.

Declarations **Conflict of interest:** The authors declare that they have no conflict of interest.

References

Adimalla, N., Venkatayogi, S., & Das, S. (2019). Assessment of fluoride contamination and distribution: A case study from a rural part of Andhra Pradesh, India. *Applied Water Science, 9*, 1–15. https://doi.org/10.1007/s13201-019-0968-y

Aouiti, S., Azaza, F. H., Fetheddine, E., Melki, E., Hamdi, M., Celico, F., & Zammouri, M. (2021). Groundwater quality assessment for different uses using various water quality indices in semi-arid region of central Tunisia. *Environmental Science and Pollution Research, 28*, 46669–46691. https://doi.org/10.1007/s11356-020-11149-5

Aravindkumar, J., Saravanakumar, K., Gokulakrishnan, M., & Indira, B. (2014). Assessment of physio-chemical parameters of water at environmentally degraded Pallikaranai marsh area, Chennai, India. *International Journal of Scientific and Engineering Research, 5*(7), 1067. nammapallikaranai.org/management-plan/

Bhunia, G. S., Keshavarzi, A., Shit, P. K., EwisOmran, E.-S., & Bagherzadeh, A. (2018). Evaluation of groundwater quality and its suitability for drinking and irrigation using GIS and geostatistics techniques in semiarid region of Neyshabur, Iran. *Applied Water Science, 8*, 168. https://doi.org/10.1007/s13201-018-0795-6

Chabuk, A., Al-Madhlom, Q., Al-Maliki, A., Al-Ansari, N., Hussain, H. M., & Laue, J. (2020). Water quality assessment along Tigris River (Iraq) using water quality index (WQI) and GIS software v. *Arabian Journal of Geosciences, 13*, 654. https://doi.org/10.1007/s12517-020-05575-5

Ebong, D., Anthony, E., & Emeka, C. N. (2017). Groundwater quality assessment using geoelectrical and geochemical approaches: Case study of Abi area, southeastern Nigeria. *Applied Water Science, 7*, 2463–2478. https://doi.org/10.1007/s13201-016-0439-7

Eldho, T. I. (2001). Groundwater contamination – The challenge of pollution control and Protection. *Journal of Indian Water Works Association, 33*, 171–180.

ESRI. (2008). *Using ArcGIS geostatistical analyst*. Environmental Systems Research Institute, Redlands (300 pp).

Ghalib, H. B. (2017). Groundwater chemistry evaluation for drinking and irrigation utilities in East Wasit province, Central Iraq. *Applied Water Science, 7*, 3447–3467. https://doi.org/10.1007/s13201-017-0575-8

Gnanachandrasamy, G., Ramkumar, T., Venkatramanan, S., Vasudevan, S., Chung, S. Y., & Bagyaraj, M. (2015). Accessing groundwater quality in lower part of Nagapattinam district, Southern India: Using hydrogeochemistry and GIS interpolation techniques. *Applied Water Science, 5*, 39–55. https://doi.org/10.1007/s13201-014-0172-z

Inson, J. G. M., Supsup, C. E., & Flores, M. J. C. (2021). Spatial mapping of groundwater quality in the municipality of Santa Ignacia, Tarlac, Philippines. *Applied Water Science, 11*, 174. https://doi.org/10.1007/s13201-021-01513-2

Juniet, M., Jose, J. M., & Ganesh, M. C. (2016). Current status of Pallikaranai wetland: A review. *International Journal of Development Research, 06*(08), 9002–9007.

Kaaviya, R., & Devadas, V. (2021). Water resilience mapping of Chennai, India using analytical hierarchy process. *Ecological Processes, 10*, 71. https://doi.org/10.1186/s13717-021-00341-1

Khan, A., Khan, H. H., & Umar, R. (2017). Impact of land-use on groundwater quality: GIS-based study from an alluvial aquifer in the western Ganges basin. *Applied Water Science, 7*, 4593–4603. https://doi.org/10.1007/s13201-017-0612-7

Kulkarni, H., Deolankar, S. B., Lalwani, A., Joseph, B., & Pawar, S. (2000). Hydrogeological framework of the Deccan basalt groundwater systems, west-central India. *Hydrogeology Journal, 8*, 368–378.

Li, C., Gao, Z., Chen, H., Wang, J., Liu, J., Li, C., Teng, Y., Liu, C., & Congcong, X. (2021). Groundwater quality assessment for different uses using various water quality indices in semi-arid region of central Tunisia. *Environmental Earth Sciences, 80*, 523. https://doi.org/10.1007/s12665-021-09823-z

Malar, A., Suriya, T., Meenakshi, R., & Priya, S. L. (2015). Hydro geochemical analysis of groundwater quality in Sriperumbudur block: A case study of Pondur Panchayat of Tamil Nadu, India. *International Journal of Applied Engineering Research*., ISSN 0973-4562*, 10*(62), 41–46.

Malleshappa, H., & Jayanthi, M. (2013). *State of environment report of Chennai Metropolitan area* (pp. 1–36). ENVIS Centre, Department of Environment.

Mohamed, A. K., Liu, D., Mohamed, A., & Song, K. (2018). Groundwater quality assessment of the quaternary unconsolidated sedimentary basin near the Pi river using fuzzy evaluation technique. *Applied Water Science, 8*, 65. https://doi.org/10.1007/s13201-018-0711-0

Mohan, S., & Gandhimathi, R. (2009). Solid waste characterization and the assessment of the effect of dumping site leachate on groundwater quality: A case study. *International Journal of Environment and Waste Management, 3*, 65–77.

Mor, S., Ravindra, K., Dahiya, R. P., & Chandra, A. (2006). Leachate characterization and assessment of ground water pollution near municipal solid waste disposal site. *Environmental Monitoring and Assessment, 118*, 435–456.

Najme, Y. (2016). Spatiotemporal mapping of groundwater quality for irrigation using geostatistical analysis combined with a linear regression method Model. *Earth Systems and Environment, 2*, 18. https://doi.org/10.1007/s40808-015-0071-9

Packialakshmi, S., & Ambujam, N. K. (2012). A hydrochemical and geological investigation on the Mambakkam mini watershed, Kancheepuram District, Tamil Nadu. *Environmental Monitoring and Assessment, 184*, 3293–3306. https://doi.org/10.1007/s10661-011-2189-1

Packialakshmi, S., Ambujam, N. K., & Prakash, N. (2011). Groundwater market and its implications on water resources in the southern peri-urban interface, Chennai, India. *Journal of Environment Development and Sustainability, 13*(2), 423–438. https://doi.org/10.1007/s10668-010-9269-1, Kluwer Publisher.

Parameswari, K., & Mudgal, B. V. (2014). Geochemical investigation of groundwater contamination in Perungudi dumpsite, South India. *Arabian Journal of Geosciences, 7*(4), 1363–1137.

Parameswari, K., & Mudgal, B. V. (2015). Assessment of contaminant migration in an unconfined aquifer around an open dumping yard: Perungudi a case study. *Environmental Earth Sciences, 74*(7), 6111–6122.

Patnaik, D. C., & Srihari, P. (2004). Wetlands – A development Paradox: The Dilemma of South Chennai, India. *SSRN Electronic Journal, 2*(July), 1114–1118. https://doi.org/10.2139/ssrn.591861

Paul, R., Prasanna, M. V., Gantayat, R. R., & Singh, M. K. (2019). Groundwater quality assessment in Jirania Block, west district of Tripura, India, using hydrogeochemical fngerprints. *Applied Sciences, 1*, 1055. https://doi.org/10.1007/s42452-019-1092-1

Piyathilake, I. D. U. H., Ranaweera, L. V., Udayakumara, E. P. N., Gunatilake, S. K., & Dissanayake, C. B. (2022). Assessing groundwater quality using the Water Quality Index (WQI) and GIS in the Uva Province. *Sri Lanka Applied Water Science, 12*, 72. https://doi.org/10.1007/s13201-022-01600-y

Ram, A., Tiwari, S. K., Pandey, H. K., Chaurasia, A. K., & Singh, S. S. (2021). Groundwater quality assessment using water quality index (WQI) under GIS framework Applied Water. *Science, 11*, 46. https://doi.org/10.1007/s13201-021-01376-7

Said, S., & Hussain, A. (2019). Pollution mapping of Yamuna River segment passing through Delhi using high-resolution GeoEye-2 imagery. *Applied Water Science, 9*, 46. https://doi.org/10.1007/s13201-019-0923-y

Salehi, S., Chizari, M., Sadighi, H., & Bijani, M. (2018). Assessment of agricultural groundwater users in Iran: A cultural environmental bias. *Hydrogeology Journal, 26*, 285–295. https://doi.org/10.1007/s10040-017-1634-9

Sonkamble, Chandra, S., Nagaiah, E., Dar, F. A., Somvanshi, V. K., & Ahmed, S. (2014). Geophysical signatures resolving hydrogeological complexities over hard rock terrain—A study from Southern India. *Arabian Journal of Geosciences, 2014*(7), 2249–2256. https://doi.org/10.1007/s12517-013-0931-4

Sridevi, M., & Ramachandran, S. (2012). Analysis of heavy metals in dying wetland Pallikaranai, Tamil Nadu, India. *Journal of Environmental Biology, 33*, 757–761. ISSN: 0254-8704.

Thambidurai, P. (2017). *Effect of forest cover on groundwater recharge for sustainable river flow "Revitalization of Rivers in India – Draft Policy Recommendation"* (pp. 284–296). Isha Foundation.

Thambidurai, P., Vignesh, K. S., & Indhiya Selvan, V. N. (2019). Assessment of groundwater potential zone in Chennai region, Tamil Nadu, India. In P. P. Adhikary, P. K. Shit, P. Santra, G. S. Bhunia, A. K. Tiwari, & B. S. Chaudhary (Eds.), *Geostatistics and geospatial technologies for groundwater resources in India* (pp. 167–191). Springer.

Vasanthi, P., Kaliappan, S., & Srinivasaraghavan. (2008). Impact of poor solid waste management on ground water. *Environmental Monitoring and Assessment, 143*, 227–238. https://doi.org/10.1007/s10661-007-9971-0

Verma, P., Singh, P. K., Sinha, R. R., & Tiwari, A. K. (2020). Assessment of groundwater quality status by using water quality index (WQI) and geographic information system (GIS) approaches: a case study of the Bokaro district, India. *Applied Water Science, 10*, 27. https://doi.org/10.1007/s13201-019-1088-4

Webster, R. (1997). Regression and functional relations. *European Journal of Soil Science, 48*, 557–566. https://doi.org/10.1111/j.1365-2389.1997.tb00222.x

Chapter 3
Catchment Scale Modeling of Land Use and Land Cover Dynamics

P. Dinagarapandi, K. Saravanan, and K. Mohan

Abstract The dynamic of Land Use and Land Cover (LULC) at the Chittar catchment is to obtain the spatial deviation for the historical and forecast period from 2001 to 2026. Spatial deviation occurred within the five LULC features such as the agricultural land, urban land, wasteland, forest, and water bodies which are classified and mapped at the spatial distribution from the years 2001, 2006, 2011, and 2016 using supervised classification. Then, LULC forecasts 2021 and 2026 using the Artificial Neural Network-based Cellular Automata (ANN_CA) method. The catchment scale LULC changes; 2001 and 2006 data are used as base maps to determine the transition potential model. Then ANN_CA is supported to simulate the LULC for the year 2011. The level of spatial matching between the simulated and field LULC for the year 2011 is measured using kappa statistics. The overall spatial matching between the two LULC is 92%, and the kappa coefficient value is 0.88. Twenty-six years of average percentage in areal contribution for agricultural, forest, urban, water bodies, and wasteland is 58%, 16%, 7.5%, 3.5%, and 15%, respectively. This LULC change data is most significant in the applications of hydrological modeling, irrigation management, urban planning, land and water resource management, etc.

Keywords LULC · ANN_CA · Change detection · Kappa statistics · Chittar catchment · Thamirabarani basin

1 Introduction

The phrase Land Use and Land Cover (LULC) generally refers to the spatial mapping of natural and anthropogenic sources of materials on the landscape within a definite time. Land cover is the physical process that generally covers the earth's surface. Land use is to describe how the land is utilized. LULC changes are one of the important parameters that affect the global environment. The LULC change also

P. Dinagarapandi · K. Saravanan (✉) · K. Mohan
School of Civil Engineering, Vellore Institute of Technology, Chennai, India
e-mail: saravanan@vit.ac.in

P. Thambidurai, A. K. Dikshit (eds.), *Impacts of Urbanization on Hydrological Systems in India*, https://doi.org/10.1007/978-3-031-21618-3_3

helps to model environmental problems such as flooding, landslides, biodiversity loss, climate change, etc. (Mousavi et al., 2019). Thus, LULC change also causes the socio-economic problem due to improper land management (Reis, 2008). Mapping and forecasting of LULC are important for environmental monitoring studies which include:

- Sustainable natural resource development and management.
- Land and water resource development and management.
- Wildlife habitat protection.
- Baseline mapping for many hydrological modeling studies.
- Urban planning.
- Coastal management.
- Urban growth modeling.
- Transport planning and management.
- Damage delineation (such as earthquake, drought, flood, forest fire, etc.)
- Guiding the real estate business investment and development.
- Target detection-identification of school, hotel, hospital, water bodies.
- Deforestation and forest conservation.

The LULC changes occur within its own features of LULC wherein the environmental hazards occur due to urbanization (alteration of cropland to an urban area), for instance, the rotation of crops in accordance with the seasons. There is a direct impact on the social-economic development with the conversion of the seasonal cropland to the uncultivated, which is the effect of the water scarcity that the fluctuation has led in seasons during the semiarid conditions. The key research for most of the developing countries revolves around water resources, as most of the researchers are centered on the changes of LULC and their impacts on the water and land resources. The findings of the availability of water present either as seasonally or annually can be achieved by the morphological analysis of the surface water body, which is led mainly by the changes in LULC; also, this LULC changes to aid in developing the hydrological model, which analyzes the hydrological response impact.

This study explores the historical and future LULC changes over the Chittar catchment of Thamirabarani Basin, Tamil Nadu (Fig. 3.1). It aligns in a semiarid climate. The catchment has been divided into five LULC classes' descriptions as shown in Table 3.1, viz., agricultural land, urban land, wasteland, forest, and water bodies (Roy & Inamdar, 2019). The historical period maps are developed from Landsat 5 Thermal Mapper, Landsat 7 Enhanced Thematic Mapper, and Landsat 8 Operational Land Imager in Geographical Information System (GIS) platform for the years 2001, 2006, 2011, and 2016. The commercially available LULC forecast model packages include CA_MARKO, Dyna-CLUE, and ANN_CA (Aarthi & Gnanappazham, 2018). This study uses an Artificial Neural Network-based Cellular Automata (ANN_CA) model to forecast the LULC over the Chittar catchment. The ANN_CA model is to learn the transition of LULC over Chittar catchment from historical data for the years 2001 and 2006 which are used to forecast LULC in 2011. The forecasted LULC in 2011 is validated with 2011 field data using kappa

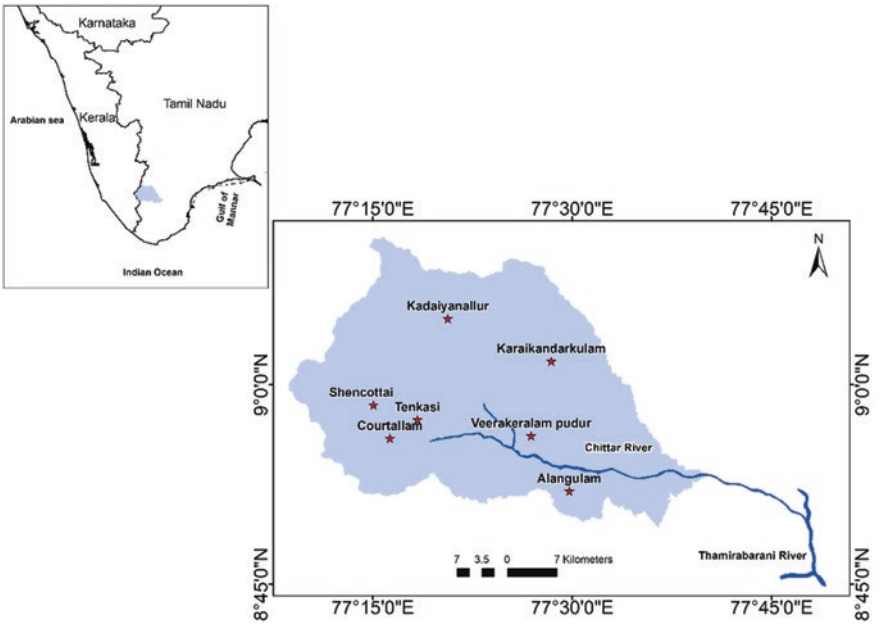

Fig. 3.1 Chittar River catchment of South Tamil Nadu, India

Table 3.1 LULC feature description

LULC features	Description
Urban land	It is an area having cluster of buildings along with human footprint such as railway station, airport, roads and streets, water bodies, park, vegetation, vacant land, and other utility area
Agricultural land	These are the lands primarily suitable for farming, which includes food, commercial and horticultural crops, dairy and animal husbandry, temporarily fallow and pasture land, etc.
Waste land	This lands which are not suitable/used for cultivation or build on or any other way. Major portion of this land possible to reclaim with reasonable effort and specific technology
Water bodies	These are natural and manmade structures to store and transport water over the earth surface. It includes wetland, reservoir, pond, channel, canal, river, etc.
Forest	The FAO defining the forest as a dense native or introduced vegetation cover with area more than 5000 m^2 and height more than 5 m with minimum 10% canopy cover. It does not include other predominant land uses like agricultural, urban land, etc.

statistics (Al-Fares, 2013). The LULC is part of the hydrological response unit, which induces the finding the certain water balance and runoff component estimations such as manning roughness coefficient and SCS-CN. By these parameters it evolves the WBC, such as runoff and infiltration. The LULC also evolves the water balance components such as interception, depression storage, and

evapotranspiration. LULC is dynamic in nature, caused by anthropogenic activity or natural causes. This concept is applied to the different time periods of LULC that link with the suitable land features with their standard parameter available in the default geodatabase.

2 Study Area

The Chittar River originated from the Courtallam hills in the southern part of Western Ghats and is one of the major tributaries of the Thamirabarani basin. Its area spans about 1300 km^2 with latitude and longitude varying from 8°45′N to 9°15′N and 77°10′E to 77°50′E, respectively (Fig. 3.1). The length of the river travels about 82 km to reach the main river. The dividing line of the catchment separates the Kerala and Tamil Nadu border. It lies in a semiarid climate zone with temperatures ranging from 25 to 40 °C. Northeast monsoon of the Chittar catchment starts from October to December and receives a 50% of annual rainfall; the Southwest monsoon starts from the month of June to August and receives a 30% of rainfall. The total rainfall of the Chittar catchment is about 880 mm. The catchment relief varies from 25 to 1710 m above MSL. The upper catchment is very steep, with a slope of more than 15%. The downstream side of the catchment is generally plain, with an average elevation of about 60–80 m and a slope of less than 1%.

3 Methodology

The LULC map is delineated from Landsat imagery (URL: glovis.usgs.gov). Landsat is a multispectral image with 30 m of spatial resolution jointly released by NASA and USGS (details shown in Fig .3.1). The visible near-infrared (VNIR) region has three bands with a spectral range of blue (0.45–0.52 μm), green (0.52–0.60 μm), and red (0.63–0.69 μm) which were captured using multispectral satellite sensors. Using three bands of Landsat imagery, LULC features were delineated in the GIS environment (Trujillo-Jiménez et al., 2022). The Resources-2 is available only within India and has a succession of 5.8 m VNIR by the Indian Space Research Organization, Government of India. The Landsat 8 OLI is launched with 30 m VNIR by the Earth Resources Observation and Science Center, NASA; it's available worldwide and has its finest provision on the coastal zone regulations and surface water resources. The Sentinel 2 was launched by European Space Agency to monitoring the morphology of land with 13 spectral bands. The Landsat satellite program series provides enormous information about LULC data. This is one of the world's largest collections of global land resources data, which is the available free and open Internet.

The Landsat imagery has a temporal resolution of 8 days starting from 1970 to the present. Lone and Mayer (2019) used the IRS LISS III and P6 to classify the

Table 3.2 Imagery data description

S. no.	Year	Type	Path/row	Resolution	Source
1	2001	Landsat TM	143/54	30 × 30	USGS
2	2006	Landsat TM	143/54	30 × 30	USGS
3	2011	Landsat ETM	143/54	30 × 30	USGS
4	2016	Landsat OLI_TIRS	143/54	30 × 30	USGS

LULC features using supervised classification. The series of Landsat imagery, as mentioned in Table 3.2, are used in this study. The Landsat imagery data are projected by Universal Transverse Mercator (UTM) zone 44 N in the World Geodetic System (WGS) datum named WGS_1984_UTM_Zone_44N to certify the consistency between the datasets during analysis. The Level 1 of the National Remote Sensing Centre classification system is used in this study (NRSC, 2014). The LULC Level 1 consists of five features (Roy & Inamdar, 2019): land use considers the urban land and agricultural land, and land cover considers wasteland, forest, and water bodies (Table 3.2). The given features are classified with the supervised classification (Vivekananda et al., 2021). The maximum likelihood classifier is one of the popular supervised classification systems that gather each trained pixel information from Landsat imagery (Lone & Mayer, 2019). Trained pixels are processed in the maximum likelihood classifier per the equation below to classify the LULC features. The maximum likelihood classifier is one of the popular algorithms for the classification of satellite images, in which a pixel with the maximum likelihood (ML_A) is classified into the corresponding class:

$$ML_A = \ln P(A) - \frac{1}{2}\ln|\Sigma_A| - \frac{1}{2}(x - X)\Sigma_A^{-1}(x - X) \tag{3.1}$$

where A = features; x = number of bands in dimensional; $p(A)$ = probability of all features; $|\Sigma_A|$ = determinant of the covariance matrix in features; Σ_A^{-1} = inverse matrix; and X = mean vector.

The maximum likelihood classifier is used in this study, which is one of the popular satellite data processing methods. The LULC data for the years 2001, 2006, 2011, and 2016 over the Chittar catchment are prepared and used for ANN model training.

The concepts of Cellular Automata (CA) were jointly induced by two great mathematicians Alan Turing and John von Neumann, during 1930s. The CA is a very popular method applied for modeling the LULC and its changes, estimating the pixel value according to its initial state. The pixel value determines according to their surrounding neighborhood effects and transition rules. A CA only effectively models the nonlinear spatially stochastic LULC change processes. The LULC is delineated in the GIS environment and prepared for the year 2001, 2006, 2011, and 2016, respectively. Here, the ANN_CA model is capable of predicting the future LULC from the transition from the previous state of LULC. Artificial Neural Network (ANN) is used for training to find the transition potential within LULC features (Mas et al., 2014). Again, the CA technique is used to simulate future data

by adopting the transition potential. Finally, ANN_CA is supported to forecast the future LULC (Li & Yeh, 2002; Qiang & Lam, 2015). Using Kappa statistics, ANN_CA-predicted 2011 LULC is validated with field 2011 LULC through the multi-resolution budget. The final model is used to forecast the LULC for the years 2021 and 2026. A flow chart of methodology to forecast LULC for 2021 and 2026 by using historical 5-year intervals of LULC is shown in Fig. 3.2.

Commercially available LULC forecasting model package includes CA_MARKOV, Dyna-CLUE, and ANN_CA. Here, the Chittar catchment is used to forecast the LULC using the ANN_CA model package (Basse et al., 2014; Qiang & Lam, 2015). Forecast LULC data for the years 2021 and 2026 are adopted for the methodology shown in Fig. 3.2. Modules for Land Use Change Simulations (MOLUSCE) is accessed as an open-source QGIS plugin to process the ANN_CA LULC change model (Measho et al., 2020). Input variables of ANN training datasets are of five stages: neighborhood pixels, learning rate, momentum, maximum iterations number, and hidden layers using multilayer perceptron. The number of hidden layers and neurons in each hidden layer has arrived arbitrarily. Input neurons are carried out as

$$\left(C_f - 1\right)\left(2N_b + 1\right)^2 + R_f\left(2N_b + 1\right)^2 \tag{3.2}$$

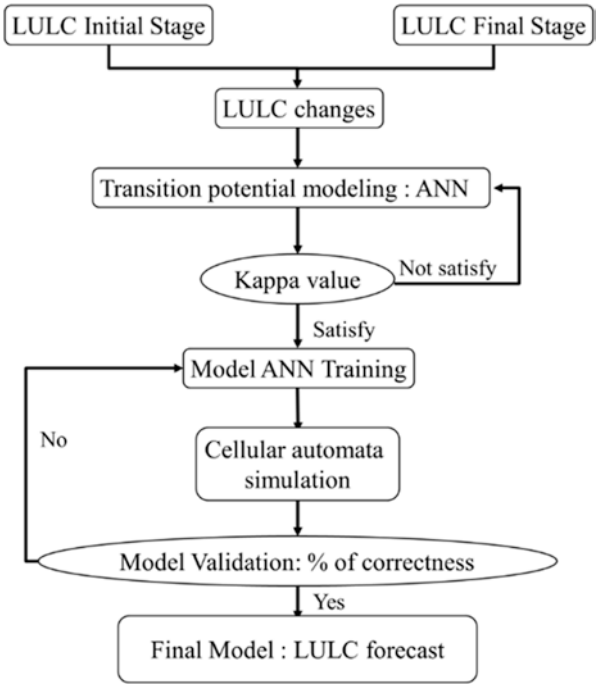

Fig. 3.2 Methodology of flow chart

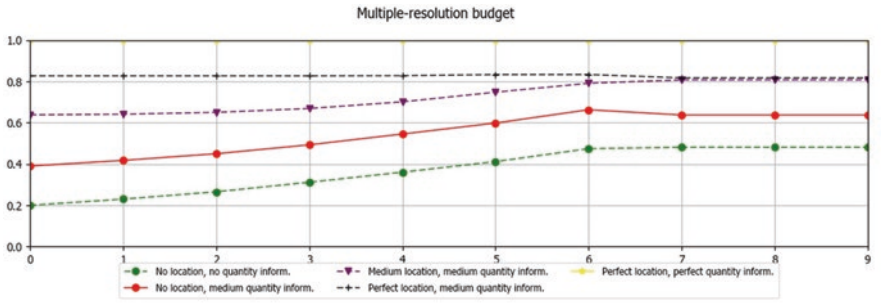

Fig. 3.3 Validation of 2011 LULC with multi-resolution budget method using ten iterations

where C_f = count of attained LULC features; N_b = neighborhood pixels size specified by the initial data; and R_f = summary band count of factor raster. Output neurons (M) usually are a count of unique features in the change map (C_f^2). The classic back propagation algorithm with momentum is used to train the ANN model. Trained data rectification is performed as

$$X(n+1) = \mathrm{L}_r^* D_x(n) + M^* D_x(n-1) \tag{3.3}$$

where X = vector of neuron trained data; D_x = vector of trained LULC changes; n = iteration number; L_r = learning rate; and M = momentum.

The initial and final LULC datasets are used to delineate the transition potential. The transition potential is mapping the areal changes between the LULC features. The ANN is used in training to find out the transition potential of LULC features (Mas et al., 2014). Transition potential is trained between the years of 2001 and 2006 of LULC. Again, CA is the technique used for the simulation of future data by incorporating the modeled transition potential. Finally, the ANN_CA is supported to predict the 2011 LULC. Multi-resolution budget validates the two datasets on the five categories of plots (Fig. 3.3). These plots are based upon the quantity and location where perfect location information and perfect quantity information plots for ten iterations have reached a high value with others. It has achieved 88% of correctness with the historical 2011 LULC. Similarly, LULC of 2011 and 2016 is used for the ANN_CA to forecast LULC data for 2021. Further, the LULC of 2026 is forecasted from the LULC of 2016 and 2021.

4 Results and Discussions

The LULC change analysis is interpreted for 2001, 2006, 2011, and 2016 (Fig. 3.4). Thus, the process of LULC change analyzes the area contribution in km^2 as shown in Fig. 3.5. Over the Chittar catchment, about 74% of the area is jointly covered by agricultural and forest land (Fig. 3.5). The remaining 26% area is covered by

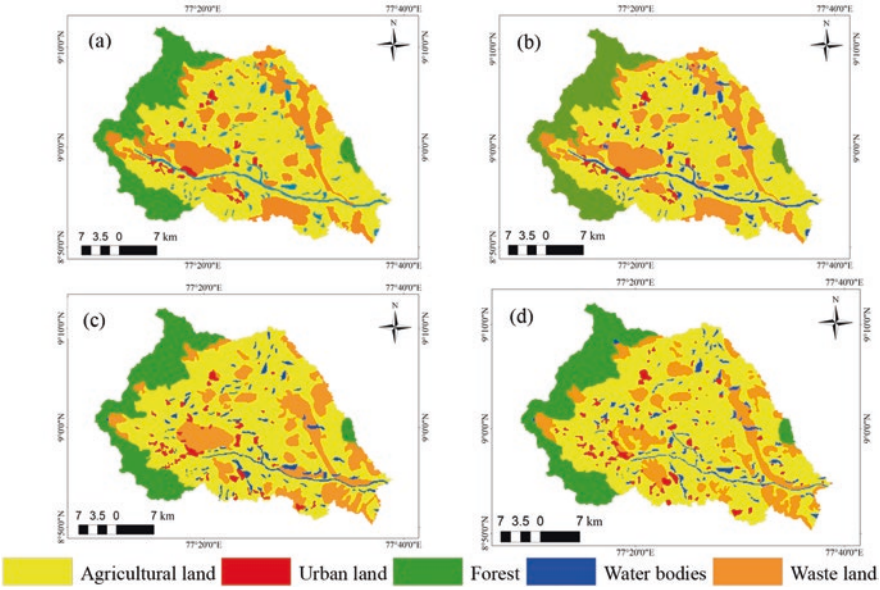

Fig. 3.4 LULC dynamics map of (**a**) 2001, (**b**) 2006, (**c**) 2011, and (**d**) 2016

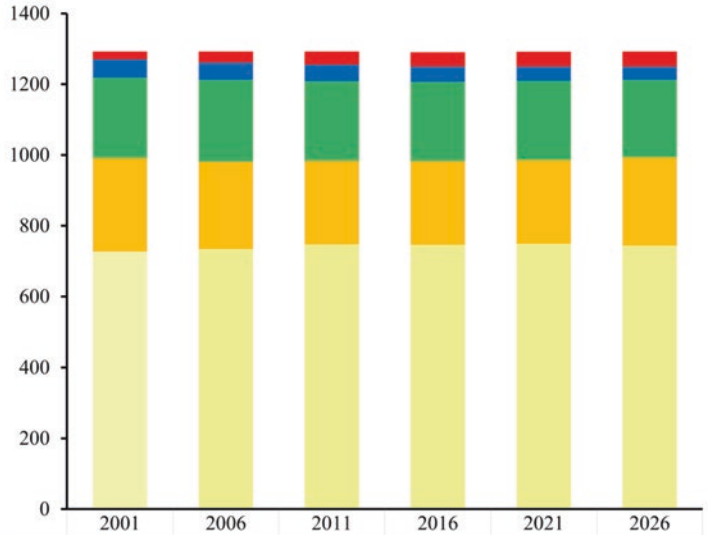

	2001	2006	2011	2016	2021	2026
Urban land (sq.km)	22	31	37	40	41	42
Water bodies (sq.km)	52	49	47	44	41	38
Forest (sq.km)	227	231	226	224	224	219
Waste land (sq.km)	264	247	237	236	237	250
Agricultural land (sq.km)	727	734	747	746	749	744

Fig. 3.5 LULC Distribution

wasteland (20%), water bodies (4%), and urban land (2%). During the 20 years from 2001 to 2021, about 22 km^2 of agricultural land gradually increased, and in the same period, 27 km^2 of wasteland decreased. The increase in farming activities reclaims the wasteland over the Chittar catchment (Awotwi et al., 2015). Approximately 1% of the forest was converted to wasteland between 2001 and 2016, resulting in increased runoff in the foothills (Danáčová et al., 2020). About 20 km^2 (i.e., 78% area) of urban land is increased from 2001 to 2016, and it's driven by population growth. It is observed that agricultural and wastelands are converted into urban land to meet the sheltering needs of the increasing population. The 16% of water bodies in the Chittar catchment decreased between the periods of 2001 to 2016. The change of agricultural and urban land leads to causes critical environmental issues, likely flooding, landslides, etc., along the catchment.

The ANN_CA is used to delineate the LULC transition between 2001 and 2006. The trained ANN_CA model is used to forecast 2021 with the LULC data for 2011 and 2016. In the subsequent year 2016 and 2021, data are used to forecast 2026 LULC (Fig. 3.5). This model is further used to forecast 2011 from 2001 and 2006. A kappa value seems to be location matching with two spatial data. Here, this is matched up to approximately 88% of the area between the simulated 2011 and field 2011 LULC data. The validation results for ten iterations are shown in Fig. 3.3. Then the 2021 and 2026 LULC is forecasted using ANN_CA. From 2001 to 2026, about 6% of wasteland decreases, and alternately 3% of agricultural land is increased in the same period. Over the middle and lower portions of the Chittar watershed, agricultural land is being maintained to its greatest extent. Forest covers the upper part of the Chittar catchment. From 2001 to 2016, the forest decreased by 3.5% area was converted to a wasteland. The wasteland covers all parts of the catchment and scatters very well. Thus, a wasteland in 2016 was converted into agricultural land (about 1.5%) due to farming practices. Then agricultural land converts into an urban area (about 0.5%) in 2026 due to the rising of the population (Fig. 3.4). The maximum urban is the low region of forest area. They are Tenkasi, Shencottai, Courtallam, Kadaiyanallur, Alangulam, etc. Finally, 2026 water bodies continuously decrease up to 26% from 2001 over the Chittar catchment. Because of human activity, water bodies are being converted to urban and agricultural land.

Forecast LULC of 2026 shows fewer areal changes compared to the historical LULC; the areal changes of 2011 to 2016 show the frequent variation from 2001 to 2011 in agricultural and wasteland. The ANN_CA model is achieved by the neural systems that delineate areal changes between the LULC features. After 2016 LULC of area contribution describes the rise in the wasteland, and drop down from the agricultural land directly denotes the conversion of wasteland to agricultural. The wasteland is mostly a salt-affected region with low productivity. Again in 2026 LULC, it achieves the gain of agricultural land of approximately 5 km^2 and a loss in the wasteland of about 13 km^2. So, it seems to be a rise in moisture content due to climate change (Fig. 3.6). If the reduction of agricultural land happens within the catchments, it leads to an impact on the social and economic effects. Agriculture is the main source of increase in the national economy. In a historically agricultural community, a rise in uncultivated land creates social instability and conflict.

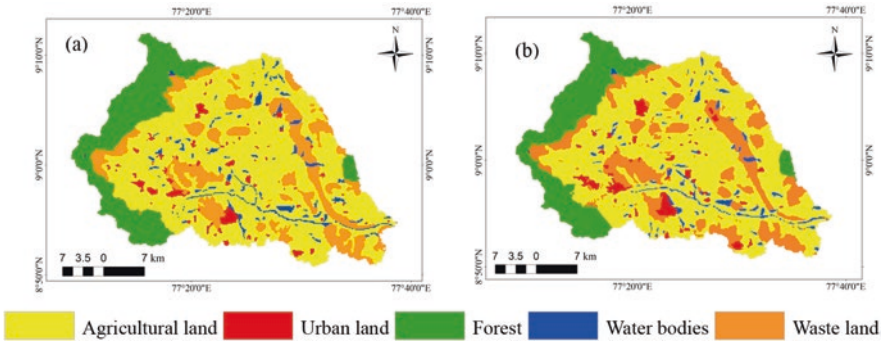

Fig. 3.6 LULC dynamics map of study area for (**a**) 2021 and (**b**) 2026

Table 3.3 Change detection for the ten years

	Ten years			
LULC types	2001–2011	2006–2016	2011–2021	2016–2026
Agricultural land	+20	+12	+2	-2
Waste land	−27	−11	0	+14
Forest	−1	−7	−2	−5
Water bodies	−5	−5	−6	−6
Urban land	+15	+11	+5	0

Furthermore, the fall in agricultural productivity raises the likelihood of food production security threats (Rasool et al., 2021).

5 Change Detection

Change detection is the proper technique for estimating the spatial deviation between the two datasets. It can be calculated with the area units in km^2. Change detection is the technique to analyze the mapped spatiotemporal LULC changes between the multi-temporal images. The change defection analysis is carried out for the period 2001 to 2026 between five subclasses over the Chittar catchment. Table 3.3 summarizes the area of increase (+) or decrease (−) in km^2 during the consecutive 10-year periods. The 10 years of LULC maximum change is detection that occurred between agricultural and wasteland. Forest, urban land, and water bodies do not change much in 10 years. Due to the dominance of agricultural land, indirectly, the Chittar catchment indicates the water resources gained by their subsurface, i.e., groundwater or its surface, led by the irrigation practices. Forest is the only feature not disturbed by other features. Even though water bodies and urban land contribute at a minor level at this LULC change detection, efficiency is larger than any other features.

It shows the maximum gain of 20 km^2 from 2011 to 2021 and 12 km^2 from 2006 to 2016 for the agricultural land. Gain and loss of agricultural land denote the amount of food productivity. Loss of wasteland continuously changes by more than 5 km^2 per decade. Suddenly, the increase of wasteland between 2016 and 2026 is 14 km^2 due to the reduction of agricultural land. These changes occurred mainly due to soil degradation, land rehabilitation, and land productivity. Then, 2016 to 2026 has low gain/loss in LULC changes. Minimum LULC change happens in the forest and water bodies that range less than 10 km^2. Agricultural and urban land was steadily incremented up to 2001–2026 and proportionally reduced in water bodies. It leads to the declination of water bodies as the massive increase in agricultural productivity in the riverbed. Similarly, the trend of 10 years is quite the same as 30 years also. The loss happened in the wasteland, forest, and water bodies and followed by gain happen in urban and agricultural land. The LULC change has been detected for 30 years and has a major impact on the hydrological model.

6 Conclusion

In the tropical climate of south India, it behaves as a seasonal variation in the temperature as well as the rainfall reflected in the landscape. In the Chittar catchment, hot weather (temperature) happens for 6 months in an annum, so it causes more evaporation and evapotranspiration in the agricultural land (70%) due to this solar energy; also, it converts the surface water bodies to dry land. However, surface irrigation completely stopped after 2011, as shown in the LULC dynamics map. Further, the probability of water resources purely depends upon rainfall and groundwater. The rest of the period leads to the direct supply of water (rainfall) into soil derived from the runoff, infiltration, and percolation characteristics over the catchments. As per the Chittar catchment, 16% of water bodies' decline is visualized in 2001–2026 LULC dynamic map. The 40% of 2001 urban area rises to 2026 LULC map. Here, 58% of agricultural land is mapped along with the uncultivated land also, so the contribution of agricultural land has a meager change in the Chittar catchment. Uncultivated land has directed the wasteland, i.e., scrubland. Due to the source of groundwater potential site, agricultural activities still have achieved their best level in this Chittar catchment. Wasteland of 25 years has contributed to all the other features. The spatial distribution of wasteland is easier to interpret from the LULC dynamics map. Change detection helps to compare the LULC features in km^2, where it interprets the major change between the agricultural land and wasteland. Other features are less contributed. Thus, the landscape phenomenon is attained by the combination of soil, LULC, and slope (i.e., HRU) of the Chittar catchment, which leads to a response of hydrologic characteristics in it. The HRU is the basis for many hydrological models at the catchment scale.

Acknowledgments Authors are very much thankful to our School of Civil Engineering, VIT, Chennai, Tamil Nadu, India, for providing research-related facilities to complete this research. Further, our institute is also sponsoring this publication. The authors are grateful to open-source Landsat series data provided by the US Geological Survey Earth explorer.

Declarations Authors declare no conflict of interest.

References

Aarthi, A. D., & Gnanappazham, L. (2018). Urban growth prediction using neural network coupled agents-based cellular automata model for Sriperumbudur Taluk, Tamil Nadu, India. *Egyptian Journal of Remote Sensing and Space Science, 21*(3), 353–362. https://doi.org/10.1016/j.ejrs.2017.12.004

Al-Fares, W. (2013). *Historical land use/land cover classification using remote sensing: A case study of the Euphrates River basin in Syria*. University of Jena, Germany, Springer Briefs in Geography, Springer. https://doi.org/10.1007/978-3-319-00624-6

Awotwi, A., Yeboah, F., & Kumi, M. (2015). Assessing the impact of land cover changes on water balance components of White Volta Basin in West Africa. *Water Environment Journal, 29*(2), 259–267. https://doi.org/10.1111/wej.12100

Basse, R. M., Omrani, H., Charif, O., Gerber, P., & Bódis, K. (2014). Land use changes modelling using advanced methods: Cellular automata and artificial neural networks. The spatial and explicit representation of land cover dynamics at the cross-border region scale. *Applied Geography, 53*, 160–171. https://doi.org/10.1016/j.apgeog.2014.06.016

Danáčová, M., Földes, G., Labat, M. M., Kohnová, S., & Hlavčová, K. (2020). Estimating the effect of deforestation on runoff in small mountainous basins in Slovakia. *Water, 12*, 3113. https://doi.org/10.3390/w12113113

Li, X., & Yeh, A. G. O. (2002). Neural-network-based cellular automata for simulating multiple land use changes using GIS. *International Journal of Geographical Information Systems, 16*(4), 323–343. https://doi.org/10.1080/13658810210137004

Lone, S. A., & Mayer, I. A. (2019). Geo-spatial analysis of land use/land cover change and its impact on the food security in district Anantnag of Kashmir Valley. *GeoJournal, 84*(3), 785–794. https://doi.org/10.1007/s10708-018-9891-2

Mas, J. F., Kolb, M., Paegelow, M., Olmedo, M. C., & Houet, T. (2014). Modelling land use/cover changes: A comparison of conceptual approaches and softwares. *Environmental Modelling & Software, 51*, 94–111. https://doi.org/10.1016/j.envsoft.2013.09.010

Measho, S., Chen, B., Pellikka, P., Trisurat, Y., Guo, L., Sun, S., & Zhang, H. (2020). Land use/land cover changes and associated impacts on water yield availability and variations in the Mereb-Gash River Basin in the Horn of Africa. *Journal of Geophysical Research – Biogeosciences, 125*(7), e2020JG005632. https://doi.org/10.1029/2020JG005632

Mousavi, S. M., Roostaei, S., & Rostamzadeh, H. (2019). Estimation of flood land use/land cover mapping by regional modelling of flood hazard at sub-basin level case study: Marand basin. *Geomatics, Natural Hazards and Risk, 10*(1), 1155–1175. https://doi.org/10.1080/19475705.2018.1549112

NRSC. (2014). *Land use/Land cover database on 1:50,000 scale.* Natural Resources Census Project, LUCMD, LRUMG, RSAA, National Remote Sensing Centre, ISRO, Hyderabad.

Qiang, Y., & Lam, N. S. (2015). Modeling land use and land cover changes in a vulnerable coastal region using artificial neural networks and cellular automata. *Environmental Monitoring and Assessment, 187*(3), 57. https://doi.org/10.1007/s10661-015-4298-8

Rasool, R., Fayaz, A., & ul Shafiq, M., Singh, H., Ahmed, P. (2021). Land use land cover change in Kashmir Himalaya: Linking remote sensing with an indicator based DPSIR approach. *Ecological Indicators, 125*, 107447. https://doi.org/10.1016/j.ecolind.2021.107447

Reis, S. (2008). Analyzing land use/land cover changes using remote sensing and GIS in Rize, North-East Turkey. *Sensors, 8*(10), 6188–6202. https://doi.org/10.3390/s8106188

Roy, A., & Inamdar, A. B. (2019). Multi-temporal Land Use Land Cover (LULC) change analysis of a dry semi-arid river basin in western India following a robust multi-sensor satellite image calibration strategy. *Heliyon, 5*(4), 01478. https://doi.org/10.1016/j.heliyon.2019.e01478

Trujillo-Jiménez, M. A., Liberoff, A. L., Pessacg, N., Pacheco, C., Díaz, L., & Flaherty, S. (2022). SatRed: New classification land use/land cover model based on multi-spectral satellite images and neural networks applied to a semiarid valley of Patagonia. *Remote Sensing Applications: Society and Environment, 26*, 100703. https://doi.org/10.1016/j.rsase.2022.100703

Vivekananda, G. N., Swathi, R., & Sujith, A. V. L. N. (2021). Multi-temporal image analysis for LULC classification and change detection. *European journal of remote sensing, 54*(sup2), 189–199. https://doi.org/10.1080/22797254.2020.1771215

Chapter 4
Urban Floods: A Case Study of Patna Floods 2019 – Natural or Anthropogenic?

Ahmad Rashiq and Om Prakash

Abstract In September 2019, Patna witnessed an urban flood due to a greater than expected rainfall. Nearly 177 mm of precipitation within 48 h broke the decade-old record of 158 mm on September 3, 2013. This was also the highest rainfall recorded in September at nearly 430 mm, eclipsing the old record of 400 mm. Five teams of NDRF were deployed in the city, which rescued nearly 5000 people from the flood-affected areas. The floods led to the loss of property, damaged structures, and the spread of waterborne diseases. In the 6 years (i.e., from 2013 to 2019), what had changed in Patna city that a rise of nearly 12% in highest rainfall during September led to such an extent of flooding? Though the deluge was immediately blamed on climate change, it cannot be understated how unplanned rapid urbanization, deforestation, exploitation of flood plain, and lack of proper drainage networks are the underlying factors which aggravate the impact of climate change. Lack of flood zoning, lack of proper action plan for disaster management, and lack of proper legislation add fuel to the fire in terms of preparedness. This case study aims to explore the different natural and anthropogenic factors which congregated to cause the Patna flood of 2019 so that appropriate mitigation strategies can be worked out and implemented to abate future urban floods in Patna.

Keywords Urban floods · Urbanization · Climate change · Remote sensing · Patna

1 Introduction

1.1 Urban Floods

Urban flooding can be defined as the inundation of any urban area as a result of meteorological and hydrological factors, which are exacerbated by anthropogenic activities. Urban floods are different from riverine floods. Unlike riverine floods,

A. Rashiq (✉) · O. Prakash
Indian Institute of Technology Patna, Bihta, Bihar, India
e-mail: ahmad_2021ce05@iitp.ac.in

P. Thambidurai, A. K. Dikshit (eds.), *Impacts of Urbanization on Hydrological Systems in India*, https://doi.org/10.1007/978-3-031-21618-3_4

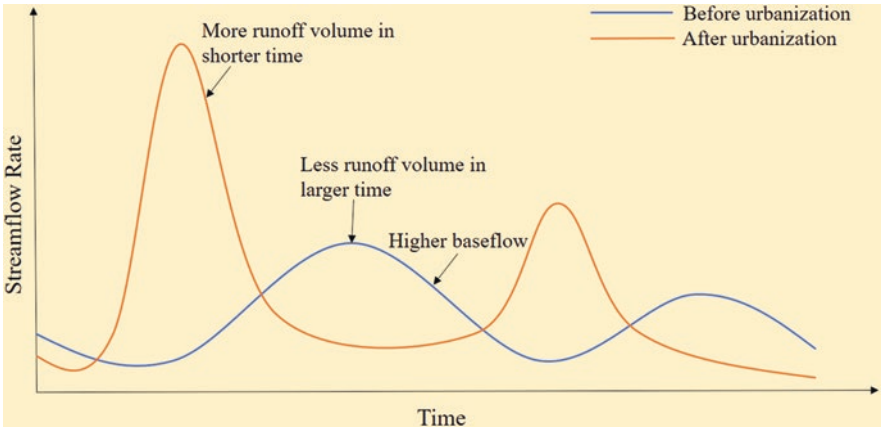

Fig. 4.1 Changes in the hydrological response of a catchment due to urbanization

which can take days to build up, urban areas act as developed catchments (Fig. 4.1) where flood volume builds up in quick time due to the impervious nature of the surface. The paved surfaces offer less resistance to the runoff, leading to a very low time for attaining peak discharge. So urban floods result in high runoff in a relatively short duration of time. Some of the most destructive urban floods of recent times are the Mumbai flood (2005) and Chennai flood (2015), which claimed hundreds of lives, while the damage due to both floods combined ran in excess of 3 billion dollars. These floods brought life to a standstill, with train and airplane services halted for days and industries shut down completely. Many people are vulnerable to the risk of urban floods in dense urban areas, making them a significant cause of concern among town planners. In recent times, city after city has experienced urban floods. The National Disaster Management Authority (NDMA) classified urban floods as separate disasters given that their causes and strategies to deal with them differ from riverine floods.

1.2 Causes of Urban Floods

Urban floods result due to a combination of meteorological, hydrological, and anthropogenic factors. These factors have been documented by various authors (Mourato et al., 2012; Rafiq et al., 2016; Mukherjee, 2016; Gupta, 2020; Vazhuthi & Kumar, 2020; Qi et al., 2021; Ranger et al., 2011) and are shown in Fig. 4.2. Like any kind of floods, be it pluvial or fluvial, intense precipitation is one of the major causes. A 100 mm of rainfall spread over a day and an hour will have different impacts, with the latter having the potential to overwhelm the drainage capacity of any urban system. Long spells of rainfall lead to saturation of soil moisture, meaning that the capacity of soil to act like a sponge to absorb incoming rainfall decreases.

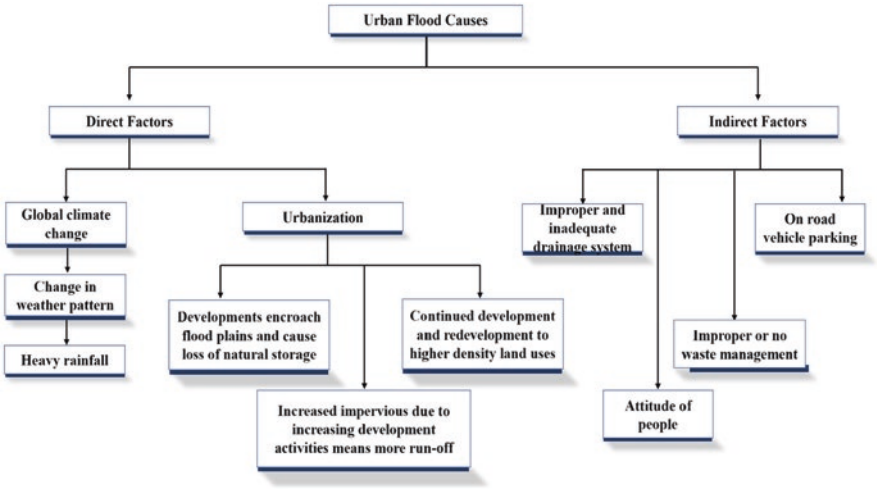

Fig. 4.2 Cause of urban floods. (Modified after Qi et al., 2021; Mukherjee, 2016; Gupta, 2007)

Rapid urbanization has led to various problems which arise because of unplanned and unmanaged urban development (Hammond et al., 2015). Encroachment and obstruction of flood plains due to construction and sand mining lead to loss of natural storage and urban water bodies, while paved surfaces decrease the perviousness of urban surfaces. Construction activities on flood plains endanger the lives of people who reside in such risk-prone areas. The drainage system in most of cases of urban floods proved to be inadequate and was poorly maintained (Berggren et al., 2014). When the intensity of rainfall is greater than the return period of rainfall for which the drainage system is designed, the excess water will appear as runoff. This scenario is aggravated due to the non-maintenance of drains which leads to siltation and choking of the drains (Gupta, 2007). Siltation of existing drains reduces their capacity to carry stormwater, and increasing population only adds more load. On top of all this, improper solid waste disposal leads to the blockage of natural and artificial drains (Huong & Pathirana, 2013).

1.3 Urban Floods and Anthropogenic Activities

The advent of the twenty-first century has brought about rapid development and urbanization in our country. As the country has grown, opportunities have attracted more people to migrate to the cities leading to a rise in the urban population. Infrastructure to support this growing population developed at a rapid pace so as to cater to everyone's needs. As urban areas have grown, more industries, vehicles, and commercial areas have come up, which not only leads to the urban heat island effect but also disrupts the hydrological processes in the urban catchment (Kug &

Ahn, 2013). Unplanned and unsustainable development has led to encroachment of urban water bodies, construction on river flood plains, non-maintenance urban stormwater networks, etc. A congregation of problems arising out of this development has choked the urban catchment's capabilities in dealing with rainfall. As more concrete structures grow, the perviousness of the surface decreases, which, in turn, decreases infiltration (Jacobson, 2011). Along with infiltration, evapotranspiration also decreased due to urbanization (Nie et al., 2009). The impact of urbanization on runoff is evident through literature and common observation by seeing a glass of water dropped on soil producing no runoff and the same glass of water on a concrete surface producing instant runoff due to the impervious nature of concrete. Further, the urban heat island effect leads to intense precipitation over cities as the air over cities gets warmer compared to the surrounding suburban areas.

1.4 Urban Floods and Climate Change

Although urban heat island has resulted in increased intense precipitation over urban areas, macroscale climate change has itself led to an increase in intensity and frequency of extreme precipitation events in general (Nie et al., 2009; Djordjević et al., 2011; Kug & Ahn, 2013). Also, the frequency of localized heavy precipitation has increased over the Indian subcontinent (Gnanaseelan et al., 2020). Climate change has led to the warming of the atmosphere due to the sustained greenhouse effect. An increase in temperature means that as the air expands, its capacity to hold moisture also increases, which in turn means that there is more potential for evaporation. Increased evaporation results in more precipitation taking place. In the Chennai flood of 2015 (Seenirajan et al., 2017), record-breaking rainfall occurred in the city, dwarfing any rainfall in the previous 100 years. Continuous heavy rainfall due to the low-pressure region over the Bay of Bengal led to intense wet spells, which lasted from November 8 to December 14, 2015. The city received almost 300 mm of rainfall on both November 16 and December 2, while rainfall values exceeded the 100 mm mark on 5 separate days, and such intense wet spells are a result of the changing climate.

2 Study Area

2.1 Patna City

Patna is the capital and largest city of Bihar state, located on the southern banks of the river Ganga. Patna city is a major agricultural hub and center of trade and is an important business brand center in eastern India. Also, it is the main administrative

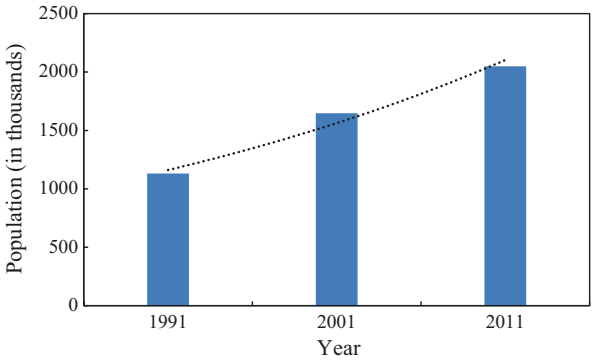

Fig. 4.3 Population of Patna city (1991–2011)

and educational center in the state. As per the census of India 2011, Patna is the 18th largest urban agglomeration in the country. The main urban area of Patna is located between coordinates of 25°35′38.74″ N and 85°8′15.23″ E with an elevation of 53 m (173 feet) above sea level.

2.2 Demography and LULC

Although the census data for the year 2021 is not available as of writing this article, the increase in urban population is apparent considering census data from the previous years. The average population density in the city is 1800 per square kilometer, which is higher than the national average of 382 per km^2. The population of Patna city has swelled from 11.31 lacs to 20.49 lacs (UDHD, 2016), an increase of nearly 81% from 1991 to 2011 (Fig. 4.3). This increase in population has been accompanied by a shift toward urban economic activities from agriculture. Given that the population of Patna district is yet to reach saturation levels, the population of the city is likely to increase considerably as the development and opportunities are going to draw in more immigrants. The growing urban area and suburban sprawls (Khan et al., 2021) are a result of the need for more infrastructure to support the growing population. Overall the entire district of Patna has shown an increase in built-up by almost 600% between 1988 and 2013 (Mishra & Rai, 2016). The average elevation of the city is about 40–60 m (Fig. 4.4a), while the topography of the city is fairly flat (Fig. 4.4b).

2.3 Climate of Patna City

Patna city receives an annual rainfall of about 911 mm (Guhathakurta et al., 2020). Almost 80–90% of this rainfall occurs during the monsoon season, which lasts from June to September. The other seasons, pre-monsoon (March–May), post-monsoon

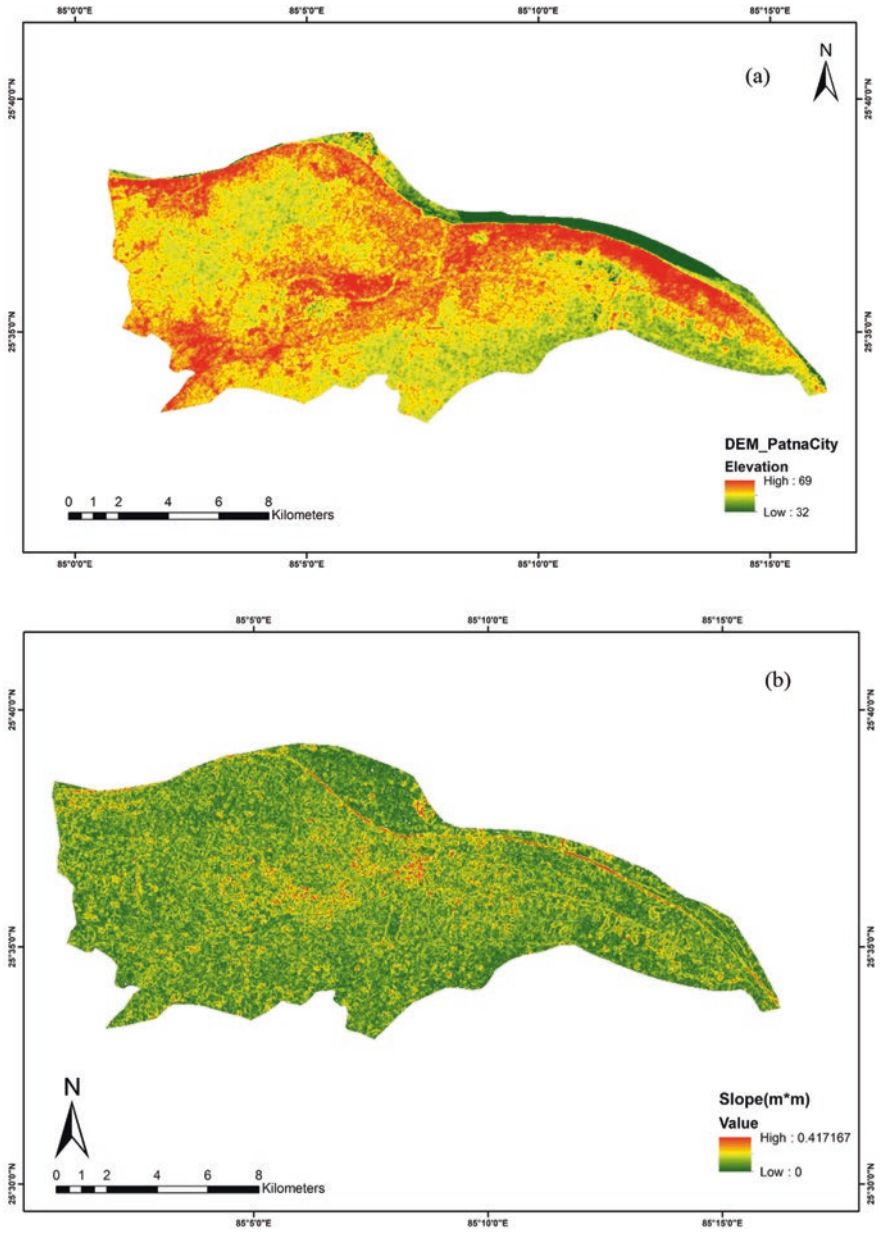

Fig. 4.4 (**a**) Digital elevation model (DEM), (**b**) Slope map of Patna city

(October–November), and winter (December–February), receive the rest of the rainfall. In Patna, the summer temperatures rise very high as the hot tropical sun beats down with all its intensity. The city, being near four large rivers, experiences rather high humidity throughout the year. The summer begins in April and peaks in June/July, with the temperature soaring up to 46 °C till the moisture-laden monsoon winds bring some much-needed relief to the parched fields. The rains last through August and September and continue into early October. The northern Indian winter brings bitter cold nights and sunny days to Patna from November to February till the arrival of the spring, which brings the weather to a full cycle.

2.4 A General Review of Patna City Flood 2019

The last week of September 2019 saw the city receive heavy rainfall due to the activation of the southwest monsoon. The Indian Meteorological Department (IMD) flashed a warning on September 27 for heavy rainfall. Consequently, the state government issued a red alert closing educational institutions and deploying rescue teams to low-lying areas. The rainfall was much greater than the initial forecasted value of 21 mm. This triggered flooding in the urban regions on September 29. Low-lying areas in the city, like Rajendra Nagar, Ramkrishna Nagar, Gandhi Maidan, Kankarbagh, and Pataliputra Colony, were the worst affected areas. Even the Nalanda Medical College was severely waterlogged. The floods left the city without power for 3 days and trapped thousands of people. Five battalions of the National Disaster Response Force (NDRF) rescued thousands of people using 16 rescue boats. The floods left city officials red-faced since the drainage maps of the city were nowhere to be found and the deluge was blamed on climate change. The city has pumping stations to draw out the water from low-lying areas, but these are unable to work at capacity due to the lack of maintenance.

3 Materials and Methodology

3.1 Data Used

Various data used in the present study are shown in Table 4.1. Point rainfall data from three IMD stations, namely, Patna Aero, Bihta, and Sripalpur, were used to prepare the average rainfall data using the inverse distance weightage (IDW) interpolation technique in ArcGIS. Even though Bihta and Sripalpur lie outside the boundary of the city, their vicinity and similarity in rainfall to that of Patna make their rainfall data useful. Land-use maps were prepared using the Landsat 8 images obtained from the earth explorer portal. These images were processed in ArcGIS, and land-use classes were defined using supervised classification. The digital

Table 4.1 Various data used in the present study and their resolution

Data	Resolution
Rainfall	Daily data
Population	Decadal
Landsat-8	30 m
CARTOSAT	30 m
Soil	1:5000000
Soil database	NA

elevation model (DEM) was obtained from CARTOSAT version 3 at 30 m resolution from the Bhuvan portal. The DEM was processed in ArcGIS to obtain the slope map. The soil map was downloaded from the Food and Agricultural Organization (FAO) portal and classified using the ArcSWAT library.

3.2 Methodology Adopted

The hydrological, meteorological, and topographical properties of the study area were evaluated using a hydrological model to derive the rainfall-runoff characteristics. Natural Resources Conservation Service-Soil Conservation Service (NRCS-SCS)-curve number (CN) is a widely used method for estimating runoff depth due to rainfall. This empirical method depends on dimensionless CN values for the calculation of runoff:

$$\mathrm{S} = \frac{25400}{CN} - 254 \tag{4.1}$$

$$Ia = 0.2S \tag{4.2}$$

$$\mathrm{Q} = \frac{\left(P - 0.2S\right)^2}{P + 0.8S} \tag{4.3}$$

The runoff (Q) was calculated as shown by Eq. (4.3). This required the calculation of maximum potential retention (S) (Eq. 4.1) and initial abstraction (Ia) (Eq. 4.2) using the CN values. If precipitation was greater than the initial abstraction, then excess rainfall would produce runoff. The CN values depend on land use, land cover type, hydrologic soil group (HSG), and the antecedent moisture condition (AMC). The land-use impacts the perviousness of the surface, HSG affects the infiltration capabilities of soil, and AMC accounts for the presence of soil moisture due to previous cumulative 5-day rainfall. The CN values increase as we go from HSG-A to HSG-D. This model has been used to prepare the runoff maps. Further, grids of 1 × 1 km were used over the study area to extract the mean rainfall and runoff values in those grids and assess the rainfall-runoff characteristics for the events of 2013 and 2019.

3.3 Use of Remote Sensing in Flood Management

Remote sensing provides a wide array of data, which are used in GIS for hydrological analysis as well for flood modelling and management. Some of the data provided by the remote sensing satellites are information regarding the water bodies and their monitoring, snow cover and glaciers, precipitation, evapotranspiration, soil moisture, and topography. The synthetic aperture radar (SAR) data has been extensively used in mapping the flood extent (Bhatt et al., 2021) as it allows observation even under the presence of cloud cover. The longer wavelength of radio waves enables them to penetrate cloud cover. Derived products from satellite images, such as DEM obtained from ASTER, SRTM, CARTOSAT, etc., are used to assess the slope, aspect, and topography of the area and can help derive the drainage network as well. Land use land cover (LULC) classification using Landsat 4, Landsat 5, Landsat 8, and Sentinel 2 is also done to identify different land covers present, such as built-up areas and vegetation. The DEM and LULC are derivatives of satellite imagery and are extensively used in flood modelling and management (Seenirajan et al., 2017; Qi et al., 2021). Flood models like HEC-HMS, SWAT, and MIKE require inputs, which are provided through spatial data. In the absence of ground-based rain gauges, derived precipitation products such as Global Precipitation Mission (GPM) and Tropical Rainfall Measuring Mission (TRMM) are used.

3.4 Runoff Estimation Using GIS

The NRCS-CN method was implemented in the ArcGIS platform by using Landsat 8 and CARTOSAT images and their derivatives along with hydrometeorological data (Fig. 4.5). This offered the advantage of visualizing the results in terms of areas are getting inundated and the depth of inundation. All the calculations were performed using the "map algebra" tool in the ArcGIS platform.

The steps to implement NRCS-CN in GIS were as follows:

1. DEM was taken as input in ArcGIS, and a slope map was prepared.
2. Supervised classification was done for the Landsat imagery to obtain the different classes of land use (LULC).
3. The soil map was processed in ArcGIS, and hydrological soil groups (HSG) were identified.
4. A rainfall map was prepared using IDW interpolation, taking the location of the stations and the corresponding rainfall values for 2013 and 2019.
5. Once all the data was ready, the LULC and soil map was combined to find the corresponding curve number (CN)-II values.
6. Once CN-II was obtained, slope correction was applied using Huang's (2006) equation (Eq. 4.4) as follows:

$$CN_{2\alpha} = CN_2 \frac{322.79 + 15.63 \alpha}{323.52 + \alpha} \tag{4.4}$$

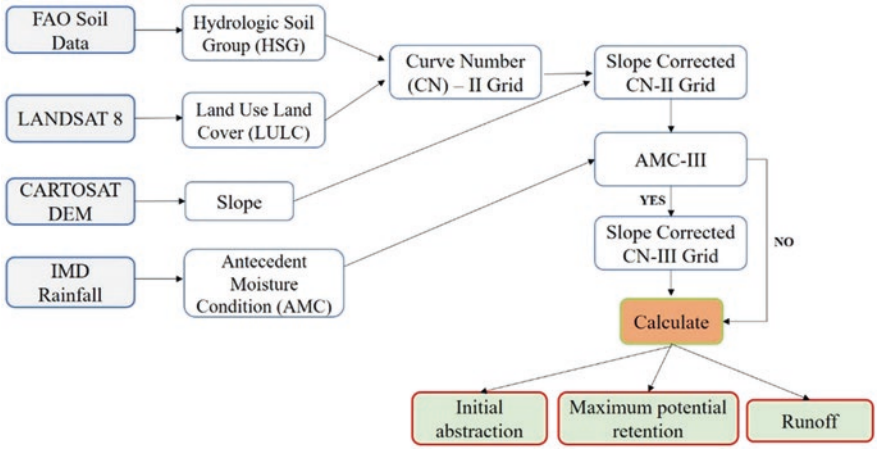

Fig. 4.5 Flowchart elaborating the various steps used to obtain the runoff maps from raw data

where $\propto$ is the slope of the area.

7. Based on the daily rainfall data, AMC was calculated. For AMC-III conditions, corrections to the slope corrected CN-II values were applied to obtain CN-III values using Hawkins's (1985) equation (Eq. 4.5) as follows:

$$CN_3 = \frac{CN_{2\propto}}{0.427 + 0.00573CN_2} \tag{4.5}$$

8. Potential maximum retention (S), initial abstraction (Ia), and runoff maps were then prepared using the equations shown in Fig. 4.5.

4 Results

4.1 Rainfall Events of 2013 and 2019

Rainfall data at three stations (Patna Aero, Bihta, and Sripalpur) were compared for the rainfall events of 2013 and 2019. The days leading to the flooding in Patna city were studied to understand the rainfall events which preceded the floods. Although the single-day rainfall recorded at Patna Aero station on September 29 (151.9 mm) was slightly lower than the value recorded on September 3, 2013 (158 mm), the distribution of rainfall in 2019 was much higher magnitude-wise as compared to 2013 (Fig. 4.6). It was also imperative to understand the built up of rainfall and soil moisture due to rainfall on preceding days. A very distinguishing picture emerged to the forefront when the 5-day total rainfall (Fig. 4.7) was obtained by adding 3-day rainfall before September 3, 2013/September 29, 2019 to the rainfall of September 3, 2013/September 29, 2019, and the rainfall on the following day. For 2013, the

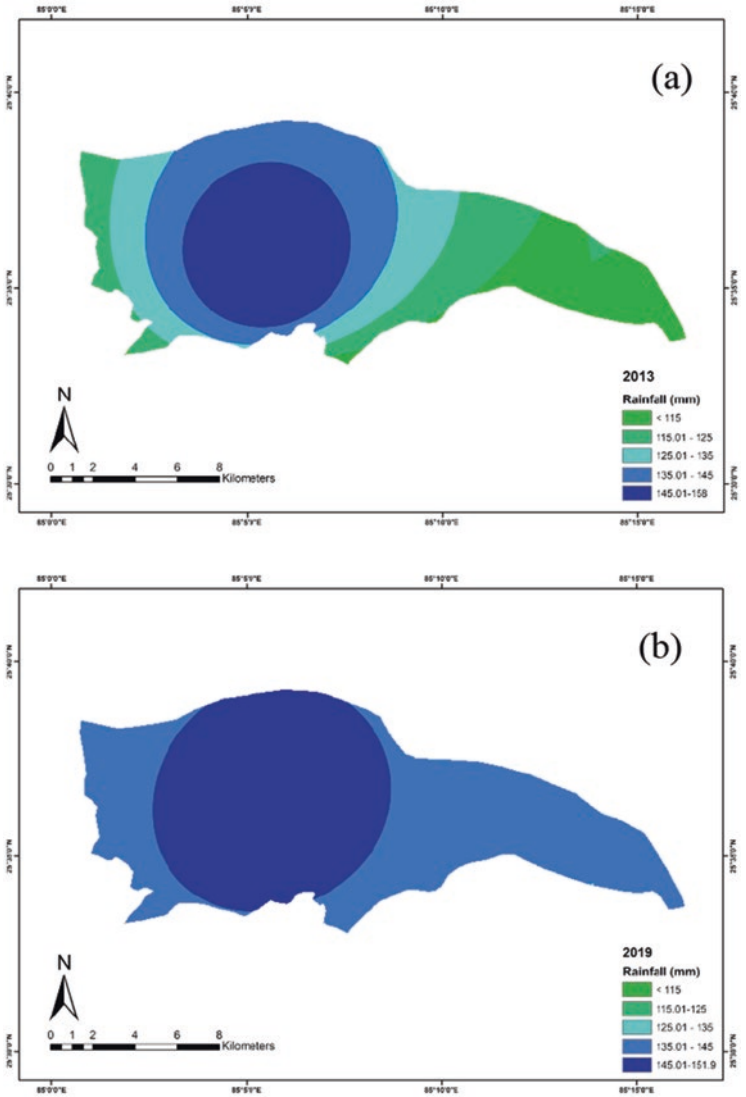

Fig. 4.6 Spatial distribution map of 1-day rainfall events for years (**a**) 2013 and (**b**) 2019

5-day rainfall recorded at Bihta, Patna Aero, and Sripalpur was 65 mm, 222.3 mm, and 62.4 mm, respectively. In 2019, the 5-day rainfall recorded at Bihta, Patna Aero, and Sripalpur were 202.6, 371, and 458.6 mm, respectively. Two conclusions can be drawn from these rainfall values:

1. The rainfall events of 2019 were much larger than the ones in 2013 when the 5-day rainfall is compared. The 5-day rainfall at Patna Aero for 2019 was 70% greater than in 2013. The Sripalpur had almost 600% greater 5-day rainfall in 2019 when compared with 2019. This highlights the intense precipitation event of 2019.

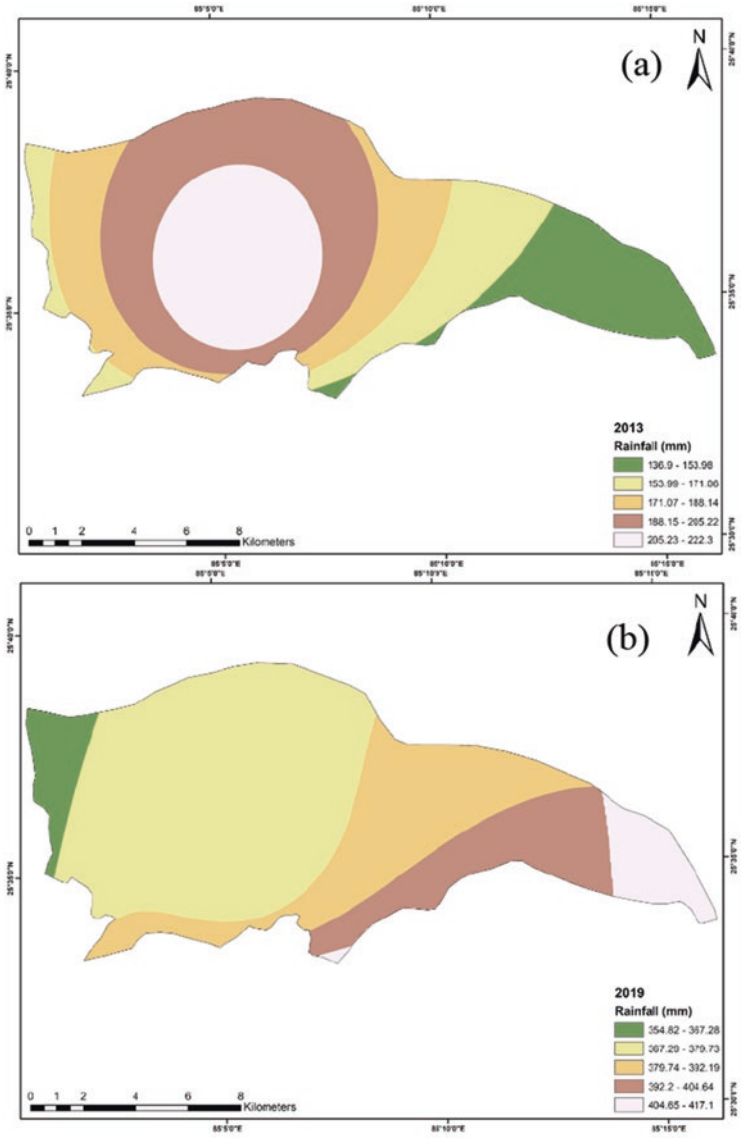

Fig. 4.7 Spatial distribution map of cumulative rainfall for 5 days (**a**) 2013 and (**b**) 2019

2. Computing the antecedent moisture condition for 2013 and 2019, it was found that the rainfall preceding the events of September 3, 2013, met the AMC-II condition, while those of September 29, 2019, met the AMC-III condition. This highlights the built-up of soil moisture in the year 2019 and how more runoff should be expected in 2019. The built-up of soil moisture in September of 2019 has been reported by Bhatt et al. (2021).

Even though the 1-day rainfall was higher in 2013, the rainfall leading to this particular day was not enough to saturate the soil moisture. However, the events of September 29, 2019, showed that rainfall events leading to the extreme 1-day rainfall were significant as the rainfall on the previous days was also high. The previous days of heavy rainfall meant that the soil moisture was saturated, leading to almost all rain appearing as runoff, consequently triggering flooding.

4.2 LULC of 2013 and 2019

Land use land cover changes (LULC) have also been assessed to bring forth the anthropogenic differences between 2013 and 2019. The LULC maps were prepared using supervised classification in ArcGIS by making use of Landsat 8 images (Fig. 4.8). The area was broadly classified into the following macro classes: water, urban/built-up, vegetation, and bare soil. Comparing the land features for the 2 years, it can be seen that there was a decrease in the water bodies by around 28%. These changes were prominent due to the exposure of the river bed downstream of the river as the river meanders. These changes were due to an increase in the river bed which is more prominent downstream of the Ganga river in 2019. Also, the drying up of urban water bodies due to unplanned urbanization is another reason for the decrease in the water bodies. Regarding urbanization, the urban area has increased by almost 18.30%, from 81.67 square kilometers in 2013 to 97 square kilometers in 2019. This increase came at the cost of vegetation, which has decreased by almost 16.50% in the same duration. An increase in urban areas led to more imperviousness of the land surface, resulting in more flood volume being generated for the same rainfall. The extent of bare soil grew by about 6% from 2013 to 2019. Vegetation helps absorb moisture and reduce runoff by interception losses and storing water in the root zone of plants, improving infiltration. Decreased vegetation consequently resulted in less infiltration and less losses, ultimately increasing runoff volume.

4.3 Runoff for 2013 and 2019

The runoff maps were prepared using the NRCS-CN model in the GIS platform. As discussed above, based on the antecedent moisture condition (AMC), the curve number grid was first formed for the study area shown in Fig. 4.9. The denser dark green areas for 2019 highlighted higher values of CN, which correspond to AMC-III conditions as compared to 2013. The corresponding initial abstraction (Ia) and maximum potential retention (S) maps based on the equation (Eqs. 4.1 and 4.2) are shown in Figs. 4.10 and 4.11, respectively. These maps revealed how both initial abstraction and maximum potential retention parameters were low for 2019. The lower values of S in 2019 indicated that the capacity of soil to retain moisture was lower than in 2013. Finally, the runoff maps were derived using Eq. 4.3 for both

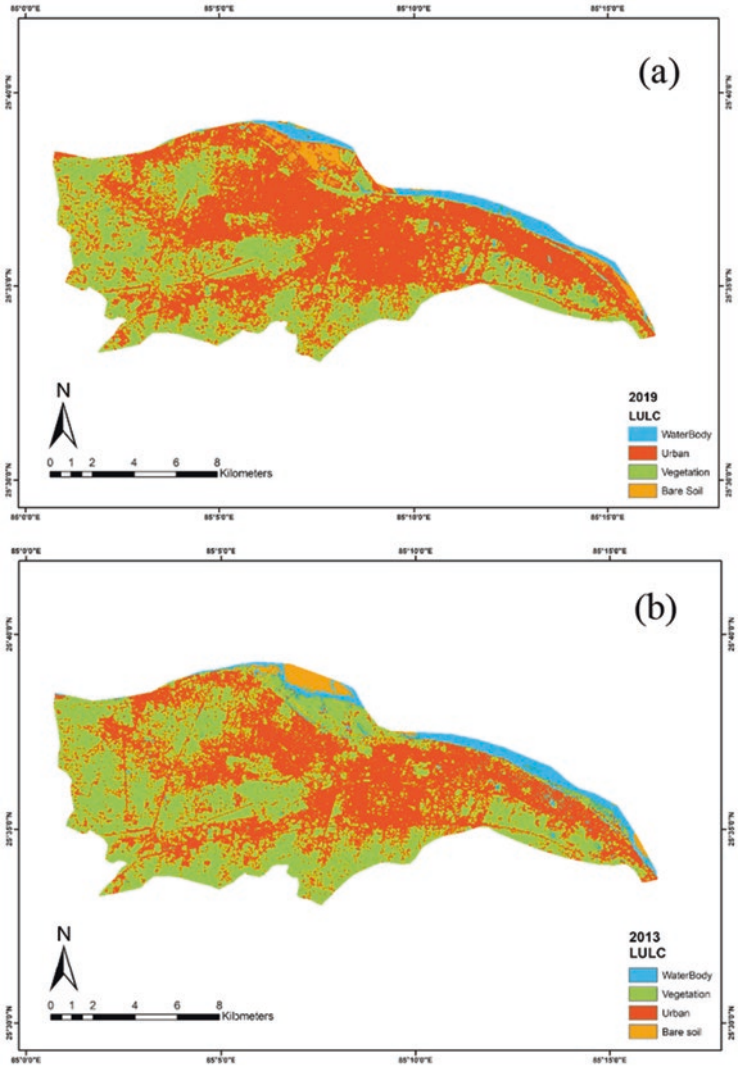

Fig. 4.8 LULC map distribution for Patna city (**a**) 2019 and (**b**) 2013

years, as shown in Fig. 4.12. These maps indicate the runoff depth (in millimeters) across the entire city. The runoff map for 2019 shows much higher and more dense runoff across the entire city, even for areas under vegetation. This is a result of extreme rainfall and the built-up of soil moisture taking place over more than 1 day. High-intensity rainfall across the entire city is more likely to overwhelm the drainage capacity of the city as it will produce high runoff across the entire city. Any choke point or blockage in the drainage system can build runoff volume and inundate the city within minutes. The runoff map for 2013 showed high runoff values, but the distribution of intense runoff was concentrated in only a small region in the

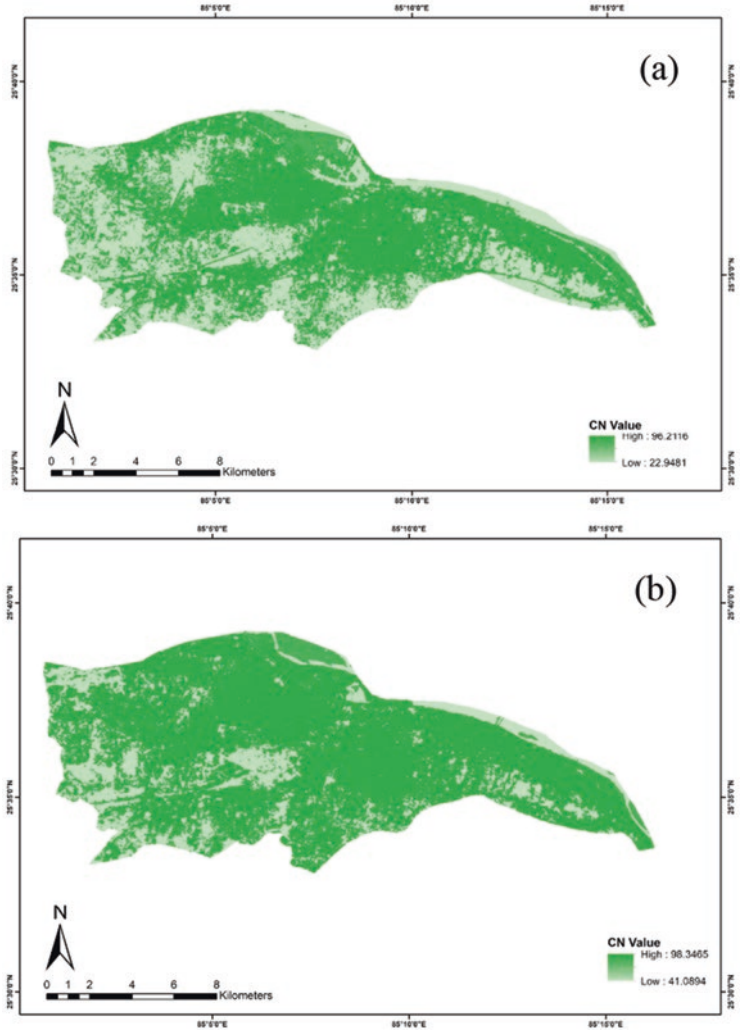

Fig. 4.9 Distribution map of curve number across Patna after accounting for AMC (**a**) 2013 and (**b**) 2019

city, unlike in 2019. In such a case, the drainage system in areas subjected to low runoff could work at capacity to drain out the water coming from high runoff areas.

5 Discussion

The present study compared the rainfall events along with the LULC of 2013 and 2019. The year 2013 was taken specifically as it had the largest 1-day rainfall. Even though there were larger rainfall events in the distant past, year 2013 was chosen as

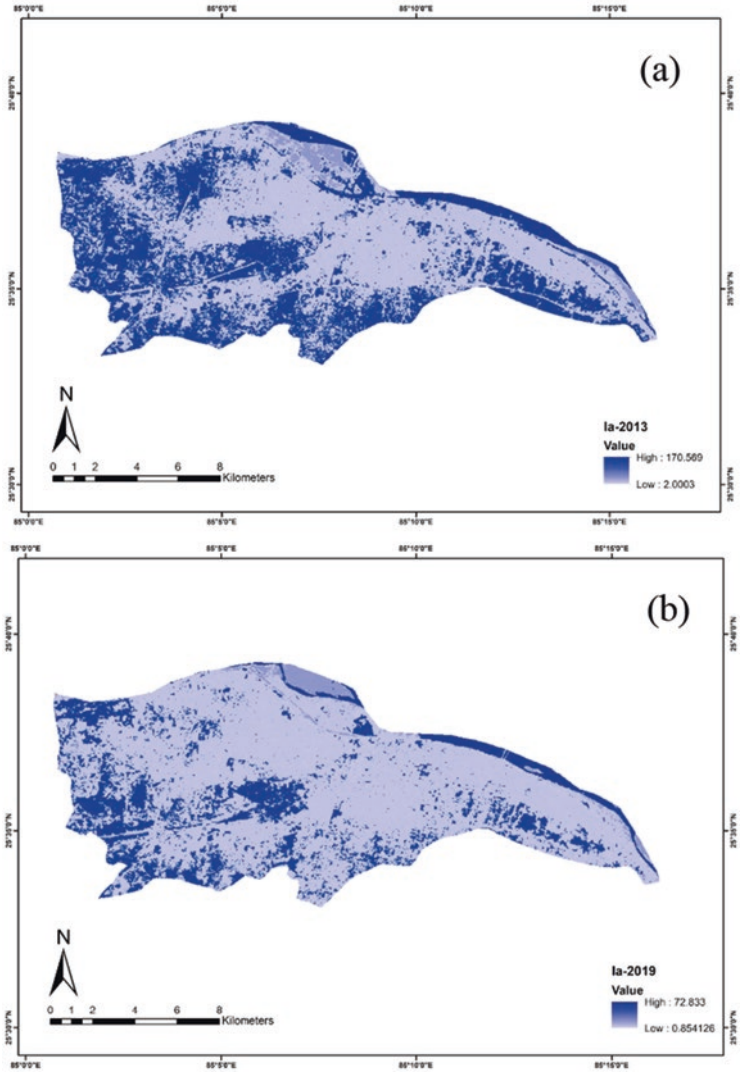

Fig. 4.10 Initial abstraction map of Patna city (**a**) 2013 and (**b**) 2019

it matched the land-use characteristics, which impacted the hydrological response of urban catchments; such dense urban areas were not there for earlier high rainfall events dating back to 1990s. Figure 4.13 shows the relationship between rainfall runoff for the years 2013 and 2019. For September 3, 2013, the runoff volumes mainly ranged between 40 and 140 mm, while for 2019 the runoff volumes ranged between 100 and 150 mm. A nearly similar amount of 1-day rainfall producing different runoff was a result of different AMC present during the two rainfall incidents. These AMC could be understood through the 5-day rainfall shown in Fig. 4.5,

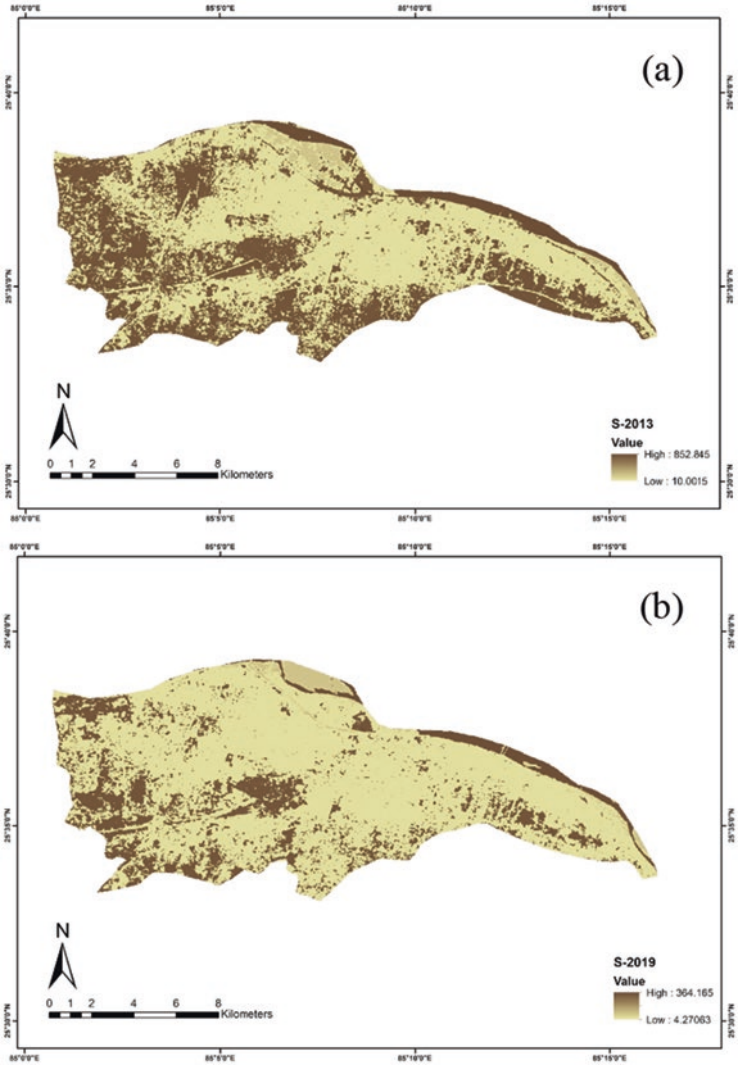

Fig. 4.11 Map of maximum potential retention of Patna (**a**) 2013 and (**b**) 2019

wherein in 2019 the rainfall was much larger and uniformly distributed across the entire Patna city.

Based on the comparison between the rainfall, runoff, and LULC results, the following observation arrived:

1. In the 6 years between 2013 and 2019, some increase in urbanization and a decrease in vegetation were seen. As the city grew, this trend continued with the dense urban areas becoming denser as every square meter of space was utilized. The dense urban areas grew in 2019 and showed high runoff values. For 2013

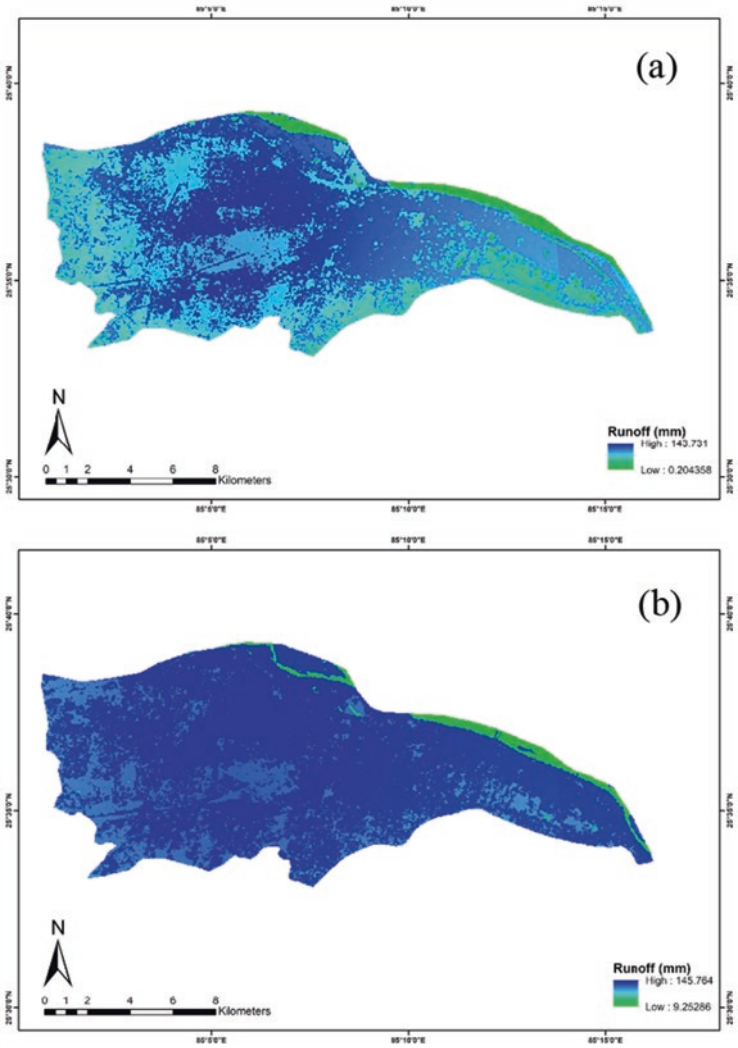

Fig. 4.12 Map of runoff depth by rainfall in Patna (**a**) 2013 and (**b**) 2019

also, the urban areas showed high runoff values. Although it could not be deduced that an increase in urban areas led to floods in 2019, in general, it can be said that the buildup area leads to more runoff and vegetation helped control runoff to some extent. However, the events of 2019 also highlighted that once saturation was reached for soil moisture (due to prolonged heavy rainfall), even vegetation could not prevent high runoff.

2. Although the 1-day peak rainfall in September of 2013 and 2019 was almost the same, comparing the cumulative 5-day rainfall at the different stations revealed the stark difference between these two events. The 5-day cumulative rainfall in

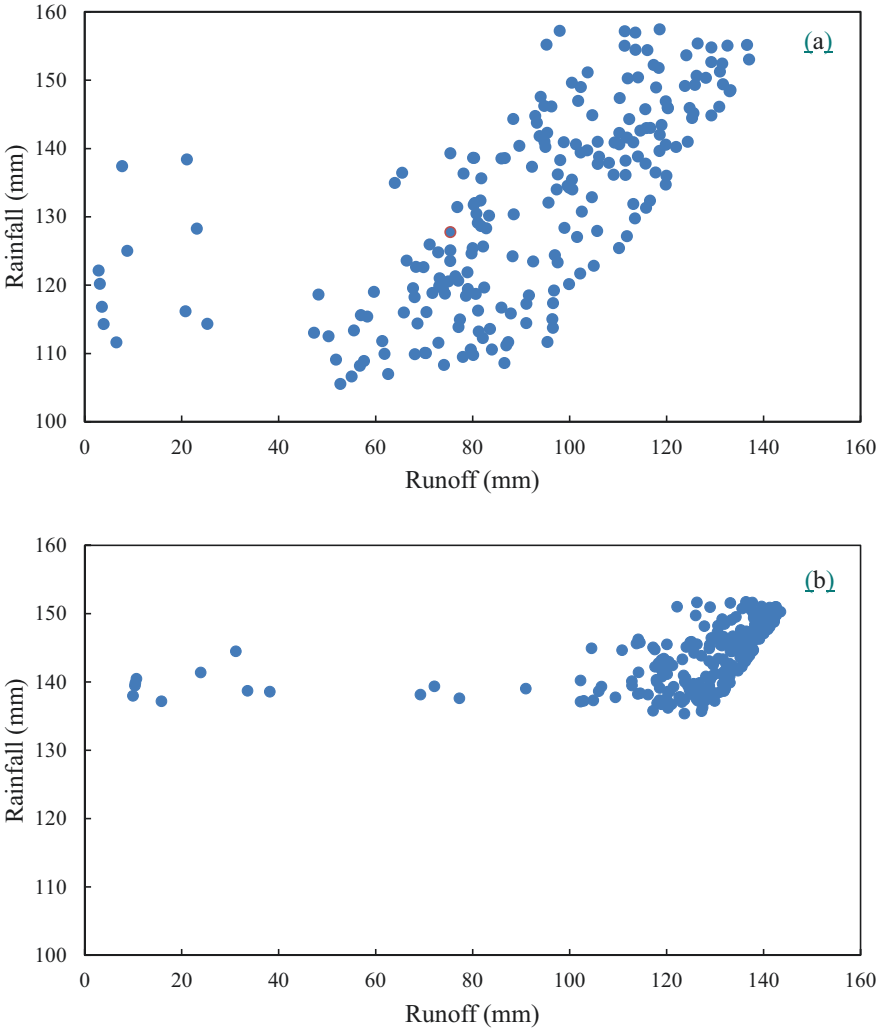

Fig. 4.13 Scatter plots of rainfall-runoff relationships for the events (**a**) 2013 and (**b**) 2019

2019 was significantly greater than that in 2013, owing to continuous heavy rainfall on previous days. Also, the distribution of rainfall was nonuniform in 2013 with other stations recording less rainfall as compared to Patna Aero. In 2019, all the stations recorded the same magnitude of rainfall. It can be concluded the events of 2019 were much greater than those in 2013 due to the strong southwest monsoon, which played an important role in the urban flooding.

3. The immediate cause of the floods of 2019 can be said to be climate change, given the extreme rainfall events. However, the later part of the deluge, when streets remained flooded even after a week of heavy rainfall, was definitely due to anthropogenic reasons where further investigation is required on the drainage network.

6 Conclusions

The research results shown in the study discuss the rainfall to runoff transformation based on the extreme rainfall events of 2013 and 2019 by accounting for the soil properties and LULC. The study helps identify extreme rainfall as the immediate cause of the urban flood of 2019, while poor drainage systems can be held responsible for subsequent ponding in low-lying areas. These findings, however, do not account for the drainage network of the city, which play a significant role in draining the floodwaters from the streets of the city. A good and well-maintained drainage system should, in theory, be capable of dealing with rainfall of high intensities. A drainage system forms the backbone of the city in removing any kind of wastewater. Detailed analysis of the drainage system of Patna is imperative to understand the present capabilities of the system and the load it is subjected. However, with climate change bringing intense rainfall, an assessment of the drainage system to combat such events needs to be done. A worst-case scenario of these drainage systems in dealing with both extreme climate and urban development can help understand the impact of both climate change and urbanization. This will also help plan future drainage facilities. The existing drainage system also needs to be maintained and cleaned annually to ensure that the drainage network works as designed.

Talking of measures to prevent such urban floods in the future, the first and foremost thing to be done is to upgrade the existing drainage network and ensure it is capable of dealing with high-intensity rainfall incidents. This design rainfall should account for variabilities arising out of climate change and urban population growth. A government body should work and maintain the drainage network, which will ensure the accountability aspect of such problems. There is a need to look into the urban planning aspect of the city. Urban local bodies and town planners need to ensure that urbanization has the least impact on the hydrological aspects of the catchment while ensuring everyone reaps the benefits of development. Construction on flood plains should be checked. Solid waste disposal in existing water bodies needs to be stopped so that these water bodies are not choked. Rejuvenation of city lakes should also be prioritized as they act as sinks for flood water. There is also a need for more automatic weather stations which can record detailed spatial and temporal variations in hydrometeorological conditions. Rainwater harvesting and managed groundwater recharge can also lessen the runoff volumes generated in urban areas. The problem of urban floods is a modern problem, and certain innovative modern methods can also help mitigate the risk of urban floods. Since the construction of a drainage system is a money and time taking process, as an alternative, the urban local bodies can also look into ecosystem-based disaster risk reduction (Eco-DRR). The Eco-DRR is the sustainable management, conservation, and restoration of ecosystems to provide services that reduce disaster risk by mitigating hazards and increasing livelihood resilience. The use of green spaces in the city like central parks, rooftop gardens, and innovative concepts like permeable pavements need to be implemented at the city level to complement the drainage system by reducing the water load. It is imperative to mitigate the growing risk of urban floods

through these structural and nonstructural measures so that the people in the city are less vulnerable. This will ensure that urban flood risk does not hamper the growth of the city, on which the livelihood of millions depends. The growth of a city comes with many challenges, and the challenge of providing people a more resilient city is of utmost importance.

Declarations No conflict of interest to declare.

References

Berggren, K., Packman, J., Ashley, R., & Viklander, M. (2014). Climate changed rainfalls for urban drainage capacity assessment. *Urban Water Journal, 11*(7), 543–556. https://doi.org/10.1080/1573062X.2013.851709

Bhatt, C. M., Gupta, A., Roy, A., Dalal, P., & Chauhan, P. (2021). Geospatial analysis of September, 2019 floods in the lower gangetic plains of Bihar using multi-temporal satellites and river gauge data. *Geomatics, Natural Hazards and Risk, 12*(1), 84–102. https://doi.org/10.1080/19475705.2020.1861113

Djordjević, S., Butler, D., Gourbesville, P., Mark, O., & Pasche, E. (2011). New policies to deal with climate change and other drivers impacting on resilience to flooding in urban areas: The CORFU approach. *Environmental Science and Policy, 14*(7), 864–873. https://doi.org/10.1016/j.envsci.2011.05.008

Gnanaseelan, C., Mujumdar, M., Kulkarni, A., Chakraborty, S., & Sciences, E. (2020). *Assessment of climate change over the Indian Region*. https://doi.org/10.1007/978-981-15-4327-2

Guhathakurta, P., Khedikar, S., Menon, P., Prasad, A. K., Sable, S. T., & Advani, S. C. (2020). Climate research and services observed rainfall variability and changes over Assam state. *IMD Annual Report, 16*, 28. ESSO/IMD/HS/Rainfall%0AVariability/16(2020)/40%0AObserved.

Gupta, K. (2007). Urban flood resilience planning and management and lessons for the future: A case study of Mumbai, India. *Urban Water Journal, 4*(3), 183–194. https://doi.org/10.1080/15730620701464141

Gupta, K. (2020). Challenges in developing urban flood resilience in India. *Philosophical Transactions of the Royal Society A: Mathematical, Physical and Engineering Sciences, 378*(2168). https://doi.org/10.1098/rsta.2019.0211

Hammond, M. J., Chen, A. S., Djordjević, S., Butler, D., & Mark, O. (2015). Urban flood impact assessment: A state-of-the-art review. *Urban Water Journal, 12*(1), 14–29. https://doi.org/10.1080/1573062X.2013.857421

Hawkins, R. H., Hjelmfelt, A. T., & Zevenbergen, A. W. (1985). Runoff Probability, Storm Depth, and Curve Numbers. *Journal of Irrigation and Drainage Engineering, 111*(4), 330–340. https://doi.org/10.1061/(asce)0733-9437(1985)111:4(330)

Huang, M., Gallichand, J., Wang, Z., Goulet, M. 2006). A modification to the Soil Conservation Service curve number method for steep slopes in the Loess Plateau of China. *Hydrological Processes, 20*(3), 579–589. https://doi.org/10.1002/hyp.5925

Huong, H. T. L., & Pathirana, A. (2013). Urbanization and climate change impacts on future urban flooding in Can Tho city, Vietnam. *Hydrology and Earth System Sciences, 17*(1), 379–394. https://doi.org/10.5194/hess-17-379-2013

Ilam Vazhuthi, H. N., & Kumar, A. (2020). Causes and impacts of urban floods in Indian cities: A review. *International Journal on Emerging Technologies, 11*(4), 140–147. www.researchtrend.net

Jacobson, C. R. (2011). Identification and quantification of the hydrological impacts of imperviousness in urban catchments: A review. *Journal of Environmental Management, 92*(6), 1438–1448. https://doi.org/10.1016/j.jenvman.2011.01.018

Khan, B., Rathore, V. S., & Krishna, A. P. (2021). Identification of Desakota region and urban growth analysis in Patna City, India using remote sensing data and GIS. *Journal of the Indian Society of Remote Sensing, 49*(4), 935–945. https://doi.org/10.1007/s12524-020-01248-8

Kug, J. S., & Ahn, M. S. (2013). Impact of urbanization on recent temperature and precipitation trends in the Korean peninsula. *Asia-Pacific Journal of Atmospheric Sciences, 49*(2), 151–159. https://doi.org/10.1007/s13143-013-0016-z

Mishra, V. N., & Rai, P. K. (2016). A remote sensing aided multi-layer perceptron-Markov chain analysis for land use and land cover change prediction in Patna district (Bihar), India. *Arabian Journal of Geosciences, 9*(4). https://doi.org/10.1007/s12517-015-2138-3

Mourato, S., Fernandez, P., & Moreira, M. (2012). Flood risk assessment in an urban area. In *Comprehensive flood risk management*, *April 2014*. https://doi.org/10.1201/b13715-97

Mukherjee, D. (2016). Effect of urbanization on flood – a review with recent flood in Chennai (India). *International Journal of Engineering Sciences & Research Technology, 5*(7), 451–455. http:%5Cnwww.ijesrt.com

Nie, L., Lindholm, O., Lindholm, G., & Syversen, E. (2009). Impacts of climate change on urban drainage systems – A case study in Fredrikstad, Norway. *Urban Water Journal, 6*(4), 323–332. https://doi.org/10.1080/15730620802600924

Qi, W., Ma, C., Xu, H., Chen, Z., Zhao, K., & Han, H. (2021). A review on applications of urban flood models in flood mitigation strategies. In *Natural hazards* (Vol. 108, Issue 1). Springer. https://doi.org/10.1007/s11069-021-04715-8.

Rafiq, F., Ahmed, S., Ahmad, S., & Khan, A. A. (2016). Urban floods in India. *International Journal of Scientific & Engineering Research, 7*(1), 721–734.

Ranger, N., Hallegatte, S., Bhattacharya, S., Bachu, M., Priya, S., Dhore, K., Rafique, F., Mathur, P., Naville, N., Henriet, F., Herweijer, C., Pohit, S., & Corfee-Morlot, J. (2011). An assessment of the potential impact of climate change on flood risk in Mumbai. *Climatic Change, 104*(1), 139–167. https://doi.org/10.1007/s10584-010-9979-2

Seenirajan, M., Natarajan, M., Thangaraj, R., & Bagyaraj, M. (2017). Study and analysis of Chennai flood 2015 using GIS and multicriteria technique. *Journal of Geographic Information System, 09*(02), 126–140. https://doi.org/10.4236/jgis.2017.92009

UDHD. (2016). *PATNA MASTER PLAN 2031 town and country planning organisation*. http://udhd.bihar.gov.in/PMP2031/data/pmp-2031-report.pdf

Chapter 5
Flood Susceptibility Zonation Using Dempster-Shafer Evidential Belief Function (EBF) Method in Chalakudy Taluk, Kerala, India

Shweta Bhardwaj and Ramesh Veerappan

Abstract This study focuses on flood susceptibility zonation (FSZ) of Chalakudy taluk, Thrissur, Kerala, using a statistical Dempster-Shafer evidential belief function (EBF) model with the aid of geoinformation techniques. This study considered 12 conditioning factors: elevation, slope, slope aspect, plan curvature, topographic wetness index, stream power index, lithology, soil type, land use, land cover, rainfall, and proximity to drainage. The flood inventory database of 159 flood locations was prepared through fieldwork and synthetic aperture radar (SAR) data, which was divided into training (70%) and test (30%) data. The relationship of each factor with inventory was established using the EBF model. The factor maps with assigned weights were integrated into geographical information systems (GIS) to map the flood susceptibility of the region. Dempster's rule of combinations and belief summation are the two integration methods adopted to integrate and prepare the FSZ maps. The prediction rate and success of the FSZ maps were quantitatively estimated using the area under curve method. The estimated area under curve (AUC) values of success and prediction rate curves for the FSZ map prepared using the Dempster rule of the combination were 0.7357 and 0.7052, respectively, whereas the estimated AUC values of success and predication rate curves for the FSZ map prepared using the belief summation method were 0.8584 and 0.8536, respectively. The AUC prediction rate and success rate of Dempster's rule of combination fall under the "fair" category, whereas the success rate and prediction of belief summation are under the "good" classification category.

Keywords Flood susceptibility zonation · Evidential belief function · Dempster-Shafer · GIS · Chalakudy

S. Bhardwaj · R. Veerappan (✉)
Centre for Geoinformatics, Jamsetji Tata School of Disaster Studies, Tata Institute of Social Sciences, Mumbai, India
e-mail: ramesh.veerappan@tiss.edu

P. Thambidurai, A. K. Dikshit (eds.), *Impacts of Urbanization on Hydrological Systems in India*, https://doi.org/10.1007/978-3-031-21618-3_5

1 Introduction

Worldwide, climate change is causing an increase in the frequency of flood occurrences triggered due to changing rainfall patterns (Rahmati & Pourghasemi, 2017). The major causes of flooding in a particular region include natural and anthropogenic activities like increase in population; unplanned urbanization; change in river channel morphology; deforestation of catchment areas; encroachment of natural habitation, particularly of floodplains; and intense rainfall, particularly in monsoon season which leads to increase in socioeconomic impacts (Tehrany et al., 2019; Ramesh & Iqbal, 2020). Flood, like any disaster, is inevitable; however, their impacts can be minimized by effective flood management. Flood zonation maps play a crucial part in demonstrating flood-prone areas and their management opportunities in the geographical context (APFM, 2013). The advancements in the fields of GIS and remote sensing have played an important role in facilitating the operations of flood risk assessment through flood mapping and brought out exceptional results, which are highly useful in effective flood management. Use of these technologies for flood management helped in visualization of floods and provided us with the potential for further analysis of these flood maps to estimate the probable damages. Flood maps can be used as an important strategic tool in land use planning of flood-prone areas. As stated by Verstappen (1995), the purpose of utilizing remote sensing and GIS techniques includes "investigating the susceptibility of the land and the vulnerabilities of the society, constructing hazard zoning maps and potential damage maps, and monitoring potential hazards to deal with emergency situations after a disaster".

Researchers have used different causative factors while evaluating flood susceptibility for different study areas. However, there are some of these factors that remain common across most of flood studies. Topographic factors such as slope gradient, elevation, and curvature are some of such factors which are commonly used for flood hazard mapping (Pradhan, 2009; Essel, 2017; Rahmati et al., 2016). Hydrological factors such as rainfall and runoff are also some of the most frequently used conditioning factors in flood studies (Kia et al., 2012; Althuwanee et al., 2012). Some of the studies by (Tehrany et al., 2014; Rahmati et al., 2016) have used other factors such as TWI, SPI, and NDVI to evaluate flood hazards. As stated in Essel (2017), "Generally, it can be said that creating of flood hazard maps can be considered as a subjective process that is strongly influenced by the availability of input data". Based on it, one can conclude that the use of input data for flood studies is not constant. Therefore, understanding and selecting of flood conditioning factors are very crucial for any such study. Since, different thematic data layers corresponding to each of the selected conditioning factors would be used as input of the study. These causative factors must be carefully selected through detailed literature reviews and field studies.

Different studies use a number of different methods with the aid of GIS and remote sensing techniques in order to prepare the flood susceptibility zonation (FSZ) maps. Some of the models employed across different studies include

frequency ratio (Samanta et al., 2018), logistic regression model (Pradhan, 2009; Tehrany et al., 2014), weights-of-evidence (Khosravi et al., 2016), evidential belief function model (Tehrany & Kumar, 2018; Ramesh & Iqbal, 2020), artificial neural network model (Kia et al., 2012; Campolo et al., 1999), analytic hierarchy process (Siddayao et al., 2014; Danumah et al., 2016), fuzzy logic (Nandalal & Ratnayake, 2011), adoptive neuro-fuzzy inference system (Ahmadlou et al., 2019), Shannon's entropy model (Jothibasu & Anbazhagan, 2016; Haghizadeh et al., 2017), support vector machines (Choubin et al., 2019), and hydrological and stochastic rainfall methods (Diakakis, 2011; Merwade et al., 2018; Wu & Adler, 2012). The objective of the research is to prepare the FSZ map of Chalakudy taluk based on various flood influencing factors using GIS and remote sensing-based techniques through the statistical Dempster-Shafer evidential belief function model.

2 Study Area

Chalakudy taluk is one of the seven taluks in the Thrissur district in the State of Kerala, India. The study area is geographically located between the 10°10′2.1″ to 10°28′37.74″ N latitude and 76°8′24.36″ to 76°53′30.56″ E longitude, as shown in Fig. 5.1. The total geographical area covered by the Chalakudy taluk is 1293.05 Sq.km. The main river that flows in the study area is the Chalakudy River. Climatically, the study area experiences a humid tropical climate, with oppressive hot summers and plentiful monsoon rainfall. The average temperature during summers (March to May) is approximately 33 °C. Chalakudy taluk receives most of its rainfall during the southwest monsoon season (May end or early June). The second spell of rainfall in the region is witnessed during the northeast monsoon seasons (between October and November). The annual rainfall received by the Taluk is about 3000 mm. The Chalakudy taluk mainly comprises metamorphic rocks and plutonic rocks. Since this area was formed in 2013, there is no census data available for it. However, based on data available for different villages and Chalakudy municipality, which comprises the Taluk, the total population is 4,32,362. As stated by CWC (2018), the storm on 15–17 August 2018 resulted in heavy flooding in four sub-basins of Kerala, including Periyar, Chalakudy, Bharathappuzha, and Pamba. The rainfall from 15–17 August 2018 was almost comparable to the historic rainfall of 16–18 July 1924 in Kerala. Between 15 and 17 August 2018, rainfall depths in Periyar, Chalakudy, and Bharathappuzha sub-basins were 588 mm, 421 mm, and 373 mm, respectively, which are of the same order as that of rainfall during the 1924 floods. Wayanad (Kabini sub-basin), Idukki (Periyar sub-basin), Ernakulam (Periyar and Chalakudy) sub-basins, Alleppey, and Pathanamthitta (both in Pamba sub-basin) were among the worst affected districts due to the floods that resulted from continuous rainfall and overflowing of river basins. After the

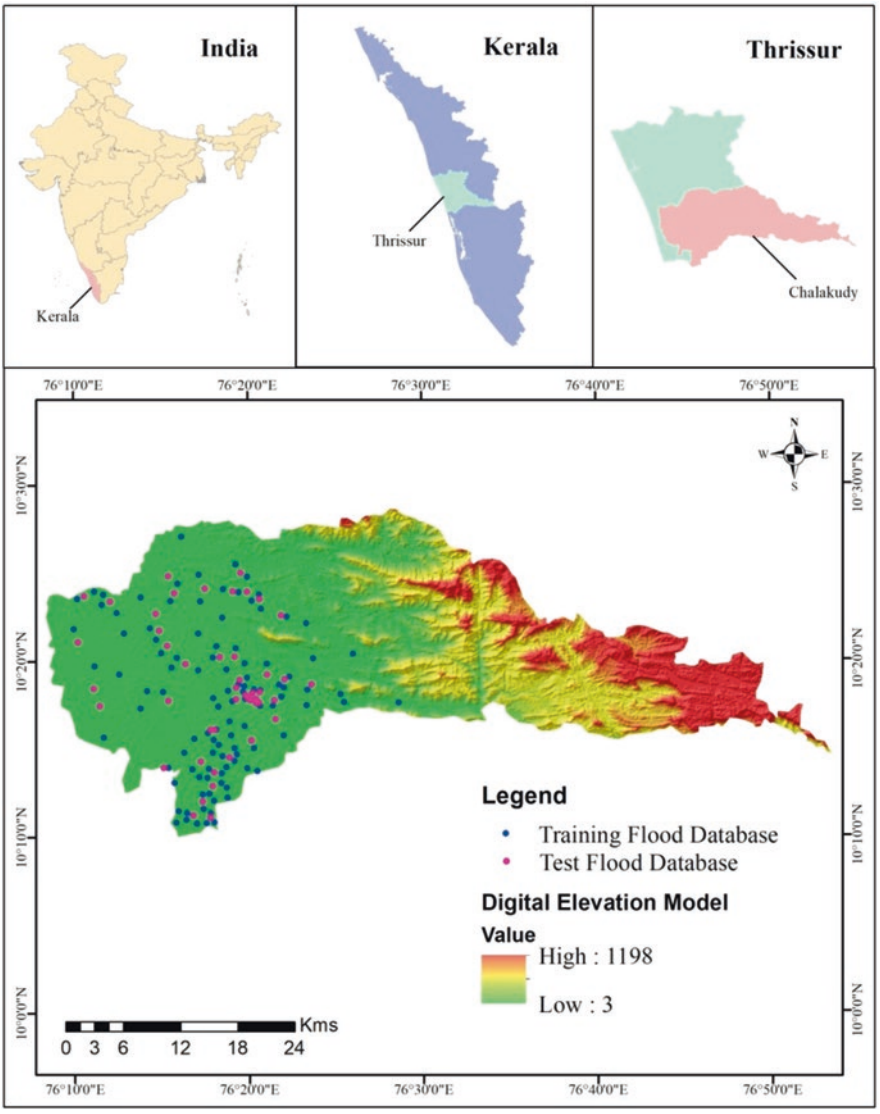

Fig. 5.1 Study area map with past flood locations overlaid on Digital Elevation Model

heavy rainfall and rise in water levels of reservoirs beyond their full reservoir level, water was released from the Parambikulam dam and Tamil Nadu's Sholayar dam into the Poringalkuthu reservoir located downstream. Almost 35,000 cusecs and 30,000 cusecs of water were released from the Parambikulam and Sholayar dams, which flowed into the Poringalkuthu reservoir, resulting in overflowing the Chalakudy River causing severe flooding in areas of Chalakudy Taluk (Fig. 5.2).

Fig. 5.2 Field photographs show flood levels in the study area

3 Methodology

The FSZ using statistical models usually involves creating a database of independent as well as the dependent variable as thematic layers. In this study, different independent layers, i.e. flood conditioning factors, were prepared using satellite imagery (high resolution), Digital Elevation Model (DEM), published lithology, and soil maps. The dependent variable, which is the flood inventory details database, was generated through fieldwork as well as through processing Sentinel 1 SAR satellite data of during flood. The Dempster-Shafer's evidential belief function (EBF) statistical model was used to set up relationships between flood conditioning

factors with flood events, in which the belief, disbelief, uncertainty, and plausibility were calculated. The factor maps with belief, disbelief, and uncertainty were integrated using Dempster's rule of combination as well as belief summation to prepare the final FSZ map of the study area. The FSZ map was classified into different susceptibility zones – very low, low, moderate, high, and very high – based on the susceptibility of a particular area towards flood occurrence. The prediction accuracy and success of the resultant FSZ map through two different integration procedures were evaluated using area under curve (AUC) method. The success rate curve was obtained by using a training dataset (70% of total flood inventory points). The prediction rate curve was obtained by using a testing dataset (30% of total flood inventory points). The detailed methodology adopted to carry out this study is represented in Fig. 5.3.

4 Geospatial Database Generation

FSZ mapping requires the mapping of different factors that can directly or indirectly affect flood occurrence. Different thematic data layers corresponding to each of these conditioning factors were prepared for the study region, which was used as an input for the study. Various remote sensing and GIS tools and techniques were adopted to acquire datasets and generate a geospatial database for various factors (Table 5.1). All the thematic layers were prepared in a GIS environment using QGIS, ArcMap 10, SAGA GIS, and ERDAS Imagine 2011 software and projected with Universal Transverse Mercator (UTM-Zone 43 N) system and WGS 84 Datum. All the thematic layers were rasterized with 10 x 10 m pixel size. The study area covers a total of 12,930,529 pixels.

4.1 Flood Inventory Mapping

Flood inventory is a database of past flood events in an area considered to be the most important factor while predicting the future occurrence of flood events in a given region. The inventory map represents the spatial distribution of past flood locations in the area, and it is also used to validate the FSZ map. The flood inventory database was prepared based on an extensive field survey and discussion with local people and administrators. During the fieldwork, spatial locations of 50 flood locations that were severely affected during the recent flood event were collected using GPS. These points were validated, and 109 more flood points were located using Sentinel 1A SAR data. Thus, a detailed inventory of 159 flood locations was mapped in the study region.

The final flood inventory was divided into two groups of 70% and 30% of total flood points to carry out training and testing of the model. The study indicated that the flooding in the study area was mainly caused by torrential rainfall, which resulted in the Chalakudy River overflow.

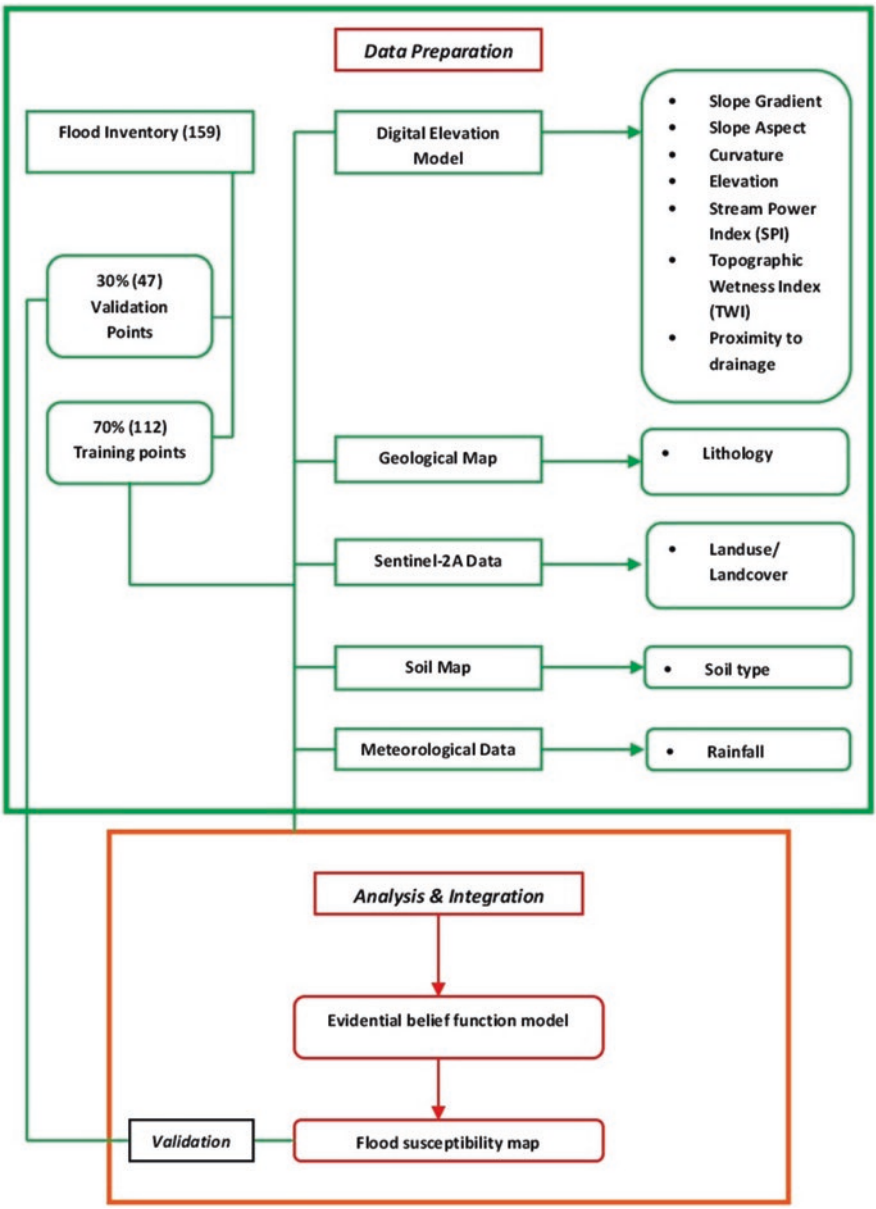

Fig. 5.3 Methodology adopted for FSZ mapping

Table 5.1 Various datasets used in this study with their specifications

Satellite/sensor/date of acquisition	Spectral resolution	Spatial resolution
Sentinel 2A satellite imagery 7 and 9 January 2019	B2 (blue) – 496.6 nm	10 m
	B3 (green) – 560.0 nm	
	B4 (red) – 664.5 nm	
	B8 (NIR) – 835.1 nm	
Advanced Spaceborne Thermal Emission and Reflection Radiometer (ASTER), Digital Elevation Model (DEM), Terra (EOS AM-1)		30 m
Topographic Rainfall Measuring Mission (TRMM) – Monthly Rainfall		0.25° × 0.25°
Sentinel 1A Synthetic Aperture Radar (SAR) Data	C-band	20 m × 22 m

4.2 Flood Conditioning Factors

4.2.1 Elevation

The elevation is considered one of the most influential flood conditioning factors, which directly influence the amount and velocity of runoff in an area. Flat regions are naturally more prone to flooding since water flows from high elevated areas towards low elevated or flat areas (Mojaddadi et al., 2017). The elevation map was directly extracted from DEM. The elevation map was further reclassified into ten classes using the quantile classification method. The elevation map for the study area is shown in Fig. 5.4. The lowest elevation in the study area was found to be 3 m, whereas the highest elevation in the area is 1198 m.

4.2.2 Slope

The slope is the angle between the horizontal datum and the ground. Slope plays an important role in the rainfall-runoff process. It influences runoff generation as well as runoff speed in an area. As stated by Mu et al. (2015), soil infiltration decreases with the increase in slope gradient, which in turn increases the runoff amount. Therefore, the slope is considered a crucial factor in hydrological analyses and is taken as one of the flood conditioning factors in this study. A slope map was prepared from DEM. The slope map was reclassified into ten classes using the quantile

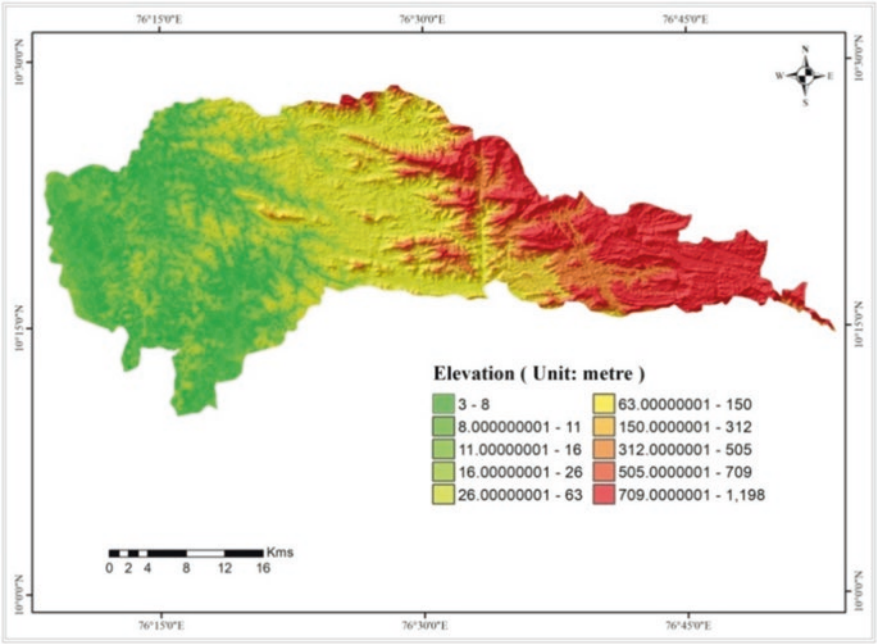

Fig. 5.4 Flood influencing factor – elevation

classification method, as shown in Fig. 5.5. The minimum and maximum values of slope gradient were found to be 0° and 68.53°, respectively.

4.2.3 Slope Aspect

The slope aspect is the horizontal direction towards which a slope face. The slope aspect is an important factor for analysing the geomorphologic stability of the soil as it controls some significant climatic parameters such as radiation received, wind, intensity of precipitation, soil moisture, and vegetation cover (Conforti et al., 2011). Slope aspect is expressed in degrees and ranges from 0° to 360°. The −1 value indicates a flat class. The slope aspect map was derived from DEM and was reclassified into 9 classes: flat (−1), north (337.5–22.5°), northeast (22.5–67.5°), east (67.5–112.5°), southeast (112.5–157.5°), south (157.5–202.5°), southwest (202.5–247.5°), west (247.5–292.5°), and northwest (292.5–337.5°) (Fig. 5.6).

4.2.4 Plan Curvature

Curvature is defined as the rate of change of slope. The curvature function output can be used in describing physical drainage basin characteristics such as erosion and runoff processes. There are two types of curvature, viz. profile and plan curvature,

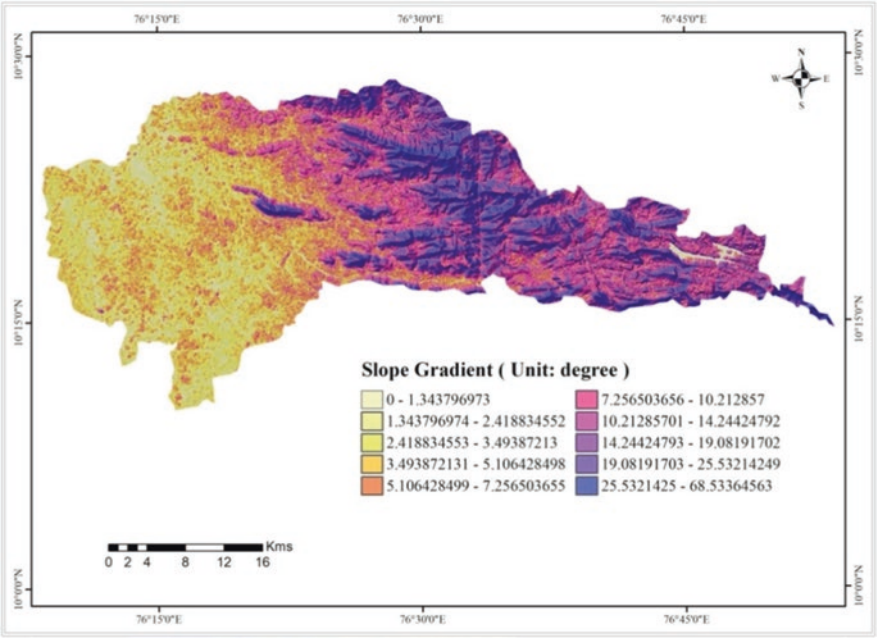

Fig. 5.5 Flood influencing factor – slope

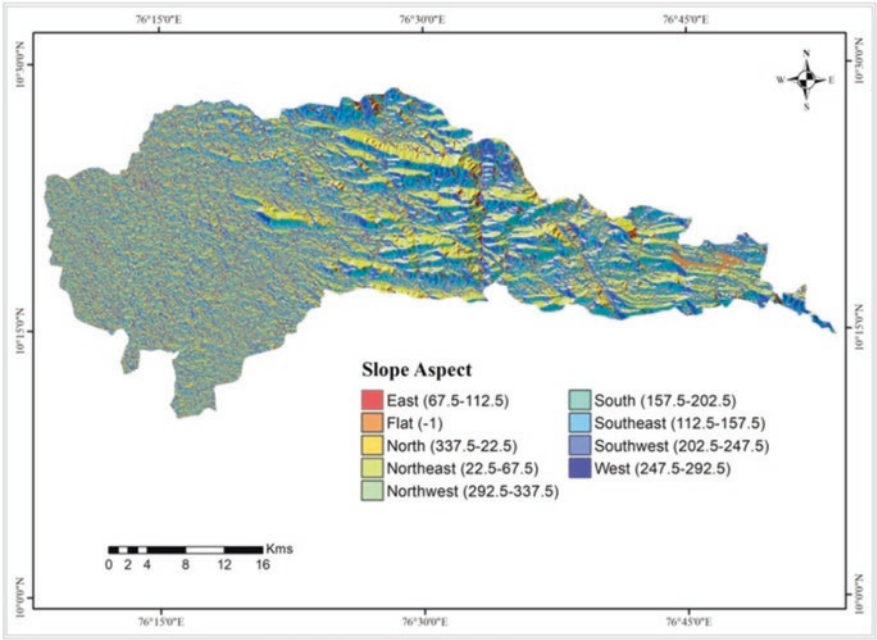

Fig. 5.6 Flood influencing factor – slope aspect

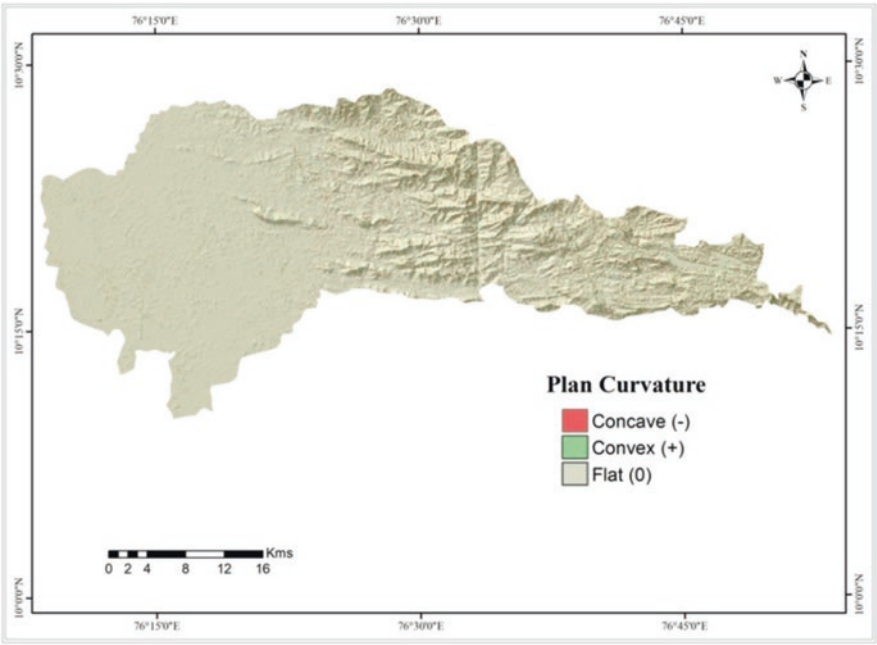

Fig. 5.7 Flood influencing factor – plan curvature

both of which can be convex, concave, or flat. According to Krebs et al. (2014), plan curvature represents curvature in a horizontal plane, whereas profile curvature represents curvature in a vertical plane in the direction of the steepest slope. In the present study, plan curvature has been used. The plan curvature influences the slope erosion processes by the converging or diverging water during a downslope flow (Conforti et al., 2011). The negative value represents concave curvature, and the positive value represents the convex curvature, whereas the zero values are classified as "flat". The curvature map was prepared from DEM, which is reclassified into three classes: flat, concave, and convex, as shown in Fig. 5.7.

4.2.5 Topographic Wetness Index (TWI)

The TWI quantifies the effect of topography on hydrological processes based on the assumption that topography control flow movement in sloped terrain and thus the spatial distribution of soil moisture or soil wetness condition (Schmidt & Persson, 2003; Sorensen et al., 2006). The TWI determines the effect of topography on a generation of runoff and the accumulation of flow in an area. It is defined as a function of slope and the specific catchment area and can be calculated using Eq. 5.1 (Gokceoglu et al., 2005; Mojaddadi et al., 2017). Higher values of the TWI are for converging, flat areas, whereas low values are usually for diverging, steep terrains.

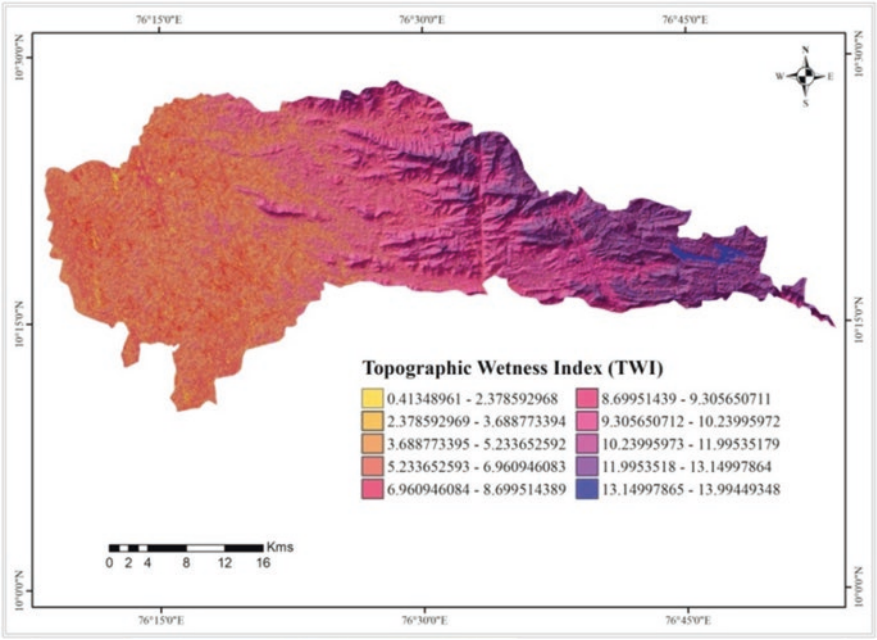

Fig. 5.8 Flood influencing factor – TWI

The TWI map was prepared from DEM. The map is reclassified into ten classes using the quantile method, as shown in Fig. 5.8. For the study region, TWI values range between 0.413 and 13.149. The highest values of TWI were mostly found across the flat and gentle slope terrains:

$$\mathrm{TWI} = \ln\left(\frac{\mathrm{As}}{\tan\beta}\right) \tag{5.1}$$

where As is the specific catchment area (m^2m^{-1}) and β is the slope gradient (°).

4.2.6 Stream Power Index (SPI)

The SPI indicates the erosive power of water flow, which assumes that discharge is directly proportional to a specific catchment area. The areas with lower values of SPI are more susceptible to flood occurrence (Mojaddadi et al., 2017). As stated in Jacoby et al. (2011) and Conforti et al. (2011), SPI can use to locate the erosion potential of an area since slope/surface erosion is significantly influenced by erosive power of running water. The SPI can be derived from the slope and catchment area using Eq. 5.2 (Althuwaynee et al., 2012). The SPI map was derived from DEM, and it was reclassified into ten classes using the quantile method (Fig. 5.9). The highest and the lowest values of SPI for the study area were found to be −2,38,254.66 and

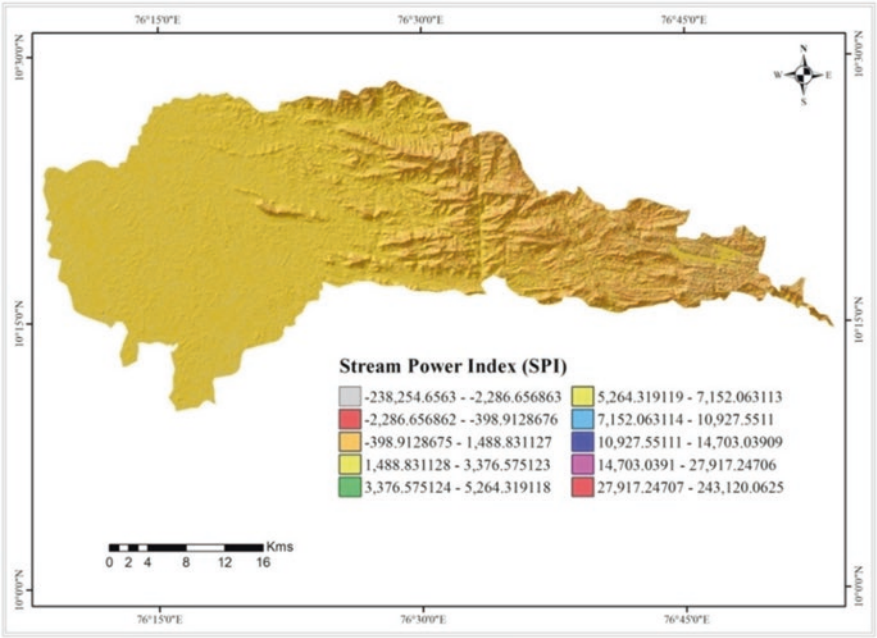

Fig. 5.9 Flood influencing factor – SPI

2,43,120.06, respectively. In the study area, higher SPI values are mostly located across hilly terrains, whereas the lower values are found across flat areas:

$$\mathrm{SPI} = \mathrm{As} \times \tan\beta \tag{5.2}$$

where As is the specific catchment area (m^2m^{-1}) and β is the slope gradient (°).

4.2.7 Land Use Land Cover (LULC)

Land use is surface cover (vegetation type, built-up type, etc.) of the earth at a specific location (Sohl & Sleeter, 2012). As stated by Rizeei et al. (2016), a thorough understanding of LULC is extremely important for assessing natural hazards. Different land use types have different levels of susceptibility towards floods. Because of the negative correlation that exists between flood events and vegetation density, vegetated areas are less susceptible to flooding (Mojaddadi et al., 2017), whereas built-up/non-vegetated areas consist of impermeable spaces and barren lands, which increases surface runoff and peak discharge, making them more prone to flooding (Abdulkareem and Elkadi, 2018). Hence, LULC is taken up as a parameter for evaluating flood susceptibility for the study. A high-resolution satellite data, Sentinel 2A with 10 m spatial resolution, was used to prepare the LULC map through the supervised maximum likelihood image classification technique. There

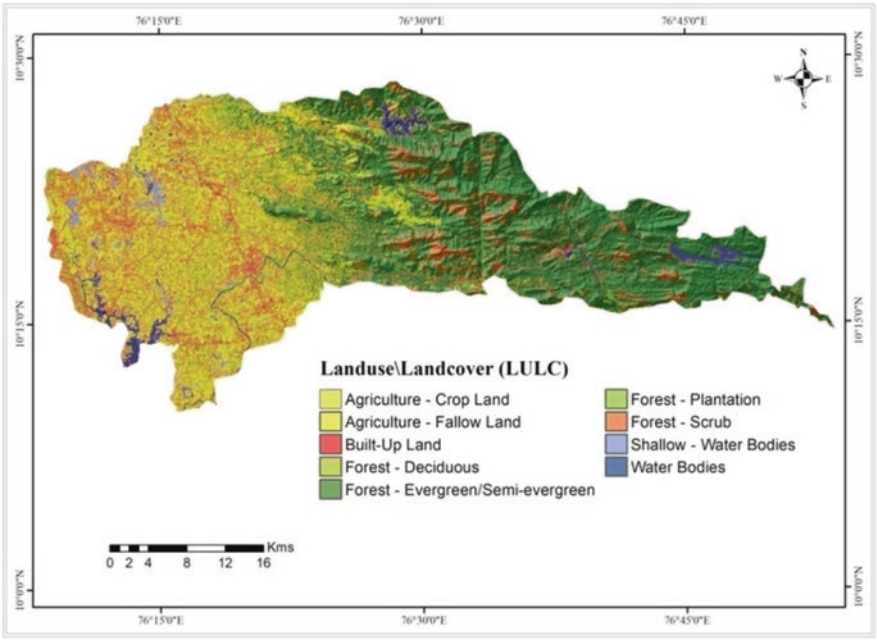

Fig. 5.10 Flood influencing factor – LULC

are nine LULC classes: agriculture-cropland, fallow land, built-up land, forest-deciduous, forest-evergreen/semievergreen, forest-plantation, forest-scrub, shallow water bodies, and water bodies, as shown in Fig. 5.10.

4.2.8 Lithology

Lithology fundamentally controls the geomorphologic features of a landscape (Dai et al., 2001). The lithology of an area significantly influences the behaviour of water on the ground (Tehrany et al., 2015). The lithology of the study region was extracted from the state lithology map downloaded from ENVIS Centre: Kerala website. The study area comprises four lithology units, viz. charnockite group, peninsular gneissic complex, migmatite complex, and quaternary complex, as shown in Fig. 5.11.

4.2.9 Soil Type

Soil properties, such as texture, permeability degree, structure, etc., play an important role in drainage processes (Mojaddadi et al., 2017). Therefore, soil type is considered a crucial flood conditioning factor. The soil types reveal properties that

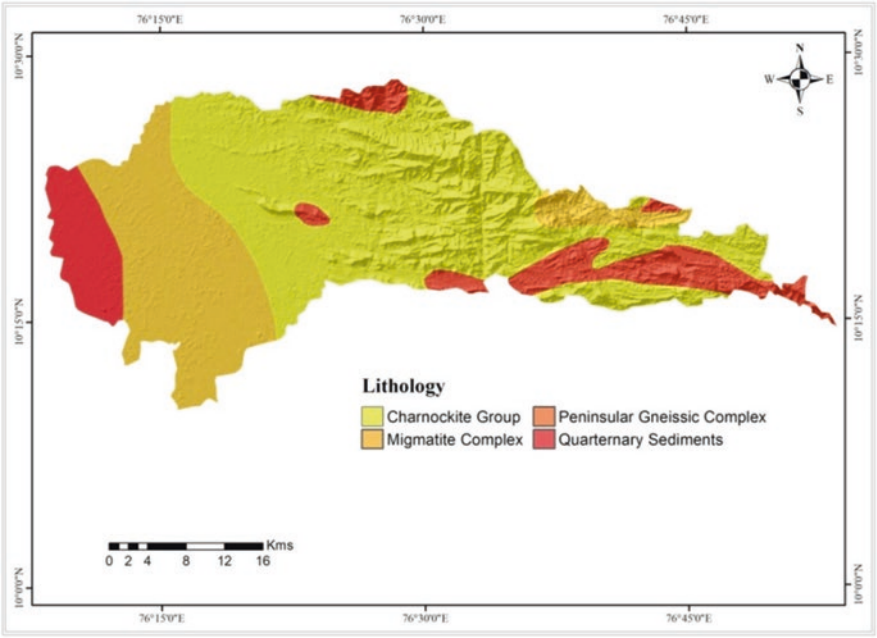

Fig. 5.11 Flood influencing factor – lithology

influence the rate of water seepage as well as the capacity of a particular soil type to retain water (Pradhan & Kim, 2016). The most sensitive variable in relation to surface runoff is infiltration rate, which is directly related to soil permeability. Soil water infiltration is an important hydrological dependent on external factors and soil properties and varies significantly across different soil types (Tejedor et al., 2013). In the case of soils with higher permeability, because of very less resistance to water, it can easily penetrate through the soil and are less prone to flooding, whereas soils with lower permeability are more prone to flooding due to higher resistance to the flow of water. The soil map for the study area was extracted from the soil map of Kerala state, which was downloaded from the ENVIS Centre: Kerala website. The study area consists of six different soil types: acid saline, alluvium, coastal soil, forest soil, hill soil, and laterite soil (Fig. 5.12).

4.2.10 Proximity to Drainage

Distance from drainage is another important flood conditioning factor. Regional spreading of floods has a direct relationship with distance from drainages. The water level in drainages usually increases during heavy rainfall, which causes an overflow of water in the areas closest to these drainages. The areas nearer to the drainages are more susceptible to flooding (Ramesh & Iqbal, 2020). This study prepared a

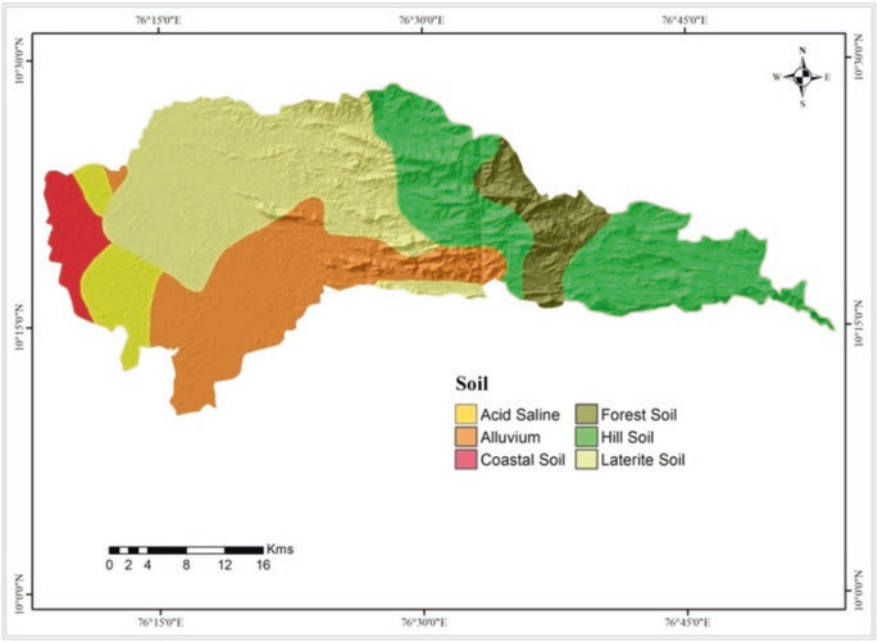

Fig. 5.12 Flood influencing factor – soil

drainage proximity map from drainages extracted from DEM using distance analyses. The drainage proximity map was reclassified into ten classes using the quantile method, as shown in Fig. 5.13.

4.2.11 Rainfall

Higher precipitation can lead to a higher runoff which can increase water accumulation, particularly in low-lying areas; hence, flood susceptibility increases with the increase in rainfall in a particular area (Essel, 2017). The severity of flood and level are directly dependent on the intensity of the rainfall. As stated by, Sangati and Borga (2009), rainfall is the primary input to most hydrological systems. Therefore, it is considered the most influential factor in flood generation, particularly in the case of river floods. The monthly rainfall data for the study area was extracted from TRMM data acquired from NASA DAAC, an online source for NASA's distributed archive. The average rainfall during the southwest monsoon season (May to October) for the last 5 years, i.e. 2014–2018, was created using Inverse Distance Weighted (IDW) interpolation method. The rainfall map of the study area is shown in Fig. 5.14. The highest and lowest amount of average rainfall received during the mentioned period in the study region was found to be 1043.29 mm and 1850.22 mm, respectively.

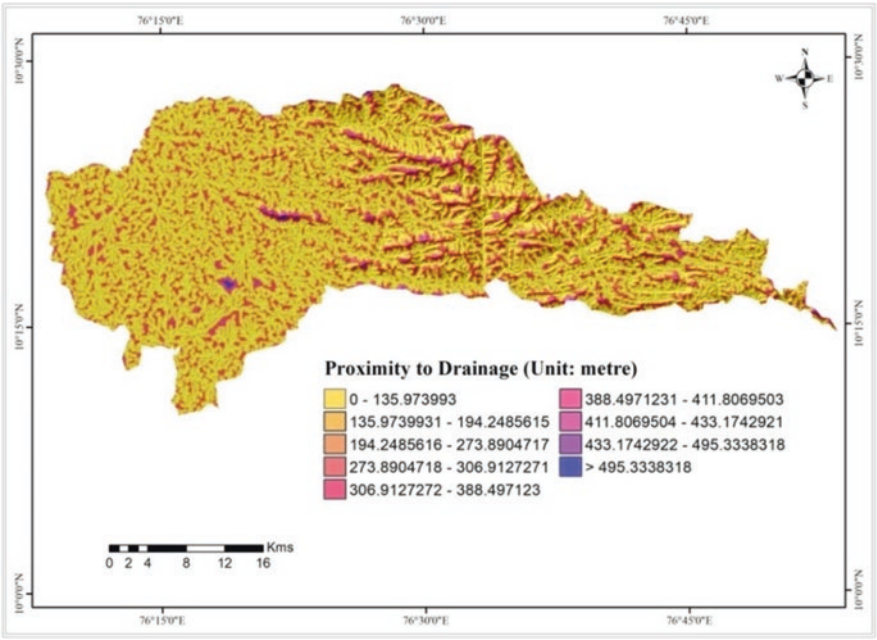

Fig. 5.13 Flood influencing factor – proximity to drainage

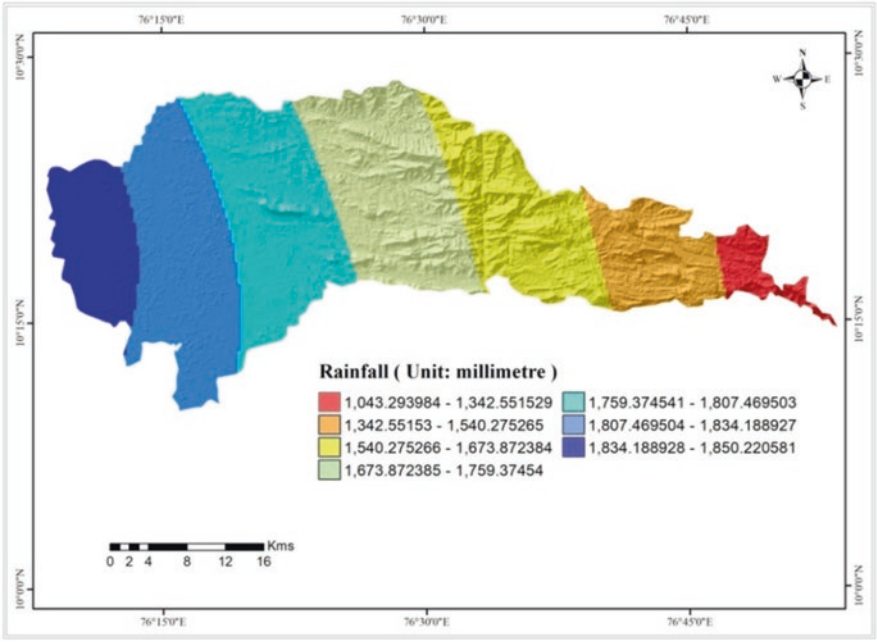

Fig. 5.14 Flood influencing factor – rainfall

5 Applying Dempster-Shafer Evidential Belief Function (EBF) Method in FSZ Mapping

Statistical methods have been widely used in hazard zonation mapping. The statistical methods are based on the functional relationship between the conditioning factors and the hazard. The evidential belief function (EBF) model is a statistical model based on Dempster-Shafer's theory of evidence which was first proposed by Dempster (1967, 1968) and later developed by Shafer (1976) and is basically a generalization of the Bayesian theory of subjective probability. Dempster-Shafer's evidential belief model is a bivariate statistical model wherein the impact of each class of every conditioning is evaluated on the particular hazard. As stated by Tehrany et al. (2018), the advantage of using Dempster-Shafer's approach lies in its capability to handle incomplete datasets or varying precision levels of information. Moreover, it not only predicts flood susceptibility, but, at the same time, it also predicts and allows the representation of the degree of uncertainty of a system. DST is relatively more flexible as it allows combining degrees of belief from different sources of evidence (Jebur et al., 2015). Dempster-Shafer's theoretical framework is used to estimate the evidential belief functions, which are bel (degree of belief), dis (degree of disbelief), unc (uncertainty), and pls (degree of plausibility). Estimation of these EBFs is relative to a hypothesis that "based on spatial evidence, a given region is susceptible to future flood occurrence". Belief and plausibility are the lower and upper probabilities, respectively, that the given evidence supports the hypothesis. Disbelief is the probability that the given hypothesis is untrue, whereas, uncertainty is doubt in the belief that the hypothesis is true. Bel, dis, and unc follow the probability approach thus bel+dis + unc = 1.

Consider that the study region consists of a total number of N(T) pixels. X_i (where i = 1,2,3…..n) represents different flood causative factors with C_{ij} (where j = 1,2,3….n) classes. $N(C_{ij})$ represents the total number of pixels in a particular class of one causative factor. $N(C_{ij} \cap F)$ would give the number of C_{ij} pixels that overlaps pixels of the flood inventory map, F, where map F contains the flood inventory points. $[N(C_{ij}) - N(C_{ij} \cap F)]$ gives the number of pixels C_{ij} not overlapping pixels of map F. Following this belief value can be calculated using Eq. 5.3:

$$\mathrm{bel}_{C_{ij}} = \frac{W_{C_{ij}F}}{\sum_{j}^{k} = 1 W_{C_{ij}F}} \tag{5.3}$$

where

$$W_{C_{ij}F} = \frac{\frac{N(Cij \cap F)}{N(C_{ij})}}{\frac{N(F) - N(C_{ij} \cap F)}{N(T) - N(C_{ij})}} \tag{5.4}$$

is the ratio of conditional probability of occurrence of flood event (F) in the presence of C_{ij} to conditional probability of occurrence of flood event (F) in the absence of C_{ij}. As stated by Tehrany (2018), Eq. 5.3, i.e. bel, represents the relative strength of $W_{C_{ij}F}$ for every class (j = 1,2,3….) of each evidential parameter. On the similar lines, disbelief values can be calculated using Eq. 5.5:

$$\mathrm{dis}_{C_{ij}} = \frac{W_{C_{ij}F}}{\sum_{j}^{k} = 1 W_{C_{ij}F}} \tag{5.5}$$

where

$$W_{C_{ij}F} = \frac{\frac{N(C_{ij}) - N(Cij \cap F)}{N(C_{ij})}}{\frac{N(T) - N(F) - \left[N(C_{ij}) - N(Cij \cap F)\right]}{N(T) - N(C_{ij})}} \tag{5.6}$$

is the ratio of the conditional probability of absence of event F in the presence of Cij to the conditional probability of absence of event F in the absence of Cij. Like belief, disbelief, as per Eqs. 5.3 and 5.5, gives the relative strength of $W_{C_{ij}F}$ for every class of each parameter.

Uncertainty and plausibility can be calculated using Eqs. 5.7 and 5.8:

$$\mathrm{unc}_{C_{ij}} = 1 - \mathrm{bel}_{C_{ij}} - \mathrm{dis}_{C_{ij}} \tag{5.7}$$

$$\mathrm{pls}_{C_{ij}} = \mathrm{bel}_{C_{ij}} + \mathrm{unc}_{C_{ij}} \mathrm{or} \mathrm{pls}_{C_{ij}} = 1 - \mathrm{dis}_{C_{ij}} \tag{5.8}$$

In the present study, the EBF model has been used based on two different approaches. The first approach uses Dempster's rule combination to prepare the flood susceptibility map. In the second approach, a flood susceptibility map is prepared by adding the belief maps of each conditioning factor.

5.1 Dempster's Rule of Combination

As per Dempster's rule of combination, at a time, only maps of two spatial evidential maps can be integrated. The formulae for integrating EBFs of two evidential maps, say, X_1 and X_2, as mentioned by Wright and Bonham-Carter (1996) are as follows:

$$\beta = 1 - \left(\mathrm{belX}_1 \times \mathrm{disX}_2\right) - \left(\mathrm{disX}_1 \times \mathrm{belX}_2\right) \tag{5.9}$$

$$\text{bel} = \frac{\left(\text{belX}_1 \times \text{belX}_2\right) + \left(\text{belX}_1 \,\text{x}\, \text{uncX}_2\right) + \left(\text{belX}_2 \times \text{uncX}_1\right)}{\beta} \tag{5.10}$$

$$\text{dis} = \frac{\left(\text{disX}_1 \times \text{disX}_2\right) + \left(\text{disX}_1 \times \text{uncX}_2\right) + \left(\text{disX}_2 \times \text{uncX}_1\right)}{\beta} \tag{5.11}$$

$$\text{unc} = \frac{\text{uncX}_1 \times \text{uncX}_2}{\beta} \tag{5.12}$$

Here, β is a normalizing factor that ensures that bel, dis, and unc follow a probability approach i.e. bel+dis + unc = 1.

The EBFs of other spatial evidence (X_3, …X_{11}) are combined by the repeated application of the above equations, one after the other. As stated by Carranza et al. (2005), the above formulae for combining the evidential maps are commutative and associative in nature, meaning that different order combinations of these evidential maps do not affect the final outcome. In the present study, the thematic maps of EBFs were paired as represented as per the scheme adopted for Dempster's rule of combination, as shown in Fig. 5.15. All of these evidential maps are combined as per Eqs. 5.9, 5.10, 5.11, and 5.12.

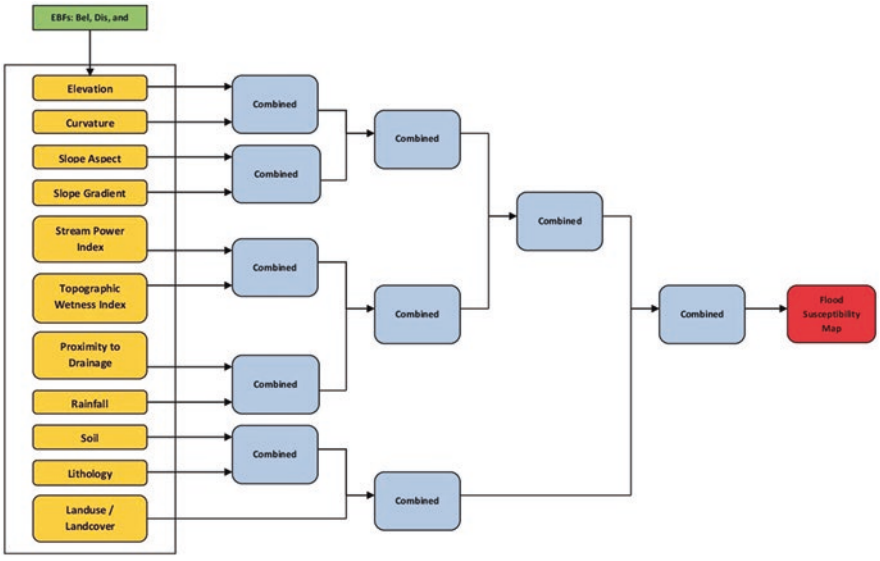

Fig. 5.15 Conceptual framework of Dempster's rule of combination for the study

5.2 Belief Summation

Dempster-Shafer's theory provides relative flexibility in its approach to integrating different datasets as it is capable of combining beliefs from different evidence. A number of previous studies have employed this approach of summing the belief maps of different thematic layers to prepare hazard susceptibility maps (Althuwaynee et al., 2012; Jebur et al., 2015; Hong et al., 2016; Rahmati & Pourghasemi, 2017). The flood susceptibility index is calculated using Eq. 5.13:

$$\mathrm{FSI} = \sum_{\mathrm{bel}=1}^{n} \mathrm{bel} \tag{5.13}$$

where FSI is flood susceptibility index and bel is the belief value of each influencing factor map.

As stated by Althuwaynee et al. (2012), a flood susceptibility map can be considered as the spatial distribution of the degree of support for the occurrence of a flood event; therefore combined belief function map can be considered a final susceptibility map.

6 Results and Discussion

6.1 Relationship Between Conditioning Factors with Past Flood Occurrence

The estimated belief, disbelief, and uncertainty values using Eqs. 5.3, 5.5, and 5.7 for each of the flood conditioning factors are shown in Table 5.2. The elevation class 3–8 m received the highest value of belief, i.e. 0.406, whereas the highest elevation class 709–1198 m received the lowest value of belief, demonstrating high potential for flooding in low elevated areas. In the case of curvature, flat curvature showed the highest degree of belief 0.817, whereas concave curvature showed the lowest degree. Flat or less steep slope classes received higher belief values compared to steep slope classes. In steep areas, the runoff velocity is more which decreases the infiltration time; hence the probability of flooding is higher in flat or less steep areas. For the slope aspect, slopes with west and northwest aspects received higher belief values. In the case of TWI and SPI, the classes 398.9128675–1488.831127 and 5.47307929–6.804550257, respectively, received the highest degree of belief indicating higher potential of flooding in the areas following under these classes. In case of proximity to drainage, classes 411.8069504–433.1742921 and 0–135.973993 showed a high chance of flood occurrence due to a higher degree of belief, 0.426 and 0.153, respectively. Rainfall class 1807.469504–1834.188927 showed a high

Table 5.2 Flood influencing factors, classes, and respective belief, disbelief, and uncertainty values estimated using EBF model

Layers	Class	Bel	Dis	Unc
Elevation (m)	3–8	0.406	0.061	0.533
	8.000000001–11	0.198	0.091	0.711
	11.00000001–16	0.185	0.093	0.722
	16.00000001–26	0.167	0.096	0.737
	26.00000001–63	0.033	0.108	0.859
	63.00000001–150	0.011	0.110	0.879
	150.0000001–312	0.000	0.110	1.000
	312.0000001–505	0.000	0.110	1.000
	505.0000001–709	0.000	0.110	1.000
	709.0000001–1198	0.000	0.110	1.000
Slope (°)	0–1.343796973	0.252	0.085	0.663
	1.343796974–2.418834552	0.302	0.075	0.623
	2.418834553–3.49387213	0.188	0.092	0.719
	3.493872131–5.106428498	0.139	0.096	0.765
	5.106428499–7.256503655	0.090	0.102	0.809
	7.256503656–10.212857	0.010	0.110	0.880
	10.21285701–14.24424792	0.010	0.110	0.880
	14.24424793–19.08191702	0.010	0.109	0.880
	19.08191703–25.53214249	0.000	0.110	1.000
	25.5321425–68.53364563	0.000	0.110	1.000
Slope aspect (°)	Southeast (112.5–157.5)	0.080	0.115	0.806
	West (247.5–292.5)	0.165	0.104	0.731
	South (157.5–202.5)	0.098	0.113	0.789
	Southwest (202.5–247.5)	0.119	0.109	0.772
	East (67.5–112.5)	0.138	0.108	0.755
	Northeast (22.5–67.5)	0.057	0.118	0.825
	Northwest (292.5–337.5)	0.142	0.106	0.751
	North (337.5–22.5)	0.073	0.117	0.811
	Flat (−1)	0.129	0.111	0.761
Plan curvature	Concave (−)	0.000	0.473	1.000
	Flat (0)	0.817	0.057	0.126
	Convex (+)	0.183	0.470	0.347
TWI	0.41348961–2.756878514	0.327	0.083	0.590
	2.756878515–4.141608321	0.023	0.117	0.860
	4.141608322–5.473079289	0.018	0.111	0.872
	5.47307929–6.804550257	0.500	0.055	0.444
	6.804550258–8.242538902	0.105	0.105	0.790
	8.242538903–9.414233354	0.027	0.107	0.866
	9.414233355–10.47941013	0.000	0.108	1.000
	10.47941014–11.75762226	0.000	0.109	1.000
	11.75762227–12.82279903	0.000	0.105	1.000
	12.82279904–13.99449348	0.000	0.101	1.000

(continued)

Table 5.2 (continued)

Layers	Class	Bel	Dis	Unc
SPI	−238,254.6563 to −2286.656863	0.463	0.105	0.432
	−2286.656862 to −398.9128676	0.000	0.113	0.887
	−398.9128675–1488.831127	0.537	0.041	0.422
	1488.831128–3376.575123	0.000	0.107	1.000
	3376.575124–5264.319118	0.000	0.106	1.000
	5264.319119–7152.063113	0.000	0.106	1.000
	7152.063114–10,927.5511	0.000	0.105	1.000
	10,927.55111–14,703.03909	0.000	0.105	1.000
	14,703.0391–27,917.24706	0.000	0.105	1.000
	27,917.24707–243,120.0625	0.000	0.105	1.000
LULC	Built-up land	0.254	0.087	0.660
	Agriculture-crop land	0.068	0.109	0.823
	Agriculture-fallow land	0.135	0.083	0.782
	Forest-evergreen/semievergreen	0.003	0.183	0.814
	Forest-deciduous	0.000	0.112	1.000
	Forest-scrub	0.042	0.113	0.844
	Forest-plantation	0.000	0.109	1.000
	Shallow-water bodies	0.473	0.094	0.433
	Water bodies	0.025	0.110	0.865
Lithology	Charnockite group	0.148	0.381	0.470
	Quaternary sediments	0.150	0.246	0.605
	Migmatite complex	0.702	0.107	0.190
	Peninsular gneissic complex	0.000	0.000	1.000
Soil	Alluvium	0.541	0.077	0.383
	Hill soil	0.000	0.226	1.000
	Forest soil	0.000	0.180	1.000
	Laterite soil	0.152	0.183	0.665
	Coastal soil	0.079	0.171	0.750
	Acid saline	0.228	0.164	0.608
Proximity to drainage (m)	0–135.973993	0.153	0.094	0.753
	135.9739931–194.2485615	0.122	0.112	0.766
	194.2485616–273.8904717	0.064	0.118	0.818
	273.8904718–306.9127271	0.064	0.116	0.820
	306.9127272–388.497123	0.033	0.115	0.852
	388.4971231–411.8069503	0.138	0.112	0.750
	411.8069504–433.1742921	0.426	0.110	0.463
	433.1742922–495.3338318	0.000	0.112	1.000
	> 495.3338318	0.000	0.112	1.000
Rainfall (mm)	1043.293984–1342.551529	0.000	0.148	1.000
	1342.55153–1540.275265	0.000	0.159	1.000
	1540.275266–1673.872384	0.000	0.170	1.000
	1673.872385–1759.37454	0.016	0.178	0.806
	1759.374541–1807.469503	0.317	0.118	0.565
	1807.469504–1834.188927	0.496	0.082	0.422
	1834.188928–1850.220581	0.171	0.145	0.684

value of belief degree of belief received by them. In LULC, the built-up land received the highest belief value, i.e. 0.254, after the shallow water body categories (shallow water bodies indicate water bodies with less depth or seasonal water flow, which are bound fill up quickly, in case of rains or flooding), indicating high probability of flooding in built-up areas.

6.2 *Flood Susceptibility Zonation (FSZ) Mapping*

The calculated EBFs (bel, dis, and unc) are then added to the attribute tables of each causative factor in the ArcGIS environment. Thereafter, rasterization of the thematic layer of each parameter was carried out with 10 m × 10 m pixel size based on each of the EBFs, i.e. belief, disbelief, and uncertainty. Therefore, each causative factor had three EBFs evidential maps, viz. belief, disbelief, and uncertainty map. The integration of these thematic layers was carried out using two approaches, first using Dempster's rule of combination and second using belief summation. The final flood susceptibility index map using Dempster's rule of combination and belief summation method is shown in Figs. 5.16 and 5.17, respectively. The flood susceptibility index map was divided into five classes, viz. very low, low, moderate, high, and very high, using the quantile classification

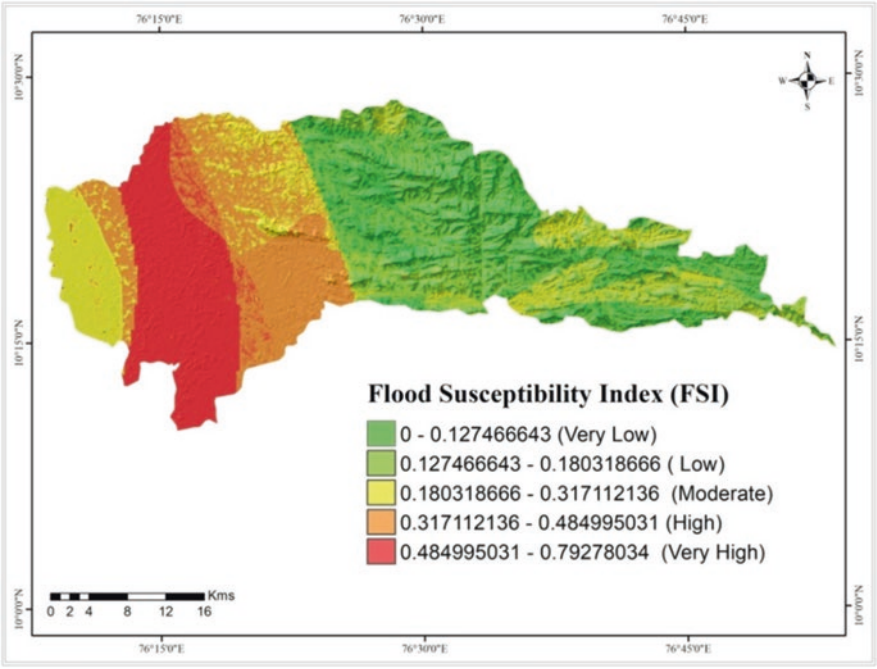

Fig. 5.16 Flood susceptibility zonation map prepared using Dempster's rule of combination

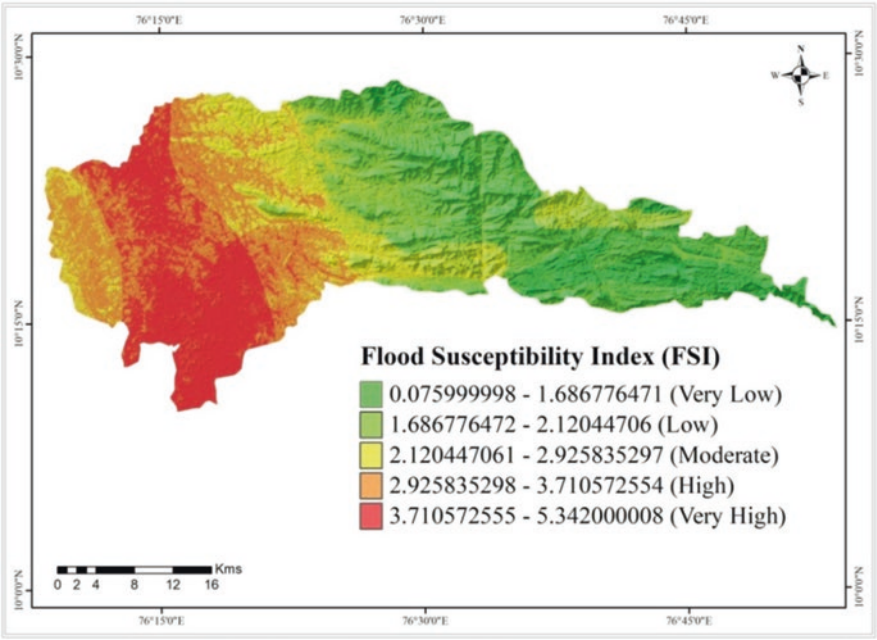

Fig. 5.17 Flood susceptibility zonation map prepared using Belief summation

Table 5.3 Spatial relationship between flood susceptibility zones and floods using Dempster's rule of combination and Belief summation

Flood susceptibility zones	Pixels in domain	% of pixels	Flood frequency	% of flood frequency domain
Using Dempster's rule of combination				
Very low	2,494,770	19.29	1	0.89
Low	2,858,214	22.10	0	0.000
Moderate	2,521,871	19.506	5	4.46
High	2,534,171	19.60	43	38.39
Very high	2,521,503	19.50	63	56.25
Using belief summation				
Very low	2,586,123	20.00	1	0.89
Low	2,586,643	20.00	0	0.00
Moderate	2,586,598	20.00	2	1.79
High	2,586,189	20.00	30	26.79
Very high	2,584,976	19.99	79	70.54

method. The final evidential belief maps from both the approaches were compared with respective belief maps, which showed belief values were high for the areas where disbelief values were low. The FSZ maps show most of the agriculture-crop land, agriculture-fallow land, and built-up land fall under high to very high flood susceptible zones, whereas forest-evergreen/semievergreen, forest-scrub, and

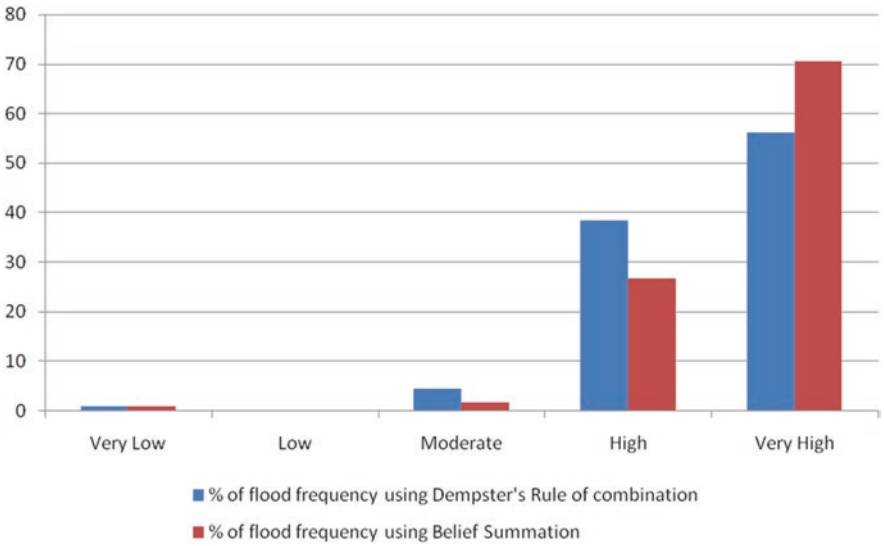

Fig. 5.18 The distribution of flood frequency percentage in each FSZ class

forest-deciduous lie under low to very low susceptible zones. The integration results show 94.64% of past flood occurrences fall in very high and high classes using Dempster's rule of the combination, while 97.33% of past flood occurrences fall in very high and high classes using belief summation (Table 5.3). The flood inventory locations were overlaid with FSZ maps to analyse the distribution of flood frequencies in each susceptibility class (Fig. 5.18).

6.3 Accuracy Assessment of the Methods

The accuracy of final flood susceptibility maps was determined by area under the curve (AUC) method. AUC is one of the most reliable methods used to validate the model. The AUC method validates a model by predicting the success rate and prediction rate for the model. In this method, the susceptibility index is classified into 100 flood susceptibility index classes on the x-axis and cumulative percentage in the y-axis. Success and prediction rates were derived by evaluating the number of training/testing flood points in each 100 class. The success rate is predicted by comparing training flood points (70% of flood inventory points) with the susceptibility map. As stated in Bui et al., (2011), since the training set is already being used in the modelling, therefore, testing data should be used to validate the result. Hence, the prediction rate is obtained by comparing testing data (30% of flood inventory points) with a flood susceptibility map. The value of AUC ranges from 0 to 1. Value 1 represents maximum accuracy, demonstrating the model was 100% successful in predicting flood susceptibility; the closer the value is to one, the more reliable the

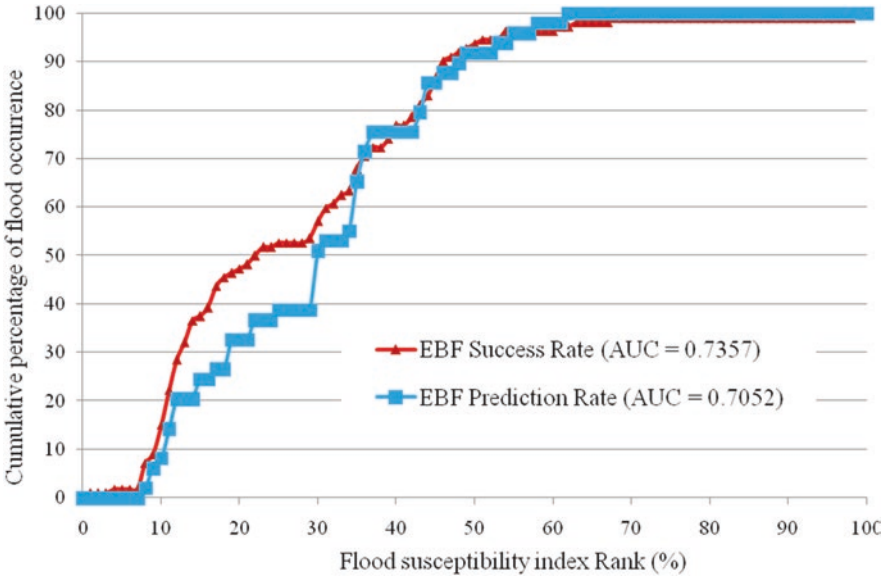

Fig. 5.19 The success and prediction rate through AUC for the FSZ map using Dempster's rule of combination

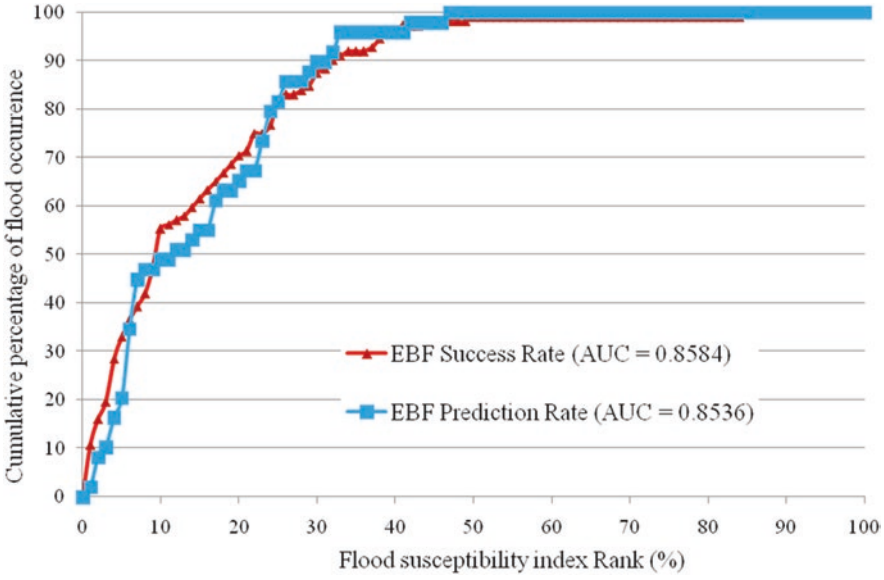

Fig. 5.20 The success and prediction rate through AUC for the FSZ map using belief summation

model and the factors in predicting floods (Pradhan, 2009; Tehrany & Kumar, 2018). The AUC method is applied to evaluate to both the flood susceptibility maps obtained by Dempster's rule of combination as well as the belief summation method.

The AUC validation curves for the flood susceptibility map using Dempster's rule of combination are shown in Fig. 5.19. The AUC values obtained for success and prediction rates are 73.57% and 70.52%, respectively. The AUC for flood susceptibility map using belief summation is shown in Fig. 5.20, with 85.84% and 85.36% being the success and prediction rates, respectively. The accuracy of results was classified as 0.90–1 (excellent), 0.80–0.90 (good), 0.70–0.80 (fair), 0.60–0.70 (poor), and 0.50–0.60 (fail) by Pradhan and Kim (2016). The AUC success rate and prediction rate of Dempster's rule of combination fall under the "fair" category, whereas the success rate and prediction of belief summation are under the "good" classification category.

7 Conclusions

The study highlights the efficient use of GIS and remote sensing techniques in susceptibility mapping, which proved to be quick as well as efficient. Different GIS software such as ArcGIS, SAGA GIS, and ERDAS Imagine is highly useful and capable of processing and analysing spatial datasets. Different conditioning parameters were used to evaluate the flood susceptibility. Each of the conditioning parameter classes has a different influence on the flood. In the present study, the most influential parameter classes included low elevated, flat curvature, low SPI, high TWI, and built-up classes. High-resolution satellite images and datasets such as Sentinel data, RADAR data, and ASTER DEM can be used for deriving thematic layers for different flood conditioning parameters accurately and efficiently. Such datasets are highly useful and necessary for carrying out flood studies, which involve accurately mapping the number of spatial and temporal data that cannot be mapped out from the field. However, getting such datasets is one of the biggest challenges as well as limitations in such types of studies.

For example, getting a cloud-free image of the area, particularly when the study area is located near the coast, can be a challenging task. Statistical models such as Dempster-Shafer's evidential belief function model are highly useful in predicting and mapping the susceptibility of an area towards flood, wherein such models can effectively classify a region into different flood susceptible zones. The accuracy of the model is well proved by the validation method. The major limitation of the model used, particularly with Dempster's rule of combination, is that each conditioning factor has to be converted into evidential data layer and requires several calculation steps and data transformation for integrating the conditioning factors to create a susceptibility map, which can be tedious and time-consuming, particularly when dealing with the large number of data layers.

References

Abdulkareem, M., & Elkadi, H. (2018). From engineering to evolutionary, an overarching approach in identifying the resilience of urban design to flood. *International Journal of Disaster Risk Reduction, 28*, 176–190. https://doi.org/10.1016/j.ijdrr.2018.02.009

Ahmadlou, M., Karimi, M., Alizadeh, S., Shirzadi, A., Parvinnejhad, D., & Shahabi, H. (2019). Flood susceptibility assessment using integration of adaptive network-based fuzzy inference system (ANFIS) and biogeography-based optimization (BBO) and BAT algorithms (BA). *Geocarto International, 34*, 1252–1272. https://doi.org/10.1080/10106049.2018.1474276

Althuwaynee, O. F., Pradhan, B., & Lee, S. (2012). Application of an evidential belief function model in landslide susceptibility mapping. *Computer & Geosciences, 44*, 120–135. https://doi.org/10.1016/j.cageo.2012.03.003

APFM. (2013). *Integrated flood management tool series: Flood mapping*. Associated Programme on Flood Management (APFM) a joint initiative of the World Meteorological Organization (WMO) and the Global Water Partnership (GWP), Issue 20, p. 88.

Bui, D.T., Pradhan, B., Lofman, O., Revhaug, I., & Dick, O.B. (2011). Landslide susceptibility mapping at Hoa Binh province (Vietnam) using an adaptive neuro-fuzzy inference system and GIS. *Computer & Geosciences, 45*, 199–211. https://doi.org/10.1016/j.cageo.2011.10.031

Campolo, M., Andreussi, P., & Soldati, A. (1999). River flood forecasting with a neural network model. *Water Resources Research, 35*(4), 1191–1197. https://doi.org/10.1029/1998WR900086

Carranza, E. J. M., Woldai, T., & Chikambwe, E. M. (2005). Application of data-driven evidential belief functions to prospectivity mapping for aquamarine-bearing pegmatites, Lundazi district, Zambia. *Natural Resources Research, 14*(1), 47–63. https://doi.org/10.1007/s11053-005-4678-9

Central Water Commission (CWC). (2018). *Study report: Kerala floods of august 2018*. Central Water Commission (CEC), Government of India.

Choubin, B., Moradi, E., Golshan, M., Adamowski, J., Sajedi-Hosseini, F., & Mosavi, A. (2019). An ensemble prediction of flood susceptibility using multivariate discriminant analysis, classification and regression trees, and support vector machines. *Science of the Total Environment, 651*, 2087–2096. https://doi.org/10.1016/j.scitotenv.2018.10.064

Conforti, M., Aucelli, P. P. C., Robustelli, G., & Scarciglia, F. (2011). Geomorphology and GIS analysis for mapping gully erosion susceptibility in the Turbolo stream catchment (Northern Calabria, Italy). *Natural Hazard, 56*, 881–898. https://doi.org/10.1007/s11069-010-9598-2

Dai, F. C., Lee, C. F., & Xu, Z. W. (2001). Assessment of landslide susceptibility on the natural terrain of Lantau Island, Hong Kong. *Environmnetal Geology, 40*, 381–391. https://doi.org/10.1007/s002540000163

Danumah, J. H., Odai, S. N., Saley, B. M., Szarzynski, J., Thiel, M., Kwaku, A., Kouame, F. K., & Akpa, L. Y. (2016). Flood risk assessment and mapping in Abidjan district using multi-criteria analysis (APH) model and geoinformation techniques, (Cote d'ivoire). *Geoenvironmental Disasters, 3*, 10. https://doi.org/10.1186/s40677-016-0044-y

Dempster, A. P. (1967). Upper and lower probabilities induced by a multivalued mapping. *Annals of Mathematical Statistics, 38*(2), 325–339.

Dempster, A. P. (1968). A generalization of Bayesian inference. *Journal of the Royal Statistical Society, 2*, 205–247.

Diakakis, M. (2011). Rainfall thresholds for flood triggering. The case of Marathonas in Greece. *Natural Hazards, 60*, 789–800. https://doi.org/10.1007/s11069-011-9904-7

Essel, B. (2017). The application of GIS in mapping of flood hazard areas and assessing of risk in Kumasi, Ghana. *Journal of Energy and Natural Resource Management, 3*(2), 97–103. https://doi.org/10.26796/jenrm.v3i3.95

Gokceoglu, C., Sonmez, H., Nefeslioglu, H. A., Duman, T. Y., & Can, T. (2005). The 17 March 2005 Kuzulu landslide (Sivas, Turkey) and landslide-susceptibility map of its near vicinity. *Engineering Geology, 81*(1), 65–83. https://doi.org/10.1016/j.enggeo.2005.07.011

Haghizadeh, A., Siahkamari, S., Haghiabi, A. H., & Rahmati, O. (2017). Forecasting flood-prone areas using Shannon's entropy model. *Journal Earth System Sciences, 126*, 39. https://doi.org/10.1007/s12040-017-0819-x

Hong, H., Naghibi, S. A., Pourghasemi, H. R., & Pradhan, B. (2016). GIS-based landslide spatial modeling in Ganzhou City. *China. Arabian Journal of Geosciences, 9*, 112. https://doi.org/10.1007/s12517-015-2094-y

Jacoby, B. S., Peterson, E. W., & Dogwiler, T. (2011). Identifying the stream erosion potential of cave levels in carter Cave State resort park, Kentucky, USA. *Journal of Geographic Information System, 3*, 323–333. https://doi.org/10.4236/jgis.2011.34030

Jebur, M. N., Pradhan, B., Shafri, H. Z. M., Yusoff, Z. M., & Tehrany, M. S. (2015). An integrated user-friendly ArcMAP tool for bivariate statistical modelling in geoscience applications. *Geoscientific Model Development, 8*, 881–891. https://doi.org/10.5194/gmdd-7-7239-2014

Jothibasu, A., & Anbazhagan, S. (2016). Flood susceptibility Appraisal in Ponnaiyar River Basin, India using Frequency Ratio (FR) and Shannon's Entropy (SE) models. *International Journal of Advanced Remote Sensing and GIS, 5*(10), 1946–1962. https://doi.org/10.23953/cloud.ijarsg.73

Khosravi, K., Nohani, E., Maroufinia, E., & Pourghasemi, H. R. (2016). A GIS-based flood susceptibility assessment and its mapping in Iran: A comparison between frequency ratio and weights-of-evidence bivariate statistical models with multi-criteria decision-making technique. *Natural Hazards, 83*, 947–987. https://doi.org/10.1007/s11069-016-2357-2

Kia, M. B., Pirasteh, S., Pradhan, B., Mahmud, A. R., Sulaiman, W. N. A., & Moradi, A. (2012). An artificial neural network model for flood simulation using GIS: Johor River Basin, Malaysia. *Environmental Earth Sciences, 67*, 251–264. https://doi.org/10.1007/s12665-011-1504-z

Krebs, P., Stocker, M., Pezzatti, G. B., & Conedera, M. (2014). An alternative approach to transverse and profile terrain curvature. *International Journal of Geographical Information Science, 29*(4), 643–666. https://doi.org/10.1080/13658816.2014.995102

Merwade, V., Rajib, M. A., & Liu, Z. (2018). An integrated approach for flood inundation modelling on large scales. In H. S. Jung & B. Wang (Eds.), *Bridging science and policy implication for managing climate extremes* (pp. 133–155). World Scientific.

Mojaddadi, H., Pradhan, B., Nampak, H., Ahmad, N., & Ghazali, A. H. B. (2017). Ensemble machine-learning-based geospatial approach for flood risk assessment using multi- sensor remote-sensing data and GIS Ensemble machine-learning-based geospatial approach for flood risk assessment using multi-sensor remote-sensing data and GIS. *Geomatics, Natural Hazards and Risk, 8*(2), 1080–1102. https://doi.org/10.1080/19475705.2017.1294113

Mu, W., Yu, F., Li, C., Xie, Y., Tian, J., Liu, J., & Zhao, N. (2015). Effects of rainfall intensity and slope gradient on runoff and soil moisture content on different growing stages of spring maize. *Water, 7*(6), 2990–3008. https://doi.org/10.3390/w7062990

Nandalal, H. K., & Ratnayake, U. R. (2011). Flood risk analysis using fuzzy models. *Journal of Flood Risk Management, 4*, 128–139. https://doi.org/10.1111/j.1753-318X.2011.01097.x

Pradhan, B. (2009). Flood susceptible mapping and risk area delineation using logistic regression, GIS and remote sensing. *Journal of Spatial Hydrology, 9*(2), 1–18.

Pradhan, A. M. S., & Kim, Y. T. (2016). Spatial data analysis and application of evidential belief functions to shallow landslide susceptibility mapping at Mt. Umyeon, Seoul, Korea. *Bulletin of Engineering Geology and the Environment, 76*, 1263–1279. https://doi.org/10.1007/s10064-016-0919-x

Rahmati, O., Pourghasemi, H.R., & Zeinivand, H. (2016). Flood susceptibility mapping using frequency ratio and weights-of-evidence models in the Golastan Province, Iran. *Geocarto International. 31*(1), 42–70. https://doi.org/10.1080/10106049.2015.1041559

Rahmati, O., & Pourghasemi, H. R. (2017). Identification of critical flood prone areas in data-scarce and ungauged regions: A comparison of three data mining models. *Water Resources Management, 31*, 1473–1487. https://doi.org/10.1007/s11269-017-1589-6

Ramesh, V., & Iqbal, S. S. (2020). *Urban flood susceptibility zonation mapping using evidential belief function, frequency ratio and fuzzy gamma operator models in GIS: A case study*

of Greater Mumbai, Maharashtra, India. Geocarto International. https://doi.org/10.1080/10106049.2020.1730448

Rizeei, H. M., Saharkhiz, M. A., Pradhan, B., & Ahmad, N. (2016). Soil erosion prediction based on land cover dynamics at the Semenyih watershed in Malaysia using LTM and USLE models. *Geocarto International, 31*(10), 1158–1177.

Samanta, S., Pal, D. K., & Palsamanta, B. (2018). Flood susceptibility analysis through remote sensing, GIS and frequency ratio model. *Applied Water Science, 8*(2), 66. https://doi.org/10.1007/s13201-018-0710-1

Sangati, M., & Borga, M. (2009). Influence of rainfall spatial resolution on flash flood modelling. *Natural Hazards and Earth System Sciences, 9*, 575–584. https://doi.org/10.5194/nhess-9-575-2009

Schmidt, F., & Persson, A. (2003). Comparison of DEM data capture and topographic wetness indices. *Precision Agriculture, 4*, 179–192. https://doi.org/10.1023/A:1024509322709

Shafer, G. (1976). *A mathematical theory of evidence* (Vol. 1, p. 314). Princetown University Press.

Siddayao, G. P., Valdez, S. E., & Fernandez, P. L. (2014). Analytic Hierarchy Process (AHP) in spatial modeling for floodplain risk assessment. *International Journal of Machine Learning and Computing, 4*(5), 450–457. https://doi.org/10.7763/IJMLC.2014.V4.453

Sohl, T., & Sleeter, B. (2012). Role of remote sensing in land use and land cover modelling. In C. Giri (Ed.), *Remote sensing and land cover: Principles and applications* (pp. 225–239). CRC press.

Sorensen, R., Zinko, U., & Seibert, J. (2006). On the calculation of the topographic wetness index: Evaluation of different methods based on field observations. *Hydrology and Earth System Sciences, 10*, 101–112. https://doi.org/10.5194/hess-10-101-2006

Tehrany, M. S., & Kumar, L. (2018). The application of a Dempster–Shafer-based evidential belief function in flood susceptibility mapping and comparison with frequency ratio and logistic regression methods. *Environmental Earth Sciences, 77*(13), 490. https://doi.org/10.1007/s12665-018-7667-0

Tehrany, M. S., Lee, M. J., Pradhan, B., Jebur, M. N., & Lee, S. (2014). Flood susceptibility mapping using integrated bivariate and multivariate statistical models. *Environmental Earth Sciences, 72*(10), 4001–4015. https://doi.org/10.1007/s12665-014-3289-3

Tehrany, M. S., Pradhan, B., Mansor, S., & Ahmad, N. (2015). Flood susceptibility assessment using GIS-based support vector machine model with different kernel types. *Catena, 125*, 91–101. https://doi.org/10.1016/j.catena.2014.10.017

Tehrany, M. S., Kumar, L., Jebur, M. N., & Shabani, F. (2018). Evaluating the application of the statistical index method in flood susceptibility mapping and its comparison with frequency ratio and logistic regression methods. *Geomatics, Natuarl Hazards and Risk, 10*(1), 79–101. https://doi.org/10.1080/19475705.2018.1506509

Tehrany, M. S., Jones, S., & Shabani, F. (2019). Identifying the essential flood conditioning factors for flood prone area mapping using machine learning techniques. *Catena, 175*, 174–192. https://doi.org/10.1016/j.catena.2018.12.011

Tejedor, M., Neris, J., & Jimenez, C. (2013). Soil properties controlling infiltration in volcanic soils (Tenerife, Spain). *Soil Science Society of America Journal, 77*, 202–212. https://doi.org/10.2136/sssaj2012.0132

Verstappen, H. T. (1995). Aerospace technology and natural disaster reduction. *Advances in Space Research, 15*(11), 3–15. https://doi.org/10.1016/0273-1177(95)00070-U

Wright, D. F., & Bonham-Carter, G. F. (1996). VHMS favourability mapping with GIS-based integration models, chisel Lake-Anderson Lake area. In G. F. Bonham-Carter, A. G. Galley, & H. GEM (Eds.), *EXTECH I: A multidisciplinary approach to massive sulphide research in the Rusty Lake–Snow Lake Greenstone Belts, Manitoba* (Vol. 426, pp. 339–401). Geological Survey of Canada, Bulletin.

Wu, H., & Adler, R. F. (2012). Evaluation of global flood detection using satellite-based rainfall and a hydrologic model. *Journal of Hydrometeorolgy, 13*, 1268–1284. https://doi.org/10.1175/JHM-D-11-087.1

Chapter 6
Impact of Urbanization on Ganga River Basin: An Overview in the Context of Natural Surface Water Resources

Ankit Modi, Chandrashekhar Bhagat, and Pranab Kumar Mohapatra

Abstract The Ganga river, a symbol of faith for hundreds of millions of Indians, provides all essentials for the development of human beings such as ample amount of freshwater for domestic-agriculture-industrial purposes, productive agricultural land for food production, and diversified flora-fauna for a sustainable ecosystem in its one million km^2 basin. Over the years, various alternatives have been introduced in the basin to feed the growing population, and in the last hundred years manifold changes have been made. Various multipurpose dam/barrages were constructed on the river's main stem and on its tributaries for hydropower production, irrigation, and drinking water supply. Similarly, forest cover changed into agricultural land, and barren land was developed for buildings to support housing and industries for an increasingly urban population of the basin. The effects of anthropogenic activities and anthropogenic activity-induced climate change have started to degrade surface water bodies in terms of their quality and quantity, and in some cases, surface water bodies have been lost completely. For example, the major tributaries of the Ganga river in upper part of the basin, Alaknanda and Bhagirathi, had been altered by ~8% and ~35%, respectively, due to dam/barrages. In the Ramganga basin (a major sub-basin of the Ganga river basin), the surface-subsurface water storage was reduced by ~0.2 MCM/km^2 during 1982–2013. The increment of lead concentration (Pb, a heavy metal) from 3 μg/L to 26.9 mg/L indicates the influence of anthropogenic activities and human encroachment. The increasing pH (>9) and metal concentration near Kanpur stretches indicate industrialization's impact on water quality. Out of 629 lakes and wetlands, 338 were entirely extinct in the Delhi district. Thus,

A. Modi (✉) · P. K. Mohapatra
Discipline of Civil Engineering, Indian Institute of Technology Gandhinagar, Gandhinagar, India
e-mail: ankit.m@iitgn.ac.in

C. Bhagat
Discipline of Civil Engineering, Indian Institute of Technology Gandhinagar, Gandhinagar, India

Department of HSE & Civil Engineering, University of Petroleum and Energy Studies, Dehradun, India

P. Thambidurai, A. K. Dikshit (eds.), *Impacts of Urbanization on Hydrological Systems in India*, https://doi.org/10.1007/978-3-031-21618-3_6

this chapter enlightens the urbanization impact on the surface water bodies in the Ganga river basin. The chapter also discusses the future research scope from the sustainable development perspective.

Keywords Ganga river basin · Urbanization · Surface water · Climate change · Anthropogenic activity

1 Introduction

India is the second largest country in population after China. Its population is increasing at an average rate of ~1% annually (Gu et al. 2021). As per the Census of India 2011, rural areas contributed ~69%, and the urban regions contributed ~31% of the total population. The population percentage was higher in the rural areas but lower than the ~89% in 1901. So, the urban population is increasing continuously. In the last 10 years, India's urban population growth rate has been reported to be between 2.3% and 2.4% annually (Gu et al., 2021). The number of towns and cities in India is also increasing rapidly, which signifies increased urbanization. It is noted that urbanization is a response to the opportunity created by better technological, economic, social, political, and geographical factors of an area (Cohen, 2006; Fox, 2012). Or in other words, urbanization means more population in cities due to better opportunities for jobs, education, and entertainment (refer – https://www.nationalgeographic.org/encyclopedia/urbanization/). As per the Census of India 2011, 7935 towns were reported in India in 2011, which were 5161 in the year 2001. In India, an area is called a town with at least 5000 persons, a population density of 400 persons per km^2, and more than 75% persons with nonagricultural occupation (Rijesh et al. 2022). The number of towns and cities with a million-plus population is also rapidly increasing in the last few decades. According to the Census of India 2001 and 1991, the number of urban cities with a million-plus population was 25 and 35, respectively. This number was 53 in 2011, as per the Census of India 2011.

Most of the cities in India were developed at the banks of the river as rivers, and surface water bodies have always been a driving force for the evolution of human civilization. Throughout history, it is evident that all great civilizations were developed at the banks of major rivers or in river valleys because water is an essential commodity for survival, routine work, and growth. For example, Varanasi (old name Kashi) and Prayagraj (old name Allahabad) at the bank of the Ganga river, Agra, Delhi, and Mathura at the bank of the Yamuna River, etc. have their cultural heritage and rich history in development and facility. With increasing industrialization and population, these cities have proliferated and expanded their spatial areas (Bhagat et al., 2021a). Many cities, including heritage cities, are growing in terms of urbanization. These cities have created more opportunities to attract more population by developing industrial clusters resulting from urban agglomeration.

Figure 6.1 demonstrates the spatial and temporal variation of the cities in India from 1991 to 2011. It may be seen from the figure that many new million-plus cities have been aroused, especially in the Ganga river basin. The exact reason behind urbanization in these cities is the livelihood opportunity created by the service sectors and industrial clusters for a growing population (Joshi, 2021). Studies on urbanization, urban agglomeration, and urban sprawl reported that these cities are continuously spreading even though they are in a stagnant situation for basic

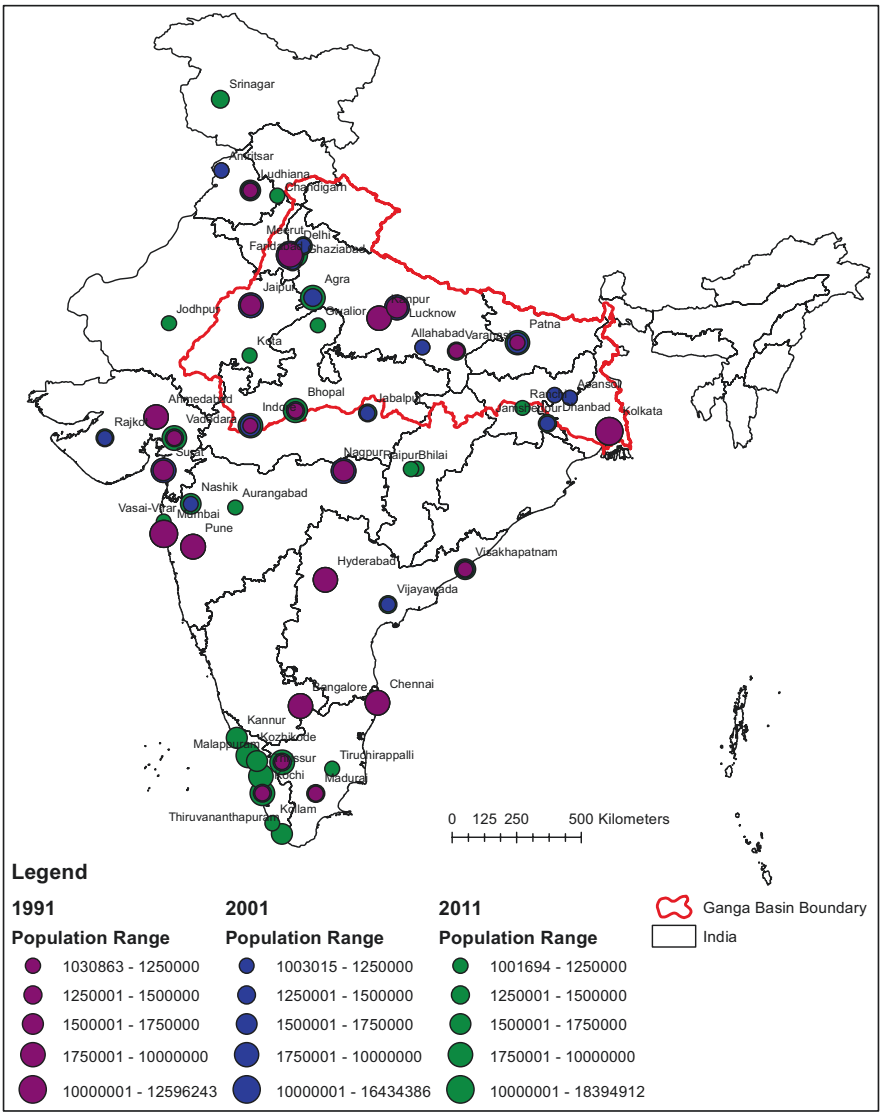

Fig. 6.1 Temporal variation of the population of the cities in India from 1991 to 2011

amenities. With better facilities for living, transportation, medical, water supply, and sanitation, these cities are capturing adjacent agricultural lands, surface water bodies, barren lands, forest areas, floodplains, etc., to develop an urban infrastructure and lead to the disturbed entire ecosystem (Modi et al. 2022a). Domestic and industrial water supply is ensured through nearby rivers, dams/barrages, and canal systems or water supply pipelines. Various water projects, river linking projects, and canal systems have been developed to fulfill the water demand, keeping in mind the nearby river systems and surface water bodies by city planners and managers (Bhagat et al., 2021b; Kumar et al., 2020; Singh et al., 2022).

Surface water storage in the Ganga river basin in northern India is a valuable source of freshwater supply for domestic, agricultural, and industrial demand (Routray, 2022). The process of urbanization and industrialization along the river stretch has put this freshwater source on high risk to vanish. The surface water bodies like ponds, lakes, and small rivers, including some parts of the floodplain Ganga river, are converted into built-up areas (Tyagi & Sahoo, 2022), leading to disturbing the entire ecosystem and biodiversity (Modi et al., 2022a). These urban areas have been spreading rapidly and creating urban sprawls to support more populations. This expansion converted forest cover and small surface water bodies into impervious zones by creating buildings for domestic and industrial purposes leading to increase the flood event and soil erosion in the watershed of River Ganga (Anand et al., 2018a). Also, lots of open lands or barren land areas are utilized only in this way. The urbanization encroached on many natural entities like natural forest cover, small surface water bodies like ponds, lakes, small river beds, floodplains, etc., in the Ganga river watershed, which supported groundwater recharge, local climate, and regional biodiversity (Mani et al., 2021; Modi and Tare, 2022). Few researchers reported that urbanization along with industrialization has disturbed many natural processes of hydrological water balance components like rainfall, surface runoff, groundwater recharge, and base flow of the Ganga river basin (Anand et al., 2018a; Modi et al., 2021; Shukla et al., 2020). It also degraded the water quality significantly of surface water bodies and groundwater aquifers. Therefore, in light of the abovementioned issue, the present chapter provides a comprehensive overview and discusses the impact of urbanization on surface water bodies in the Ganga river basin in detail.

2 Urbanization and Surface Water Bodies in the Ganga River Basin

Since immemorial, the Ganga river basin has been a cradle of human civilization. The oldest civilization reported in the Ganga river basin is the Indus Valley Civilization (Sameer et al., 2018; Singh, 2019). The basin has variations in climate (rainfall pattern, temperature range), cropping pattern, and ecology (flora and fauna). The human settlement with different social and cultural life had progressed

over time through this diversity. Many cities with more than one million population had been developed at the river banks and their tributaries. The Ganga river basin is the largest river basin of India among 22 river basins in India, with an 861,452 km^2 drainage area (Duttagupta et al., 2021). This 26.3% of the geographical area of India supports 42% of the total population of India. The basin's average annual surface water storage potential is assessed as ~230 km^3 (Shamsudduha & Panda, 2019). The average annual rainfall is not uniform in the basin, and it varies from east to west as 2000 to 350 mm, respectively (Anand et al., 2018b). The basin is spread in eleven states of the country, viz., Uttar Pradesh, Madhya Pradesh, Rajasthan, Bihar, West Bengal, Uttarakhand, Jharkhand, Haryana, Chhattisgarh, Himachal Pradesh, and Delhi. The river basin covers Uttarakhand, Uttar Pradesh, Bihar, Jharkhand, and Delhi. Table 6.1 shows state-wise drainage area and population variation in the last three decades as per the census of India. From Table 6.1, it is evident that Delhi's contribution is lowest in the drainage of the basin, but its contribution in the

Table 6.1 State-wise drainage area and population variation in the Ganga river basin in the last three decades

State	Drainage area (km^2)	Million-plus cities	Population (2011) millions	Population (2001) millions	Population (1991) millions
Uttar Pradesh	241392 (~28%)	Meerut	1.42	1.16	–
		Agra	1.76	1.33	–
		Kanpur	2.92	2.71	2.03
		Lucknow	2.90	2.24	1.67
		Allahabad	1.21	1.04	–
		Varanasi	1.43	1.20	1.03
Madhya Pradesh	181070 (~21%)	Bhopal	1.88	1.46	1.06
		Gwalior	1.10	–	–
		Indore	2.17	1.50	1.11
Rajasthan	112496 (~13%)	Jaipur	3.04	2.32	1.52
		Kota	1.00	–	–
Bihar	93580 (~11%)	Patna	2.05	1.69	1.10
West Bengal	71489 (~8%)	Asansol	1.24	1.06	–
		Kolkata	14.05	13.20	11.02
Uttarakhand	52989 (~6%)	–	–	–	–
Jharkhand	50390 (~6%)	Dhanbad	1.20	1.06	–
Haryana	34343 (~4%)	Faridabad	1.41	1.06	–
Chhattisgarh	17908 (~6%)	–	–	–	–
Himachal Pradesh	4317 (~1%)	–	–	–	–
Delhi	1484 (~0.2%)	Delhi	16.35	12.87	8.41

population is highest. It is located on the banks of the Yamuna River. The stretch of the Yamuna River in Delhi is highly degraded and polluted, which shows the impact of urbanization on the river (Arora and Keshari 2021). The geographical extent of the Ganga basin, covered states, and million-plus cities are shown in Fig. 6.2.

Urbanization in the Ganga river basin has increased manifold in the last five decades. Over time, many new million-plus population cities have emerged along the river and its tributaries. The existing million-plus population cities have been significantly expanded. In Fig. 6.3, different land use-land cover (LULC) maps are prepared for the Ganga river basin for different periods using various public domain resources. The LULC maps for 1985, 1995, and 2005 are prepared using the data provided by ORNL DAAC (Roy et al., 2016). The LULC map for 2021 is prepared using the data provided by ESRI (Karra et al., 2021). From Fig. 6.3, it can be seen that the urban area (shown in black color) is expanded over the period. The yellow dotted circle over the Delhi region shows a spatial expansion clearly during the last four decades. Many other black areas show the increment of the urban areas of the Ganga river basin. The LULC maps clearly show that urbanization had increased in the basin.

The basin's surface water bodies mainly comprise the Ganga river and its tributaries, lakes, ponds, and man-made reservoirs. The Ganga river, whose main stem length is 2525 km, is joined by many different order tributaries. The rivers, Yamuna, Ramganga, Kali, Gomti, Ghaghra, Gandak, Kosi, Son, and Tons are the major tributaries of the Ganga river. A line diagram in Fig. 6.4 shows the major tributaries of the Ganga river along with dam/barrages and canal systems. For other surface water bodies, the basin has 1750 ponds and lakes with a minimum of 0.030 km^2 size (Raju et al., 2015). The reduction in the level of the Ganga river water was observed as -6.03 ± 0.76 $cm.year^{-1}$ using in situ water level data during the pre-monsoon season from 1999 to 2013 (Mukherjee et al., 2018). Also, the reduction in base flow was observed at around 50% during the summer season in the last three decades and 75% compared to 1970 (Mukherjee et al., 2018).

Urbanization and surface water bodies have a close correlation as water bodies provide many goods and services to fulfill the requirements of urbanization. In goods, water, sand, boulders, food, and energy are supplied by surface water bodies. In services, recreational activities, conveyance, nutrient recycling, sediment transport, water quality alteration, and spiritual and aesthetic values are received by water bodies.

3 Impact of Urbanization on Surface Water Bodies in the Ganga River Basin

The rapid growth of population and industrialization has caused severe problems in the Ganga river basin that are discussed in the forthcoming sections.

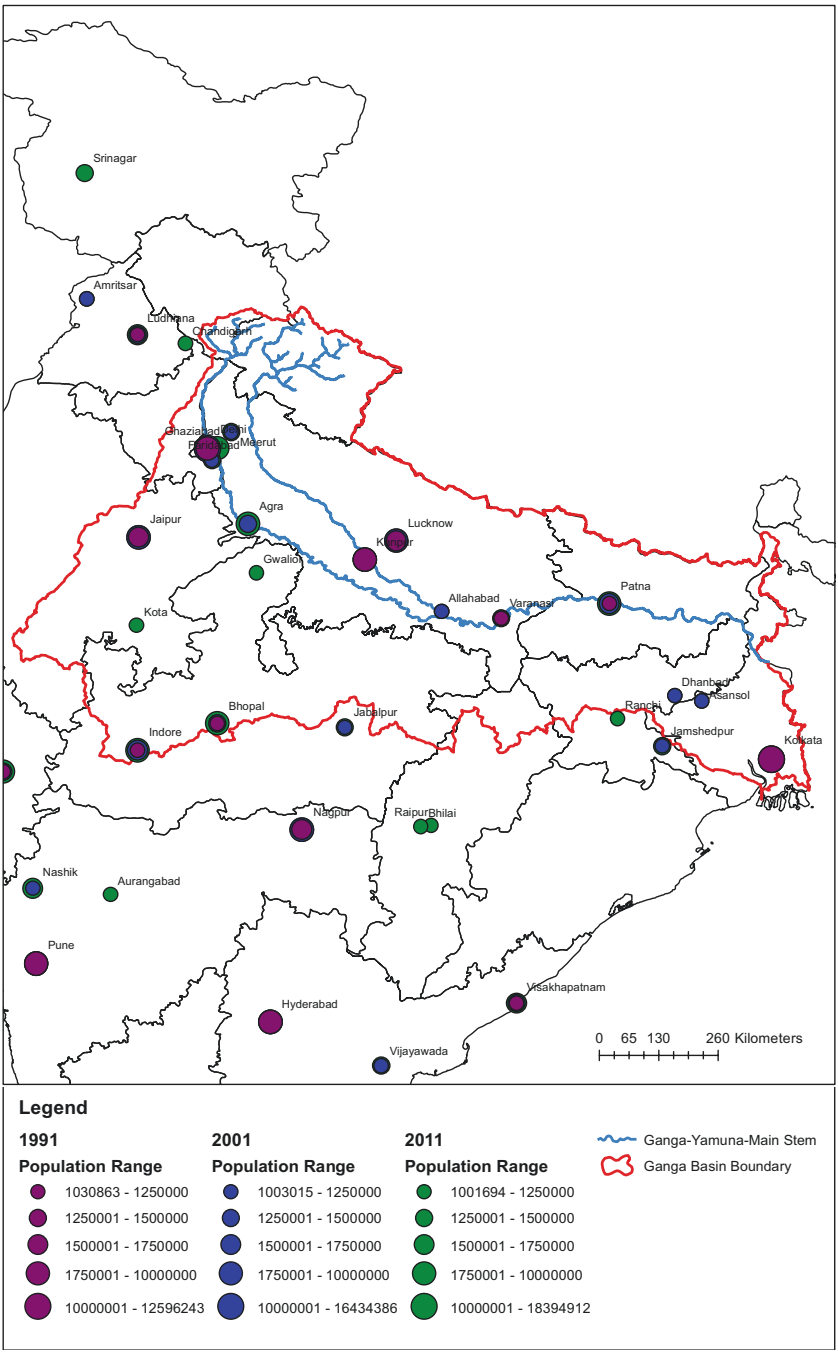

Fig. 6.2 Geographical extent of the Ganga basin, covered states, and million-plus cities

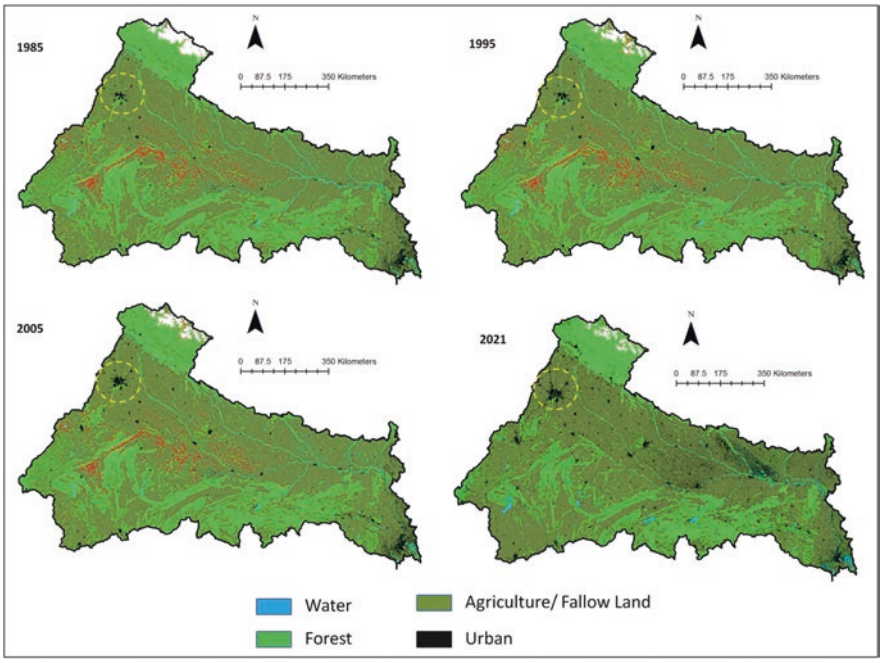

Fig. 6.3 Decadal LULC maps of the Ganga river basin

3.1 Extinction of Lakes, Ponds, and Wetlands

Urbanization has impacted the ecological, environmental, social, economic, and limnological aspects of the basin's lakes, ponds, and wetlands (Bassi et al., 2014). Many studies found the significant conversion of the lakes and ponds into built-up areas and its negative impact on the various functioning of the system. Delhi had faced the severe impact of urbanization on the extinction of these water bodies. Chaudhuri et al. (2022) pointed out that between 1970 and 2013, out of 629 lakes and wetlands, 338 were entirely extinct in the Delhi district due to urbanization, which ultimately resulted in the loss of the ecosystem. In another study on the extinction of the Delhi region's ponds and lakes, Singh et al. (2013) highlighted the impact of the extinction of lakes and ponds in the Delhi district on groundwater recharge and eco-hydrology of the study area. They found that the only reason for the extinction of these surface water bodies was rapid urbanization in the Delhi district. Similar studies have been done for water bodies of Uttar Pradesh and Bihar. The Upper Ganga stretch (Brijghat to Narora stretch of the Ganga river in Uttar Pradesh) is a type of floodplain-wetland. It has significant importance in the context of the eco-hydrology of the basin. It was declared a Ramsar site in 2005 to protect this water body from encroachment for agriculture and dumping of domestic-agriculture-industrial effluents/wastes. Sharma and Singh (2021) studied the status of wetlands and ponds in Bihar and found that many wetlands and ponds have

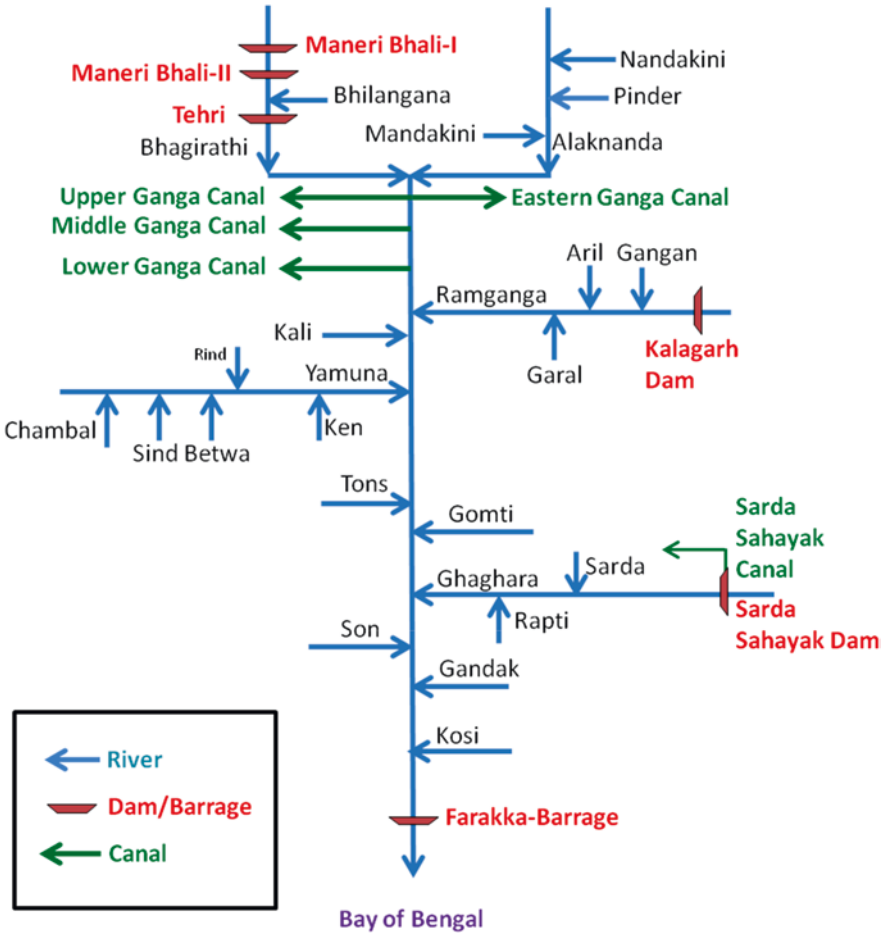

Fig. 6.4 A diagram of major tributaries, dam/barrages, and canal systems in Ganga river basin. (Jain et al., 2007)

become extinct due to urbanization. Kabartal wetland in Bihar, which was declared a Ramsar site in 2020, had faced severe encroachments by agricultural and urban activities.

3.2 Fragmentation of Rivers

The continuity of the river flow is an essential aspect of the river's biotic components. Due to urbanization, water demand for drinking and industrial purposes became high. For that, various multipurpose projects were developed on the main stem of the Ganga river and its tributaries. Tehri multipurpose project in Tehri

(Uttarakhand), commissioned in 2017, is used for supplying drinking water to Delhi and generates electricity to cater to the demand for energy for household and industrial needs. Other projects include Kalagarh multipurpose project on the Ramganga River for drinking water supply, irrigation, and electricity generation, the Upper Ganga canal project on Bhimgoda barrage (Haridwar, Uttar Pradesh) for irrigation and domestic water supply, and and the Lower Ganga canal project on Narora barrage (Narora, Uttar Pradesh) for irrigation. However, these projects have fragmented the rivers significantly (Modi et al. 2022b). This fragmentation had caused a severe impact on the biodiversity of the system. The Ganga river dolphins that are considered an indicator of the excellent health of the Ganga river are found only in a few reaches of the river, while these were found in the entire stretch of the Ganga river pre-dam era (Behera et al., 2014; Sinha & Kannan, 2014). The river's sediment transportation, self-cleaning properties, and influent-effluent mechanism have been affected severely due to the fragmentation of the river imposed by urbanization (Bawa et al., 2014; Khan et al., 2018, 2022; Simon & Joshi, 2022). S. Khan et al. (2018) modeled sediment load for the middle stretch of the Ganga river and found that present-day sediment peaks are lower than half of the simulated peaks due to dam/barrage abstraction. Khan et al. (2022) assessed the hydro-geo-chemical parameters of the Saman wetland (Uttar Pradesh) in the Ganga basin. They found that degradation in the wetland water quality and quantity was due to the loss of the influent-effluent relationship of the wetland with the Ganga river.

3.3 Degraded Water Quality

The untreated wastewater from households, industries, and other commercial activities of the cities near the river and its tributaries goes directly into the river and causes degradation in water quality. Many reaches and tributaries have now been converted into wastewater drains to carry out sewage and industrial effluents. On average, around 900 MLD of sewage reaches the main stem of the Ganga river directly or through its tributaries, responsible for 75% of the total pollution load of the river (Jain et al., 2007; Kumar & Tortajada, 2020). The river is exposed to partly treated effluents from pharmaceutical industries in the upper reaches of the Ganga river, between Rishikesh and Haridwar (Mariya et al., 2019). Also, municipal wastewater load is high in this reach due to the local population and religious visits by pilgrims. The water quality at Haridwar stretch was highly contaminated due to heavy metals, as the concentration of Cr was observed to be 43–196 $\mu g.L^{-1}$ (permissible limit is 100 $\mu g.L^{-1}$ by WHO), and Pb concentration was reported to be 108–690 $\mu g.L^{-1}$ (permissible limit is 50 $\mu g.L^{-1}$ by WHO) (Siddiqui & Pandey, 2022). These high concentrations indicate that river water quality at this stretch is no longer suitable for potable use. Further downstream, cities like Bijnor, Garhmukteshwar, Narora, and Kannauj do not add much pollution load to the river due to the absence of industrial clusters. This reach contributes base flow of the river during the non-monsoon season (Jain et al., 2007). Downstream of Kannauj city, the

river water quality is inferior due to the industrial clusters and domestic wastewater in Kanpur city. The main stem of the Ganga river between Kanpur city and Buxar city is found to be significantly degraded due to industrial and domestic waste from the urban population and industries (Shukla et al., 2018). The leather industries in Kanpur are the main contributor of chromium and other chemicals to the river (Khwaja et al., 2001). In this stretch, the concentration of trace metals found in river water was very high, ranging from a few $\mu g.L^{-1}$ to 27.596 $mg.L^{-1}$ (Nazir et al., 2022). The wide range of heavy metals exceeding their permissible limits in the river water and the sediment deposits indicates water quality degradation (Bhattacharjee et al., 2022). A high level of pH range was reported near the Kanpur city stretch, indicating the alkaline river water due to the discharge of untreated wastewater (Nazir et al., 2022). In Allahabad city, the pollution load is mainly contributed by domestic wastewater due to its dense population (Chakarvorty et al., 2015). The range of heavy metals found at this stretch varies from a few $\mu g.L^{-1}$ to 11.9 mg of $Fe.L^{-1}$ which exceeded the permissible limit, indicating that river water is not suitable for domestic use and therefore needs a good treatment before supply to the communities. After that, in Varanasi city, a similar kind of situation is being faced by the river. Varuna and Assi are two tributaries, mainly wastewater drains that carry sewage from the city and dump it into the Ganga river. Another factor that causes river pollution is having the cremation ghats at the river banks in the stretch of Varanasi city. It is reported that around 40 thousand dead bodies are cremated at these ghats every day, and their ashes or remains (partially burnt or unburnt corpses) are dumped into the river (Arnold, 2016). The river water quality at the different ghats in Varanasi stretch was heavily polluted due to the heavy metals. The heavy metal concentration varies with very high concentrations of Zn (15.32 $mg.L^{-1}$), Cr (1090 $\mu g.L^{-1}$) Pb (240 $\mu g.L^{-1}$), and Cu (1700–2000 $\mu g.L^{-1}$) that indicates degraded situation of the river water due to the anthropogenic activities (Kumari et al., 2021). After that, in Bihar, cities like Patna contributes pollution load to the river through fertilizer industries, oil refineries, and domestic sewage. In West Bengal, Kolkata city also contributes to pollution through domestic sewage and numerous industrial effluents.

Apart from the main stem of the Ganga river, a major tributary, the Yamuna River is also facing severe challenges in terms of water quality and quantity due to urbanization (Misra, 2011; Sarker et al., 2021). The main cause of pollution load is untreated domestic sewage and industrial effluents from households and industries of the cities situated at the river banks. Major towns in Uttar Pradesh (Saharanpur, Muzaffarnagar, Ghaziabad, Noida, Vrindavan, Mathura, Agra, and Etawah) and Haryana (Yamuna Nagar, Karnal, Panipat, Sonipat, Gurgaon, Faridabad, Chhachhrauli, Indri, Radaur, Gharaunda, Gohana, and Palwal) are responsible for the pollution load in the Yamuna River (Singh et al., 2021b). Alone, Delhi state contributes a considerable amount of pollution load in the river due to the densely populated situation. The area nearby Delhi has expanded so much that all agricultural lands have been converted into colonies, shops, and industries. It affects the river in two ways – one is the domestic pollution load increment, and the second is the wastewater used earlier in agricultural irrigation, which is now dumped into the

river without any treatment. Also, the river's floodplains are encroached by illegal human settlements, which have affected the local hydrology of the river system. Other than rivers, the surface water bodies like lakes, ponds, and wetlands are highly polluted due to changes or alterations in the natural landscapes due to urbanization. The recreational activities and waste discharge have increased manifolds that have caused eutrophication, sediment deposition, and degraded water quality. Also, these water bodies are being used as waste dumping sites which have degraded water quality mainly due to eutrophication, other physiochemical processes, and water temperature rise. Various studies have also reported the rise in the temperature of surface water bodies like rivers, lakes, and ponds due to the mixing of industrial effluent and thermal power projects (R. Sharma et al., 2021).

3.4 Decreased Water Quantity

Urbanization has increased the demand for water for domestic and industrial usage. Water purifiers, washing machines, dishwashers, and flushing systems in toilets require more water than actual necessity. So, in comparison to rural living, the urban lifestyle demands more water. Also, industries like tanneries, pulp-paper, distilleries, diaries, etc. are water-based industries that consume ample amounts of water to get the ultimate products and release large amounts of effluent (Singh et al., 2021a; Sonawane & Murthy, 2022). The water supply is made by groundwater pumping and canal systems from dams/barrages. These dams/barrages are responsible for lowering water volume in the river downstream of the abstraction. Sometimes no water is released through these abstractions due to the heavy demand for water for domestic-agricultural-industrial usage. In the Ramganga basin (a major sub-basin of the Ganga river basin), surface-subsurface water storage was reduced by ~0.2 MCM/km^2 from 1982–2013 (Modi et al., 2021). The reduced flow in the river was found due to upstream storage in the river. So urbanization is responsible for decreasing water volume downstream in rivers, lakes, ponds, and wetlands.

3.5 Increased Sediment Load

Vegetation cover helps protect against soil erosion through surface runoff. During the process of urbanization, vegetation cover gets converted into a wide variety of built-up areas with two implications, increased surface runoff, and the second decreased groundwater recharge. With increased surface runoff, soil erosion increases and causes more sediment deposition in lakes, ponds, wetlands, rivers, or water depressions. Ultimately, it reduces the storage capacity of lakes due to sediment deposits. Due to the lack of a proper waste management system in the city, dumping of waste also causes a reduction in the storage capacity of these water bodies. For example, Saha et al. (2010) studied the ponds of Brij (near Mathura

district in Uttar Pradesh) for silting problems. They found that the rapid urbanization caused a loss of vegetation cover in the study area. Due to that, the erosion of sand was high and deposited in the ponds through surface runoff in the rainy season.

3.6 Disturbed Hydrology of the Region

Urbanization has impacted the basin's hydrology by changing the land use-land cover (LULC) of the basin. For any river basin, runoff volume, flood peak, and groundwater recharge (including base flow) depend on the amount of perviousness of the basin. Urbanization is responsible for increasing the basin's imperviousness as the forest-barren-shrub land cover is converted into built-up areas. Consequently, it negatively impacted the soil integrity, exchange of nutrients, infiltration rate, surface roughness, leaf area index, rooting depth of vegetation cover, and albedo. These changes ultimately affect groundwater recharge, evaporation, evapotranspiration, and other water balance components. Urbanization also affects the microclimate of a specific region if the evapotranspiration-rainfall relationship is highly correlated. LULC changes due to urbanization had also affected the variation in the flood frequency due to a shift in the curve number of the surface. Many researchers have also studied LULC changes and their impact on base flow. Many researchers have also studied LULC change and soil erosion. Small ponds were/are being converted into built-up areas, which have wholly vanished the local hydrology of the surface water bodies and negatively impacted the pond's local ecosystem. Also, these water bodies have been used as waste dumping sites, reducing water storage capacity. For example, Anand et al. (2018b) assessed the impact of anthropogenic activities impact on the hydrology of the Ganga river basin. Through simulated results, they found that in the present situation, annual water yield had lower down by ~35% in the Ganga basin in comparison to the virgin condition (the condition with no anthropogenic activities). Further they pointed out that in the upper reaches of the basin, stream flow had increased while it had been reduced in the lower reaches and tributaries. They also found the availability of water in water resources had decreased significantly in the basin. The change in LULC, e.g., conversion of small ponds into built-up areas, has changed the basin's hydrology and negatively impacted the basin's local ecosystem.

4 Discussion and Conclusion

Population growth is a natural process that can be managed up to a certain level if the legislation is implanted strictly by the government and with the support of communities. Based on that, urbanization can also be handled up to a certain level in the Ganga river basin. So, to handle the problematic situation, three approaches can be taken: stabilizing the population, strict implementation of environmental protection

law, and raising and protecting the existing water resource. These things cannot be achieved totally, as every approach has restrictions. So, by maintaining an equilibrium approach, surface water bodies can be managed sustainably with urbanization development in the Ganga river watershed. It is the only solution for mitigating the problems aroused by urbanization to the river Ganga and different surface water bodies.

India's economy has changed from an agricultural-based economy to a service-based economy over the last few decades. So, water-related policies have shifted from surface water development to surface water management. In surface water management, the main focus has been on urban river management, as urbanization significantly impacted surface water bodies. It is now time to manage surface water bodies integrated with urban planning. So following provisions can be adopted for surface water management:

- Provision for sewerage systems and effluent treatment can help remain surface water bodies unpolluted. The mismanagement of domestic and industrial waste was frequently reported in the entire Ganga river stretch.
- Mapping surface water bodies and their geotagging is also imperative to conserve surface water bodies from exploitation.
- The provision of environmental flows from diversion structures is also a sustainable solution to managing water bodies and urban development.
- Hydro-geological studies for surface water management can also prepare urban river management plans to effectively, efficiently, and sustainably manage the surface water bodies.
- The implementation and monitoring of river water quality should be displayed the water quality parameter to the nearby localities so that the local people are aware of the impacts of wastewater discharge in the river. It will help to reduce water demand as treated water can be utilized for various purposes in domestic industries, the agricultural sector, the horticulture sector, and other commercial activities.
- Frequent water quality monitoring at the specific locations across the stretch must be implanted, and data should be displayed. It will increase their concerns about the water contamination-related issue, which may lead to the cooperation of local communities to protect the water bodies and maintain the water quality of surface water bodies.
- Increasing the awareness about rainwater management and motivating the local communities to implement the rainwater harvesting system in their house, which may lead to reducing urban flooding, degradation of water quality of surface water bodies, and reducing the stress on water resources.

Overall, the present study concludes that urbanization is critical for surface water bodies and should be managed sustainably.

Acknowledgments Nothing to declare.

Declarations No Conflict of interest to declare.

References

Anand, J., Gosain, A. K., & Khosa, R. (2018a). Prediction of land use changes based on Land Change Modeler and attribution of changes in the water balance of Ganga basin to land use change using the SWAT model. *Science of the Total Environment, 644*, 503–519.

Anand, J., Gosain, A. K., Khosa, R., & Srinivasan, R. (2018b). Regional scale hydrologic modeling for prediction of water balance, analysis of trends in streamflow and variations in streamflow: The case study of the Ganga River basin. *Journal of Hydrology: Regional Studies, 16*, 32–53. https://doi.org/10.1016/j.ejrh.2018.02.007

Arnold, D. (2016). Burning issues: Cremation and incineration in modern India. *NTM Zeitschrift für Geschichte der Wissenschaften, Technik und Medizin, 24*(4), 393–419.

Arora, S., & Keshari, A. K. (2021). Pattern recognition of water quality variance in Yamuna River (India) using hierarchical agglomerative cluster and principal component analyses. *Environmental Monitoring and Assessment, 193*(8), 1–18.

Bassi, N., Kumar, M. D., Sharma, A., & Pardha-Saradhi, P. (2014). Status of wetlands in India: A review of extent, ecosystem benefits, threats and management strategies. *Journal of Hydrology: Regional Studies, 2*, 1–19.

Bawa, N., Jain, V., Shekhar, S., Kumar, N., & Jyani, V. (2014). Controls on morphological variability and role of stream power distribution pattern, Yamuna River, western India. *Tropical rivers of South and South-east Asia: Landscape evolution, morphodynamics and hazards, 227*, 60–72. https://doi.org/10.1016/j.geomorph.2014.05.016

Behera, S. K., Singh, H., & Sagar, V. (2014). Indicator species (Gharial and Dolphin) of riverine ecosystem: An exploratory of River Ganga. In *Our National River Ganga* (pp. 121–141). Springer.

Bhagat, C., Mohapatra, P. K., & Kumar, M. (2021a). Unveiling the extent of salinization to delineate the potential submarine groundwater discharge zones along the North-western coast of India. *Marine Pollution Bulletin, 172*, 112773. https://doi.org/10.1016/j.marpolbul.2021.112773

Bhagat, C., Puri, M., Mohapatra, P. K., & Kumar, M. (2021b). Imprints of seawater intrusion on groundwater quality and evolution in the coastal districts of south Gujarat, India. *Case Studies in Chemical and Environmental Engineering, 3*, 100101. https://doi.org/10.1016/j.cscee.2021.100101

Bhattacharjee, R., Gupta, A., Das, N., Agnihotri, A. K., Ohri, A., & Gaur, S. (2022). Analysis of algal bloom intensification in mid-Ganga river, India, using satellite data and neural network techniques. *Environmental Monitoring and Assessment, 194*(8), 1–20.

Chakarvorty, M., Dwivedi, A. K., Shukla, A. D., Kumar, S., Niyogi, A., Usmani, M., & Pati, J. K. (2015). Geochemistry and magnetic measurements of suspended sediment in urban sewage water vis-à-vis quantification of heavy metal pollution in Ganga and Yamuna Rivers, India. *Environmental Monitoring and Assessment, 187*(9), 1–17.

Chaudhuri, A. S., Gaur, N., Rana, P., Pallavi, & Verma, P. (2022). Ecohydrological perspective for environmental degradation of Lakes and Wetlands in Delhi. In P. K. Rai, V. N. Mishra, & P. Singh (Eds.), *Geospatial technology for landscape and environmental management: Sustainable assessment and planning* (pp. 143–163). Springer. https://doi.org/10.1007/978-981-16-7373-3_7

Cohen, B. (2006). Urbanization in developing countries: Current trends, future projections, and key challenges for sustainability. *Technology in Society, 28*(1–2), 63–80.

Duttagupta, S., Bhanja, S. N., Dutta, A., Sarkar, S., Chakraborty, M., Ghosh, A., et al. (2021). Impact of Covid-19 lockdown on availability of drinking water in the arsenic-affected Ganges River Basin. *International Journal of Environmental Research and Public Health, 18*(6), 2832.

Fox, S. (2012). Urbanization as a global historical process: Theory and evidence from sub-Saharan Africa. *Population and Development Review, 38*(2), 285–310.

Gu, D., Andreev, K., & Dupre, M. E. (2021). Major trends in population growth around the world. *China CDC Weekly, 3*(28), 604.

Jain, S. K., Agarwal, P. K., & Singh, V. P. (2007). *Hydrology and water resources of India* (Vol. 57). Springer.

Joshi, S. (2021). Key determinants of urbanization in India: Evidence from State-Level data. In *Urban growth and environmental issues in India* (pp. 55–67). Springer.

Karra, K., Kontgis, C., Statman-Weil, Z., Mazzariello, J., Mathis, M., & Brumby, S. (2021). Global land use/land cover with Sentinel-2 and deep learning. In *IGARSS 2021–2021*. IEEE.

Khan, S., Sinha, R., Whitehead, P., Sarkar, S., Jin, L., & Futter, M. N. (2018). Flows and sediment dynamics in the Ganga River under present and future climate scenarios. *Hydrological Sciences Journal, 63*(5), 763–782. https://doi.org/10.1080/02626667.2018.1447113

Khan, I., Umar, R., & Izhar, S. (2022). Hydrogeochemical and health risk assessment in and around a Ramsar-designated wetland, the Ganges River Basin, India: Implications for natural and human interactions. *Environmental Monitoring and Assessment, 194*(7), 1–24.

Khwaja, A., Singh, R., & Tandon, S. (2001). Monitoring of Ganga water and sediments vis-a-vis tannery pollution at Kanpur (India): A case study. *Environmental Monitoring and Assessment, 68*(1), 19–35.

Kumar, M. D., & Tortajada, C. (2020). *Assessing wastewater management in India*. Springer.

Kumar, M., Deka, J. P., & Kumari, O. (2020). Development of water resilience strategies in the context of climate change, and rapid urbanization: A discussion on vulnerability mitigation. *Groundwater for Sustainable Development, 10*, 100308.

Kumari, A., Sinha, S. K., Rani, N., & Sinha, R. K. (2021). Assessment of heavy metal pollution in water, sediment, and fish of the river Ganga at Varanasi, India. *Arabian Journal of Geosciences, 14*(22), 1–11.

Mani, N., Wajih, S. A., Gupta, A. K., Narain, V., & Prakash, A. (2021). *Peri-urban ecosystems and urban resilience: Knowledge compendium of case studies*. IDRC.

Mariya, A., Kumar, C., Masood, M., & Kumar, N. (2019). The pristine nature of river Ganges: Its qualitative deterioration and suggestive restoration strategies. *Environmental Monitoring and Assessment, 191*(9), 1–33.

Misra, A. K. (2011). Impact of urbanization on the hydrology of Ganga Basin (India). *Water Resources Management, 25*(2), 705–719.

Modi, A., & Tare, V. (2022). Baseflow index assessment for agriculture-industry led Ramganga river basin. *Journal of Applied Water Engineering and Research,* 1–15. https://doi.org/10.1080/23249676.2022.2132306

Modi, A., Tare, V., & Chaudhuri, C. (2021). Usage of long-term river discharge data in water balance model for assessment of trends in basin storages. *Modeling Earth Systems and Environment, 7, 953–966*. https://doi.org/10.1007/s40808-020-00941-4

Modi, A., Kapoor, V., & Tare, V. (2022a). River space: A hydro-bio-geomorphic framework for sustainable river-floodplain management. *Science of the Total Environment, 812,* 151470. https://doi.org/10.1016/j.scitotenv.2021.151470

Modi, A., Tare, V., & Sharma, D. (2022b). Hydro-energy potential assessment in the context of E-flows for Himalayan upland rivers. *Water, Air, & Soil Pollution, 233,* 304. https://doi.org/10.1007/s11270-022-05788-2

Mukherjee, A., Bhanja, S. N., & Wada, Y. (2018). Groundwater depletion causing reduction of baseflow triggering Ganges river summer drying. *Scientific Reports, 8*(1), 12049. https://doi.org/10.1038/s41598-018-30246-7

Nazir, A., Khan, M. A., & Ghosh, P. (2022). Assessment of variations in metal concentrations of the Ganges River water by using multivariate statistical techniques. *Limnologica, 95*, 125989.

Raju, K. P., Sarkar, S., & Pandey, M. K. (2015). Indus and Ganga river basins in India: Surface water potentials. *Water resources: Rejuvenation of surface water resources of India: Potential, problems and prospects* (pp. 43–53).

Rijesh, N., Mohammed, F. C., Susan, C., & Sruthi, K. V. (2022). Sustainable spatial planning for the Rural–Urban continuum settlements of Kerala, India. In *Sustainable urbanism in developing countries* (pp. 117–141). CRC Press.

Routray, J. K. (2022). Water resource development and sustainable initiatives of India: Present and future. In *Climate, environment and disaster in developing countries* (pp. 173–187). Springer.

Roy, P. S., Meiyappan, P., Joshi, P. K., Kale, M. P., Srivastav, V. K., Srivasatava, S. K., et al. (2016). *Decadal land use and land cover classifications across India, 1985, 1995, 2005*. https://doi.org/10.3334/ORNLDAAC/1336.

Saha, A., Kansal, M., Mishra, G., & Gupta, R. (2010). Restoration of the traditional small water bodies in Braj. *South Asian Journal of Tourism and Heritage, 3*(2), 19–29.

Sameer, M. A., Juzhong, Z., & Miao, Y. M. (2018). Approaching the origins of rice in China and its spread towards Indus valley civilization (Pakistan, India): An Archaeobotanical Perspective. *Asian Journal of Research in Crop Science, 2*(3), 1–14.

Sarker, B., Keya, K. N., Mahir, F. I., Nahiun, K. M., Shahida, S., & Khan, R. A. (2021). Surface and ground water pollution: Causes and effects of urbanization and industrialization in South Asia. *Scientific Review, 7*(3), 32–41.

Shamsudduha, M., & Panda, D. K. (2019). Spatio-temporal changes in terrestrial water storage in the Himalayan river basins and risks to water security in the region: A review. *International Journal of Disaster Risk Reduction, 35*, 101068.

Sharma, S., & Singh, P. (2021). *Wetlands conservation: Current challenges and future strategies*. Wiley. https://books.google.co.in/books?id=RVBDEAAAQBAJ

Sharma, R., Kumar, R., Sharma, D. K., Sarkar, M., Mishra, B. K., Puri, V., et al. (2021). Water pollution examination through quality analysis of different rivers: A case study in India. *Environment, Development and Sustainability, 24*, 1–22.

Shukla, A. K., Ojha, C. S. P., Mijic, A., Buytaert, W., Pathak, S., Garg, R. D., & Shukla, S. (2018). Population growth, land use and land cover transformations, and water quality nexus in the Upper Ganga River basin. *Hydrology and Earth System Sciences, 22*(9), 4745–4770.

Shukla, A. K., Ojha, C. S. P., Garg, R. D., Shukla, S., & Pal, L. (2020). Influence of spatial urbanization on hydrological components of the Upper Ganga River Basin, India. *Journal of Hazardous, Toxic, and Radioactive Waste, 24*(4), 04020028.

Siddiqui, E., & Pandey, J. (2022). Atmospheric deposition: An important determinant of nutrients and heavy metal levels in urban surface runoff reaching to the Ganga River. *Archives of Environmental Contamination and Toxicology, 82*(2), 191–205.

Simon, M., & Joshi, H. (2022). Story of the Ganga River: Its pollution and Rejuvenation. In A. Mukherjee (Ed.), *Riverine systems: Understanding the hydrological, hydrosocial and hydro-heritage dynamics* (pp. 21–55). Springer. https://doi.org/10.1007/978-3-030-87067-6_2

Singh, R. (2019). Early description of numerical and measuring system in Indus Valley Civilization. *Journal of Applied Social Science, 6*, 1586–1589.

Singh, R. B., Gahlot, S., & Singh, A. (2013). Ecohydrological perspectives of declining water sources and quality in traditional water bodies in Delhi. *Proceedings of the H, 4*, 361–368.

Singh, P., Itankar, N., & Patil, Y. (2021a). Biomanagement of hexavalent chromium: Current trends and promising perspectives. *Journal of Environmental Management, 279*, 111547.

Singh, G., Patel, N., Jindal, T., & Ranjan, M. R. (2021b). Heavy metal contamination in soils and crops irrigated by Kali River in Uttar Pradesh, India. *Bulletin of Environmental Contamination and Toxicology, 107*(5), 931–937.

Singh, S., Singh, V., & Kumar, S. (2022). Assessment of water resources in development of Rajasthan. In *Wastewater assessment, treatment, reuse and development in India* (pp. 239–260). Springer.

Sinha, R. K., & Kannan, K. (2014). Ganges River dolphin: An overview of biology, ecology, and conservation status in India. *Ambio, 43*(8), 1029–1046.

Sonawane, A. V., & Murthy, Z. (2022). Synthesis and characterization of ZIF-8-based PVDF mixed matrix membranes and application to treat pulp and paper industry wastewater using a membrane bioreactor. *Environmental Science: Water Research & Technology, 8*(4), 881–896.

Tyagi, N., & Sahoo, S. (2022). Assessing the status of changing regimes of water bodies in Gorakhpur District, Uttar Pradesh, India. *Environmental Monitoring and Assessment, 194*(2), 1–21.

Chapter 7
Urban Water Scarcity: A Global Challenge and Impending Solutions

Paulami Sahu and Chitrangada Debsarma

Abstract Water of good quality and quantity has become a gradually vital subject, facing shortages in numerous urban areas around the globe. Population explosion, hasty urbanization, economic and industrial developments, and climate change led to growing pressure on water resources. Urban citizens around the globe are dealing with water shortages, which is projected to upsurge from 933 million in 2016 to 2.373 billion by the year 2050. In India, the water-scarce urban population of 153 million in 2016 is projected to increase up to 422 million in 2050. Urban water consumption is exceeding the water supply capacity, creating prominent water shortages in numerous cities of underdeveloped, developed, and developing countries. Several cities, especially in the semiarid and arid areas, have already exceeded their local water supply capacities. The entire groundwater sources are being tapped and exploited in an unsustainable way. The number of large cities exposed to water scarcity is projected to increase from 193 (in 2016) to 284 (in 2050), including 10–20 megacities by 2050. Moreover, an increased number of cities will be relied on remote water resources, inter-basin water transfers, domestic virtual water trade, seawater desalination, etc., to cope with the rising demands for water. Presently many urban areas share a similar aim to deal with valuable water resources in a sustainable manner. Resilient building, nature-based solutions, including green infrastructures, aquifer recharge, stormwater management, reducing nonrevenue water, gray water usage, planning of smart cities, etc., should be implemented for sustainable urban water management.

Keywords Groundwater · Nature-based solutions · Population growth · Urban water scarcity · Water quality

P. Sahu (✉) · C. Debsarma
School of Environment and Sustainable Development, Central University of Gujarat, Gandhinagar, India
e-mail: paulami_sahu@cug.ac.in

P. Thambidurai, A. K. Dikshit (eds.), *Impacts of Urbanization on Hydrological Systems in India*, https://doi.org/10.1007/978-3-031-21618-3_7

1 Introduction

The expeditious urbanization, population explosion, and lifestyle change around the globe increase per-capita urban water consumption and physical water insufficiency (Ray & Shaw, 2016). Over 50% of inhabitants reside in urban areas, and the urban water utilization for domestic and industrial purposes has increased due to the high rate of urbanization (Gleick, 2003; Jury & Vaux, 2005). Figure 7.1 shows the region-wise urban population distribution (in millions) worldwide. It is projected that about 95% of the urban development will happen in the less developed nations, and the worse effect will be on the Asian ones. The number of inhabitants of metropolis around the globe has expanded from 29.6% (0.8 billion) to 56.2% (4.4 billion) from 1950 to 2020. The increasing trend of the population is predicted to hit 68.4% (6.7 billion) by 2050 (He et al., 2021). The urban areas around the world, including secondary towns and cities, are experiencing severe water scarcity, with one in four cities being called "water-stressed" (Zero, 2021). Watkins (2006) has described that one-fifth of the inhabitants around the globe reside in areas with physical water shortage where insufficient water resources are available to meet the entire water requirement of human beings and the ecosystem. Deteriorating local environmental conditions and surface or subsurface water resources are the common indications of physical water shortage. Funding deficiency for technology and infrastructures to drain water from surface water bodies, aquifers, or other resources is denoted as economic water shortage, which is faced by one more quarter of residents of the globe.

Economic water shortages are the inadequacy of local infrastructural facilities for dependable and good-quality drinking water that makes the local people fetch

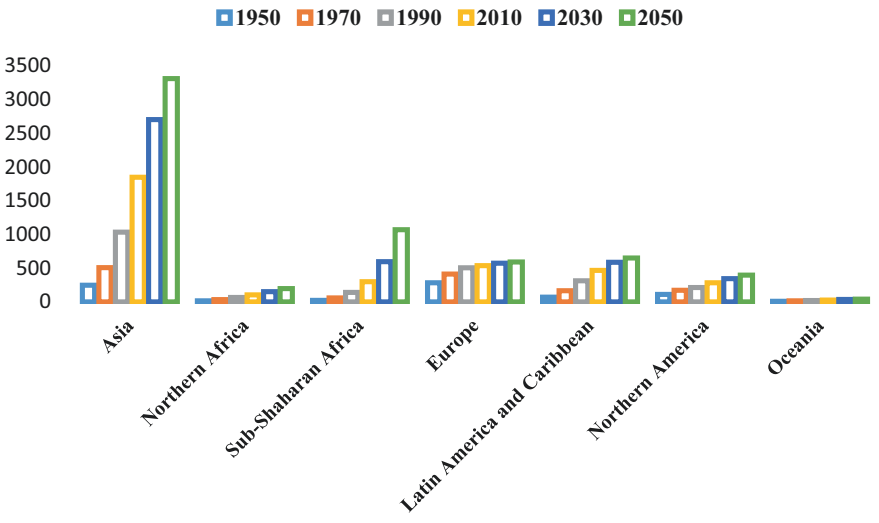

Fig. 7.1 Region-wise population distribution in millions. (Branch 2012)

water from a great distance (Ray & Shaw, 2016). Briefing (1998) reported that higher anthropogenic consumption, deprived management, and increasing pollution make water resources more vulnerable and cause global water scarcity. This shortage is aggravated by climate change and even affects the third-world metropolises' water scenario. The global and regional climate alterations interfere with the hydrological cycle of that area, alter rainfall pattern and amount, and sometimes causes short-term droughts (Easterling et al., 2000; Tudhope et al., 2001; Royer et al., 2002; Arnell, 2004; Giorgi & Bi, 2005; Thomson et al., 2005). Rapid urbanization, population explosions, enhanced per-person water demand, poor water management, pollution, and climate change are threatening the quality as well as quantity of available natural freshwater. Urban areas are more vulnerable to this situation as cities have highly compacted and condensed populations. To meet the water need of the residents and to maintain the economy, cities require dependable, consistent, and good-quality water resources. So, the present chapter focuses on the global situation of urban water scarcity, its causes, and sustainable urban water solutions.

1.1 Current and Projected Urban Water Scarcity

In 2016, around the world, about 32.5% urban population lived in areas with water scarcity. Out of which, 20% of residents face seasonal water scarcity (when per-capita monthly water availability is <100 L per day of the year), and the rest, 12.5%, are experiencing perennial water scarcity (when per-capita surface and groundwater consumption is <100 L per day within that urban extent). It is reported that cities and towns in India and China have the maximum number of urban residents experiencing water scarcity. Out of 30 megacities that carry more than 10 million residents, 9 are experiencing water insufficiency. Six of them (Delhi, Bangalore, Lahore, Los Angeles, Moscow, and Beijing) are facing perennial water shortages, and rest three of them (Karachi, Mexico City, and Istanbul) are suffering from seasonal water deficiencies (He et al., 2021). The quantity of water-scarce urban citizens is hastily snowballing every year. By the year 2050, the number is projected to touch about 2.065 billion (on average) residents, which is about 121.3% more than that of 2016. Almost 50% of the mega towns and cities around the world are expected to experience water shortages by the year 2050. Globally the perennial and seasonal water shortages are expected to experience 840 million and 1.23 billion people (on average), respectively, by the year 2050. India's entire water-scarce citizens are 26.7% of the total urban populations around the globe facing water deficiency. It is projected that in India, the number of water-scarce urban residents is much larger than the other nations and the number will upsurge from 222 million to 550 million by the year 2050 (He et al., 2021). Case studies of urban water scarcity reported from different regions of the world are summarized in Table 7.1.

Table 7.1 Case studies of urban water scarcity around the world

Water-scarce cities	Situation description	Reason of scarcity	Management measures	References
Cape Town, 2018	Severe drought situation over 3 consecutive years	1. Lower rainfall than average, water levels in dams gradually dropped, finally up to 20% capacity in 2018	1. To avoid reservoirs running empty and prompting widespread efforts to reduce water use 2. Encouraging the use of water efficiently 3. Public awareness campaigns 4. Leak repairing initiatives 5. Implementation of restriction levels 6. Finding substitute water resources 7. Installation of metering systems 8. Application of tax or tariff systems for a great number of water users to pay as they consume a large quantity of water	Zero (2021)
La Paz, Bolivia, 2016	An emergency drought situation (associated with influences from El Niño) throughout Bolivia for 25 years was declared by the government	1. Climate change and high temperatures are the reasons for the melting of glaciers, which are the chief water sources of that region 2. Poor water management and infrastructures include leaking pipes, illegal connections, inadequate investment in new infrastructures for water sources and energy 3. Mining activity limits water resources	1. Change in a new water distribution system 2. Introduction of a strict water rationing system 3. Launching numerous infrastructural projects to improve water supply capacity, including newer dams and reservoirs to capture more rainwater	Zero (2021)

(continued)

Table 7.1 (continued)

Water-scarce cities	Situation description	Reason of scarcity	Management measures	References
Amman, Jordon	Reported fifth most water-stressed country in the world Experiencing severe water scarcity	1. Leakages in the water distribution system 2. Illegal network connections 3. Illegal boreholes	1. Wastewater reuse 2. Wastewater blended with fresh water and used in irrigation 3. Replacement of the leakage systems	Zero (2021)
City of Melbourne, Australia, 1997–2009	"Millennium drought" situation arose	1. Lower average rainfall for over a decade	1. Water-saving actions such as campaigns for behavioral change and water use awareness 2. Saving on per-capita domestic water use 3. Publishing data on the water level in dams 4. Discounts on water-saving goods 5. Water restrictions 6. Rating to reward water saving 7. Requirements for industrial water audits 8. Target for per-capita water usage of 155 L per day (target 155)	Zero (2021)
Shandong, China, 2000–2010	661 cities in China were experiencing water deficiency, out of which 110 cities are facing severe conditions Widespread spreading of groundwater depression cone Natural springs dried up	1. Population increase 2. Industrial activities 3. Rapid urbanization	1. Scientific urban planning 2. Water-saving infrastructures to reduce industrial water use 3. Sewage purification 4. Seawater desalination 5. Inter-basin projects: *Water diversion project from Yellow River to Qingdao*	Wu and Tan (2012)

(continued)

Table 7.1 (continued)

Water-scarce cities	Situation description	Reason of scarcity	Management measures	References
Singapore	Inadequate water convenience against water demand	1. High population density	1. Extensive funding for research and technology to conserve, treat, recycle, and increase water supplying capacity 2. "Four National Taps" program such as: a. Rainwater harvesting, green solutions, and stormwater managing b. Reuse of water ("NEWater" program) c. Desalinization of seawater d. Import water from the Johor River of Malaysia	Zero (2021)
Chennai, India, 2019	1. Availability of water was nil during the summer of 2019 2. Heat waves 3. Severe drought 4. Public toilets were closed	1. Unsustainable groundwater extraction 2. Poor water management	1. Short-term solutions a. Investment in desalination plants b. Transport water from distant water sources 2. Long-term solutions a. Improve technical capacities b. Continuous monitoring of water resources c. Efficient use of water d. Behavioral changes	Zero (2021)

(continued)

Table 7.1 (continued)

Water-scarce cities	Situation description	Reason of scarcity	Management measures	References
Delhi, India	1. Poor quality and inadequate water supply 2. Urban poor are worse affected	1. Mismanagement of the supplying authority 2. Groundwater level was dropping owing to increased exploitation by private wells	1. Supply-based partnerships between government and private sectors 2. Installing advanced water treatment plants 3. Repairing leakages	Janakarajan et al. (2006)
Kolkata, India	Issue of land subsidence	1. Rapid urbanization 2.Overexploitation of groundwater	1. Finding alternate resources 2. Rainwater harvesting 3. Artificial recharge	Sahu and Sikdar (2011)

2 Causes for Alteration in Urban Water Environment

Water scarcity is both a natural and anthropogenic phenomenon. The expansion of urbanization generates the growth of the urban population and a per-capita increase in urban water consumption. The key factors that cause urban water scarcity are as follows.

2.1 Population Growth

Overcrowding in urban cities is putting tremendous pressure on the water supply. An increase in life expectancy and other factors are causing the urban population to increase. Owing to several socio-economic reasons, there are influxes of rural inhabitants toward urban centers. As the population migration from rural to urban continues, water consumption is also rising along with a consequential extra load on freshwater resources. Hasty urbanization resulted in an increase in poorly planned infrastructures and paved areas, which decreased the soil's natural drainage, reduced recharge areas and reservoir capacity, and led to local urban flooding (Chakraborti et al., 2019).

2.2 Over Consumption

Increased groundwater extraction more than the recharge of the same by the rainfall causes aquifer water level depletion, and it is very prominent in several areas. This situation leads to an increase in concentrations of salts, heavy metals, TDS, and various other chemicals in groundwater. For instance, according to Central

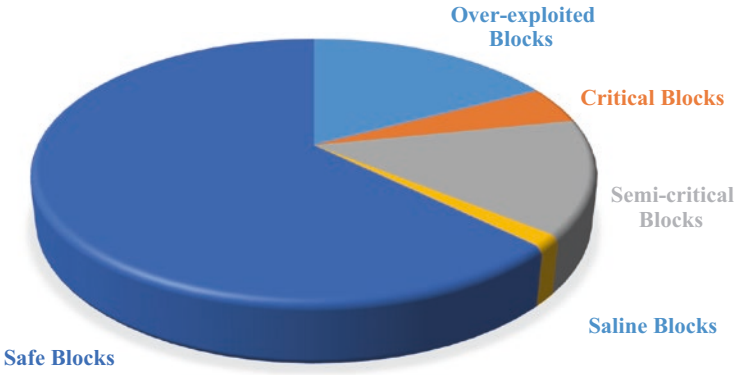

Fig. 7.2 Categorization of Indian Blocks according to their groundwater conditions (CGWB)

Groundwater Board (CGWB, 2019), about 29% of India's blocks necessarily require better groundwater basin management. Figure 7.2 shows that, out of 6881 blocks/talukas in India, 4310 are safe, 100 are saline, 972 are semi-critical, and 313 are critical in condition, whereas 1186 blocks are overexploited (CGWB, 2019).

2.3 Water Pollution

Population increase, industrial activities, and urbanization together create stress on local surface and subsurface water quantity and quality. Several point sources like untreated industrial wastes and sewage are polluting the rivers, local streams, and other surface water bodies, causing serious health issues. UNICEF (2013) reported that inappropriate sanitation and underprivileged hygiene practices cause diarrhea, pneumonia, and other waterborne diseases, which are the reasons for one-third of all deaths of children (under the age of five) in India. Oil spills and landfill leakages are seeped underground and contaminate groundwater. Deforestation and the increase of concreted surfaces lead to alteration of precipitation along with higher temperatures in urban areas (Chakraborti et al., 2019).

2.4 Erratic Monsoon

Numerous urban areas are experiencing drought situations, especially in summers owing to insufficient availability of water and lack of infrastructural facilities. Citizens become dependent on subsurface water resources to meet their needs. About 70% of rainfall occurs in the monsoon season resulting in dry conditions for the rest of the year in India, and 2018 was the fifth successive year to register as a shortfall of monsoons (Pandey & Sengupta, 2018).

2.5 Saltwater Intrusion in Coastal Cities

Groundwater is extracted much quicker than it can be recharged in the coastal areas, and the seawater moves toward the inland side of the coast and mixes with freshwater in the aquifer. Seawater intrusion toward the inland area can worsen local freshwater quality, abolish farmlands, and create a freshwater crisis. For instance, excessive groundwater extraction caused a severe water crisis in Shandong (China) from 1970 to 2010 by deteriorating the quality of local freshwater (Wu & Tan, 2012).

2.6 Groundwater Depletion and Spreading the Cone of Depression

Excessive pumping of groundwater rather than its natural replenishment by rainfall/recharge resulted in a dropping of water-table and aquifer depletion in a widespread area. For instance, China's cone of depressions of Zibo-Weifang covered 5475 km^2, and Shenxian-Xiajin covered 4004 km^2 in 2009. The area of depression has been continuously spreading since 1979 due to hasty urbanization, overexploitation, and unsustainable utilization of groundwater (Wu & Tan, 2012).

2.7 Issue of Land Subsidence

Sometimes certain kinds of formations, such as fine-grain sediments, hold groundwater, and the compaction of the sediments is partially accountable for holding up the ground. When a huge volume of water is withdrawn from that type of aquifers, the piezometric head drops, which results in vertical compaction of the subsurface materials and lateral flow of groundwater, causing subsidence of the land surface. In India, London, Venice, Mexico, Jakarta, Tokyo, etc., there are visible shreds of evidence of land subsidence due to overexploitation of groundwater (Sahu & Sikdar, 2011; Bose et al., 2020).

3 Urban Water Scarcity Solutions

3.1 Urban Water Management

Water management systems are currently dominated by conventional, concrete-based, man-made infrastructures or "gray" infrastructures. Harnessing the opportunities and advantages of nature-based solutions ("green" solutions) still remain underused. Gray infrastructures like sewers and sewage treatment systems usually

do not provide multiple environmental advantages like green infrastructures. But its efficiency can be magnified by the integration of green-engineering technologies to restore the local hydrological cycle. Bhat (2014) propounded that the average supply of per-capita water could reduce from 24 GDP to 21 GDP by the year 2025 and calculated to drop to 18 GDP by the year 2050. In these circumstances, it is necessary to regulate anthropogenic behavior and check interferences to improve the condition by making certain changes in technology and policy guidelines.

3.1.1 Green Infrastructures

"Green" solutions for urban water management are more advanced approaches than conventional ones. Capturing and exploiting stormwater to recharge the aquifer of an area are a good way as a "green" infrastructural solution. Capturing and management of runoff of stormwater from streets, footpaths, parking lots, rooftops, etc. and directing it to engineered systems are coming under nature-based ways of urban water management. "Green" solutions include natural and man-made wetlands and riparian buffer strips, which help to improve the water quality of that place. Green roofs in urban areas also serve against high temperatures and climate change (Chakraborti et al., 2019).

3.1.2 Virtual Water Trade

Virtual water trade is the implied exchange of water for the manufacture of goods and to perform several services. Water-intensive goods get more expensive to produce when water becomes scarce, and the economy compensates through higher water imports. It is the most effective solution to overcome urban water shortages for 71.2% of the world's big cities. But it may disturb the regional economy, increase GHG emissions of GHGs from the transportation sector, and aggravate social inequality. Virtual water trade is recognized as a possible solution for an urban area if the area is situated in a country without national-scale water shortages. For instance, a big city like Los Angeles can adopt virtual water trade as a possible water scarcity solution. Cities of developing countries like Delhi in India are restricted by their geography and economic development levels to adopt this method as a possible solution to urban water scarcity (He et al., 2021).

3.1.3 Aquifer Recharge

Artificial recharge by injection and infiltration of treated surface water into aquifers should be done by governmental organizations in scarce groundwater areas. Rapid urbanization is ignoring the natural groundwater recharge mechanisms in terms of surface water bodies, which are shrinking daily. For that, the restoration of wetlands

and watersheds is part of supporting green infrastructure by reducing impervious surfaces. Before seeking the permission to establish the construction of groundwater withdrawal systems, registration of drilling agencies and proper record keeping of all abstraction structures should be made mandatory (Chakraborti et al., 2019).

3.1.4 Inter-basin Water Transfer

Inter-basin water transfer is a potential solution for urban water scarcity, in which a large amount of water is transferred from one river basin to another. It could be effective for 68.2% of large cities in the world. But this has potential negative impacts on the environment. For instance, inter-basin water transfer, reservoir construction, etc., would harm the native hydro-ecosystem, hydrogeology, and eventually the local climate (He et al., 2021). In India, the National River Linking Plan was proposed in 2002 and was implemented by the National Water Development Agency, GoI (Gurung, 2015), for better management of the water scarcity problem.

3.1.5 Stormwater Management

The building of groundwater recharge channels or shafts between cemented surfaces, porous pavements, and effluent systems for stormwater along the footpaths and roads should be fortified. The digging processes should be encouraged to increase surface water bodies' water storage capacity. Moreover, governments and authorities should necessarily emphasize technical investments and efficient usage of prevailing resources. Awareness spreading and people's participation in regulating the water pollution and maintenance of surface water as well as groundwater are the need of the hour (Chakraborti et al., 2019).

3.1.6 Nonrevenue Water

Lack of proper mapping, illegitimate water connections, an unestimated water supply, leaks in the supplying pipelines, lack of timely maintenance, etc. are responsible for generating nonrevenue water. Metered connections and well-spread water distribution networks with advanced, satisfactory, and effective pumping facilities are required for reliable water supply (Chakraborti et al., 2019).

3.1.7 Reuse of Water

The untreated gray water generated from different sources can be utilized for toilet flushing, car washing, industrial processing, etc. Saltwater is also reused for different purposes after adopting a proper desalination process (Chakraborti et al., 2019).

3.2 Resilient Approaches for Sustainable Water Use

Generally, resilient approaches are the need of the hour to avoid the forthcoming ambiguous state of water. Nations need to prioritize sustainable ways to conserve and utilize water as per their situations.

3.2.1 Smart Cities

Smart cities signify diverse area-based inclusive land-use planning and development, including physical, economic, and social infrastructure. It comprises efficient computer-assisted transportation and competent water and energy infrastructures, controls various pollutions, manages native resources, and improves the local economy. Smart planning includes encouraging green substructures, minimizing urban heat island effects, exploring renewable energy resources, installing advanced technologies for water management, and conserving and creating new open spaces. These kinds of infrastructures, such as playlands, urban greens, and other recreational grounds, improve the residents' quality of life overall, endorsing ecological balance (Smart Cities Mission, 2019). It is expected that the physical, economic, and social development of smart cities will provide water resources with the maximum grade and improved water management facilities. Indian cities like Pune, Chandigarh, etc. are shifted to the smart meter-based water distribution system for monitoring on water management system (Ramos et al., 2020).

3.2.2 Climate-Resilient Planning

Service providers and organizations should find and manage the climate hazards affecting water systems using a framework. This framework will provide climate-resilient adaptation strategies, assessment of possible threats, and sustainable water systems. For instance, after Hurricane Sandy occurred in 2012 in the New York metropolitan region was redesigned with climate resilient infrastructures. They integrated hard structures with the soft landscape to increase coastal resistance mechanism, a network of interrelated green infrastructures for straight rainwater recharge to aquifers, water pumps, and alternative ways for provision of drainage, etc. (Dolman, 2021).

3.2.3 Exploring Alternative Water Sources

It is the appropriate time to explore alternative, climate-resilient, and sustainable water resources to maintain the balance between naturally available potable water and the over-exploitation by humans, increasing the surface water storage capacity, rainwater harvesting on rooftops of urban buildings, desalination of seawater by exploiting renewable energy and harmless saline release, finding of altered water

resources by hydrological investigations and remote sensing techniques, etc. (UNICEF, 2013).

3.2.4 Citizen's Behavioral Change

An effective, resilient solution through educational clubs may be helpful to build a future generation who can practically apply their knowledge to solve the water scarcity problem by educating students about water scarcity and the impact of climate alteration. Incentives and public awareness campaigns would help to change the citizen's behavior regarding water consumption and will set up optimistic social customs (UNICEF, 2013).

3.2.5 Taxes and Investments

Tariff systems are necessary for proper operation and perpetuation of the water system to work effectively as well as in a sustainable manner. Taxes, rates, quotas, etc. are very effective in lessening the consumption rate. The private sector investments and carbon credits are also beneficial for the maintenance of water and wastewater services (UNICEF, 2013).

4 Conclusions

Fresh and potable water is a vital natural resource with finite quantity. Urban sprawl, population explosion, and economic growth create stress on the quality and quantity of urban water, showing an increasing trend. Several pieces of literature reported that half of the world's megacities will experience urban water deficiencies by 2050. Therefore, improved water management systems, smart cities integrating "green" solutions, aquifer recharge, water reuse, policy changes, investments in newer technologies, etc. could be possible ways to secure the consistent and sustainable supply of desirable water resources to future generations.

References

Arnell, N. W. (2004). Climate change and global water resources: SRES emissions and socio-economic scenarios. *Global Environmental Change, 14*(1), 31–52.

Bhat, T. A. (2014). An analysis of demand and supply of water in India. *Journal of Environment and Earth Science, 4*(11), 67–72.

Bose, S., Mazumdar, A., Basu, S. (2020). Review on Present Situation of Groundwater Scenario on Kolkata Municipal Area. In *IOP Conference Series: Earth and Environmental Science, 505(1)*, IOP Publishing.

Branch, S. (2012). *United nations statistics division*,13–35.
Briefing, P. (1998). *Liquid assets is water privatisation the answer to access*.
CGWB. (2019).*Ground water year book – India 2019–20*. http://cgwb.gov.in/Ground-Water/GW%20YEAR%20 BOOK%2020 1920%20ALL%20INDIA%20FINAL%20752021%20(1).pdf
Chakraborti, R. K., Kaur, J., Kaur, H. (2019). Water Shortage Challenges and a way forward in India. *Journal: American Water Works Association*, *111*(5), 42–49.
Dolman, N. (2021). Integration of water management and urban design for climate resilient cities. In *Climate resilient urban areas* (pp. 21–43). Palgrave Macmillan.
Easterling, D. R., Meehl, G. A., Parmesan, C., Changnon, S. A., Karl, T. R., & Mearns, L. O. (2000). Climate extremes: Observations, modeling, and impacts. *Science, 289*(5487), 2068–2074.
Giorgi, F., Bi, X. (2005). Regional changes in surface climate interannual variability for the 21st century from ensembles of global model simulations. *Geophysical Research Letters*, *32*(13), 1–5.
Gleick, P. H. (2003). Water use. *Annual Review of Environment and Resources, 28*(1), 275–314.
Gurung, P. (2015). *Inter-basin water transfer: is this a solution for water scarcity*.
He, C., Liu, Z., Wu, J., Pan, X., Fang, Z., Li, J., & Bryan, B. A. (2021). Future global urban water scarcity and potential solutions. *Nature Communications, 12*(1), 1–11.
Janakarajan, S., Llorente, M., & Zérah, M. H. (2006). *Urban water conflicts in Indian cities: Man-made scarcity as a critical factor. Urban water conflicts: An analysis of the origins and nature of water-related unrest and conflicts in the urban context* (pp. 91–111). UNESCO.
Jury, W. A., & Vaux, H. (2005). The role of science in solving the world's emerging water problems. *Proceedings of the National Academy of Sciences, 102*(44), 15715–15720.
Pandey, K., Sengupta, R. (2018, October 1). India had a deficit monsoon in 13 of the last 18 years. *Down to Earth*.
Ramos, H. M., McNabola, A., López-Jiménez, P. A., & Pérez-Sánchez, M. (2020). Smart water management towards future water sustainable networks. *Water, 12*(1), 58.
Ray, B., Shaw, R. (2016). Water stress in the megacity of Kolkata, India, and its implications for urban resilience. In *Urban disasters and resilience in Asia* (pp. 317–336). Butterworth-Heinemann.
Royer, J. F., Cariolle, D., Chauvin, F., Déqué, M., Douville, H., Rong-Ming, H., & Valcke, S. (2002). Simulation of climate changes during the 21. Century including stratospheric ozone; simulation des changements climatiques au cours du 21. Siecle incluant l'ozone stratospherique. *Comptes Rendus Geoscience, 334*(3), 147–154.
Sahu, P., & Sikdar, P. K. (2011). Threat of land subsidence in and around Kolkata city and East Kolkata wetlands, West Bengal, India. *Journal of Earth System Science, 120*(3), 435–446.
Smart Cities Mission. (2019). *Smart city features*. Ministry of Housing and Urban Affairs, Government of India. https://smartcities.gov.in/
Thomson, A. M., Brown, R., Rosenberg, N. J., Srinivasan, R., & Izaurralde, R. C. (2005). Climate change impacts for the conterminous USA: An integrated assessment. *Climatic Change, 69*(1), 67–88.
Tudhope, A. W., Chilcott, C. P., McCulloch, M. T., Cook, E. R., Chappell, J., Ellam, R. M., & Shimmield, G. B. (2001). Variability in the El Niño-Southern Oscillation through a glacial-interglacial cycle. *Science, 291*(5508), 1511–1517.
UNICEF (United Nations International Children's Emergency Fund), FAO (Food and Agriculture Organization of the United Nations), & SaciWATERs. (2013). *Water in India: Situation and Prospects*.
Watkins, K. (2006). *Human development report 2006-beyond scarcity: Power, poverty and the global water crisis*. UNDP Human Development Reports.
Wu, P., & Tan, M. (2012). Challenges for sustainable urbanization: A case study of water shortage and water environment changes in Shandong, China. *Procedia Environmental Sciences, 13*, 919–927.
Zero, P. D. (2021). Urban water scarcity guidance note. *UNICEF*, 6–45.

Chapter 8
Groundwater Scarcity in Urban Areas Is a Major Issue: Case Studies from West Bengal

Mayank Sharma

Abstract The supply of freshwater is important for day-by-day existence. Groundwater issues are a social construct, so also are the solutions. This particular chapter deals with the case studies on identifying water scarcity in the two hard rock cities of West Bengal, namely, Purulia and Bankura. A general consideration of the surface and subsurface sources of water is done in this chapter. The surficial water sources include the river systems, dams, lakes, and rainfall, which were studied and well researched from the past Central Ground Water Board and Indian Meteorological Department reports. Furthermore, geophysical investigations were also indicated to determine the depth of aquifers in the research regions. An electrical resistivity survey of geophysical exploration was used to know the aquifer zones of the area. The vertical electrical sounding (VES) method was employed to know the subsurface geology of the area. For the cities of Purulia and Bankura, ten and eight locations were assessed, respectively. The VES data were processed, analyzed, and interpreted for the groundwater availability in the areas using Resist v1.07fc. At the end of the chapter, it is evident that depending upon the population, per-capita-water needs and the amount of water available for consumption in these cities, they are water-scarce, and in the near future, the sources may dry up. Also some suggestive measures for overall balanced groundwater development in the short term and long term are discussed to preserve water.

Keywords Groundwater · Vertical electrical sounding · Scarcity

M. Sharma (✉)
St. Xavier's College, Ranchi, India
e-mail: mayank@sxcran.org

P. Thambidurai, A. K. Dikshit (eds.), *Impacts of Urbanization on Hydrological Systems in India*, https://doi.org/10.1007/978-3-031-21618-3_8

1 Introduction

All the water above the earth's surface is accounted under surface water such as dams, rivers, lakes, ponds, rainfall-runoff, etc. But, apart from this, any water source below the surface of the earth falls under the subsurface water or groundwater. Water, including surface water and groundwater, is one of the most vital resources. All life on earth depends on it. Water availability and its use are critical for our society's progress. This valuable resource is sometimes rare, sometimes plentiful, but it is unevenly distributed. Groundwater is the world's second largest source of freshwater, accounting for ~30% of all freshwater resources. Subsurface water is used as drinking water by about 1.5 billion people worldwide. Water is present in various strata, and the strata which have the tendency to produce stored water are called aquifers.

1.1 Geophysical Survey for Groundwater Exploration

Exploration geophysics is a discipline of geophysics that employs surface methods to determine the physical attributes of the earth's subsurface. Exploration geophysics is the use of physical methods (such as seismic, gravitational, magnetic, electrical, and electromagnetic) to determine the physical attributes of the earth's beneath and, in particular, to identify measurable physical changes in the earth's subsurface formation. Geophysical surveys are used to gather geological information prior to subsurface excavation. Drills or trenches must be dug in specific locations to ensure that the conclusions drawn from geophysical investigations are true, and the inferred data must be compared to observational data. As a result, geophysical investigations reduce test drilling by allowing for a better selection of test borehole locations. Applied geophysics, exploratory geophysics, geophysical prospecting, and other terms are used to describe geophysics devoted to mineral exploration, including groundwater exploration. Electrical, gravitational, magnetic, seismic, thermal, or radioactive properties are the most common properties recorded in surveys. Electrical resistivity is a typical method for detecting and locating the existence of water-bearing rocks (Zohdy et al., 1974; Ashok Kumar & Thambidurai, 2022). Vertical electrical sounding (VES) can reveal important details about the earth's crust and mantle's interior structure. Electrical surveys rely on natural current and potential sources. This method is now widely used in the scientific examination of environmental issues. They are employed to understand the variation in the resistivity values of different underlying strata and are used to explore groundwater aquifers. In hard rock areas, cracks and fractures are observed to have porosity to store water, whereas on the other hand, in the alluvial plains, water is present in the sand layer. This method detects the resistivity values of different layers, and then after analysis and interpretation of data, the depth of aquifers is delineated.

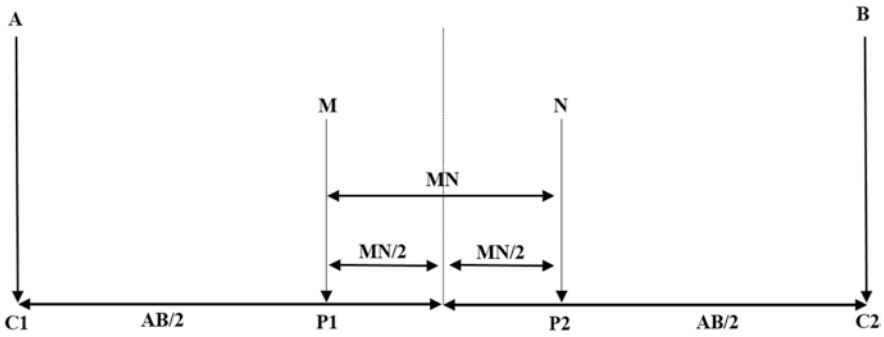

Fig. 8.1 Schlumberger electrode configuration

The VES at specific locations with a Schlumberger electrode set up in all regions is used to delineate the aquifers. The Schlumberger arrangement is shown in Fig. 8.1; the potential and current terminals are aligned, with the current electrodes placed slightly wider apart than the potential electrodes.

The formula for calculating apparent resistivity (ρ) is as follows in Eq. (8.1):

$$\rho = \pi . \left[\frac{\left(\mathrm{AB}/2\right)^2 - \left(MN/2\right)^2}{MN} \right] . \frac{\mathrm{V}}{\mathrm{I}} \tag{8.1}$$

where AB represents the distance between current electrodes C_1 and C_2 (in m), MN depicts the distance between potential electrodes P_1 and P_2 (in m), I refers to the current measured (in amps), and V is the voltage supplied (in volts). AB is much greater than MN, with AB to be greater than or equal to five times MN for accurate results (Todd, 1980). AB/2 is usually kept in the range of 250–300 m, having a north-south orientation.

2 Literature Review

2.1 Water Scarcity

Freshwater resources are essential in daily life since they feed people, power the economies, and maintain the land and marine habitats (Postel, 2000). Though water is ubiquitous across the world, most of it is unavailable for us and for ecological use. Freshwater sources are not uniformly allocated over the world, and freshwater supply can fluctuate significantly over time. Frequently, locations with a high concentration of economic ventures or thick populations need not conflict geographically with places with abundant freshwater supplies (Kummu et al., 2010). Regardless of the fact that 10% of the world's freshwater resources are used (Oki & Kanae, 2006),

many cities are facing water shortages, and these provinces are home to no less than one-third of the world's population (Kummu et al., 2010, 2016; Hanasaki et al., 2013; Schewe et al., 2014; Mekonnen & Hoekstra, 2016). Crop failures, food scarcity and mass starvation, economic losses due to business interruption, and the deterioration of terrestrial and marine ecosystems are only a few of the consequences of water scarcity.

2.2 *Use of Electrical Resistivity Method in Groundwater Hydrogeology*

Niwas and Singhal (1980) calculated aquifer transmissivity in porous materials using Dar-Zarrouk characteristics. Using two universal laws, Darcy law and Ohms law of fluid flow, the analytical relationships were established between transmissivity and transverse resistance, as well as transmissivity and longitudinal conductance. Wadatkar (1984) employed the electrical resistivity-sounding method to determine the subsurface stratum parameters, such as depth and resistivities, in the Salkuti area of Midnapur District, West Bengal. This would allow the aquifer to be identified, as well as its depth, thickness, and horizontal extent. The countryside of Dhiwarwadi, District Nagpur, is located in a fault zone, according to Kaore and Kokil (1990). The area is divided into blocks based on profile information, VES graphs, and true resistivity of prior plotted curves, demonstrating the presence of fractures and fault zones in the Deccan Traps of Nagpur and Wardha districts. According to the data, resistivity investigation and exploratory drilling failed to reveal the entire depth of weathering on the fault zone. The prevalence of faults can be detected using certain forms of curves and resistivity data. Kelekar (1990) investigated the use of electrical resistivity to identify a well, excavated well, or subsurface structure location. The shape and thickness of a causal body are inferred from the fluctuation in apparent resistivity values. For electrical resistivity survey work, he recommended using the Schlumberger method. This is because the effect of horizontal inhomogeneity may be measured and adjusted to some amount using this approach which is also a speedier technique. Murthy (1990) discovered that the occurrence of lineament is indicated by the alignment of low resistivity in a specific direction. Depending on the hydrological circumstances, this lineament could serve as a good aquifer that could be accessed through a bore well.

The river Bhogawati, which is a branch of the Sina, drains cretaceous Eocene Deccan basalts (Sawant, 1999). The basin is roughly 1950 km^2 in size and is located in the Solapur district of Maharashtra, which is prone to drought. Suitable locations for bore wells, dug wells, and dug-cum-bore wells for drinking water have been satisfactorily recommended using lithological, geomorphological, and structural features, as well as resistivity sounding. The chronological, geomorphological, as well as structural features and resistivity sounding have all proved useful in proposing prime areas for drinking water dug wells, bore wells, and dug-cum-bore wells.

Ghosh (2001) used the resistivity approach to investigate groundwater in the Bharatpur district of Rajasthan. A maximum of 184 Schlumberger soundings were done utilizing maximum current electrode spacing at different locations. The district's geoelectrical maps (S = h) are somewhat similar to the district's longitudinal conductivity map that was constructed using sounding information at electrode separations of AB/2 = 10 m, 50 m, 100 m, and 200 m. Half current electrode spacing (AB/2) is approximately 50 m on the district's apparent resistivity maps, showing that the apparent resistivity spread is similar. Subrahmanyam (2001) conducted research in the Sanathnagar and Santoshnagar neighborhoods of Hyderabad, Andhra Pradesh, on geoelectrical investigation for groundwater. These studies used 42 Sanathnagar resistivity values and 50 Santoshnagar soundings. Resistivity-sounding statistics show a three-layer succession in the bulk of the locations, with the first layer possessing resistivity ranging from 23 to 100 ohm-m. Weathered granite is represented by the second layer, which has resistivities ranging from 20 to 130 ohm-m, and semi-weathered to massive granite is represented by the third layer, which has resistivities of 400 ohm-m and higher. A few sites reported greater resistivity values between 1000 and 1400 ohm-m in the relatively close dry soil layer. A weathered zone with a large thickness for shallow bore wells is commonly considered acceptable. As a consequence, weathered zones with sufficient thickness and adequate hydrogeological parameters were investigated for the purpose of suggesting bore wells.

Drozhko et al. (2002) investigated the hydrological parameters of heterogeneous cracked rock. They give a comparison of preliminary hydrogeological results as well as descriptions of various hydrological and geophysical data acquisition and processing methods. The coincidence of hydraulic conductivity measurements utilizing various field testing and data processing methods allows us to endorse the processes presented for use in extensive investigations of fractured rock subsurface transmissivity. In the chromite mines in Sukinda Valley, Orissa, Dhakate (2003) conducted research on the development of groundwater resources. The Sukinda Valley is well-known for its massive chromite ore reserves. A complete hydrological and geophysical examination is carried out to examine the subsurface regime and its quality, which provides vital information about the groundwater in this location. Israil (2003) investigated the use of apparent resistivity data to determine layer boundaries. In the absence of abrupt limits, he devised a method for establishing geologically influenced layer boundaries using an inverse model constructed using a smooth inversion methodology. Chandra et al. (2004) used a mixture of Schlumberger as well as axial pole dipole configurations to investigate groundwater in hard-rock settings. Using field examples from Dharwar (Archean granitic) or Vindhya, scientists show that the relatively close inhomogeneity effect may be recognized in the sounding contour using a combination of Schlumberger and axial pole-dipole setups. Jat and Jain (2007) conducted research at the CTAE instructional farm in Udaipur on establishing aquifer characteristics using the least square technique in fractured rocks under linear flow circumstances, validating that the least square technique has benefits over the plotted graph because it eradicates the issue of subjectivity affiliated with curve-matching methodology.

3 Case Study I: Water Scarcity in Purulia

Purulia covers a total land area of 6259 km^2, and it is the fifth largest in the state. It is adjoined by Jharkhand, Hazaribagh, and Dhanbad to the north, Singhbhum to the south, and Ranchi to the west. The eastern flank is covered by the West Bengal districts, including Burdwan, Bankura, and Midnapore. Purulia is divided into three subdivisions, namely, Purulia Sadar (east), Purulia Sadar (west), and Raghunathpur. There seem to be 28 urban divisions in the district, with 3 municipalities and 25 census towns. Three municipalities are named Raghunathpur, Jhalda, and Purulia. The district witnesses a great change in the temperature during the summers and the winters. The temperature varies between 23 and 45 °C during summers and 3 and 20 °C in winters. Purulia is among West Bengal's drought-prone districts. It does have hot and humid summers with significant evaporation and little precipitation. The yearly rainfall averaged 1368 mm. In the latter half of August, the showers are unpredictable, with the unusual drought somewhere between. Storms or severe depressions form in the Bay of Bengal during the month of May and after the monsoon season. Depressions throughout the monsoon season and heavy thunderstorms in the afternoons during the summertime are among the district's unique weather occurrences. The district is well-known for its harsh weather. The average total annual precipitation in the last 50 years has been 1355 mm. During the monsoons, relative humidity levels range from 72% to 81%. The majority of the Purulia region is peneplain, with a minor uneven surface pattern. It is essentially an extension of the Ranchi peneplain. The presence of a very few minor eroded hills such as Ayodhya, Baghmundi, Joychandi Pahar, and Panchet, as well as an absolute altitude and somewhat low relief, suggests that this area is still in the early stages of the degradation cycle. To the west, hills abound and plains come gradually to the east. In the west and south, absolute elevation increases.

3.1 Study Area

The city is the district headquarter of Purulia itself, being the nearest railway station and bus stand. Figure 8.2 shows the location of the city. The study area is well connected to other villages through roadways. Villages and towns like Baligara, Chakda, and Ramnagar are in the west of the city, whereas Gopalpur, Bengra, and Bhagabandh are in the east. Bongabari and Dumdumi are located toward the north, while the Kangsabati River flows through the south of the city. Jharkhand-West Bengal border lies toward the north and northeast of the city. In order to carry out the electrical resistivity prospecting method, ten points, namely, S1–S10, were selected and evenly distributed.

Geographic position of each point S1–S10 shown in Fig. 8.3 was recorded in the tabular form as given in Table 8.1.

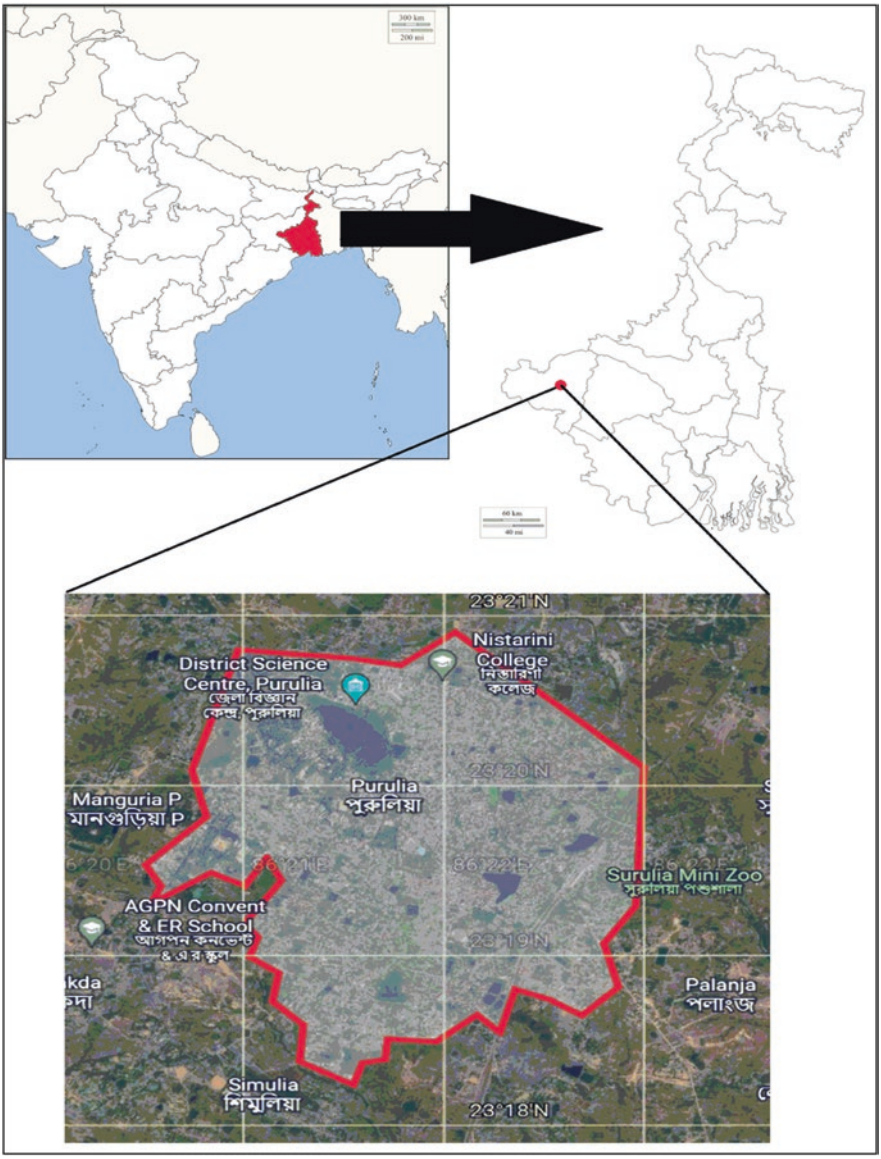

Fig. 8.2 Location of the city

3.1.1 Geology

Except for a tiny section in the northeastern half, where sediments of the Gondwana age prevail, pre-Cambrian age rocks dominate the district of Purulia. Recent age unconsolidated sediments are limited to small stream channels and valleys. The city of Purulia shows a variation in geology and lithology. Basically, the topsoil in the

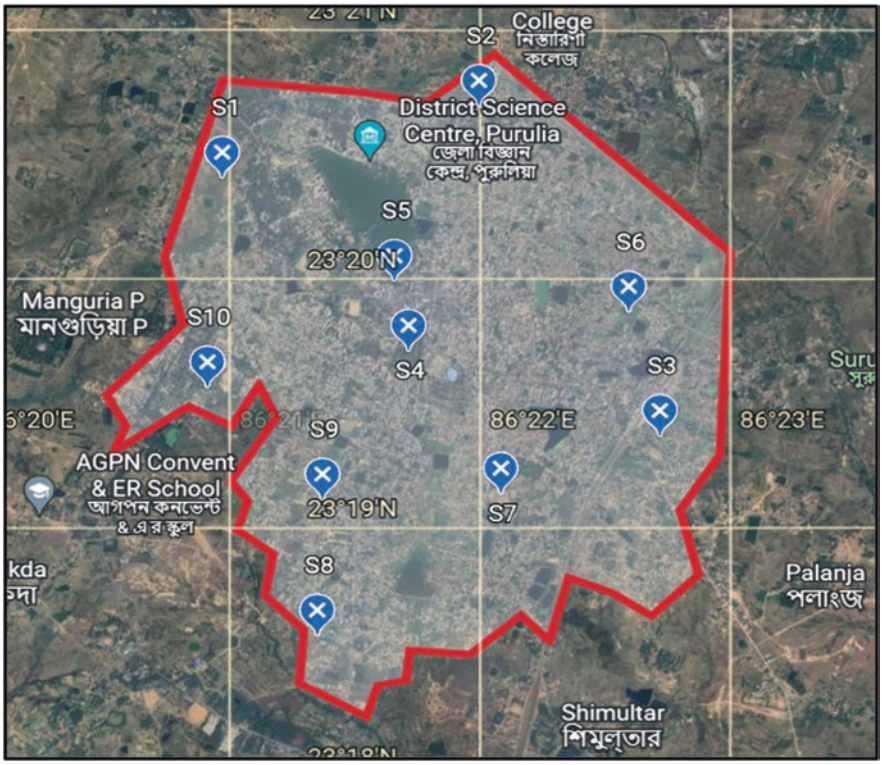

Fig. 8.3 The location of investigation points S1–S10 in the study area

Table 8.1 The GPS locations of investigation points

Points	Latitude	Longitude
S1	23° 20′ 21.17″N	86° 21′ 17.39″E
S2	23° 20′ 36.82″N	86° 21′ 59.03″E
S3	23° 19′ 26.67″N	86° 21′ 46.47″E
S4	23° 19′ 41.85″N	86° 21′ 43.49″E
S5	23° 19′ 58.62″N	86° 21′ 31.2″E
S6	23° 19′ 46.49″N	86° 22′ 30.72″E
S7	23° 19′ 09.07″N	86° 21′ 42.43″E
S8	23° 18′ 35.99″N	86° 21′ 29.02″E
S9	23° 19′ 04.81″N	86° 21′ 22.85″E
S10	23° 19′ 31.65″N	86° 20′ 55.42″E

area is shallow, well-drained, and gravelly loamy and is underlain by intrusive granites in the northern part covering a major area of the city. The southern part is rich in granitic gneiss and migmatites. The Ajodhya hill in the north shares its lithology with the Chotanagpur Gneissic Complex of Jharkhand and is hence rich in intrusive

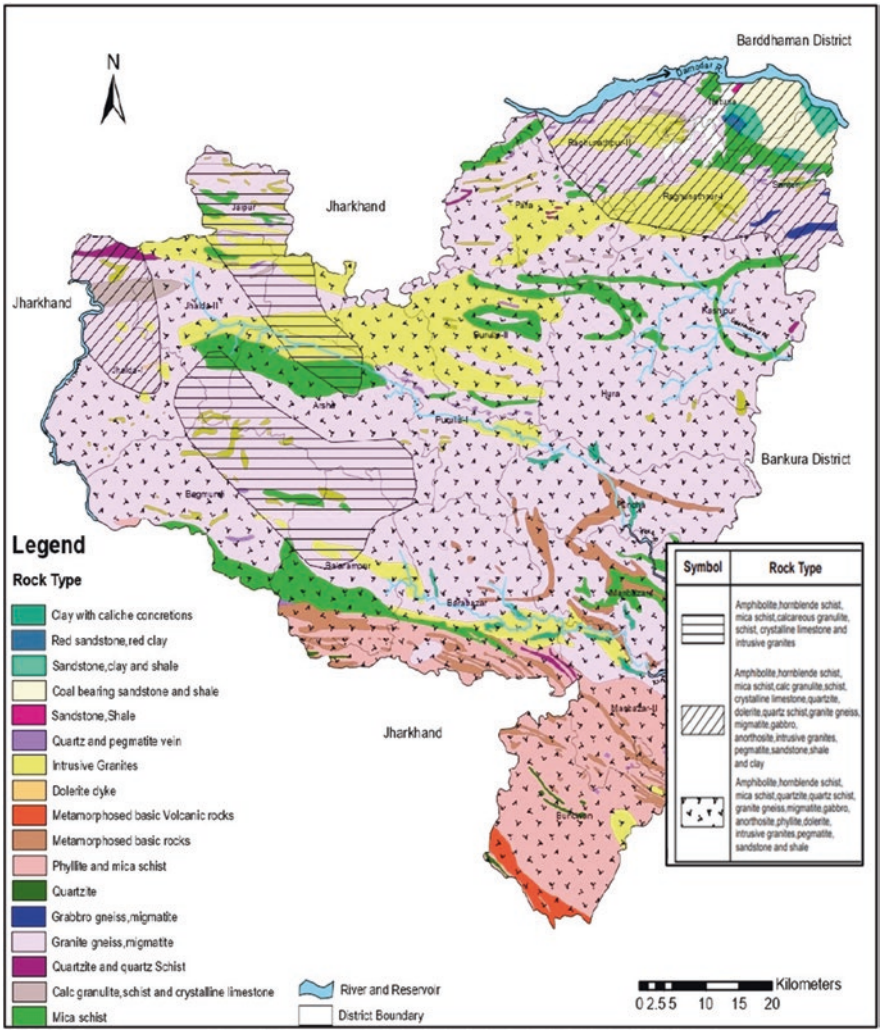

Fig. 8.4 Hydrogeological map of Purulia district. (WBWRIDD website – http://wbwridd.gov.in/swid/mapimages/PURULIA.pdf)

granites and gneiss. Apart from this, Mica Schist is also found in the southeastern part of the city. The thickness ranges from 15 to 24 m. Rocks in the area are of Pleistocene to Recent times consisting of open joints, faults, bedding, and foliation planes. Groundwater is mainly found in minor cracks and fractured rocks at great depths. According to the map in Fig. 8.4 from Water Resources Investigation & Development Department (WBWRIDD) website, the main rocks observed to predominate here are amphibolite, pegmatite, hornblende schist, gabbro, mica schist, dolerite, shale, intrusive granites, and sandstone.

3.1.2 Hydrogeology

Purulia, the extension of Chota Nagpur Plateau and the westernmost district of West Bengal, is characterized by a paucity of groundwater due to its difficult hydrogeological condition. The country rocks are principal of hard Archaean crystalline like granite, granite-gneiss, anorthosite, epidiorite, and paraschist, whereas the northern part of Damodar River embankment (Neturia and Santuri blocks) is constituted of Gondwana sediments like sandstones and shales with or without the cover of the weathered counterpart (residue) of host rocks. The thickness of weathered residue may vary from 0 m to 15 from higher reaches to lower reaches. Higher surface runoff due to a steeper gradient, lack of extensive large primary aquifer with the less retentive capacity of rainwater in the weathered residue of underlying crystallines, and high evaporation rate make it difficult for sufficient water availability in this semiarid region. The entire district can be divided into several sub-river basins like Damodar, Dwarakeswar, Kansai, Kumari, and Subarnarekha. Each river basin shows its own characteristics and hydrogeological condition depending on geology, morphology, tectonic history, and met-condition of the river basin system. Figure 8.4 shows the hydrogeological map of the Purulia district.

3.1.3 Drainage Pattern

The streams that pass through the district are small but dry for most of the year. Just during the monsoon do these rivers become extremely tumultuous. Rainwater harvesting is used in Purulia, where rainwater is gathered during the monsoons. However, that evaporates during the other seasons, particularly whenever the area is experiencing drought, resulting in water scarcity. Subarnarekha, Kumari, Dwarakeswar, Damodar, and other rivers run through this district. The drainage pattern of the rivers in this region is parallel and trellis. The Kangsabati River, which flows from the south, is an important supply of water for the city.

3.2 Prospecting the Potential Aquifers

3.2.1 Vertical Electrical Sounding Data Acquisition

Data acquisition is the most difficult part of any field study as there are scopes of committing errors while recording data. In order to perform the VES method, Schlumberger electrode configuration was used to collect data at the site of investigation. The resistivity values were obtained for a current electrode spacing of 600 m, resulting in the current penetration depth of nearly 190–200 m since the penetration depth of current ranges between 0.25AB and 0.5AB. VES1 to VES10 were implemented at locations S1to S10, respectively, in the Purulia study region. After the electrode configuration was set up, the experimental readings were now noted for

different AB/2 and MN/2 spacings. The first data was noted down with half current electrode spacing equal to 1.5 m which commenced until the spacing turned to 300 m. On the other hand, the observations started with MN/2 at 0.5 m and subsequently increased with the AB/2 spacing up to a maximum extent of 300 m. For MN/2 equal to 0.5 m: the M and N electrodes were separated by 1 m, and the current electrodes A and B were separated by 3 m, resulting in AB/2 equal to 1.5 m for the first observation. The resistivity meter provided the resistance value. The AB/2 spacing was then extended to 2 m, 3 m, and 4 m, respectively. As the AB/2 spacing was already ten times MN/2, it was now time to alter the MN/2 value by increasing the gap between M and N electrodes. For improved results, the MN/2 was increased to 1 m. As soon as the MN/2 spacing equaled 1 m, we repeated the same steps that we followed when MN/2 spacing equaled 0.5 m; the current electrodes were then shifted with AB/2 varying from 4 m to 10 m. MN/2 was then further increased to 2 m at 10 m AB/2 spacing, and successive values of resistance were recorded. This procedure continued until AB/2 equaled 300 m and MN/2 spacing equaled 40 m. At the end of the VES, data up to the depth of 190–200 m was obtained.

3.2.2 Analysis of Data

The values of apparent resistivities and AB/2 values obtained from field data were used as input in Resist v.1 fc7 software to get the true resistivity (ohm-m) and thickness (m) of layers. Table 8.2 shows the analyzed result.

On the basis of analyzed data and its correlation with the available borehole data, the probable lithologs corresponding to the true resistivity values have been inferred, as represented in Table 8.3.

Analysis of data reveals the presence of minorly cracked hard rocks which act as an aquifer in this area. The section is encountered within a depth of 94–108 m (having a resistivity range of 403–417ohm-m). At points S2, S6, and S10, the resistivity of the third layer are lower than that of compact rocks at S1, S3, S4, S5, S7, S8, and S9, indicating the presence of minor cracks. Hence at S2, S6, and S10, drilling up to

Table 8.2 The analyzed field data

S. no.	ρ1 (ohm-m)	ρ2 (ohm-m)	ρ3 (ohm-m)	T1 (m)	T2 (m)	T3 (m)	Curve type
VES 1	28	110	532	22	76	102	A
VES 2	18	97	409	23	79	98	A
VES 3	22	95	513	18	64	118	A
VES 4	22	95	586	20	70	110	A
VES 5	24	110	581	18	87	95	A
VES 6	22	86	417	23	85	92	A
VES 7	22	95	586	21	73	106	A
VES 8	24	110	581	18	87	95	A
VES 9	22	86	515	23	85	92	A
VES 10	26	90	403	20	74	106	A

Table 8.3 Inference of lithology

True resistivity values (ohm-m)	Probable lithology
<50	Soft overburden
50–110	Decomposed rocks
110–250	Fractured rocks
250–390	Partially fractured rocks
390–430	Hard rocks with minor cracks
>430	Hard and compact rocks

a depth of 190–200 m can be done. After drilling a borehole at these points using down-the-hole (DTH) drilling rigs, it was established that the amount of water in these aquifers is very less. A yield test was performed, and a very low yield of 900–1200 liters per hour was observed from the deep tube wells, which was very low to meet the needs of the expanding population. Apart from this, the rest of the points consisted of hard and undisturbed rock strata with no possibility of aquifers up to the depth of 200 m. The interpretation was done using data inversion models in Resist v1.07fc software. Following Fig. 8.5 shows the VES curves for all the points in the city of Purulia.

3.3 Conclusion

The groundwater table sharply declines during the summer period in this semiarid region. The problem is more critical for higher reaches areas where the water sources become dry during the summer season. Moreover, the existing structures of water sources are insufficient to meet the entire requirement for drinking and irrigational purposes and only fulfill the partial demand. Hence proper monitoring of these structures and finding new renewable potential zones of groundwater are essential to tackle this problem. All these factors have led Purulia to be a water-scarce city that is unable to quench the thirst of its people.

4 Case Study II: Water Scarcity in Bankura

The study area is situated in Midnapore and Hooghly in the east, Burdwan in the north, Purulia in the west, and Purulia and Midnapore in the south, encircling the Bankura district. In the north, the River Damodar divides Bankura from Burdwan province. Hooghly district borders the district's southeastern portion to some degree. The district's two biggest rivers are Dwarakeswar and Kangsabati, Silabati, Joyponda, Gandheswari, Sali, Birai, and Amoda. The district's principal harvest is rice. Although the district is vulnerable to drought, favorable rainfall seasons might result in increased agricultural production. Bankura (Sadar), Bishnupur, and Khatra

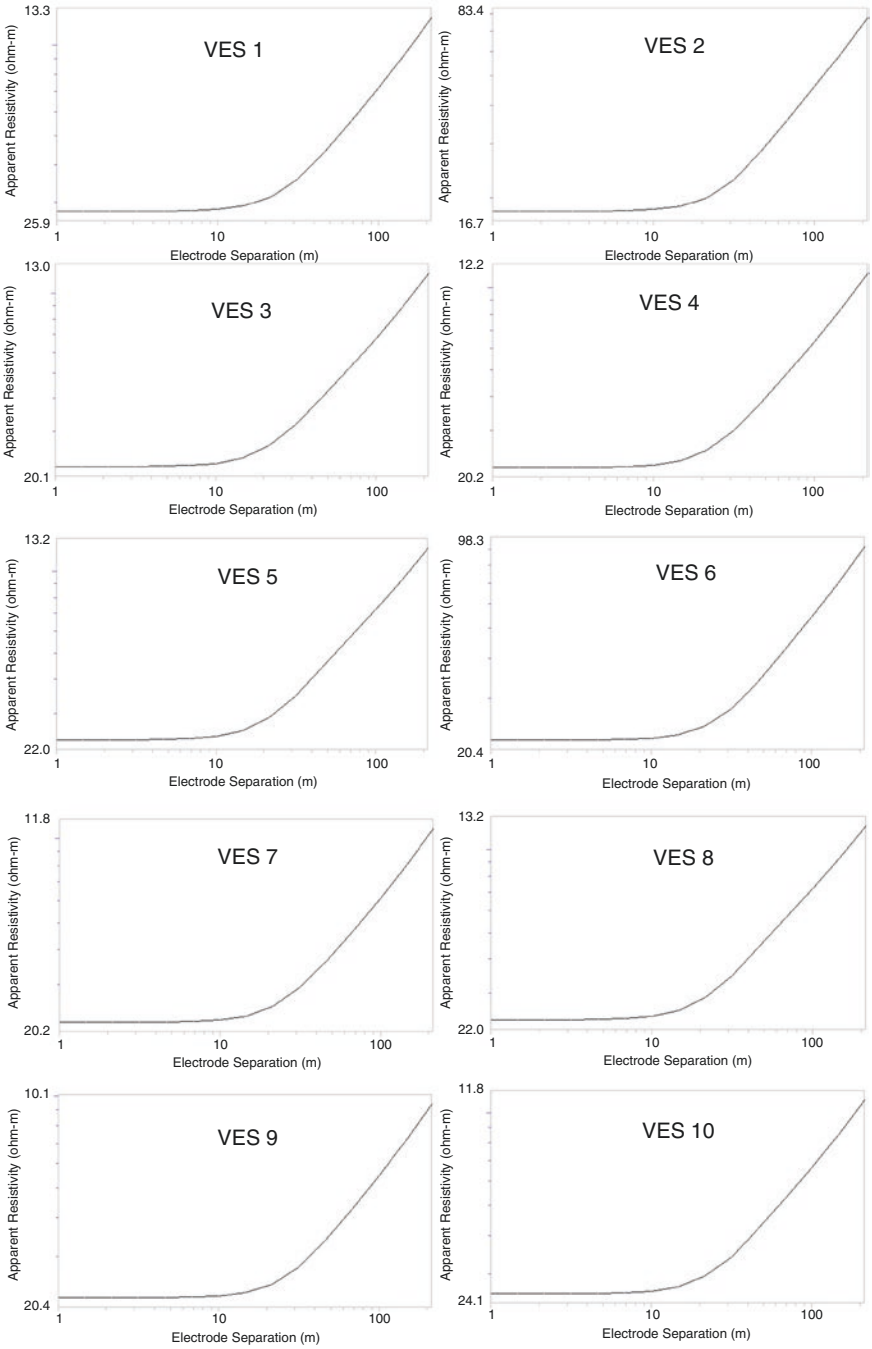

Fig. 8.5 Vertical electrical sounding curves for points S1–S10 in Purulia

are the major subdivisions of the district Bankura. The district of Bankura experiences an extreme climate with a high range of temperatures. The climate of the district is characterized by oppressive heat and high humidity in summer with the average daily maximum temperature varying between 26 and 39 °C. Winter is generally dry and cold, with an average winter temperature of around 15 °C. In summer, the Rarh plain of Bankura district is humid and warm, while the winter is dry and cold. The yearly rainfall averages between 130 and 140 cm. The average winter temperature is 15 °C, whereas the average summer temperature rises to around 30 °C (Nandi et al., 2007). Rainfall in the district of Bankura is generally scanty, even though good rainfalls occur in the eastern part of the district. The average annual rainfall ranges from 130 to 140 cm. Relative humidity remains high throughout the year. The annual average rainfall ranges between 130 and 140 cm. The average percentage of humidity varies from 50 in April to 82 in August (Nandi et al., 2007). The Bankura district covers 6955 km^2.

4.1 Study Area

Bankura is a city located within the state of West Bengal. Bankura city was considered a study area in order to understand the groundwater potential. Compared to other cities in West Bengal, Bankura is fairly large, having high population density. Considering the location of the city, it is well connected with other cities through roads and railways. Furthermore, toward the south flows the Dwarkeswar River, and toward the northeast flows the Gandheswari river. The closest railway station is the Bankura railway station itself. Toward the north lies Raghunathpur, and toward the east lies Bejgram, Bhuteshwar, and Sendra. Villages like Barut and Katgaria are in the west, whereas Dhaldanga and Debagram lie toward the south of the city. All the villages are well connected with Bankura through roadways. Figure 8.6 shows the location of the study area. Now, as per the geophysical investigation, eight points were selected, namely, S1–S8, and VES was performed. The map in Fig. 8.7 shows the eight points spread evenly around the urban area for aquifer delineation. The geographic position of each point S1–S8 was recorded in the tabular form as in Table 8.4.

4.2 Geology and Hydrogeology

The district of Bankura is underlain by Archean rocks. Bankura shares the same lithology as the Chotanagpur Gneissic Complex. Anorthosite, Gondwana sandstone, clay, and grit dominate the hard rock area. These hard rocks age back to the Archean to tertiary age and possess faulted structures and joints having low to moderate permeability. Subsurface water is mainly present in the cracks and fractures of these hard rocks. In the western part of the district, crystalline granite gneiss of the

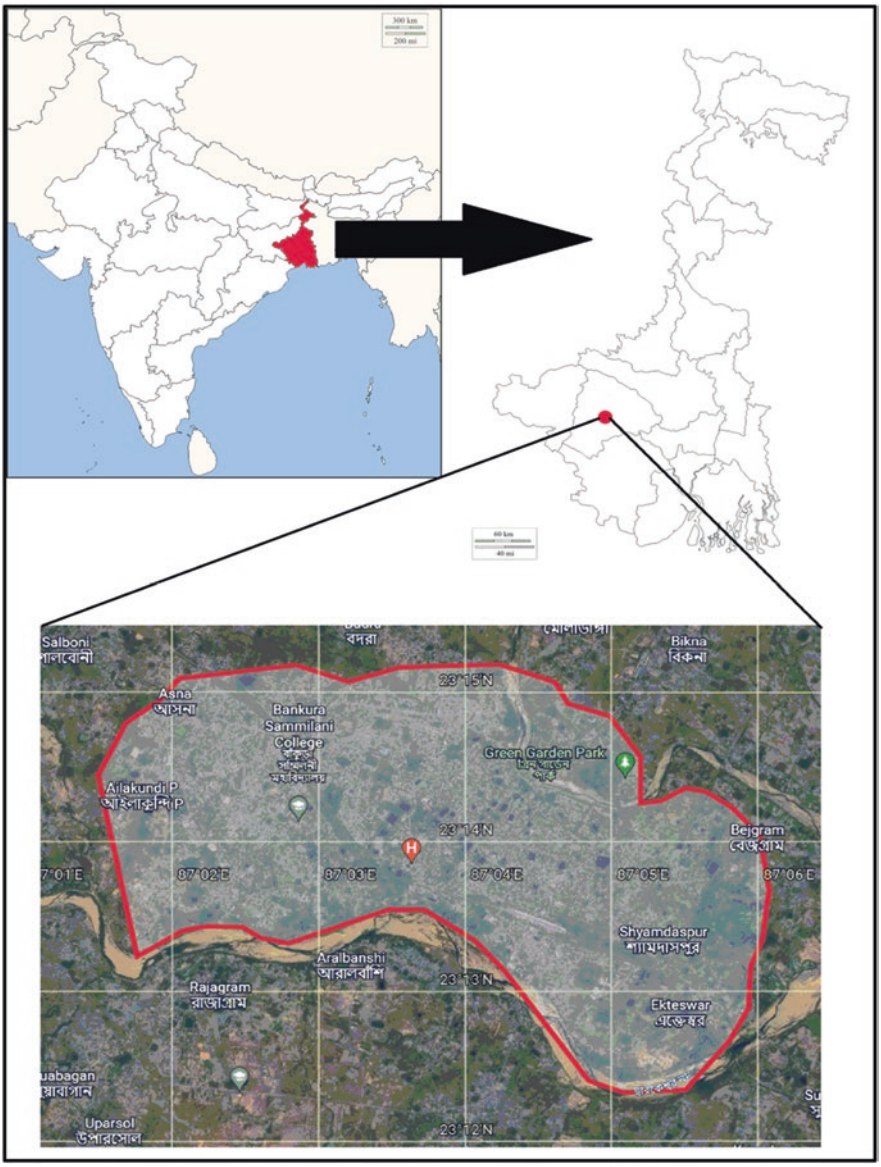

Fig. 8.6 Location of the city

Archaean age covers the major blocks of the district. The district of Bankura has varied types of hydrogeological characteristics. Figure 8.8 shows the geology of the district. The hard rock area comprises the western and southern parts of the district. It is composed of hard Archaean crystalline rock and, in some places, overlaid by sedimentary rocks belonging to the Gondwana group. Groundwater in this area is

Fig. 8.7 The layout of investigation points S1–S8 in the study area

Table 8.4 The GPS location of investigation points

Points	Latitude	Longitude
S1	23° 14′ 16.43″N	87° 03′ 34.46″E
S2	23° 13′ 25.01″N	87° 04′ 32.13″E
S3	23° 15′ 19.45″N	87° 02′ 12.27″E
S4	23° 15′ 00.06″N	87° 02′ 32.62″E
S5	23° 13′ 55.58″N	87° 04′ 41.5″E
S6	23° 14′ 41.65″N	87° 03′ 52.76″E
S7	23° 14′ 47.45″N	87° 03′ 05.01″E
S8	23° 13′ 32.6″N	87° 05′ 05.04″E

restricted and available in limited quantum and occurs in the cracks and fissures and in the weathered zone of the hard crystalline rocks. Aquifers are discontinuous, mostly unconfined, and at places confined to low-yielding secondary aquifers. Depth to water level is between 5 and 10 m bgl in peak summer. In this area, only dug wells are feasible. Dug wells are excavated to a depth of 10 m–15 m depth and having a diameter of 3–4 m. This area is covered by thick lateritic cappings followed by sand and silty clay with kankar. Moderately thick to thin unconfined to semi-unconfined aquifers host groundwater in this region. In the eastern alluvial area, as in Indus, Kotalpur, and Jaypur, block groundwater occurs under confined conditions below a blanket of clay whose thickness varies between 10 and 30 m.

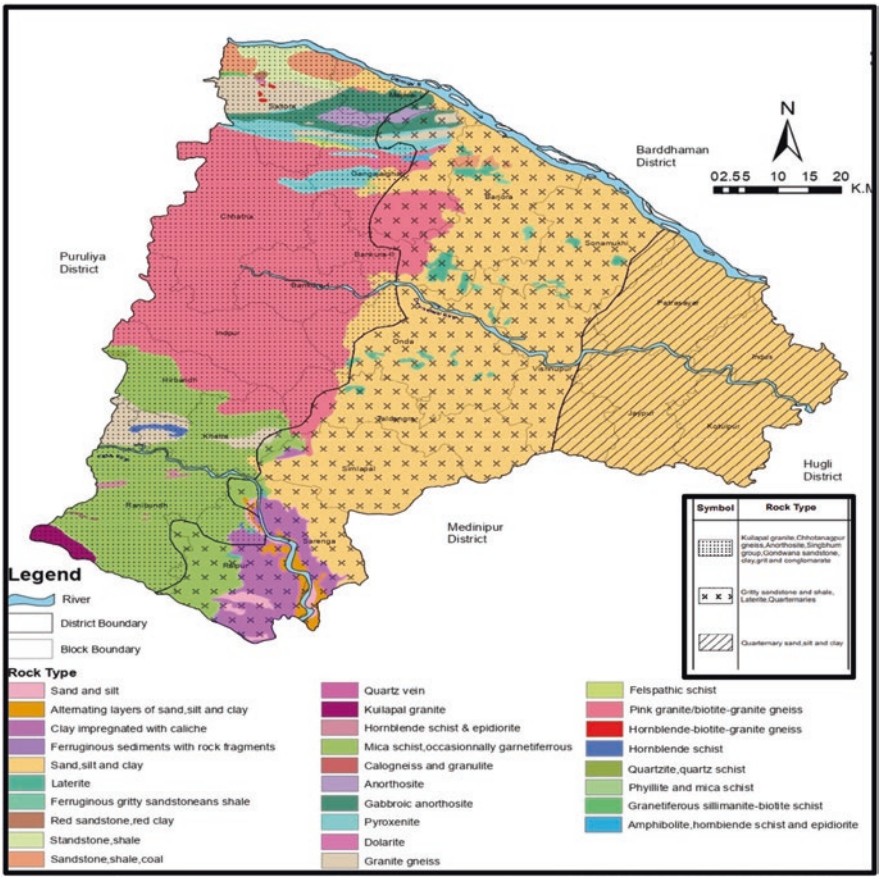

Fig. 8.8 Hydrogeological map of Bankura district. (WBWRIDD website – http://wbwridd.gov.in/swid/mapimages/BANKURA.pdf)

This area is suitable for low depth tube wells with depth up to 100 m, and high-depth tube wells are feasible at Bishnupur, Joypur, Kotulpur, Sonamukhi, Patrasayar, Indus, and part of Barjora and Onda blocks, where the depth may be about 150–200 m bgl having yield 94–184 cubic m/h.

4.2.1 Drainage Pattern

Bankura district is irrigated by the rain-fed Damodar, Dwarkeswar, and Kangsabati rivers, as well as its tributaries, the most important of which is the Gandheswari, Silabati, and Kumari. The streams in the area flow almost parallel to each other from north to south. They are generally hill streams that originate in the western hills. After heavy rains, rivers overflow and then decrease as quickly as they rise. Their sand beds are virtually usually dry in the summertime. Among the various

rivers that flow through to the south of the study region, Dwarakeswar is among the most important. Gandheswari, Kukhra, and Birai are the primary tributaries of the Dwarakeswar stream. Shilabati and Kangsabati, both of which approach the district from Purulia and travel through Bankura's boundaries before entering West Medinipur district, are two more notable rivers. There are a few minor waterfalls along the Shilabati near Harmasra and the Kangsabati near Raipur. Jaypanda, a tributary of Shilabati, and Bhairabanki are two minor rivers in the district.

4.3 Prospecting the Potential Aquifers

4.3.1 Vertical Electrical Sounding Data Acquisition

Data acquisition is the most difficult part of any field study as there are scopes of committing errors while recording data. In order to perform the VES method, Schlumberger electrode configuration was used to collect data at the site of investigation. The values were obtained for a current electrode spacing of 500 m, resulting in the current penetration depth of nearly 160–170 m, since the penetration depth of current ranges between 0.25AB and 0.5AB. VES1 to VES8 were implemented at locations S1 to S8, respectively, in the Bankura study region. After the electrode configuration was set up, the experimental readings were now noted for different AB/2 and MN/2 spacings. The first data was noted down with half current electrode spacing equal to 1.5 m which commenced until the spacing turned to 250 m. On the other hand, the observations started with MN/2 at 0.5 m and subsequently increased with the AB/2 spacing up till a maximum extent of 250 m. For MN/2 equals 0.5 m: the M and N electrodes were separated by 1 m, and the current electrodes A and B were separated by 3 m, resulting in AB/2 equal to 1.5 m for the first observation. The resistivity meter provided the resistance value. The AB/2 spacing was then extended to 2 m, 3 m, and 4 m, respectively. As the AB/2 spacing was already ten times MN/2, it was now time to alter the MN/2 value by increasing the gap between M and N electrodes. For improved results, the MN/2 was increased to 1 m. As soon as the MN/2 spacing equaled 1 m, we repeated the same steps that we followed when MN/2 spacing equaled 0.5 m; the current electrodes were then shifted with AB/2 varying from 4 m to 10 m. MN/2 was then further increased to 2 m at 10 m AB/2 spacing, and successive values of resistance were recorded. This procedure continued until AB/2 equaled 250 m and MN/2 spacing equaled 40 m. At the end of the VES, data up to the depth of 170 m were obtained.

Table 8.5 The analyzed field data

S. no.	ρ1 (ohm-m)	ρ2 (ohm-m)	ρ3 (ohm-m)	T1 (m)	T2 (m)	T3 (m)	Curve type
VES 1	29	79	567	25	95	50	A
VES 2	16	94	512	24	66	80	A
VES 3	33	78	521	18	42	110	A
VES 4	27	72	406	16	61	93	A
VES 5	31	98	498	15	50	105	A
VES 6	30	82	539	12	48	110	A
VES 7	29	108	430	13	62	95	A
VES 8	36	110	410	15	49	106	A

Table 8.6 Inference of lithology

True resistivity values (ohm-m)	Probable lithology
<50	Soft overburden
50–110	Decomposed rocks
110–250	Fractured rocks
250–390	Partially fractured rocks
390–430	Hard rocks with minor cracks
>430	Hard and compact rocks

4.3.2 Analysis of Data

The values of apparent resistivities and AB/2 values obtained from field data were used as input in Resist v.1 fc7 software to get the true resistivity (ohm-m) and thickness (m) of layers. Table 8.5 shows the analyzed result.

Here, ρ1, ρ2, and ρ3 stand for the true resistivities of layers, namely, 1, 2, and 3 whereas T1, T2, and T3 represent the thickness of respective layers On the basis of analyzed data and its correlation with the available borehole data, the probable lithologs corresponding to the true resistivity values are represented in Table 8.6.

Analysis of data reveals the presence of minorly cracked hard rocks which act as an aquifer in this area. The section is encountered within a depth of 64–77 m (having a resistivity range of 406–430 ohm-m). At points S4, S7, and S8, the resistivity of third layer is lower than that of compact rocks at S1, S2, S3, S5, S6, and S7, indicating the presence of minor cracks. Hence at S2, S6, and S10, drilling up to a depth of 170 m can be done. After drilling a borehole at these points using DTH drilling rigs, it was established that the amount of water in these aquifers is very less. A yield test was performed, and very low yield of 1200–1500 liters per hour was observed. On the other hand, the rest of the points consisted of hard and compact rock strata with no porosity up to the depth of 170 m. The sounding curves obtained from the inversion data model in Resist v1.07fc software are represented in the following Fig. 8.9.

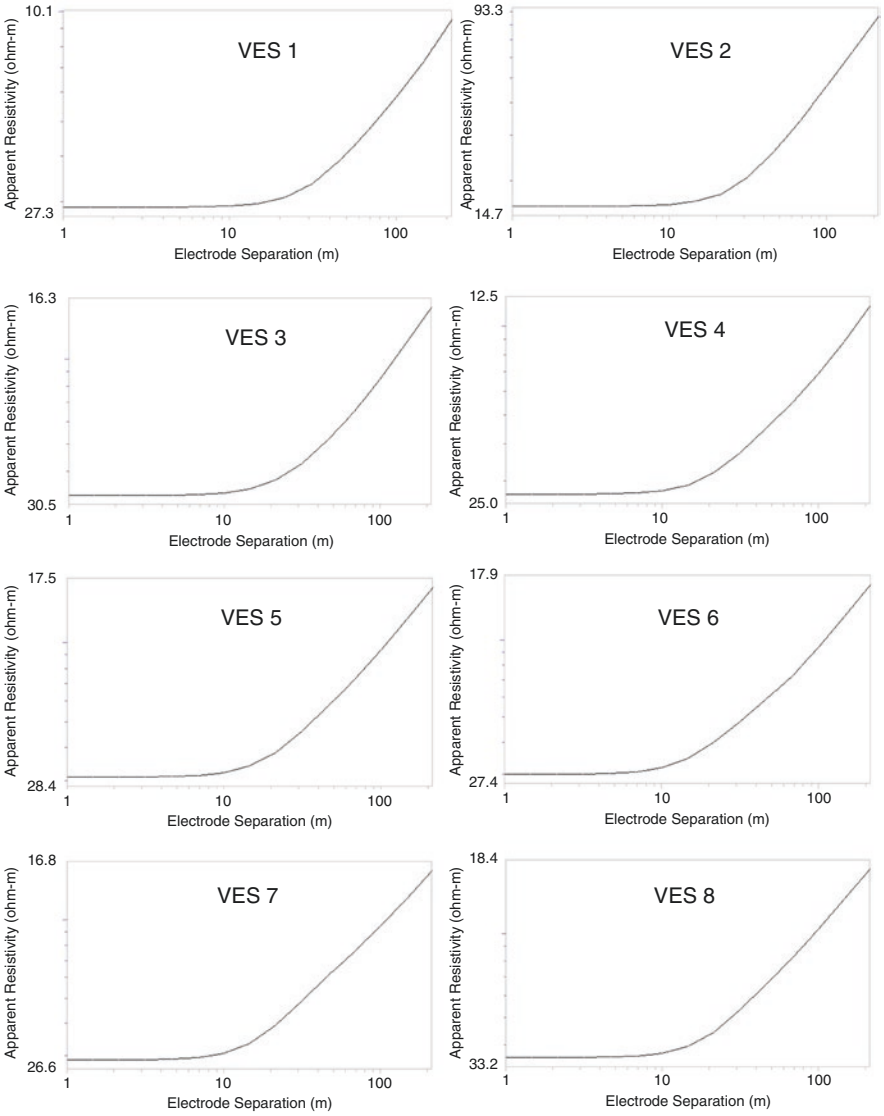

Fig. 8.9 Vertical electrical sounding curves for points S1–S8 in Bankura

4.4 Conclusion

Despite sufficiently high annual rainfall (1430 mm), intervention of drought breathes down the neck of the Bankura district owing to uneven distribution of rainfall. The main problems are due to the high runoff, low soil moisture retaining capacity, low

atmospheric humidity, undulatory topography, and presence of lateritic subsoil etc. In case of the city of Bankura, it was observed that the water sources for the population are the two rivers, namely, Dwarkeswar and Gandheswari, which are the main source of irrigation. But during the summer season, the Dwarkeswar River reduces to a thin hairline stream, whereas its tributary Gandheswari almost dries up. Furthermore, the people of Bankura have to depend upon the dug wells, hand pumps, and tube wells. But due to overexploitation of groundwater, the aquifers have started drying up and yielding a mere 1200–1500 LPH for low powered pumps that cannot meet the water consumption demands. These factors have led Bankura to become a water-scarce city.

5 Recommendations

Being water-scarce cities with huge problems of water crisis, some suggestive measures to overcome the drought situations are mentioned below. These measures are divided into two categories, and one is the short-term measure while the other is long-term.

5.1 Short-Term Measures

The short-term measures for overall balanced groundwater development are:

1. Preservation and maintenance of existing water structures like ponds, dug wells, and bore wells in good condition
2. Setting up of check dams in topographic depressions to store water for summer seasons

5.2 Long-Term Measures

The long-term measures for overall balanced groundwater development include:

1. Optimum utilization of surface running water in the streams by building dams and reservoirs
2. Soil conservation measures like afforestation, contour banding, terracing, and trenching to store water
3. Rainwater harvesting methods must be implemented
4. Artificial recharge should be established at the most suitable site to recharge

References

Chandra, S., Rao, A. V., & Singh, V. S. (2004). A combined approach of Schlumberger and axial pole-dipole configurations for groundwater exploration in hard-rock areas. *Current Science, 86*(10), 1437–1443.

Dhakate, R. (2003). Development and management of ground water resources in chromite mines of Sukinda valley, Orissa. In V. P. Singh & R. N. Yadav (Eds.), *Water and environment ground water pollution* (pp. 51–60). Allied Publisher Pvt. Limited.

Drozhko, E., Ivanov, I., Samsonova, L., Glagolev, A., Glinsky, M., Ter-Saakian, N., Skokov, A., Looney, B., Nichols, R., Hutter, A., & Wollenberg, H. (2002). Assessment of hydrological parameters in heterogeneous fractured rock. *Environmental Geology, 42*(2–3), 178–186.

Ghosh, A. K. (2001). Groundwater investigations of Bharatpur district, Rajasthan, using resistivity method. In *Proceedings of national seminar on ground water resources* (pp. 68–79). Department of Geology, MLS University.

Hanasaki, N., Fujimori, S., Yamamoto, T., Yoshikawa, S., Masaki, Y., Hijioka, Y., Kainuma, M., Kanamori, Y., Masui, T., Takahashi, K., & Kanae, S. (2013). A global water scarcity assessment under Shared Socioeconomic Pathways – Part 2: Water availability and scarcity. *Hydrology and Earth System Sciences, 17*, 2393–2413.

Israil, M. (2003). Determining layer boundaries from apparent resistivity data. In V. P. Singh & R. N. Yadav (Eds.), *Water and environment ground water pollution* (pp. 60–67). Allied Publisher Pvt. Limited.

Jat, M. L., & Jain, L. K. (2007). Determination of aquifer parameter by least squares method under linear flow condition in fractures rocks. *Journal of Agricultural Engineering, 44*(2), 34–37.

Kaore, M. P., & Kokil, A. S. (1990). Discovery of fault zone by resistivity surveys at Dhiwarwadi Taluka Katol, District Nagpur. In *Proceeding Vol. of All India seminar on Modern Techniques of Rain Water Harvesting Water Conservation and Artificial Recharge* (pp. 299–302). GSDA.

Kelekar, A. D. (1990). Identification of potential areas for artificial recharge by resistivity method and use of advanced geophysical technique for its implementation. In *Proceeding of All India seminar on Modern Techniques of Rain Water Harvesting. Water Conservation and Artificial Recharge* (pp. 292–294). GSDA.

Kumar, A., & Thambidurai, P. (2022). Relationship between topography with weathering and water table of Usri watershed of Chota Nagpur Plateau, India. *Arabian Journal of Geosciences, 15-504*, 1–16.

Kummu, M., Ward, P. J., de Moel, H., & Varis, O. (2010). Is physical water scarcity a new phenomenon? Global 226 assessment of water shortage over the last two millennia. *Environmental Research Letters, 5*, 034006.

Kummu, M., Guillaume, J. H. A., de Moel, H., Eisner, S., Flörke, M., Porkka, M., Siebert, S., Veldkamp, T. I. E., & Ward, P. J. (2016). The world's road to water scarcity: Shortage and stress in the 20th century and pathways towards sustainability. *Scientific Reports, 6*, 38495.

Mekonnen, M. M., & Hoekstra, A. Y. (2016). Four billion people facing severe water scarcity. *Science Advances, 2*, 500323.

Murthy, C. S. (1990). Identification of lineaments by electrical resistivity method. In *Proceeding of All India seminar on Modern Techniques of Rain Water Harvesting, Water Conservation and Artificial Recharge for Drinking Water, Afforestation, Horticulture and Agriculture* (pp. 295–297). GSDA.

Nandi, N. C., Venkataraman, K., Das, S. R., & Das, S. K. (2007). Wetland faunal resources of West Bengal. 5. Bankura and Puruliya districts. *Records of the Zoological Survey of India, 107*(2), 61–91.

Niwas, S., & Singhal, D. C. (1980). Estimation of aquifer transmissivity from Dark-Zarrouk parameters in porous media. *Journal of Hydrology, 50*(2), 393–399.

Oki, T., & Kanae, S. (2006). Global hydrological cycles and world water resources. *Science, 313*, 1068–1072.

Postel, S. L. (2000). Entering an era of water scarcity: The challenges ahead. *Ecological Applications, 10*, 941–948.

Sawant, K. (1999). Ground water potential of Bhogawati river basin Solapur distt. Maharashtra. *Journal of Applied Hydrogeology, 12*(1), 1–9.

Schewe, J., Heinke, J., Gerten, D., Haddeland, I., Arnell, N. W., Clark, D. B., Dankers, R., Eisner, S., Fekete, B. M., Colón-González, F. J., Gosling, S. N., Kim, H., Liu, X., Masaki, Y., Portmann, F. T., Satoh, Y., Stacke, T., Tang, Q., Wada, Y., et al. (2014). Multimodel assessment of water scarcity under climate change. *Proceedings of the National Academy of Sciences of the United States of America, 111*, 3245–3250.

Subrahmanyam, K. (2001). Geoelectrical investigation for groundwater in Sanathnagar and Santoshnagar areas of Hyderabad city, Andhra Pradesh. In *Proceedings of national seminar on groundwater resources* (pp. 80–85). Department of Geology, MLS University.

Todd, D. K. (1980). *Groundwater hydrology* (2nd ed., pp. 413–420). Wiley.

Wadatkar, S. B. (1984). *Geophysical exploration for groundwater resources around salkuti, Dist. Midnapore* (Unpublished M. Tech. Thesis, IIT Kharagpur).

WBWRIDD website. (2022a). *Hydrogeological map of Bankura*. Accessed Mar 2022. http://wbwridd.gov.in/swid/mapimages/BANKURA.pdf

WBWRIDD website. (2022b). *Hydrogeological map of Bankura*. Accessed Mar 2022. http://wbwridd.gov.in/swid/mapimages/PURULIA.pdf

Zohdy, A. A., Eaton, C. P., & Mabey, D. R. (1974). *Application of surface geophysics to groundwater investigation* (Tech. water resources investigation). U.S. Geo/Surveys.

Chapter 9
Impact of Urbanization and River Morphology on Groundwater System in Patna Urban Area, Bihar, India

Ashok Kumar and P. Thambidurai

Abstract The impact of increased groundwater demand due to vertical urban growth and a shift in the course of the river Ganges in the Patna urban area (PUA) has been analyzed through a numerical groundwater flow model in this chapter. The model simulation indicated a large cone of depression in the deeper aquifer in the central parts of PUA. The cone of depression of each tube well is interfering with each other. Depending on the pumping rate (2000–7000 m^3/day) of the individual tube well, the radius of influence of wells is between 100 and 200 m. The hydraulic head of the deep aquifer in the central part of PAU has declined by 2 m (maximum) from 1990 to 2002, which has now declined to 4–6 m (maximum) in 20 years. The simulated results with the existing stress conditions on the aquifer system indicate that there is a 0.5 m/year decline in the hydraulic head of the deep aquifer in the central parts of PAU.

Keywords Groundwater · Groundwater flow model · Patna urban area

1 Introduction

Patna urban settlement is situated in a vast Indo-Gangetic plain and on the river Ganges bank (Figs. 9.1 and 9.2). Being on the bank of a huge perineal river, even then, the water supply to Patna UrbanArea (PUA) is met solely from groundwater. It is mostly due to a cost-benefit analysis between surface and groundwater. The Patna Municipal Corporation (PMC), responsible for the drinking water supply, made 110 high-yielding deep tube wells in different localities within the PUA limit.

A. Kumar (✉)
Consultant Hydrogeologist, Dwarka, New Delhi, India
e-mail: ashok.kumar@wateraquifers.com

P. Thambidurai
Department of Coastal Disaster Management, School of Physical, Chemical and Applied Sciences, Pondicherry University-Port Blair Campus, Port Blair, Andaman and Nicobar Islands, India

P. Thambidurai, A. K. Dikshit (eds.), *Impacts of Urbanization on Hydrological Systems in India*, https://doi.org/10.1007/978-3-031-21618-3_9

Fig. 9.1 Google Map of the study area – an extent of model boundary for Patna urban

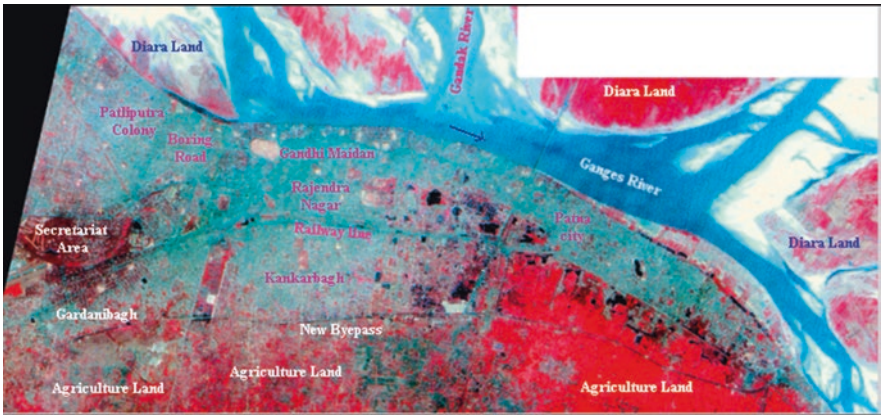

Fig. 9.2 IRS-1D satellite data of Patna urban area and river Ganges (2000)

These tube wells are in a depth range of 150–200 m below ground level. The pumping rate of these well is in between 4000 and 8000 m^3/day, except a few are abstracting in between 3000 and 4000 m^3/day. About 418,000 m^3/day of water is required to provide drinking water to an estimated population of 2.48 million in the municipal area of the city. To meet the demand, the municipal corporation is approximately abstracting 698,000 m^3/day of groundwater through 110 deep high-yielding tube wells in different municipal wards. In 2001, there were 77 operational tube wells, which could abstract a total of 141,000 m^3/day of groundwater against a water demand of 215,240 m^3/day (Table 9.1). Besides, individual residential houses and multistoried apartments are also abstracting groundwater from shallow as well as deep aquifers to meet the water demand for drinking and domestic water. This is additional unaccounted stress to the aquifer system. Patna urban development plan

Table 9.1 Patna urban water demand

Years	2001	2011	2021 (estimated)
Population (million)	1.43	1.73	2.48
Domestic water demand, including commercial/ institutional (m^3/day)	183,700	221,100	372,230
Industrial demand (m^3/day)	21,500	25,900	31,200
Floating population demand (m^3/day)	10,000	12,100	14,641
Total demand (m^3/day)	215,200	259,000	418,071
Designed water supplying capacity (m^3/day)	153,700	96,000	205,000
Deficit (m^3/day)	61,500	163,000	213,071

indicates there will be a need to construct additional 43 new tube wells to meet the projected urban population by 2038 (BRJP, 2003), apart from the existing 77 tube wells in 2001. To be more conservative in estimation, taking minimum efficiency of pumping tube wells, the annual withdrawal of groundwater comes to be 56.10×10^6 m^3/year. There are approximately 1700 apartments in the PUA. Most of the apartments are operating a 5HP submersible pump, which pumps water at a rate of 200 m^3/day. The total conservative withdrawal from the deep aquifer comes around 68.51×10^6 m^3/year, which is higher than the annual replacement of the deep aquifer. So, it may be concluded that pumping is currently being done beyond the sustainable limit.

The hydraulic head of the deep aquifer has a declining trend, whereas the water table in the phreatic aquifer has an increasing trend in PUA (Maitra & Ghose, 1992; CGWB, 2000, 2007, 2015, 2016). The historical data on groundwater level indicates a 1 m decline in the hydraulic head of the deep aquifer between 1990 and 2000. The shallow low-yielding aquifer is already in stressful conditions, and now private tube wells are targeting the deep aquifer from where the municipal corporation is making bulk groundwater supply. This provides an opportunity to study the temporal and spatial behavior of aquifers with the projected groundwater abstraction. The aquifer geometry, dynamic and static storage, interconnection with other hydrological systems, and its spatial and temporal variation require to be understood for its sustainable utilization and development of a long-term management plan for the deep aquifer.

1.1 Study Area

Patna town is situated on the bank of the Ganga river, which is the largest river in India. The study area is the urban limit of Patna town, and this study considers a 210 km^2 geographical area. The study area is located between latitude 25°30′–25°40′ and latitude 85°–85°20′. The old town is located along the natural levee of the river, whereas the new town is spread over the depressional area just after the natural

levee, which is mainly in the eastern part of the town (Fig. 9.2). In topographic elevation within PUA is varying between 45 and 60 m MSL. The western town is at higher elevation and traces of paleochannel of Son River have also been observed. In general, depressional area elevation is about 50–55 m MSL, whereas natural levee elevation ranges between 60 and 65 m MSL. The southwestern has a higher elevation, and the maximum elevation is within the 65 m MSL.

1.2 River Bank Morphology

There is a narrow linear stretch of natural levee that exists all along the river bank in the mid part to eastern part and followed by backside depression land (Fig. 9.3). Natural levee runs all along the river bank, with the eastern side being at a higher elevation which gradually merges with normal ground elevation in the western part. There is a sharp drop in elevation between the river bank and ground where the natural levee gradually ends on the western side and reaches normal ground elevation.

The change in elevation between ground and river bank is also gradual. The lateral flood plain of the river is very wide, and it is up 10 km, whereas the northern bank of the river is stable. The river main flow channel is very dynamic, and it changes every year during the flood period. The river reaches at the high stage during the monsoon period and remains at the lowest stage during summer. The river water level fluctuates between 42 m MSL to 48 m MSL. The flat and wide, low-lying flood plain of the river is likely to act as a recharge area for the shallow as well as deeper aquifers. The river main channel has a very significant role in controlling and inflow and outflow of the aquifer system near PAU. The shifting of the river channel away from the historical southern bank is likely to affect the groundwater sustainability of the aquifer system both in terms of availability and quality. In the

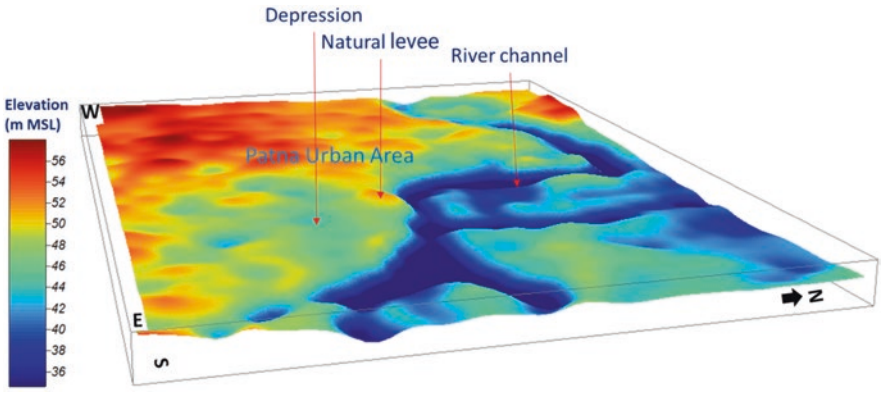

Fig. 9.3 Digital elevation model of landforms in Patna urban area along with the Ganga river

year 2000, the river's main course was away from the historical river bank in the western part (Fig. 9.4), which gradually shifted further north in 2010 (Fig. 9.5). However, the river's main course remained unchanged in the eastern parts. Now in the period of 2019–2021 the river main course will be reached closer to the historical river bank (Fig. 9.6). This dynamic behavior of the main river course, which is unpredictable has a direct impact on the groundwater system of PUA and creates uncertainty in the groundwater recharging capacity of the river.

1.3 Hydrogeology

The PUA is a part of the vast Gangetic plain. The alluvial deposit near Patna has been derived from the transportation of the Himalaya and Chota Nagpur Plateau sediments. The basement depth near Patna is more than 1000 m (Bose et al., 1966). Both the sediments have different hydro-geophysical characteristics (Ashok Kumar & Thambidurai, 2022). It has also been observed that the river Ganges was the dividing line for the sediments brought from the Chota Nagpur plateau and Himalaya. There is the presence of alternate layers of sand and clay (Fig. 9.7).

Broadly, three aquifers are packaged beneath the PUA (Fig. 9.7). The top aquifer is mainly a fluvial deposit dominated by clayey on the back side of the natural levee. The second aquifer, which dominantly consists of fine-grained sand, is beneath the first layer but has reached the ground surface on the western side. The thickness second aquifer is variable over the PUA. There is also a well-defined paleochannel of the river Son, which occupies comparatively high ground level and is a part of the second layer. However, its surface exposure is limited. This acts as a recharge area to the middle-level aquifer and, at the same time, due to its high transmissivity, may pose a risk for contaminant migration to the middle aquifer. The third aquifer is

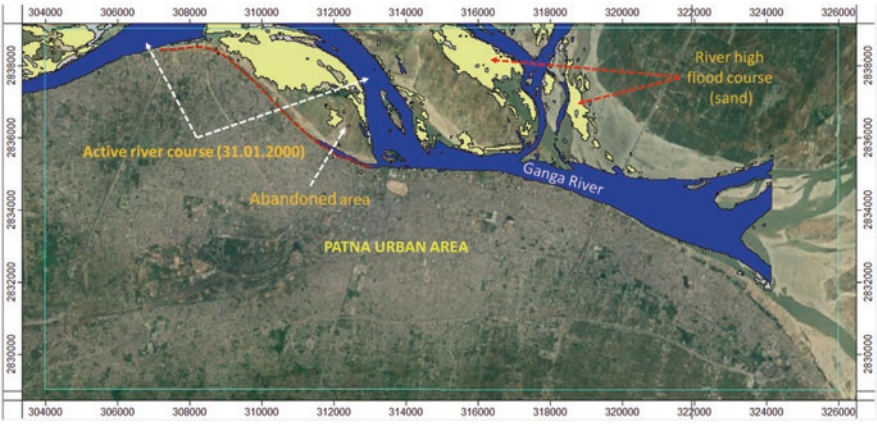

Fig. 9.4 Ganga river main course during January 2000 (lean period) based on satellite data

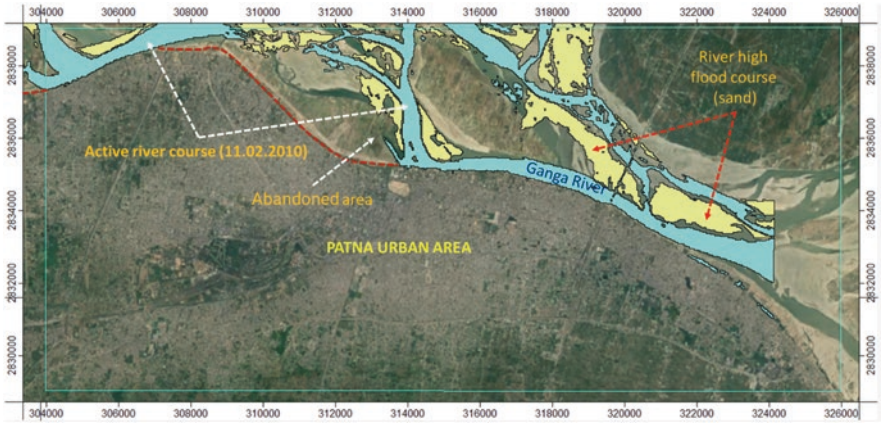

Fig. 9.5 Ganga river main course during February 2010 (lean period) based on satellite data

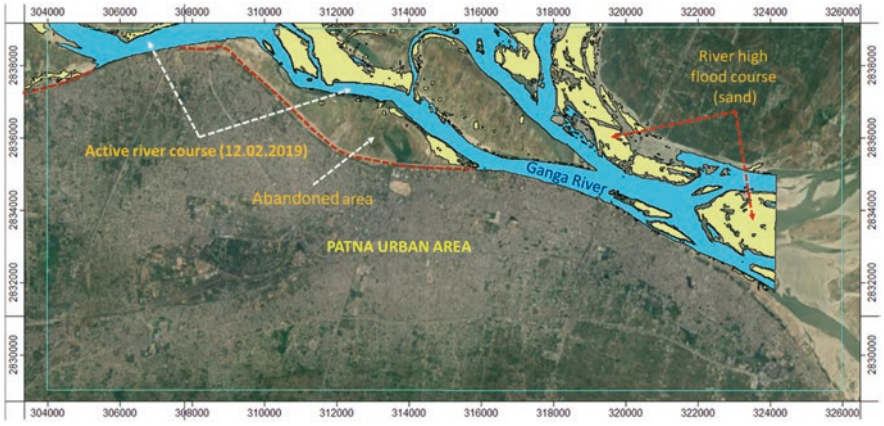

Fig. 9.6 Ganga river main course during February 2019 (lean period) based on satellite data

below the second aquifer, separated by a 30- to 50-m-thick clay layer. The upper portion of the third aquifer consists of medium sand and gradually changes to gravel and pebbles in depth. The third aquifer is very thick and widespread. This aquifer serves as the principal aquifer for the Patna urban water supply. The water table data for 1985 (Fig. 9.8) depicts regional groundwater flow patterns. But rapid urbanization after 1985 has resulted in a change in flow patterns. The water level of the unconfined aquifer has a rising trend (BRJP, 2003). This is mainly due to increased recharge from urban drainage and soaks pits. The hydraulic head of the deep aquifer has decreasing trend due to the high abstraction of urban water supply. The hydraulic head (Fig. 9.9) of the third aquifer varies between 41 and 45 m MSL. The higher head value is in the upper reaches compared to the head value near the river. In the

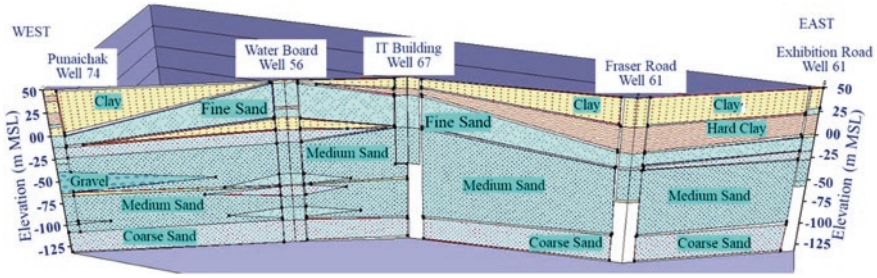

Fig. 9.7 Fence diagram of multilayer aquifer system in the urban area of Patna

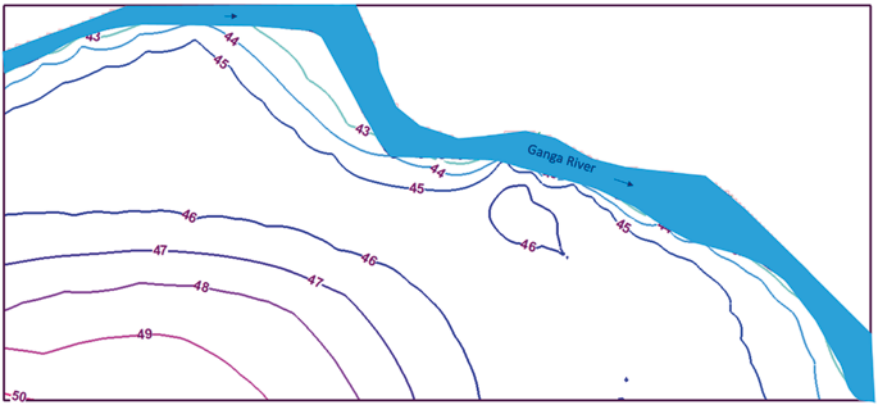

Fig. 9.8 Hydraulic head of unconfined aquifer (layer-1) in 1985

deep aquifer (third aquifer), the dominant flow direction of groundwater is from SW to NE direction.

The unconfined aquifer has been less explored in the earlier scientific study, and very limited data is available on aquifer parameters. The present study has been characterized based on available published information (Maitra & Ghose, 1992). The third aquifer (confined) has been explored in detail by the CGWB (1981, 1996, 2000). It has been observed that the transmissivity value of the aquifer varies from 3500 to 17,000 m^3/day. The storage coefficient varies from 0.005 to 0.0001 (Table 9.2).

1.4 Groundwater Recharge Potential

Presently 210 km^2 area of PUA is under consideration, and the average annual rainfall is 996 mm in the area. However, the mid-eastern parts of PAU are dominated by a thick clayey layer, and it is expected that recharge to lower aquifer is likely to be

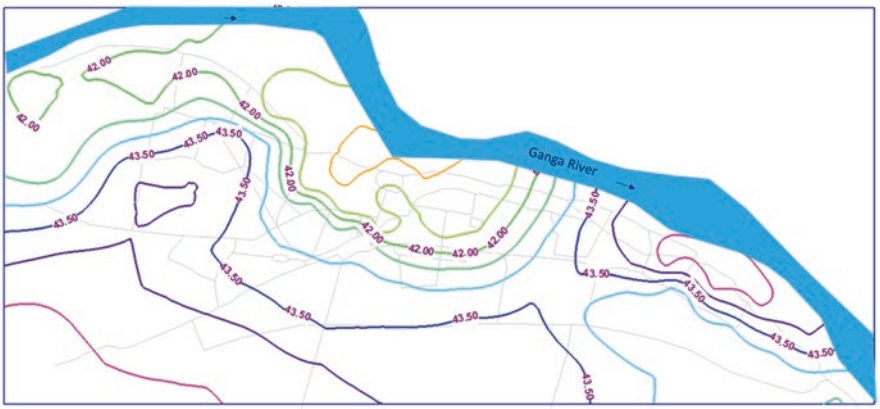

Fig. 9.9 Hydraulic head of confined aquifer (layer-4) in 1985

Table 9.2 Transmissivity of the deep aquifer (layer-4) at different location in PUA

Name	Transmissivity (m^3/day)	Name	Transmissivity (m^3/day)
Takiyapur, Danapur[a]	5775	Anisabad[b]	6621
Danapur[a]	15,984	Begampur[b]	3786
Raj bhawan[a]	6989	Chhajjubagh[b]	7114
Sanskrit Vidya Parishad[a]	3600	Congress maidan[b]	5892
CDA (MES), Kadamkuan[a]	4982	Goalghar[b]	14,113
P&T colony, Kidwaipuri[a]	4908	Harding road[b]	6820
Bata shoe co., Digha[a]	4393	Karbigahiya[b]	8057
Press field, Gilzarbagh[a]	3529.9	Khagaul[b]	17,000
PESC ltd., Mithapur[a]	8163	Khajekalan[b]	10,246
Chandmari road[b]	13,650	Phulwari Sharif[b]	7894
TW no.2, Kankarbagh[b]	5144	Sanatan dharamshala[b]	6980
Mangal Talab, Patna City[b]	7896	Digha[b] ***	7068
Phulwari changar[b]	2008.9	Malsalami[b]	12,235
Aalamganj[b]	9882	Harding park[b]	9924

Source: [a]Maitra & Ghose (1992), [b]BRJP (2003)

limited in this area, whereas the western parts have better groundwater recharge prospects both due to comparatively better hydraulic characteristics of the unconfined aquifer. The historical data has indicated that the average seasonal variation in the third (confined) aquifer is approximately 1.5 m in groundwater level. The recharge to the groundwater system has been estimated, assuming rainfall infiltration as 15% and specific yield as 0.10. The annual increment in groundwater has

been computed on the basis of seasonal variation of water level as well as rainfall infiltration factor. The annual groundwater increment on the basis of the rainfall infiltration method is 31.50×10^6 m^3/year, whereas the methodology based on specific yield and seasonal rise in water is 78.50×10^6 m^3/year. This difference between the two methodologies indicates that seasonal rise in water level of deep aquifers is not only governed by rainfall recharge from the top surface, but recharge from Ganga river and inflow from surrounding parts of the aquifer also contribute. This estimate requires a better understanding of the entire groundwater system in the PUA. The numerical groundwater model is one of the better tools to visualize the entire groundwater system and forecast the long-term behavior of the groundwater system with current and projected stresses to the entire groundwater system.

2 Numerical Groundwater Model

The numerical groundwater flow model has been developed using MODFLOW 2005 package with available data. The deep tube wells drilled by the BRJP (2003) has provided vital information about the aquifer property. Earlier studies carried out by Chatterjee and Garrett (1953), Nath (1981), Pandey et al. (1982), Maitra and Ghose (1992), Nath and Tripathy (1996), and BRJP (2003) have provided historical data. Data on temporal and spatial variations in the hydraulic head of the third aquifer was limited, and it has been generalized over a large area. Therefore, the developed groundwater model is based on various assumptions or generalizations. The model has been tested for 10 years by considering monthly stresses to the aquifers. This has been done mainly to observe the influence of the Ganga river stage on the aquifer behavior.

2.1 Aquifer Geometry

Based on the available lithologs, aquifer geometry has been conceptualized. It has been found that it is more appropriate to consider four layers aquifer system to reasonably apply the stresses to different layers (Figs. 9.10 and 9.11).

2.2 Hydraulic Properties

The lithological evidence indicates each layer is not completely isolated from the others. It has some interconnection between them in many places. Therefore, the hydraulic properties of each layer have been subdivided into different zones to take care of the spatial variation in aquifer property (Table 9.3).

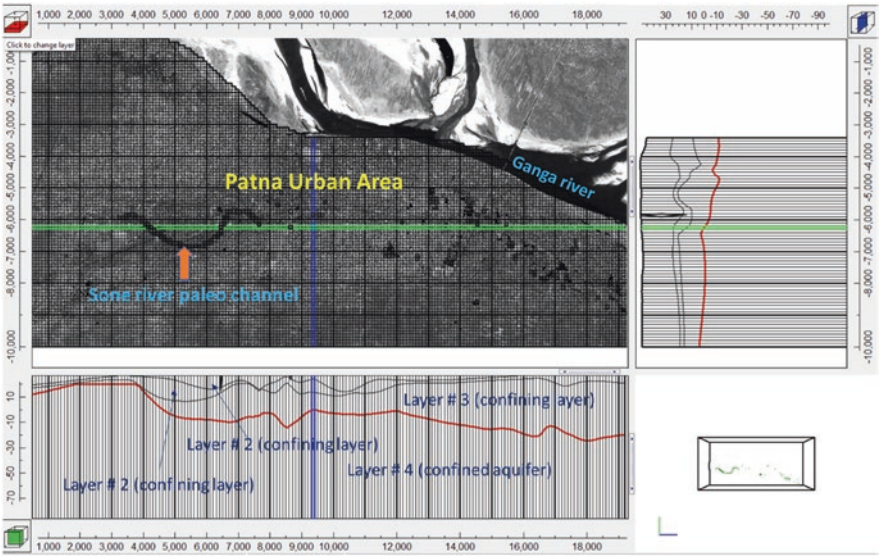

Fig. 9.10 Conceptual layer geometry within Patna urban settlement in modelling environment

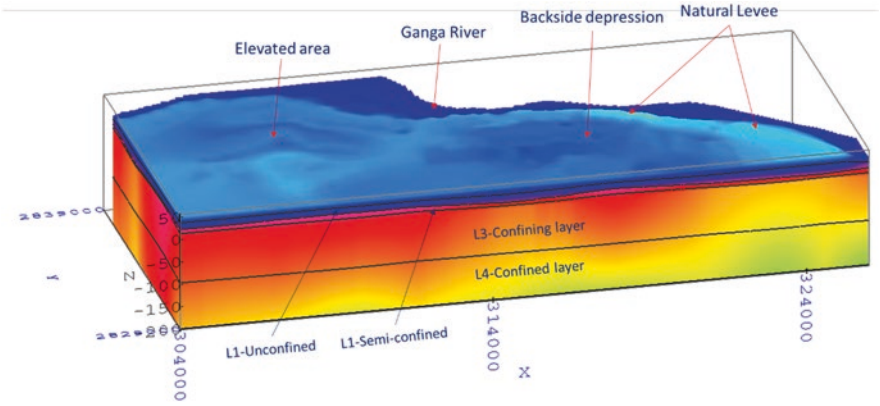

Fig. 9.11 3D visualization of layer geometry within Patna urban settlement in modelling environment

2.2.1 Initial Head

The initial head has been derived from the historical data and its trend. Based on the trend of the long-term hydraulic head of different layers, the historical water level of 1985 has been extrapolated up to 2003. The interpolated head has been further smoothed by running the model in steady state conditions (Figs. 9.12 and 9.13). The transient head of the middle aquifer (layer-2) and lower aquifer (layer-4) shows the cone of depressions in the pumping well area (Fig. 9.14). The historical data

Table 9.3 Model parameter for aquifer system of Patna urban area

	Layer-1	Layer-2	Layer-3	Layer-4
	Fine sand clay intermixed	Fine to coarse sand	Dominantly clay, fine to coarse sand	Coarse sand and gravel
Hydraulic conductivity (m/day)	0.1–1	–	–	–
Transmissivity (m^2/day)	–	6000	500–4000	8000
Primary storage coefficient	0.001–0.18	0.0025	0.001–0.00001	0.005
Aquifer porosity	0.18–0.20	0.27	0.1–0.21	0.25
River bed conductance (m^2/day)	10,000 (assumed on the basis of best fit case)			
Recharge (m/day)	0.0005			
Evapotranspiration (m/day)	0.0003			

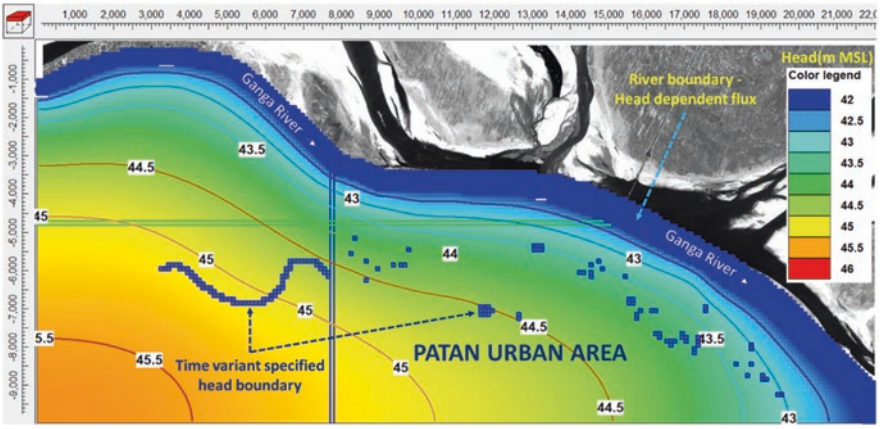

Fig. 9.12 Model of initial steady state hydraulic head (2003) of layer # 1 (unconfined aquifer)

indicates that the upper unconfined aquifer (layer-1) and deep confined aquifer (layer-4) have a different hydraulic head. The upper aquifer (layer-1) has a higher hydraulic head and is more uniform than the lower aquifer (layer-4). This is mainly due to the upper aquifer's negligible utilization of the upper aquifer, whereas the lower confined aquifer is being heavily utilized for town water supply as well as for individual households for drinking and domestic water needs.

2.2.2 Model Boundary Conditions

The considerable part of the eastern side of PUA is located on the back side depression of the natural levee. Many permanent water bodies/waterlogged area exist. Similarly, a water-filled paleochannel of Son River is present. These water bodies

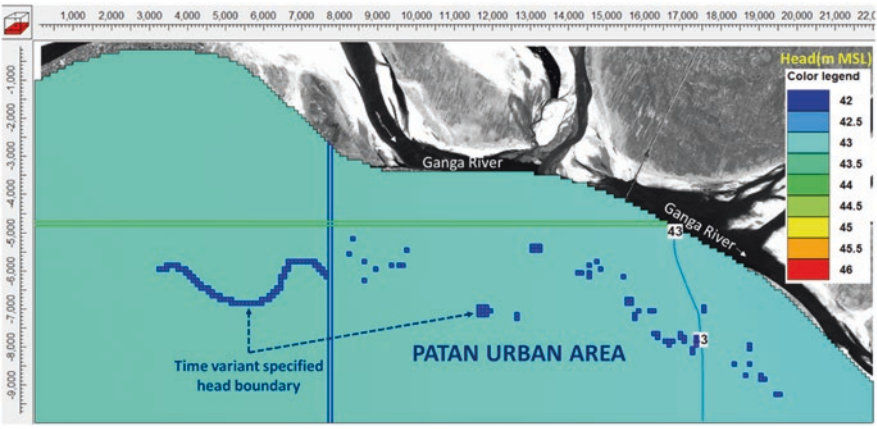

Fig. 9.13 Model of initial steady state hydraulic head (2003) of layer # 4 (confined aquifer)

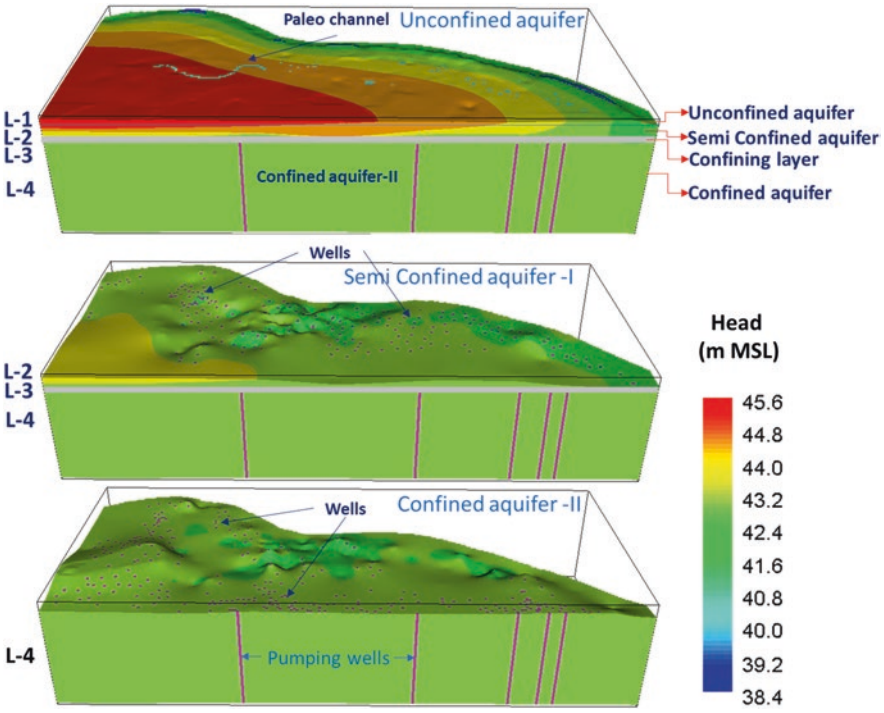

Fig. 9.14 Model Transient hydraulic initial heads of different aquifers

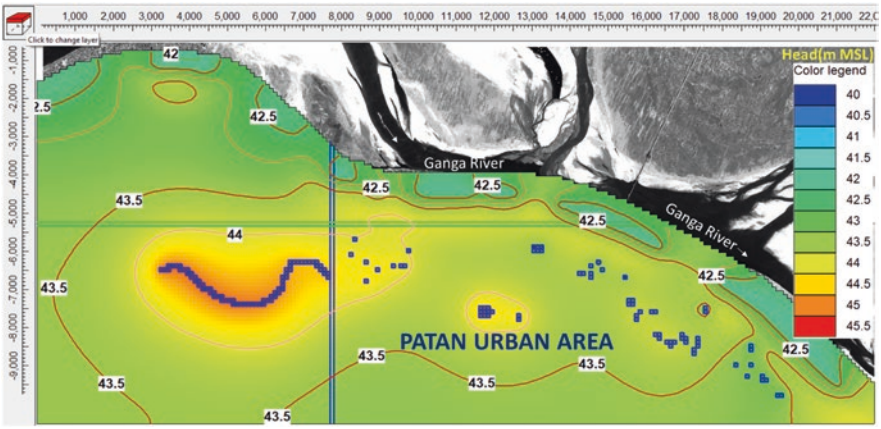

Fig. 9.15 Simulated head of the upper aquifer (layer-1) at the end of 10th year

have been treated as time-variant specified head boundaries in the development of the model (Figs. 9.12 and 9.13). The vast stretch of the Ganga river has been treated as a head-dependent flux boundary in the development of the model (Figs. 9.12 and 9.13). This model boundary varies with monthly river flow stages.

2.3 Model Simulation

Aquifer behavior has been simulated for 10 years (Figs. 9.15 and 9.16) with projected population growth and urban water need. The model has been simulated on a monthly stress period mainly to understand the impact of fluctuating river flow stages of the Ganga river. The model has been calibrated with the initial observed value, and it has been used for long-term prediction (Fig. 9.17). The 10 years of simulation has been found reasonable to understand the river and aquifer interactions as well as long-term aquifer behavior of the upper and lower aquifer (layer-1 and layer-4) under different external stresses. This has helped to predict the likely impact on the aquifer due to the heavy utilization of the lower aquifer to meet the drinking and domestic water demand of the entire Patna urban population.

3 Results and Discussion

The simulated results of the 10-year period with a stress period length of 1 month have indicated that the water table in some parts of the upper aquifer (unconfined) has a rising trend (Fig. 9.19). This may be due to negligible utilization of groundwater from this aquifer, and water logging has increased with time due to drainage

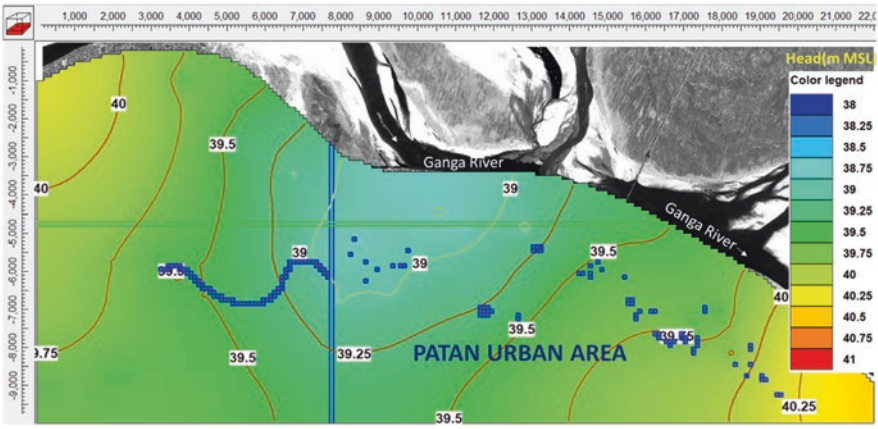

Fig. 9.16 Simulated head of the deep aquifer (layer-4) at the end of 10th year

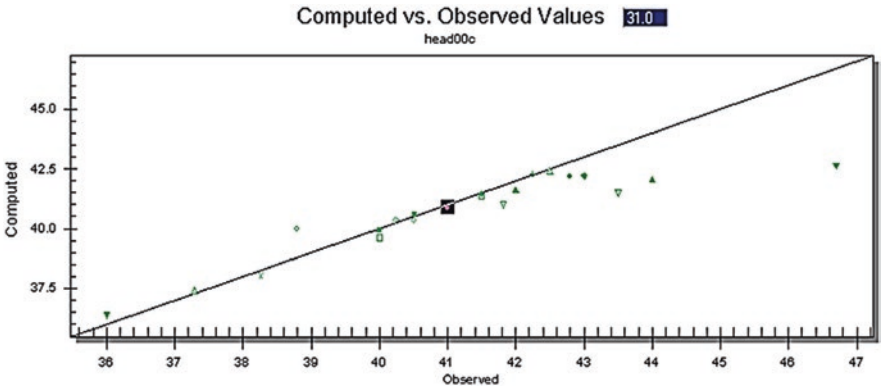

Fig. 9.17 Observed and computed head plot showing model calibration

congestion. Leaking soak pits and underground drainage systems are another source of recharge to the upper aquifer. The model simulation has indicated a 4.5–5.5 m decline in the hydraulic head during 10 years in the central area close to the river bank (Fig. 9.18). This area is part of the densely populated old part of town and a greater number of closely spaced high discharge tube wells operate in the area to meet the water demand of the urban population. It has also been observed that there will be an overall drop of more than 3 m in the hydraulic head within the entire PUA. It is likely to be a 0.3 m/year drop in the hydraulic head. The interfering cone of depressions of individual large volume pumping wells is now in the lower (confined) aquifer which has created a large cone of depression in the central part of the urban area. The hydraulic head of the lower (confined) aquifer near Patna maintains the level of river Ganga river in the north and Purpun river in the east and south, and observed seasonal fluctuation in the hydraulic head is due to direct or indirect interconnection between river and aquifer.

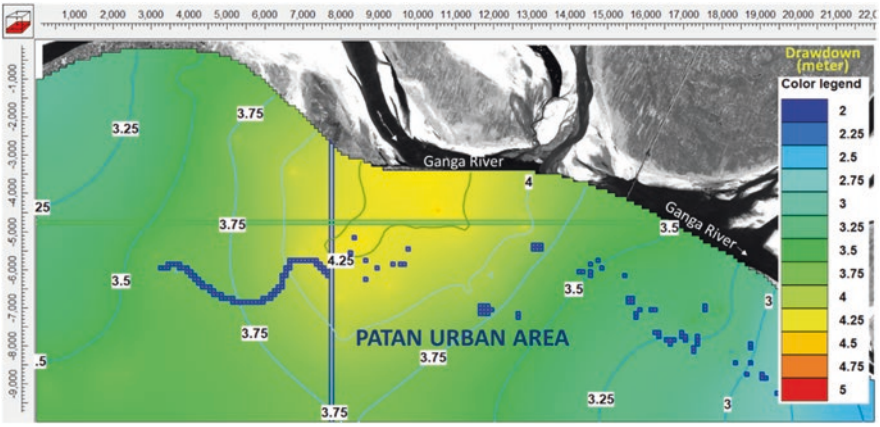

Fig. 9.18 Simulated drawdown of the deep aquifer (layer-4) at the end of 10th year

The model simulation has also indicated that the aquifer system of PUA is actively connected with the Ganga river and the river stages control the hydraulic head with time (Figs. 9.19 and 9.20). Its effects are more visible in the upper aquifer (Fig. 9.19). During the peak summer, the hydraulic head is about 43 m MSL near the river, whereas the river stage during this period remains at a level of 42 m MSL. During this period, aquifer outflow comes to the river. But during the peak flood period, i.e., the river at the highest flow stage (47 m MSL) situation reverses, river flow contributes to the near bank parts of the aquifers, and a rise in the hydraulic head has been overserved during this period. As the river flow stage decreases, the hydraulic head also starts declining. The effect of the river stage on the hydraulic head of the upper aquifer is visible up to 200–500 m inward from the river bank. The impact on the hydraulic head due to time-varying river stages is not visible in the lower (confined) aquifer (Fig. 9.20). But it cannot be concluded that there is no impact of river stage on the lower (confined) aquifer mainly because depletion in hydraulic head heavy pumping dominates and the aquifer has a continuous declining trend. Also, inflow from river to lower (confined) aquifer is relatively less than the rate of continuous constant outflow from aquifer, i.e., abstraction. This understanding is based on the flow water budget of the model (Fig. 9.21).

The river leakage to the aquifer system is about 116,000 m^3/day at the end of the stress period 10, i.e., the end of September, which is also when the Ganga river flows at the highest stage. Once the river flow stage starts to decline, leakage from the river into the aquifer also starts to decline. At the end of December, situation gets reversed; aquifer system started contributing to the river. It has been found that outflow from the aquifer to the river will be 71,000 m^2/day at the end of the stress period 13, i.e., the end of December, whereas river inflow to the aquifer will be negligible. The maximum inflow into the groundwater system surpasses the rainfall recharge to the aquifer system. Therefore, any long-term change in the river system in terms of flow volume and morphology will likely impact heavily on the groundwater system of PUA.

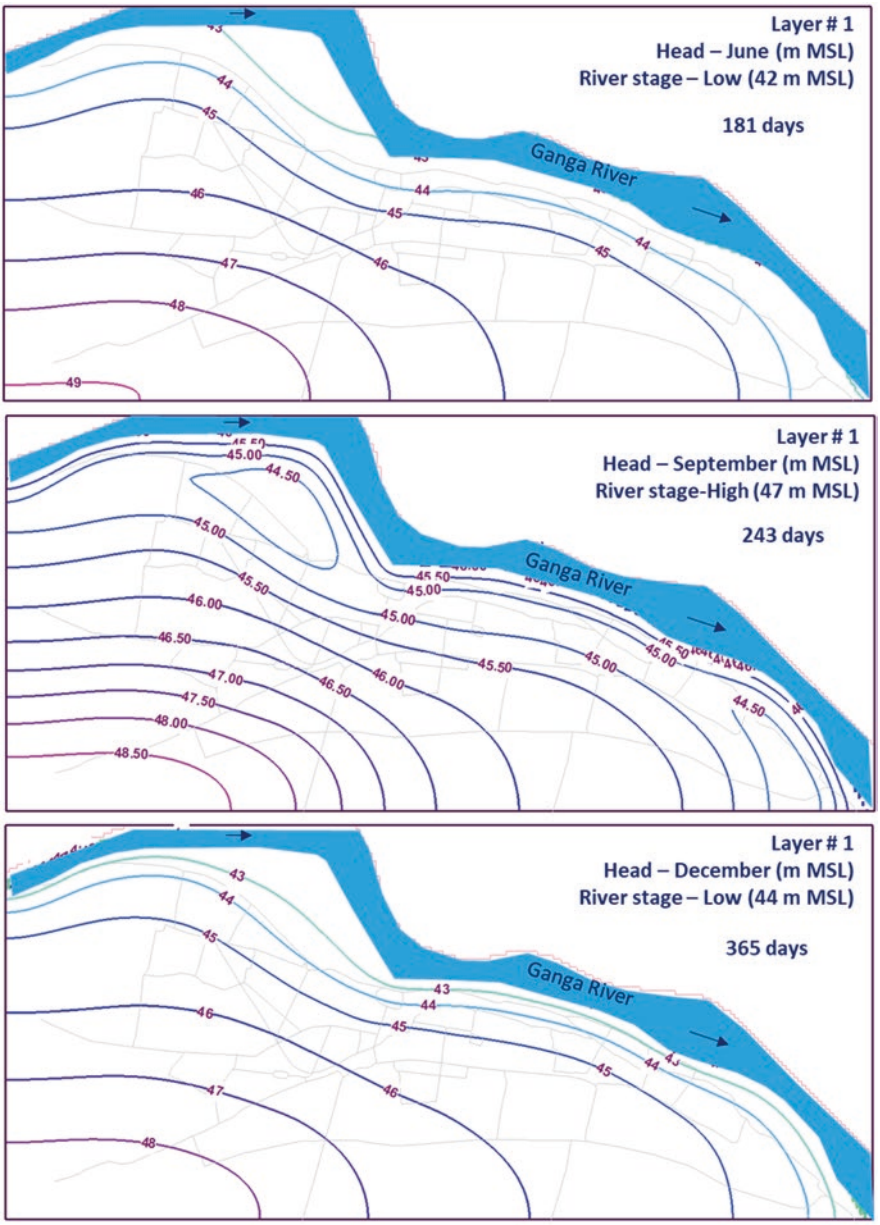

Fig. 9.19 Simulated hydraulic head of upper (unconfined) aquifer at different river stages

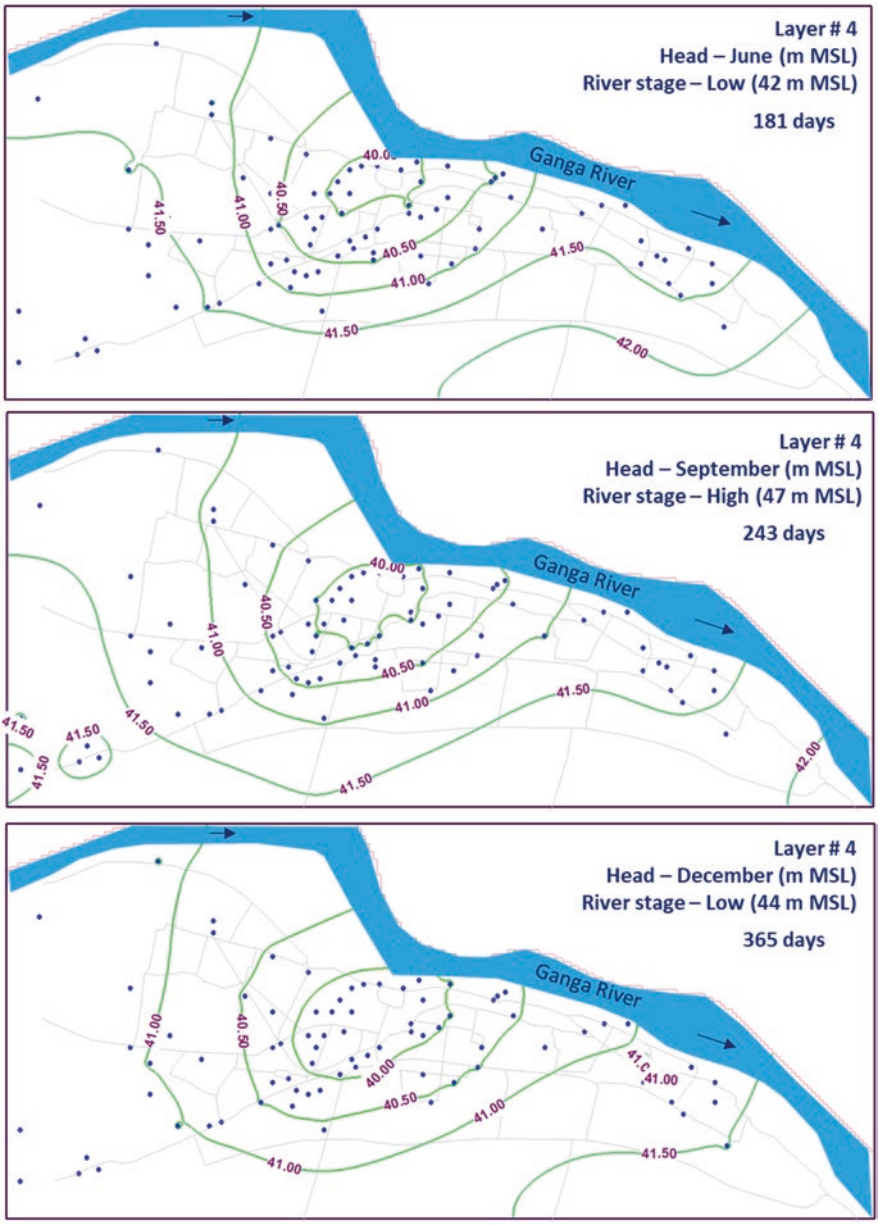

Fig. 9.20 Simulated hydraulic head of lower (confined) aquifer at different river stages

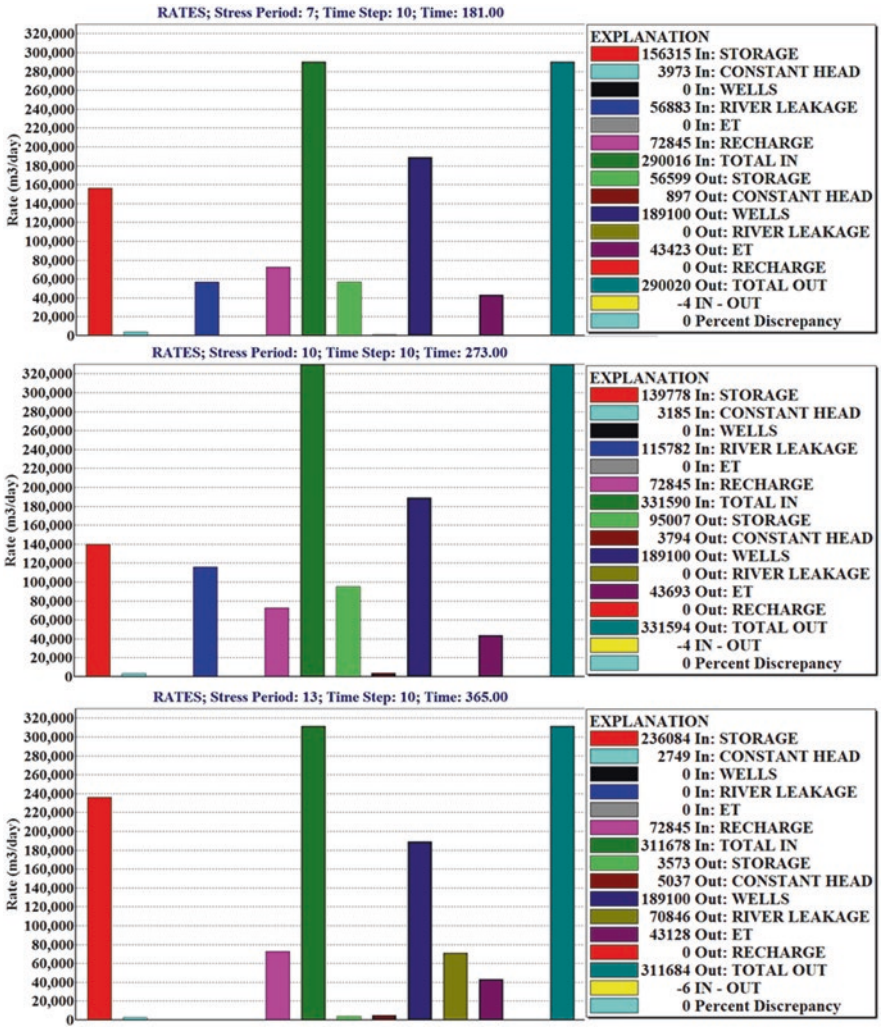

Fig. 9.21 Flow budget components during different stress periods (SP) of the year

4 Conclusions

The conceptual model has helped to understand the temporal and spatial behavior of the unconfined and confined aquifers under natural and human-induced stress conditions. It has been observed that there is a continuous decline in hydraulic heads in the lower (confined) aquifer. The hydraulic head of the lower (confined) aquifer is likely to decline at the rate of 0.3 m/year. This indicates that large volume abstraction from the lower aquifer for the town water supply is not sustainable. Results also indicated that high-rate pumping by individual tube wells interferes with each other, and in the long run, a large composite cone of depression will be created within the central part of the urban area. The new well fields must be shifted outside the

composite cone of depression to avoid further deepening and should be uniformly distributed over large areas. The overused confined aquifer cannot be replenished through artificial recharge due to the high hydraulic head of both the upper and lower aquifer. At the same time, the artificial recharge system likely creates a risk of aquifer contamination as recharged water will directly reach into the capture zone of operating tube wells. Engineering measures need to be adopted be to keep the water level of the upper aquifer below the ground level; otherwise, there will be risk of entering urban pollutants into the aquifer. The study has indicated a strong interaction between the Ganga river and the aquifer system inflow, and outflow from the aquifer is significant compared to the other components of inflow into the aquifer. It has been observed that the river morphology of the Ganga river has dynamic flow and drastic changes in the river course near Patna town, which is connected to the groundwater system. The vast low-lying flood plain is the main source of recharge to the aquifers, and it guides the seasonal fluctuation in the aquifer. Therefore, protection of flood plain from urbanization is one of the important aspects of avoiding long-term abrupt changes in aquifer behavior.

References

Bose, P. K., Saikia, B. C., & Mukherjee, B. B. (1966). Refraction seismic survey for groundwater in Patna and Gaya, Patn*a and Munger districts, Bihar*. Geological Survey of India.

BRJP. (2003). *Modified pre-feasibility report for water supply project of Patna town under Integrated Development Scheme of Patna*. Bihar Rajya Jal Parshad, Urban Development Department, Government of Bihar.

CGWB. (1981). Exploratory well Drilled in Patna Urban Area, Unpublished report, Central Ground Water Board, Mid Eastern Region, Patna.

CGWB. (1996). Exploratory well Drilled in Patna Urban Area, Unpublished report, Central Ground Water Board, Mid Eastern Region, Patna.

CGWB. (2000). Exploratory well Drilled in Patna Urban Area, Unpublished report, Central Ground Water Board, Mid Eastern Region, Patna.

CGWB. (2007). *Ground Water Information Booklet of Patna District, Bihar State*. Central Ground Water Board, Ministry of Water Resources, Government of India.

CGWB. (2015). *Report on Pilot Project on Aquifer Mapping in Maner-Khagaul Area, Patna District, Bihar* (Watershed-GNDK013). Central Ground Water Board, Ministry of Water Resources, River Development & Ganga Rejuvenation, Government of India.

CGWB. (2016). *Report on Aquifer Mapping in parts of Saran, Vaishali, Samastipur, Begusarai and Patna districts, Bihar* (NAQUIM_Phase-II). Central Ground Water Board, Ministry of Water Resources, River Development & Ganga Rejuvenation, Government of India.

Chatterjee, G. C., & Garrett, A. A. (1953). *Observation on a deep tube well at Patna, Bihar*. Geological Survey of India.

Kumar, A., & Thambidurai, P. (2022). Relationship between topography with weathering and water table of Usri watershed of Chota Nagpur Plateau, India. *Arabian Journal of Geosciences, 15-504*, 1–16.

Maitra, M. K., & Ghose, N. C. (1992). *Groundwater management – An application* (pp. 1–301). Efficient Offset Printers.

Nath, S. (1981). *Groundwater resources and development potential of Patna district, Bihar* (Technical Report, Series D). Central Ground Water Board.

Nath, S., & Tripathy, P. K. (1996). *Groundwater in Patna District*. Central Ground Water Board (MER).

Pandey, K. S., Nath, S., & Khan, H. A. (1982). *Basic data report on production well at Rajbhawan, Patna district* (Bihar Technical Report., Series C, No. 109). Central Ground Water Board.

Chapter 10
Aquifer Storage and Recovery: Key Issues and Feasibility

Gopal Krishan and Rahul Garg

Abstract Water is abundant on our planet, but its disparate occurrence at the spatial and temporal scale is causing panic. Apart from the sporadic availability of water resources, contamination is another major threat to the water supply. Developing countries like India, with a humongous population to sustain and minimum water infrastructure, stands at a vulnerable spot. As a resilient society, there is a need to devise innovative methods or improve the existing technologies of freshwater supply. This study also aims to comprehend, identify, and improve the global understanding of groundwater remediation methods based on the dilution of contaminants. We constructed a sand-based aquifer model to experiment with the well-known method of aquifer storage and recovery (ASR) as a model to ameliorate the water crisis in regions that have water scarcity and contamination problems. The benefits, historical developments, and recent advancements are thoroughly discussed. Along with the experimentation, key technical issues and methods to enhance the feasibility of the ASR are explored in detail and how the advancement in the hydrological investigation techniques facilitates the implementation of the ASR with time.

Keywords Geochemistry · Groundwater remediation · Sandbox experiment · Water scarcity

1 Introduction

In the face of climate change and the burgeoning human population, keeping an adequate freshwater supply is essential. The sporadic occurrence of freshwater resources is further exacerbated by land-use changes, vast agricultural developments, deforestation, and contamination. Groundwater accounts for 30% of all available freshwater on the earth and is still the most reliable source of water supply. In regions with no access to surface water resources, communities, agriculture, and

G. Krishan (✉) · R. Garg
National Institute of Hydrology, Roorkee, India
e-mail: drgopal.krishan.nihr@gov.in

P. Thambidurai, A. K. Dikshit (eds.), *Impacts of Urbanization on Hydrological Systems in India*, https://doi.org/10.1007/978-3-031-21618-3_10

industries are heavily dependent upon groundwater. However, many such areas are threatened by groundwater scarcity due to over-abstraction, climate change, and groundwater contamination, both anthropogenic and (geo)genic. All these threats make it more difficult for societies to access free water and do their daily chores. As a resilient society, we have to devise some cost-effective and efficient ways to remediate these natural resources and make them available for common use. Many methods for groundwater remediation have been invented in the last century. The use of each and every method depends primarily upon the hydrogeology and chemical, physical, economic, and social feasibility of the technique. Among them, one such technique is aquifer storage and recharge, which has emerged as a boon to semiarid areas in providing freshwater supply at a very low cost. Aquifer storage and recharge (ASR) is a water management technique for actively storing excess freshwater during wet periods and recovering it during dry periods. It presents a viable option to harness the full potential of groundwater. As the name suggests, freshwater from different surface sources like rainwater, reservoirs, ponds, rivers, and desalinated water can be stored temporarily in a subsurface environment for future recovery and use. Think of the ASR as a storage unit, either physically or chemically bound from all sides to confine freshwater within the unit. Physical boundaries are impermeable stratigraphic units that do not allow water movement. However, chemical boundaries are created by the difference in fluid properties like salinity and density; se boundaries emerge as a mixed zone in the system. Throughout the world, the ASR has been successfully implemented at numerous sites and proved very efficient. More than 175 active ASR well fields are operational in the United States (Dillon et al., 2019), followed by Australia, Europe (Sprenger et al., 2017), Latin America, the Arabian Peninsula, and South America. The ASR is more suitable and effective than other available remediation options because of several reasons:

1. Large quantities of water can be recovered. Since ASR harnesses the potential at the aquifer level, a huge volume of water can be stored and recovered from the ground, providing freshwater supply from household level to state level. The stored water can be used for seasonal or yearly groundwater supply.
2. The biggest advantage of ASR is that it is cost-effective and easy to implement. A simple injection of freshwater with prior subsurface knowledge is required to implement this method. Due to its cost-effectiveness, it's very favourable for developing or low-income communities. The easy and handy implementation makes it a very common method of remediation.
3. Stored water free from environmental or organic pollutants. If we store the excess water in open surface storage like ponds, rivers, and lakes, they are prone to developing more organic and inorganic contaminants. Several diseases like malaria and dengue may rise if large quantities of water are left open. To further use them, we need an extra step to check for contamination and clean for organic pollutants. However, ASR is closed from all sides, and it's very unlikely that they develop any organic contaminants, but care must be taken in choosing the specific site of the ASR because the presence of organic sediments in the subsurface

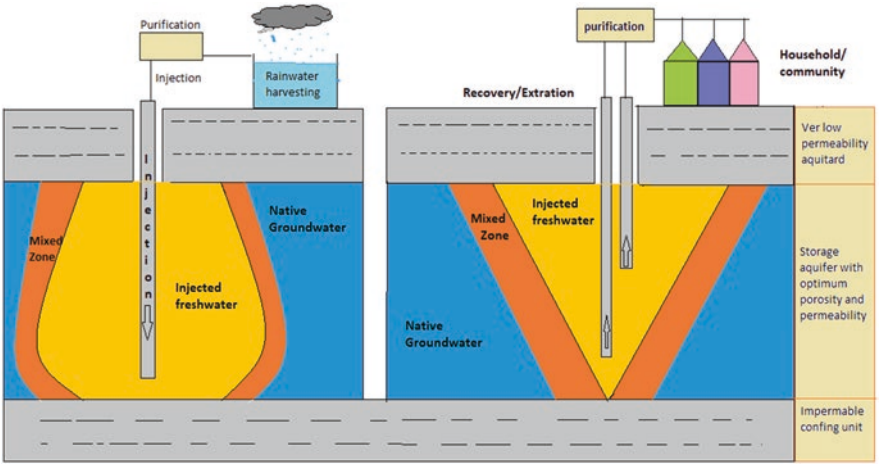

Fig. 10.1 Aquifer storage and recovery injection phase (left) and recovery phase (right)

might pollute the water. Moreover, surficial processes like runoff and dumping cannot affect subsurface storage.

4. Negligible surface footprint. Neither it needs any kind of treatment nor any large surface facility, so the surface below which ASR is operating can be used for all purposes and would not affect the community.
5. Lastly, no evapotranspiration losses in ASR operations. Since the stored water is not in direct contact with the sunlight or plant species, evaporation losses are negligible in this method. Evaporation is a major concern for water-stressed communities and significantly accounts for losses from surface storage. Some studies have shown that ET can take up to 30% of stored water which is very significant and can increase the salinity of the stored water (Fig. 10.1).

2 Historical Development

The concept of ASR in brackish water was first proposed by Cederstrom (1947), after which a lot of literature came describing the phenomenon of water bubbles. The most common factors that lead to mixing freshwater and saline water are dispersion and gravity segregation or free convection. Anthropogenic factors like sporadic pumping lead to mixed/forced convection. According to Esmail & Kimbler (1967), dispersion effects mean if two miscible fluids are in sharp contact, they will slowly diffuse into each other. After some time, initially, sharp contact will form a mixed zone. This diffusion results from the random motion of ions of two fluids. The distribution of ions across an arbitrary plane can be represented through Fick's Law. The density contrast between the native saline water and stored freshwater causes the density/buoyancy-driven flow and causes the mixing of the saline and

freshwater. Since freshwater is less dense compared to saline water, it tends to flow and remain above the saline-fresh interface. The buoyancy-driven flow causes the saline water to intrude in the lower part of the ASR zone and reduces the recovery efficiency. To reduce these effects, reservoir operation must be taken care of, and sites with very low vertical hydraulic conductivity should be selected to restrict the vertical flow of groundwater. The density effect is also called "gravity segregation" or "buoyancy stratification". He experimentally studies the dispersion and gravity segregation in the synthetic sandstone aquifer model and later confirms the observed results with then available computer programs. He finds that the density effect impacts recovery efficiency more strongly than dispersion effects. He also observed the wider mixing zone suppressing the interface tilt. He concluded that storage of freshwater in saline water is feasible under low permeability, small density contrast, low storage period, and high flow rate. The previously thought cylindrical plume is now viewed as a conical plume and reduces the recovered water volume. For this experiment, he used separate models to study the density and dispersion effects. Later Kumar and Kimbler (1970) combined both models and used a pear-shaped model representing 45° of a circle. The major objective of the experiment is to validate the assumption that previously sought the effect of gravitation segregation in the now-flowing system by expanding it to the radial flow system. Furthermore, it was found that recovery efficiency can be increased by increasing the injection-abstraction cycle.

Furthermore, a numerical modelling approach was used in an array of papers by Ward to explore the influence of controlling variables on ASR in saline water. Ward et al. (2007) concluded that widening the mixing zone reduces the density contrast and hence the impact of the density effect, confirming the assertion of Kumar and Kimbler (1970). Ward et al. (2008) further found that the greater the permeability contrast in layer aquifer and higher the anisotropy inhomogeneous aquifer restrict the vertical flow due to density effect and increase the recovery efficiency (Ward et al., 2009). Zuurbier et al. (2014) set up multiple partially penetrating wells, which inject freshwater into deeper aquifers and recover water from the open well casing in shallow aquifers to encounter the negative impacts. The numerical modelling demonstrated that 40% recovery efficiency could be achieved compared to 15% efficiency in a single penetrated well. To further investigate Witt et al. (2021) built a plexiglass tank and dyes to visualise the shape of both fresh and saline water bodies and investigate the recovery efficiency due to multiple penetrating wells. The results corroborate the previous efficiency. In order to further maximise the recovery efficiency, Zuurbier et al. (2015) experimented with horizontal directional drilled wells (HDDW) in the Netherlands, where they achieved 100% recovery efficiency of injected 4200 m^3 injected water, demonstrated by a numerical groundwater flow model.

3 Material and Methods

The lab experimentation was commenced to measure the viability of aquifer storage and recovery (ASR) as a remediation option in the saline aquifers of Mewat, Haryana. The experiment was conducted in an experimental sandbox model having dimensions: 120 cm in length, 60 cm in width, and 120 cm in height (Fig. 10.2). Separate fresh and saline water injection sources were built. Two sprinklers are used to create saturated saline conditions, and four injection wells are used to inject freshwater into the aquifer. The wide distribution of injection wells allows four different pockets of freshwater to observe for ASR phenomenon. A saline solution of concentration 8500 μs/cm was prepared of sodium chloride salt. The temperature was measured with an EC meter (Eutech). 150 litres of this saline solution at a temperature of 25 °C was inserted in the sand of size ranging between 0.075 and 1.00 mm till saturation. The sand was kept in an experimental model for a prototype artificial aquifer.

Figures 10.3, 10.4, 10.5, 10.6, and 10.7 are showing the transverse profile of the model. The x-axis represents the depth inserted for sampling. The z-axis represents the various ports in the horizontal direction. The y-axis represents the electrical conductivity value in micro-siemens per meter. The plot (Fig. 10.3) shows the spatial variation in EC just after the injection of freshwater in saline water. The middle-high in different plots represents the high salinity. The low mixing between freshwater and surrounding saline water is represented by high relief in salinity variation. The plot (Fig. 10.4) represents EC values after a few hours of injection. The H1A blue plot and H10A green plot represent the two extreme parts of the model where most of the freshwater is injected. Sharpe highs and lows can visualise the same in the curve. For instance, in the green graph between 25 and 40 cm, we

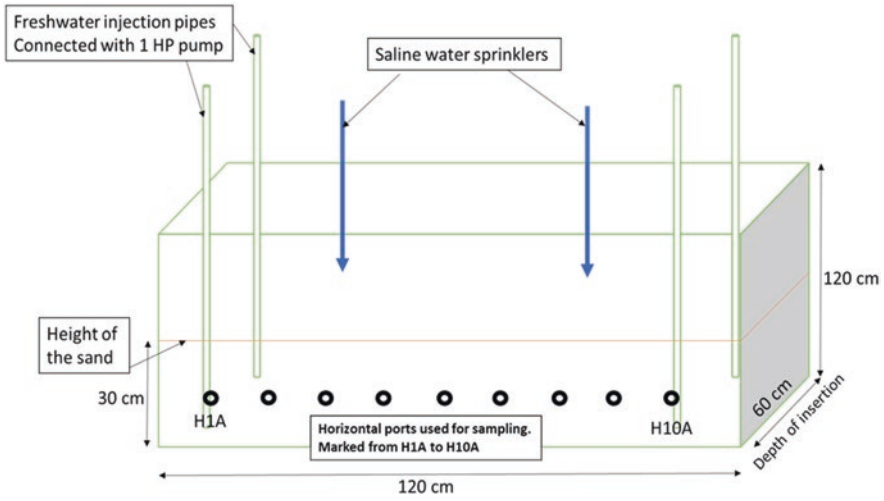

Fig. 10.2 Experimental model layout

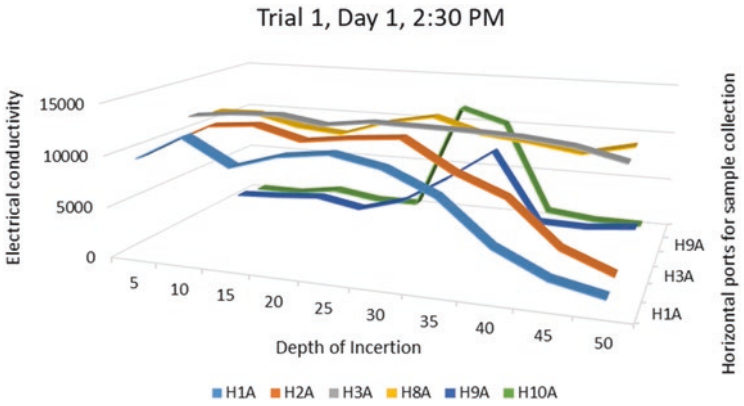

Fig. 10.3 Plot of ASR trial 1 day 1 AN

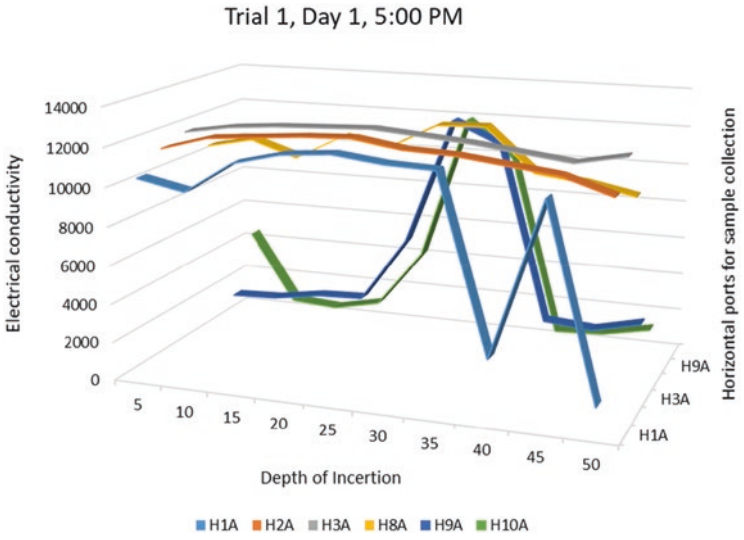

Fig. 10.4 Plot of ASR trial 1 day 1 AN

can see the maximum EC value due to placing injection points at 10 cm and 45–50 cm distance causing low salinity values at these points. Figure 10.5 shows EC values after 1 day of experimentation. Due to freshwater saline water mixing, the contrast between middle position values and values position values has subsided. For instance, the H10A, compared to the previous plot, greatly flattened at extreme ends. The grey and yellow plots are taken from extreme middle ports where no injection point was present; hence we see an overall constant profile. Figure 10.6 represents the EC observations after 2 days of injection. Still, we could obtain water of standard quality at the H1A and H10A ports at 45–50 cm depth. Elsewhere, the saline water is thoroughly mixed with freshwater. The slight lower can also be seen

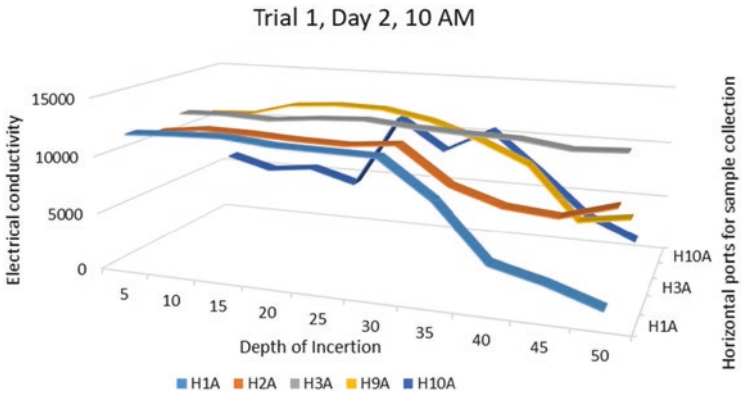

Fig. 10.5 Plot of ASR trial 1 day 2 FN

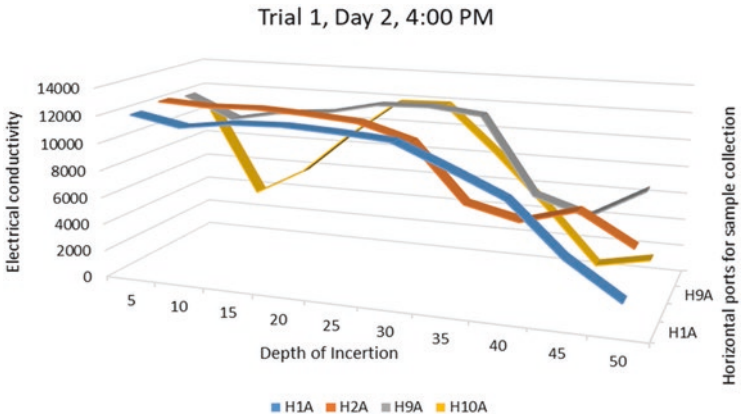

Fig. 10.6 Plot of ASR trial 1 day 2 AN

at 10 cm depth in the H10A port. After 3 days of experimentation, the injected freshwater was thoroughly mixed with ambient saline water, and the average salinity reached up to 12,500 micro-siemens per meter. Since no pockets of freshwater were found, we decided to halt our experimentation (Fig. 10.7).

4 Feasibility Issues

Although ASR operation can be traced back to 600 AD in the Indian subcontinent (Ramaswamy, 2007), the ability to store freshwater in brackish-saline aquifers is still technically questionable, mainly because of several physical and chemical reasons. These concerns hang around this method and cannot be ignored, such as fluid-rock interactions, biogeochemical reactions which arise due to the injection of

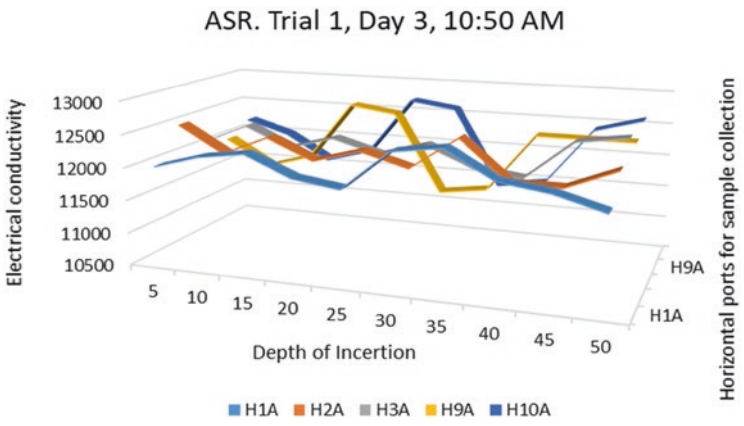

Fig. 10.7 Plot of ASR trial 1 day 3 FN

foreign substances, and interaction between stored water and native groundwater. For the proper feasibility and recovery of the stored water, the byzantine subsurface aquifer system needs to be thoroughly scrutinised, and several intricate interactions and factors need to be taken into account. This approach is not a panacea to all groundwater problems everywhere. However, it depends heavily upon the hydrogeology of the region. Factors like aquifer heterogeneity, anisotropy, grain size, dispersivity, and density contrast between native and stored groundwater. Physical, biological, and chemical clogging of water and infiltration sites causes a reduction in infiltration rates and is often a major problem in ASR sites. Another problem with ASR is liquefaction, a very shallow water table formed in geologic media and frequently shaken by the earthquake, further exacerbating the damage.

Transmissivity significantly affects the ability to recover injected water from the aquifer system in two ways. First, the transmissivity must be high enough to allow economic injection and groundwater extraction to achieve project goals and targets. Second, it should not be high enough so that the injected water is lost to aquifers and cannot be recovered. So, the site selection must consider the transmissivity effects. For instance, a Florida north lake test site attempted to test outside the prescribed transmissivity rates in a highly conductive limestone aquifer. It could not recover a significant fraction of injected water. Other risks associated with aquifer storage and recovery are subsidence. Although one of the utilities of the ASR is reducing subsidence, the abstraction of groundwater during the recovery phase poses a great threat to the subsidence of the area. In Kelley et al. (2020) a pre-feasibility study was done to minimise the impact of groundwater extraction during peak months on land subsidence. The performance of the ASR system is estimated by recovery efficiency, which is the percentage of recovered water of standard quality to the injected water. Normally it ranges from 10% to 60% depending upon hydrogeology, stored water volume, recovery time, and chemistry of native water. Reservoir operations play a significant role in the recovery efficiency of an ASR site.

4.1 ASR Feasibility Studies

The essential phase for the success of any project is the initial feasibility studies and development strategies. One can maximise the success of the project by accurately understanding the objective and following a set of logical steps. More careful attention to initial planning and details can identify and resolve the key issues well in advance, which saves time and energy and prevents losing the momentum of the project. Although the ASR project heavily depends upon site-specific hydrogeology and socio-economic feasibility, a set of phased guidelines can be followed for the implementation of ASR. The technical experts from geochemistry, hydraulics, modelling, economics, water quality, water treatment, pumping design, pipelines, and water utility systems are required for a transdisciplinary approach for an easy-going project and to maintain a balance between science and engineering. Phase 1 of development involves preliminary feasibility and conceptual design. Several elements comprise this phase. First is the clearly defined objective of recharge. Other subsequent factors depend upon the objective, failing to conclude that could lessen the benefits that could have been achieved, for instance, selection of the wrong site, etc. The objectives could be simple seasonal storage and recovery of water (Wasif & Hasan, 2020), restoring depleted groundwater levels Sheng (2005), reducing subsidence (Kelley et al., 2020), improving water quality (Appelo & De Vet, 2003), or preventing saline water intrusion (Zuurbier & Stuyfzand, 2017).

Next comes the source of water supply or recharge. Selecting a supply source is essential because of fluctuating flow rate, average flow, and quality which could impact the recharge amount and water standards. A typical situation is the peace river ASR site in Florida, which stores water from a river source that has a highly variable quality and flow. The most common method of water supply is rainwater harvesting; it is suitable in those areas that have seasonal raining periods and a dearth of dynamic surface water resources. Similarly, water demand is another key factor to assess. The location and scale of the ASR plant depend upon the community's monthly, seasonal, and annual demands. Understanding the local hydrogeology is one of the most time-consuming and important factors to consider before applying the ASR in the field, which leads to careful selection of appropriate storage zones, recharge water sources, and treatment required. The following factors in hydrogeology are needed to be considered: hydrostratigraphy, aquifer and aquitard, aquifer geometry, confining layer, lithology, aquifer physical parameters, mineralogy presence of clay, geochemical and redox environment, subsurface heterogeneities, rechargeable sites and potential zones, discharge zones, water table level, local and regional flow directions, proximity to potential contaminants plumes, and groundwater abstraction.

Maliva et al. (2019) defined optimum hydrogeological conditions for the ASR facility in saline aquifers. These are moderate hydraulic conductivity (5–20 m/d), primary porosity-dominated lithology with effective porosity higher than 5%, and low degrees of heterogeneity. The 4D operational monitoring systematic survey used the method, survey design, data acquisition, processing, and quantitative

interpretation and studied the Leyden Colorado ASR facility: an abandoned mine to fill the winter surplus water and use in summer. Using the time-lapse gravity survey successfully detected the distribution and movement of general water. A set of geological, hydrogeological, geochemical, water quality, geophysics, and remote sensing techniques can be used in identifying suitable hydrogeology and field sites for the objective. The remote sensing techniques provide a good alternative to the time- and resource-consuming geophysical and geological techniques. Just like the remote sensing techniques used in reconnaissance surveys in metal exploration, Amineh et al. (2017) integrate the spatial multi-criteria decision-making and GIS for delineating suitable zones for ASR. Moreover, remote sensing and GIS can also be used to identify recharge sites and storage sites. The advancement in modelling tools has facilitated the accurate representation of subsurface processes. The groundwater models are increasingly being used to test recharge rate, aquifer parameters essential for ASR feasibility, residence time, optimum pumping and extraction rates, and locating subsurface sites for ASR establishment.

LaHaye et al. (2021) used the integrated approach of numerical modelling and geospatial technology to predict the ASR feasibility in Louisiana. They constructed a 3D numerical model based on hydrostratigraphy of the region to calculate four aquifer parameters such as depth to thickest sand layer (DS), hydraulic gradient (HG), storage zone thickness (ZT), and transmissivity (TM). The model results are further coupled with geospatial parameters like land use, groundwater quality, TDS of surface water, stream thickness, well density, cumulative crop cover, excess surface water, and groundwater availability. Wasif and Hasan (2020) used the finite-difference MODFLOW numerical model to simulate seasonal water storage in the Flemish alluvial plains of Belgium. The steady-state model was initially utilised for transient analysis, scenario analysis, and prediction simulation. The water balance component showed an increase in heads during water-stressed winter months. Moreover, the individual ASR wells achieved a recovery efficiency of 97%, and multiple wells achieved the RE of 100%. Apart from simulating the feasibility and site assessment, modelling can be expanded to other ASR management applications like simulation-optimisation, approach, and examining operation factors, for example, surface water minimising in aquifers, minimising injection time. Chinnasamy et al. (2018) use the MODFLOW to access the ASR operation protocols to prevent surface ponding during recharge and air locking during extraction and minimise pump adjustment. They run the model to do this in assumed aquifer conditions and simulate the head values. If overflow is observed, then they reduce the recharge rate by half and then run the model again to estimate the head. If no overflow is observed this time, they check for saturation head and top the model.

5 Geochemical Technical Issues

The most concerning threat and speculation over the ASR projects are the standards of recovered water quality, which encompasses a wide range of contaminants and parameters that need to be checked at pre-feasibility and continuous monitoring stages. The physical parameters are TDS, EC, Ph, Eh, alkalinity, temperature,

dissolved oxygen, colour, and turbidity; the inorganic parameters include chloride, fluoride, sulphate, major ions, nitrate, phosphate, ammonia, arsenic, cadmium, etc.; the organic contaminants include TOC, hydrocarbons, total coliform, chloroform, bromodichloromethane, dibromochloromethane, bromoform, total trihalomethane, etc. Since the majority of reactions occurred at the interface of native groundwater, foreign water, and aquifer matrix or sediments, analysing their respective geochemistry is essential to track down future reaction pathways and possibilities. The first step of the geochemical pre-feasibility test is to check recharging groundwater for these parameters by extensive sampling and laboratory analysis of recharging water and native groundwater followed by the geochemical assessment. Using this data and model, simulation reactions involving various proportions of aquifer water and recharging water can be simulated to find the set of geochemical reactions like precipitation and dissolution that could cause problems like clogging of aquifers. However, these simulations often do not give conclusive results as we are unknown about the subsurface geology. So, the next logical step is to identify the mineralogy and geochemistry of aquifer material which is done by analysing the core data. The core is highly valuable in knowing the aquifer characteristics, organic activity, captain exchange capacity, mineralogy, redox potential, and potential of plugging. The physical characteristics include permeability, porosity, grain size distribution, and specific gravity. The colour indicates homogeneity in the aquifer, organic activity, and quick reference to oxidation and reduction potential. For instance, High organic activity, reduced iron, and manganese are marked by blue or grey colour. The oxidised iron forms a yellow or red formation that indicates abiotic conditions. To analyse the presence of major phase and clay minerals, optical petrography and X-ray diffraction (XRD) are implemented. The relative abundance and types of clay provide an indication of geochemical reaction or physical plugging. For example, montmorillonite clays are more sensitive to changes in TDS. Similarly, kaolinite is more likely to cause plugging. Another useful parameter is cation exchange capacity which is obtained when the core is flushed with ammonium acetate solution to determine cation concentration that is in an exchangeable position. For instance, if the recharge water has a different chemistry than the subsurface environment, the clay will become unstable and release various cations to achieve equilibrium. Lately, using scanning electron microscopy, it is possible to determine how clay minerals occur in formation pores.

Finally, the interface and interactions between the three reacting components are monitored through observations and monitoring wells and also computer simulations. The advancement in geochemical modelling is proving as a boon in the mixing assessment. These models are user-friendly, highly efficient, feed on large geochemical reactions and processes databases, and can be operated once you have preliminary data. A few common examples are PHREEQC, MINTEQ, and WATEQ. These models can be used to determine the products of the geochemical reactions and the reaction kinematics and pathways that could be possible. The kinematics is the rate of reactions; if the kinematics is slow, it can be ignored. The geochemical processes give rise to a plethora of problems that ultimately lead to decreased ASR feasibility. The immediate mechanisms are physical clogging, bacterial activity, adsorption processes, surface ponding, and ion exchange. The slower reactions like dissolution processes appear after several months of running. Physical

clogging is one of the fatal processes for ASR systems. The suspended solids in the recharge water can reduce the hydraulic conductivity of the aquifer matrix and filter, decreasing the recharge rate, storage capacity, and filtration rate. Gas entrapment and biogenic gases can also cause physical clogging. The physical clogging further leads to biological clogging with an accumulation of biomass and the growth of microorganisms. The chemical precipitation of reacting minerals further exacerbates the clogging (Jeong et al., 2018). Pretreatment includes coagulation, sedimentation, filtration, advanced oxidation, and disinfection. However, clogging can still happen in the running phase. At that time the treatment methods that can be used are scrubbing, surging, backwashing, jetting, biociding, acidification, and underreaming. Among all the surface infiltration systems proved to be highly efficient and economical. Stuyfzand and Osma (2019) analyse the biological-chemical-physical clogging mechanisms during pre-feasibility tests due to diatoms, algae, and colloidal or precipitating $Fe(OH)_3$, $Al(OH)_3$, and MnO_2. They first identify the contribution, combination of the membrane filter index (MFI) method, and an amendment of the exponential bacterial growth method to optimise it.

Adsorption can further threaten ASR viability. Although adsorption occurs at every level, from deposition of flocs to ion adsorption, the one stick on the pore is highly dangerous for ASR as it reduces the hydraulic conductivity. Acidification can be used to recover the permeability, and however, if severe adsorption happens, it can restrict the flow of acids from reaching the affected area. Ion exchange is another geochemical process that can significantly affect the ASR system. For instance, sodium on clay minerals is in an exchangeable position in brackish water conditions and remains stable until the TDS isn't lowered. Once freshwater is injected, the exchange between calcium and sodium commences, which convert the clay minerals and mobilise ions to accumulate in pore throats. Similarly, kinetics, oxidation, and dissolution further control the processes.

Arsenic (As) release from ASR sites is the major source of concern worldwide. Many large sites had to be abandoned due to the release of As in initially non-contaminated water. Since the As is present in various hydroxides and sulphide minerals, they remain stable in particular redox conditions. It can be mobilised through the oxidation of sulphides like pyrite when the subsurface has a reducing environment, and surface water is of high oxidation potential. Another release mechanism is the dissolution of hydroxides and releases through other mobile elements like U, Mn, and Fe. Moreover, oxidation-reduction of organic matter can also mobilise As. Appelo and De Vet (2003) reported high As concentration during the removal of in situ iron, where oxygenated water was recharged into anoxic siliciclastic sediments. The geochemical modelling suggested the native groundwater containing phosphate was the main mobilisation mechanism of As. Wallis et al. (2010) investigated the elevated As concentration in the ASTR site in a siliciclastic aquifer. Here, As release was related to oxidation of pyrite due to injection of oxygenated water.

Even after the geochemical modelling prediction and steps taken, in-field water quality problems exist. To tackle them, detailed laboratory analysis of core and aquifer material is required to ensure the water quality standards and simulate the exact field conditions in the lab environment. Such lab testing includes column experiments and batch testing. Rinck-Pfeiffer et al. (2000) conducted column

experiments on drill cores to experiment with clogging mechanisms before proceeding to field trials. They observed the above-mentioned interrelation among physical, chemical, and biological clogging mechanisms. Even in low suspended solid conditions, the hydraulic conductivity is maintained between 20% and 50% of the original. In the first 7 days of the experiment, the accumulation of suspended solids and biomass decreased the hydraulic conductivity from 0.78 m/s to 0.068 m/s. However, this significant decrease is countered by the chemical dissolution of calcite at the inflow end, opening the pore spaces. The re-precipitation of calcite at the outflow end is verified from SEM images. Batch testing is another lab experiment. It is inexpensive as compared to column experiments. The sample core materials are mixed together and are subjected to progressive series of leaching tests at steadily increasing pH values to estimate chemical reactions occurring at each step.

6 Case Study: El-Paso Texas

El Paso, Texas, is situated in the Chihuahuan Desert and often experiences prolonged river drought and a heavy burden on groundwater resources (Cliett, 1969). The two major aquifers in the region are Hueco Bolson (Sheng et al., 2001) and the Mesilla Basin, and surface water from the Rio Grande. In the 1980's El Paso Water Utilities started investigating alternative water resources to substitute for future water supply. They investigated the technical and administrative feasibility of ASR for prolonged water storage. The investigation by the New Mexico-Texas water commission concluded that northeast El Paso has favourable hydrogeological conditions for the implementation of large-scale recharge features. The ASR system is proposed to serve three purposes: reuse of reclaimed freshwater and preservation of the native groundwater, restoration of depleted groundwater levels by artificial recharge; prevention of brackish water intrusion. The treated wastewater up to the level of standard drinking quality is used to recharge the Hueco Bolson aquifer. The aquifer is unconfined to semi-confined within a long sediment-filled trough. The sediments consist of fine- to medium-grained sand with the interbedded lens of clay, silt, gravel, and caliche and have a thickness of 2743 m. The pivot injection test found a horizontal hydraulic conductivity of 8.13 m/day (Heywood & Yager, 2003). The northeast well field site was chosen for storage purposes mainly because of three reasons. First is enough storage space and depth to build up hydraulic heads within recharge wells. Second, injection wells are situated in such a way to allow maximum recovery of freshwater and minimise the cost. Last, adequate residence time will provide enough to further purify the groundwater (Sheng, 2005). The water quality assessment of native groundwater and treated freshwater demonstrate the compatibility between both; the higher sodium and calcium concentration ratios are comparable. The $HCO_3 + CO_3$ ratio of treated water is higher than groundwater, and the sulphate ratio is almost the same. Both are sodium chloride-type water. The system faced one threat: transporting pathogens and microbes in the water system. It is recommended that additional data collection and water testing be conducted to better understand transport mechanisms.

Acknowledgments This work was carried out in a purpose-driven study under National Hydrology Project (NHP) funded by World Bank. The funding received is duly acknowledged.

Declarations The authors declare no conflict of interest.

References

Amineh, Z. B. A., Hashemian, S. J. A. D., & Magholi, A. (2017). Integrating Spatial Multi Criteria Decision Making (SMCDM) with Geographic Information Systems (GIS) for delineation of the most suitable areas for aquifer storage and recovery (ASR). *Journal of Hydrology, 551*, 577–595.

Appelo, C. A. J., & De Vet, W. W. J. M. (2003). Modelling in situ iron removal from groundwater with trace elements such as As. In *Arsenic in ground water* (pp. 381–401). Springer.

Cederstrom, D. J. (1947). Artificial recharge of a brackish water well. The Commonwealth, Va., Dec. 1947, pp. 31.

Chinnasamy, C. V., McIntyre, W. C., & Mays, D. C. (2018). Technical and administrative feasibility of alluvial aquifer storage and recovery on the South Platte River of northeastern Colorado. *Water Policy, 20*(4), 841–854.

Cliett, T. (1969). Groundwater occurrence of the El Paso area and its related geology. In *Guidebook of the border region, Chihuahua and the United States: New Mexico Geological Society Twentieth Field Conference*, pp. 209–214.

Dillon, P., Stuyfzand, P., Grischek, T., Lluria, M., Pyne, R. D. G., Jain, R. C., et al. (2019). Sixty years of global progress in managed aquifer recharge. *Hydrogeology Journal, 27*(1), 1–30.

Esmail, O., & Kimbler, O. (1967). Investigation of the technical feasibility of storing fresh water in saline aquifers. *Water Resources Research, 3*(3).

Heywood, C. E., & Yager, R. M. (2003). *Simulated ground-water flow in the Hueco Bolson, an alluvial-basin aquifer system near El Paso, Texas* (Vol. Vol. 2, No. 4108). US Department of the Interior, US Geological Survey.

Jeong, H. Y., Jun, S. C., Cheon, J. Y., & Park, M. (2018). A review on clogging mechanisms and managements in aquifer storage and recovery (ASR) applications. *Geosciences Journal, 22*(4), 667.

Kelley, V., Turco, M., Deeds, N., Petersen, C., & Canonico, C. (2020). Assessment of subsidence risk associated with aquifer storage and recovery in the Coastal Lowlands Aquifer System, Houston, Texas, USA. *Proceedings of the International Association of Hydrological Sciences, 382*, 487–491.

Kumar, A., & Kimbler, O. K. (1970). Effect of dispersion, gravitational segregation, and formation stratification on the recovery of freshwater stored in saline aquifers. *Water Resources Research, 6*(6), 1689–1700.

LaHaye, O., Habib, E. H., Vahdat-Aboueshagh, H., Tsai, F. T. C., & Borrok, D. (2021). Assessment of aquifer storage and recovery feasibility using numerical modelling and geospatial analysis: Application in Louisiana. *JAWRA Journal of the American Water Resources Association, 57*, 505.

Maliva, R. G., Manahan, W. H., & Missimer, T. M. (2019). Aquifer storage and recovery using saline aquifers: hydrogeological controls and opportunities. Groundwater. https://doi.org/10.1111/gwat.12962

Ramaswamy, S. (2007). The groundwater recharge movement in India. In *The agricultural groundwater revolution: Opportunities and threats to development* (pp. 195–210). https://www.iwmi.cgiar.org/Publications/CABI_Publications/CA_CABI_Series/Ground_Water/protected/Giordano_1845931726-Chapter10.pdf

Rinck-Pfeiffer, S., Ragusa, S., Sztajnbok, P., & Vandevelde, T. (2000). Interrelationships between biological, chemical, and physical processes as an analog to clogging in aquifer storage and recovery (ASR) wells. *Water Research, 34*(7), 2110–2118.

Sheng, Z. (2005). An aquifer storage and recovery system with reclaimed wastewater to preserve native groundwater resources in El Paso, Texas. *Journal of Environmental Management, 75*(4), 367–377.

Sheng, Z., Mace, R. E., & Fahy, M. P. (2001). The Hueco Bolson: An aquifer at the crossroads. In R. E. Mace, W. F. Mullican III, & E. S. Angle (Eds.), *Aquifers of West Texas* (pp. 66–67). Texas Water Development Board.

Sprenger, C., Hartog, N., Hernández, M., Vilanova, E., Grützmacher, G., Scheibler, F., & Hannappel, S. (2017). Inventory of managed aquifer recharge sites in Europe: Historical development, current situation and perspectives. *Hydrogeology Journal, 25*(6), 1909–1922.

Stuyfzand, P. J., & Osma, J. (2019). Clogging issues with aquifer storage and recovery of reclaimed water in the brackish werribee aquifer, Melbourne, Australia. *Water, 11*(9), 1807. https://doi.org/10.3390/w11091807

TY-JOUR T1. – Multi-influence factor method to determine groundwater potential zone using GIS and RS (Remote sensing) techniques in parts of Rajasthan, India. AU – Adya Aiswarya Dash AU – Abhijit Mukherjee AU – Rahul Garg N1 – https://doi.org/10.1002/essoar.10509547.1 DO – https://doi.org/10.1002/essoar.10509547.1 T2 – Earth and Space Science Open Archive JF – Earth and Space Science Open Archive PB – Earth and Space Science Open Archive M3 – https://doi.org/10.1002/essoar.10509547.1 UR – https://doi.org/10.1002/essoar.10509547.1 Y2 – 2022/3/10 ER.

Wallis, I., Prommer, H., Simmons, C. T., Post, V., & Stuyfzand, P. J. (2010). Evaluation of conceptual and numerical models for arsenic mobilization and attenuation during managed aquifer recharge. *Environmental Science & Technology, 44*(13), 5035–5041.

Ward, J. D., Simmons, C. T., & Dillon, P. J. (2007). A theoretical analysis of mixed convection in aquifer storage and recovery: How important are density effects? *Journal of Hydrology, 343*(3–4), 169–186.

Ward, J. D., Simmons, C. T., & Dillon, P. J. (2008). Variable-density modelling of multiple-cycle aquifer storage and recovery (ASR): Importance of anisotropy and layered heterogeneity in brackish aquifers. *Journal of Hydrology, 356*(1–2), 93–105.

Ward, J. D., Simmons, C. T., Dillon, P. J., & Pavelic, P. (2009). Integrated assessment of lateral flow, density effects and dispersion in aquifer storage and recovery. *Journal of Hydrology, 370*(1–4), 83–99.

Wasif, M. R., & Hasan, M. M. (2020). Modeling aquifer storage and recovery potential for seasonal water storage in the Flemish alluvial plains of Belgium using MODFLOW. *Arabian Journal of Geosciences, 13*(5), 1–12.

Witt, L., Müller, M. J., Gröschke, M., et al. (2021). Experimental observations of aquifer storage and recovery in brackish aquifers using multiple partially penetrating wells. *Hydrogeology Journal, 29*, 1733–1748. https://doi.org/10.1007/s10040-021-02347-7

Zuurbier, K. G., & Stuyfzand, P. J. (2017). Consequences and mitigation of saltwater intrusion induced by short-circuiting during aquifer storage and recovery in a coastal subsurface. *Hydrology and Earth System Sciences, 21*(2), 1173–1188.

Zuurbier, K. G., Zaadnoordijk, W. J., & Stuyfzand, P. J. (2014). How multiple partially penetrating wells improve the freshwater recovery of coastal aquifer storage and recovery (ASR) systems: a field and modeling study. *Journal of Hydrology, 509,* 430–441. https://doi.org/10.1016/j.jhydrol.2013.11.057

Zuurbier, K. G., Kooiman, J. W., Groen, M. M., Maas, B., & Stuyfzand, P. J. (2015). Enabling successful aquifer storage and recovery of freshwater using horizontal directional drilled wells in coastal aquifers. *Journal of Hydrologic Engineering, 20*(3), B4014003.

Chapter 11
Temporal Prediction of Groundwater Levels: A Gap in Generalization

N. Ramsundram, Mohammad Taghi Sattari, R. Kaviya, M. Kaarthic, and M. Niveditha

Abstract Groundwater serves the significant demand created by the human ecosystem across the globe. In this scenario, primary dependence on the groundwater scenario, the prediction of its availability will be valuable information for the stakeholders. Researchers in the current decade have widely used the prediction of the resources based on the available/historical database. Above made researchers generalize the selection models depending on the domain of study (application domain). In the generalization process, the introduction of risk towards dependability on the predicted outputs has been increased. This study tries to identify the performance of two well-known predictive algorithms, which have their footprints both in data-driven, and data mining models, namely, (a) artificial neural network (ANN) and (b) support vector machine (SVM). The performance analysis has been performed to understand the impact of neurons in ANN and Kernel functions in cases of SVM. The developed framework is allowed to explore three well locations in the same basin to explicitly show the performance of the algorithms. The prediction capability is measured in Nash-Sutcliffe efficiency (NSE) and root mean square error (RMSE). The results inferred that even though the study groundwater wells are pertaining to the same basin (where climate and lithology are almost similar), the algorithms may not be generalized for the domain application. The above observation may be due to the draft and land use pattern variability.

Keywords Artificial neural network · Database modeling · Groundwater · Support vector machine · Temporal prediction

N. Ramsundram (✉) · R. Kaviya · M. Kaarthic · M. Niveditha
Department of Civil Engineering, Kumaraguru College of Technology, Coimbatore, India
e-mail: ramsundram.civil@kct.ac.in

M. T. Sattari
Department of Water Engineering, University of Tabriz, Tabriz, Iran

Department of Water Engineering, Ankara University, Ankara, Turkey

P. Thambidurai, A. K. Dikshit (eds.), *Impacts of Urbanization on Hydrological Systems in India*, https://doi.org/10.1007/978-3-031-21618-3_11

1 Introduction

Groundwater is an indispensable source of freshwater that satisfies the requirements of the agriculturist, the industrialist, and the inherent need of all living organisms, which plays a significant function in the balance of the ecosystem (Yoon et al., 2011). This demands preciseness in the quantification procedure, which made the researchers utilize the strength of the modeling approach (numerical/data analytics) for estimating the groundwater fluctuations concerning withdrawal through pumping. Numerical modeling has been used widely to simulate groundwater levels considering the recharge through rainfall and surface water bodies. Most of this recharge condition is given to the topsoil layers/zones during model development, assuming that current period rainfall will not influence the water level of deep aquifers. In this study, an attempt is made to understand the behavior of rainfall and groundwater levels, especially in deep aquifers. Numerical modeling is widely prepared in the case of groundwater level prediction is concerned as it is highly effective with spatial variation visualization (Behzad et al., 2010). The accuracy/dependability of the results is based on the effectiveness of the calibration process and the certainty in the input data (hydrogeology, mesh size, surface water bodies bathymetry, stage height, rainfall, draft from aquifer) during the model development process. This high data requirement and associated uncertainty resulted in researchers looking for knowledge recovery from available historical data. The development of artificial intelligence found its wide application in this research domain of groundwater level prediction on a temporal scale (Xu et al., 2014). Temporal prediction, in particular, is a unique process of extracting inherent knowledge from the existing database to enumerate a temporal pattern or model. A few well-known data-driven modeling techniques are (a) artificial neural network (ANN) (Daliakopoulos et al., 2005), (b) linear regression, (c) support vector machine (SVM) (Yoon et al., 2011), (d) self-organizing map (SOM) (Chang & Zhang 2016), and (e) adaptive neuro-fuzzy inference systems (ANFIS) (Gong et al., 2016). The ANN has been positioned as an essential tool by most data-driven modeling researchers. Badouiet al. (2013) used linear regression and multilayer perceptron (MLP) neural network for predicting global solar irradiation. The study confirmed that MLP seems to be promising compared to linear regression. Patel and Yalamalle (2014) predicted the stock market price using ANN. By the results, it may be inferred that, among many different algorithms of neural networks, the feed-forward MLP technique gives better prediction results. Isa et al. (2010) studied the suitability of the activation functions in neural networks (NN) to classify breast cancer datasets and detect thyroid disease. The research work has deduced that the hyperbolic tangent activation function holds good for the breast cancer dataset and the neuronal activation function is proficient for the thyroid dataset. From the inferences, it is concluded that the choice of the activation function plays the most significant role in the accuracy of the algorithm. The safe pumping rate to preserve the groundwater salinity in the island aquifer was estimated by Banerjee et al. (2011). The above study was executed using a

feed-forward ANN model with quick propagation and mathematical models. From the analysis, it is proven that ANN is more competent in the case of island hydrological prediction. Tsanis et al. (2008) studied the groundwater level variations using various architectures in the Messara valley in Crete (Greek). The research study proved that, among various network architectures, neural network trained with the Levenberg-Marqdart algorithm is promising to perform the efficient prediction process. Using numerous methods, Panchal et al. (2011) performed the behavior analysis of MLP with different network architectures. The analysis concluded that the performance seems to improve with an increase in the network architecture. The above research also inferred that selection of the network architecture is made as per the requirement of whether the accuracy of the time is concerned in the prediction process. Alsmadi et al. (2009) analyzed the efficiency of various methods of training and testing datasets using MLP. The above-stated investigation proved that the feed-forward, backpropagation algorithm outperforms the rest. Khan and Coulibaly (2006) compared the proficiency of SVM with MLP and seasonal autoregressive model (SAR) in predicting the lake water levels at Lake Erie. The aforementioned comparative analysis concludes that SVM performs better than MLP and SAR. The author justified that the unique capability of SVM to solve the linearly constrained quadratic equation is the reason for its extensive performance. Osowskil et al. (2004) performed a comparative study between ANN and SVM by conducting numerical experiments. Through the analysis, it is inferred that SVM is the best algorithm for classification, and ANN has competent performance in the case of regression. Sakr et al. (2011) made certain the results mentioned above through their investigation on predicting the probability of the occurrence of the fire using ANN and SVM. The climatic variables, namely, relative humidity and cumulative rainfall, were considered to perform the above study. The results concluded that ANN performs better in prediction, with 17% higher efficiency than SVM. It is also inferred that SVM, the binary classifier, outperforms ANN in the case of classifying the fire danger and non-fire scenarios. Behzad et al. (2010) utilized the robustness of the data-driven modeling approaches, namely, ANN and SVM, for predicting groundwater level variations. The above analysis considers the variation in pumping and weather conditions of the study area for the prediction process. The forecasting includes daily, weekly, monthly, and bimonthly horizons. Through the study, it is inferred that SVM achieved superior performance, particularly over longer horizons. The groundwater levels of two wells in coastal aquifers in South Korea are studied by Yoon et al. (2011) using ANN and SVM. The precipitation and the tidal levels are the two input parameters considered in addition to the groundwater levels in developing the model. The results show that the RMSE value is lower in ANN than in SVM, but in terms of the overall performance of the models, SVM is equivalent to or even better than ANN. From the above. it may be concluded that ANN and SVM have been reported as effective algorithms for exploring hidden knowledge in the historical database. In the present study, an attempt has been made to utilize the strengths of ANN and SVM to predict the temporal variation of groundwater levels, considering the meteorological variable (rainfall).

2 Case Study

The groundwater levels at three different observation wells in the Parambikulam Aliyar Pasanam (PAP) Basin have been considered for this study to execute the prospective methodology. Table 11.1 represents the statistical characteristics of the groundwater level dataset of the three observation wells from June 1988 to June 2001 every month. The statistical study on the database revealed that the groundwater levels are fluctuating with gradual surge and drop. The fact mentioned above may be due to the influence of the meteorological variables. Hence, rainfall data of the nearest gauge stations, namely, Anaimalai, Vettaikaranputhur, and Nallar for the observation wells mentioned in Table 11.3, are considered input parameters for the prediction. The historical database is generally susceptible to missing data estimated using the arithmetic mean method. Figure 11.1a shows the location of Tamilnadu, 11.1b location of Parambikulam Aliyar Pasanam basin, and 11.1c locations of observation wells considered for the study with respective wells in maps.

3 Material and Methods

The proposed methodology (Fig. 11.2) has three major components, namely, (a) data preprocessing, (b) data-driven modeling (training and testing), and (c) performance evaluation of the algorithms. The above three components are integrated into a sequential flow to predict the temporal groundwater levels. The developed framework begins with exploring the historical database for noise and missing data. The outliers and the missing data are filled by the arithmetic mean of the previous temporal data. The temporal relation between rainfall and groundwater levels is explored by correlation analysis. From this analysis, the independent variables related to the dependent variable are identified. The identified database is analyzed using data-driven models to explore the hidden relationship between the variables. The knowledge recovery process is done in two phases, namely, (a) training and (b) testing. The entire database is split into 80% for the training phase and the remaining 20% database to test/validate the developed data-driven model. The developed framework utilizes well-proven artificial neural network (ANN) and support vector regression (SVR) for exploring the database. The performance of the developed data-driven

Table 11.1 Specifications of the case study

Location ID	Latitude (DMS)	Longitude (DMS)	Groundwater level depth (m)		
			Maximum	Minimum	Mean
63,712	10°35′00″	76°56′00″	11.62	1.10	6.61
63,714	10°32′30″	76°58′50″	11.10	2	6.28
63,715	10°32′45″	77°02′30″	11.90	1	6.50

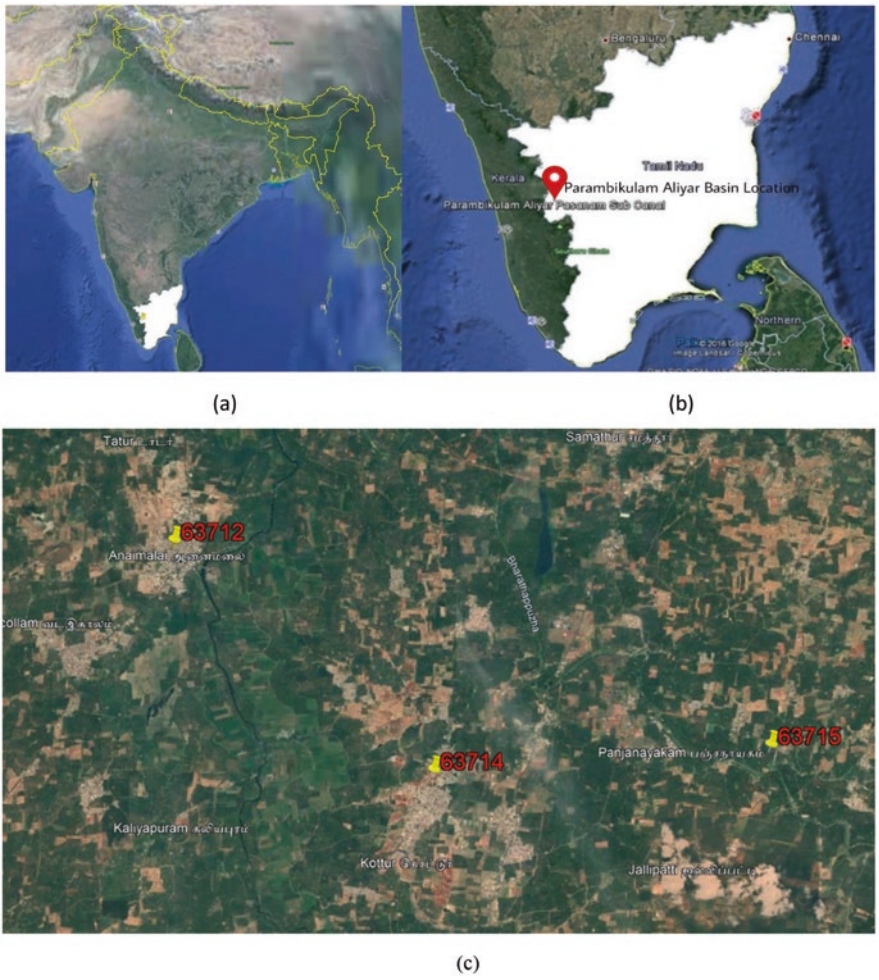

Fig. 11.1 Maps showing (**a**) representing administrative boundary of Tamil Nadu state, (**b**) location of Parambikulam Aliyar Pasanam basin, and (**c**) locations of observation wells considered for the study with respective wells

models is evaluated based on Nash-Sutcliffe efficiency NSE (for peak prediction) and root mean square error RMSE (for mean prediction) (Tables 11.2 and 11.3).

3.1 Data Selection

The historical groundwater piezometer database has records on the level of water from the topsoil with respect to the time period and also rainfall record pertaining to the corresponding time period. The temporal correlation analysis is performed to

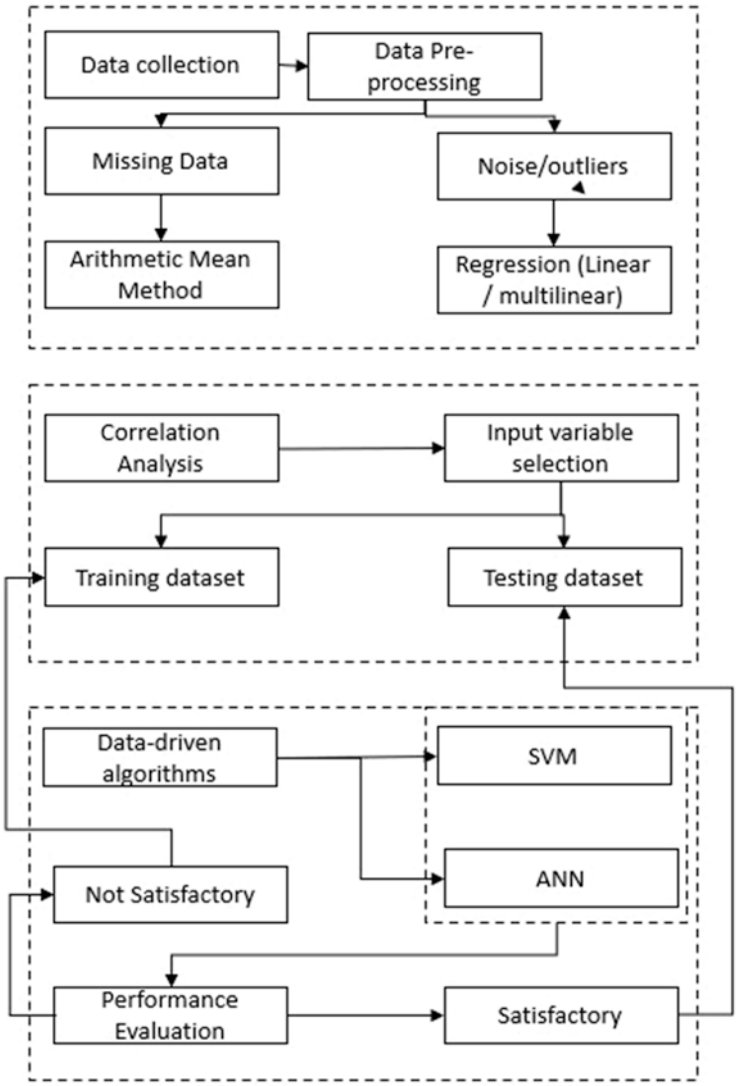

Fig. 11.2 Flowchart of methodology

identify the influence of time "t-1" to "t-n" piezometer level on piezometer level at time "t":

$$\text{Temporal correlation} = \frac{\sum\left(x-\bar{x}\right)\left(y-\bar{y}\right)}{\left(n-1\right)S_x S_y} \tag{11.1}$$

where S_x and S_y represent the sample standard deviations of the x and y data values, respectively (Mohan & Ramsundram, 2016).

Table 11.2 Statistics on water level depths at various observation wells under study (monthly basis)

	Location ID – 63,712				Location ID – 63,714				Location ID – 63,715			
	Anaimalai				Vettaikararpudhur				Anaimalai			
Month	Mean (m)	Max (m)	Min (m)	Var (m^2)	Mean (m)	Max (m)	Min (m)	Var (m^2)	Mean (m)	Max (m)	Min (m)	Var (m^2)
JAN	5.68	11.2	2.0	12.12	5.98	11.1	2.6	5.29	6.06	9.01	1.40	5.48
FEB	6.44	11.5	3.16	9.45	5.95	9.33	4.2	3.19	5.96	8.90	3.10	4.32
MAR	7.10	11.62	4	8.46	6.43	9.12	4	2.97	6.21	9.73	3.5	3.8
APR	7.63	11.1	4.35	5.82	6.96	10.05	4.4	3.34	6.53	10.44	3.65	3.46
MAY	8.04	11.27	4.65	6.04	7.05	9.43	5.6	1.88	6.43	11.35	3.2	4.68
JUN	8.26	11.55	5.10	4.88	6.93	10	5.75	1.80	5.77	7.98	3.8	1.81
JUL	7.36	11.17	3.15	5.72	6.63	9.24	4.80	1.64	6.9	9.6	4.6	2.94
AUG	6.60	10.73	2.44	5.59	6.08	8.91	3.95	1.98	7.02	10.58	3.15	5.60
SEP	6.49	10.74	3.71	3.90	6.25	9.32	4.2	2.04	7.54	11.9	3	6.82
OCT	6.21	10.35	2.00	5.63	6.44	9.47	4.50	2.43	8.01	11.86	4	6.31
NOV	4.72	9.72	1.10	10.46	5.7	11.04	2.15	5.63	6.77	11.65	1.25	10.95
DEC	4.91	10.32	1.45	8.15	5.45	10.9	2	6.35	6.13	10.40	1	9.57

Table 11.3 Statistics on the rainfall data at the nearest gauge station of the respective study locations

	Location ID – 63,712				Location ID – 63,714				Location ID – 63,715			
	Anaimalai				Vettaikararpudhur				Nallar			
Month	Mean (m)	Max (m)	Min (m)	Var (m^2)	Mean (m)	Max (m)	Min (m)	Var (m^2)	Mean (m)	Max (m)	Min (m)	Var (m^2)
JAN	9	50	0	258.9	6.8	52.5	1	262.5	21.1	190	0	3041.2
FEB	7.9	58	0	337.4	3.3	35.4	0	103.6	1.1	8	0	6.8
MAR	23.3	95	0	1111	20.2	89	0	1063.6	10	35	0	224.4
APR	123.8	261	28.2	5096	40.4	87.1	0	603.8	62.6	180	0	3020.6
MAY	181.6	519	20	27,850	58.6	114.6	2	1637.3	31.5	82.2	0	816
JUN	706.1	1026	441	35,994	70.9	106.5	17.4	920.6	44.6	142	0	2255
JUL	1107.9	1358	774.4	26,427	129.2	214.2	95	1312	73	199	13	3259.2
AUG	641	831	438.9	16,309	73.2	226	13	3159	37.9	118	3	17192.2
SEP	389.9	582	114.8	29,122	36	143.6	0	1562	50.7	218	0	4062
OCT	397.5	686	164	28,384	145.1	320.5	0	14,573	139	396.5	3	17192.2
NOV	182.1	283	36	8436	147.7	448	6.2	15,146	186	440	41	15429.2
DEC	43.3	150	0	2722.5	47	280	0	6874.8	69.9	174	0	3014.2

3.2 Data-Driven Models

3.2.1 Artificial Neural Network (ANN)

ANN is well known for its temporal prediction data-driven model and found its wide application in water resources research, namely, (a) rainfall-runoff modeling (Hughes et al., 2019), (b) climatic variable prediction (Chang et al., 2015), (c)

reservoir operation (Safavi et al., 2010), and (d) groundwater level prediction. ANN mimics the behavior of human brain neural communication to map any independent vector matrix to a dependent vector. Haykin (1999) described the behavior of the ANN modeling framework. The basic network architecture has three layers, namely, (a) input layer which are the independent variables that might influence the mapping of dependent variable/vector; (b) hidden layer, which communicates/transfer the information between the input and output layer; and (c) the output layer which describes the dependent variable. The ANN tries to map the independent variable matrix to the dependent variable through various training algorithms such as backpropagation (Wagh et al., 2016), GRNN (Barzegar & Asghari Moghaddam, 2016), and GA(Dash et al., 2010). However, from various research applications, it is proven back propagation network is very popular for training the network. During the process of training, the network architecture and the associated weights are estimated based on the performance of the network to map the observed groundwater levels. The weights are adjusted/estimated based on the overall error "E" while mapping the predicted output to the actual output (Ghasemi et al., 2011):

$$\mathrm{E} = \frac{1}{P} \sum E_P \tag{11.2}$$

$$E_P = \frac{1}{2} \sum \left(T_r - O_r \right)^2 \tag{11.3}$$

where "P" is the total number of training patterns, "Tr" is the actual output measured, and it's the predicted output of the "kth" node.

3.2.2 Support Vector Regression (SVR)

The basic idea of SVR is to learn the nonlinear classifier in the most elegant manner. The SVR algorithm executes the abovementioned task of transforming the data into a higher-dimensional space. The nonlinear classifier in the original space is thus learned as the linear classifier in the hyperspace. The mapping of data in the hyperspace is facilitated using the kernel functions. The statistical mapping capability of SVR enhances its strength in capturing the non-linear relationship that exists between the independent and dependent variables (Salem et al., 2017). The performance of SVR depends on the kernel function that is employed to solve the dot matrix (Naghibi et al., 2017). The selection of kernel function plays a major role in SVR, and it varies based on the statistical characteristics of the database. There are three well-known kernel functions, namely, (a) poly kernel (Raheja et al., 2021), (b) RBF (Natarajan & Sudheer, 2020), and (c) Pearson-type IV(Zhou et al., 2017); the training process estimates the suitable kernel function and respective shape parameters.

3.2.3 Performance Evaluation Measures

Root mean squared error:

$$\mathrm{RMSE} = \sqrt{\frac{\sum_{i=1}^{t}\left(y_i^o - y_i^c\right)^2}{n-1}} \tag{11.4}$$

Nash-Sutcliffe efficiency:

$$NSE = 1 - \frac{\sum_{i=1}^{t}\left(\mathrm{y_i^o} - y_i^c\right)^2}{\sum_{i=1}^{t}\left(y_i^o - \overline{y}^o\right)^2} \tag{11.5}$$

where y_i^o and y_i^c are the observed and the predicted values, respectively.

4 Results and Discussions

The developed framework is allowed to explore the rainfall and piezometer database pertaining to three wells locations in the PAP basin. The knowledge recovered from the training phase is allowed to predict the future piezometer levels at a temporal scale.

4.1 Artificial Neural Network

Figure 11.3 indicates the variation of the efficiency with respect to the parameters, namely, learning rate momentum and the network architecture, in the case of ANN.

4.1.1 Estimation of Network Architecture

Considering the observation well at location ID-63712 (Table 11.1), it is observed that the efficiency fluctuates with the increase in the influencing parameters. From Fig. 11.3a, b, it is observed that the efficiency during the training phase is higher for the network architecture 3:4:2:1. The network architecture of 3:2:2:1 yields the training efficiency of 0.67, with the learning rate and the momentum of 0.5 (Table 11.4a) and 0.2 (Table 11.4b), respectively. The above-stated network (3:2:2:1) is quite less proficient in mapping compared to the network architecture 3:4:2:1. From Table 11.4b, it is observed that the architecture 3:2:2:1 is capable of mapping the test datasets with the NSE of 0.63. The architecture 3:4:2:1 can test the datasets

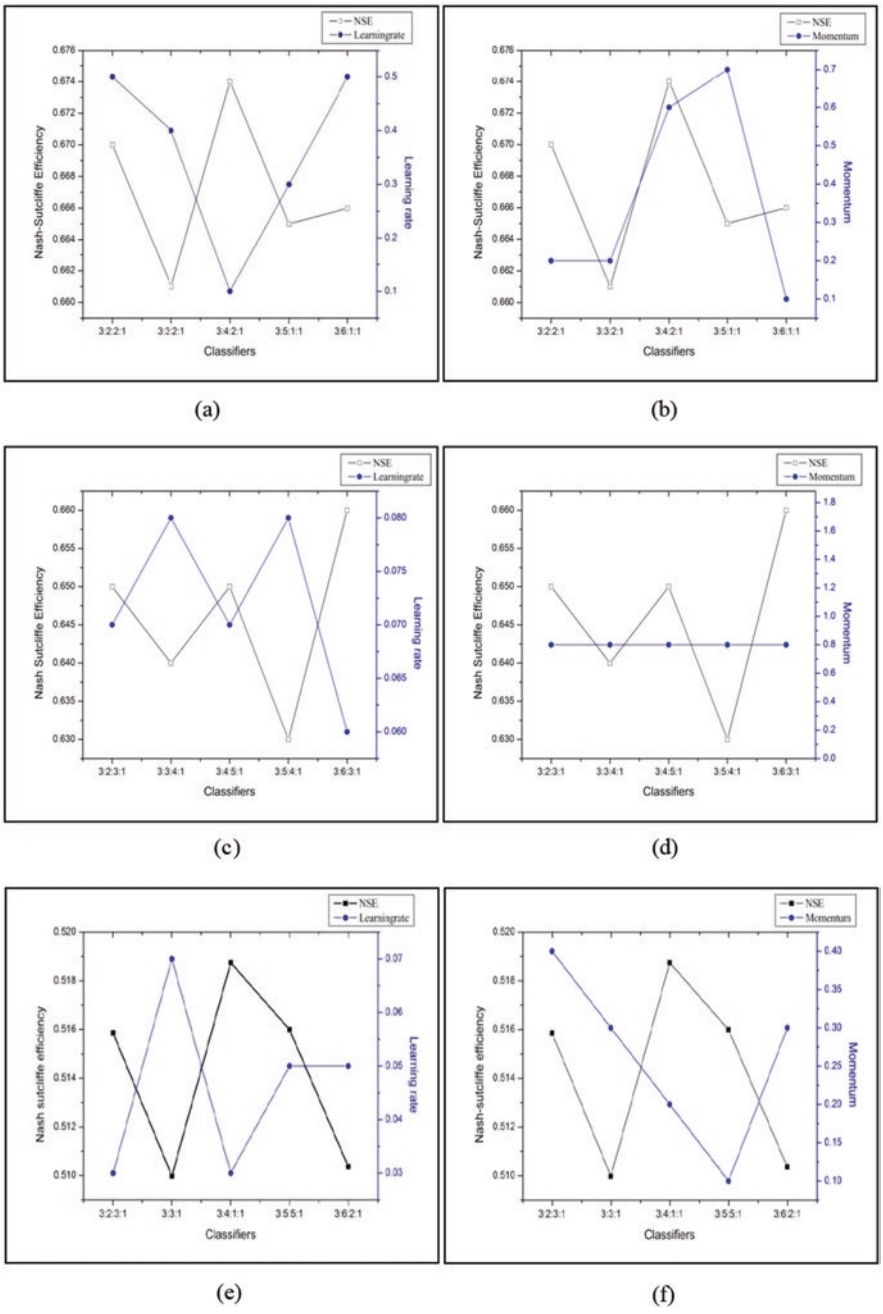

Fig. 11.3 The variation of parameters with respect to the NSE in ANN (**a**–**f**) and the variation of kernel parameters with respect to NSE in SVM (**g**–**k**)

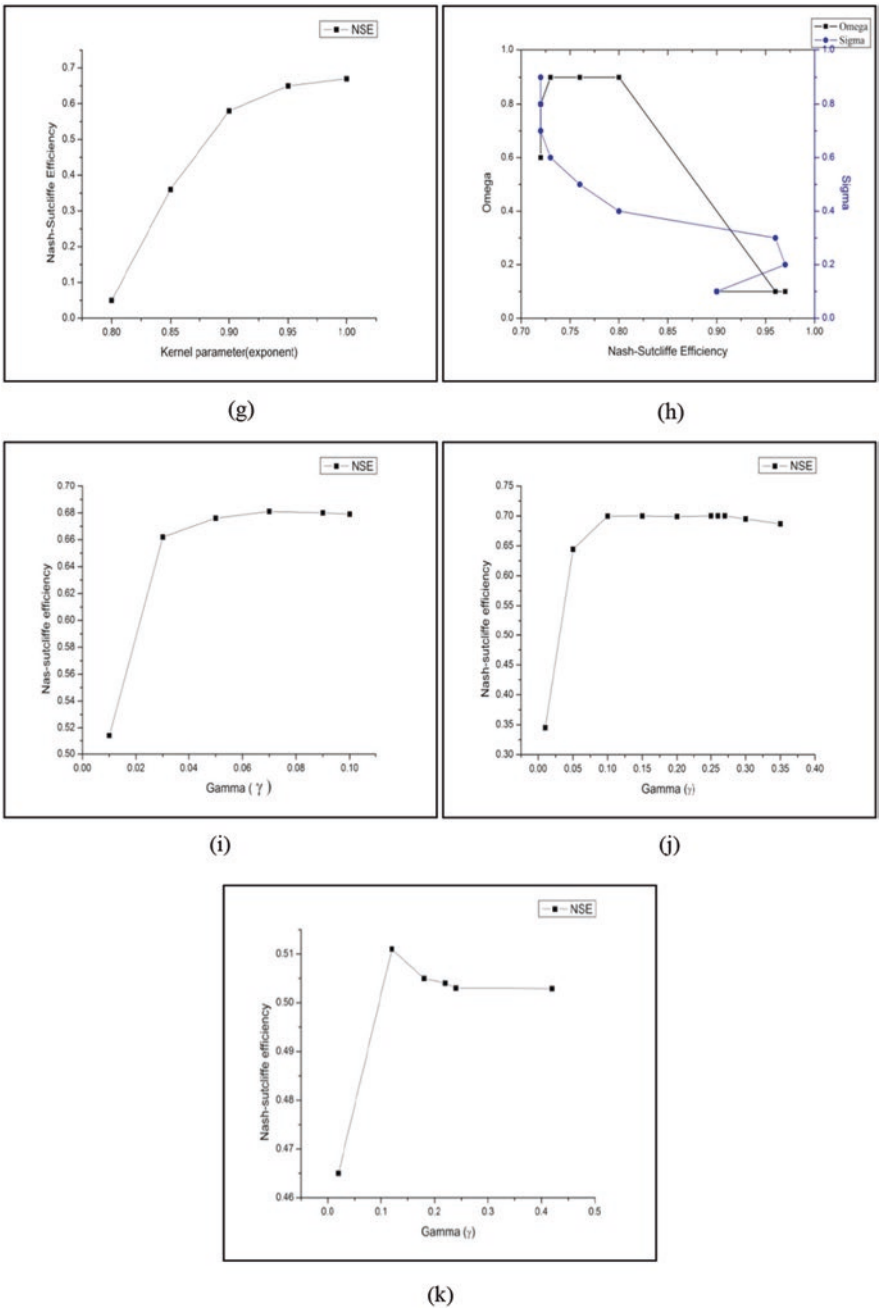

Fig. 11.3 (continued)

Table 11.4 The training and the testing phase results for ANN (a and b) and also the training and the testing phase results for SVM (c to h)

ANN							
Location	**Architecture**	**(a)**			**(b)**		
		Training phase			**Testing phase**		
		Correlation	**RMSE (m)**	**NSE**	**Correlation**	**RMSE (m)**	**NSE**
63,712	3:2:2:1	0.83	1.63	0.67	0.822	0.95	0.63
63,714	3:2:3:1	0.84	1.01	0.65	0.76	0.80	0.58
63,715	3:2:3:1	0.72	1.52	0.516	0.82	1.06	0.62
SVM-linear polynomial							
Location		**(c)**			**(d)**		
		Training phase			**Testing phase**		
		Correlation	**RMSE (m)**	**NSE**	**Correlation**	**RMSE (m)**	**NSE**
63,712		0.83	1.63	0.67	0.79	1.09	0.52
63,714		0.84	0.93	0.69	0.76	0.88	0.50
63,715		0.72	1.53	0.52	0.82	1.06	0.62
SVM-Pearson-type VII kernel							
Location		**(e)**			**(f)**		
		Training phase			**Testing phase**		
		Correlation	**RMSE(m)**	**NSE**	**Correlation**	**RMSE (m)**	**NSE**
63,712		0.98	0.46	0.97	0.79	1.10	0.50
63,714		0.85	0.92	0.70	0.7	0.94	0.43
63,715		0.74	1.52	0.52	0.82	1.60	0.60
SVM-radial basis function kernel							
Location		**(g)**			**(h)**		
		Training phase			**Testing phase**		
		Correlation	**RMSE (m)**	**NSE**	**Correlation**	**RMSE (m)**	**NSE**
63,712		0.83	1.59	0.68	0.79	1.06	0.54
63,714		0.84	0.93	0.69	0.76	0.85	0.53
63,715		0.72	1.53	0.502	0.84	1.09	0.66

with less NSE compared to the architecture 3:2:2:1. Hence, architecture 3:2:2:1 has efficiency in prediction. It means that the three input signals from the datasets are individually required to be continuously subjected to two activation functions in two subsequent layers to be stabilized with their respective weights for producing the desired output signal. The network architecture, other than the abovementioned, is not sufficient to compromise the complexity of the function to be learned. The above result shows that in architecture 3:4:2:1, the model has attempted to capture maximum efficiency in the training phase, which in turn has generalized the model, and so the corresponding test results are poor.

Figure 11.3c, d represent the variation of the efficiency with respect to the parameters in the observation well at location ID-63714 (Table 11.1). Figure 11.3c, d show that the network architecture 3:2:3:1 results in the maximum NSE of 0.65 (Table 11.4a) in the training phase and 0.58 (Table 11.4b) in the testing phase. It is also observed that the learning rate is inversely proportional to the NSE and the momentum is

constant for various forms of network architecture (Fig. 11.3c, d). The learning rate and momentum corresponding to the maximum NSE are 0.07 and 0.8, respectively. The result proves that the model requires two hidden layers, as the output from the activation function in the first layer is not completely stabilized to produce efficient output predictions. It is also inferred that further change in the network architecture led to a reduction in efficiency as the complexity of the dataset to be learned does not match the complexity of the model. Figure 11.3e, f represent the efficiency of the model versus the parameters to be estimated for the observation well at location ID-63715. The network architecture 3:2:3:1, with a learning rate of 0.03(Fig.11.3e) and momentum of 0.4 (Fig. 11.3f) results in the NSE of 0.516 (Table 11.4a) in the training phase. The corresponding testing phase NSE is 0.62 (Table 11.4b). The above result is the best prediction efficiency for the developed model to forecast the groundwater levels at the specified observation well. It means that the amplitude of output signals from the two hidden nodes in the first layer and three hidden nodes in the second layer is required in order to provide the best fit output.

4.1.2 Pattern Analysis for the Training and the Testing Sets

Comparing the efficiency of the best fit models in the three different observation models, the most proficient learning has occurred in the case of the dataset collected at location ID-63712 (Table 11.1). Figure 11.4a, b represent the actual and the predicted water level depth at the observation well (location ID-63712) (Table 11.1). The training phase has shown the appearance of a cyclic pattern, which may be the reason for the best fit when applying the ANN algorithm, the mimic of the human brain, which is capable of learning the cyclic occurrence efficiently. Figure 11.4c, d indicate the actual and the predicted values of the dataset at the observation well with location ID 63714. Though it is observed to be less cyclic in its pattern, the adequacy of ANN to capture all the points during the training phase worked up to NSE of 0.65 (Table 11.4a) Nash efficiency, and the corresponding testing efficiency is 0.58 (Table 11.4b). The abovementioned capability of the model to capture 65% of the samples in the training phase and 58% of the sample in the testing phase may be because of the gradual surge and drop down in the water level, throughout the dataset, without any sudden dropdown. The model failed to capture 35% of the datasets in the training phase and failed 42% in the testing phase. The reason for the above instability of the model may be due to a few sudden peaks and drop-downs in the water levels at the end of the year 1998. Figure 11.3e, f illustrate the actual and the predicted water level depths in both training and testing datasets at location ID-63715 (Table 11.1). The efficiency in the training and the testing phase is 51.6% (Table 11.4a) and 62% (Table 11.4b), respectively. It is observed that the model is more proficient in capturing the testing data than the training samples. The abovementioned fact is justified as follows. From Fig. 11.4e, it is noted that the algorithm has attempted to capture an irregular pattern, sudden variation in the groundwater levels (water-level variation between August 1996 and September 1996 is 7.4 m, which is recorded as the maximum sudden peak in the case of the training dataset).

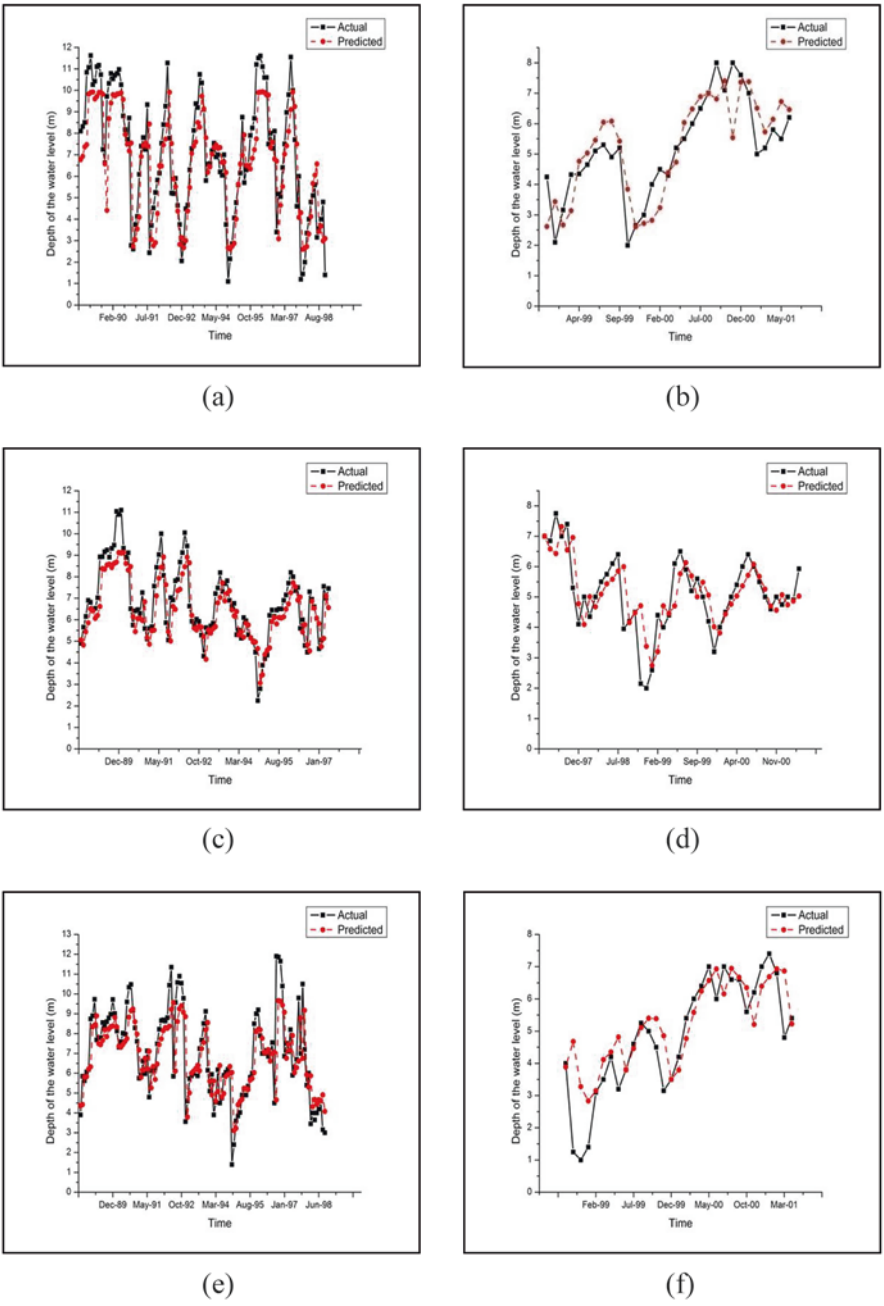

Fig. 11.4 The actual and the predicted groundwater levels using ANN (a to f) and the actual and using SVM (g to p) for the case study

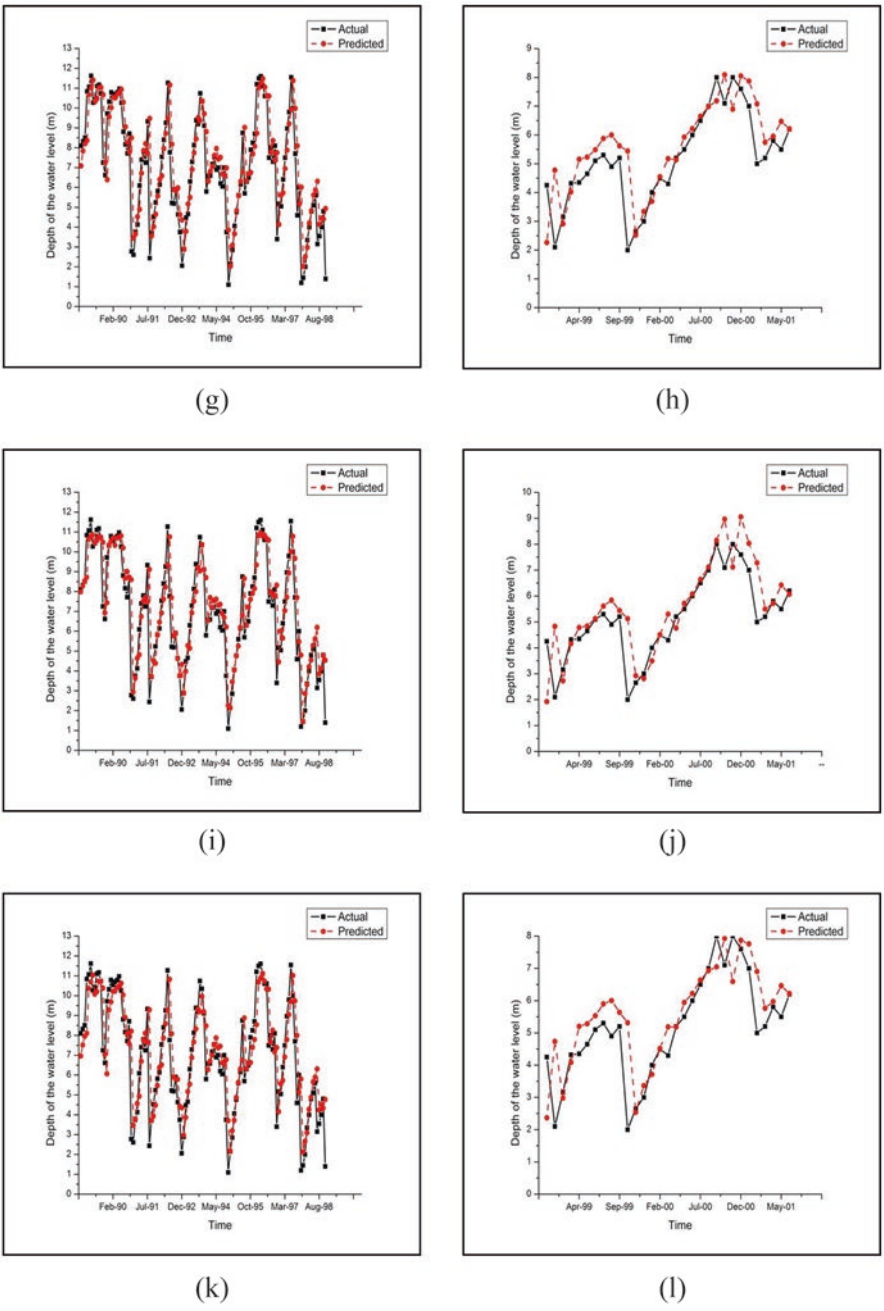

Fig. 11.4 (continued)

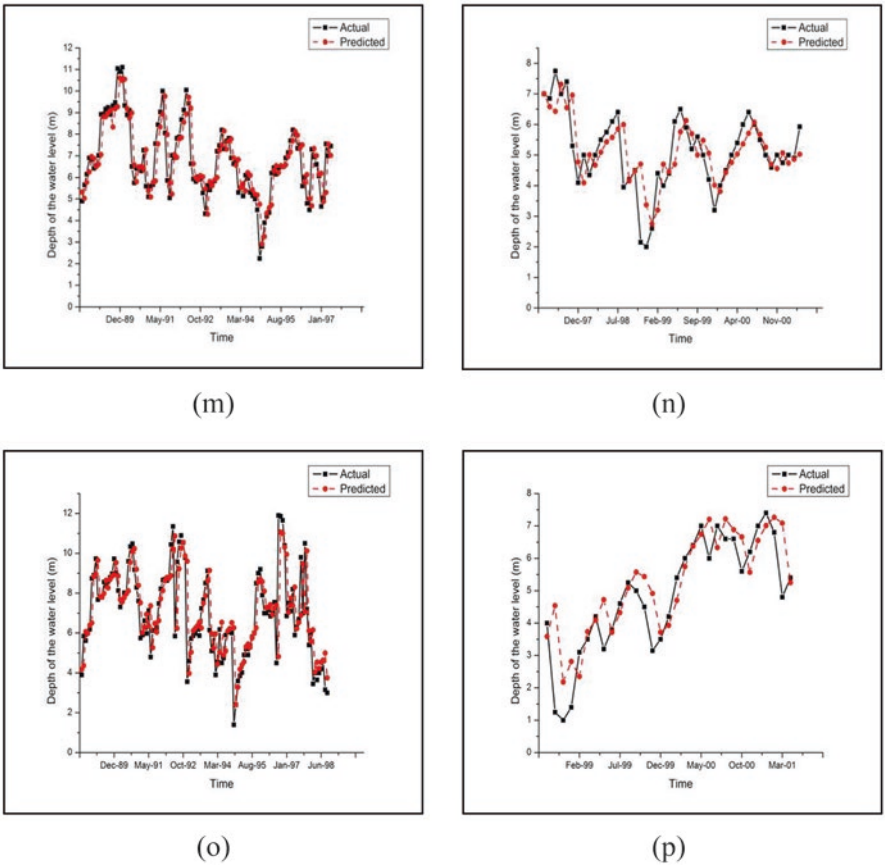

Fig. 11.4 (continued)

Figure 11.4f representing the variation in the groundwater level depths for the testing phase does not exhibit the maximum sudden peaks as in the training phase (water-level variation between October 1998 and November 1998 is 2.5 m, which is recorded as the maximum sudden variation in case of the testing dataset). From the above observations, it is inferred that the algorithm has learned a pattern with sudden peaks in the training phase and has been subjected to testing the datasets whose values are more towards the gradual mean. Hence, the resulting efficiency in the testing phase is 62% (NSE)which is higher than the efficiency of the training phase.

4.2 Support Vector Machine

Support vector machine (SVM), in general, is a statistical model which utilizes the strengths of kernel functions to facilitate the learning of the nonlinear classifiers in the hyperspace (Sect. 3.2). The choice of Kernel has an impact on the prediction ability (Cui et al., 2012), as the knowledge for mapping is available within the kernel function. The support vector machine has three basic kernel functions, namely, (a) linear, (b) polynomial, and (c) radial basis function.

4.2.1 Choice of Kernel

The section comprises a discussion on the results from the performance evaluation of each Kernelin in terms of mash efficiency for the groundwater level estimation in the observation well at location ID-63712 (Table 11.1). The kernel function, which assists the best fit model from the above-stated analysis, is thus fixed for the prediction of the groundwater levels at the observation wells (location ID-63714 and ID-63715) (Table 11.1). The tendency of the dataset (63712-Table 11.1), utilized to fix an appropriate kernel function for the present study, is observed to be fluctuating with gradual surge and drop down and with the occurrence of the cyclic pattern.

4.2.2 Linear Polynomial Kernel Function

Variation of Kernel Parameters for NSE (Linear Polynomial Kernel)
Figure 11.2g represents the variation of the NSE concerning the kernel parameter (exponent) for the training phase. The maximum efficiency is achieved for the maximum value of the exponent.

Pattern Analysis of Training and Testing Phase (Linear Polynomial Kernel)
Figure 11.4g, h represent the predicted results with a 1-D linear polynomial kernel. The kernel function performs the mapping process with the prediction efficiency of 0.67 (Table 11.4c) in the learning/ training phase and 0.52 (Table 11.4d) in the validation/ testing phase. The above-stated efficiency of the model shows that, though SVM with linear polynomial regression is capable of mapping 67% of the datasets in the training phase, the testing efficiency is only up to 52%. It is observed in Fig. 11.4g, h that the number of datasets towards the gradual mean is high in the training phase compared to the testing phase. The results stated above may be because the linear polynomial kernel function efficiently captures the datasets that are towards the gradual mean. The phenomenon of the linear polynomial kernel explained above has already been stated by Liu et al. (2014) (Sect. 3.2).

4.2.3 Pearson-Type VII Kernel Function

Variation of Kernel Parameters with Respect to NSE (Pearson-Type VII Kernel)
Figure 11.2h represents the variation of the SVM-Pearson-type VII kernel parameters, namely, (a) omega and (b) sigma, with respect to NSE in the training phase. It is observed that the NSE corresponds to the omega and sigma, 0.1 and 0.2, respectively, which is the best result yielded. The NSE value for the above-stated kernel parameters is 0.97 (Table 11.4e). Though the regression model is developed so effectively that most of the training data are captured accurately, the corresponding NSE in the testing phase is 0.50 (Table 11.4f). The result proves that the shape functions omega and sigma are calibrated, with a complete concentration towards capturing the training datasets. The flexibility of the abovementioned shape functions to change the curve according to the dataset has led to the formation of the regression curve, which captures only the training dataset. The consequence of the above phenomena is the development of a non-generalized model, that is, incapable of capturing around 50% of the testing datasets. The nature of the Pearson-type VII kernel function explained above is also stated by Uestuen et al. (2006).

Pattern Analysis of Training and Testing Phase (Pearson-Type VII Kernel)
Figure 11.3h represents the variation of kernel parameters in the SVM-Pearson-type VII kernel for the observation well at location ID 63712 (Table 11.1). The regression model developed using the SVM-Pearson-type VII kernel function shows an NSE of 0.97 (Table 11.4e) in the training phase. Although the learning/training has occurred to the maximum efficiency, the model failed to retain the performance level in the testing phase and has resulted in a decline of 47% NSE. The above-stated instability of the model in the testing phase is due to the fact that the shape functions omega and sigma have been estimated to provide a better fit for the training dataset. The analysis shows that the best fit model in the Person-type VII kernel is possible only if the training and testing datasets hold the same kind of pattern. Due to the difference in pattern between the training and testing datasets, the developed regression model has resulted in reduced testing efficiency compared to the training phase.

4.2.4 Radial Basis Kernel Function

Variation of Kernel Parameters with Respect to NSE (Radial Basis Function)
The variation of efficiency in the SVM-RBF kernel is controlled by three parameters, namely, (a) gamma (γ), (b) regularization parameter (c), and (c) loss function (ϵ). Gamma (γ) acts as the shape function. Relative to the dataset under study, the variation in gamma value has the maximum impact on the efficiency of the model. The regularization parameter represents the complexity of the model. The value of "c" controls the empirical error due to the outliers. An increase in the complexity attempts to reduce the error, and hence the model may result in high efficiency. With

reference to the processing time and the negative impacts of a highly complex model, the value of "c" is limited. Epsilon is the loss function which denotes the range within which the error is zero. Generally, the tube is expected to be narrow for high precision in modeling. The impact of the loss function for the datasets under study was up to the third decimal point; hence, its influence on the efficiency of the model is neglected. Figure 11.3i represents the variation of the kernel parameter in RBF named gamma (γ). Figure 11.4k, l represents the actual and the predicted results of the water-level depth, using SVM in combination with the RBF kernel. The gamma value of 0.07 (Fig. 11.3i) has resulted in the training efficiency of 0.68 (Table 11.4g) and the testing efficiency of 0.54 (Table 11.4h). The smaller the value of gamma (0.07), the higher its dependency on the support vectors will be, and subsequently, the margin might be less. The least gamma (0.07) value reported in the present study shows that the model is highly accurate (mentioned in the same section). The value of the kernel parameter is restricted to overfitting.

The linear polynomial kernel has comparatively less than that of the RBF kernel in terms of NSE in the testing phase. Though Pearson-type VII shows in Table 11.4e, good training NSE (0.97), the model developed does not retain its efficiency in the testing phase and has been subjected to a decline of 47% efficiency. The above-stated drawbacks in previously mentioned kernels are not seen in the case of RBF kernel functions. The RBF kernel is infinitely differentiable as it contains an exponential squared term. The above phenomena assist the RBF kernel in deriving an appropriate complex regression model relative to the complexity of the dataset. The same characteristics of the RBF kernel have been stated by Pecli et al. (2015).

4.2.5 Comparison of Different Kernel Functions

Comparing the results of the previously discussed kernels for the observation well at location-63712, RBF shows better testing NSE. The testing efficiency of the RBF kernel is 2% higher than the polynomial Kernel (compare Table 11.4d, h) and 4% higher than the Pearson-type VII kernel (compare Table 11.4f, h). It is also shown that RBF has supported to development of a highly stable regression model. Hence, from the results of SVM with RBF kernel in the prediction of water levels at location ID-63712, it may be concluded that RBF is the best fit kernel for forecasting the groundwater levels in the observation wells. The strength of the RBF kernel is thus utilized to predict the groundwater level variations in the observation wells at locations ID-63714 and ID-63715 (Table 11.1).

4.2.6 Application of the Appropriate Kernel (Radial Basis Function)

The section comprises a discussion on the prediction results obtained by using SVM with RBF kernel for the observation wells at locations ID-63714 and ID-63715 (Table 11.1).

Variation of Kernel Parameters with Respect to NSE (RBF)

Figure 11.3j represents the variation of the kernel parameter with respect to NSE for the groundwater level variations in the observation well at location ID-63714 (Table 11.1). It is observed that an increase in gamma value resulted in high efficiency up to 0.1, and the further increase in gamma did not influence the NSE to a greater extent. The highest training efficiency of 0.69 (Table 11.4g) and testing efficiency of 0.53 (Table 11.4h) note the gamma value of 0.35. The kernel parameter value other than 0.35 (gamma) may show better training results, but the corresponding testing efficiency is lower than that of 0.35 (gamma). The appearance of the above-stated phenomena may be due to the overfitting of the model toward the training dataset. Figure 11.3k represents the variation of the kernel parameter with respect to training/learning NSE for the groundwater-level variations in the observation well at location ID-63715 (Table 11.1). The gamma value corresponding to the best-fit regression model for the study is 0.3. The training and the testing NSE are 0.502 (Table 11.3g) and 0.66 (Table 11.3h), respectively. From Fig. 11.3k, it is observed that the highest NSE is recorded for the gamma value of 0.12 (NSE = 0.51), but the corresponding testing phase NSE of 0.63 is less than 0.66, which is the efficiency of the regression model actually developed. Hence, the gamma value, thus estimated to forecast the groundwater-level variations at the observation well located at location ID-63715, is 0.30. Table 11.4c to illustrates the NSE of the SVM in combination with three different kernels for the observation wells of locations ID-63712, ID-63714, and ID-63715. The RBF kernel in the testing phase has resulted in a 3% higher NSE compared to the polynomial Kernel and 10% higher NSE compared to the Pearson-type VII kernel (Table 11.4c–h), in the case of the observation well at location ID 63714. Similarly, the above phenomenon may be observed in the testing phase of the models pertaining to the well ID-63712 and ID-63715 (Table 11.4c–h), justifying that RBF is the best fit kernel function (Table 11.5).

From the percent deviation computed, it is inferred that the model calibration is sufficient enough to predict more than 50% of the datasets with 90% accuracy, and the confidence limit of 75% is achieved by more than 77% of the data sets. In addition to the above, the comparison between ANN and the SVM-RBF kernel reveals

Table 11.5 Percent of deviation between the actual and the predicted test data sets in terms of the percentage of sample numbers for ANN and for SVM

Data set	10% deviation (%)	20% deviation (%)	50% deviation (%)
Ann			
63,712	45.16	32.26	6.25
63,714	43.48	15.22	6.52
63,715	45.17	22.58	16.13
SVM-radial basis function kernel			
63,712	51.61	19.35	6.45
63,714	41.30	21.74	6.52
63,715	45.16	29.03	12.9

that ANN is capable of fitting into the confidence level of 90% for more than 54% of the data, but the SVM-RBF is capable of predicting 48% of datasets with 90% accuracy. The above statement may prove that ANN may be suggested as the most appropriate model for performing groundwater-level prediction in the case of datasets pertaining to the case study.

Pattern Analysis of SVM-RBF Kernel and Comparison with ANN
Figure 11.4k, l exhibit the actual and the predicted water level depth for the observation well ID-63712 (Table 11.1). The efficiency achieved is 0.68 (Table 11.4g) in the training phase and 0.54 (Table 11.4h) in the testing phase. In the prediction process, when carried out using the ANN algorithm, the efficiency resulting is 0.67 (Table 11.4a) in the training phase and 0.63 (Table 11.4b) in the testing phase, which is comparatively better than SVM. Figure 11.4m, n detail the results of the prediction of water-level depth at the observation well at location ID-63714. The illustration in Fig. 11.4c, d, and the discussion on the results, which corresponds to the same dataset using the ANN algorithm, explain the tendency of the dataset and justify its best performance in ANN. The training phase NSE is 0.65 (Table 11.4a), and the test in phase NSE is 0.58 (Table 11.4b) for the model developed using ANN, while training and the testing NSE in the case of SVM with RBF kernel are 0.69 (Table 11.4g) and 0.53 (Table 11.4h) respectively. From the results, it may be inferred that ANN seems to be the best algorithm to predict the water level variations for the well ID-63714 (Table 11.1). Figure 11.4o, p illustrate the variation in water levels for both the training and the testing phase in the observation well at ID-63715 (Table 11.1), using SVM with RBF kernel. The NSE of the ANN model in the training phase for the same dataset is 0.52 (Table 11.4a) and in the testing is 0.62 (Table 11.4b). The reason for the testing result being more proficient than the training is explained in Sect. 4.1.2 (discussion in Fig. 11.4e, f). The SVM, with RBF kernel, has shown the training phase has an NSE of 0.50 (Table 11.4g), and in the testing phase NSE of 0.66 (Table 11.4h). The above-stated results show that the SVM has performed better than ANN, and the reason may be due to the difference in the nature of the dataset between the training and the testing phase (Fig. 11.4e, f). The characteristic of SVM, to learn the chaotic dynamic properly, resulted in the condition where SVM outperformed ANN.

5 Conclusions

The comparative analysis of the two supervised learning algorithms, namely, ANN and SVM, in predicting the groundwater levels at the observation wells shows that both algorithms have equivalent efficiency in performing the pattern recognition. The ANN works better for two observation wells, and the SVM does better at the third one in which the test data fit the grade mean. The fact mentioned above is based on the analysis of the testing dataset in terms of NSE. The complexity of SVM is high in terms of computation, as it takes into account the empirical error in

addition to the model error. Though ANN considers only the model error, it is intelligent to compete with SVM in the specified database. From this study, it may be concluded that ANN with the backpropagation technique is the best-suggested algorithm for the prediction of the groundwater levels pertaining to the historical database having similar statistical characteristics used in this research. The future scope is to extend the research toward analyzing the relationship that may be prevailing between the groundwater variables, both in terms of temporal and spatial characteristics.

Declarations The authors declare that no funds, grants, or other support were received during the preparation of this work.

References

Alsmadi, M. K. S., Omar, K. B., & Noah, S. A. (2009). Back propagation algorithm: The best algorithm among the multilayer perceptron algorithm. *IJCSNS International Journal of Computer Science and Network Security, 9*(4).

Banerjee, P., Singh, V. S., Chattopadhyay, K., Chandra, P. C., & Singh, B. (2011). Artificial neural networkmodel as a potential alternative for groundwatersalinity forecasting. *Journal of Hydrology, 398*(2011), 212–220.

Barzegar, R., & Asghari Moghaddam, A. (2016). Combining the advantages of neural networks using the concept of committee machine in the groundwater salinity prediction. *Modeling Earth Systems and Environment, 2*(1), 1–13. https://doi.org/10.1007/s40808-015-0072-8

Behzad, M., Asghari, K., & Coppola, E. A. (2010). Comparative study of SVMs and ANNs in aquifer water level prediction. *Journal of Computing in Civil Engineering, 24*(5), 408–413. https://doi.org/10.1061/(asce)cp.1943-5487.0000043

Chang, J., Wang, G., & Mao, T. (2015). Simulation and prediction of suprapermafrost groundwater level variation in response to climate change using a neural network model. *Journal of Hydrology, 529*, 1211–1220. https://doi.org/10.1016/j.jhydrol.2015.09.038

Chang, D., Zhang, F. (2016). Resolving temporal variations in data-driven fow models constructed by motion tomography. In: IFAC-Papers OnLine, vol. 49, pp. 182–187. Elsevier, Amsterdam

Cui, Y., Sachdev, P. S. Lipnicki, D. M., Jin, J. S., Luo, S., Zhu, W., Kochan, N. A. Reppermund, S., Liu, T., Trollor, J. N. Brodaty, H., & Wen, W. (2012). Predicting the development of mild cognitive impairment: A new use of pattern recognition, *NeuroImage, 60*(2), 894–901. ISSN 1053–8119, https://doi.org/10.1016/j.neuroimage.2012.01.084.

Daliakopoulos, I. N., Coulibaly, P., & Tsani, I. K. (2005). Groundwater level forecasting using artificial neural networks. *Journal of Hydrology, 309*(2005), 229–240.

Dash, N. B., Panda, S. N., Remesan, R., & Sahoo, N. (2010). Hybrid neural modeling for groundwater level prediction. *Neural Computing and Applications, 19*(8), 1251–1263. https://doi.org/10.1007/s00521-010-0360-1

Ghasemi, H., Malek-Mohammadi, M., Babaie-Zadeh, M., Jutten C., (2011). SRF: Matrix Completion Based on Smoothed Rank Function. ICASSP 2011 - IEEE International Conference on Acoustics, Speech and Signal Processing, Prague, Czech Republic. pp.3672–3675. ffhal-00596777

Gong, Y., Lan, Y. S., & Wang, H. (2016). A comparative study of artificial neural networks, support vector machines and adaptive neuro-fuzzy inference system for forecasting groundwater levels Lake near Lake Okeechobee, Florida. *Water Resource Management, 30*, 375–391.

Hicham, El Badaoui & Abdelaziz, Abdallaoui & Samira, Chabaa. (2013). Using MLP neural networks for predicting global solar radiation. *The International Journal of Engineering and Science (IJES). 2*. 48–56.

Hughes, L., Dwivedi, Y. K., Misra, S. K., Rana, N. P., Raghavan, V., & Akella, V. (2019). Blockchain research, practice and policy: Applications, benefits, limitations, emerging research themes and research agenda. *International Journal of Information Management, 49*(February), 114–129. https://doi.org/10.1016/j.ijinfomgt.2019.02.005

Isa, I. S., Saad, Z. S., Omar, S., Osman, M. K., Ahmad, K. A., & Sakim, H. A. M. (2010). Suitable MLP network activation functions for breast cancer and thyroid disease detection. In *Second international conference on computational intelligence, modelling and simulation*, 978-0-7695-4262-1/10 $26.00 © 2010 IEEE, https://doi.org/10.1109/CIMSiM.2010.93

Khan, M. S., & Coulibaly, P. (2006). Application of support vector machine in Lake water level prediction. *Journal of Hydrologic Engineering, 11*(3), 199–205.

Haykin, S. S. (1999). Neural Networks: A Comprehensive Foundation, PrinticeHall Inc., NJ, USA.

Liu, L., Shen, B., & Wang, X. (2014). Research on kernel function of support vector machine. *Journal of Computers, 25*(1).

Mohan, S., & Ramsundram, N. (2016). Predictive temporal data-mining approach for evolving knowledge-based reservoir operation rules. *Water Resources Management, 30*, 3315. https://doi.org/10.1007/s11269-016-1351-5

Naghibi, S. A., Ahmadi, K., & Daneshi, A. (2017). Application of support vector machine, random forest, and genetic algorithm optimized random forest models in groundwater potential mapping. *Water Resources Management, 31*(9), 2761–2775. https://doi.org/10.1007/s11269-017-1660-3

Natarajan, N., & Sudheer, C. (2020). Groundwater level forecasting using soft computing techniques. *Neural Computing and Applications, 32*(12), 7691–7708. https://doi.org/10.1007/s00521-019-04234-5

Osowskil, S., Siwek, K., & Markiewicz, T. (2004). MLP and SVM networks – A comparative study. In *Proceedings of the 6th Nordic signal processing symposium – NORSIG 2004*, IEEE, June 2004.

Panchal, G., Ganatra, A., Kosta, Y. P., & Panchal, D. (2011). Behaviour analysis of multilayer perceptrons with multiple hidden neurons and hidden layers. *International Journal of Computer Theory and Engineering, 3*(2), 332–337.

Patel, M. B., & Yalamalle, S. R. (2014). Stock Price prediction using artificial neural network. *International Journal of Innovative Research in Science, Engineering and Technology, 3*(6) ISSN: 2319-8753.

Pecli, A., Giovanini, B., Pacheco C. C., Moreira, C., Ferreira, F., Tosta, F., Tesolin J., et al. (2015). Dimensionality Reduction for Supervised Learning in Link Prediction Problems. In ICEIS (1), pp. 295–302.

Raheja, H., Goel, A., & Pal, M. (2021). Modeling of water quality index of Haryana: A comparison of deep neural network and support vector machine. In 1st *international online conference on Sustainable Development in Civil and Electrical Engineering (SDCEE-2021)*, National Institute of Technology, 17–19 December, 2021.

Safavi, H. R., Darzi, F., & Mariño, M. A. (2010). Simulation-optimization modeling of conjunctive use of surface water and groundwater. *Water Resources Management, 24*(10), 1965–1988. https://doi.org/10.1007/s11269-009-9533-z

Salem, G. S. A., Kazama, S., Shahid, S., & Dey, N. C. (2017). Impact of temperature changes on groundwater levels and irrigation costs in a groundwater-dependent agricultural region in Northwest Bangladesh. *Hydrological Research Letters, 11*(1), 85–91. https://doi.org/10.3178/HRL.11.85

Sakr, S. et al. (2011). A survey of large scale data management approaches in cloud environments. *IEEE communications surveys & tutorials 13*(3), 311–336.

Tsanis, I. K., Paulin C. and Ioannis N. D., "Improving groundwater level forecasting with a feedforward neural network and linearly regressed projected precipitation." Journal of Hydroinformatics 10.4 (2008): 317–330.

Uestuen, B., Melssen, W. J., Buydens, L. M. C., (2006). Facilitating the application of support vector regression by using a universal Pearson VII function based kernel. *Chemometrics and Intelligent Laboratory Systems 81*(1), 29–40.

Wagh, V. M., Panaskar, D. B., Muley, A. A., Mukate, S. V., Lolage, Y. P., & Aamalawar, M. L. (2016). Prediction of groundwater suitability for irrigation using artificial neural network model: A case study of Nanded tehsil, Maharashtra, India. *Modeling Earth Systems and Environment, 2*(4), 1–10. https://doi.org/10.1007/s40808-016-0250-3

Xu, T., Valocchi, A. J., Choi, J., & Amir, E. (2014). Use of machine learning methods to reduce predictive error of groundwater models. *Groundwater, 52*(3), 448–460. https://doi.org/10.1111/gwat.12061

Yoon, H., Jun, S. C., Hyun, Y., Bae, G. O., & Lee, K. K. (2011). A comparative study of artificial neural networks and support vector machines for predicting groundwater levels in a coastal aquifer. *Journal of Hydrology, 396*(1–2), 128–138. ISSN 0022-1694, https://doi.org/10.1016/j.jhydrol.2010.11.002

Zhou, T., Wang, F., & Yang, Z. (2017). Comparative analysis of ANN and SVM models combined with wavelet preprocess for groundwater depth prediction. *Water (Switzerland), 9*(10). https://doi.org/10.3390/w9100781

Chapter 12
Suitability of Groundwater for Drinking and Agricultural Use in Patna District, Bihar, India

Yash Aryan, P. Thambidurai, and Anil Kumar Dikshit

Abstract Groundwater is the most important source of freshwater, with nearly one-third of the world's population depending on it for drinking. The demand for groundwater has increased tremendously in developing countries, including India, due to the rapid growth of population, urbanization, and industrialization. The quality of groundwater is also important, along with the quantity. The present study highlights the scenario of groundwater in India and in the study area, which is Patna district in the state of Bihar. The study aims to evaluate the groundwater suitability for drinking and irrigation purposes. The chemical characteristics of groundwater samples at 37 locations were obtained from the Central Ground Water Board 2021 report. The study found that the groundwater samples in most parts of the study area were appropriate for drinking and irrigation purposes as most of the parameters such as pH, EC, TDS, and TH were within the maximum allowable limit or maximum permissible limit specified by WHO and BIS. The major anions and cations were found to be within the maximum limit permitted for drinking. The various parameters indicating the groundwater suitability for irrigation were found to be excellent to permissible range, while the magnesium hazard parameter was observed to be greater than 50% at 12 locations indicating groundwater samples were not desirable for irrigation. Although most of the above parameters were within the range, parameters such as coliform value and arsenic content are also equally important and need to be measured before declaring groundwater fit for drinking.

Keywords Agriculture · Drinking · Groundwater · Industrialization · Urbanization · Water quality

Y. Aryan · A. K. Dikshit (✉)
Environmental Science and Engineering Department, Indian Institute of Technology Bombay, Mumbai, Maharashtra, India
e-mail: dikshit@iitb.ac.in

P. Thambidurai
Department of Coastal Disaster Management, School of Physical, Chemical and Applied Sciences, Pondicherry University-Port Blair Campus, Port Blair, Andaman and Nicobar Islands, India

P. Thambidurai, A. K. Dikshit (eds.), *Impacts of Urbanization on Hydrological Systems in India*, https://doi.org/10.1007/978-3-031-21618-3_12

1 Introduction

Water is an essential and vital resource for the existence of all life forms. Groundwater is the major source of freshwater for human life (Vignesh et al., 2021). Around one-third of the global population depends on groundwater for drinking water (Li et al., 2021). The presence of freshwater on the earth is estimated at around 36 Mkm^3; out of this, about 22% exists as groundwater (Sarath Prasanth et al., 2012). Groundwater availability has been taken for granted as it is a replenishable resource, resulting in the overexploitation of groundwater as a resource. The demand for groundwater has increased tremendously in developing countries, including India, due to the increase in population and growth of industries. The overexploitation of groundwater resulted in groundwater stress in many parts of India, along with degradation in the quality of groundwater mostly due to anthropogenic activities.

2 Groundwater Scenario in India

The extraction of groundwater is not uniform in different parts of India. The majority of extracted groundwater (90%) is used for irrigation, and groundwater supplies primarily support about 60% of the irrigated land in India (Chindarkar & Grafton, 2019). According to an assessment conducted by Central Ground Water Board (CGWB) in 2017, 432 billion cubic meters (bcm) was the total annual groundwater recharge, and 393 bcm was the annual extractable groundwater resource. The problem gets worsened due to the disparity in basin-wise water availability across the country because of variation in population density and uneven rainfall in the country. The availability of water in the Brahmaputra/Barak basin is very high, around 14,057 m^3/year/person, and very low in the Sabarmati basin (307 m^3/year/person). There are many basins like Pennar, Tapi, Mahi, etc., which are already water-stressed. In the study conducted by CGWB, 17% of blocks in various states (mainly Rajasthan, Punjab, and Haryana) were in an overexploited condition indicating the groundwater extraction exceeded the annually replenishable groundwater recharge, while 5% of blocks were in a critical stage where the groundwater extraction is between 90% and 100%. Around 14% of blocks fell under the semi-critical stage, with groundwater extraction between 70% and 90%, and 63% of the blocks had been categorized as safe, having groundwater extraction less than 70% (CGWB, 2020). The water level in India during pre-monsoon in 2018 was 5–10 m bgl (below ground level) in most parts of the country (Fig. 12.1). A few states such as Maharashtra, Odisha, Assam, and Andhra Pradesh had water level depth less than 2 m bgl in some of the locations. Most parts of Assam and some parts of Odisha, Andhra Pradesh, Uttar Pradesh, and Bihar showed a water level of 2–5 m bgl. The major western states and northwestern states such as Punjab, Haryana, Rajasthan, and Gujarat had a deeper depth to the water level of 10–40 m bgl or greater than 40 m bgl (CGWB, 2018). The groundwater level in India for pre-monsoon in 2018

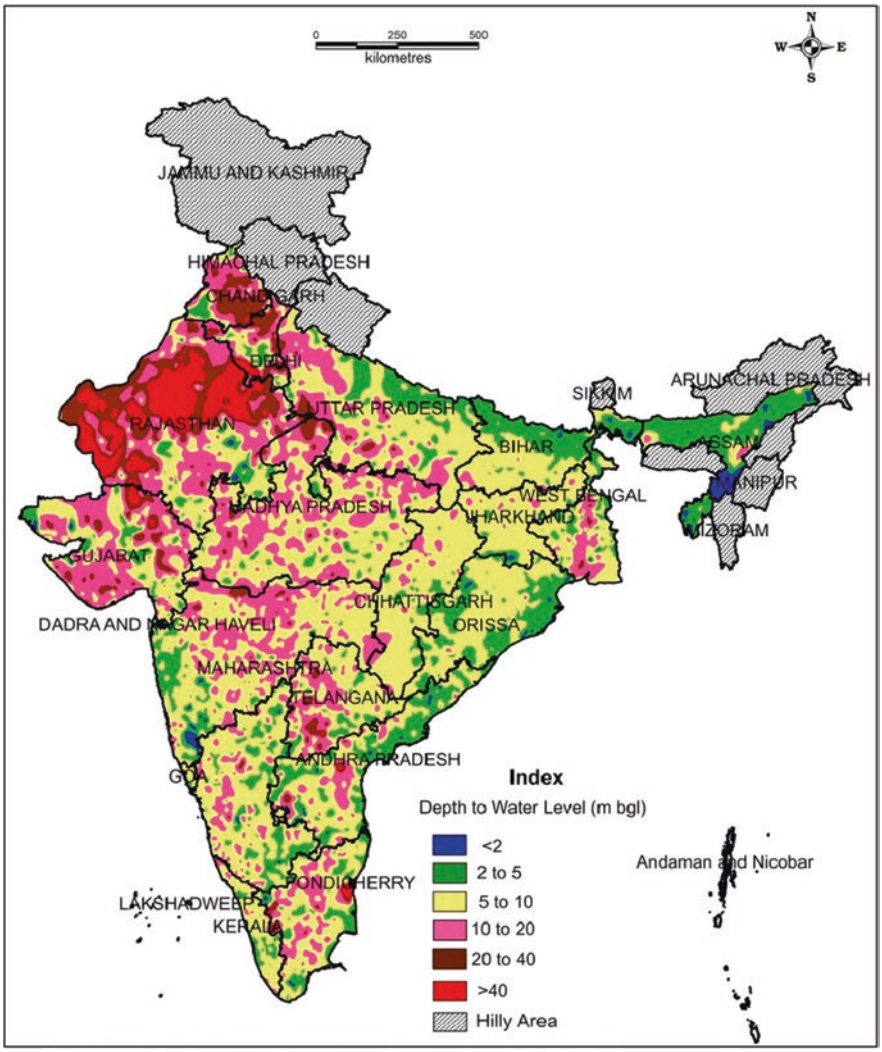

Fig. 12.1 Depth to water level map of pre-monsoon 2018

is shown in Fig. 12.2. Out of the total of 14,591 wells assessed, the majority of wells, around 5886 (41 %), had water levels in the range of 5–10 m bgl (CGWB, 2018). The fluctuations of water level during pre-monsoon in 2018 compared to pre-monsoon in 2017 have been shown in Fig. 12.3. The CGWB (2018) report revealed that water levels had both risen and fallen in the entire country. Out of 13,255 wells monitored, 6941 (52%) showed an increase in water depth, whereas 5721 (43%) showed a decrease. The water level did not change in the remaining 593 (4%) wells. Most of the wells showed fluctuation of 0–2 m. The water level rise was

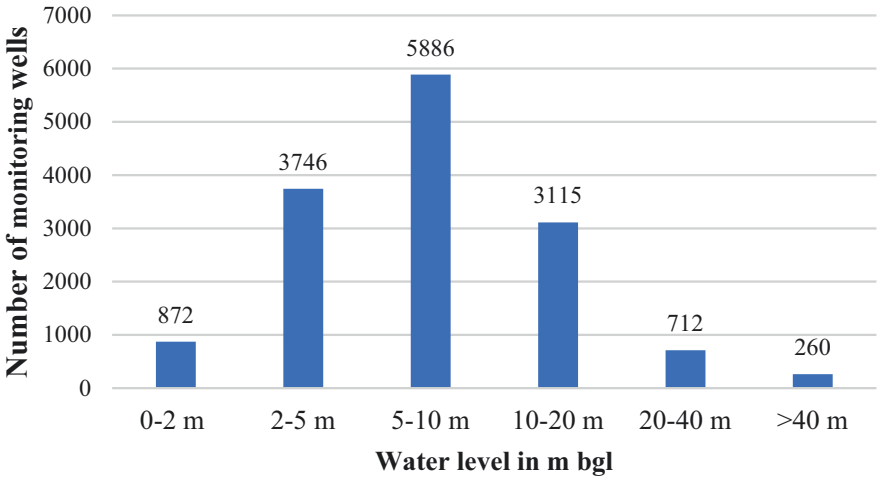

Fig. 12.2 Number of wells showing water level during pre-monsoon 2018

observed in the states of Jharkhand, Kerala, Meghalaya, Assam, Karnataka, Odisha, and parts of West Bengal, Maharashtra, and Tamil Nadu.

The fall of 0–2 m was seen in different parts of the states of Madhya Pradesh, Haryana, Bihar, Goa, Jammu and Kashmir, Chandigarh, Himachal Pradesh, Delhi, and Uttar Pradesh, while a fall of above 4 m prevailed in the states of Uttarakhand, Gujarat, Rajasthan, Chhattisgarh, Madhya Pradesh, Delhi, Goa, Gujarat, Telangana, and Madhya Pradesh. The wells showing water level depth during different periods, such as pre-monsoon, mid-monsoon, post-monsoon, and recession, have been presented in Fig. 12.4. It has been observed that once the monsoon starts, the wells are getting recharged, and more wells are coming under the range of 0–5 m bgl (Fig. 12.4). Whereas less variation in numbers has been observed in the wells having water level depth greater than 40 m bgl. The less variation in numbers of these wells may be attributed to the fact that these wells (>40 m bgl) mainly lies in the western states of India, having less rainfall, and hence these wells are not recharged from the rainfall to a great extent.

3 Groundwater Scenario in Bihar

Most of the parts of the state of Bihar have been blessed with plenty of water resources, but overexploitation and improper management of the groundwater have led to water scarcity in the state of Bihar. The administrative map of the state of Bihar is shown in Fig. 12.5.

According to the study conducted by CGWB in 2021, the water level out of the total of 209 wells monitored, 23 wells (11%) had water level of 0–2 m bgl observed in the northern part (Gopalganj, Siwan, Sitamarhi, and Muzaffarpur) and as patches

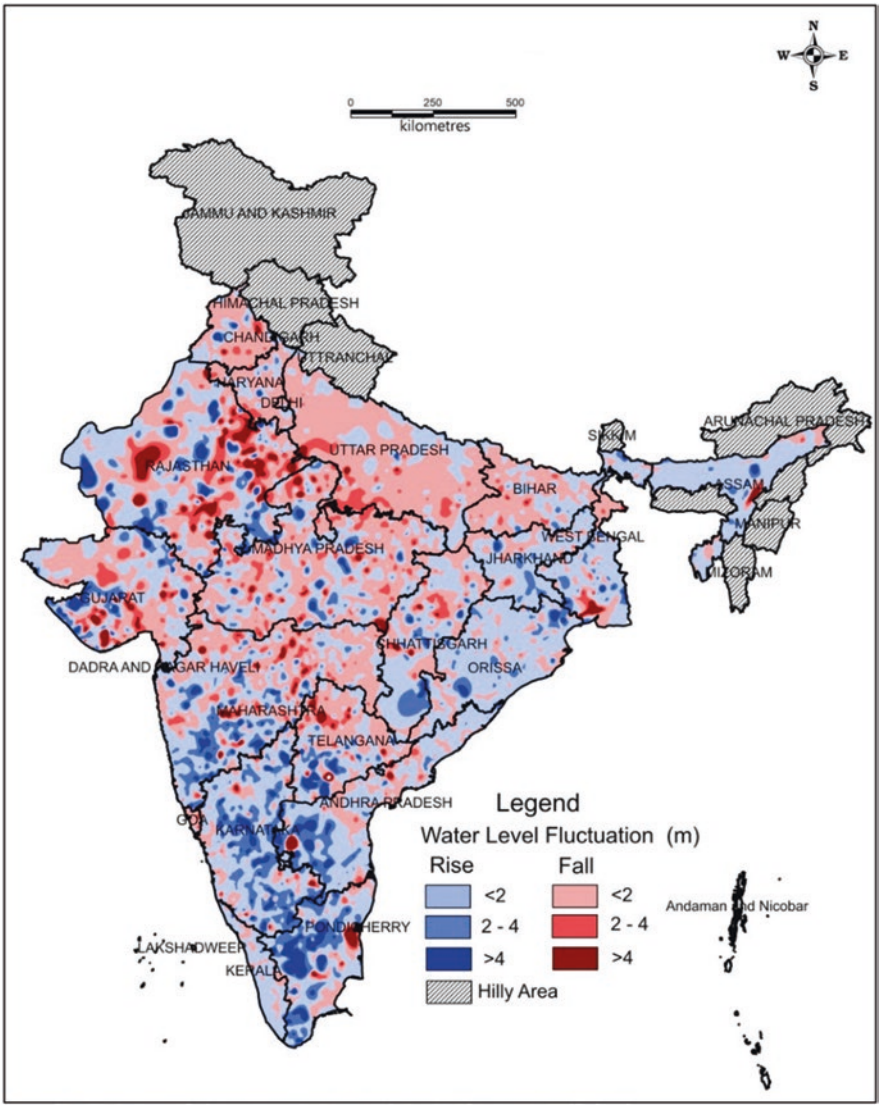

Fig. 12.3 Water level fluctuation during pre-monsoon 2017–2018

in the South Bihar Plain (SBP), while 96 wells (46%) fell in 2–5 m bgl water depth lied in the central part of Bihar (Saran, Vaishali, Arwal, Jehanabad, Gaya, Bhojpur, and Patna) and 90 wells (43%) had water level depth of 5–10 m bgl observed scattered in different districts of the state such as Bhojpur, Patna, Begusarai, Samastipur, Vaishali, Nalanda, and Nawada. During mid-monsoon (August 2020), a total of 327 wells were monitored. The water level depth during this period varied from 0.04 in Muzaffarpur to 11.00 m bgl in Nawada. The major number of wells ~86% across the

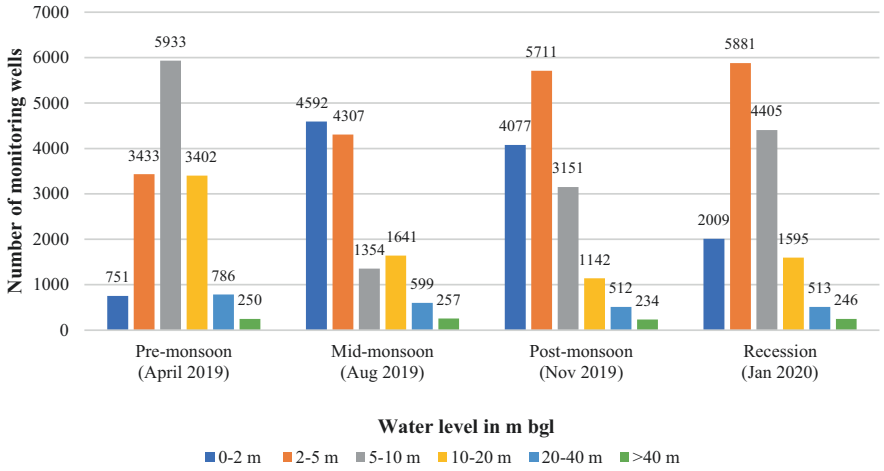

Fig. 12.4 Number of wells showing water level during different months

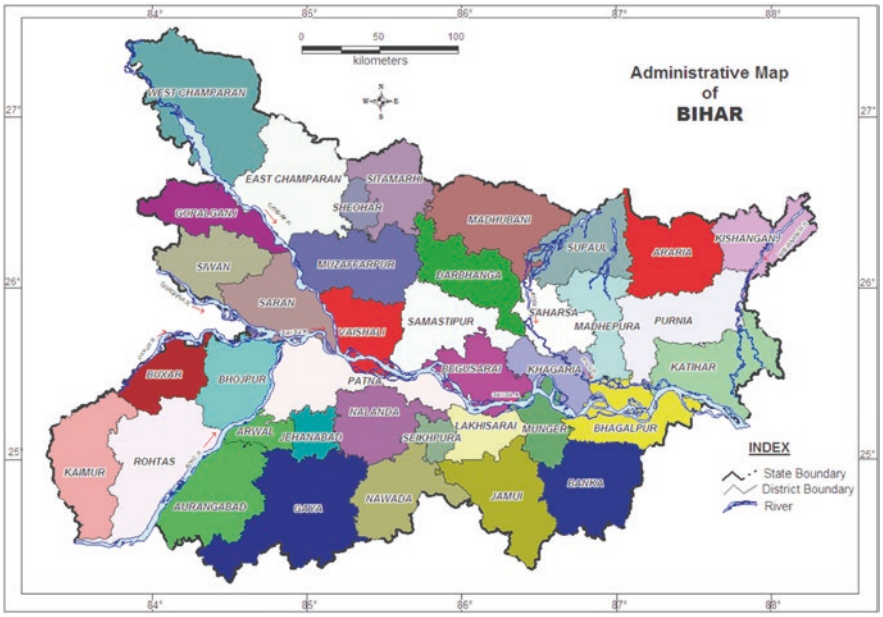

Fig. 12.5 Administrative map of Bihar state

state (except that some locations in Samastipur and Begusarai district) had water level depth ranging from 0 to 5 m bgl as the monsoon rainfall recharged the groundwater level rising the depth of water level in wells. Out of a total of 327 wells, 47 wells (13%) mostly in the Begusarai district, had a water level depth of 5–10 bgl, while water-level depth above 10 m bgl found only in 1 well located in Nawada. The

shallow water level depth of range 0–2 m bgl was in Sitamarhi, Sheohar, Darbhanga, Madhubani districts, and many localized areas, mostly in NBP. About 12% of wells observed a water level of 5–10 m bgl, covering small areas at many locations of various districts such as Kaimur, Rohtas, Jamui, and Banka lying in SBP. The water level of above10 m bgl was found in about 15 numbers of wells (3%) present in the parts of Patna, Bhagalpur, Rohtas, Kaimur, and many other places as small patches. A total of 663 wells were monitored during the recession period (January 2020). The Muzaffarpur district had a minimum water level of 0.47 m bgl, while the Rohtas district had a maximum water level of 15.8 m bgl. In most regions of the state (64%), water levels were reported to be 2–5 m bgl. The water level in m bgl for different monsoon periods has been shown in Fig. 12.6. The number of wells having a water depth of 0–2 m bgl and 2–5 m bgl was observed to be increased during mid-monsoon and post-monsoon. This increase is completely justified due to the recharging of groundwater levels from the rainfall during the monsoon period.

3.1 Seasonal Fluctuation

The seasonal fluctuation showing rise and fall of water in wells (% of wells) has been shown in Fig. 12.7. A total of 180 wells were monitored to identify the variation in water level during August 2020 compared to May 2020. Out of a total of 180 wells, 176 wells (97%) showed a rise, and 4 wells (3%) showed a fall in the water table. Also, 181 wells were monitored to compare the fluctuations in water level in November 2020 compared to May 2020. The number of wells showing a rise was 157 (87%), and the number of wells showing a fall was 24 (13%). The wells

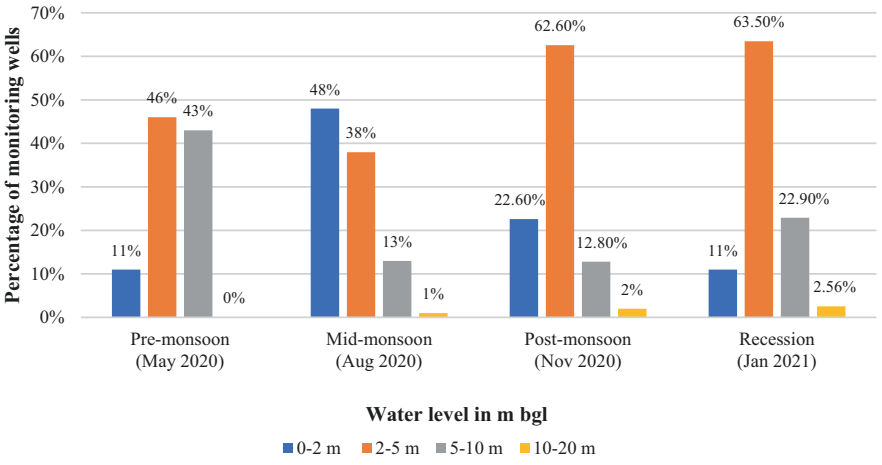

Fig. 12.6 Water level in wells during different periods in Bihar

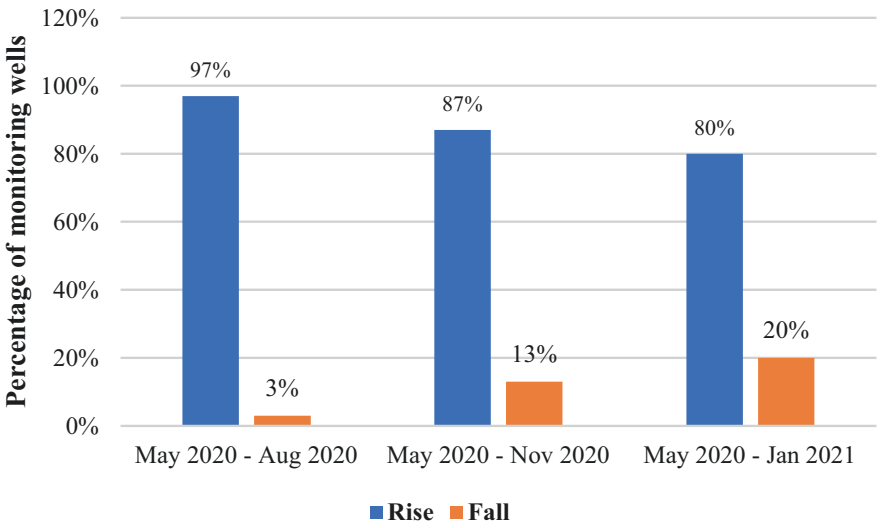

Fig. 12.7 Seasonal fluctuation in water level in Bihar state

showing falls were present in the major part of the Madhubani district and localized areas of Patna, Jehanabad, and Gopalganj districts.

Again, to compare the fluctuations in January 2021 compared to May 2020, a total of 184 wells were analyzed, and out of these, 147 wells (80%) observed a rise while 37 wells (20%) showed a fall in the water table. The falls were seen in the wells located in the Madhubani district and in patches areas of Gopalganj, Patna, Nawada, Nalanda, Bhojpur, and East Champaran districts.

3.2 Annual Fluctuation

The annual fluctuation in terms of the rise and fall of water level (% of wells) has been shown in Fig. 12.8. The monitoring wells represented a limited area of the state of Bihar during the assessment done for May 2019 to May 2020 indicated that 158 wells (91%) out of 174 wells showed a rise in the water level and covered the major part of the state while 16 wells (9%) indicated fall in the water level covering mainly parts of the Nalanda, Samastipur, Buxar and Begusarai districts. Similarly, water table variation between August 2019 and August 2020 showed that out of a total of 283 wells, 226 wells (80%) indicated a rise while 57 wells (20%) indicated a fall. The fall was observed mostly in districts located in SBP, such as Arwal, Aurangabad, and Jehanabad districts (Fig. 12.8). From November 2019 to November 2020, the wells were monitored in the entire state, and the analysis showed that out of a total of 582 wells, the number of wells indicating rise was 239 (41%) and 343 wells (59%) showed fall in the water level. Similarly, from January 2020 to January

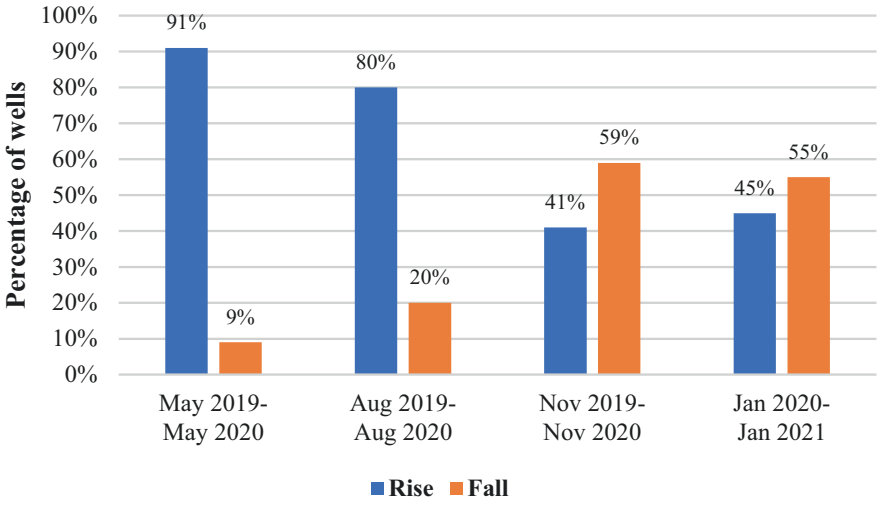

Fig. 12.8 Annual fluctuation in water level in Bihar state

2021, a total of 619 was analyzed, covering the whole state. Out of 619 wells, 277 wells (45%) indicated a rise, while 343 wells (55%) indicated a fall in the water level (Fig. 12.8).

3.3 Decadal Fluctuation

The decadal fluctuation in terms of the rise and fall of the water table (% of wells) has been shown in Fig. 12.9. The water-level fluctuation in May 2020 related to the decadal mean of May had been reported and a total of 202 wells were analyzed, covering a limited area of the state of Bihar. Out of a total of 202 wells, 175 wells (86%) showed a rise in the water level while 27 wells (14%) indicated a fall in the water level, covering mainly parts of the Samastipur, Begusarai, Nalanda, Nawada, Sitamarhi, and Bhojpur districts. Similarly, variation in water depth between August 2010 and August 2020 showed that out of a total of 320 wells, 253 wells (79%) indicated a rise while 67 wells (21%) indicated a fall mostly observed in major parts of Begusarai, and some parts of Saran, Vaishali, Bhojpur, Nalanda, Arwal, Aurangabad, Nawada, East Champaran, and Gaya district (Fig. 12.9). From November 2010 to November 2020, 626 wells were monitored in the entire state, and the analysis showed that out of a total of 626 wells, the number of wells indicating rise was 396 (63%), and 230 wells (37%) showed fall in the water level. The falls were observed mainly in the areas of East Bihar, covering various districts such as Supaul, Araria, Kishanganj, Purnea, Katihar, Banka, Jamui, Munger, and in some areas of West Champaran, East Champaran, Kaimur, Buxar, Rohtas, Arwal, and Aurangabad. Similarly, from the decadal mean of January 2011 to January 2021, a

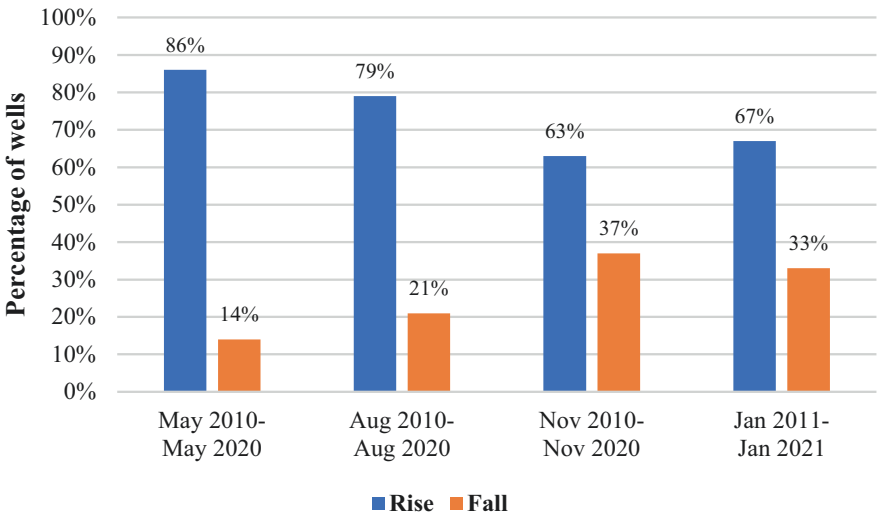

Fig. 12.9 Decadal fluctuation in water level in Bihar state

total of 627 were analyzed, covering the whole state. Out of 627 wells, 418 wells (67%) indicated a rise, while 209 wells (33%) indicated a fall in the water level (Fig. 12.9).

3.4 Groundwater Contamination

Groundwater contamination is a global challenge as everyone must have access to sufficient and affordable clean water for drinking and other purposes. The rapid population, urbanization, and industrialization resulted in severe groundwater contamination, posing a major problem all over the world. The groundwater contaminants are mainly geogenic in nature. The natural mineral deposits within the Earth's crust dissolve, resulting in contamination, but now, the release of contaminants of anthropogenic origin from industries and various other human activities has worsened the scenario. The contamination of groundwater is different from surface water contamination as it is not visible, and resource recovery is difficult at the current level of technology (Li et al., 2021). The groundwater contaminants are generally colorless and odorless, and their impact on human health is chronic (Chakraborti et al., 2015). Groundwater pollution can negatively impact human health and environment and can create social issues among citizens. The high levels of chemical constituents in drinking water, such as fluoride, metals, nitrate, etc., adversely affects the human health and leads to soil contamination. Contamination of groundwater also reduces freshwater availability, causing conflicts among citizens and leading to socio-economic crises and even wars (Li et al., 2021).

The major challenges and concerns in India are groundwater contamination from arsenic, fluorides, and nitrates. Several studies have been performed in the field of groundwater contamination from these contaminants in various parts of India (Ahamed et al., 2006; Thapa et al., 2019; Suthar et al., 2009; Chakraborti et al., 2016). Arsenic contamination affected 107 countries all over the world, having concentrations beyond the maximum limit of 10 ppb specified by WHO (Shaji et al., 2021). In terms of population, around 200 million people all over the world have been adversely affected by arsenic contamination above the specified limit of WHO (Jha & Tripathi, 2021). Asia has the highest number of reports (32), followed by Europe (31) and then Africa (20). South Asia, including India, appears to be the worst affected by arsenic groundwater contamination. Shaji et al. (2021) stated that over 50 million population in India is exposed to arsenic groundwater contamination. A total of 17 states and one union territory in India have been reported to have arsenic values beyond the limit of 50 ppb specified by BIS. About 19% of the Indian population is at risk of arsenic poisoning (Shukla et al., 2020). The shallow aquifers from 10 states in India had reported high arsenic value in groundwater (>10 ppb), while deeper aquifers greater than 100 m are free from arsenic. The worst affected states are Bihar, West Bengal, Assam, and Tripura. More than 10 million people in rural Bihar are exposed to the high level of naturally occurring arsenic, covering 46% of the geographical area (Chakraborti et al., 2016). Chakraborti et al. (2016) found that the magnitude of the arsenic contamination in the groundwater was severe in the Patna district, and around 61% of analyzed tube wells in five blocks of Patna had arsenic above 10 μg/l. The groundwater of the Bhojpur district in Bihar was also found to have arsenic concentrations higher than 50 ppb in most of the groundwater samples (Maity et al., 2020). Chronic arsenic exposure causes arsenicosis and various other adverse effects on human health, such as liver damage, cancer, and coronary heart disease. The fluoride contamination exceeding 1.5 mg/l is affecting around 260 million worldwide. Globally, citizens of around 25 nations are exposed to adverse health effects due to the high concentration of fluoride (Jha & Tripathi, 2021). Mostly, the reason for high fluoride is geogenic in nature, and fluoride content in the groundwater in India has been increasing mainly due to the excessive withdrawal of groundwater. Around 62 million people are exposed to the risk of excess fluoride contamination in India (Jha & Tripathi, 2021). The groundwater in many states (Odisha, Rajasthan, Haryana, Punjab, Gujarat, West Bengal, Bihar, Gujarat, Uttar Pradesh, and Andhra Pradesh) of India has high fluoride concentrations. The concentration of fluoride in groundwater in Rohtas district in Bihar varied from 0.10 to 2.50 mg/l, while groundwater contamination due to fluoride in Gaya district (Bihar) varied from 0.19 to 14.4 mg/l. At the same time, the fluoride value in the groundwater of Bhagalpur district (Bihar) ranged from 0.00 to 1.34 mg/l. The low concentration (0.5–1.0 ppm) is necessary as it prevents dental caries, while a high concentration of fluoride causes fluorosis, while prolonged exposure to high fluoride content of above 4 ppm causes calcification in bones resulting in the formation of osteoporosis and osteosclerosis.

Nitrate contamination in drinking water is widely spread contaminations globally (Thapa et al., 2019). The sources of nitrate contamination in the groundwater

are mainly the application of fertilizer, unlined drainage, sewerage lines, and human and animal wastes. There are various studies on nitrate contamination in groundwater performed in various parts of India, such as Thapa et al., (2019), Ahamad et al. (2018), and Ahada and Suthar (2018). The groundwater of Gharbar village in Jharkhand, India, had nitrate contamination from 34.10 to 319.10 mg/l, which is much more than the specified limit of 45 mg/l as per BIS (Thapa et al., 2019). The groundwater in Varanasi, Uttar Pradesh, India, was found to have nitrate content ranging from 40.32 to 78.97 mg/l, and around 80% of the groundwater samples exceeded the specified limit of 45 mg/l (Ahamad et al., 2018). Similarly, the groundwater nitrate concentration in the southern district of Punjab, India, varied from 38.45 to 198.05 mg/l, and over 92% of sites showed a high level of nitrates exceeding the specified limit (Ahada & Suthar, 2018). 26% of groundwater samples of Nirmal province in the South exceeded the specified limits and were found to have a significantly high nitrate concentration (Adimalla et al., 2018). The groundwater nitrate concentration in the rural areas of Rajasthan, India, also exceeded the specified limits and ranged from 7.10 to 82.0 mg/l (Suthar et al., 2009). The risk of nitrate-contaminated groundwater was also found in Anantapur District in Andhra Pradesh, India, where 65% of groundwater samples had nitrate content higher than the specified limit examined during the pre-monsoon (Reddy et al., 2009). The existing studies revealed that the problem of high nitrate content in the groundwater is prevailing in most parts of India. The high nitrate content has numerous adverse health effects such as methemoglobinemia in infants and causes gastric cancer and thyroid gland hypertrophy, respiratory trouble and multiple sclerosis in adults.

4 Study Area

The study area is Patna district, located in South Bihar alluvial plains. It is located at an elevation of 174 feet on the southern bank of Ganges'. It is surrounded by the Samastipur and Saran districts in the north, Begusarai in the east, and Bhojpur in the west, and the river Ganges separates it from the Vaishali district. The present study area lies between 25°21′45.83"N, 85°42′19.54″E, and 25°28′22.78"N 83°51′51.40″E. The climate of the district is extreme in nature, with high temperatures during summer and low temperatures during winter. The monsoon starts in June and lasts till September. The Patna district lies in the flat region, having a high presence of alluvium, making it fertile for agricultural use (Chettry & Surawar, 2021). Despite its location on the banks of the Ganges, water needs of the city are fulfilled entirely by underground aquifers (Saha et al., 2014). The water level ranged from 0.54 m bgl to 8.92 m bgl during the pre-monsoon period (May 2020) in the Patna district, while during mid-monsoon (August 2020) ranged from 0.12 m bgl to 5.03 m bgl. Similarly, the water table varied from 1.82 m bgl to a maximum of 11.47 m bgl during the post-monsoon (November 2020) and during the recession (January 2021) ranged from 0.78 m bgl to 7.99 m bgl (CGWB, 2021). The decadal

mean variation of the water table between January 2011 and January 2021 revealed a rise in the water table in 87% of wells and a decline in 13% of wells (CGWB, 2021).

5 Methodology

The physicochemical and ion-related data for groundwater samples in the Patna district have been taken from CGWB (2021). A total of 35 dug wells known as hydrograph network stations (HNS) were examined in the district. These HNSs were monitored for pre-monsoon, mid-monsoon, post-monsoon, and recession periods. The present study assessed the suitability of groundwater for drinking and irrigation purposes by comparing the physicochemical and ion concentration data of groundwater samples in the study area to the water quality parameters specified by the World Health Organization (WHO, 2004) and the Bureau of Indian Standards (BIS 2012). The groundwater samples were collected in airtight polypropylene bottles having capacity of 1 L and standard American Public Health Agency (APHA) (2017) and BIS methods were adopted to analyze the samples for basic parameters. Various parameters included in the study were pH, EC, TDS, TH, Ca^{2+}, Mg^{2+}, Na^{+}, K^{+}, HCO_3^{-}, Cl^{-}, NO_3^{-}, SO_4^{2-}, and F^{-}. Coliform and arsenic were not within the scope of study. The data published in the report (CGWB, 2021) were verified, and error balance percentage of the analyzed geochemical data of the water samples was within the range of acceptability (±5%).

6 Results and Discussion

This section evaluates and discusses the appropriateness of groundwater in the Patna district for drinking and irrigation, considering significant physicochemical characteristics such as pH, electrical conductivity (EC), total dissolved solids (TDS), and so on, as well as major ions such as Ca^{2+}, Mg^{2+}, Na^{+}, K^{+}, HCO_3^{-}, Cl^{-}, NO_3^{-}, SO_4^{2-}, and F^{-}.

6.1 Suitability for Drinking Purposes

The physicochemical characteristics and values of the major ions present in groundwater samples of different locations in the Patna district have been presented in Table 12.1. All the values are in mg/l except for the pH and EC values. The range of physicochemical parameters value in the study area is shown in Table 12.2.

Table 12.1 Physicochemical characteristics of groundwater in the study area

S.No.	Block	pH	EC (µs)	TDS	TH	Ca^{2+}	Mg^{2+}	Na^{+}	K^{+}	HCO_3^{-}	Cl^{-}	NO_3^{-}	SO_4^{2-}	F^{-}
1	Bihta	7.38	1649	1072	420	130	23	150	60	622	142	51	49	0
2	Paliganj	8.23	908	590	170	24	27	103	35.6	476	18	14	21	0.3
3	Dulhin bazar	8.29	841	547	355	80	38	30	1.49	238	89	48	45	0
4	Bikram	8.1	980	637	245	58	24	104	15.1	348	60	51	61	0.2
5	Bikram	7.5	463	301	205	24	35.2	13	0.49	234	11	1	5.2	0.112
6	Abarh	7.91	518	337	175	42	17	33	2.91	252	15	0	7.5	0.257
7	Bihta	8.05	327	213	135	26	17	10	1.58	166	9	0	3.9	0.211
8	Phulwari	7.82	578	376	215	40	27.9	22	2.07	301	25	0	6.1	0.27
9	Bakhtiyarpur	8.23	621	404	155	10	31.6	57	2.94	332	23	0	16.6	0.09
10	Bihta	8.07	654	425	170	36	19.4	40	37.12	228	48	41.3	18.1	0.17
11	Barh	8.19	946	615	220	8	48.6	94	0.09	572	8	0.2	4.6	0.78
12	Bihta	8.06	560	364	200	38	25.5	23	2.61	289	10	1.4	9.9	0.28
13	Daniyawan	7.95	515	335	190	36	24.3	20	1.19	295	4	0	3.1	0.36
14	Danapur	8.02	376	244	150	28	19.4	15	1.57	221	2	0	2.5	0.37
15	Punpun	8.0	464	302	165	32	20.7	17	1.62	271	6	0	4.3	0.16
16	Bikram	8.1	497	323	205	32	30.4	9	1.07	320	3	0	2.2	0.3
17	Dulhinbazar	8.16	398	259	160	34	18.2	12	1.02	197	9	3	4.4	0.14
18	Phulwari	7.87	839	545	300	58	37.7	43	10.21	443	26	2.7	13.6	0.38
19	Naubatpur	8.05	504	328	200	26	32.8	19	2.09	283	10	0	3.3	0.4
20	Fatuha	8.07	655	426	260	16	53.5	49	2.81	301	39	12.8	10.1	0.11
21	Danapur	7.99	664	432	255	42	36.5	22	1.95	381	13	5.4	6.8	0.3
22	Maner	7.9	729	474	250	48	31.6	36	4.75	264	80	14.7	27.8	0.3
23	Danapur	8.15	416	270	190	34	25.5	5	1.82	228	3	0	2.6	0.4
24	Patna Sadar	8.08	554	360	205	40	25.5	19	2.87	338	10	0	6.7	0.33
25	Maner	8.18	1033	671	435	52	74.1	30	8.21	480	104	5	24.5	0.43

S.No.	Block	pH	EC (µs)	TDS	TH	Ca^{2+}	Mg^{2+}	Na^{+}	K^{+}	HCO_3^{-}	Cl^{-}	NO_3^{-}	SO_4^{2-}	F^{-}
26	Maner	7.98	986	641	380	54	59.5	28	6.4	449	52	18.5	21.5	0.49
27	Mokama	8.03	736	478	265	38	41.3	48	2.66	351	41	0.2	24.3	0.25
28	Bikram	8.07	511	332	185	34	24.3	22	1.84	197	67	0	3.9	0.33
29	Patna Sadar	7.94	819	532	280	50	37.7	42	1.89	264	110	0	16.6	0.19
30	Mokama	8.18	474	308	150	28	19.4	34	2.43	221	16	0	11.3	0.48
31	Maner	8.32	401	261	175	30	24.3	13	1.86	209	15	0	4.4	0.26
32	Bikram	8.2	400	260	150	20	24.3	15	1.3	240	5	0	3.1	0.39
33	Phulwari	8.11	418	272	140	22	20.7	25	1.93	252	6	0	3.4	0.35
34	Patna City	8.06	439	285	190	22	32.8	22	2.82	240	12	0	6.6	0.14
35	Barh	8.0	509	331	200	36	26.7	20	1.74	308	9	4.5	4.9	0.5
36	Barh	7.96	538	350	194	28	30.2	23	4.4	308	0	0	0	0
37	Naubatpur	8.06	590	384	235	40	32.8	24	1.14	308	13	0	0	0

[a]All units are in mg/l except pH and EC

Table 12.2 The range of physicochemical parameters in the study area

Sl. No.	Water quality parameters[a]	WHO standards 2004		Indian standard (BIS 10500, 2012)		Range in the study area
		Most desirable limit	Max. allowable limit	Highest desirable	Max. permissible	
1	pH	6.5	8.5	6.5–8.5	6.5–9.5	7.38–8.32
2	EC (µs/cm)	1500	–	–	–	327–1649
3	TDS	500	1500	500	2000	213–1072
4	TH (as $CaCO_3$)	100	500	300	600	135–435
5	Ca^{2+}	75	200	75	200	8.0–130
6	Mg^{2+}	50	150	30	100	17.0–74.1
7	Na^{+}	–	200	–	200	5.0–150
8	K^{+}	–	12	–	–	0.09–60
9	HCO^{-}_{3}	–	–	–	–	166–622
10	Cl^{-}	200	400	200	400	0.0–142
11	F^{-}	1.00	1.5	1.00	1.5	0.0–0.78
12	NO^{-}_{3}	–	50	–	45	0.0–51.0
13	SO^{2-}_{4}	200	400	200	400	0.0–61.0

[a]All units are in mg/l except pH and EC

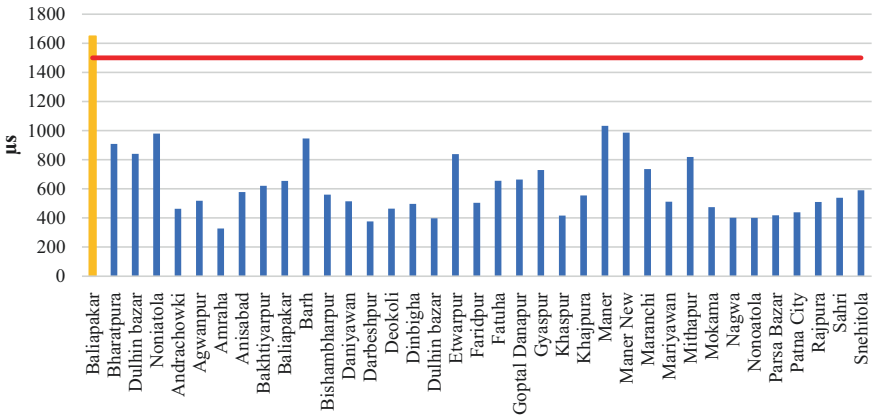

Fig. 12.10 EC values in the groundwater samples of different locations in the Patna district

pH

The quantitative measure of the basicity or acidity of an aqueous solution is called pH. The pH of drinking water must be within the standard limit of 6.5–8.5 mentioned by the WHO and BIS. The pH of groundwater samples of the study area ranged from 7.38 to 8.32, with the average value of 8.03 indicating that the groundwater was somewhat alkaline or basic in character. The alkaline nature of groundwater in the Patna district can be attributed due to the absence of any major industry in the study area.

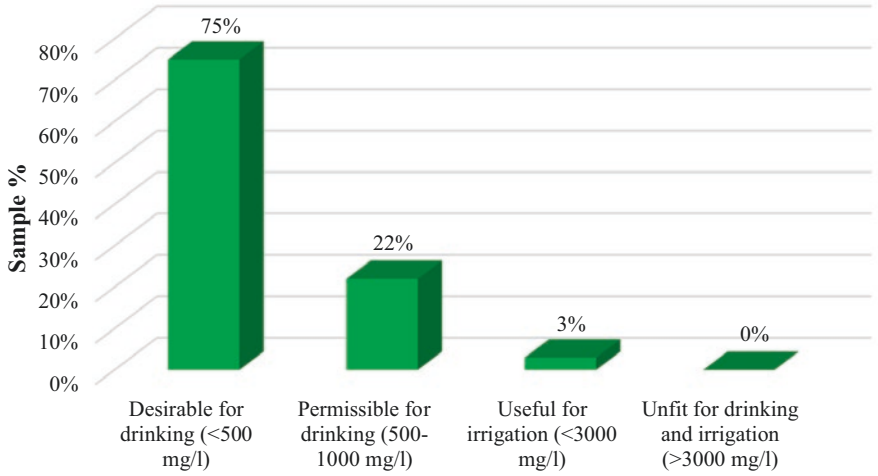

Fig. 12.11 Groundwater quality in the study area based on TDS

Electrical Conductivity

Electrical conductivity (EC) refers to the capacity of water to carry electricity. It varies directly with the variation of dissolved material in the water. According to WHO (2004), the recommended level in drinking water is 1500 μhos/cm. The EC of groundwater in the Patna district varied from 327 to 1649 μs at 25 °C, having an average of 635.40 μs. The EC values of groundwater samples of different locations are shown in Fig. 12.10. The EC was found to be within the desirable limit as mentioned by WHO (2004) in all the study area at all locations except one. The location is Baliapakar in block Paliganj of Patna district with an EC of 1649 μs. The low values of EC in the research region indicated groundwater samples with less dissolved salts. The high value of EC at one location in the study area may be due to some anthropogenic causes. The EC value less than 1500 μmhos/cm is classified as type I where enrichment of salts is low; type II, when EC is between 1500 and 3000 μmhos/cm in which the enrichment of salts is medium; and type III, when EC > 3000 μmhos/cm having high enrichments of salts. According to the aforementioned classification, 97% of groundwater samples are classified as type I, which has little salt concentration, while 3% of total groundwater samples under type II have medium salt enrichment.

Total Dissolved Solids

Total dissolved solids (TDS) in groundwater is the overall concentration of dissolved solids. TDS majorly include inorganic salts such as potassium, calcium, sodium, carbonate, and bicarbonate. According to WHO, the highest recommended TDS level is 500 mg/l, while the maximum is 1500 mg/l. As per BIS, the acceptable level is 500 mg/l, but the maximum permitted is 2000 mg/l. TDS values ranged from 213 to 1072 mg/l, having an average of 413 mg/l in the study area. Out of the total 37 locations, TDS values at 28 locations are found to be within the highest desirable

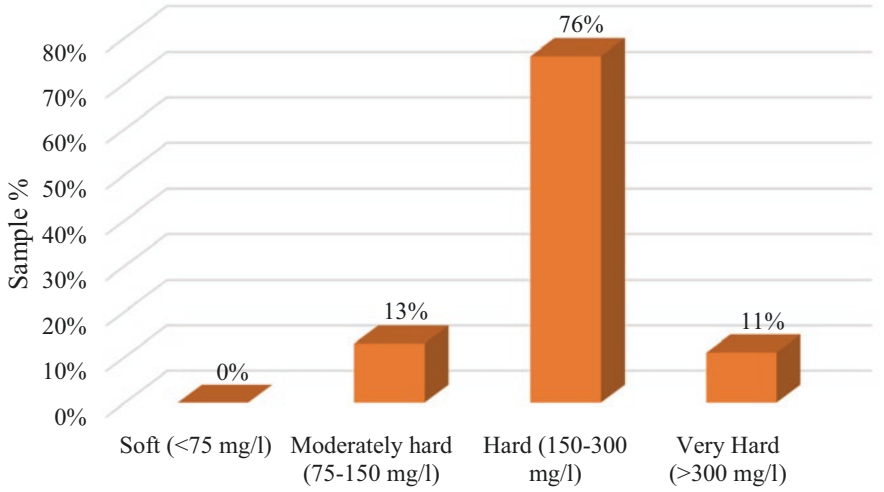

Fig. 12.12 Groundwater quality for drinking in the study area based on TH

or acceptable limit, while TDS at the remaining 9 locations falls under max allowable or permissible limit. TDS values have not exceeded the permissible limit at any of the locations in the Patna district. The reason for high TDS values at some locations may be the percolation of sewage into the groundwater or the leaching of salts from the soil. Groundwater has been classified based on TDS values by Davis and De Wiest (1966). Based on this classification, it was found that 75% of the groundwater samples (TDS < 500 mg/l) are fit for drinking, while 22% of the samples (500–1000 mg/l) are permissible for drinking (Fig. 12.11).

Total Hardness

Total hardness (TH) is the amount of dissolved magnesium and calcium in the water. The TH values varied from 135 to 435 mg/l, having an average of 221 mg/l in the Patna district. As per WHO (2004), the most desirable limit of hardness is 100 mg/l, and the maximum allowable limit is 500 mg/l, while BIS (2012) specifies 300 mg/l as the highest desirable limit and 500 mg/l as the maximum permissible limit. The hardness at all the locations of the research area was found to be greater than the most desirable limit (100 mg/l) as specified by WHO, while none of the locations had hardness values greater than the maximum allowable limit. According to BIS (2012), 4 out of a total of 37 sites had hardness levels higher than the highest recommended limit of 300 mg/l. None of the locations had hardness values greater than the maximum permissible limit. Based on TH, Sawyer and McCarthy (1967) classified groundwater. According to this classification, none of the groundwater samples was soft (TH < 75 mg/l); 13% were moderately hard (75–150 mg/l); 76% were hard (150–300 mg/l) while 11% were very hard (TH > 300 mg/l) (Fig. 12.12).

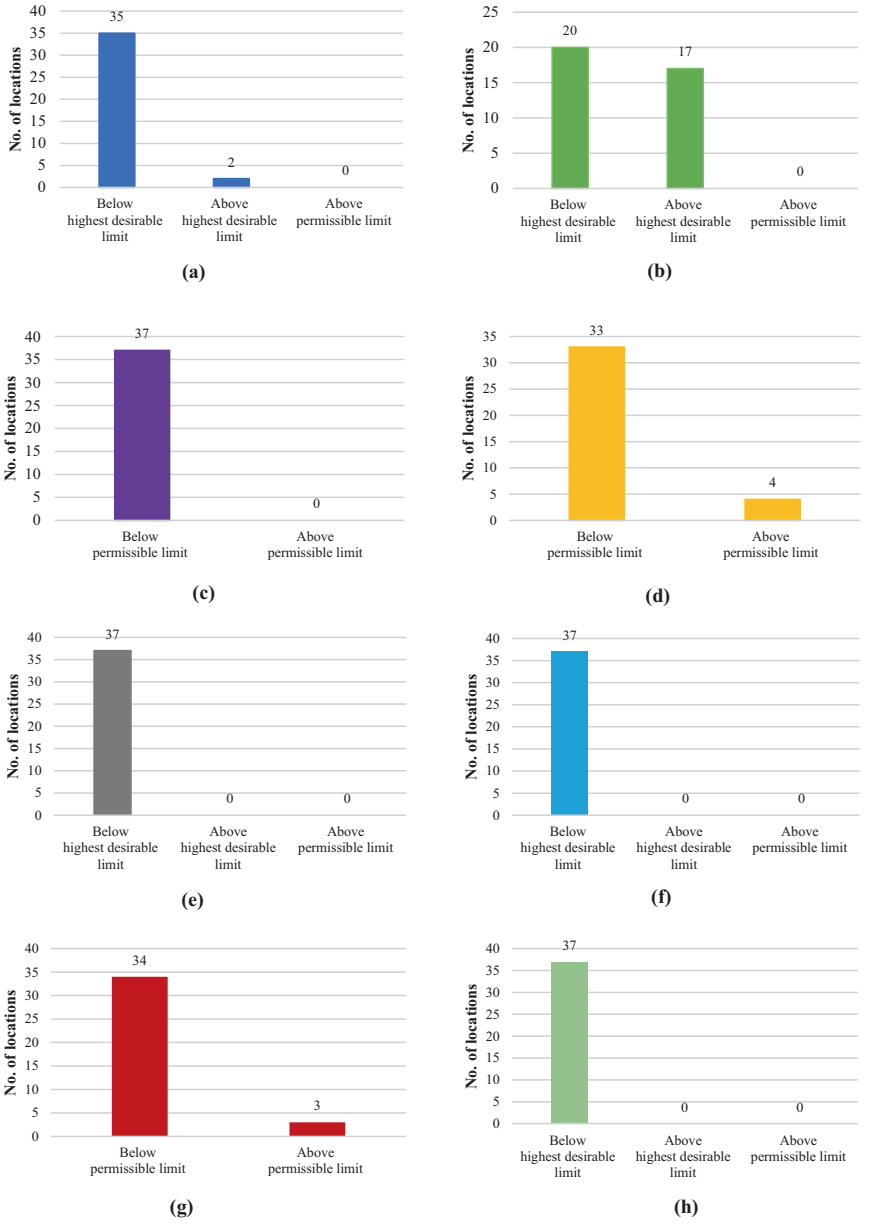

Fig. 12.13 Concentration in the groundwater of (**a**) Calcium (Ca^{2+}), (**b**) Magnesium (Mg^{2+}), (**c**) Sodium (Na^{+}), (**d**) Potassium (K^{+}), (**e**) Chloride (Cl^{-}), (**f**) Flouride (F^{-}), (**g**) Nitrate (NO_3^{-}), and (**h**) Sulfate (SO_4^{2-})

Calcium and Magnesium

The Ca and Mg are present mostly in the form of bicarbonates and to a less extent in the form of chloride and sulphate. When the groundwater comes in contact with certain rocks and minerals, these minerals get dissolved, releasing calcium and magnesium. Ca and Mg deficiency in drinking causes oncological diseases, gastrointestinal, respiratory systems, and cardiovascular diseases (Rapant et al., 2017). The Ca^{2+} concentration in groundwater samples ranged from 8 mg/l to 130 mg/l having an average 38 mg/l. As seen in Fig. 12.13a, the value of Ca^{2+} exceeded the most or highest desirable limit of 75 mg/l at two of the locations in the study area, while at the rest 35 locations, the value was within the highest desirable limit (<75 mg/l). In the study area, none of the locations exceeded the value of the maximum allowable or maximum permissible limit (>200 mg/l) of Ca^{2+}. Similarly, the value of Mg^{2+} varied from 17 mg/l to 74.1 mg/l with an average of 31 mg/l (Fig. 12.13b). Out of total 37 locations, 20 locations had Mg^{2+} value below highest desirable limit (< 30 mg/l). The value of Mg^{2+} at 17 locations (46%) in the study region surpassed the value of the highest desired limit of 30 mg/l as per BIS (2012) while at all the locations, the value of Mg^{2+} was within the maximum permitted limit of 100 mg/l as specified in BIS (2012). When compared to the most desirable limit of 50 mg/l specified by WHO, the value of Mg^{2+} exceeded at 3 locations out of a total of 37 locations in the study area.

Sodium and Potassium

Sodium is present in most groundwater and is a highly reactive alkali metal. The source of sodium in groundwater is the rocks containing sodium compounds which dissolve to release sodium in groundwater. The various health issues due to high Na-concentrated groundwater intake are hyperosmolarity, high blood pressure, oedema, and not suitable for agricultural use. The Na content of the groundwater samples in the Patna district varied from 5 mg/l to 150 mg/l. Na content in the groundwater was found to be within the limit of maximum allowable or maximum permissible limit (<200 mg/l) as specified by WHO and BIS and none of the locations had groundwater sapmles exceeding the highest permissible limit (> 200 mg/l) (Fig. 12.13c). The K content in the groundwater across the locations in the study area varied from 0.09 to 60 mg/l having an average value of 6.31 mg/l. The K content in the groundwater was found to be in low concentrations (< 10 mg/l) in most of the locations, while at 5 locations out of 37 locations, the concentration was found to be more than 10 mg/l. As per WHO, the maximum allowable limit is 12 mg/l, and the K concentration at 4 locations exceeded the above limit (>12 mg/l) (Fig. 12.13d). Whereas groundwater samples from 33 locations had K concentration below permissible limit (<12 mg/l). The high potassium content in a few locations can be attributed due to the leaching of potassium through the soil into the groundwater from the use of fertilizer containing potassium.

Bicarbonate

Bicarbonate is present in the groundwater majority due to the carbonate rocks such as limestone and dolomite. The reaction involved between carbonate rocks and carbon dioxide in the aqueous environment produces an alkaline environment. The

bicarbonate concentration varied from 166 mg/l to 622 mg/l. The oxidizing organic matter in the aquifer can be the reason for the high bicarbonate content (Saha et al., 2019).

Chloride and Fluoride

The sources of chloride in the groundwater are intrusion of saltwater, municipal and industrial effluents, weathering, leaching of sedimentary rocks and soils, etc. (Karanth, 1987). Usually, chlorides do not have adverse effects on human health, but the sodium part of table salt may lead to heart and kidney disease. The groundwater sample had chloride concentrations ranging from 0 to 142 mg/l. The chloride content across all the locations was found to be within the most desirable limit (<200 mg/l) specified by WHO and BIS (Fig. 12.13e). The source of fluoride in the groundwater is mainly geogenic in nature (Ram et al., 2021; Karunanidhi et al., 2020), resulting from the presence of added minerals such as pyroxene, and biotite, fluorite, and apatite in the rocks (granite and hornblende). These minerals release fluoride ions into groundwater during silicate weathering and dissolution processes. Industries that use fluoride minerals as raw material, such as brick and ceramics manufacture, mining, and pottery, also contribute to the occurrence of fluoride in groundwater (Yadav et al., 2019). Fluoride intake in small quantities (<0.5 mg/l) is recommended as it reduces dental caries, whereas intake of higher concentrations (>1.5 mg/l) leads to fluorosis (Jha et al., 2013). Fluoride concentrations in groundwater and various sources of water are causing severe concerns in India (Mukherjee & Singh, 2018). The high fluoride-contaminated groundwater exists in 20 states out of a total of 29 states of India (Subba Rao et al., 2020). The groundwater samples in the study region had fluoride concentrationss varying from 0 to 0.78 mg/l which is well below the maximum permissible limits of 1.5 mg/l and also below highest desirable limit (<1 mg/l) specified by the WHO and BIS (Fig. 12.13f).

Nitrate and Sulfate

The presence of nitrate in the groundwater in higher concentrations is a common and alarming problem all over the world, including in India. The various sources of nitrate contamination are leaching and oxidation of nitrogenous compounds, fixation, intensive agriculture, and unsewered sanitation. The maximum allowable limit of nitrate is 50 mg/l specified by WHO and 45 mg/l specified by BIS (Adimalla, 2020). In India, the nitrate concentration is generally higher than the specified limit in the intensively cultivable states such as Delhi, Maharashtra, Punjab, Haryana, Andhra Pradesh, West Bengal, Rajasthan, Uttar Pradesh, and Delhi (Suthar et al., 2009). The intake of groundwater containing a high concentration of nitrate above the specified limit causes several health problems such as methemoglobinemia, increases the risk of certain cancers, and impacts fetal development during pregnancy (Mathewson et al., 2020). The consumption of groundwater containing high nitrate content is also harmful to animals causing various diseases such as gastrointestinal cancer, vascular dementia, Alzheimer's disease, multiple sclerosis, absorptive, and hypertrophy of the thyroid (Suthar et al., 2009). Above 13 million people in India are drinking water having nitrate above the maximum allowed limit of 50 mg/l (Adimalla, 2020). The nitrate level in the study area's groundwater ranged

from 0 mg/l to 51 mg/l, with an average of 7.42 mg/l. The value of nitrate in groundwater is below 10 mg/l across 30 locations (81%) out of 37 locations. Whereas nitrate content at four locations was found to be higher than 40 mg/l out of which three locations had nitrate content in the groundwater above the specified maximum

Table 12.3 Na%, SAR, MH, and KR values of groundwater samples

S. No.	Block	Location	Na%	SAR	MH	KR
1	Paliganj	Baliapakar	48.99	3.2	15.03	0.98
2	Paliganj	Bharatpura	61.19	3.4	52.94	2.02
3	Dulhin bazar	Dulhin bazar	15.82	0.7	32.20	0.25
4	Bikram	Noniatola	50.14	2.9	29.27	1.27
5	Bikram	Andrachowki	12.44	0.4	59.46	0.22
6	Abarh	Agwanpur	30.06	1.1	28.81	0.56
7	Bihta	Amraha	14.84	0.4	39.53	0.23
8	Phulwari	Anisabad	19.07	0.7	41.09	0.32
9	Bakhtiyarpur	Bakhtiyarpur	45.18	2.0	75.96	1.37
10	Paliganj	Baliapakar	44.19	1.3	35.02	0.72
11	Barh	Barh	48.19	2.7	85.87	1.66
12	Bihta	Bishambharpur	21.06	0.7	40.16	0.36
13	Daniyawan	Daniyawan	19.16	0.6	40.30	0.33
14	Danapur	Darbeshpur	18.70	0.5	40.93	0.32
15	Punpun	Deokoli	19.14	0.6	39.28	0.32
16	Bikram	Dinbigha	9.43	0.3	48.72	0.14
17	Dulhinbazar	Dulhin bazar	14.58	0.4	34.87	0.23
18	Phulwari	Etwarpur	26.21	1.1	39.39	0.45
19	Naubatpur	Faridpur	18.09	0.6	55.78	0.32
20	Fatuha	Fatuha	29.75	1.3	76.98	0.71
21	Danapur	Goptal Danapur	16.53	0.6	46.50	0.28
22	Maner	Gyaspur	25.28	1.0	39.70	0.45
23	Danapur	Khaspur	6.56	0.2	42.86	0.08
24	Patna Sadar	Khajpura	18.06	0.6	38.93	0.29
25	Maner	Maner	14.79	0.6	58.76	0.24
26	Maner	Maner new	15.41	0.6	52.42	0.25
27	Mokama	Maranchi	28.94	1.3	52.08	0.61
28	Bikram	Mariyawan	21.40	0.7	41.68	0.38
29	Patna Sadar	Mithapur	25.11	1.1	42.99	0.48
30	Mokama	Mokama	33.95	1.2	40.93	0.72
31	Maner	Nagwa	15.00	0.4	44.75	0.24
32	Bikram	Nonoatola	18.55	0.5	54.85	0.34
33	Phulwari	Parsa bazar	28.92	0.9	48.48	0.59
34	Patna city	Patna city	21.36	0.7	59.85	0.40
35	Barh	Rajpura	18.61	0.6	42.58	0.32
36	Barh	Sahri	22.24	0.7	51.89	0.40
37	Naubatpur	Snehitola	18.53	0.7	45.05	0.33

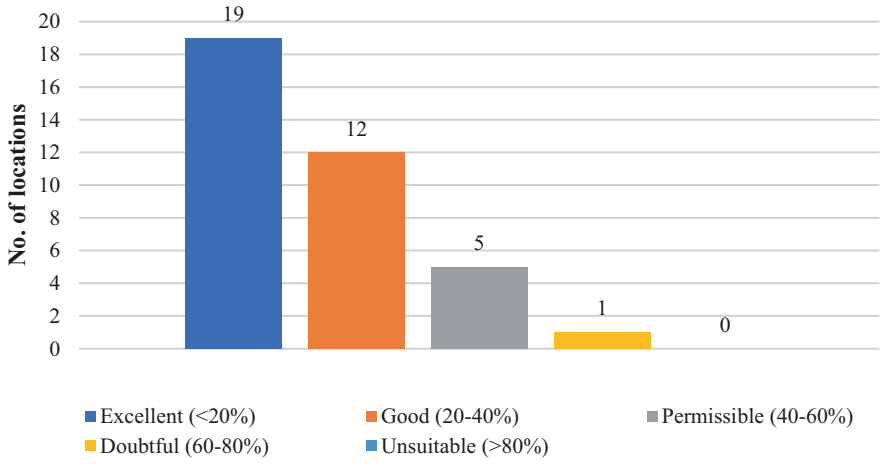

Fig. 12.14 Groundwater quality for irrigation in the study area based on sodium percentage

permitted limit (>45 mg/l) as specified by WHO and BIS (Fig. 12.13g). The nitrate concentration in the groundwater samples at 34 locations found to be below permissible limit (<45 mg/l). The sources of sulfate in the groundwater are both natural and anthropogenic. The natural sources include deposition from the atmosphere, sulfate mineral dissolution and oxidation, and sulfide mineral oxidation, while the anthropogenic sources include power plants, coal mines, power plants, metallurgical and phosphate refineries (Miao et al., 2012). The intake of sulfate higher than the specified limits causes diarrhea in humans. The recommended sulfate limit in groundwater is 200 mg/l, but the allowed maximum is 400 mg/l, as specified by WHO and BIS. Sulfate levels in groundwater in the study region varied from 0 to 61 mg/l, with an average of 12.43 mg/l. The sulfate content in groundwater did not reach the highest recommended limit (<200 mg/l) in any of the study area locations (Fig. 12.13h).

6.2 Irrigation Suitability

The groundwater suitability for irrigation purposes has been assessed based on various salinity indices such as sodium percentage (Na%), sodium absorption ratio (SAR), magnesium hazards (MH), and Kelly's ratio (KR). The calculated values of various water quality parameters to be used for irrigation of the groundwater samples in the study area are shown in Table 12.3.

Sodium Percentage (Na%)

The presence of excess sodium in groundwater combines with carbonates forming alkaline soils, while a combination of sodium with chlorine causes saline soils resulting in reduced permeability of the soil, affecting the plant or crop growth adversely. The sodium percentage was calculated using the equation below (Rao & Latha, 2019):

$$Na(\%) = \left(\frac{Na^{+} + K^{+}}{Ca^{2+} + Mg^{2+} + Na^{+} + K^{+}} \right) \times 100 \tag{12.1}$$

The water used for irrigation should have a sodium percentage of less than 60%. The sodium percentage varied from 6.56% to 61.19% (Table 12.3). The sodium percentage was within the suitable range in all the locations of the Patna district except at Paliganj block in Bharatpura. Wilcox (1955) categorized the suitability of groundwater for irrigation based on Na%. According to this classification, groundwater samples of 19 locations had excellent suitability for irrigation purposes, while groundwater samples of 12 locations were of good category for irrigation. The groundwater samples at five locations fall in the permissible category based on sodium percentage, whereas the groundwater sample of one location fall in the doubtful category. There were no groundwater samples under the not suitable category for the irrigation purpose based on sodium percentage (Fig. 12.14).

Sodium Absorption Ratio (SAR)

SAR is a measure of water quality used for irrigation because the concentration of sodium reduces soil permeability (Todd, 1959; Richards, 1954). The SAR values in the samples of groundwater in the Patna district ranged from 0.2 to 3.4, indicating that the groundwater is observed to be of an excellent category as SAR values are less than 10 and can be used for irrigation (Table 12.4).

Magnesium Hazard (MH)

The presence of magnesium and calcium ions is essential as they cause friability of soil. However, high content of magnesium and calcium increases the pH of soil causing phosphorus loss. The groundwater having MH < 50% is suitable for irrigation (Szabolcs & Darab, 1964):

$$MH = \left(Mg^{2+} \times 100 \right) / \left(Ca^{2+} + Mg^{2+} \right) \tag{12.2}$$

Table 12.4 Classification of groundwater as per SAR values

Water quality	SAR values	Number of samples
Excellent	<10	37
Good	10–18	–
Permissible	18–26	–
Doubtful	>26	–

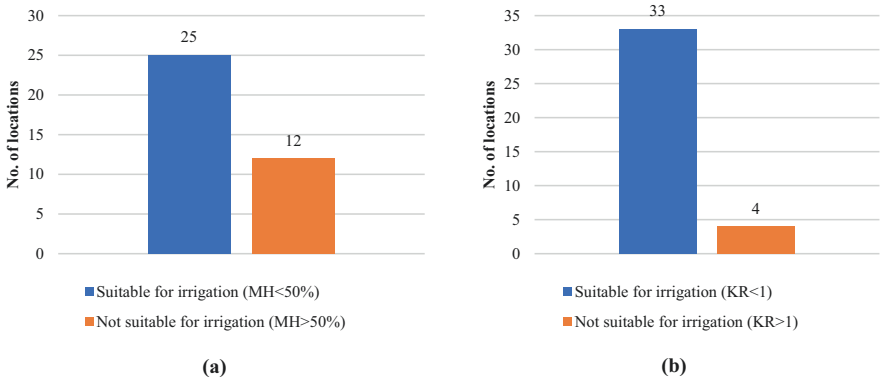

Fig. 12.15 Groundwater quality for irrigation in the study area based on (**a**) magnesium hazard values and (**b**) Kelly's ratio values

The MH values in the groundwater samples varied from 15.03 to 85.87% (Table 12.3). In the study area, the groundwater samples at 12 locations (32%) had MH values above 50% and are considered not suitable for irrigation with respect to magnesium concentration in the groundwater, as shown in Fig. 12.15a.

Kelly's Ratio (KR)

Kelly ratio value also indicates the suitability of the groundwater for irrigation purposes and is expressed as Kelley (1951):

$$KR = \left(\frac{\mathrm{Na}^{+}}{\mathrm{Ca}^{2+} + \mathrm{Mg}^{2+}} \right) \tag{12.3}$$

where the cations concentration is in mg/l.

KR values <1 indicate groundwater to be of good quality and suitable for irrigation, while KR >1 indicates groundwater is not suitable for irrigation. The KR values in the groundwater sample of the study area varied from 0.08 to 2.02. Out of the total 37 locations, 33 locations groundwater samples were suitable for irrigation as KR <1, while groundwater samples at 4 locations were not suitable for irrigation as KR >1 (Fig. 12.15b).

7 Conclusions

The groundwater in most parts of the Patna district was suitable for drinking, as most parameters were within the specified limits of WHO and BIS. The pH was found to be within range in all the locations while EC value exceeded in one location (Baliapakar in Paliganj). TDS was also within the specified limit, while TH values did not exceed the maximum allowable limit. The foremost anions and

cations such as Ca^{2+}, Na^{+}, Mg^{2+}, Cl^{-}, F^{-} and SO^{2-}_{4} were found to be within the maximum permissible limit, while K^{+} concentration exceeded the maximum allowable limit at four locations [Baliapakar (Paliganj), Bharatpura (Paliganj), Noniatola (Bikram), and Baliapakar (Paliganj)] in the study area. The concentration of NO^{-}_{3} surpassed the maximum permitted level of 45 mg/l stipulated by BIS in 3 of the 37 research locations [Baliapakar (Paligang), Dulhin Bazar, and Noniatola (Bikram)]. Although most of the above parameters were within the range, parameters such as coliform value and arsenic content are also equally important and need to be measured before declaring groundwater fit for drinking. The majority of the groundwater in the study area was acceptable for irrigation as per the presence of Na% at all the locations was within the permissible range except for one location (Bharatpura in Paliganj), the SAR values also fall in the excellent category. The KR value was more than 1 in the groundwater samples at four locations [Bharatpura (Paliganj), Barh, Bakhtiyarpur, Noniatola (Bikram)] indicating unsuitable for irrigation, whereas the study found that the MH values of the groundwater were high in a few locations. The MH values were observed to be greater than 50% at 12 locations [Barh, Fatuha, Bakhtiyarpur, Patna City, Andrachowki (Bikram), Maner, Faridpur (Naubatpur), Bikram, Palihanj, Maranchi (Mokama), Sahri (Barh)] indicating groundwater samples were not suitable for irrigation.

Acknowledgments The first author would like to acknowledge the Ministry of Education, Government of India, for providing financial assistance for part of the research work. The authors sincerely acknowledge the Central Ground Water Board (CGWB), Department of Water Resources, Government of India, for the data used in this study.

Declaration All the authors of this manuscript do not have any competing interests.

References

Adimalla, N. (2020). Spatial distribution, exposure, and potential health risk assessment from nitrate in drinking water from semi-arid region of South India. *Human and Ecological Risk Assessment, 26*(2), 310–334.

Adimalla, N., Li, P., & Qian, H. (2018). Evaluation of groundwater contamination for fluoride and nitrate in semi-arid region of Nirmal Province, South India: A special emphasis on human health risk assessment (HHRA). *Human and Ecological Risk Assessment, 25*(5), 1107–1124.

Ahada, C. P., & Suthar, S. (2018). Groundwater nitrate contamination and associated human health risk assessment in southern districts of Punjab, India. *Environmental Science and Pollution Research, 25*(25), 25336–25347.

Ahamad, A., Madhav, S., Singh, P., Pandey, J., & Khan, A. H. (2018). Assessment of groundwater quality with special emphasis on nitrate contamination in parts of Varanasi City, Uttar Pradesh, India. *Applied Water Science, 8*(4), 1–13.

Ahamed, S., Sengupta, M. K., Mukherjee, A., Hossain, M. A., Das, B., Nayak, B., & Chakraborti, D. (2006). Arsenic groundwater contamination and its health effects in the state of Uttar Pradesh (UP) in upper and middle Ganga plain, India: A severe danger. *Science of the Total Environment, 370*(2–3), 310–322.

American Public Health Agency (APHA). (2017). *Standard methods for the examination of water and wastewater* (23rd ed.). American Public Health Association.

BIS (Bureau of Indian Standard). (2012) *Indian standard drinking water specification* (pp. 1–16), second revision.

CGWB. (2018). *Groundwater scenario in India pre-monsoon 2018*. Available at: http://cgwb.gov.in/Ground-Water/AllIndiaGWReportMay2018.pdf

CGWB. (2020). *Master plan for artificial recharge to groundwater in India – 2020*. Available at: http://cgwb.gov.in/Master%20Plan%20to%20GW%20Recharge%202020.pdf

CGWB. (2021). *Ground water year book, Bihar*. Available at: http://cgwb.gov.in/Regions/MER/Reports/Ground%20Water%20Year%20Book%202021%20Bihar.pdf

Chakraborti, D., Rahman, M. M., Mukherjee, A., Alauddin, M., Hassan, M., Dutta, R. N., et al. (2015). Groundwater arsenic contamination in Bangladesh—21 years of research. *Journal of Trace Elements in Medicine and Biology, 31*, 237–248.

Chakraborti, D., Rahman, M. M., Ahamed, S., Dutta, R. N., Pati, S., & Mukherjee, S. C. (2016). Arsenic groundwater contamination and its health effects in Patna district (capital of Bihar) in the middle ganga plain, India. *Chemosphere, 152*, 520–529.

Chettry, V., & Surawar, M. (2021). Assessment of urban sprawl characteristics in Indian cities using remote sensing: Case studies of Patna, Ranchi, and Srinagar. *Environment, Development and Sustainability, 23*(8), 11913–11935.

Chindarkar, N., & Grafton, R. Q. (2019). India's depleting groundwater: When science meets policy. *Asia & the Pacific Policy Studies, 6*(1), 108–124.

Davis, S. N., & De Wiest, R. J. M. (1966). *Hydrogeology*. Wiley.

Jha, P. K., & Tripathi, P. (2021). Arsenic and fluoride contamination in groundwater: A review of global scenarios with special reference to India. *Groundwater for Sustainable Development, 13*, 100576.

Jha, S. K., Singh, R. K., Damodaran, T., Mishra, V. K., Sharma, D. K., & Rai, D. (2013). Fluoride in groundwater: Toxicological exposure and remedies. *Journal of Toxicology and Environmental Health, Part B, 16*(1), 52–66.

Karanth, K. R. (1987). *Ground water assessment: Development and management*. Tata McGraw-Hill Education.

Karunanidhi, D., Aravinthasamy, P., Subramani, T., Roy, P. D., & Srinivasamoorthy, K. (2020). Risk of fluoride-rich groundwater on human health: Remediation through managed aquifer recharge in a hard rock terrain, South India. *Natural Resources Research, 29*(4), 2369–2395.

Kelley. (1951). *Alkali soils-their information properties and reclamation*. Reinhold Publishing Corp.

Li, P., Karunanidhi, D., Subramani, T., & Srinivasamoorthy, K. (2021). Sources and consequences of groundwater contamination. *Archives of Environmental Contamination and Toxicology, 80*(1), 1–10.

Maity, S., Biswas, R., & Sarkar, A. (2020). Comparative valuation of groundwater quality parameters in Bhojpur, Bihar for arsenic risk assessment. *Chemosphere, 259*, 127398.

Mathewson, P. D., Evans, S., Byrnes, T., Joos, A., & Naidenko, O. V. (2020). Health and economic impact of nitrate pollution in drinking water: A Wisconsin case study. *Environmental Monitoring and Assessment, 192*(11), 1–18.

Miao, Z., Brusseau, M. L., Carroll, K. C., Carreón-Diazconti, C., & Johnson, B. (2012). Sulfate reduction in groundwater: Characterization and applications for remediation. *Environmental Geochemistry and Health, 34*(4), 539–550.

Mukherjee, I., & Singh, U. K. (2018). Groundwater fluoride contamination, probable release, and containment mechanisms: A review on Indian context. *Environmental Geochemistry and Health, 40*(6), 2259–2301.

Ram, A., Tiwari, S. K., Pandey, H. K., Chaurasia, A. K., Singh, S., & Singh, Y. V. (2021). Groundwater quality assessment using water quality index (WQI) under GIS framework. *Applied Water Science, 11*(2), 1–20.

Rao, K. N., & Latha, P. S. (2019). Groundwater quality assessment using water quality index with a special focus on vulnerable tribal region of Eastern Ghats hard rock terrain, Southern India. *Arabian Journal of Geosciences, 12*(8), 1–16.

Rapant, S., Cvečková, V., Fajčíková, K., Sedláková, D., & Stehlíková, B. (2017). Impact of calcium and magnesium in groundwater and drinking water on the health of inhabitants of the Slovak Republic. *International Journal of Environmental Research and Public Health, 14*(3), 278.

Reddy, A. G. S., Niranjan Kumar, K., Subba Rao, D., & Sambashiva Rao, S. (2009). Assessment of nitrate contamination due to groundwater pollution in north eastern part of Anantapur District, AP India. *Environmental Monitoring and Assessment, 148*(1), 463–476.

Richards, L. A. (1954). *Diagnosis and improvement of saline and alkaline soils* (p. 60). U.S Department of Agriculture Hand Book.

Saha, D., Dwivedi, S. N., & Singh, R. K. (2014). Aquifer system response to intensive pumping in urban areas of the Gangetic plains, India: The case study of Patna. *Environmental Earth Sciences, 71*(4), 1721–1735.

Saha, S., Reza, A. S., & Roy, M. K. (2019). Hydrochemical evaluation of groundwater quality of the Tista floodplain, Rangpur, Bangladesh. *Applied Water Science, 9*(8), 1–12.

Sarath Prasanth, S. V., Magesh, N. S., Jitheshlal, K. V., Chandrasekar, N., & Gangadhar, K. (2012). Evaluation of groundwater quality and its suitability for drinking and agricultural use in the coastal stretch of Alappuzha District, Kerala, India. *Applied Water Science, 2*(3), 165–175.

Sawyer, G. N., & McCarthy, D. L. (1967). *Chemistry of sanitary engineers* (2nd ed., p. 518). Mc Graw Hill.

Shaji, E., Santosh, M., Sarath, K. V., Prakash, P., Deepchand, V., & Divya, B. V. (2021). Arsenic contamination of groundwater: A global synopsis with focus on the Indian peninsula. *Geoscience Frontiers, 12*(3), 101079.

Shukla, A., Awasthi, S., Chauhan, R., & Srivastava, S. (2020). The status of arsenic contamination in India. In S. Srivastava (Ed.), *Arsenic in drinking water and food* (pp. 1–12). Springer.

Subba Rao, N., Ravindra, B., & Wu, J. (2020). Geochemical and health risk evaluation of fluoride rich groundwater in Sattenapalle region, Guntur district, Andhra Pradesh, India. *Human and Ecological Risk Assessment: An International Journal, 26*(9), 2316–2348.

Suthar, S., Bishnoi, P., Singh, S., Mutiyar, P. K., Nema, A. K., & Patil, N. S. (2009). Nitrate contamination in groundwater of some rural areas of Rajasthan, India. *Journal of Hazardous Materials, 171*(1–3), 189–199.

Szabolcs, I., & Darab, C. (1964). The influence of irrigation water of high sodium carbonate content of soil. *Proceedings of 8th International Congress Issue Transactions, 2*, 803–812.

Thapa, R., Gupta, S., Kaur, H., & Baski, R. (2019). Assessment of groundwater quality scenario in respect of fluoride and nitrate contamination in and around Gharbar village, Jharkhand, India. *HydroResearch, 2*, 60–68.

Todd, D. K. (1959). *Groundwater hydrology* (p. 535). Wiley.

Vignesh, K. S., Thambidurai, P., & Selvan, V. N. (2021). Geospatial assessment of groundwater potential zone in Chennai region, Tamil Nadu, India. In P. P. Adhikary et al. (Eds.), *Geostatistics and geospatial technologies for groundwater resources in India* (pp. 167–191). Springer.

WHO. (2004). *Guidelines for drinking water quality*. World Health Organisation.

Wilcox, L. V. (1955). *Classification and use of irrigation waters*. USD Circular No. 969, p. 19.

Yadav, K. K., Kumar, V., Gupta, N., Kumar, S., Rezania, S., & Singh, N. (2019). Human health risk assessment: Study of a population exposed to fluoride through groundwater of Agra city, India. *Regulatory Toxicology and Pharmacology, 106*, 68–80.

Chapter 13
Groundwater Potential Assessment Using GIS-Based Weighted Linear Combination Technique: A Case Study of Hard Rock Terrain Around Bhopal, India

Prafull Singh

Abstract The objective is to find out groundwater potential zone (GWPZ) in hard rock terrain, and no such work on an integrated approach has been reported in the area for groundwater management. In the primary phase, the relevant, effective thematic layers important for assessing water resources were generated in the GIS platform, such as lithology, hydrogeomorphology, land use/land cover, drainage density, and slope. An integrated knowledge-based weighted linear combination (WLC) method was applied for the assessment of groundwater potential. In last, integrated groundwater prospect was evaluated and grouped as very good, good, moderate, and poor. The very good GWPZ comes along the major river courses having good thickness with 50–600 liter per minute (lpm) yielding capacity. The second aquifer formations were weathered, jointed, and fractured basalt under unconfined conditions, which made the major aquifer an upper level. Sandstone under the jointed and fractured conditions in the low-lying areas made the surface water storage and the very shallow aquifer formation with yield capacity limited to 10–50 lpm.

Keywords Groundwater potential · GWPZ · Hard rock · Weighted linear combination · GIS

P. Singh (✉)
Department of Geology, Central University of South Bihar (CUSB), Gaya, India
e-mail: prafullsingh@cusb.ac.in

P. Thambidurai, A. K. Dikshit (eds.), *Impacts of Urbanization on Hydrological Systems in India*, https://doi.org/10.1007/978-3-031-21618-3_13

1 Introduction

The rapid growth in urban population and overexploitation of precious groundwater reservoirs, climate change, and day-to-day reduction of the natural groundwater recharge are serious issues in the present century (Murray, 2013). The proper groundwater recharge and large-scale aquifer mapping using advanced field technology, space-borne technology, capacity building, and people participation are only the options for management and sustainable development of groundwater resources, especially in the hard rock formation and fast rate of groundwater-level fluctuations (Singh et al., 2013a). The dynamics of groundwater occurrence and movements are very complex, and a systematic approach is necessary to adopt for the collection of field data and their processing in an integrated manner to understand groundwater availability (Jha et al., 2007; Jasmin & Mallikarjuna, 2011; Vignesh et al., 2019; Verma et al., 2020a, b; Chaudhuri et al., 2021). Space-based earth observation technology with better spatial and temporal resolution availability makes it a very promising tool for primary level landscape evaluation and further integration of large data sets in GIS environment to develop the groundwater prospect for sustainable groundwater recharge (Krishnamurthy et al., 1996; Saraf & Choudhury, 1998; Singh et al. 2013a, b). Remote sensing and GIS techniques have been used for groundwater exploration and development of groundwater recharge for a long time (Brunner et al., 2007; Leblanc et al., 2007; Sawaya et al., 2003). Besides these are Jaiswal et al. (2003), Prasad et al. (2008), Rokade et al. (2007), and Saraf et al. (2004).

Remote sensing data provide very cost-effective and fast information about groundwater-controlling factors that directly or indirectly control the occurrence and movement of groundwater, such as geology, geomorphology, structure/lineaments, land use/land cover, soil types, topography/slope, drainage patterns, etc. (Boutt et al., 2001; Chenini et al., 2010; Singh et al., 2013b). Most of the research on groundwater based on remote sensing and GIS-based analysis for the groundwater potential prediction was based study of groundwater controlling factors mapping and their reclassification using statistical and machine learning approaches under GIS and other software. Researchers have widely applied the knowledge-driven approach for groundwater recourse assessment coupled with remote sensing and GIS techniques (Madrucci et al., 2008; Avtar et al., 2010; Lee et al., 2012; Manap et al., 2013). The present study was carried out for the Bhopal region, the capital city of Madhya Pradesh, India. Any agency does not cover the groundwater development in the area except for some regional-level surveys from the state and central groundwater department of the district. With the growing demand for groundwater, rapid urbanization, increasing population, rapid industrialization, and economic development in the area, it is necessary to predict the groundwater potential of the area. The objective of the present work is to assess the groundwater conditions of the area by developing various important surface hydrological layers from the remotely sensed satellite images and the utility of a GIS-based modeling approach for predicting groundwater potential zones in the Bhopal area. The specific

objective of the paper is to explore the important groundwater storage and movement controlling factors such as geology, geomorphology, land use/land cover, slope and drainage density of the area from IRS satellite images, Aster DEM, and other available supporting maps, reports, and survey of the area. The developed groundwater contributing parameters are analyzed through filed data and expert opinions before the assignment of ranking and weighted under the GIS environment.

2 Study Area and Geological and Hydrogeological Setting

The present study area covers the major part of Bhopal City and its surrounding landscape as Bhopal is the capital city of Madhya Pradesh in central India and is globally known for its large number of lakes and natural water bodies. The city forms a part of the Malwa plateau and has a very varying topographical landscape under the geographic latitudes 23° 5′–23° 25′N and longitudes 77° 15′–77° 35′E (Fig. 13.1). The normal average annual rainfall of the city is about 1260.2 mm. The southern part of the city receives more rainfall than the northern part of the city. The maximum rainfall takes place during the month of July. Bhopal is characterized by a hot summer, and the daily mean normal temperature in May is about 40.7 °C, and the minimum is 26.4 °C. The winter commences in the middle of November and lasts till the end of February. The summer season stretches from March to the first week of June, and May is the hottest month. Black cotton soil covers the major part of the area, whereas the central part of Bhopal occupies Vindhyan sand with laterite

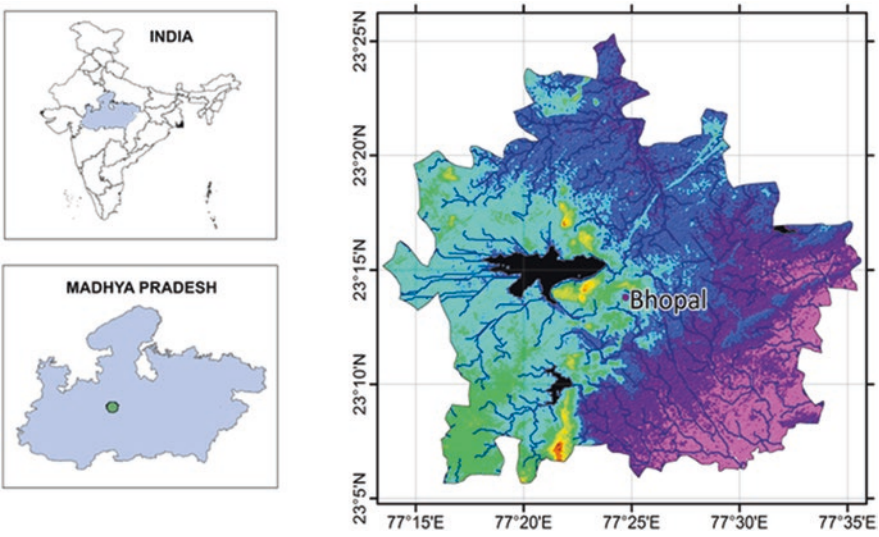

Fig. 13.1 Location map of the study area

and kankar. The majority of land in the area is drained by river Betwa downstream and its contributing tributaries.

In the study area, Deccan traps are sporadically distributed mainly in the form of linear patches. On the satellite image, this rock type is seen with distinct gray color with a rough texture. The derivatives of Deccan trap rock are the black soils, which are seen on the satellite image as a dark grey tone with a smooth texture. Hydrogeological analysis of the Deccan basalt requires a detailed study of the physical characteristics of the sequences of Deccan basalt lavas, particularly the nature and arrangement of openings through which groundwater moves. Hydrogeologically, basaltic rocks have been considered low-permeability rocks, but the main source of groundwater in the basaltic rock is its high degree of inhomogeneity. The groundwater accumulation and movement within basaltic lava flows are controlled by the nature and the degree of secondary openings, which include vertical and horizontal joints, contacts between lava flows and individual units (Kulkarni et al., 2000; Limaye, 2010; Singh & Singh, 2012; Rai et al., 2013). The hydrogeological framework of the area around Bhopal city is characterized by its undulating topography with hills formed by Vindhyan formations and valleys occupied by alluvium and basalts. The Vindhyan sandstones occur with the intercalation of shale and conglomerates at deeper depths. The weathered basalt overlying the Vindhyans is reported to be thin, shallow, and poor in groundwater potential. The potential groundwater potential is trapped in shallow depth in confined situations in weathered formations. The outmost prospect of groundwater confined in alluvium, weathered, jointed, and fractured Deccan traps make the good aquifer, where the thickness of weathered and vesicular basalt is present. A thick layer of clay was also observed in the topographically low-lying valley fill area, and the aquifer was made under confined conditions.

3 Data Used and Methodology

3.1 Development of Thematic Layers and Weightage Criteria

Assessment and management of groundwater or any other natural resource evaluation require multisource data, including satellite data, field hydrogeological information, lithology, and bore well yield, to establish the suitable methodology to achieve the best possible site for groundwater recharge and potential targeting (Table 13.1). It is very important to apply image classification and enhancement to extract meaningful information from satellite-based data sets. There is an established protocol for extracting and mapping information related to groundwater. Lithological, hydrogeomorphological, and LULC were prepared from the satellite data by applying image processing techniques such as contrast enhancement, principle component analysis, and nonlinear edge enhancement. These techniques have been applied to enhance lithological boundaries and variations in landforms based on their spectral variation and spatial arrangement. A geological map has been prepared mainly by refining the boundaries

Table 13.1 Data sets used in the present work

Type of data/software	Details of data	Sources
Survey of India, Toposheets	Toposheet Nos. Scale: 1:50,000	Survey of India (SOI), Dehradun, India
IRS LISS - III satellite data	Raw/path/57/97, year 2010	NRSC, Hyderabad
ASTER DEM	30 m spatial resolution	http://www.gdem.aster.ersdac

of the various lithological units, as shown in the published geological map of GSI, using image characteristics of tone and textural variations in remote sensing data. Extensive field verification was also conducted to check the results based on the report and previous studies in the area, and pre- and postediting were performed before the finalization of maps. The hydrogeomorphological map is prepared based on the satellite image characteristic and associated land use activities within the geomorphic units. The hydrogeomorphic map is validated through the field survey using the topographic information and drainage pattern. The depositional environment was also considered during the finalization of the units. The LULC map is prepared based on the satellite image characteristics by applying the standard supervised image classification techniques, and classes were assigned as per their water requirement. The six major categories of LULC classes were mapped in the area and validated through the field survey using the OREGON-550 GPS receiver before the finalization of the LULC map. The drainage density map was created from the drainage map created by Survey of India (SOI) topo sheets and updated from ASTER DEM using the standard techniques in Arc GIS software. Finally, the drainage density (D_d) was created by applying the method proposed by Haan (2002):

$$D_d = \frac{\sum_{i=1}^{n} SL_i}{A} \tag{13.1}$$

where D_d = drainage density (km^2), SL_i = cumulative length of ith stream (km), A = area (km^2), and n = total number of streams present within the area "A."

Slope map of the area created by ASTER raster digital elevation model (DEM) in a grid where each cell is a value referenced to a common datum. Dedicated software packages are required to extract elevation from satellite images, but most GIS packages have routines for point or contour line interpolation. Any two points on the grid will be sufficient to ascertain a slope. Once the slopes have been calculated, then the maximum difference can be found, and the gradient can be determined.

3.2 Ranking Criteria of Hydrological Parameters

The dynamic of groundwater availability and its distribution is very complex and controlled by a number of hydrogeological variables such as geology, geomorphology, tectonic setup, soil type and its texture, amount and duration of rainfall, drainage

pattern and its density, local and regional topographical features, land use pattern and its water requirement, and historical water-level data (Singh et al. 2013a, b; Jaiswal et al., 2003). The demarcation of potential groundwater exploration sites and selecting areas for further groundwater development in hard rock areas required detailed surface and subsurface investigation. The availability of required data sets and equipment is a major concern in hydrological research. The present case study of Bhopal, which is known as a city of lakes and one of the major cities of Central India, comprises hard rock terrain and faces an acute water crisis. The water distribution system of the city depends on the surface water resources, and a very small amount of water is explored from groundwater resources (Singh et al., 2016). Present work discusses the major five controlling factors such as lithology, hydrogeomorphology, land use, slope, and drainage density were mapped using remote sensing and GIS techniques to assess the groundwater potential in the area and their weightages (Table 13.2). Lithologically, the area is grouped into various classes, i.e., alluvium along the river course, basalt weathered and fractured, and sandstone. Alluvium consists of loose sand, silt, and clay and has been given the highest preference among the geological units. Weathered and fractured basalt is given as a moderate to good zone, and sandstone is given as poor weightage. The geomorphology plays a major role in the groundwater reservoir and its distribution of groundwater, and the major hydrogeomorphological units identified are pediplains, Structural sills, pediment, and denudational hills. Among all the hydrogeomorphological features, the peneplain and structural hills are given high

Table 13.2 Weights and score assigned to themes and their groundwater prospect

Theme	Weight	Class	Score	Groundwater prospect
Geomorphology	5	Waterbody	9	Very good
		Pediplains	8	Good
		Structural hills	6	Good
		Pediment	7	Moderate
		Denudational hills	4	Poor
Lithology	4	Alluvium	9	Very good
		Basalt	6	Good
		Sandstone	4	Moderate to poor
Land use/land cover	3	Agriculture	9	Very good
		Forest	7	Good
		Wasteland	5	Moderate
		Built-up land	4	Moderate to poor
		Water body	2	Moderate to poor
Slope	2	< 3	6	Very good
		3–8	4	Good
		8–15	3	Moderate
		15–30	2	Poor
		> 30	1	Very poor
Drainage density	1	Low	7	Good
		Medium	5	Moderate
		High	2	Poor

preference over the pediments and denudational hills. Land use is also an important hydrological unit showing direct or indirect prospects of water resources. The major categories of LULC are water body, agriculture, wasteland, and built-up land. Among the identified land use, agriculture and forest are considered an excellent class for groundwater management and development. The highest preference was given, and water bodies and the urban area have poor groundwater potential. Drainage density is an important surface indicator for understanding the subsurface formations and their permeability characteristics based on the density it considers for groundwater potential. The topographical setup is considered an important indicator for surface runoff and recharge and general slope of the area comes between 3% and more than 30%.

3.3 Methodology for Groundwater Potential Mapping

Groundwater potential mapping has been carried out by a number of researchers for groundwater resource prediction in diversified geological and hydrological terrains through the use of GIS-based modeling approaches (Dar et al., 2011). Most of the studies discussed by researchers are based on the parameters which are derived from different sources such as satellite data, field survey data, hydrometrological data sets, hydrological soil data, and geophysical data (Solomon & Quiel, 2006; Prasad et al., 2008; Singh et al., 2011a). Groundwater modeling, including recharge, potential, and estimation of runoff through the satellite data and GIS techniques coupled with weighted linear combination (WLC) has been carried out (Madrucci et al., 2008; Pradhan, 2009; Agarwal et al., 2013; Manap et al., 2013; Samy & Mohamed, 2014) and weighted aggregation method (Prasad et al., 2008; Chowdhury et al., 2009; Pradhan, 2009).

In the present paper, a numerical modeling approach has been utilized for the final integration of different thematic layers and assessment of groundwater potential. The experts' weights were provided to different themes and their classes based on the investigator finding in the area and his experience in the assessment of conditioning factors for developing the recharge and yielding potential. The final integrated model in the present study was developed by considering extensive review literature of published work on integration and modeling of groundwater potential using the multicriteria decision-making (MCDM) technique. The importance of value, field knowledge, and hydrological characteristics were used to assign the importance of each layer. All thematic layers and their corresponding class were assigned a knowledge base ranging from 1 to 9 depending on their suitability to store groundwater and their movement. The maximum/minimum importance was given based on the groundwater potential prospect (Table 13.2). The suitability can be calculated as:

$$S = \sum W_i X_i \tag{13.2}$$

where S is suitability, Wi is the weight of factor i, and Xi is the criterion score of factor i.

4 Result and Discussion

Groundwater availability in different geological formations controlled by lithological fabrics and aquifer characteristics. In literature, a number of methods and techniques are applied to ascertain groundwater resources and show variations in results; however, they use the same techniques and data (Al Saud, 2010; Singh et al., 2011a). The hydrogeomorphological setup represents an important surface indication of the landform characteristics and subsurface formation. Geomorphological mapping supports understanding the deposition processes, lithology/structure, and various geological controls. Overall hydrogeomorphological interpretation has been carried out from the satellite data along with detailed field surveys and available hydrogeological data. The specific characteristic of each of the units is classified in terms of the shape, size, and thickness of the overburdened material, underlying rock type, permeability, and porosity. The major hydrogeomorphic landforms demarcated are peneplain, water body, denudation hill, structural hill, and pediments (Fig. 13.2). On the basis of various characteristic features such as thickness and type of weathered material and spatial distribution coupled with pediplain, shallow-weathered pediplain and moderate-weathered pediplain are considered as a promising zone for groundwater recharge and potential. Moderate-weathered pediplains are mainly observed in southeastern and southwestern portions of the study area with moderate to deep thickness and are characterized as good zone for groundwater exploration. Denudational hills and pediments are characterized by highly sloping topography and high surface runoff; therefore, they are categorized as "poor." Structural hills like linear ridges are the linear surface exposure characterized by hard rocks of Vindhyan sandstone and act as run-off zone and hence are categorized as "poor." In the study area, Deccan traps are sporadically distributed mainly in the form of linear patches. On the satellite image, this rock type is seen with distinct grey color with a rough texture.

Alluvium deposits are also spotted in small amounts along river courses, which are associated with different grades of clay, silt, sand, gravel, and pebbles. The sandy graveling formations are categorized as a very good formation for groundwater development. The Deccan trap basalt covers the major part of the study area; the possibility of groundwater is limited to weathered, vesicular flow contacts, jointed fractured zones, etc. The groundwater occurs mainly under phreatic conditions and generally confined conditions. The red bole horizon generally acts as semi-confining and confining layers in the deep aquifers. A small portion of Vindhyan formations is found in the study area with Denudational and ridge-like structural hills comprising sandstones, shale, and quartzite. The Vindhyans are, in general, poor aquifers; however, these formations, when subjected to weathering or jointing and fracturing, gives rise to moderate potential for groundwater prospect (Fig. 13.3). The land use pattern and type of practices performed on land and consider as an important influencing factor for groundwater development and management which affect the groundwater recharge and runoff. However, a number of parameters are responsible for groundwater depletion. Still, the major causes are vegetation type, soil type,

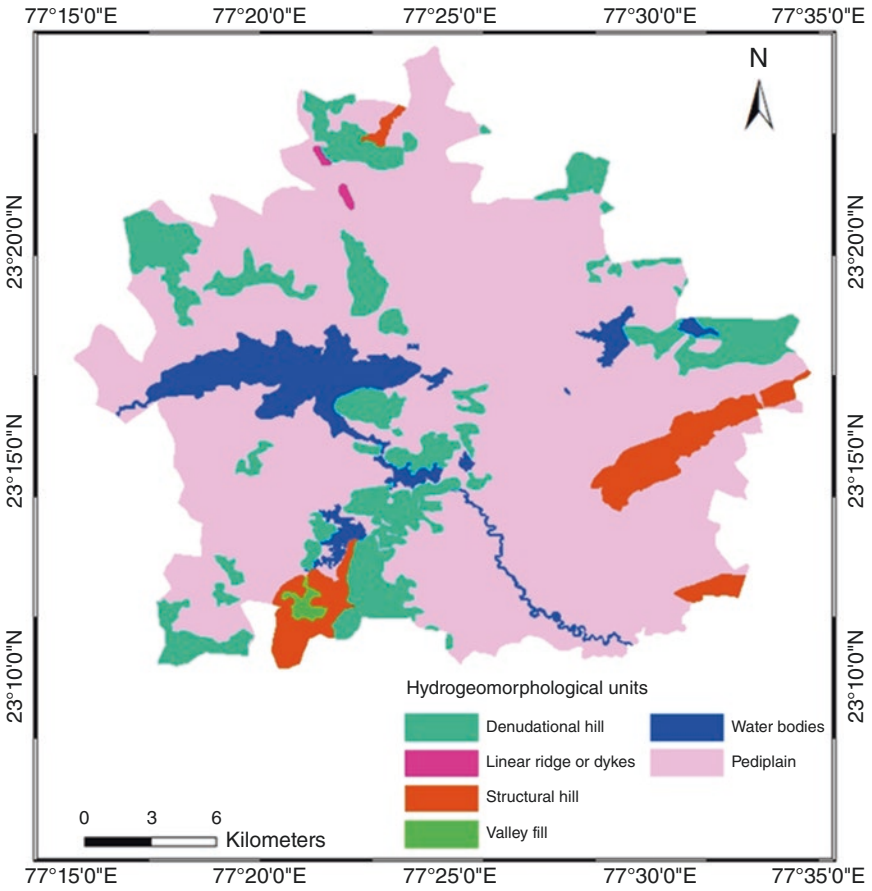

Fig. 13.2 Hydrogeomorphological map of the study area

texture and thickness, bare rocks, human settlements, and climate of the area. As per the groundwater prospect in highly urbanized cities like Bhopal, there is not much open space to allow water to infiltrate, and they create a barrier layer for the movement of water. This is because of the high density of population and anthropogenic activities in and around the cities (Al Saud, 2010; Singh et al., 2011b). The area consists of agriculture, urban plantation, forested area, reservoirs, wastelands, and settlements; from the land use point of view, agriculture is an "excellent" site for groundwater exploration.

Agricultural lands, which are not presently being used, are classified as fallow lands and hence categorized under "good." Though forest and plantation fall under good groundwater prospects, wasteland and barren land are rated poor zone since vegetation cover promotes percolation. The urban settlement is grouped as poor zones because it discontinues water percolation. Therefore, the study area considers many classes in terms of groundwater recharge and management based on the type

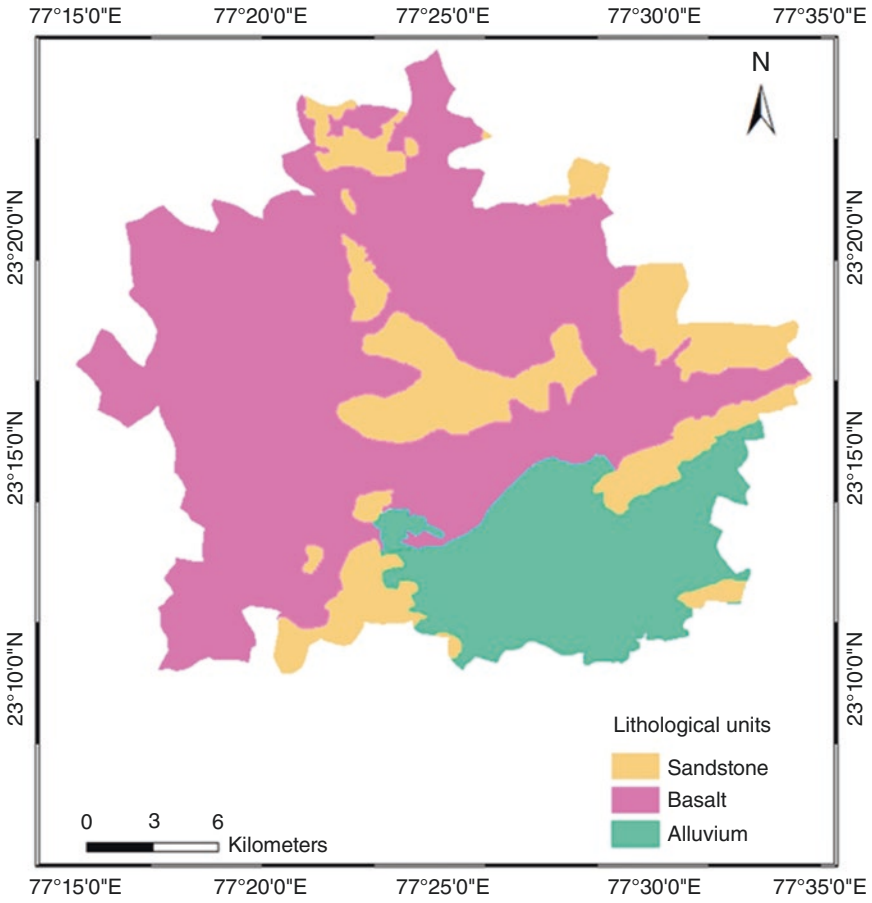

Fig. 13.3 Lithological map of the study area

of practices and water requirements (Fig. 13.4). Slope is always considered an important component for groundwater recharge and management practices and its support to runoff and infiltration. The topographic analysis was carried out using ASTER DEM data, and the minimum and maximum slope was prepared and classified in degrees (Fig. 13.5). The highest elevations in the area are 650 m in the central region of the city and are covered by hills, which support high runoff and less infiltration due to topography and geology. The low elevations are found in the southeast and southwest portion. A slope analysis was carried out by ArcGIS software and grouped into four classes from 0 to 3%, 3–8%, 8–15%, 15–30%, and > 30% (Fig. 13.5).

The drainage system and its characteristics govern the amount and rate of groundwater recharge. Therefore, drainage morphometric and pattern and density analysis are important to understand the sub-surface material and its

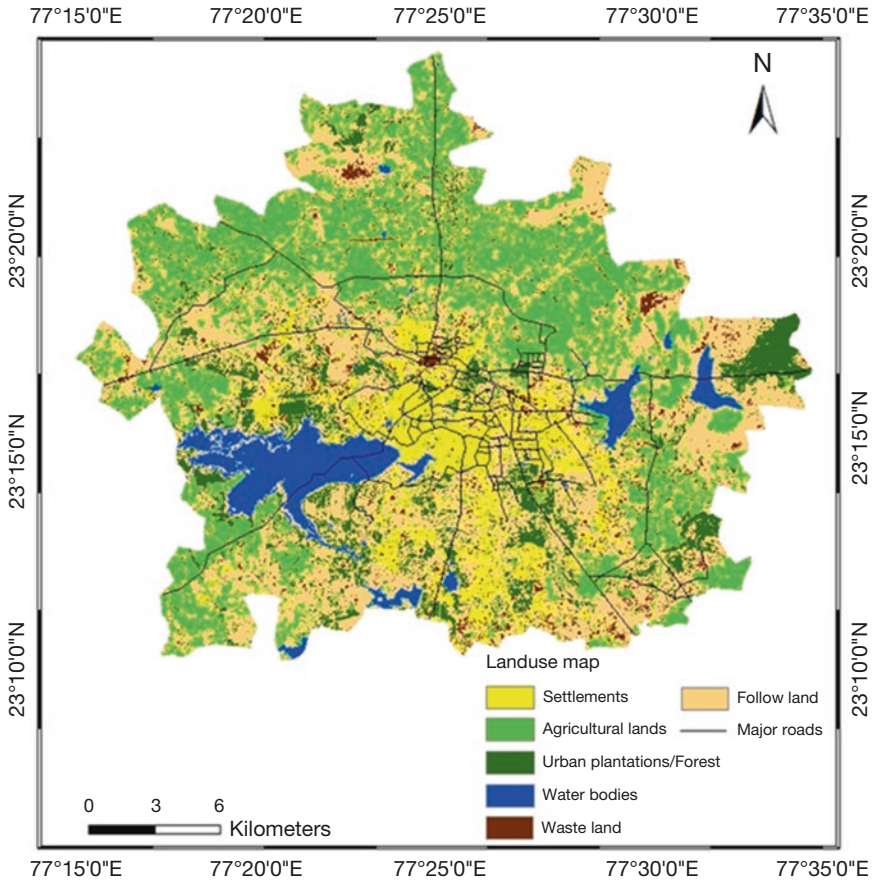

Fig. 13.4 Land use/land cover map of the study area

hydrogeological properties before the development of groundwater recharge and development plan. As a common hydrological behavior of drainage, the denser or higher the stream order the lower the recharge rate and low drainage density favors high groundwater percolation and accumulation (Singh et al., 2013a, 2014). A standard approach was used to calculate drainage characteristics and its network analysis using the spatial analyst tool of ArcGIS software. Higher drainage density supports high surface runoff and lowers the recharge, that is why drainage assessment is useful for understanding landform, climate, lithology, and structures. Drainage analysis has been carried out using ASTER satellite and spatial analyst tool in ArcGIS software, and it has been grouped into three class's high, medium, and low drainage density (Fig. 13.6). Based on drainage density, they are interpreted respectively for groundwater prospect.

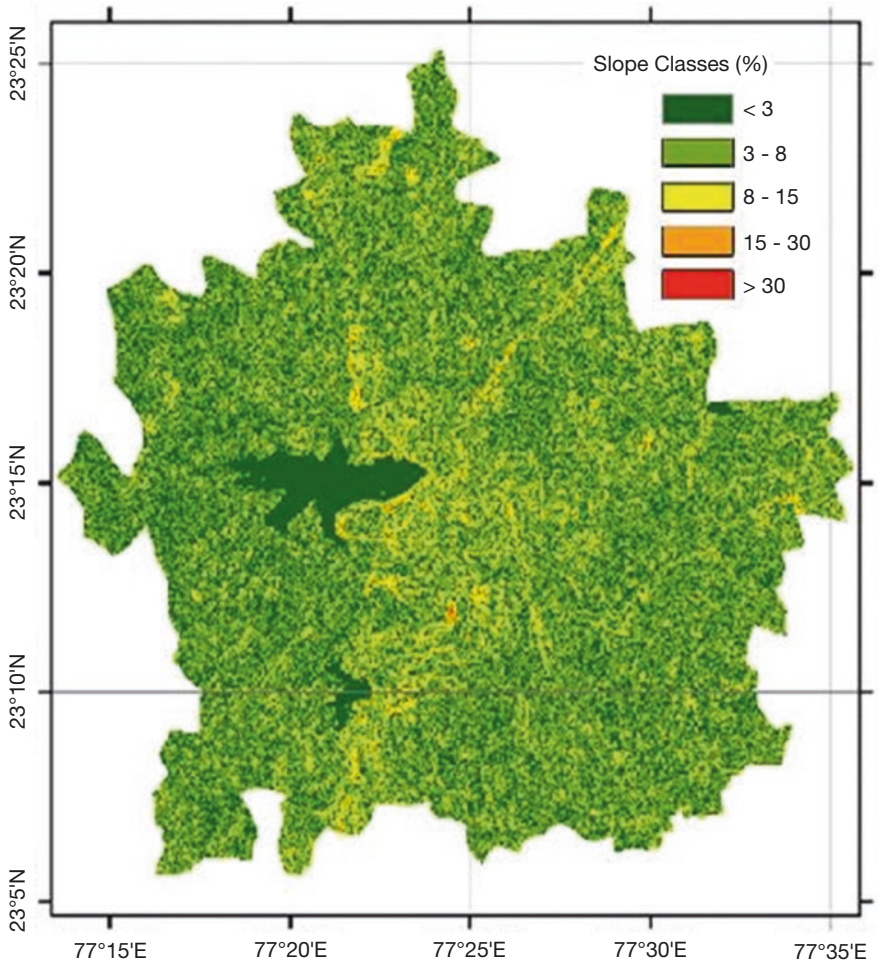

Fig. 13.5 Slope map of the study area

5 Field Validity of Groundwater Potential Map

The development of groundwater potential zones by integrating various parameters derived from satellite data and other sources must be cross-checked through the field survey of the area by considering questionnaires for different rural and urban localities to find out the status of water-yielding capacity. The groundwater potential (Fig. 13.7) inferred from integrating important thematic layers was validated with the borehole/well yield data in different hydrological setups within the study area. Many case studies on groundwater recharge and potential targeting have been carried out for hard and soft rock formation using satellite data and field investigation. It is observed that most of the excellent and good groundwater potential is found in weathered, fractured, jointed and vesicular units of basalts, pediplains, low drainage

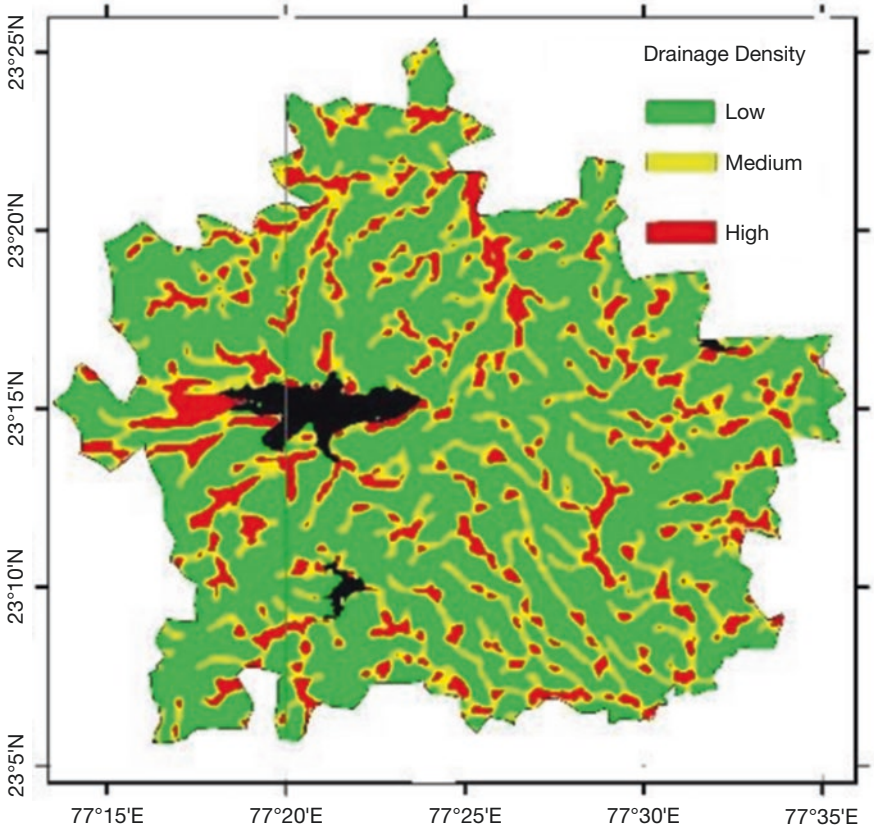

Fig. 13.6 Drainage density map of the study area

density, and gentle slope. The results were supported by the dug well and bore well number and yielding capacity. The general depth of dug wells/bore wells was observed between the range of 15–200 m below ground level (mbgl), and the water yielding varies from 10 to 600 liters per minute (lpm) as per the depth and conditions of the aquifer formation. Major aquifer formations of the area are soft rock mainly composed of unconsolidated deposits, and they are found near the river channels and marked as very good. Mostly dug wells have a yielding capacity from 50–600 lpm at 15–25 mbgl (CGWB, 2013).

6 Conclusion and Recommendations

The present work is the first remote sensing and GIS-based details scientific investigation for the Bhopal area based on an integrated modeling approach for evaluation of groundwater potential and generation of hydrological features responsible

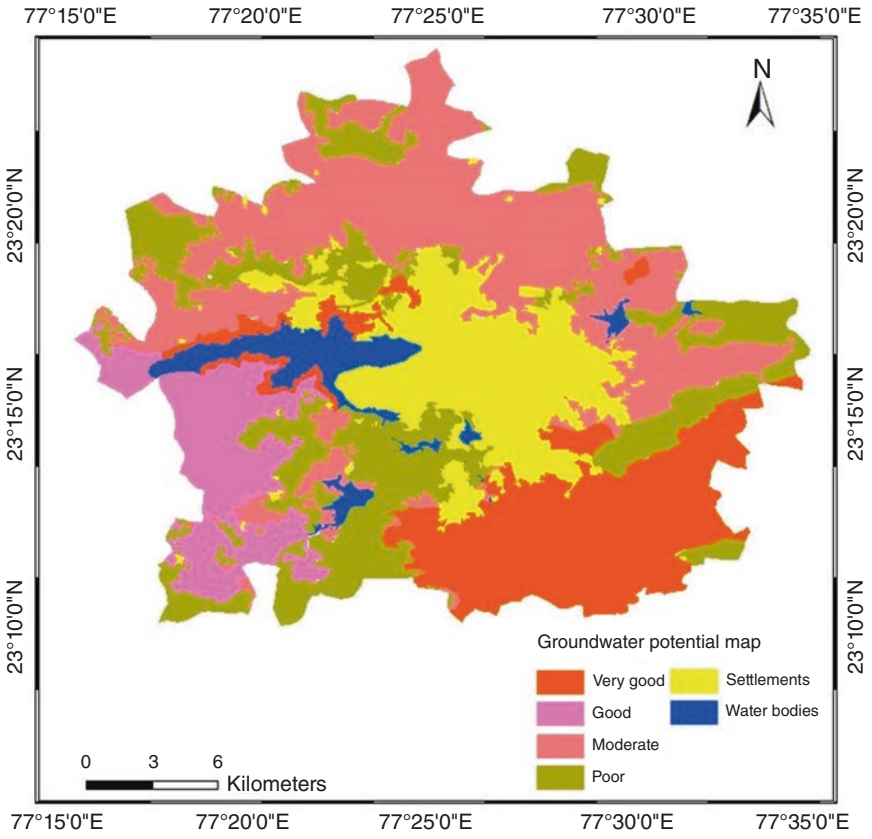

Fig. 13.7 Groundwater potential map of the study area

for storage and movement of groundwater. The work clearly concluded that the integrated use of geospatial technology and field survey data sets are promising tools for predicting groundwater reservoirs in hard rock areas. The derived GPM can be used to select suitable locations for groundwater withdrawals and management. The observed results from the present work are grouped into poor to very good based on a detailed study of terrain conditions, and it could be a better database for future groundwater development and selection of suitable possible structures for groundwater recharge and surface water storage tanks. The present work results will be a very good scientific database for decision-makers to develop a sustainable plan for groundwater resources. It is also suggested that the detailed survey based on watershed and geophysical investigation shall be a useful assessment for proper guidelines for future groundwater development.

References

Agarwal, E., Agarwal, R., Garg, R. D., & Garg, P. K. (2013). Delineation of groundwater potential zone: An AHP/ANP approach. *Journal of Earth System Science, 122*(3), 887–889.

Al Saud, M. (2010). Mapping potential areas for groundwater storage in Wadi Aurnah Basin, western Arabian Peninsula, using remote sensing and geographic information system techniques. *Hydrogeology Journal, 1*(15).

Avtar, R., Singh, C. K., Shashtri, S., Singh, A., & Mukherjee, S. (2010). Identification and analysis of groundwater potential zones in Ken–Betwa river linking area using remote sensing and geographic information system. *Geocarto International, 25*(5), 379–396.

Boutt, D. F., Hyndman, D. W., Pijanowski, B. C., & Long, D. T. (2001). Identifying potential land use-derived solute sources to stream baseflow using ground water models and GIS. *Ground Water, 39*, 24–34.

Brunner, P., Hendricks, F. H. J., Kgotlhang, L., Bauer-Gottwein, P., & Kinzelbach, W. (2007). How can remote sensing contribute in groundwater modeling. *Hydrogeology Journal, 15*, 5–18.

Chaudhuri, A. S., Singh, P., & Verma, P. (2021). Computation of groundwater recharge prospect in urban environment for sustainable water security. *Arabian Journal of Geosciences, 14*, 606. https://doi.org/10.1007/s12517-021-06904-y

CGWB (2013) District Groundwater Information Booklet, Bhopal.

Chenini, I., Mammou, A., & El May, M. (2010). Groundwater recharge zone mapping using GIS-based multi-criteria analysis: A case study in Central Tunisia (Maknassy Basin). *Water Resources Management, 24*, 921–939.

Chowdhury, A., Jha, M., Chowdary, V., & Mal, B. (2009). Integrated remote sensing and GIS-based approach for assessing groundwater potential in West Medinipur district, West Bengal, India. *International Journal of Remote Sensing, 30*, 231–250.

Dar, I. A., Sankar, K., & Dar, M. A. (2011). Deciphering groundwater potential zones in hard rock terrain using geospatial technology. *Environmental Monitoring and Assessment, 173*, 597–610.

Haan, C. T. (2002). *Statistical methods in hydrology*. Iowa State Press. 496 pp.

Jaiswal, R. K., Mukherjee, S., Krishnamurthy, J., & Saxena, R. (2003). Role of remote sensing and GIS techniques for generation of groundwater prospect zones towards rural development – An approach. *International Journal of Remote Sensing, 24*, 993–1008.

Jasmin, I., & Mallikarjuna, P. (2011). Satellite-based remote sensing and geographic information systems and their application in the assessment of groundwater potential, with particular reference to India. *Hydrogeology Journal, 19*, 729–740.

Jha, M. K., Chowdhury, A., Chowdary, V., & Peiffer, S. (2007). Groundwater management and development by integrated remote sensing and geographic information systems: Prospects and constraints. *Water Resources Management, 21*, 427–467.

Krishnamurthy, J., Venkatesa, K. N., Jayaraman, V., & Manivel, M. (1996). An approach to demarcate ground water potential zones through remote sensing and a geographical information system. *International Journal of Remote Sensing, 17*, 1867–1884.

Kulkarni, H., Deolankar, S., Lalwani, A., Joseph, B., & Pawar, S. (2000). Hydrogeological framework of the Deccan basalt groundwater systems, west-central India. *Hydrogeology Journal, 8*, 368–378.

Leblanc, M., Favreau, G., Tweed, S., Leduc, C., Razack, M., & Mofor, L. (2007). Remote sensing for groundwater modelling in large semiarid areas: Lake Chad Basin, Africa. *Hydrogeology Journal, 15*, 97–100.

Lee, S., Song, K. Y., Kim, Y., & Park, I. (2012). Regional groundwater productivity potential mapping using a geographic information system (GIS) based artificial neural network model. *Hydrogeology Journal, 20*, 1511–1527.

Limaye, S. D. (2010). Groundwater development and management in the Deccan Traps (basalts) of western India. *Hydrogeology Journal, 18*, 543–558.

Madrucci, V., Taioli, F., & de Araújo, C. C. (2008). Groundwater favorability map using GIS multicriteria data analysis on crystalline terrain, São Paulo State, Brazil. *Journal of Hydrology, 357*, 153–173.

Manap, M., Sulaiman, W., Ramli, M., Pradhan, B., & Surip, N. (2013). A knowledge-driven GIS modeling technique for groundwater potential mapping at the Upper Langat Basin, Malaysia. *Arabian Journal of Geosciences, 6*, 1621–1637.

Murray, S. J. (2013). Present and future water resources in India: Insights from satellite remote sensing and a dynamic global vegetation model. *Journal of Earth System Science, 122*(1), 1–13.

Pradhan, B. (2009). Groundwater potential zonation for basaltic watersheds using satellite remote sensing data and GIS techniques. *Central European Journal of Geosciences, 1*, 120–129.

Prasad, R., Mondal, N., & Singh, V. (2008). Evaluation of groundwater resource potential using GIS in Kurmapalli watershed of Andhra Pradesh. *Journal Geological Society of India, 71*, 661–669.

Rai, S. N., Thiagarajan, S., Ratna Kumari, Y., Rao, V. A., & Manglik, A. (2013). Delineation of aquifers in basaltic hard rock terrain using vertical electrical soundings data. *Journal of Earth System Science, 122*(1), 29–41.

Rokade, V., Kunda, I. P., & Joshi, A. (2007). Groundwater potential modelling through remote sensing and GIS: A case study from Rajura Taluka, Chandrapur district, Maharashtra. *Journal-Geological Society of India, 69*, 943–948.

Samy, I. E., & Mohamed, M. M. (2014). Groundwater potential modelling using remote sensing and GIS: A case study of the Al Dhaid area, United Arab Emirates. *Geocarto International, 29*, 433–450.

Saraf, A. K., & Choudhury, P. R. (1998). Integrated remote sensing and GIS for groundwater exploration and identification of artificial recharge sites. *International Journal of Remote Sensing, 19*, 1825–1841.

Saraf, A. K., Choudhury, P. R., Roy, B., Sarma, B., Vijay, S., & Choudhury, S. (2004). GIS based surface hydrological modelling in identification of groundwater recharge zones. *International Journal of Remote Sensing, 25*, 5759–5770.

Sawaya, K. E., Olmanson, L. G., Heinert, N. J., Brezonik, P. L., & Bauer, M. E. (2003). Extending satellite remote sensing to local scales: Land and water resource monitoring using high-resolution imagery, remote Sens. *Environment, 88*, 144–156.

Singh, P., & Singh, M. (2012). *A GIS based hydrogeomorphological mapping of basaltic terrain: Implications for water resource evaluation and management*. In 13th Esri India user conference. 1–8.

Singh, P., Kumar, S., & Singh, U. (2011a). Groundwater resource evaluation in the Gwalior area, India, using satellite data: An integrated geomorphological and geophysical approach. *Hydrogeology Journal, 19*, 1421–1429.

Singh, P., Thakur, J. K., Kumar, S., & Singh, U. C. (2011b). Assessment of land use/land cover using geospatial techniques in a semi-arid region of Madhya Pradesh, India. In J. K. Thakur, S. K. Singh, A. Ramanathan, M. B. K. Prasad, & W. Gossel (Eds.), *Geospatial techniques for managing environmenal resources* (pp. 152–163). Springer and Capital Publication.

Singh, P., Thakur, J. K., & Kumar, S. (2013a). Delineating groundwater potential zones in a hard-rock terrain using geospatial tool. *Hydrological Sciences Journal, 58*, 213–223.

Singh, P., Thakur, J. K., & Singh, U. C. (2013b). Morphometric analysis of Morar River Basin, Madhya Pradesh, India, using remote sensing and GIS techniques. *Environmental Earth Sciences, 68*, 1967–1977.

Singh, P., Gupta, A., & Singh, M. (2014). Hydrological inferences from watershed analysis for water resource management using remote sensing and GIS techniques. *The Egyptian Journal of Remote Sensing and Space Sciences, 17*, 111–121.

Singh, S. K., Singh, P., & Gautam, S. K. (2016). Appraisal of urban lake water quality through numerical index, multivariate statistics and earth observation data sets. *International Journal of Environmental Science and Technology, 13*, 445–456.

Solomon, S., & Quiel, F. (2006). Groundwater study using remote sensing and geographic information systems (GIS) in the central highlands of Eritrea. *Hydrogeology Journal, 14*, 729–741.

Verma, P., Singh, P., & Srivastava, S. K. (2020a). Impact of land use change dynamics on sustainability of groundwater resources using earth observation data. *Environment, Development and Sustainability, 22*, 5185–5198. https://doi.org/10.1007/s10668-019-00420-6

Verma, P., Singh, P., & Srivastava, S. K. (2020b). Development of spatial decision-making for groundwater recharge suitability assessment by considering geoinformatics and field data. *Arabian Journal of Geosciences, 13*, 306. https://doi.org/10.1007/s12517-020-05290-1

Vignesh, K. S., Thambidurai, P., & Indhiya Selvan, V. N. (2019). Assessment of groundwater potential zone in Chennai region, Tamil Nadu, India. In P. P. Adhikary, P. K. Shit, P. Santra, G. S. Bhunia, A. K. Tiwari, & B. S. Chaudhary (Eds.), *Geostatistics and geospatial technologies for groundwater resources in India* (pp. 167–191). Springer Nature.

Chapter 14
The Effect of Urbanization on Groundwater Quality and Hydrochemical Characteristics in Ennore Coastal Aquifers of Chennai, South India

S. Senthilkumar, K. Srinivasamoorthy, and B. Gowtham

Abstract An effort has been made to understand the impacts of urban growth on groundwater quality and its variations vis-à-vis hydrochemical characteristics in the Ennore coastal aquifers, Chennai. For the present investigation, 95 groundwater samples were composed of the surface bore wells and dug wells for dual seasons (pre-monsoon and post-monsoon) in the interval of August 2019 and January 2020 in and around Ennore, north of Chennai metropolitan city, South India. Groundwater levels in 44 wells generally decline before the monsoon because of overdrafts. Every sample was estimated for a significant chemical constituent in Ion Chromatography, adopting standard procedures. Higher electrical conductivity (21,200 mg/l) and salinity (12,500 mg/l) were perceived alongside the southeastern portions of the aimed extent dominated by urban clusters. Due to urban anthropogenic influences, a higher nitrate (157 mg/l) was noted laterally in the southern province of the aimed area. Piper plot classified groundwater types as NaCl, mixed CaMgCl, and $CaHCO_3$, suggesting impact due to rock weathering, anthropogenic, and saline water intrusion. Ionic ratio plots like $Cl/CO_3 + HCO_3$, $Mg^{2+}/Ca^{2+,}$ and Cl^{-}/HCO_3^{-} suggest groundwater are influenced by salinization confined to north, southern, and coastal sections of the aimed domain and impact due to ion exchange and mineral weathering from aquifers. A trivial rise in groundwater quality was noted in the post-monsoon session, suggesting an impact due to freshly recharged groundwater. Groundwater quality is generally influenced by lithological variations, land use, and urban impact. Groundwater is found unsuitable for drinking and domestic utilities with fewer exceptions irrespective of seasons in most locations.

S. Senthilkumar (✉) · K. Srinivasamoorthy
Department of Earth Sciences, Pondicherry University, Puducherry, India
e-mail: siva.senthil.geo@gmail.com

B. Gowtham
Department of Geology, Presidency College, Chennai, India

P. Thambidurai, A. K. Dikshit (eds.), *Impacts of Urbanization on Hydrological Systems in India*, https://doi.org/10.1007/978-3-031-21618-3_14

Keywords Ennore · Ion exchange · Rock water interaction · Salinization · Urban impact

1 Introduction

The primary water source is groundwater for agricultural, domestic, and other industrial purposes. India is covered by 2.2% of the universal terrestrial area, 4% of the global's aquatic wealth, and 16% of the earth's inhabitants (Senthilkumar et al., 2021). In the past few decades, the need on behalf of freshwater resources has enlarged fabulously towards the rapid habitant development and industrial development. The situation has been predictable that almost one-third of the global inhabitants utilize groundwater for intake and home utility purposes. The quantity and purity of this water are mainly influenced by land use (Jiang & Yan, 2010; Senthilkumar et al., 2017). The proposed focused area is known for its high-water vulnerability payable to the quick rise in people growth, industrial development, and urbanization. The overexploitation of groundwater is one of the substantial causes of aquatic vulnerability in the region. Salinity in groundwater is another major issue in this study area. The chemical configuration of groundwater is able to designate its source and past movements over subsurface constituents that water particles have been connected within narrow and innate conditions. The sources like natural, chemical, anthropogenic, and biogeochemical components have significantly altered groundwater quality recently (Ayotte et al., 2011; Senthilkumar et al., 2014). Groundwater superiority is influenced by climate, soil properties, water movement through the aquifers, elevation, saline water intrusion, and human perturbance (Srinivasamoorthy et al., 2011; Gopinath & Srinivasamoorthy, 2015; Thambidurai & Vazhacharickal, 2021). It is affected by numerous artificial causes such as industrial and agricultural waste, sanitary sewage, marine pollution, and nuclear waste disposal activity. The land use character plays a principal part in identifying the hydrological characteristics such as overland flow, infiltration rate, interceptions, and evaporation (Senthilkumar et al., 2017; Thambidurai, 2017). The location of Manali and Ennore, industrial activities, and the populace strongly impact the coastal aquifers over time. Hence, this study attempt to understand and demarcate the affected area due to the urbanization impact on groundwater resources.

2 Study Area

The study area, Manali and Ennore, and their adjoining areas fall within Thiruvallur District, representing the northeastern part of Tamil Nadu, India, casing an extent of 1402.79 km^2. The Bay of Bengal bounds the proposed area in the east, Andhra

Pradesh state in the north, Chennai city in the southeast, Kanchipuram district in the south, and Vellore region in the west. The yearly rainfall is around 1200 mm, of which the northeast monsoon contributes about 60%, which occurs from October to December, and the other 40% of the rainfall is by the southwest monsoon from July to September. The period of April to June usually is dry and hot, and its annual lowest and extreme temperatures are 24.2 and 32.8 °C, correspondingly. The current research area extends from 12°15′ N towards 13°15′ N and 79°15′ E to 80°20′ E geocoordinates and is covered in the Survey of India Topo. No., 66C3, 66C4, 66C7, and 66C8 (Fig. 14.1). The significant drainage patterns confined to the study region are tanks, the Korattalayar River, and the Buckingham canal. The Buckingham Canal navigates north to south, reaches the Korattalayar River, and finally configures the Bay of Bengal.

The Korattalayar river bottom encompasses unconsolidated coarse grain sands, gravels, pebbles, clay, and sandstones that path east. Patches of rain-fed tanks cover the dedicated area and fill out during the monsoon period. The research area's geology includes clay and sandstones of the Jurassic period, marine deposits of the Cretaceous dated, sandstones, shale, and clay of the tertiary age, and younger coastal alluvial deposits (Fig. 14.1). The quaternary formations comprise chiefly sands, silt, and clay and are restricted to significant units of the study area. The groundwater occurs under unconfined to semi-confined environments in the intergranular open places at sandstone formations, sheet planes, and skinny shale fractures (CGWB, 2007). The central geomorphological units of the study area are a typical landscape with a moderate slope near the east in the north and central portions and towards the south direction on the southern side. The essential geomorphic elements identified in this region through analysis of satellite imagery are coastal plains, alluvial plains, built-up land, flood plains, and high sedimentary lands. The sedimentary plain containing numerous landforms such as swale and marshy part, lagoon/backwater coastal plain, natural levee, and beach elevations are detected in the southern part of the region (CGWB, 2007). Soil types identified in the study area were categorized into five kinds: clay soil, clay loam soil, loamy sand, and miscellaneous. The primary area is covered by clay and clay loam type of soil, and small patches of loamy sand type of soil were detected in the coastal portion of this study location (Senthilkumar et al., 2021). The land-use pattern of this region is enclosed by large to small-scale industries, agricultural lands, domestic buildings, wastelands, and water bodies like rivers, lakes, and ponds. The agricultural lands occupy the western portion and around 579.27 km^2 are covered in its total area extends; the barren land is occupied around 388.36 km^2; some other covers are known as waste and places. The large liquid bodies occupy 187.43 km^2, and small water forms like tiny tanks and ponds are covered by 74.17 km^2 out of the total extent. The build-up structures and other flora cover 164.82 km^2 of this region (Fig. 14.2).

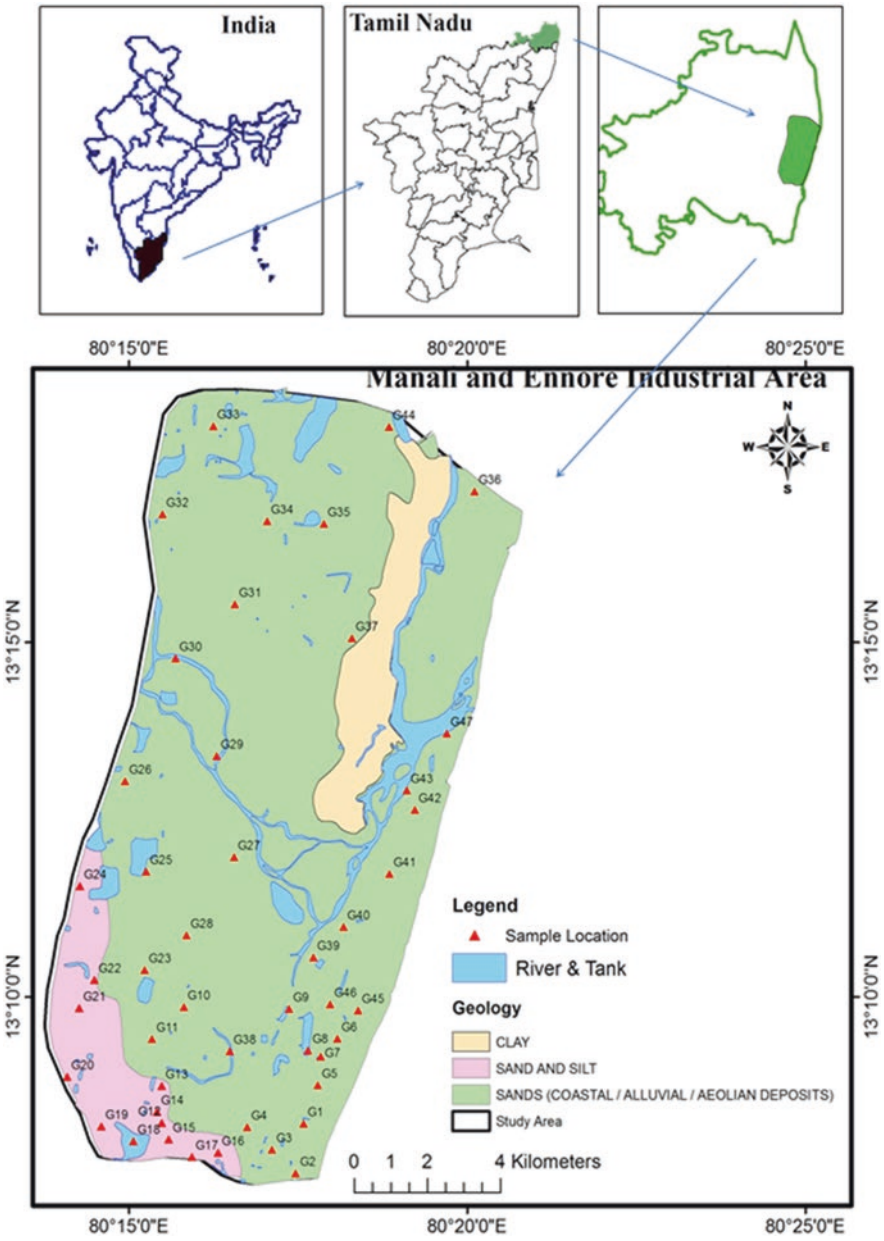

Fig. 14.1 Lithology and groundwater locations map

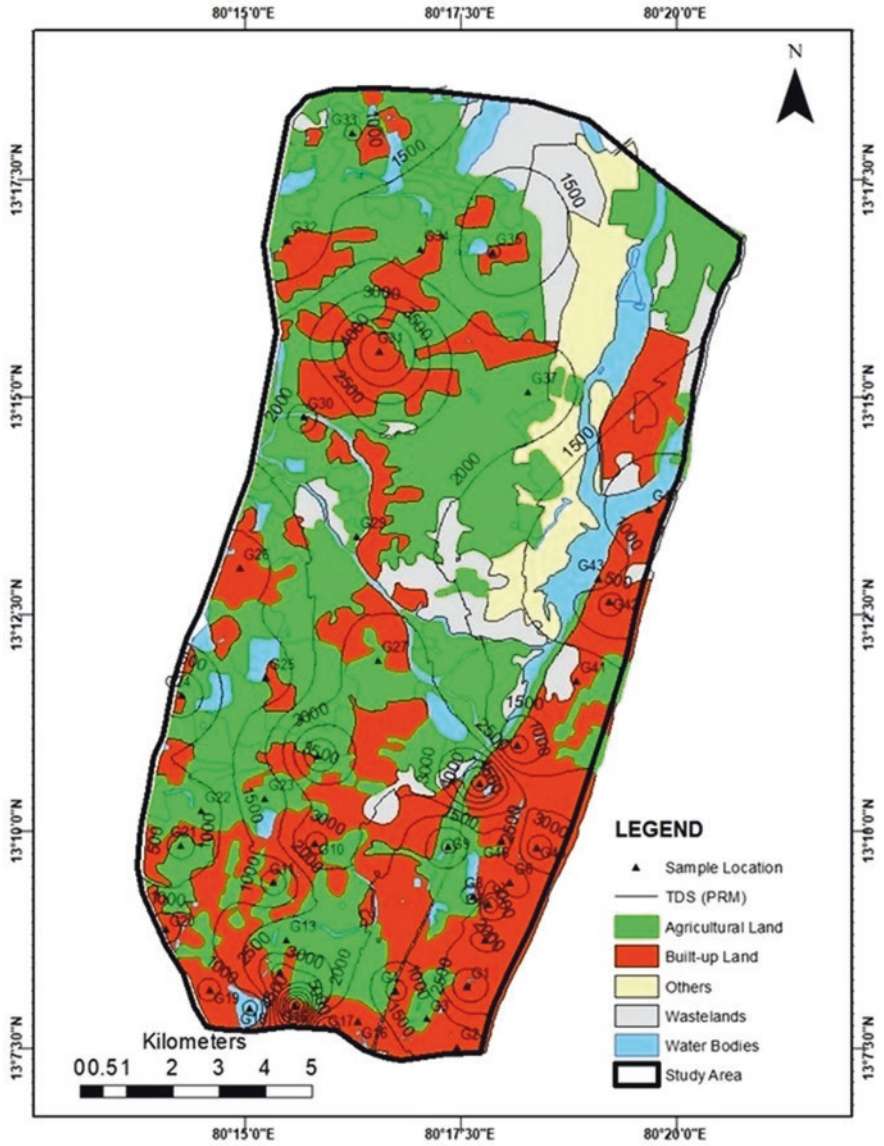

Fig. 14.2 Land use map vs. total dissolved solids contour level of the study area in pre-monsoon (PRM)

3 Methodology

In total, 94 subsurface water samples were collected for the summer period (PRM, August 2019) and winter (POM, January 2020). Groundwater samples collected were confined to bore wells and open wells in clean polyethylene 1-l bottles rinsed with nitric acid. The sampling bottles were completely washed with the aid of groundwater before being sampled. Physical parameters like total dissolved solids (TDS), electronic conductivity (EC), salinity, pH, temperature, and turbidity of groundwater were measured instantly immediately after sample collection using a multiparameter water analyzer (Hanna-Model, HI98194). For further investigation, samples were transferred to the laboratory and filtered to remove suspended particles using 0.4 μm screen paper. The cations and anions analysis are attempted using standard procedures for the collected groundwater samples (APHA, 1998). Ion chromatography was used to determine major cations such as sodium (Na^+), potassium (K^+), calcium (Ca^{2+}), magnesium (Mg^{2+}), and anions such as sulphate (SO_4^{2-}), chloride (Cl^-), and nitrate (NO_3). The carbonate (CO_3) and bicarbonate (HCO_3) were identified by the standard titration method with H_2SO_4 (0.02 N) standard solution. The analytical precession for calculating ionic error balance varies between 5 and 10%. The statistical analysis software (SPSS v17.0) generated groundwater samples' most petite, extreme, average, and standard deviation values. The correlation analysis was also attempted to realize the groundwater quality and the characterization of fresh and contaminated water quality irrespective of seasons. Statistical analysis also infers spatial and temporal variations caused due to regular and anthropogenic processes irrespective of seasonal variations (Singaraja et al., 2014; Gopinath et al., 2016). From the major ions, Chadha's plot (Vandenbohede et al., 2010) was utilized to understand the salinity and to evaluate the hydrochemical process activated in the coastal groundwater.

3.1 Outcomes and Argument

The statistical summary of the physicochemical limitations aimed at the collected subsurface water samples in the course of PRM and POM times is represented (Table 14.1). The hydrogen ion concentration (pH) during PRM varies from 6.0 to 8.3 through middling of 6.7, and the POM, arrays from 6.1 to 7.7 by a mean rate of 7.0. It is inferred that significant groundwater samples during POM were alkaline, likely due to the dissolved carbonate in the form of bicarbonate. During POM waters, samples tend to represent neutral, suggesting impact due to recent precipitation (Nagarajan et al., 2010).

Electrical conductance (EC) is the conductance of a cubic centimeter of any material equated with an equal volume of water at an average temperature of 25 °C (Driscoll, 1986). EC of water samples during PRM ranges from 692.1 to 19,093.3 μs/cm using a moderate rate of 3977.2 μs/cm, and POM samples suggest lower EC

Table 14.1 Statistical implications of groundwater chemical constituents in PRM and POM sessions

Parameter	PRM				POM			
	Min	Max	Av	St. Dev.	Min	Max	Av	St. Dev.
pH	6.0	8.3	6.7	0.4	6.1	7.7	7.0	0.4
EC (µs/cm)	692.1	19093.3	3977.2	3359.8	12.6	9564.0	3259.4	2280.6
TDS (mg/l)	442.9	12219.7	2545.4	2150.3	226.0	6167.9	1762.5	1274.0
Ca (mg/l)	41.8	1066.9	254.1	168.8	28.9	393.3	157.0	74.7
Mg (mg/l)	32.3	514.3	112.2	94.8	10.6	155.2	56.1	29.2
NH_4 (mg/l)	0.5	163.6	8.1	24.6	0.0	25.3	4.5	4.8
Na (mg/l)	41.8	3428.4	556.4	612.5	24.4	1965.1	434.8	424.2
K (mg/l)	12.1	151.4	64.3	30.7	6.0	195.6	52.6	43.0
Br (mg/l)	0.1	30.0	1.7	5.5	0.0	0.0	0.0	0.0
Cl (mg/l)	73.6	5974.9	842.0	1028.7	45.3	2291.8	601.3	565.1
HCO_3 (mg/l)	109.8	815.0	358.6	131.0	41.0	406.8	187.7	97.8
SO_4 (mg/l)	4.2	1883.3	262.6	338.8	11.2	1113.8	181.9	206.7
NO_2 (mg/l)	0.1	18.9	1.3	3.1	0.0	144.7	23.3	33.5
NO_3 (mg/l)	0.5	157.0	27.5	36.8	0.0	144.7	22.9	33.1
F (mg/l)	0.0	1.6	0.7	0.3	0.0	0.0	0.0	0.0
TH (mg/l)	274.0	4775.7	1095.1	772.1	116.0	1619.3	622.7	294.8

values (12.6 to 9564.0 µs/cm) by the middling value of 3259.4 µs/cm. The highest EC (19093.3 µs/cm) was well-known in the south-eastern part during PRM, and values were found to decrease in the POM gradually owed to the dissolution of ions for consequent precipitation through the rainy period (Senthilkumar et al., 2017)**.** The total dissolved solid (TDS) results during PRM range between 442.9 mg/l and 12219.7 mg/l using a middle value of 2545.4 mg/l, and during POM, TDS ranges from 226.0 mg/l to 6167.9 mg/l with a moderate value of 1762.5 mg/l. Greater TDS observed along the SE, and the NW regions of the study portion regardless of seasons (Figs. 14.2 and 14.3) suggest impact due to the excess withdrawal of groundwater in urbanized areas and seawater disturbance in the aquifers of this coastal region (Senthilkumar et al., 2017).

The supremacy of cations existing the arrange as $Na^+ > Ca^{2+} > Mg^{2+} > NH_4^+ > K^+$ and anion as $Cl^- > SO_4^- > HCO_3^- > NO_3^-$ irrespective of seasons. The Na^+ ranges from 41.8 mg/l to 3428.4 mg/l with a moderate value of 556.4 mg/l in PRM. During POM, it ranges from 24.4 mg/l to 1965.1 mg/l with a moderate value of 434.8 mg/l, signifying a greater concentration popular the PRM might be due to the seawater intrusion by anthropogenic sources and enduring of plagioclase feldspar (Gopinath et al., 2019) in the southern and eastern coastal portion of the aimed region nevertheless of seasons. During PRM, the Ca^{2+} concentration in the study area ranges from 41.6 mg/l to 1066.9 mg/l, with an average of 254.1 mg/l. The value decreased during POM with ranges of 28.9 mg/l to 393.3 mg/l through a middle value of 157.0 mg/l, and the greater importance observed in the PRM season might be due to precipitation and dissolution of $CaCO_3$ with Ca Mg $(CO_3)^2$ minerals interested in

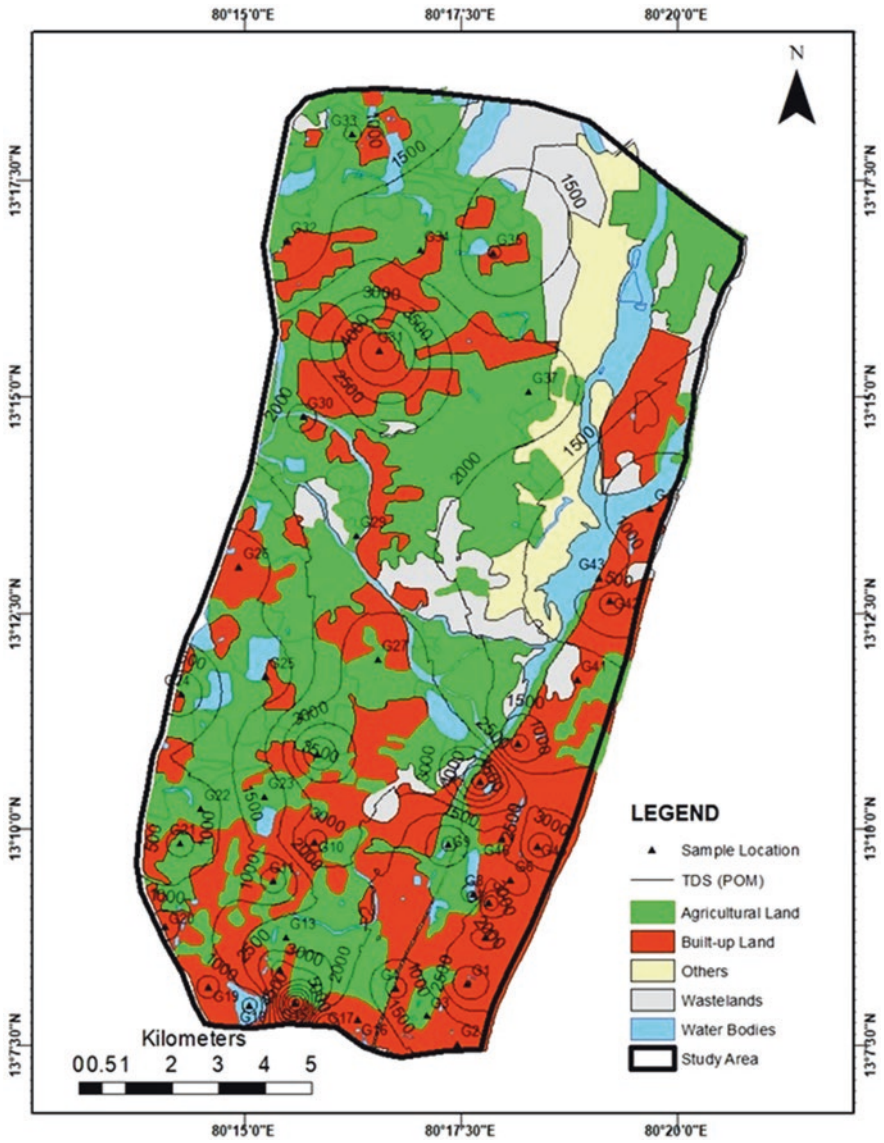

Fig. 14.3 Land use vs. total dissolved solids contour level of the study area in post-monsoon (POM)

aquifer restore in the south and eastern coastal portion of this area (Senthilkumar et al., 2021). In this fused area, Mg^{2+} during PRM differs from 32.3 mg/l in near 514.3 mg/l with middling of 112.2 mg/l, and during POM, it ranges from 10.6 mg/l to 155.2 mg/l average of 56.1 mg/l. The maximum magnesium values detected in the PRM session influence due to the leaching of dolomite, sulfate, and silicate minerals recognized in the litho-units of the aimed region (Appelo & Postma, 2005). NH_4^+ levels in groundwater samples range from 0.5 mg/l to 163.6 mg/l with an

average of 8.2 mg/l during PRM and 0.0 mg/l to 25.3 mg/l with an average of 4.5 mg/l during POM. Compared with PRM, lower NH_4 is noted in POM, irrespective of sample locations. The suggested impact is due to the agricultural and urban runoff process, various industrial inadequate treated discharges, and municipal waste treatment plants (USEPA, 1999) in this study area. In the south-central region of this area, upper ammonium concentration with all seasons might be a source due to the presence of rich settlements and the industrial cluster of this area. The K^+ ions range from 12.1 mg/l to 151.4 mg/l through a normal of 64.3 mg/l in the course of PRM, but POM values range from 6.0 mg/l towards 195.6 mg/l with a normal of 52.6 mg/l, respectively. A higher concentration K^+ in PRM season in the northeastern and southern part might be payable to urban landfills and fertilizer discharge from agricultural activities nevertheless of the monsoon (Natesan et al., 2022).

Among the anionic values, the Cl^- is the leading concentration in the analyzed standards, ranging from 73.6 mg/l to 5974.9 mg/l through a normal of 842 mg/l in PRM period. In the course of POM, it decreased from 45 mg/l to 2291.8 mg/l by a common of 601.3 mg/l. Greater Cl − concentration in groundwater samples observed at the time of PRM in and around the southern part of the coastal lands of this area denotes the consequence of seawater disruption due to the surplus taken out by the urbanized region and evaporation augmented irrigation return flow (Gopinath et al., 2016). Next to chloride, the SO_4 concentration is the leading value in the pre-monsoon, ranging from 4.2 mg/l to 1883.3 mg/l with a middling value of 262.6 mg/l; then POM values vary from 11.2 mg/l to 1113.8 mg/l by means of an average of 181.9 mg/l its reveal that sulfate values are increased gradually in few locations. The maximum value of SO_4^- is experiential in the southern part of the area in all seasons due to mineral dissolution, bacterial fascination, fertilizers, and other anthropogenic causes (Chidambaram et al., 2012; Natesan et al., 2022).The HCO_3^- ions vary from 109.8 mg/l to 815.0 mg/l with a common point of 358.6 mg/l during the pre-monsoon seasons; it reduced up to 41.0 mg/l 406.8 mg/l with an average of 187.7 mg/l in the post-monsoon stage. The highest HCO_3^- values detected in the PRM season, irrespective of sample location, may be due to the carbonate dissolution, and silicate enduring due to the presence of topsoil CO2 discharging HCO3− was the chief key to the existence of extraordinary bicarbonate in groundwater (Moquet et al., 2011). The nitrate value of the studied sites varied between 0.5 and 157.0 mg/l with an average of 27.5 mg/l in the course of the PRM, and it decreased in the POM season from 0.0 mg/l to 144.7 mg/l with a mean of 22.9 mg/l. For the duration of the PRM period, the highest value is witnessed in the densely urbanized south and the eastern province of the focused location, revealing that the source might be resulting from decayed tank leakages and animal wastes, irrigation follows, poultry farms, and decaying of domestic rubbishes (Narsimha & Sudarshan, 2017). The fluoride ion in the focused study area is diverse from 0.1 to 1.5 mg/l with a middle of 0.7 mg/l in PRM, and it is almost nil in POM. Higher values are mainly due to varying aquifer mineral composition, aquifer dynamics, temperature, pH, and continuous contact with additional ions (Tahaikt et al., 2008). The total hardness (TH) of the research area in the maximum of the studied locations witnessed difficult water type (TH > 300 mg/l) popular the pre-monsoon time, and it converted

from moderately complex water type (TH > 150 mg/l) to hard water type in the post-monsoon periods. The prolonged consumption of hard water might cause urolithiasis, prenatal mortality, anencephaly, cancer, and cardiovascular complaints that affect human health (Agrawal & Jagetai, 1997; Senthilkumar et al., 2017).

3.2 Groundwater Facies

The Piper trilinear diagram is applicable to evaluate the progress of groundwater and the relationship between the rock type and water composition. The diagram contains three different fields; triangular fields are two and a single diamond-shaped field derived by Piper (1944). In the triangular field, the percentage values of cations and anions (in meq/l) such as Mg and Ca (limy earth) and Na and K were plotted. The HCO_3 (weak acid), SO_4 (strong acid), and Cl (strong acid) are all distinct. The entire representation of the aquatic is denoted in the diamond-shaped portion using the prominent point of the diagrams in the trilateral portion of many authors (Najib et al., 2017).

According to Piper plots, maximum of the groundwater shows in alkaline (Na^+, K^+) field, and controlling excess of the basic earth metals ($Ca2^+$, $Mg2^+$) and more acid (Cl^-, SO_4^{2-}) beat the weak acid (CO_3^{2-}, HCO_3^-) in nature with irrespective of seasons (Fig. 14.4). In both seasons, the dominant hydrogeochemical facies in the

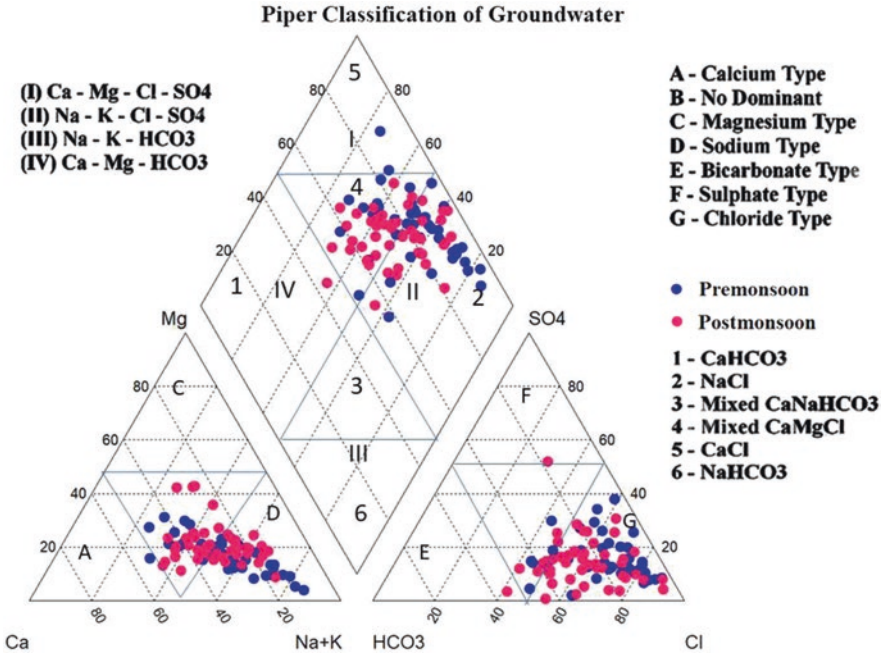

Fig. 14.4 Piper classification of groundwater for pre- and post-monsoon seasons

area falls in NaCl> Mixed CaMgCl>CaCl> $CaHCO_3$. However, samples are also associated with NaCl and mixed CaMgCl fields irrespective of the seasons. The highest groundwater types of this region, such as NaCl and mixed CaMgCl, irrespective of periods, suggest mingling high-salinity water initiated from surface pollution bases like inland wastewater, irrigation reappearance flow, besides septic seepages confined alongside by way of southern and eastern portions of the study extent (Saravanan et al., 2016; Senthilkumar et al., 2019). Few $CaHCO_3$ water types indicate the current recharge of native water controlled to the studied location covered by dint of deposited aquifers. The CaCl water types are observed in the premonsoon time of year due to mutual practices like equilibrium in the cation exchange and natural withstanding (Thivya et al., 2015). The maximum Cl (Na-Cl system) is 2974 mg/l all along the coastal extents. As to the Piper graph, the chemical composition broad tendency of groundwater varies beginning with mixed Ca-Mg-Cl type towards Na-Cl type of waters after the inner to near the coastline.

3.3 Seawater Contamination Studies

Seawater intrusion is apparent as the immigration of salty seawater into the aquifers that remain hydraulically attached to the marine. In densely populated coastal areas that rely heavily on groundwater, the withdrawal rate frequently exceeds the recharge rate, resulting in seawater intrusion. An attempt has been made to study the impact of saltwater intrusion keen on the aquifer by adopting various ionic ratios (Senthilkumar et al., 2019: Selvakumar et al., 2022).

$Cl/CO_3 + HCO_3$ Ratio

The Cl^- and HCO_3 help identify the seawater disturbance due to chloride content dominance in marine water. At the same time, bicarbonate exists merely in minimal quantities. Simpson's ratio, or chloride to bicarbonate, isolates seawater contamination of freshwater (Todd, 1980). There are five categories in the Simpson classification: 0.5 is classified as good water, 1.3 as slightly contaminated by seawater, 2.8 is moderately contaminated water, 6.6 is injuriously contaminated by seawater, and 15.5 as highly contaminated by seawater. The ratios of $Cl/CO_3 + HCO_3$ charts prepared for both seasons (Fig. 14.5) show that most samples represent slightly, moderately, and injuriously pretentious by seawater intrusion. The higher impact is confined to the study area's central, southern, and western parts irrespective of seasons. Most of the injuriously affected locations during PRM alter to moderately and slightly contaminated zones during POM, suggesting impact due to recently recharged water due to precipitation (Senthilkumar et al., 2017).

Chadha Plots

Chadha (1999) plot has been cast off to realize the hydrochemical process activated in the study point. The same plot has been utilized by Thilagavathi et al. (2012) to determine the hydrochemical process activated in coastal aquifers. For understand the hydrochemical process and its dominance, the weak acid anions ($CO_3 + HCO_3$) and

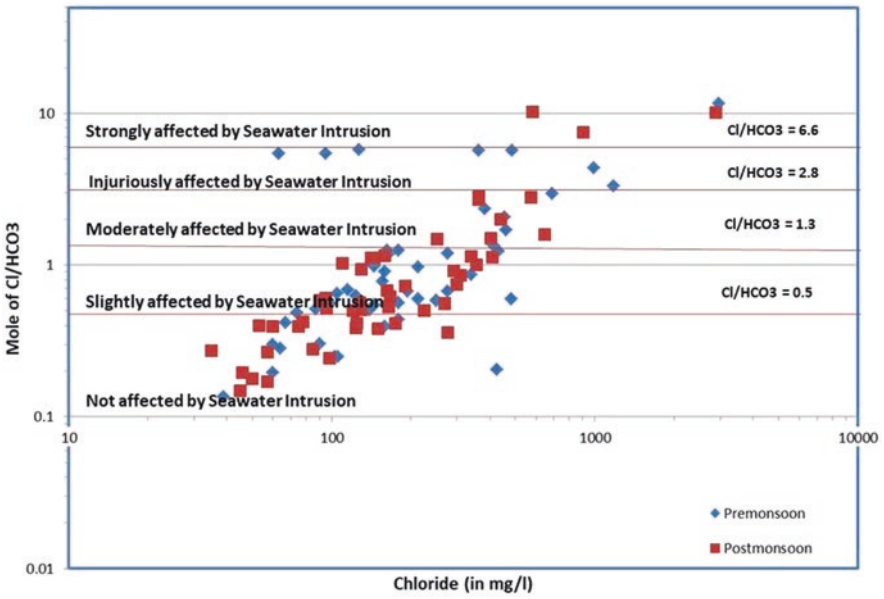

Fig. 14.5 Association of mole relation of Cl/HCO3 to chloride chart of the study area

strong acidic anions (SO_4 + Cl) were improved to one hundredth (milli-equivalent percentages) and articulated as the variance between alkali metals (Na + K) and alkaline earth (Ca + Mg) of cations. Chadha (1999) recommended hydrochemical processes for four quadrants of the graph, which can be stated as follows:

Field-1: Ca-HCO_3 kind- recharging waters.
Field-2: Ca-Mg-Cl kind- reverse ion-exchange waters.
Field-3: Na-Cl kind- seawater end member waters.
Field-4: Na-HCO_3 kind- base ion-exchange waters.

Figure 14.6 shows the maximum samples drop in Field-3 (Na-Cl) irrespective of seasons, signifying the waters show distinctive seawater mixing, generally controlled to southern and densely populated coastal areas (Senthilkumar et al., 2019). The majority of samples were collected in field 2 (reverse ion exchange field) next to this field, indicating that the waters are less well characterized and less common. However, it suggests that Ca + Mg ions are more abundant than Na + K ions, moreover due to the higher discharge of Mg and Ca from exposed bedrock mineral enduring or potentially due to reverse base cation-exchange processes of Mg + Ca into solution and succeeding Na adsorption on mineral faces (Karmegam et al., 2010).

Mg^{2+}/Ca^{2+} and Cl^{-}/HCO_3^{-} Ratios

Calcium ions predominate in freshwater, while magnesium ions predominate in seawater. As a result, the Mg^{2+}/Ca^{2+} ratio might be used as a marker for identifying the saltwater-freshwater boundary. Mondal et al. (2008) found that extremely short HCO_3/Cl and high Mg^{2+}/Ca^{2+} (molar fractions) suggest the modification of renewed groundwater to salty water. The presently studied sample ratios plotted in Fig. 14.7

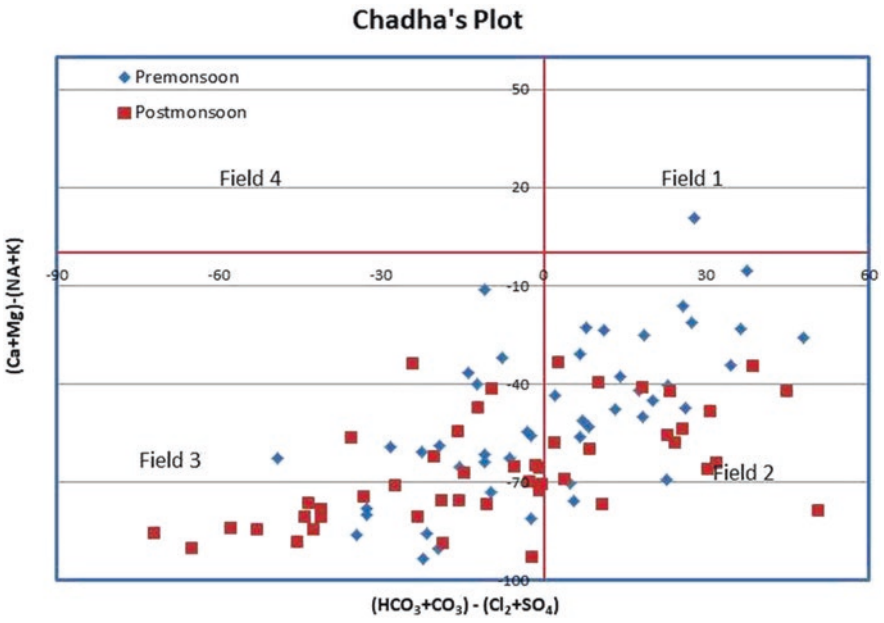

Fig. 14.6 Chadha's plot of the groundwater sample during PRM and POM seasons

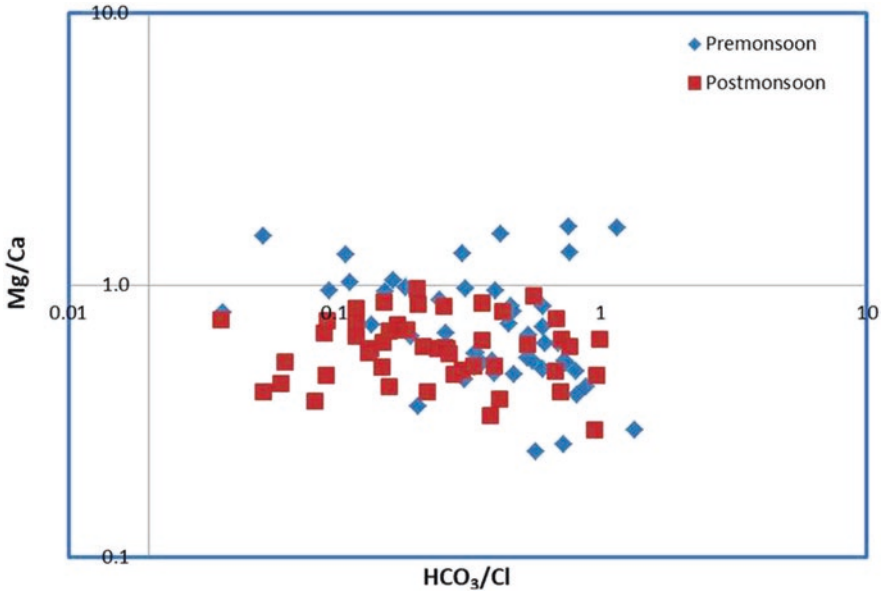

Fig. 14.7 Relationship of Mg/Ca vs Cl/HCO_3 ratio plot

designate Mg/Ca values varying from 0.1 to 1, with higher Ca ions in most samples. Fewer water samples were recorded with a higher ratio (> 1.0) during both seasons, suggesting higher Mg ions due to saltwater contamination (Senthilkumar et al., 2019).

4 Statistical Analysis

Correlation Analysis

The Pearson correlation matrix for 14 variables was prepared using SPSS 23 software during both seasons (Table 14.2). EC strongly and positively correlates with most parameters such as Ca^{2+}, $Mg^{2+,}$ Na^{+}, TH, Cl^{-}, and $SO_4^{2-.}$ The strong correlation of EC with Ca^{2+}, Mg^{2+}, Na^{+}, and poor correlation with nitrate, fluoride, and bicarbonate during PRM infers the leaching of salts, chemical weathering, and anthropogenic activity such as agricultural inputs, domestic seepages in the aquifers (Chidambaram et al., 2008; Srinivasamoorthy et al., 2009; Natesan et al., 2022). During PRM, a good correlation of ions like Na-Ca, Na-Mg, Na-Cl, Ca-Cl, Mg-Ca, Mg-Cl, Ca-Cl, and Na-SO_4, represents the leaching process of ancillary salts in the aquifer, chemical weathering of sodic feldspar, and anthropogenic influence of this area (Srinivasamoorthy et al., 2009). A noble correlation concerning Na and Cl ions suggests that the saline water incursion into the aquifer system (Senthilkumar et al., 2017). During the PRM seasons, seawater disturbance, chemical weathering, salt leaching, and anthropogenic impact are all significant contributors to the study area. The correlation matrix for 13 variables has been projected in Table 14.3 which during the POM seasons shows a good correlation with the ions of Na-K, Na-Cl, Na-Ca, Na-SO_4, Mg-Ca, and Ca-Cl, suggesting the ion-exchange developments under the effect of boosting water then deposition states of the minerals in the groundwater (Tyagi & Sarma, 2021). A decent correlation among Na-Cl suggests higher salinity during POM determined the common origin due to coastal incursion, free industrial effluents, and domestic sewage discharges of this area.

5 Conclusions

The current study emphasizes the impact of groundwater quality due to the urbanization in and around Ennore coastal area, Thiruvallur district of Tamil Nadu in South India. The land use pattern with respective total dissolved solids of this area indicates that the study area's southern and eastern coastal part is intensively affected by urbanization activity and overconsumption of groundwater resources. Regardless of the season, the groundwater was normally alkaline, had a hard to very hard water variety, and was brackish to saline. The supremacy of geochemical ions is present in arrange of $Na^{+} > Ca^{2+} > Mg^{2+} > NH_4^{+} > K^{+}$ for the cations and $Cl^{-} > SO_4^{-} > HCO_3^{-} > NO_3^{-}$ for the anions irrespective of seasons. The analytical

Table 14.2 Correlation matrix for groundwater chemical constituents during the pre-monsoon

	pH	EC	Na	NH_4	K	Mg	Ca	H_4SiO_4	HCO_3	F	Cl	SO_4	NO_3
pH	1.000												
EC	−0.162	1.000											
Na	−0.150	0.991	1.000										
NH_4	−0.179	0.067	−0.016	1.000									
K	0.002	0.389	0.301	0.382	1.000								
Mg	−0.183	0.958	0.936	0.151	0.358	1.000							
Ca	−0.095	0.842	0.811	0.031	0.375	0.814	1.000						
H_4SiO_4	0.061	−0.315	−0.333	−0.120	−0.034	−0.294	−0.061	1.000					
HCO_3	−0.152	0.462	0.420	0.072	0.380	0.379	0.401	−0.160	1.000				
F	0.082	0.048	0.051	−0.076	−0.059	0.038	0.106	0.047	0.033	1.000			
Cl	−0.157	0.972	0.973	0.074	0.320	0.960	0.833	−0.323	0.311	0.061	1.000		
SO_4	−0.098	0.721	0.702	0.036	0.387	0.623	0.435	−0.303	0.532	−0.023	0.561	1.000	
NO_3	−0.085	−0.207	−0.217	0.056	0.118	−0.237	−0.094	0.374	−0.302	−0.218	−0.206	−0.201	1.000

Table 14.3 Correlation matrix for groundwater chemical constituents during the post-monsoon

	pH	EC	Na	NH_4	K	Mg	Ca	H_4SiO_4	HCO_3	F	Cl	SO_4	NO_3
pH	1.000												
EC	−0.307	1.000											
Na	−0.141	0.703	1.000										
NH_4	0.180	−0.355	−0.406	1.000									
K	−0.162	0.389	0.647	−0.226	1.000								
Mg	−0.283	0.701	0.569	−0.286	0.394	1.000							
Ca	−0.139	0.641	0.640	−0.193	0.443	0.842	1.000						
H_4SiO_4	0.024	−0.346	−0.211	−0.076	−0.190	−0.315	−0.390	1.000					
HCO_3	−0.070	0.517	0.434	−0.352	0.321	0.431	0.408	0.133	1.000				
F	−0.218	0.764	0.981	−0.384	0.630	0.646	0.679	−0.263	0.430	1.000			
Cl	−0.264	0.067	−0.051	0.200	0.358	−0.024	0.042	−0.262	−0.197	−0.034	1.000		
SO_4	0.131	0.337	0.749	−0.352	0.576	0.430	0.534	−0.117	0.215	0.647	−0.162	1.000	
NO_3	−0.274	0.070	−0.048	0.187	0.363	−0.021	0.042	−0.255	−0.194	−0.030	0.998	−0.160	1.000

results of water samples disclosed that ionic sodium concentration was leading to cations and ionic chloride concentration was leading among the anions. The dominant hydrogeochemical facies fall in NaCl> Mixed CaMgCl>CaCl> $CaHCO_3$ during all seasons. The excess utilization of groundwater by the domestic utility and several industrial activities besides this region's southern and coastal regions has led to this water's poor quality condition. Various chemical ionic ratios like Cl/CO_3^+ HCO_3 ratio, Chadha's plots, and Mg^{2+}/Ca^{2+} again to Cl^-/HCO_3^- showed the seawater intrusion is present in southern, northwestern, and coastal parts of the focus area. According to correlation analysis of geochemical data with Na-Cl and other ions, the main governing variables of groundwater in the research area are saltwater intrusion, anthropogenic influences, and secondary salt percolating. The analysis of land use patterns and groundwater quality finds that low groundwater quality exists in the study areas in highly urbanized zones.

Acknowledgments The first author would like to thank the University Grant Commission, New Delhi, for the financial support of the D.S. Kothari Postdoctoral Fellowship (Grant No.F.4-2/2006(BSR)/E.S./18-19/0006 dated 26/12/2018).

References

Agrawal, V., & Jagetai, M. (1997). Hydrochemical assessment of groundwater quality in Udaipur city, Rajasthan, India. In *Proceedings of National conference on dimensions of environmental stress in India* (pp. 151–154). Department of Geology, MS University.

APHA (American Public Health Association). (1998). *Standard methods for the examination of water and wastewater* (19th ed.). Public Health Association.

Appelo, C. A. J., & Postma, D. (2005). *Geochemistry, groundwater and pollution* (2nd ed.). Taylor and Francis.

Ayotte, J. D., Szabo, Z., Focazio, M. J., & Eberts, S. M. (2011). Effects of human-induced alteration of groundwater flow on concentrations of naturally occurring trace elements at water-supply wells. *Applied Geochemistry, 26*(5), 747–762. https://doi.org/10.1016/j.apgeochem.2011.01.033. ISSN 0883-2927.

CGWB. (2007). *Central ground water board, district groundwater brochure, Thiruvallur district, Tamil Nadu*. CGWB.

Chadha, D. K. (1999). A proposed new diagram for geochemical classification of natural waters and interpretation of chemical data. *Hydrogeology Journal, 7*(5), 431–439.

Chidambaram, S., Ramanathan, A. L., Anandhan, P., Srinivasamoorthy, K., Prasanna, M. V., & Vasudevan, S. (2008). A statistical approach to identify the hydrogeochemically active regimes in ground waters of Erode district, Tamilnadu. *Asian Journal of Water, Environment and Pollution, 5*, 123–135.

Chidambaram, S., Karmegam, U., Prasanna, M. V., & Sasidhar, P. (2012). A study on evaluation of probable sources of heavy metal pollution in groundwater of Kalpakkam region, South India. *Environmentalist, 32*, 371–382. https://doi.org/10.1007/s10669-012-9398-1

Driscoll, F. G. (1986). *Ground water and Wells* (2nd ed.). Johnson Division.

Gopinath, S., & Srinivasamoorthy, K. (2015). Application of geophysical and hydrogeochemical tracers to investigate salinisation sources in nagapatinam and Karaikal coastal aquifers, South India. *Aquatic Procedia, 4*, 65–71.

Gopinath, S., Srinivasamoorthy, K., Saravanan, K., Suma, C. S., Prakash, R., & Senthilnathan, D. (2016). Modeling saline water intrusion in Nagapattinam coastal aquifers Tamilnadu, India. *Modeling Earth Systems and Environment, 12*. https://doi.org/10.1007/s40801-015-0058-6

Gopinath, S., Srinivasamoorthy, K., Saravanan, K., Prakash, R., & Karunanidhi, D. (2019). Characterizing groundwater quality and seawater intrusion in coastal aquifers of Nagapattinam and Karaikal. South India using hydrogeochemistry and modeling techniques. *Human and Ecological Risk Assessment: An International Journal, 25*, 314–334. https://doi.org/10.1080/10807039.2019.1578947

Jiang, Y., & Yan, J. (2010). Effects of land use on hydrochemistry and contamination of karst groundwater from Nandong underground river system, China. *Water, Air, and Soil Pollution, 210*, 123–141. https://doi.org/10.1007/s11270-009-0229-z

Karmegam, U., Chidambaram, S., Sasidhar, P., Manivannan, R., Manikandan, S., & Anandhan, P. (2010). Geochemical characterization of groundwaters of shallow coastal aquifer in and around Kalpakkam, South India. *Research Journal of Environmental and Earth Sciences, 2*(4), 170–177.

Mondal, N. C., Singh, V. S., Saxena, V. K., & Prasad, R. K. (2008). Improvement of ground water quality due to fresh water ingress in PotharlankaIsland, Krishna delta, India. *Environmental Geology, 55*(3), 595–603.

Moquet, J. S., Crave, A., Jerome, V. S., Patrick, A., Elisa, B., Luc, C., Eduardo, L., Christelle, L., Alain, W. S. L. C., Rodrigo, P., Noriega, L., Vera, A., & Guyot, J. L. (2011). Chemical weathering and atmospheric/ soil CO_2 uptake in the Andean and Foreland Amazon basins. *Chemical Geology, 287*, 1e26.

Nagarajan, R., Rajmohan, N., Mahendran, U., & Senthamilkumar, S. (2010). Evaluation of groundwater quality and its suitability for drinking and agricultural use in Thanjavur City, Tamil Nadu, India. *Environmental Monitoring and Assessment, 17*, 1289–1308. https://doi.org/10.1007/s10661-0091279-9

Najib, S., Fadili, A., Mehdi, K., Riss, J., & Makan, A. (2017). Contribution of hydrochemical and geoelectrical approaches to investigate salinization process and seawater intrusion in the coastal aquifers of Chaouia, Morocco. *Journal of Contaminant Hydrology, 198*(2017), 24–36.

Narsimha, A., & Sudarshan, V. (2017). Contamination of fluoride in groundwater and its effect on human health: A case study in hard rock aquifers of Siddipet, Telangana State, India. *Applied Water Science, 7*, 2501–2512.

Natesan, D., Sabarathinam, C., Kamaraj, P., Mathivanan, M., Haji, M., Viswanathan, P. M., Chandrasekaran, T., & Rajendran, T. (2022). Impact of monsoon shower on the hydrogeochemistry of groundwater along the lithological contact: A case study from South India. *Applied Water Science, 12*(36), 10.1007/s13201-021-01538-7.

Piper, A. M. (1944). A graphical procedure in the geochemical interpretation of water analysis. *Transactions American Geophysical Union, 25*, 914–928.

Saravanan, K., Srinivasamoorthy, K., Gopinath, S., Prakash, R., & Suma, C. S. (2016). Investigation of hydrogeochemical processes and groundwater quality in Upper Vellar sub-basin Tamilnadu, India. *Arabian Journal of Geosciences, 9*, 372. https://doi.org/10.1007/s12517-016-2369-y

Selvakumar, S., Chandrasekar, N., Srinivas, Y., Selvam, S., Kaliraj, S., Magesh, N. S., & Venkatramanan, S. (2022). Hydrogeochemical processes controlling the groundwater salinity in the coastal aquifers of Southern Tamil Nadu, India. *Marine Pollution Bulletin, 174*, 2022. https://doi.org/10.1016/j.marpolbul.2021.113264

Senthilkumar, S., Balasubramanian, N., Gowtham, B., & Lawrence, J. F. (2014). Geochemical signatures of groundwater in the coastal aquifers of Thiruvallur district, South India. *Applied Water Science, 7*, 263–274. https://doi.org/10.1007/s13201-014-0242-2

Senthilkumar, S., Gowtham, B., Sundararajan, M., Chidamparam, S., Lawrence, L. F., & Prasanna, M. V. (2017). Impact of landuse on the groundwater quality along coastal aquifer of Thiruvallur

district, South India. *Sustainable Water Resources Management, 4*, 849–873. https://doi.org/10.1007/s40899-017-0180-x

Senthilkumar, S., Vinodh, K., Johnson, B. G., Gowtham, B., & Arulprakasam, V. (2019). Integrated seawater intrusion study of coastal region of Thiruvallur district, Tamil Nadu, South India. *Applied Water Science, 9*, 124.

Senthilkumar, S., Gowtham, B., Srinivasamoorthy, K., & Gopinath, S. (2021). Hydrogeochemical delineation of groundwater fitness for drinking and agricultural utilities in Thiruvallur district, South India. *Arabian Journal of Geosciences, 14*, 526. (2021). https://doi.org/10.1007/s12517-021-06547-z

Singaraja, C., Chidambaram, S., Prasanna, M. V., Thivya, C., & Thilagavathi, R. (2014). Statistical analysis of the hydrogeochemical evolution of groundwater in hard rock coastal aquifers of Thoothukudi district in Tamil Nadu, India. *Environment and Earth Science, 71*, 451–464. https://doi.org/10.1007/s12665-013-2453-5

Srinivasamoorthy, K., Nanthakumar, C., Vasanthavigar, M., et al. (2009). Groundwater quality assessment from a hard rock terrain, Salem district of Tamilnadu, India. *Arabian Journal of Geosciences, 4*, 91–102. https://doi.org/10.1007/s12517-009-0076-7

Srinivasamoorthy, K., Nanthakumar, C., Vasanthavigar, M., Vijayaraghavan, K., Rajivgandhi, R., Chidambaram, S., Anandhan, P., Manivannan, R., & Vasudevan, S. (2011). Groundwater quality assessment from a hard rock terrain, Salem district of Tamilnadu, India. *Arabian Journal of Geosciences, 4*, 91–102. https://doi.org/10.1007/s12517-009-0076-7

Tahaikt, M., Haddou, A., El-Habbani, R., et al. (2008). Comparison of the performances of three commercial membranes in fuoride removal by nanofltration. Continuous operations. *Desalination, 225*, 209–219. https://doi.org/10.1016/j.desal.2007.07.007

Thambidurai, P. (2017). *Effect of forest cover on groundwater recharge for sustainable river flow "Revitalization of Rivers in India – Draft policy recommendation"* (pp. 284–296). Isha Foundation.

Thambidurai, P., & Vazhacharickal, P. J. (2021). Wastewater irrigation and quality-practices, safe reuse and perspectives: Scenarios from urban agriculture production across railway gardens and farms across the Mumbai Metropolitan Region (MMR), India. In A. K. Tiwari, A. Kumar, A. K. Singh, T. N. Singh, E. Suozzi, G. Matta, & S. L. Russo (Eds.), *Water resources: Scarcity, contamination and management* (pp. 451–464). Elsevier Publisher.

Thilagavathi, R., Chidambaram, S., Prasanna, M. V., et al. (2012). A study on groundwater geochemistry and water quality in layered aquifers system of Pondicherry region, Southeast India. *Applied Water Science, 2*, 253–269. https://doi.org/10.1007/s13201-012-0045-2

Thivya, C., Chidambaram, S., Rao, M. S., et al. (2015). Assessment of fluoride contaminations in groundwater of hard rock aquifers in Madurai district, Tamil Nadu (India). *Applied Water Science, 7*, 1011–1023. https://doi.org/10.1007/s13201-015-0312-0

Todd, D. K. (1980). *Groundwater hydrology* (2nd ed., p. 535). Wiley.

Tyagi, S., & Sarma, K. (2021). Expounding major ions chemistry of groundwater with significant controlling factors in a suburban district of Uttar Pradesh, India. *Journal of Earth System Science, 169*. https://doi.org/10.1007/s12040-021-01629-8

USEPA. (1999). *Update of ambient water quality criteria for ammonia*. U.S. Environmental Protection Agency. EPA-822-R-99-014. pp. 153.

Vandenbohede, A., Courtens, C., & William de Breuck, L. (2010). Fresh–salt water distribution in the central Belgian coastal plain: An update. *Geologica Belgica, 11*(3), 163–172.

Chapter 15
Groundwater Contamination in Parts of Northwestern Hyderabad: A Hydrogeochemical and Geospatial Approach

Pothuri Ramesh Chandra Phani and Kanchi Rajendra Prasad

Abstract The northwestern part of Hyderabad is known to have its groundwater contaminated due to the influence of several industries. The area is a focal point for many educational institutes and residential gated communities; the required water quantum is increasing yearly. The groundwater is polluted due to the existence of industries for decades together. The present work focuses on groundwater contamination during the pandemic in Patancheru and its northern part covering 282 km^2 area in view of increasing urbanization which is 3 times more than that in 1985. The Patancheru area has been declared a "groundwater problem area" by the Central Pollution Control Board. Pre- and post-monsoon samples (n = 30), from the bore and dug wells, were collected adapting standard procedures and analyzed for major constituents such as cations like Ca^{2+}, Mg^{2+}, Na^{+}, K^{+}, and CO_3^{-}; anions like HCO_3^{-}, Cl^{-}, SO_4^{2-}, NO_3^{-}, and F^{-}; and metallic trace elements such as Bi, Co, Cr, Fe, Pb, Mn, and Ni. The Piper diagrams revealed highly mixed type groundwater. Geospatial plotting of trace metal concentrations reveals that a high concentration regime of heavy metals occurs around Patancheru and Pashamylaram areas. The physicochemical parameters show no correlation, which is attributed to erratically high heavy industrial contamination, lack of complete effluent treatment, insufficient recharge, poor sanitation, increasing civil constructions, and other anthropogenic activities than geogenic factors. From this investigation, it is opined that either recent COVID-19 lockdowns or excess precipitation have no influence on remediating the problem.

Keywords Groundwater · Contamination · Industrial effluents · Urbanisation

P. R. C. Phani (✉) · K. R. Prasad
Department of Geology, Osmania University, Hyderabad, India
e-mail: Ramesh.Pothuri@cyient.com

P. Thambidurai, A. K. Dikshit (eds.), *Impacts of Urbanization on Hydrological Systems in India*, https://doi.org/10.1007/978-3-031-21618-3_15

1 Introduction

The chemical quality of groundwater depends on several aspects such as (i) the amount and composition of recharging water, (ii) lithological assemblage, (iii) anthropogenic activity, and (iv) environmental conditions. These factors affect the geochemical mobility of certain constituents of the groundwater (Kumar et al., 2006; Palanisamy & Kavitha, 2010). Hydrogeochemical data plays a major role in the assessment of groundwater quality. The data is plotted in several geochemical diagrams to assess the quality and character (Rao, 2006; Raju, 2007; Rashid & Izrar, 2007; Niranjan Kumar et al., 2009; Venkateswara Rao et al., 2016; Rama Mohan et al., 2021). Groundwater is the prime resource as surface water sources have become scarce, and some water bodies are no longer potable due to brackishness or contamination. The increasing urbanization demands more quantum of water for drinking and domestic purposes. The ever-increasing population and, in turn, the spread of residential colonies and the conversion of agricultural lands to gated residential communities are making the situation worse. Groundwater is contaminated either by geogenic or anthropogenic factors or both. In some cases, geogenic factors significantly impact groundwater quality, especially in igneous terrains where lithology is homogenous. Still, in such cases, anthropogenic activities may contaminate the groundwater, where the industries exist, and their effluents are let out to the open environment, the imminence of groundwater contamination is high. Therefore, a periodical assessment of groundwater is inevitable in the areas where industrial effluents are released into the environment and in upcoming urban regions.

Hyderabad city is growing rapidly in all directions in terms of infrastructure and urbanization. The industrial zones, a few tens of kilometers away from the city in the past, are now merging into the growing city. One such area is the northwestern part of Hyderabad, engulfing the Patancheru Industrial Area (PIA). In this area, several industries are actively producing their products. The industries include aquaculture, automobile, batteries, bio-products, cement and concrete products, chemicals, cold storages, dairy, electrical and electronics, fly ash, food products, metal fabrication, machinery and mechanical equipment, mineral-based products, paints and pigments, pharmaceuticals, plaster of Paris, petroleum-polymer-plastic products, paper products, poultry, rubber, seed processing, stone polishing, tannery, textiles, wood products, etc. Due to the continuous release of industrial wastes and effluents for decades, the area has been exposed to pollutants that spread into surface waters as well as percolate into groundwater. In addition, the increased urbanization in this area due to manifold increase in population and the necessity for new livable areas has drastically disturbed the drainage system. PIA was established in 1962, with 56 acres containing 67 plots and 34 units. In due course of time, it grew rapidly since 1973 with the initiative of Andhra Pradesh Industrial Infrastructural Corporation (APIICC) in the united Andhra Pradesh. Currently, 500+ industrial units of small-medium- and large-scale groups are operating. The PIA has seen flamboyant development in the mid-1980s. As per the latest information, about 323 industries are currently actively running after the COVID-19 pandemic. The PIA

covering Patancheru, Pashamylaram, Indrakaran, Isnapur, Rudraram, etc. areas is the prime location where the focal point of industrial waste generation occurs. The groundwater of Patancheru and adjoining areas have been reported to contain toxic elements such as arsenic (As), bismuth (Bi), chromium (Cr), copper (Cu), iron (Fe), selenium (Se), and zinc (Zn) (Kumar et al., 1997). Although preventive measures are implemented, massive urbanization and industrialization severely damage natural resources such as soil, vegetation, surface, and groundwater. The two main streams in the area are Peddavagu and Nakkavagu, along with the other two, Chinnavagu and Pamlavagu, which remain dry whole through the year. However, they flow sometimes, with effluent water in seasons of increased precipitation than usual.

The government has implemented several remedial measures to control groundwater contamination in this area. However, the projects halted abruptly due to several reasons. The Central Industrial Effluent Treatment Plant (CETP) is located in the PIA, is not fully equipped or upgraded to the day-to-day technology, and is not efficient in treating different types of effluents. The final effluents not completely treated are openly released into the streams, causing toxic pollutants to the open environment and subsurface by percolation through fracture systems, contaminating the groundwater. Water is vital for the livelihood of human, animal, and plant life, its contamination will raise environmental imbalance. In areas of industrial contamination, the extent of damage will be more pronounced and have immediate percussions on the natural resources, especially the groundwater resources, as they have limited movement and flushing capacity. In India, groundwater contamination will be intense in regions of industrial contamination, as industrial waste material is often released into drainages, abandoned open wells, and lakes, which is point contamination and, in many cases, to open river systems.

During the last five decades, the northwestern part of Hyderabad witnessed a prominent growth in industries and urbanization. Many residential colonies, educational institutes of national importance, shopping centers, etc. have emerged in the recent past, engulfing and amidst the industrial area. The Patancheru area has been declared problematic for groundwater contamination. Owing to the presence of a variety of industries, the northwestern part of Hyderabad has been impacted by the industrial effluents contaminating the groundwater (Saibaba, 2005; Saibaba et al., 2007; Hussain & Prasad Rao, 2014; Johnson, 2016; Venkateswara Rao et al., 2016). The state and central governments have taken up several measures to attenuate the pollution. However, there has been no improvement in the quality of groundwater. This is because of several factors, such as inefficient or incomplete effluent treatment, negligence of industries in effluent disposal, reduced rainfall and recharge, excess groundwater drawdown due to an increase in an urban area, and so on. The groundwater of the northwestern part of Hyderabad is observed to contain very high concentrations of many ions and heavy metals such as arsenic (As), barium (Ba), cadmium (Cd), chromium (Cr), copper (Cu), iron (Fe), molybdenum (Mo), selenium (Se), strontium (Sr), vanadium (V), and zinc (Zn) (Rao et al., 2001; Govil et al., 2001). A plethora of diseases is developed by the people living in the PIA and its proximity (Reddy et al., 2011). A substantial amount of land in the peripheries of

major water bodies is subjected to encroachments by rampant constructions. The emergence of industries and other residential encroachments in the lake beds in the buffer zones has defeated the primary purpose of irrigation and the general ecosystem due to the release of industrial and domestic sewerage pollutants. The PIA is well-equipped for infrastructural development and urbanisation, but the sewerage system is poorly built, which is a vital basic means for properly channeling the effluents.

Considerable research has been published on the groundwater quality of other localities during the pandemic period (Patel et al., 2020; Selvam et al., 2020; Venkatcharyulu et al., 2020; Krishan et al., 2021; Rahimi et al., 2021; Shanmugamoorthy et al., 2021). However, the northwestern part of Hyderabad, although known as a groundwater pollution hot spot, has not been touched upon. This work focuses on account of chemical assessment of groundwater involving physicochemical parameters and some trace elements in the northwestern part of Hyderabad graphically and geospatially, along with a briefing on the pace of urbanization in this area. This investigation showed that no significant impact of pandemic and/or lockdowns occurred in the study area; the groundwater contamination continued to persist.

2 Location and Study Area

The study area lies between geographic coordinates 17°36′6.10″N; 78° 6′56.05″E and 17°29′43.05″N; 78°20′25.65″E (Fig. 15.1). The area falls in the Medak district of Telangana, which is geographically merged with the Hyderabad city. The study area falls within the Manjira river basin. The area has national institutes like the Indian Institute of Technology Hyderabad (IITH) at Kandi, GITAM University at Rudraram, Ordnance Factory at Edulamailaram, Toshiba Transmission &

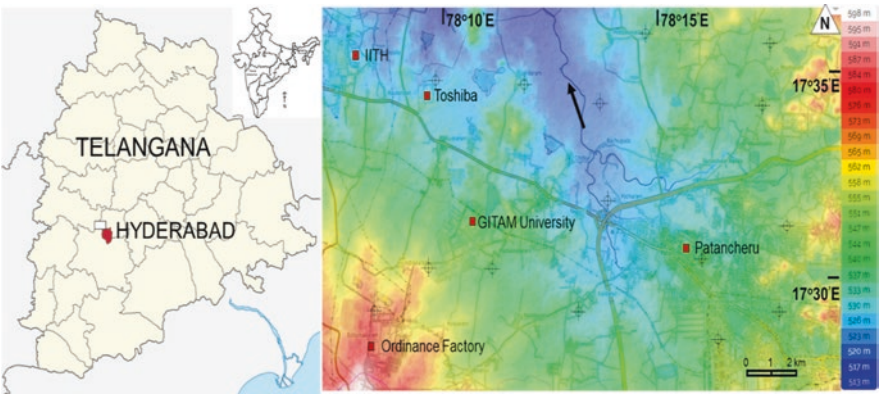

Fig. 15.1 Map showing study area and sampled well locations on elevation map (www.topographic-map.com). Arrow indicates stream course flow to meet Manjira river in the north

Distribution Systems (India) Private Limited at Degloor, and so on. In connection to the proposed regional ring road (RRR), the area is rapidly developing with many satellite townships and is soon expected to become a busy extended urban component of Hyderabad. At many locations in the selected area, the ground is being leveled for the purpose of civilian constructions such as private educational institutes, new industrial units, residential colonies, etc. As the area is leveled down, the individual watersheds are getting disturbed and disappearing, causing geomorphological imbalance. Many surface streams ranging from first order to fifth order exist in the area, which was leveled and used for agriculture, many of which are now being converted as real estate plots. Hence, the study area was chosen in such a way that it covers the span of urbanization.

3 Geology and Hydrogeomorphology

The study area is endowed with granites and granite gneisses of the Archaean age. The granites are massive, coarse to medium-grained, and occasionally display gneissosity. The granites are traversed by quartz and pegmatite veins ranging from a few cm to a few feet in width and extend for a few tens of meters. The quartz and pegmatite are rich in quartz and feldspar; however, non-mineralized. The granites are medium to coarse-grained, mesocratic studded with mafic enclaves. The granites are cut across by dolerite dykes in NE-SW, NE-SW, NNE-SSW, and EW trends. Occasionally, small laterite patches occur in the study area's western part. The granites are weathered and moderately fractured. The thickness of the weathered zone ranges from 6 to 20 m. More than two sets of joints trending in NNE-SSW and NNW-SSE are present. The streams are filled with assorted valley fill gravel and boulders. The streams are filled with densely grown acacia. The stream banks are filled with Quaternary alluvium comprising boulder to sand sized material. As observed in the stream sections and well inventory, the thickness of alluvium ranges from 5 to 60 m. The highest elevation in the study area is 598 m in the SW and western part, and the lowest is 510 m in the northern part towards the Manjira basin. Geomorphologically, the area comprises undulated terrain, including subtle mounds, hillocks, pediplain, forming a pediment-inselberg-pediplain complex. In the pediplain areas, the groundwater potential is more when compared to the pediment areas. The soil thickness ranges from 0.5 to 1.5 m. The dug wells (depth 8–22 m) are of low capacity, and tap water from shallow aquifers is controlled by weathered and fractured zones. In dug wells in weathered granitic and alluvial zones, the full recuperation is attained in 5–10 h, while it is 12–16 h and 15–45 h in laterite zones and hard rock terrains, respectively. The depth of groundwater in May 2020 ranged from 20 to 40 m, while it was raised to 10–20 m depth by November 2020 (CGWB, 2021). The area forms part of the Godavari main valley, having the Manjira River as the main tributary on the northern side of the study area. Several streams and tanks exist in the area. The total area under tank command is approximately 75,000 ha, land irrigated by canals, and life irrigation is 3400 ha. The area belongs to the

tropical savannah type. The average temperature ranges from 22 °C in winter and more than 45 °C in peak summer. The average annual rainfall is 800–900 mm. The humidity ranges from 55 to 75%, with an annual mean of 65%. The potential annual evaporation is 1940 mm.

4 Materials and Methods

Groundwater samples ($n = 30$) were collected in the second year of the COVID-19 pandemic during the 2021 lockdowns, and fieldwork has been carried out. The samples for pre- and post-monsoon from 15 locations were collected in March 2021 and December 2021, respectively. The area covered is about 282 km^2, with a sample interval is about 3 km. The sampling is carried out in areas where urbanization is spreading. The groundwater samples have been collected from dug wells, bore wells fitted with hand pumps, and submersible pumps. The sampling, preservation, and chemical analyses of samples have been carried out following the Central Pollution Control Board (n.d., 2007), and APHA (2012).

The physical parameters such as temperature and pH of water were measured using a normal mercury thermometer and digital pH meter (EI make, 1997 model). The EC and TDS were determined by the EC/TDS analyzer (CM183, Elico). The chemical methods were conducted at Lucid Laboratories Pvt. Limited, Hyderabad, accredited by the National Accreditation Board for Testing and Calibration Laboratories (NABL). For determining the total hardness (TH), calcium (Ca^{2+}), magnesium (Mg^{2+}), carbonate (CO_3^-), bicarbonate (HCO_3^-), and chloride (Cl^-). Sodium (Na^+), and potassium (K^+) were analyzed by the flame photometry method (CL345, ELICO). Sulfate was estimated by the turbidity method with the aid of Nephelo Turbidity meter (Model 132, Systronics). Nitrate was estimated by using the UV-VIS screen technique using a UV-VIS spectrophotometer (UV1201, Shimadzu). Fluoride is determined by the ion-selective electrode technique (Orion 290A+, Thermoelectron Corp.). The TDS was determined by calculating EC (Hem, 1991). The trace elements such as bismuth (Bi), iron (Fe), lead (Pb) and manganese (Mn) are determined by Atomic Absorption Spectrophotometer (AA6500, Shimadzu) while cadmium (Cd), chromium (Cr), cobalt (Co), copper (Cu), nickel (Ni), and zinc (Zn) were estimated using inductively coupled plasma (ICP) (1000IV, Shimadzu). The normalized inorganic charge balance method was adopted to obtain accurate results (Huh et al., 1998). For the majority of the samples, the ion exchange balance was <15% confirming the precision of analysis. The accuracy of analyses was controlled by including certified reference NIST1640a (National Institute of Standards and Technology, USA). The precision of analyses was checked by including blank and duplicate samples. Trace element distribution maps were constructed using ArcGIS (v10.3) software. Land use mapping, specific to built-up areas, was carried out using Google Earth imagery of the years 1985 and 2020. The built-up area polygons were digitized, and their area was measured from the latest imagery using ArcGIS (v10.3) and compared with the past imagery.

5 Results and Discussion

5.1 Increased Urbanization

A temporal-spatial assessment using a satellite (Google Earth) indicates there has been a drastic increase in urbanization in the northwestern part of Hyderabad. The satellite image of 1985 shows that there were certain very distant and sporadic habitations, especially the native villages, in this area. In 1985, there were no constructions north of Patancheru, and however, by the year 2020, the area had become like a concrete jungle (Fig. 15.2a, b). Ever since the Telangana state was separated from Andhra Pradesh in 2014, urbanization has taken a greater pace. Since the year 2015, there has been a plethora of urban development in northwestern Hyderabad, interfusing the adjacent rural areas. It is believed that industrialization causes pollution of the natural environment; however, domestic sewage alone can also remarkably increase pollution despite industrial effluents (Patel et al., 2020). The fast-growing residential colonies are also contaminating the study area groundwater due to incipient sewerage systems.

Several high-rise towers for residential purposes are coming up in the area, increasing the spatial spread of concrete jungles (Fig. 15.3a). Several granite quarries have also been opened up in the area to meet the requirement of construction material (Fig. 15.3b). Spatial analysis of study area (282 km^2) reveals that, in the year 1985, the urban area was about 68.78 km^2 (24.39%) which has been increased to 156.67 km^2 (55.55%) in 2021 with approximately an additional area of 78.9 km^2 (27.97%) with upcoming real estate plots in 2022. In other words, including upcoming residential plots, there has been a three-fold increase in urbanization. Prominent educational institutes have been developed in recent times. The residential colonies encroach into the borders of water bodies, thereby blocking the drainage system. The disused and/or abandoned metal and solid waste are dumped openly on the ground allowing certain toxic metals into the soil and therefrom to the subsurface aqueous systems (Fig. 15.3c, image source: Google Earth Photos). Due to the effluents released to the surface water bodies, the water has become unpotable irrespective of the amount of precipitation to dilute it. The effluents are released to first-order streams, making them severely contaminated (Fig. 15.3d). The mainstream of Nakkavagu, which had a valley of approximately 1 km width, now has been reduced to a few meters at a few locations and shortened as a sewerage pond at Rudraram village. The partially treated industrial effluents are directly released to the streams causing visibly severe contamination (Fig. 15.3e, f). The contamination of surface waters is being carried down to the groundwater, thereby causing heavy pollution in the groundwater. There is an increasing demand for drinking water in the study area. The available groundwater is not potable even at deeper depths (>400 m). As groundwater is not easily available, people depend on canned water. Recently, the number of mineral water plants has tremendously increased in the study area.

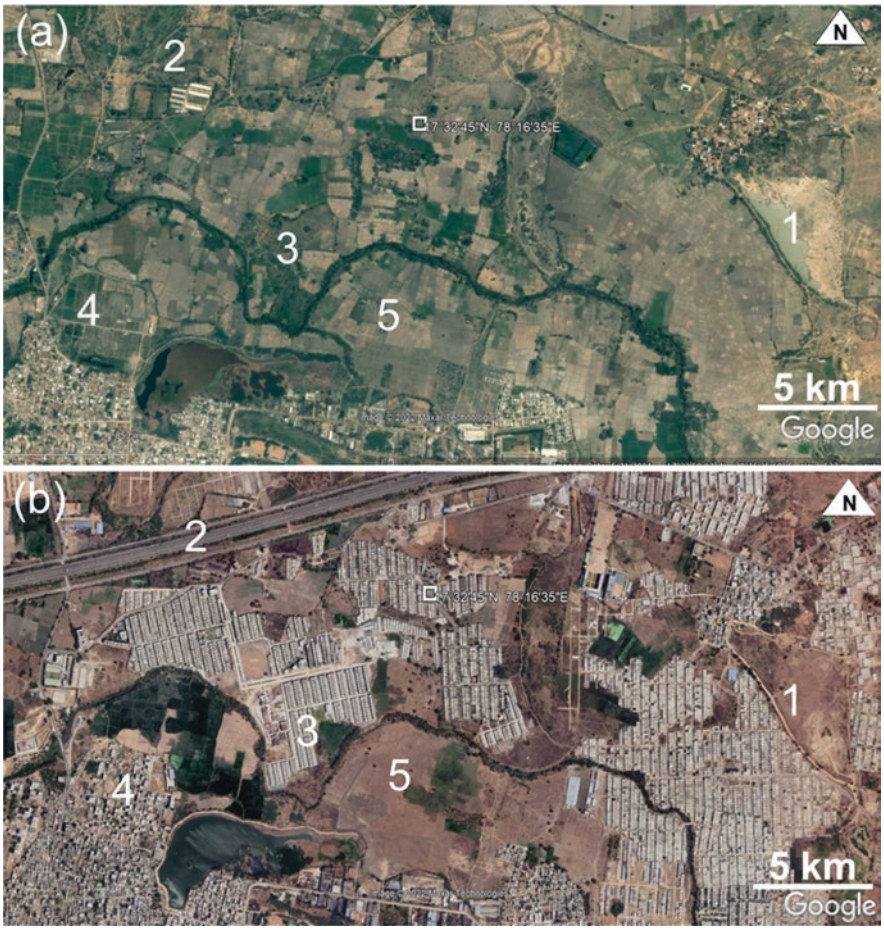

Fig. 15.2 Google Earth imagery showing the density of urbanization through time. (image source: Google Earth). (**a**) No constructions, with much of the area under cultivation in 1985, (**b**) highly dense constructions came up by 2020. 1. Water body in 1985, now dried up completely. 2. Development of outer ring roads. 3 and 4 Agricultural land replaced by residential colonies. 5 agriculture land turned to barren land. The imagery shows a part of study area reflecting intensity and increase in the built-up area

5.2 Physicochemical Characteristics

The anions in pre-monsoon and post-monsoon groundwater samples are shown in Tables 15.1 and 15.2, respectively. The pH is high, ranging from 7.42 to 8.9 in pre-monsoon samples and 73 to 8.88 in post-monsoon samples. The turbidity ranges from 4 to 8 in both pre- and post-monsoon samples. TDS ranges from 500 to 1700 mg/l and 820 to 1500 mg/l in pre- and post-monsoon samples. Total alkalinity ranges from 340 to 610 and 340 to 560 in pre- and post-monsoon samples,

Fig. 15.3 Field photographs of the study area showing various sources of groundwater contamination. (**a**) Growing urbanization in Patancheru near the outer ring road and solid waste dump in open land in the background and front ground, respectively. (**b**) An abandoned granite quarry with stagnant water at Mantrikunta (**c**) dumping of solid metal waste in open land. (**d**) Surface water contamination at Muthangi turned green and brackish due to influx of industrial effluents. (**e**) A higher order stream converted to a sewerage canal contaminated by industrial effluents at Rudraram. (**f**) Industrial effluents draining into a higher order stream at Patancheru

respectively. The total waste from animal farms, nitrogenous fertilizers, etc. are sources of nitrate in groundwater. Cations such as Ca and Mg are also in a higher range with a median of 110 and 44 mg/l in pre-monsoon samples and 140 and 48 mg/l in post-monsoon samples, respectively. Sulfate ranges from 15 to 230 mg/l for pre-monsoon samples and 70 to 230 mg/l for post-monsoon samples. The fluoride ranges from 0.86 to 5 in pre-monsoon samples, while in post-monsoon samples, it ranges from 0.9 to 1.2 mg/l. The samples show an affinity of anthropogenic influence rather than geogenic character when plotted NO_3 with conductivity

Table 15.1 Major ion composition of groundwater in pre-monsoon

Sample	Location	Easting	Northing	pH	C (µs/Cm)	T (NTU)	TDS (mg/l)	Total Alkalinity as CaCO3 (mg/l)	TH	Ca^{2+} (mg/l)	Mg^{2+}(mg/l)	Cl-(mg/l)	SO_4^{2-} (mg/l)	NO3 (As N) (mg/l)	TOC (mg/l)
W1	Patancheru	78°17′4.89″E	17°31′46.39″N	7.8	2340	5	1600	360	1010	290	110	110	230	8	11
W2	Lakdaram	78° 9′49.08″E	17°34′44.57″N	7.9	1180	4	800	480	980	205	54	55	115	8.7	9
W3	Patancheru	78°18′35.89″E	17°30′31.66″N	8.23	870	6	1560	390	165	49	21	450	15	11.9	8
W4	Patancheru	78°18′56.43″E	17°32′15.84″N	7.9	2870	5	1630	610	980	110	98	130	210	10	10
W5	Patancheru	78°17′22.22″E	17°29′52.51″N	7.6	1880	7	1500	570	700	155	148	250	130	8	6
W6	Janakampet	78°18′40.58″E	17°34′16.55″N	7.19	1580	8	1700	420	750	90	136	130	66	10	9
W7	IDA Pashamylaram	78° 9′33.71″E	17°31′49.35″N	7.42	1100	5	1400	500	450	75	80	200	77	18.1	7
W8	Inole	78°15′53.63″E	17°35′29.09″N	7.53	890	6	1100	400	330	230	38	60	50	11	5
W9	Pashamylaram	78°11′41.10″E	17°31′42.60″N	8.1	910	5	700	340	220	110	44	50	30	10	4
W10	Muthangi	78°14′35.99″E	17°32′40.00″N	7.9	879	4	500	440	230	230	50	50	25	11	4
W11	Indresamdarga	78°14′5.85″E	17°34′26.53″N	7.9	710	5	600	450	140	120	30	45	40	8	5
W12	Madaram	78°18′40.67″E	17°35′24.51″N	7.4	650	6	530	350	130	110	29	120	45	10	6
W13	Patighanpur	78°13′35.85″E	17°30′34.64″N	7.5	610	5	670	480	120	50	29	90	30	16	4
W14	Ordinance factory	78° 8′37.65″E	17°31′16.89″N	8.2	580	5	540	380	115	60	44	80	25	8	4
W15	Nandigama	78°14′5.85″E	17°34′26.53″N	7.8	720	4	510	380	130	130	30	80	60	8	4

Table 15.2 Major ion compositions in groundwater, post-monsoon

Sample	Location	Easting	Northing	pH	Conductivity (µs/Cm)	Turbidity (NTU)	TDS mg/l	Total Alkalinity (as CaCO3)	TH	Ca^{2+} mg/l	Mg^{2+} mg/l	Cl^{-}mg/l	SO_4^{2-}mg/l	Nitrates (As N)	TOC
W1	Patancheru	78°17′4.89″E	17°31′46.39″N	7.81	2240	5	1400	550	950	270	120	387	180	11	11
W2	Lakdaram	78° 9′49.08″E	17°34′44.57″N	7.68	2180	7	1100	500	700	140	89	210	139	23	10
W3	Patancheru	78°18′35.89″E	17°30′31.66″N	7.88	1100	7	1200	400	750	250	25	110	140	22	7
W4	Patancheru	78°18′56.43″E	17°32′15.84″N	7.76	2450	8	1100	450	780	220	130	389	210	7	13
W5	Patancheru	78°17′22.22″E	17°29′52.51″N	7.75	1280	6	1500	550	730	185	90	240	230	18	8
W6	Janakampet	78°18′40.58″E	17°34′16.55″N	7.81	2560	6	1350	400	820	210	45	160	130	18.7	14
W7	IDA Pashamylaram	78° 9′33.71″E	17°31′49.35″N	7.84	1370	7	1270	550	740	280	63	180	140	4.8	7
W8	Inole	78°15′53.63″E	17°35′29.09″N	7.77	2450	7	1300	530	770	170	42	230	150	8.9	8
W9	Pashamylaram	78°11′41.10″E	17°31′42.60″N	8.1	1100	5	1100	450	670	130	34	130	110	7	9
W10	Muthangi	78°14′35.99″E	17°32′40.00″N	7.3	560	5	980	560	780	120	35	120	130	8	10
W11	Indresamdarga	78°14′5.85″E	17°34′26.53″N	8.2	710	6	1020	390	700	90	40	110	80	11	8
W12	Madaram	78°18′40.67″E	17°35′24.51″N	7.5	440	5	990	420	600	110	65	50	85	17	8
W13	Patighanpur	78°13′35.85″E	17°30′34.64″N	7.3	570	4	820	510	580	140	50	90	90	9	12
W14	Ordnance factory	78° 8′37.65″E	17°31′16.89″N	7.6	820	7	930	340	710	110	40	110	110	10	13
W15	Nandigama	78°14′5.85″E	17°34′26.53″N	7.65+	650	7	1100	430	550	130	48	120	70	15	`4

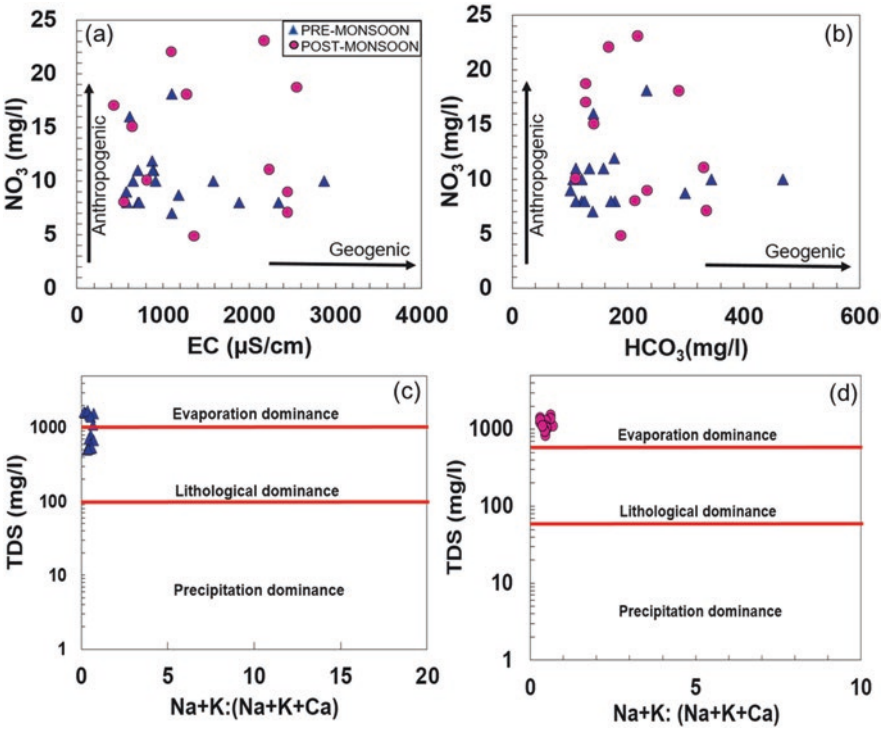

Fig. 15.4 Hydrogeochemical plots depicting anthropogenic sources of pollution and dominant character, (**a**) electrical conductivity versus nitrate, (**b**) bicarbonate (HCO_3^-) versus nitrate (NO_3^-). (**c**) Gibb's plot showing cations versus TDS in pre-monsoon samples. (**d**) Gibb's plot showing cations versus TDS in post-monsoon samples

(Fig. 15.4a) and with HCO_3 (Fig. 15.4b). Also, the major cations with TDS display a conspicuous non-geogenic character of groundwater contamination. The lithological dominance is negligible (Fig. 15.4c, d) (adopted from Brindha et al., 2020).

The cations and anion concentrations are plotted in Piper's trilinear diagram (Fig. 15.5). The samples showed the mixing nature of calcium chloride, magnesium bicarbonate, and sodium chloride type. While the cations are mixed, some samples show the dominance of Na, Mg, and Ca. The anions are also of similar behavior, showing no specific type. However, in some samples, bicarbonate and chloride are dominant. The mixed nature of groundwater in the area is attributed to the heavy influx of industrial wastewater, lack of recharge due to hard rock, and urbanization in the study area. The pre-monsoon samples are calcium chloride, magnesium bicarbonate, sodium chloride and mixed type, Mg, Ca, Na, and K type, bicarbonate, chloride, and some belong to no dominant type. The post-monsoon samples belong to the no dominant to chloride type.

The industries were dumping solid waste on their premises until the year 2002. The then Andhra Pradesh Pollution Control Board (APPCB) decided to mobilize the solid waste at a common hazardous waste treatment, storage, and disposal

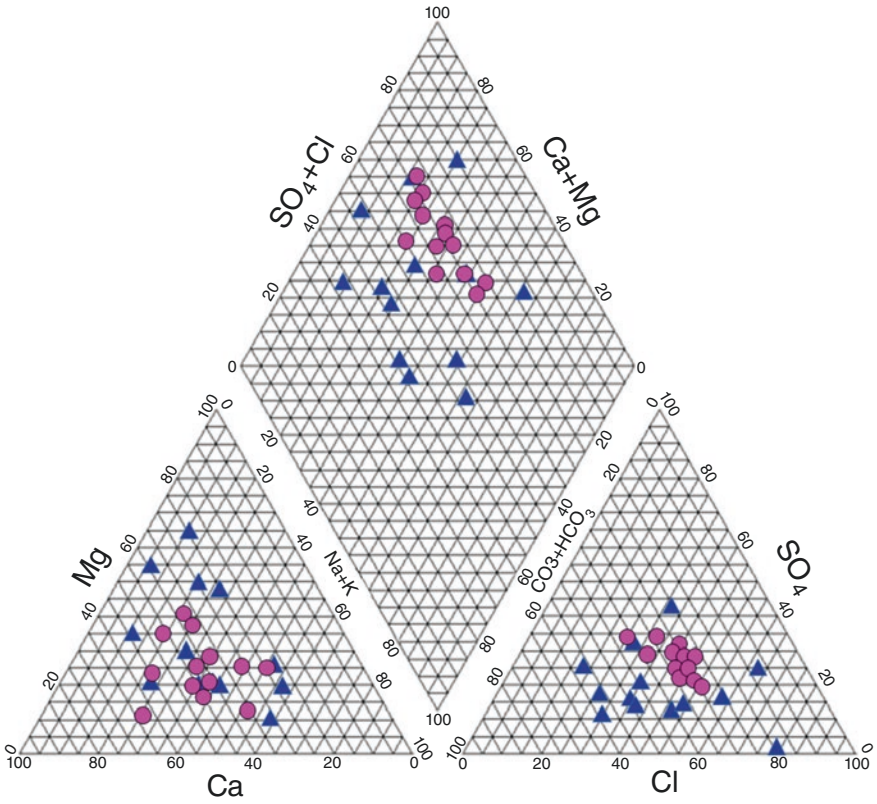

Fig. 15.5 Piper's trilinear diagrams for pre-monsoon and post-monsoon samples. Symbols as in Fig. 15.4

facility (TSDF) at Dundigal, RR district (APPCB, 2010). However, industries are still dumping the waste in open lands, causing pollution to the ground topsoil and allowing the toxic material to infiltrate into the subsurface waters. As a general phenomenon, nitrate is often naturally present in groundwater in feeble concentrations. Nitrate is sourced from anthropogenic factors such as domestic sewerage, industrial disposals, or agriculture. The correlation coefficients of various physicochemical parameters were determined to understand their interrelations. It is observed that nitrate shows a negative relationship with calcium (Ca^{2+}) and sodium (Na^{+}) while it shows positive correlation with magnesium (Mg^{2+}), potassium (K^{+}), bicarbonate (HCO_3^{-}), total alkalinity, sulfate (SO_4^{-}), chloride (Cl^{-}), and conductivity (EC) (Table 15.2). The pre-monsoon samples show a positive correlation between conductivity, TDS, and total hardness, while the rest of the physicochemical parameters show a negative correlation (Table 15.3). The correlation matrix for post-monsoon samples shows distinct positive correlations between conductivity and the majority of other parameters. The majority of physicochemical parameters are in a negative correlation with turbidity. The positive correlation decreases with parameters TDS,

Table 15.3 Correlation matrix of major cations and anions in groundwater, pre-monsoon (green, positive; red, negative)

	pH	EC	T	TDS	TA	TH	Ca	Mg	Cl	SO_4	NO_3	TOC	*F*
pH	1												
EC	0.26	1											
T	0.26	0.21	1										
TDS	0.20	0.75	0.58	1									
TA	0.33	0.54	0.05	0.38	1								
TH	0.05	0.87	0.14	0.67	0.47	1							
Ca	-0.31	0.33	-0.23	0.04	-0.09	0.46	1						
Mg	0.14	0.78	0.53	0.72	0.47	0.75	0.22	1					
Cl	0.33	0.14	0.42	0.59	0.15	0.01	-0.37	0.15	1				
SO_4	0.08	0.92	-0.01	0.59	0.44	0.88	0.48	0.66	-0.01	1			
NO_3	-0.43	-0.21	-0.02	0.12	0.20	-0.21	-0.39	-0.15	0.24	-0.26	1		
TOC	0.14	0.77	0.24	0.78	0.26	0.85	0.25	0.56	0.32	0.77	-0.09	1	
F	0.40	0.65	-0.08	0.30	0.58	0.39	-0.10	0.21	-0.04	0.53	-0.06	0.37	

Table 15.4 Correlation matrix of major cations and anions in groundwater, post-monsoon (green, positive; red, negative)

	pH	EC	T	TDS	TA	TH	Ca	Mg	Cl	SO_4	NO_3	TOC	F
pH	1												
EC	0.34	1											
T	0.06	0.42	1										
TDS	0.42	0.61	0.24	1									
TA	-0.06	0.21	-0.26	0.37	1								
TH	0.27	0.67	0.11	0.61	0.29	1							
Ca	0.60	0.56	0.28	0.67	0.35	0.63	1						
Mg	0.19	0.52	0.18	0.34	0.36	0.39	0.42	1					
Cl	0.12	0.77	0.33	0.56	0.42	0.69	0.60	0.84	1				
SO_4	0.06	0.61	0.30	0.68	0.48	0.65	0.61	0.67	0.81	1			
NO_3	0.46	0.09	0.12	0.24	-0.26	-0.08	-0.01	-0.01	-0.17	0.02	1		
TOC	-0.07	0.40	-0.14	-0.14	-0.13	0.41	0.06	0.27	0.29	0.25	-0.14	1	
F	-0.34	0.13	-0.08	-0.05	0.11	-0.11	-0.11	0.40	0.34	0.32	-0.44	0.27	1

TA, and TH prevail between the physicochemical parameters in both pre- and post-monsoon samples. This is attributed to the severe influx of effluents to the aquifers and a lack of adequate recharge (Table 15.4).

5.3 Trace Elements

The trace element distribution is a vital aspect to be noted in the study area (Table 15.5). As the industrial effluents are being let out into the open ground, the heavy metals are absorbed into the ground and interact with the aquifer, contaminating the groundwater. While Bi and Cd are not detected in the analysis, the other elements, namely, Cr, Fe, Ni, Pb, Mn, and Ni, are of higher range. Cr concentration ranges from 0.01 to 0.08 and 0.02 to 0.04 mg/l in pre- and post-monsoon samples, respectively. Fe content ranges from 1.12 to 1.61 and 1 to 1.84 in pre- and post-monsoon samples. Pb concentration ranges from 0.03 to 0.7 and 0.02 to 0.45 mg/l in pre- and post-monsoon samples. Mn content ranges from 0.24 to 0.68 and 0.23 to 0.5 in pre- and post-monsoon samples. Ni content is of negligible amounts in very few samples. The geospatial analysis gives a glimpse of the dispersion of heavy

Table 15.5 *Trace* element concentrations in pre-and post-monsoon groundwater samples

Sample	Location	Trace element concentration (mg/l)					
		Cr	Cr	Fe	Pb	Mn	Ni
Pre-monsoon							
W1	Patancheru	61	0.05	1589	0.08	0.54	0.005
W2	Lakdaram	12	0.02	1610	0.05	0.24	0.004
W3	Patancheru	32	0.01	1340	0.05	0.3	0.004
W4	Patancheru	60	0.08	1450	0.06	0.45	0.004
W5	Patancheru	58	0.04	1200	0.055	0.42	0.005
W6	Janakampet	59	0.03	1120	0.065	0.63	0.004
W7	IDA Pashamylaram	48	0.03	1578	0.035	0.68	0.004
W8	Inole	61	0.02	1330	0.056	0.32	0.004
W9	Pashamylaram	18	0.04	1290	0.08	0.33	0.003
W10	Muthangi	16	0.02	1120	0.04	0.44	0.003
W11	Indresamdarga	15	0.03	1340	0.03	0.3	0.002
W12	Madaram	21	0.04	1540	0.06	0.34	0.002
W13	Patighanpur	20	0.05	1490	0.7	0.33	0.003
W14	Ordnance factory	27	0.06	1340	0.07	0.45	0.002
W15	Nandigama	22	0.05	1440	0.06	0.54	0.002
Post-monsoon							
W1	Patancheru	62	0.03	1625	0.078	0.4	0.004
W2	Lakdaram	15	0.03	1298	0.045	0.5	0.004
W3	Patancheru	16	0.04	1190	0.047	0.23	0.004
W4	Patancheru	72	0.04	1745	0.066	0.32	0.004
W5	Patancheru	58	0.04	1840	0.07	0.34	0.004
W6	Janakampet	56	0.03	1745	0.06	0.45	0.004
W7	IDA Pashamylaram	12	0.03	1200	0.45	0.34	0.004
W8	Inole	11	0.03	1500	0.06	0.29	0.004
W9	Pashamylaram	23	0.02	1600	0.07	0.3	0.003
W10	Muthangi	20	0.03	1560	0.04	0.4	0.004
W11	Indresamdarga	21	0.04	1340	0.02	0.5	0.003
W12	Madaram	18	0.02	1700	0.04	0.4	0.003
W13	Patighanpur	18	0.04	1450	0.05	0.3	0.004
W14	Ordnance factory	16	0.04	1480	0.03	0.4	0.03
W15	Nandigama	14	0.02	1300	0.04	0.4	0.03

elements in groundwater in the study area. In the pre-monsoon samples, chromium, the chromium (Cr) content is higher on the western side of Patancheru and lower towards the northern part of the study area, i.e., the downstream side (Fig. 15.6a). In the post-monsoon samples, it shows the highest concentration in addition to Patancheru area, and the downstream portion is also enriched in Cr (Fig. 15.6b). The iron (Fe) content in pre-monsoon groundwater samples is higher in the NW part of the study area (Fig. 15.6c), and it shows higher concentrations on the western side of Patancheru in post-monsoon samples (Fig. 15.6d). The manganese (Mn) is higher

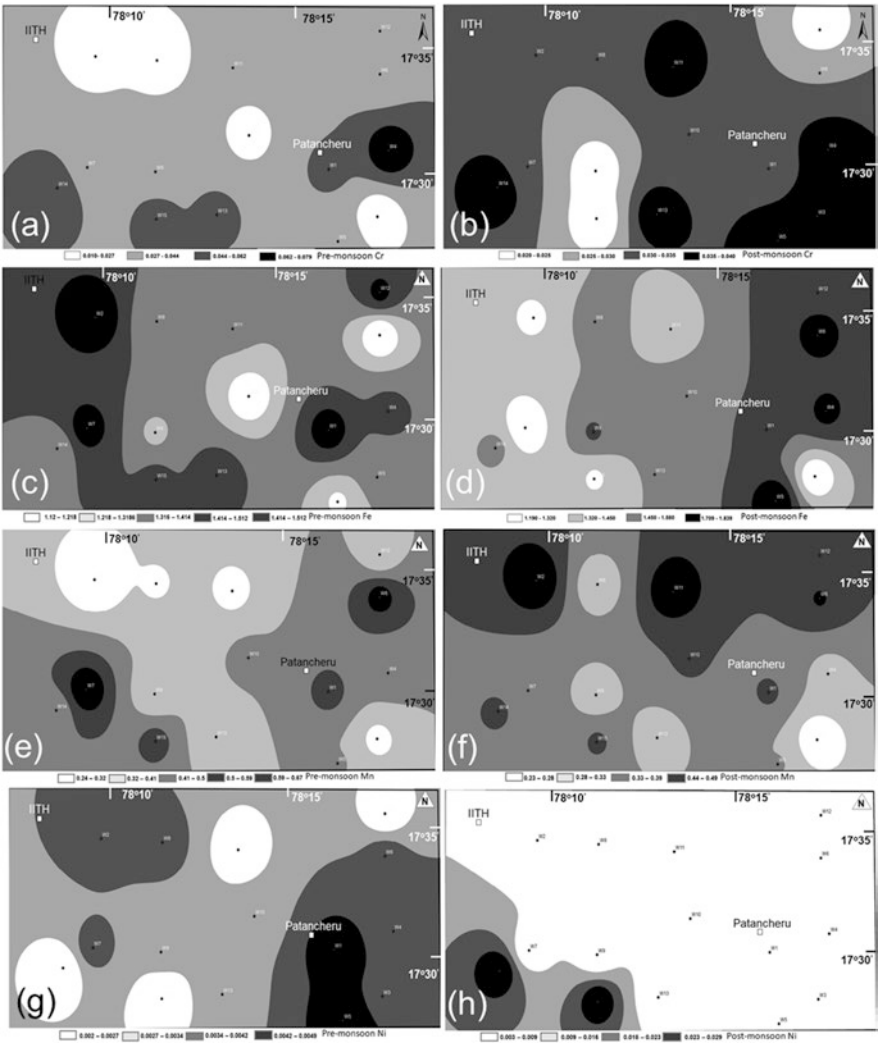

Fig. 15.6 Spatial distribution of trace elements. (**a**) Cr in pre-monsoon, (**b**) Cr in post-monsoon, (**c**) Fe in pre-monsoon, (**d**) Fe in post-monsoon, (**e**) Mn in pre-monsoon, (**f**) Mn in post-monsoon, (**g**) Ni in pre-monsoon, (**h**) Ni in post-monsoon. White and black zones represent the lowest and highest concentrations, respectively, with grey shades as intermediate ranges

in the SE and western part in pre-monsoon samples (Fig. 15.6e) while it is higher in the northern part (Fig. 15.6f).

The nickel (Ni) content is higher in the Patancheru area in pre-monsoon samples (Fig. 15.6g), while the post-monsoon samples show a higher concentration in the west of the Patancheru area (Fig. 15.6h). The Ni concentrations for most of the area are no signs in post-monsoon samples. The trace element distribution on overall shows that they are more concentrated in the Patancheru area, which is attributed to

the disposal of heavily contaminated industrial effluents to the ground, which infiltrated to interact with the aquifer and contaminate the groundwater.

5.4 Impact on Health

The people living within a radius of 5 km of PIA are reported to suffer from genetic disorders. The wastewater released from the industries, both treated and untreated, is being discharged to the open ground or roads or outside the industry campuses and finally ends either as a pool of sewerage or joining streams that are tributaries of the Manjira River course. The elevated concentrations of toxic heavy metals in the groundwater of the study area are causing disorders in chromosomes with thread-like cells called organelle. These organelles carry DNA and form genes that enter the body of biota upon consumption of contaminated groundwater. The field inventory in the villages during this study reveals that genetic disorders are up to 8% in people living within the proximity of 2 km radius from the industrial zones of Patancheru, Pashamylaram, and Rudraram and 2–3% away from the industrial area. Consultations with senior medical professionals revealed that the causative factor for the genetic damages is the presence of heavy metals in the groundwater, which are sourced from industrial effluents in the area. A survey conducted by the National Environmental Engineering Research Institute (NEERI), Nagpur, revealed that a plethora of ailments such as epilepsy, skin and throat problems, respiratory diseases, cancer, and paraplegia (paralysis of both the legs), while pregnant women are giving birth to still-born children. There are two common effluent treatment plants (CETP) in the Patancheru and Bollarum industrial areas. The tankers will transport the effluents to the CETP, from where the treated or semi-treated effluent water will be released to the surface drainage system. The CETPs do not comply with the standard operating procedures (SOP) of pollution control measures for instance, such as physical properties TDS, colour or pH (Reddy et al., 2011).

5.5 Contamination Schema

A schematic diagram pertaining to the study area has been drawn. The industrial effluents are let out for open ground, and natural stream courses are getting percolated to the subsurface through riverbeds and fractures in hard rock areas. The toxic elements are also mobilized and mixed with the groundwater. Thus, the toxic elements are, in turn, drawn out through groundwater pumping, upon consumption of which the people and environment are impacted (Fig. 15.7).

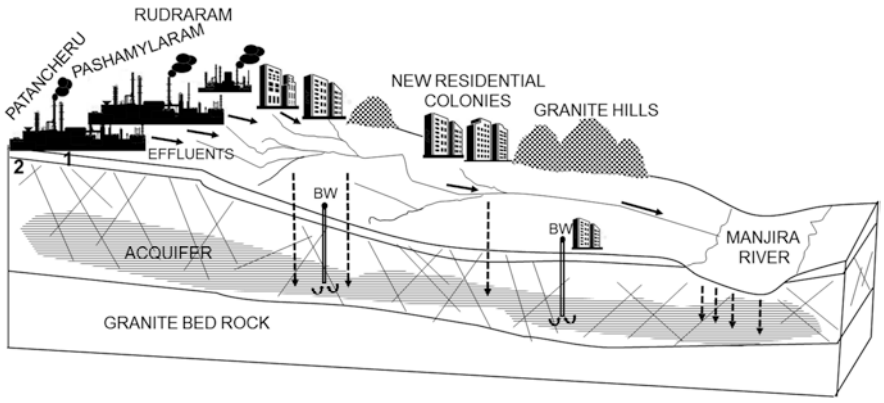

Fig. 15.7 Pictorial representation showing the process of groundwater contamination in the study area 1. Top layer containing mix of soil and weathered rock at places. 2. Fractured rock BW, bore well (not to scale)

6 Conclusions

This investigation showed that there has been a tremendous change in the landscape in the northwestern part of Hyderabad city in the past three decades. An intense urbanization three times more than that in 1985, in addition to the existing industries, has been noticed. The groundwater analysis (n = 30) revealed that a highly mixed type of groundwater exists in the area which is attributed to severe contamination. The geospatial analysis showed that the Patancheru and Pashamylaram industrial areas have a high concentration of heavy metals such as Cr, Fe, Ni, Pb, Mn, and Ni while Bi and Cd are not detected in the analysis. The physicochemical parameters show no correlation to each other owing to the influx of strong effluents of different compositions from multiple industrial sources, insufficient recharge, poor sanitation system, erratically increasing residential colonies irrespective of terrain morphology, and so many other anthropogenic activities. The geogenic factors have nil or negligible influence on the groundwater contamination. The natural drainage system is observed to be disturbed at a faster rate by the ever-increasing residential colonies. The lockdowns or temporary shutdown of industries due to recent COVID-19 pandemic or surplus rainfall in the last few years have no impact to improve the quality of groundwater which is already severely contaminated through decades of time.

Acknowledgments Google Earth is acknowledged for temporal imagery. The authors thank G. Ramesh, Environment Training and Research Institute (EPTRI), Hyderabad, for the necessary support. Field support by G. Ramakrishna and B. Srinivasa Rao, Cyient Limited is duly acknowledged. PRCP acknowledges the Department of Geology, Osmania University, for freelance research affiliation and Cyient Limited, Hyderabad, for computer facilities. This work did not receive any financial support from any agency.

Declarations This investigation has no conflict of interest with any person or organization.

References

APHA. (2012). *Standard methods for the examination of water and wastewater* (22nd ed.). American Public Health Association.

APPCB. (2010). *Final action plan for improvement of environmental parameters in critical polluted area of Patancheruv-Bollaram Cluster, Andhra Pradesh*. A.P. Pollution Control Board. 64p.

Brindha, K., Paul, R., Walter, J., Tan, M. L., & Singh, M. K. (2020). Trace metals contamination in groundwater and implications on human health: Comprehensive assessment using hydrogeochemical and geostatistical methods. *Environmental Geochemistry and Health, 42*, 3819–3839.

CGWB. (2021). *Ground water yearbook (2020–2021)*. Telangana state. http://cgwb.gov.in/Regions/SR/Reports/GWYB%20Telangana%202020-2021.pdf. https://doi.org/10.1007/s10661-011-2208-2

CPCB. (2007). *Status of groundwater quality in India, Part-I* (Groundwater quality series, GWQS/09/2006–2007). 262p.

CPCB. (n.d.). *Guide manual: Groundwater and wastewater analysis*. https://cpcb.nic.in/openpdffile.php?id=UmVwb3J0RmlsZXMvMjA0XzE1MjQ2NTA4OTNfbWVkaWFwaG90bzEyODI3LnBkZg

Govil, P., Reddy, G., & Krishna, A. (2001). Contamination of soil due to heavy metals in the Patancheru industrial development area, Andhra Pradesh, India. *Environmental Geology, 41*(3–4), 461–469. https://doi.org/10.1007/s10653-020-00637-9(0)

Hem, J. D. (1991). *Study and interpretation of the chemical characteristics of natural water* (US Geological Survey Water Supply Paper-2254:264) (3rd ed.). Scientific Publications.

Huh, Y., Tsoi, M. Y., Zaitiser, A., & Edward, J. N. (1998). The fluvial geochemistry of the river of Eastern Siberia-1 tributaries of Lena river drainage the sedimentation platform of the Siberia Craton. *Geochimica et Cosmochimica Acta, 62*, 1657–1676.

Hussain, M., & Prasad Rao, T. V. D. (2014). Toxic trace element contamination in ground water of Bollaram and Patancheru, Andhra Pradesh, India. *American Journal of Chemistry, 4*(1), 1–9. https://doi.org/10.5923/j.chemistry.20140401.01

Johnson, M. E. C. (2016). Heavy metals in the groundwater of Medak and Hyderabad districts of Telangana, India. *International Journal of Current Research, 8*(06), 32269–32277.

Krishan, G., Taloor, A. K., Sudarsan, N., Bhattacharya, P., Kumar, S., Ghosh, N. C., Singh, S., Sharma, A., Rao, M. S., Mittal, S., Sidhu, B. S., Vasisht, R., & Kour, R. (2021). Occurrences of potentially toxic trace metals in groundwater of the state of Punjab in northern India. *Groundwater for Sustainable Development, 15*, 100665.

Kumar, S. K., Pande, A. K., & Biksham, G. (1997). Toxic trace element pollution in groundwater around Patancheru and Bollarum industrial areas Andhra Pradesh, India. A graphic approach. *Environmental Monitoring and Assessment, 45*(1), 57–80.

Kumar, M., Ramanathan, A. L., Rao, M. S., & Kumar, B. (2006). Identification and evaluation of hydrogeochemical processes in the groundwater environment of Delhi, India. *Environmental Geology, 50*, 1025–1039. https://doi.org/10.1007/s00254-006-0275-4

Niranjan Kumar, K., Reddy, A. G. S., Mallikarjuna, R., Srinivas, R., & Varma, K. (2009). Preliminary investigations of groundwater quality in Hyderabad city, Andhra Pradesh, India. *International Journal of Chemical Sciences, 7*(1), 59–70.

Palanisamy, P. N., & Kavitha, S. K. (2010). An assessment of the quality of groundwater in a textile dyeing industrial area in Erode City, Tamil Nadu, India. *E-Journal of Chemistry, 7*(3), 1033–1039.

Patel, P. P., Mondal, S., & Ghosh, K. G. (2020). Some respite for India's dirtiest river? Examining the Yamuna's water quality at Delhi during the COVID-19 lockdown period. *Science of the Total Environment, 744*(140851), 1–16.

Rahimi, N. R., Fouladi-Fard, R., Aali, R., Shahryari, A., Rezaali, M., Ghafouri, Y., Ghalhari, M. R., Asadi-Ghalhari, M., Farzinnia, B., Gea, O. C., & Fiore, M. (2021). Bidirectional association between COVID-19 and the environment: A systematic review. *Environmental Research, 194*(110692), 1–20.

Raju, J. (2007). Hydrogeochemical parameters for assessment of groundwater quality in the upper Gunjanaeru River basin, Cuddapah District, Andhra Pradesh, South India. *Environmental Geology, 52*, 1067–1074.

Rama Mohan, K., Sravya Sai, G., Anjana, N., & Kishore, V. E. V. R. (2021). Assessment of leachate contaminated groundwater quality near Mandur solid waste dumping site, Bangalore. *Current World Environment, 15*(2), 194–203.

Rao, N. S. (2006). Seasonal variation of groundwater quality in a part of Guntur district, AP, India. *Environmental Geology, 49*, 413–429.

Rao, V. V. S. G., Dhar, R. L., & Subrahmanyam, K. V. (2001). Assessment of contaminant migration in groundwater from an industrial development area, Medak district, A.P, India. *Water, Air, and Soil Pollution, 128*(3–4), 369–389.

Rashid, U., & Izrar, A. (2007). Hydrochemical characteristics of groundwater in parts of Kushva-Yamuna basin, Muzaffarnagar district, UP. *Journal of the Geological Society of India, 69*, 970–982.

Reddy, A. G. S., Saibaba, B., & Sudarshan, G. (2011). Hydrogeochemical characterization of contaminated groundwater in Patancheru industrial area, southern India. *Environmental Monitoring and Assessment*, 1–23. https://doi.org/10.1007/s10661-011-2208-2

Saibaba, B. (2005). *Groundwater quality studies in Patancheru industrial area and environs, Medak District, Andhra Pradesh (AAP 2004-05)* (Central Ground Water Board (CGWB) Report). Ministry of Water Resources, Government of India.

Saibaba, B., Reddy, A. G. S., Niranjan Kumar, K., & Sudarshan, G. (2007). Effect on groundwater quality in Patancheru industrial area and environs, Medak district, AP, India. *Journal of the Indian Academy of Geosciences, 50*(2), 45–56.

Selvam, S., Jesuraja, K., Venkatramanan, S., Chung, S. Y., Roy, P. D., Muthukumar, P., & Kumar, M. (2020). Imprints of pandemic lockdown on subsurface water quality in the coastal industrial city of Tuticorin, South India: A revival perspective. *The Science of the Total Environment, 738*(139848), 1–7. https://doi.org/10.1016/j.scitotenv.2020.139848

Shanmugamoorthy, M., Subbaiyan, A., Elango, L., & Velusamy, S. (2021). Risk assessment of groundwater quality for drinking purposes during COVID-19 pandemic period around industrial areas, Perundurai, Erode, Tamil Nadu, India. *Research Square, 1*, 1–17. https://doi.org/10.21203/rs.3.rs-1000678/v1

Venkatcharyulu, S., Rathod, R., Kamala Raju, Y. (2020). Evaluation of groundwater quality of Bachupally, Nizampet and Pragathinagar Village. *E3S Web of Conferences 184*, 01105. ICMED 2020. https://doi.org/10.1051/e3sconf/202018401105

Venkateswara Rao, B., Kavitha, C., Murthy, N. N., & Lakshminarayana, P. (2016). Heavy metal contamination of groundwater in Nacharam industrial area, Hyderabad. *Journal of Indian Geophysical Union, 20*(2), 171–177.

Chapter 16
Spatio-temporal Dynamics of Groundwater Recharge in Dras Sub-Basin of Upper Indus River Basin, Western Himalayas

Suhail A. Lone and Ghulam Jeelani

Abstract Groundwater is one of the substantial sources of freshwater and plays an important role in sustaining the biodiversity of the Himalayas. However, with the limited availability of surface water resources due to global warming and anthropogenic practices, groundwater resource is under the severe threat of reduction and contamination. Hence, it becomes a prerequisite to study the stable isotope composition revealing the spatiotemporal dynamics of groundwater recharge in the Dras sub-basin of Upper Indus River Basin (UIRB), India, to understand the controls of physiographic and hydrometeorological processes. The isotopic values of groundwater showed wide spatial and temporal variance suggesting the dominant effect of physiographic and meteorological conditions. The slope and intercept of groundwater [$\delta^2H = 8.7(\pm1.8) \times \delta^{18}O + 26\ (\pm2.6)$ $R^2 = 0.81$; $p = 0.001$] are higher than local meteoric waterline and global meteoric waterline of precipitation but similar to snow and glaciers. The study indicated that groundwater recharge is mainly controlled by meltwater derived from high-altitude snow and glaciers. The study further suggested that climate warming, variation in precipitation pattern, form, and continuous glacier mass loss may negatively impact the groundwater resources of the region.

Keywords Climate change · Groundwater recharge · Himalayas · Indus River Basin · Snow melt

S. A. Lone · G. Jeelani (✉)
Department of Earth Sciences, University of Kashmir, Srinagar, India
e-mail: geojeelani@uok.edu.in

P. Thambidurai, A. K. Dikshit (eds.), *Impacts of Urbanization on Hydrological Systems in India*, https://doi.org/10.1007/978-3-031-21618-3_16

1 Introduction

Groundwater being a significant freshwater resource is vital for physical, chemical, and biological activities. However, recent global climate warming has laid acute stress on groundwater resources, mostly in dry climatic regions of the globe (Barnett et al., 2005; Mays, 2013; Gleeson et al., 2020; Lone, 2020; Lone et al., 2021b). Thus, the proper use of groundwater is needed for an hour (Taylor et al., 2013; Jeelani et al., 2020; Lone et al., 2021b). Identifying the spatiotemporal dynamics and groundwater recharge sources poses challenges due to large-scale spatiotemporal variance of groundwater recharge zones (IAEA, 1980; Abbott et al., 2000; Clark & Fritz, 1997; Lone et al., 2016; Jeelani et al., 2017; Beria et al., 2018; Shah & Lone, 2019; Jeelani et al., 2021a, b). Over the last 50 years, the application of stable isotopes to comprehend the variance of groundwater recharge has proved highly significant (Payne & Yurtsever, 1974; Gat, 1996; Gates et al., 2008; Costelloe et al., 2009; Lone et al., 2017; Keesari et al., 2017; Jeelani & Lone, 2019; Jeelani et al., 2021b; Cherry et al., 2020). The isotopes of oxygen (i.e., $\delta^{18}O$ values) and hydrogen (i.e., $\delta^{2}H$ values) are often used to comprehend the variance, source water, and residence time (Jeelani & Deshpande, 2017; Jeelani et al., 2018; Lone & Jeelani, 2019; Jeelani et al., 2020; Lone et al. 2021a, b). Numerous studies on groundwater recharge across the world based on water isotopes have been carried out over the last 60 years, focusing on estimating recharge, altitude, and sources of groundwater recharge, etc. (Lone et al., 2021a, b). However, the spatiotemporal variability and groundwater recharge sources in the Himalayas are yet to be systematically evaluated. Although groundwater is an important contributor to regional hydrology across the Himalayas, limited studies have examined the groundwater, particularly in Upper Indus River Basin (UIRB), India (Lone et al., 2020, 2021a, b). Hence, it becomes critical to study the stable isotope composition revealing the spatiotemporal dynamics of aquifer recharge in the Dras sub-basin of UIRB, India, to understand the controls of physiographic and hydrometeorological processes.

2 Study Area

The Dras sub-basin also known as the "Gateway of Ladakh" is situated within the geographic coordinates of latitude 34° 25′ 50″ N and longitude 75° 45′ 85″ E (Fig. 16.1). The sub-basin occupies an area of 3465 km^2 and is one of the coldest places in the world, situated along the Indus suture zone. The altitude of the Dras sub-basin varies from ~2700 m, asl to more than ~5500 m, asl. The Dras sub-basin experiences a continental Mediterranean climate (Köppen classification system) with an average annual precipitation of 550 mm from December to March, mostly in solid form. The rest of the months remain almost dry. The yearly average temperature observed in the Dras is 5.2 °C, with monthly maximum and minimum of 23 °C and − 23 °C in June and January, respectively. Westerlies and southwest

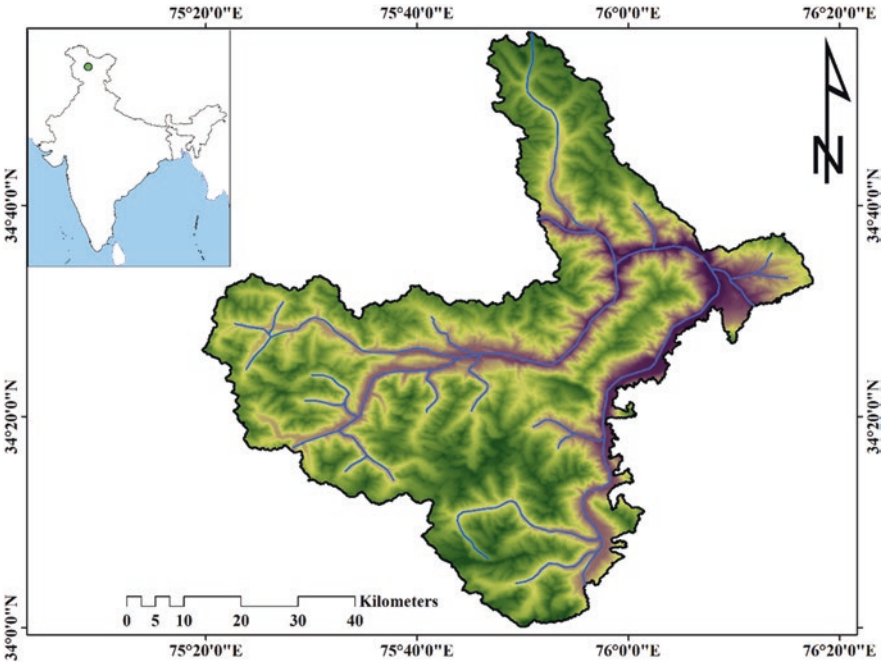

Fig. 16.1 Study area map of UIRB, Ladakh showing sampling sites on SRTM DEM of 30 m resolution downloaded from Earth Explorer website (https://earthexplorer.usgs.gov/). The blue on the map depicts the drainage network of the Dras sub-basin

monsoons mainly control precipitation in the Dras sub-basin. The major portion of precipitation received in solid form generates meltwater, which sustains the regional hydrology of the sub-basin. High altitude glaciers, alpine and moraine-dammed lakes, cold springs, and perennial streams are very common. Numerous glaciers are present in the Dras sub-basin, among which Machoi is a major glacier with an aerial extent of 5 km^2 lying at an altitude of ~4000–5500 m, asl. Meltwater from these glaciers generates groundwater recharge and runoff, hence playing a substantial role in the local and regional hydrology of the sub-basin.

3 Methodology

3.1 Sampling and Laboratory Analysis

Samples (n = 68) were collected from tube wells and cold springs across the study area for stable water isotopic analysis (Fig. 16.2). The water samples were collected on a spatial and temporal scale. The water samples were collected in 10 mL high-density polyethylene bottles (HDPE). The bottles were filled to the brim to avoid

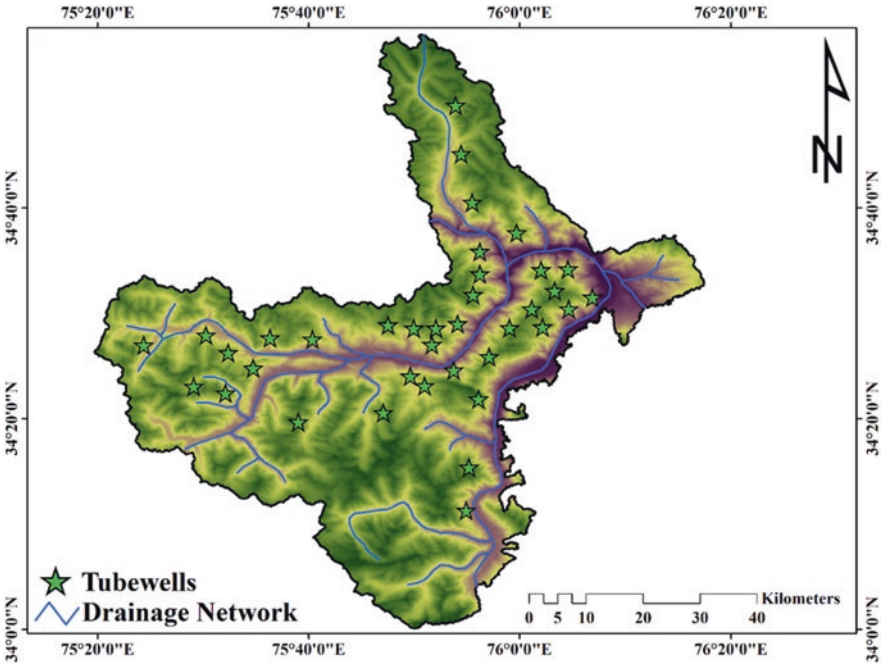

Fig. 16.2 Map of the Dras sub-basin presenting the locations of groundwater samples

evaporation and sealed in situ to avoid further contamination. All collected samples were analyzed at the Geosciences Division of Physical Research Laboratory (PRL), Ahmadabad (India). The relationship of oxygen ($^{18}O/^{16}O$) and hydrogen ($^{2}H/^{1}H$) was measured using an Isotope ratio mass Analyser (Delta V plus, Thermo Scientific) following the standard gas equilibration method. During the analysis, water (300 µL) was equalized with CO_2 for 960 minutes, and the equalized gas obtained was analyzed for the relations of $^{18}O/^{16}O$ or $^{2}H/^{1}H$ (Maurya et al., 2011). The accuracy of results obtained was better than 0.1‰ for $\delta^{18}O$ and 1‰ for $\delta^{2}H$.

4 Results and Discussions

4.1 Isotopic Variation in Groundwater

The $\delta^{18}O$ and $\delta^{2}H$ values of groundwater samples ranged from −14.6‰ to −11.4‰ and −115‰ to −80‰ with mean values of −13.3‰ and −93‰, respectively (Fig. 16.3). During the observation period, it was found that the isotopic values of groundwater are lower than the isotopic values of annual precipitation (Lone, 2020; Lone et al., 2021b). It was also perceived that the isotope values of groundwater are more similar to glaciers and snowmelt (Lone et al., 2021b) rather than precipitation

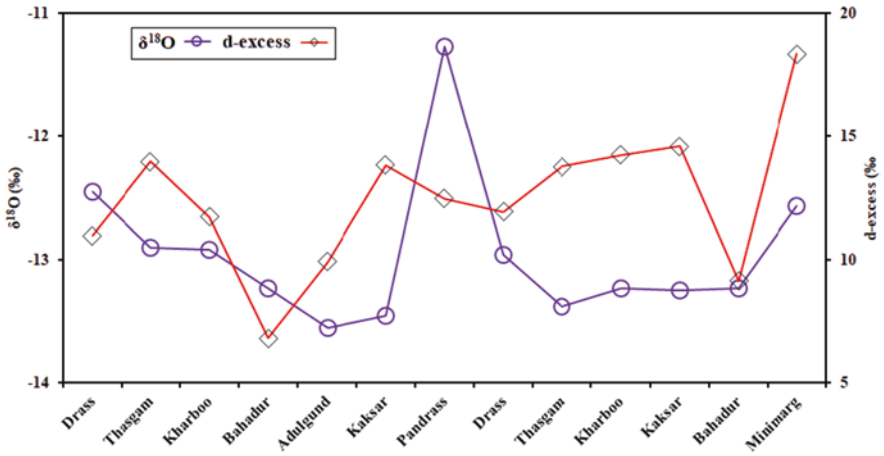

Fig. 16.3 Variance of $\delta^{18}O$ and d-excess values in groundwater across Dras sub-basin of UIRB, India

suggesting the dominance of meltwaters in controlling the groundwater recharge. The $\delta^{18}O$ values of groundwater vary significantly across the study area (Fig. 16.3). The depleted $\delta^{18}O$ values in groundwater were perceived in Minmarg (mean altitude: 3200 m, asl; $\delta^{18}O$: −14.6‰; Fig. 16.3) whereas enriched values were observed at Dras (mean altitude: 2730 m, asl; $\delta^{18}O$: −11.4‰). This discrete variance within the basin demonstrates the main role of micro-climate and topographic settings in amending the isotopic values of recharging waters. The groundwater samples across the Dras sub-basin showed noteworthy temporal variation. It was observed that groundwater samples collected in April have high $\delta^{18}O$ values ($\delta^{18}O$: −13.0‰ to −11.2‰ and $\delta^{2}H$: −102‰ to −76‰) than in August ($\delta^{18}O$: −13.8‰ to −12.4‰ and $\delta^{2}H$: −111‰ to −74‰), and October ($\delta^{18}O$: −14.6‰ to −13.8‰ and $\delta^{2}H$: −115‰ to −80‰) suggesting that with increasing melting season, the groundwater recharge is mainly controlled by waters derived from meltwater leads in lowering the isotopic signatures in November (Fig. 16.4).

4.2 Groundwater Recharge Sources

The slope of groundwater samples in the Dras sub-basin [$\delta^{2}H = 8.7(\pm1.8) \times \delta^{18}O + 26$ (±2.6) $R^2 = 0.81$; $p = 0.001$] is higher than the local meteoric waterline (LMWL) (Lone et al., 2019, 2021b) and global meteoric waterline (GMWL) (Fig. 16.5). The isotopic values ($\delta^{18}O$ and $\delta^{2}H$) in groundwater have been used to ascertain the sources of recharge and discharge (Gates et al., 2008; Costelloe et al., 2009; Lone et al., 2021b). The water collected in the Dras (mean $\delta^{18}O$: −12.3‰) has lower isotopic values ($\delta^{18}O$) than yearly precipitation (average $\delta^{18}O$: −11.7‰) but falls close to the snow and glacier data (Lone et al., 2021b) suggesting recharging water in this

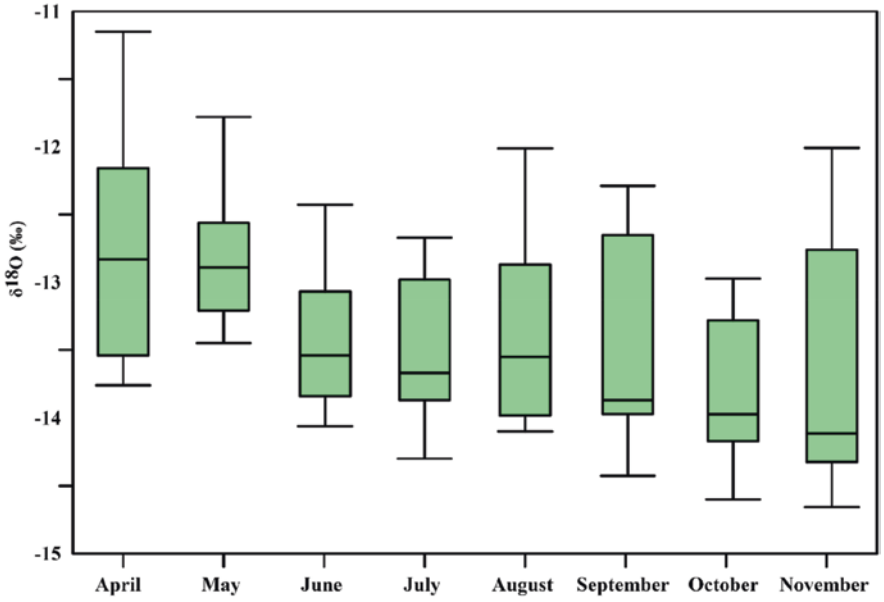

Fig. 16.4 Box and whisker plot showing the $\delta^{18}O$ values of groundwater samples collected in Dras sub-basin The $\delta^{18}O$ values tend to be higher in May than in September

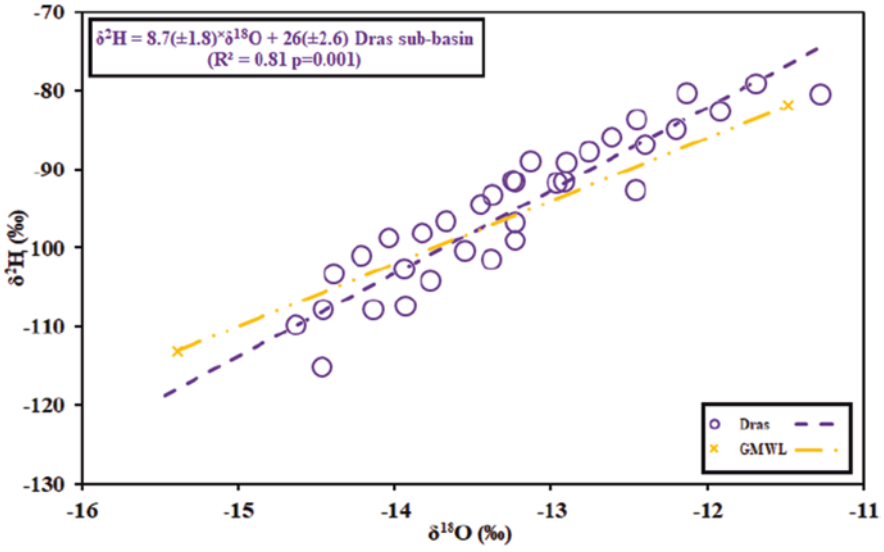

Fig. 16.5 Relation of the groundwater regression line with the global meteoric waterline. The plot depicts that the slope and intercept of groundwater samples are higher than the local meteoric waterline. (Lone et al., 2019, 2021b; Lone, 2020)

sub-basin is possibly controlled by water derived from meltwaters (snow and glacier), at higher altitude rather than the elevation at groundwater was collected. Hence, recharging water in the Dras sub-basin is a mixture of snow and glacial melt. The deviation of the regression equation slope also corroborates the above findings. Hence, the recharging water generated from high altitudes of the Dras sub-basin will be strongly affected by the variance in glacier cover and winter precipitation, with the least effect from rain.

4.3 Impact of Warming on Groundwater Recharge

In light of the discussion from the previous section, the aquifer recharge in the Dras sub-basin is governed by snow and glacier meltwaters. However, due to recent climate change, the annual variance in snow and the negative mass balance of the glacier have disturbed the accessibility of water for various physical, chemical, and biological activities. Recent global warming is expected to decrease winter precipitation and induce further glacial loss, early snow melting, and less groundwater recharge in summer (Eckhardt & Ulbrich, 2003; Lone et al., 2021a, b). Continuous increase in yearly maximum and minimum temperature and reduction in solid white mass during winter across the Western Himalayas (Lone et al., 2019, 2022a, b) may decline the volume of winter precipitation in the region. Numerous studies of the Himalayas have proposed that modification in surface and subsurface hydrology is typically due to changing climatic variables (Bibi et al., 2018; Azam et al., 2018; Singh et al., 2021; Lone et al., 2022a). These negative climatic variances are more noticeable in the Western Himalayas, where hydrological pools are dominantly controlled by the water instigating from the cryospheric cover (Lone, 2020; Lone et al., 2021b, 2022a, b). Variability in precipitation amount, type, and differential melting behaviors of cryospheric cover will negatively affect groundwater recharge. The present study highlights the role of meltwater controlling recharge in the Dras sub-basin, suggesting changes caused due to global warming will affect the groundwater recharge and, ultimately, the social and economic aspects locally and regionally.

5 Conclusions

We analyzed the spatiotemporal variance of $\delta^{18}O$ and $\delta^{2}H$ to understand groundwater recharge dynamics in the Dras sub-basin. Our results suggested that stable water isotopic signatures of groundwater vary spatially and temporally controlled by topographic and hydrometeorological conditions of the sub-basin. The slope and intercept of the groundwater regression line are higher than LMWL and GMWL of precipitation but similar to snow and glacier melt of UIRB, India. The results indicated meltwater derived from high altitudes dominates the groundwater recharge. The global climate warming observation suggests the dependence of recharge on

meltwaters obtained from snow and glacier melt in the Dras sub-basin. The study further indicated that variation in precipitation pattern, form, and shift in regional glacier mass might negatively influence the local and regional groundwater resources and, eventually, the social and economic aspects of the region.

References

Abbott, M. D., Lini, A., & Bierman, P. R. (2000). $\delta^{18}O$, δD and ^{3}H measurements constrain groundwater recharge patterns in an upland fractured bedrock aquifer, Vermont, USA. *Journal of Hydrology, 228*(1–2), 101–112.

Azam, M. F., Wagnon, P., Berthier, E., Vincent, C., Fujita, K., & Kargel, J. S. (2018). Review of the status and mass changes of Himalayan-Karakoram glaciers. *Journal of Glaciology, 64*(243), 61–74.

Barnett, T. P., Adam, J. C., & Lettenmaier, D. P. (2005). Potential impacts of a warming climate on water availability in snow-dominated regions. *Nature, 438*(7066), 303–309.

Beria, H., Larsen, J. R., Ceperley, N. C., Michelon, A., Vennemann, T., & Schaefli, B. (2018). Understanding snow hydrological processes through the lens of stable water isotopes. *Wiley Interdisciplinary Reviews: Water, 5*(6), e1311.

Bibi, S., Wang, L., Li, X., Zhou, J., Chen, D., & Yao, T. (2018). Climatic and associated cryospheric, biospheric, and hydrological changes on the Tibetan Plateau: A review. *International Journal of Climatology, 38*, e1–e17.

Cherry, M., Gilmore, T., Mittelstet, A., Gastmans, D., Santos, V., & Gates, J. B. (2020). Recharge seasonality based on stable isotopes: Nongrowing season bias altered by irrigation in Nebraska. *Hydrological Processes, 34*(7), 1575–1586.

Clark, I. D., & Fritz, P. (1997). *Environmental isotopes in hydrology*. Lewis Publishers.

Costelloe, J. F., Irvine, E. C., Western, A. W., & Herczeg, A. L. (2009). Groundwater recharge and discharge dynamics in an arid-zone ephemeral lake system, Australia. *Limnology and Oceanography, 54*(1), 86–100.

Eckhardt, K., & Ulbrich, U. (2003). Potential impacts of climate change on groundwater recharge and streamflow in a central European low mountain range. *Journal of Hydrology, 284*, 244–252.

Gat, J. (1996). Oxygen and hydrogen isotopes in the hydrologic cycle. *Annual Review of Earth and Planetary Sciences, 24*(1), 225–262.

Gates, J. B., Edmunds, W. M., Darling, W. G., Ma, J., Pang, Z., & Young, A. A. (2008). Conceptual model of recharge to southeastern Badain Jaran Desert groundwater and lakes from environmental tracers. *Applied Geochemistry, 23*(12), 3519–3534.

Gleeson, T., Cuthbert, M., Ferguson, G., & Perrone, D. (2020). Global groundwater sustainability, resources, and systems in the Anthropocene. *Annual Review of Earth and Planetary Sciences, 48*, 431–463.

IAEA (1980). Arid zone hydrology: Investigations with isotope techniques. In: IAEA (ed.) Proceedings of an Advisory Group Meeting, IAEA, .

Jeelani, G., & Deshpande, R. D. (2017). Isotope fingerprinting of precipitation associated with western disturbances and Indian summer monsoons across the Himalayas. *Journal of Earth System Science, 126*, 108.

Jeelani, G., & Lone, S. A. (2019). Establishing the effect of aridity on the stable isotopes ($\delta^{18}O$ and δD) of precipitation in cold desert, Ladakh. *International Journal of Water Resources in Arid Environment, 8*(2), 161–168.

Jeelani, G., Deshpande, R. D., Shah, R. A., & Hassan, W. (2017). Influence of southwest monsoons in Kashmir Valley, western Himalayas. *Isotopes in Environmental and Health Studies, 53*, 400–412.

Jeelani, G., Deshpande, R. D., Galkowski, M., & Rozanski, K. (2018). Isotopic composition of daily precipitation along the southern foothills of the Himalayas: Impact of marine and continental sources of atmospheric moisture. *Atmospheric Chemistry and Physics, 18*(12), 8789–8805.

Jeelani, G., Lone, S. A., Nissa, A., Mukherjee, A., & Deshpande, R. D. (2020). Sources and processes of groundwater arsenic mobilization in upper Jhelum basin, Western Himalayas. *Journal of Hydrology, 591*, 125292.

Jeelani, G., Lone, S. A., Nisa, A. U., Deshpande, R. D., & Padhya, V. (2021a). Use of stable water isotopes to identify and estimate the sources of groundwater recharge in an alluvial aquifer of Upper Jhelum Basin (UJB), western Himalayas. *Hydrological Sciences Journal, 66*(16), 2330–2339.

Jeelani, G., Lone, S. A., Lone, A., & Deshpande, R. D. (2021b). *Groundwater resource protection and spring restoration in Upper Jhelum Basin (UJB), western Himalayas* (p. 100685). Groundwater for Sustainable Development.

Keesari, T., Sharma, D. A., Rishi, M. S., Pant, D., Mohokar, H. V., Jaryal, A. K., & Sinha, U. K. (2017). Isotope investigation on groundwater recharge and dynamics in shallow and deep alluvial aquifers of Southwest Punjab. *Applied Radiation and Isotopes, 129*, 163–170.

Lone, S. A. (2020). *Hydrogeochemical and isotopic evidence of groundwater evolution and recharge in Indus Basin Ladakh (J&K India)*. Doctoral dissertation, University of Kashmir. http://hdl.handle.net/10603/314053

Lone, S. A., & Jeelani, G. (2020, November 16–30). Stable water isotopic evidence for the moisture source and composition of surface runoff in Ladakh, Upper Indus River Basin (UIRB). In *Proceedings of the 5th International Electronic Conference on Water Sciences*. MDPI. https://doi.org/10.3390/ECWS-5-07903

Lone, S. A., & Jeelani, G. (2022a, June 19–24). Assessing the hydrological processes controlling spatio-temporal patterns of snowmelt in high altitude arid-climatic environment of Upper Indus River Basin (UIRB), India. *Frontiers in Hydrology, Future of Water*.

Lone, S. A., & Jeelani, G. (2022b, June 19–24). Quantifying the dominance of source waters to river flow in high altitude arid climatic environment of Upper Indus River Basin (UIRB), western Himalayas. *Frontiers in Hydrology, Future of Water*.

Lone, S. A., Lone, A. A., & Jeelani, G. (2016). Characterization of groundwater potential of Sindh Watershed Western Himalayas. *Journal of Research & Development, 16*(2016) ISSN 0972-5407.

Lone, S. A., Jeelani, G., & Deshpande, R. D. (2017). Evaluating the sensitivity of glacier toclimate by using stable water isotopes and remote sensing. *Environment and Earth Science, 76*, 598. https://doi.org/10.1007/s12665-017-6937-6

Lone, S. A., Jeelani, G., Deshpande, R. D., & Mukherjee, A. (2019). Stable isotope ($\delta^{18}O$ and δD) dynamics of precipitation in a high altitude Himalayan cold desert and its surroundings in Indus river basin, Ladakh. *Atmospheric Research, 221*, 46–57.

Lone, S. A., Jeelani, G., Mukherjee, A., & Coomar, P. (2020). Geogenic groundwater arsenic in high altitude bedrock aquifers of Upper Indus River Basin (UIRB) Higher Himalayas. *Applied Geochemistry, 113*, 104497.

Lone, S. A., Jeelani, G., Mukherjee, A., & Coomar, P. (2021a). Arsenic fate in Upper Indus River Basin (UIRB) aquifers: Controls of hydrochemical processes, provenances, and water-aquifer matrix interaction. *Science of the Total Environment, 795*, 148734.

Lone, S. A., Jeelani, G., Deshpande, R. D., Mukherjee, A., Jasechko, S., & Lone, A. (2021b). Meltwaters dominate groundwater recharge in the cold arid desert of Upper Indus River Basin (UIRB), western Himalayas. *Science of the Total Environment, 786*, 147514.

Lone, S. A., Jeelani, G., Padhya, V., & Deshpande, R. D. (2022a). Identifying and estimating the sources of river flow in the cold arid desert environment of Upper Indus River Basin (UIRB), western Himalayas. *Science of the Total Environment, 832*, 154964.

Lone, S. A., Jeelani, G., Alam, A., Bhat, M. S., & Farooq, H. (2022b). Effects of changing climate on the water resources of Upper Jhelum Basin (UJB), India. In A. Mukherjee (Ed.),

Riverine systems: Understanding the hydrological, hydrosocial and hydroheritage connections (pp. 139–154). Springer Capital Publishing.

Maurya, A. S., Shah, M., Deshpande, R. D., Bhardwaj, R. M., Prasad, A., & Gupta, S. K. (2011). Hydrograph separation and precipitation source identification using stable water isotopes and conductivity: River Ganga at Himalayan foothills. *Hydrological Processes, 25*, 1521–1530.

Mays, L. W. (2013). Groundwater resources sustainability: Past, present, and future. *Water Resources Management, 27*, 4409–4424.

Payne, B. R., & Yurtsever, Y. (1974). Environmental isotopes as a hydrogeological tool in Nicaragua. In International Atomic Energy Agency (Ed.), *Proceedings of symposium on isotope techniques in groundwater hydrology* (Vol. I, pp. 207–216).

Shah, R. A., & Lone, S. A. (2019). Hydrogeomorphological mapping using geospatial techniques for assessing the groundwater potential of Rambiara river basin, western Himalayas. *Applied Water Science, 9*(3), 64.

Singh, V., Jain, S. K., & Goyal, M. K. (2021). An assessment of snow-glacier melt runoff under climate change scenarios in the Himalayan basin. *Stochastic Environmental Research and Risk Assessment, 35*(10), 2067–2092.

Taylor, R. G., Scanlon, B., Döll, P., Rodell, M., Van Beek, R., Wada, Y., Longuevergne, L., Leblanc, M., Famiglietti, J. S., Edmunds, M., & Konikow, L. (2013). Ground water and climate change. *Nature Climate Change, 3*(4), 322–329.

Chapter 17
Impact of Urbanization on Groundwater in Changing Climatic Scenario: A Case Study

Alifia Ibkar, Arunangshu Mukherjee, Nidhi Didwania, and Sneha Rai

Abstract The world is facing rapid urbanization in various aspects. It is predicted that India will have 50% of its population in urban centers by the end of 2030. Thus, understanding the urban characteristic to cope with reducing natural resources has produced a huge challenge. Groundwater, the primary drinking water source in many Indian cities, has faced a crisis of over-extraction and quality deterioration. Changing climatic condition has further added to the complexities of the urban hydrogeological condition. The present study is about two locations in the National Capital Region (NCR). In Haryana, Faridabad, one of the important urban centers of NCR, has witnessed a 32.5% decadal increase in population and rapid urbanization due to a considerable number of migrants. Manesar, one of the industrial townships of the NCR, has also witnessed intense urbanization due to industrial growth and migration. The average temperature of the area has increased by 2° with a corresponding increase in rainfall intensity along with a reduction in rainy days while maintaining the overall average rainfall of the area. The urbanization and associated industrialization resulted in groundwater level depletion at 0.7 m/year in parts of Faridabad and Manesar area and categorized as overexploited. The average groundwater electrical conductivity (EC) has increased. The impact also includes land subsidence in a few patches. The climate change-induced increased rainfall intensity and simultaneous urbanization have resulted in a reduction in infiltration. This has been further added by intensive extraction of groundwater to meet the essential requirements of the growing population. The chapter has discussed in depth the change in short-duration morpho-hydrogeological conditions due to overgrowth in the urban and industrial township.

Keywords Urbanization · Groundwater depletion · Climate change · Land subsidence · Rainfall intensity · Faridabad-Khoh Manesar

A. Ibkar · A. Mukherjee (✉) · N. Didwania · S. Rai
Manav Rachna Centre for Advance Water Technology & Management (MRCAWTM), Manav Rachna International Institute of Research and Studies (MRIIRS), Faridabad, India
e-mail: arunangshu.fet@mriu.edu.in

P. Thambidurai, A. K. Dikshit (eds.), *Impacts of Urbanization on Hydrological Systems in India*, https://doi.org/10.1007/978-3-031-21618-3_17

1 Introduction

Urbanization has been a global and significant socio-economic phenomenon that has occurred all over the world. Currently, about 55% of the world's population of 7.7 billion and about 35% of the Indian population of 1.4 billion live in urban areas, respectively (United Nations, 2018). The hydrogeological condition of the urban area widly differs from surrounding regional hydrogeological conditions due to urbanization and industrialization. Characterization of the urban hydrogeological condition of an area is significant for its resource management. The impact of urbanization on groundwater quantity and quality has been a growing concern for most urban areas. By 2030 half of the Indian population will be urban (United Nations, 2018). About 50% of the total requirement of urban water is drowned from aquifers (CGWB, 2021) where numerous small and medium towns completely depend on groundwater resources. Thus, the groundwater of urban areas is under great stress. As the second most populated country in the world, where groundwater is an essential resource for the sustainability of livelihoods, growth, and ecosystems, India is witnessing rapid groundwater depletion in many parts of the country (CGWB, 2021; Danger et al., 2021; Saha et al., 2018).

Further, changing climatic scenario has added to the complexities of the urban hydrogeological condition. Several institutions and individuals have studied the impact of changing climate in depth in the Delhi NCR area. Chauhan et al. (2022) worked on spatiotemporal distribution of rainfall and rainy day trends of the districts of Haryana State, India, during various seasons from the year 1901 to 2020. The study evaluated and analyzed the descriptive features of seasonal rainfall patterns to plan the well-organized usage of groundwater resources and sustainable groundwater management at the district level. Numerous investigations indicated an increase in the frequency of intense rainfall events in certain parts of the Indian subcontinent while it showed a reduction in the number of rainy days and total annual precipitation (Lal, 2003; Goswami et al., 2006; Dash et al., 2007, 2009; Sinha & Srivastava, 2000). Swain et al. (2022) assessed the groundwater quality of Gurgaon and Faridabad districts of Haryana with the help of geospatial and statistical methods. The study revealed the influence of human activities such as industrialization and rapid urbanization on the groundwater quality of these two areas. It is recommended that groundwater use for municipal water supply be managed to prevent the risk of health hazards. Dandge and Patil (2021) analyzed the spatial distribution of groundwater quality index with the help of remote sensing and GIS techniques. The research further addressed conducting frequent groundwater analysis to monitor the rate and type of contamination. Several eminent scholars, such as Chakraborty et al. (2014), Sati and Mohan (2017), and Mohan et al. (2011), carried out investigations over a span of 50 years on the impact of urbanization on urban climate, which identified urban settlement as a major cause of the rise in temperature in the past two decades. Garg et al. (2022) worked in Delhi NCR explaining a case study of the Faridabad city area on implications of unsustainable groundwater

use correlating the groundwater depletion issue with land subsidence, revealing that overextraction of groundwater, particularly from its unconsolidated alluvial deposits, makes the region prone to subsidence.

1.1 Location of Study Area

In the present study, apart from general urbanization consequences on groundwater resources, two growing urban and industrial areas of the National Capital Region of Haryana are considered to investigate the impact of urbanization on groundwater conditions (Fig. 17.1). The locations are the urban area of Faridabad and Manesar of Gurgaon District, Haryana, India. Khoh (76°55′ 44″; 28° 21′ 15″) is situated in the foothill zone of residual Aravali hill near Manesar, having an area of 2 km^2 (200 ha), while Faridabad city lies between latitude 28°15′N to 28°30′N and

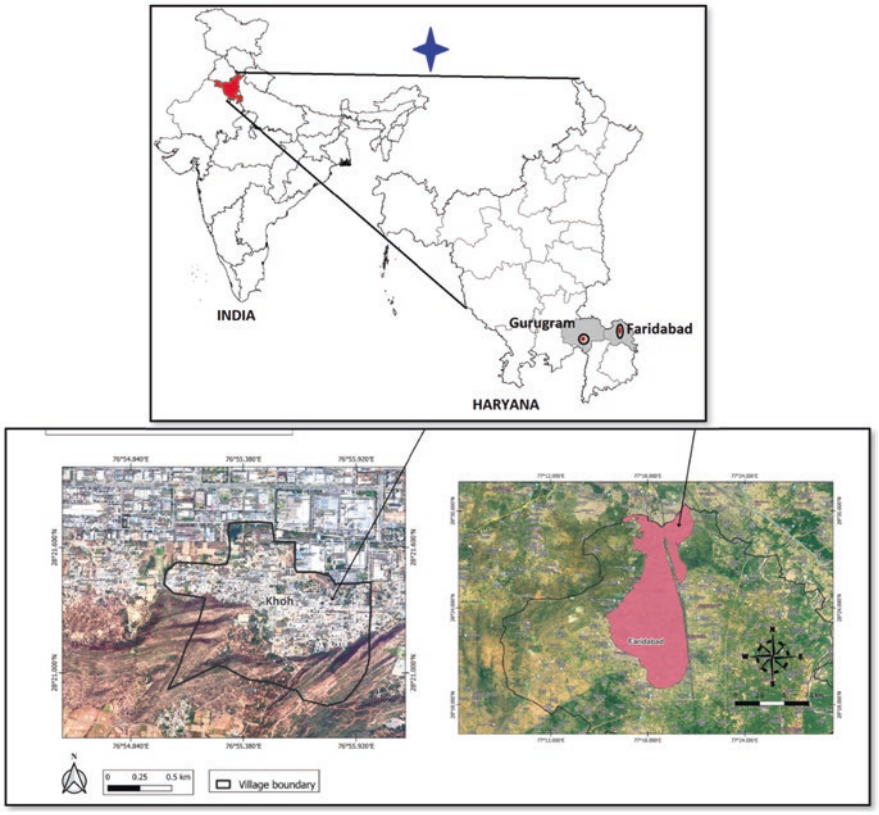

Fig. 17.1 Location map of two study areas, Khoh and Faridabad, Haryana

longitude 77°09′E to 77°30′E having 98.2% of the total urban population of the district concentrated in Faridabad Municipal Corporation area and covers 182 km^2.

2 Factors Influencing Urban Hydrogeological Conditions

Several factors influence the urban hydrogeological conditions more compared to the corresponding rural area. Though many of them are similar for both urban and rural areas, their intensity has been found to various degrees based on the density and extent of the urban area. In changing climatic scenarios, these factors became more relevant for urban areas due to their diverse land use and land cover pattern. The factors which influence the hydrogeological condition of an urban area can be divided into dynamic and static parameters. On the one hand, geology, macro-geomorphology, aquifer dimension, groundwater flow direction, transmissivity, and storativity remain static. On the other hand, population, micro-geomorphological features, land use land cover, rainfall pattern and intensity, runoff generation, rate of infiltration, groundwater abstraction, groundwater recharge, and its quality, surface water quantity, and quality are the main dynamic factors. These factors affect hydro-geological conditions differently in the urban area, particularly the recharge-discharge phenomena. The impact of these changes has been discussed in detail, considering the two study areas of Faridabad and Khoh, Manesar.

2.1 Geomorphology and Geology

Geomorphologically the area comes under the Yamuna sub-basin of the Ganga Basin. Bhuriya Nala is the main tributary that drains the Faridabad area. Other third to fourth-order streams that exist in the Faridabad area are Gochi Nala, Pakhal Nala, Jauhar Naala, Paliwaal Nala, Mehandwari Nadi, and Jair Nala which originate from Aravalli Hills and drain into either river Yamuna or disappear in the alluvial terrain. Faridabad city is bounded by Aravalli Hills in the west and the river Yamuna in the east. The altitude varies from 190 to 280 (Saini et al., 2017). The area has two distinct geomorphological units: the residual/denudational hills of Aravalli and the Yamuna Alluvial plains of lowland and upland. The Yamuna Alluvial plains can be further subdivided into active floodplain and older alluvial plains. A small portion of the area is also covered by Aeolian sand. The topography of the district is undulated plain, having linear ridges of quartzite running NS to NNE-SSW direction. The general slope of the area is NW to SE, west to east (CGWB, 2015; Saini et al., 2017). A large part of the Manesar area is occupied by scattered, isolated strike ridges of old rocks of Aravalli Mountain chain of Pre-Cambrian and alluvium sand of Recent to Subrecent origin. Geologically the Aravalli hills are folded meta-sedimentary rocks consisting of quartzite and argillite and belong to the Ajabgarh

Table 17.1 Stratigraphic succession of the study area with the corresponding geomorphology

Period	Age	Group/ formation	Geomorphic unit	Land use/ land cover	Description
Quaternary	Holocene	Newer Alluvium Disconformity and lacustrine deposits	Lowland (190–195 m RL)	Water use, sand quarrying, agriculture	Consists of unconsolidated interbedded, inter-fringing deposits of sand, clay, gravel, kankar, moderately sorted with alternation of fine fluvial sediments
	Late Pleistocene	Older Alluvium Unconformity and Aeolian deposits	Upland (190–200 m RL)	Agriculture, built-up land, brick kiln, forest, water bodies, wasteland	
Pre-Cambrian	Mid Proterozoic	Delhi Supergroup – Quartzites	Denudational Hills (220–280 m RL)	Wasteland, quarrying, forest, tourism	Massive gray colored with buff to brown leached surfaces at places, highly fractured and jointed. It is intruded locally by pegmatites and quartz veins and is interbedded with mica schist at places

After Saini et al. (2017) and Rahman et al. (2016)

Group of Delhi Supergroup of Mid Proterozoic age. The Ajabgarh Group of rock comprises mainly hard and massive bedded quartzite with local phyllitic intercalations (Table 17.1). These rocks are exposed as conspicuous ridges all along the western part of Faridabad and the southern part of Khoh, running roughly north-south in the direction. The ridge is locally known as Harchandpur-Badhkal Ridge and is formed of an anticlinal plunging fold. The fold axis trends along the N-S direction. The beds are steeply dipping between 50 and 80 degrees. The ridge is predominant in the south and subducted towards the north. Quartzites are light to dark gray to pinkish in color, hard, and highly jointed, having textural variations of fine-grained to gritty units. In Pali and Mohbatabad, the clipped ridge attains a height of more than 20 m. Marginal faults along the ridge produce 70–90-m-thick alluvial deposition along the foothill.

Quaternary alluvium unconformably overlies the Delhi Supergroup of rocks as 30–140 m thick over-burdened by loose unconsolidated sediments. On the basis of typical lithology, stratigraphic position, and continuity with the established sequence of the Ganga basin, the alluvium can be classified into Older and Newer Alluvium. The Newer alluvium disconformably overlies the Older alluvium. Older alluvium comprises horizontally bedded brown to yellowish clay-silt, brown, and gray sand. The sequence appears to gain thickness towards the east. It forms the main soil surface of the study. The Newer Alluvium is a 10–25-m-thick sequence of gray, very fine sand to silt, which disconformably overlies the Older Alluvium within the

Yamuna palaeo-banks in the lowland. It consists of Terrace Alluvium and Recent Alluvium. The Terrace Alluvium forms the bulk of Newer Alluvium and comprises loose, gray, very fine sand, slit, and clay. The Aeolian deposits comprise brownish, well-sorted, fine sand occurring as sand dunes on the sandy and slit-clay facies of Older Alluvium. Vertisol is a precious natural resource that is increasingly lost due to urbanization in Faridabad (Saini et al., 2017).

2.2 Hydrogeology

Hydrogeologically, Faridabad and Khoh areas can be divided into hard and soft rock terrains. The Khoh area is highly diversified in the mode of occurrence of groundwater, nature, and extent of the aquifer and its hydrogeological properties to groundwater flow characteristics under prevailing hydrodynamic and hydrochemical conditions. The hard and fractured quartzite up to a depth of 90 m produces a phreatic aquifer. At places, the lower part of hard and fractured rock forms a semi-confined aquifer, which remains in partial hydraulic connectivity with the phreatic aquifer. The groundwater level in the hard rock varies from 10 to 70 m in depth. The alluvial formation has a phreatic aquifer for the upper 60 m, and many a time produces semi-confined to the confined condition due to the presence of local clay horizon forming aquitard and aquiclude. Patchy occurrence of wind-blown Aeolian sand forms local phreatic aquifer. At places, perched aquifers of very local extent hanging on regional aquifers have been observed. In Faridabad, the urban area groundwater level in alluvial aquifer varies from water-logged conditions to deep as 60–70 m bgl. In alluvium, sand of various grades from the different potential aquifer zones. Shallow water levels have been observed towards Yamuna River. The water table has been found deeper along National Highway No 19, indicating that groundwater-stressed area has been formed traversing north-south due to heavy pumping along the highway caused by a dense network of tube wells due to the concentration of habitation and industries. The unconfined conditions prevail in alluvium and in weathered and jointed quartzites. In quartzites, it occurs in the weathered zones and interspaces within interconnected joints and fractures. The altitude of the water table ranges from 171.5 to 199.7 m amsl. It is observed that the groundwater flow is towards the central part of Faridabad from east and west. This phenomenon indicates heavy groundwater pumping along the National Highway for industrial and domestic purposes.

2.3 Long-Term Rainfall and Temperature

Environmental change-related investigations assume paramount significance these days because of its effect, which is observed to influence the rainfall pattern and temperature globally. According to the Intergovernmental Panel on Climate Change

(IPCC, 2007), future climate change is likely to affect agriculture, increase the potential hunger issues and the possibility of water scarcity, and lead to more rapid melting of glaciers (Jain & Kumar, 2012). It is very important to analyze the prevailing patterns in climatic conditions to interpret the impact of changing climate. On the basis of meteorological data, most of the distinguished patterns have been focused on rainfall and temperature indices (Chauhan et al., 2022). The study area, situated in the northern part of India, represents prevailing characteristics of humid subtropical to semiarid with generally dry winters extending from November to January (DES, 2014). The state of Haryana shows a normal rainfall of 558.02 mm (WRIS, 2022), whereas the normal rainfall for Faridabad and Gurgaon districts, in particular, was 521.4 mm and 583.2 mm, respectively, for the entire study period (Figs. 17.2 and 17.3). An analysis has been done to understand the Spatio-temporal change in the number of rainy days during different seasons for a duration of 120 years from 1901 to 2020 in several districts of Haryana. The study has revealed that the maximum number of rainy days was noticed during the monsoon season. The least number of rainy days were observed in post-monsoon, followed by winter and pre-monsoon season. Faridabad and Gurgaon are located in the southeastern parts of the Haryana state. A further recent analysis by IMD of the past 30 years of data (1989–2018) shows Faridabad district having 29–34 rainy days with an annual mean of 618.8 mm and Gurugram district having 25–29 rainy days with a mean annual rainfall of 529 mm (Guhathakurta et al., 2020). The rainfall data has been collected from WRIS (2022) and a decadal variation in rainfall has been analyzed for Faridabad and Gurgaon districts of Haryana.

Global climate projections, given inherent uncertainties, indicated several changes in India's future climate. One of the significant impacts of climate change will definitely include warming of 0.5 °C in overall India by the year 2030

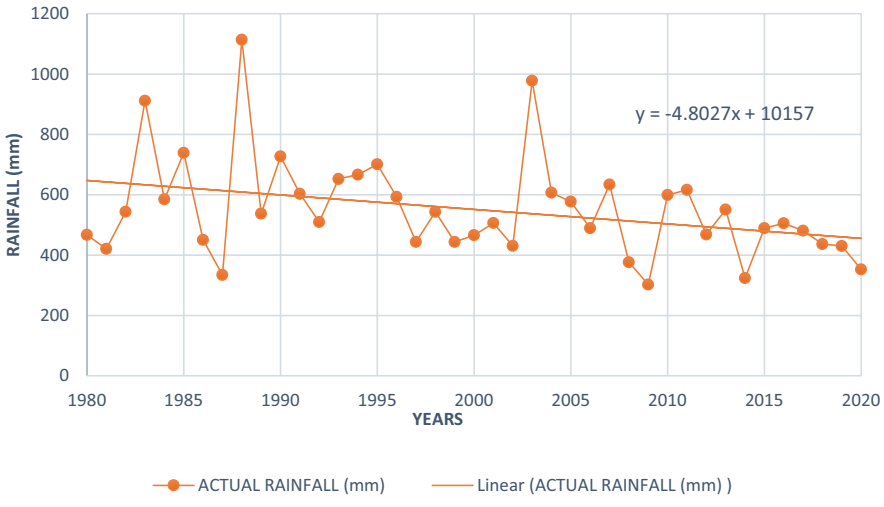

Fig. 17.2 Decadal variation in annual rainfall pattern of Faridabad during 1980–2020

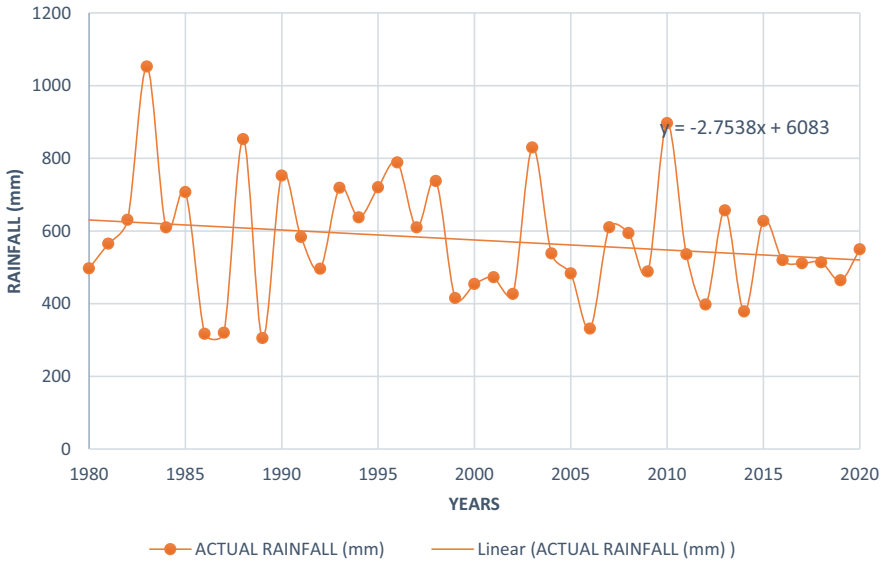

Fig. 17.3 Decadal variation in annual rainfall pattern of Gurgaon during 1980–2020

(approximately equal to the warming over the twentieth century) and warming of 2–4 °C by the end of this century, with the maximum increase over northern India (NIC, 2009). Eminent researchers have developed and analyzed the climatic indices based on long-term meteorological datasets of temperature and rainfall, which are further used to conduct a quantitative evaluation of the variations in weather patterns due to climate change (Duan et al., 2014; Talchabhadel & Karki, 2019; Ferreira et al., 2021; Teixeira et al., 2021; Chauhan et al., 2022). Chakraborty et al. (2014) addressed that urban settlement area, which mainly includes residential area and industrial area, shows much higher variation in temperature. In the year 2000, the industrial area shows a 22.3 °C temperature in winter and a rise of 10 °C in summer, which shows a 32.5 °C temperature. Observing the variation in 2010, it can be noticed that the industrial area is showing 24.2 °C in winter and 34.5 °C in summer. It can be concluded that the increase is around ±2 °C during the last 10 years in the urban areas. Sati and Mohan (2017) carried out investigations on Delhi NCR for a duration of 50 years to correlate the rapid change in land use land cover with the dramatic rise in surface temperature. The study found an almost 17-fold increase in the urban settlement areas from 1972 to 2014, including a 40% reduction in water bodies (from 221 km^2 in 1972 to 136 km^2 in 2014). The study based on model simulations has inferred that there is a change of 1.5 °C in the surface temperature due to land use land cover changes alone that have occurred because of urbanization over the same period. However, a study by Mohan et al. (2011) indicated a similar variation in temperature (2 °C) during 1906–2004. This study shows that the actual rise in temperatures that occurred in urban and its adjacent areas is more prominent in

the city areas (1.5–2 °C) compared to the increase in temperature due to global warming of 0.6–0.9 °C according to IPCC (2007). Thus, from the studies conducted by various scholars, it can be concluded that rapid urbanization has remarkably affected the urban climate in the last few decades.

2.4 Demographic Changes

As globalization and urbanization are becoming integral in the present scenario, half of the country's population will be living in urban areas by 2030 (United Nations, 2018). In India, natural population increase, economic growth, and rural-urban migration result in rapid urbanization and a dynamic transformation of peri-urban areas (Dikshit, 2011; Follman et al., 2018). At the current rate of growth, the urban population in India is estimated to reach a staggering 60 crores by 2030 (United Nations, 2018). According to Census 2011, as many as 53 cities in India had a million plus population. It is projected that more than 50% of the country's population will be urban by 2050 (WUP, 2018). Faridabad, one of the fastest-growing north-western Indian cities and part of the Delhi-National Capital Region (NCR), has followed an increasing trend in the urban population from 7.16% in 1971 to 79.51% in 2011 (Teotia & Kumar, 2015; Ranjan et al., 2021). Similarly, Gurgaon, which is situated adjacent to Delhi NCR has followed an increasing trend in the urban population from 10.62% in 1951 to 68.82% in 2011 (Fig. 17.4).

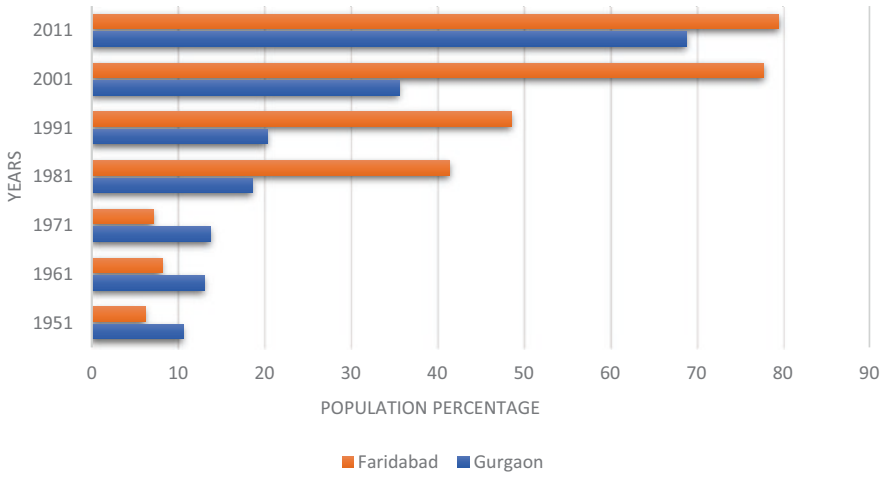

Fig. 17.4 Bar graph showing the decadal change in percentage of urban population to total population in Faridabad and Gurgaon

3 Discussions

The investigation has been carried out on the basis of both primary and secondary data. The study area has been demarcated using Google Earth to get the exact boundary and to identify the locations for sample collection. RS-GIS and Google earth has extensively used to compare and analyze land use, land cover change, and level of urbanization with time. The investigation of the quality of groundwater in the Faridabad and Khoh areas has been undertaken on the basis of samples collected from the locations and further multiple laboratory examinations. The locations of each sampling point were noted using GPS. The samples of groundwater have been collected, and laboratory experiments were done to measure EC (electrical conductivity), TDS (total dissolved solids), pH, nitrate, total hardness, alkalinity, fluoride, chloride, etc. using standard methods. A topographical survey was carried out to identify of elevation profile at the microlevel. Geophysical investigations of the Faridabad area were done to delineate the basement position, identify the freshwater saline water interface in the identified locations, and assess its hydrogeological suitability. Geophysical investigations at Manesar were done to locate community water well sites and artificial recharge sites by using Gradient Resistivity Profiling and Vertical Electrical Sounding. Borehole data were collected to understand the sub-surface lithology. Data so obtained were archived for use. The results were discussed as suitable in the following para.

3.1 Change in Land Use Landcover

3.1.1 Micro Morphometric Changes

The present-day Faridabad city covers an area of about 182 km^2, but during 1989 was restricted to only 67 km^2. In the last 33 years, the urban area has expanded about 275% by converting the peri-urban areas to urban areas (Fig. 17.5). This has not only changed the land use land cover (LULC) character of Faridabad but also significantly modified the micro morphometric features and altered the hydrogeological conditions in this area. Further detailed remote sensing and GIS study have revealed that within the core urban area of Faridabad city (67 km^2) itself, the LULC has changed a lot (Fig. 17.6). The built-up area has risen from 46% to 71% (including road) during last 33 years. At the same time area under waterbodies has reduced from 5 to <1%, and the area under vegetation and cultivation shrinked from about 31% to 20%. Further, the bare lands were also converted to built-up areas (Fig. 17.5).

Therefore, the density of built-up areas has increased by 154%. In general, runoff co-officiant for the paved area is considered 70%, but the increase of built-up area density will likely increase runoff and further reduce infiltration. This is considered one of the major causes of the generation of flash floods in old parts of the cities. Gradual reduction of open space produces larger runoff from the paved area (Table 17.2), and pre-existing drainage systems cannot carry the additional runoff

Fig. 17.5 Google map of the present (2022 in red 182 km^2) and past (1989 in blue 67 km^2) area under Faridabad city

load. Urban flash floods have become a major concern in many cities in India, including Faridabad. Streets get submerged for many hours or even days, and life becomes measurable in several parts of the city, particularly in the low-lying areas. The changing climate conditions aggravated such a phenomenon. This feature of urbanization needs detailed investigation and deliberation.

The estimated runoff generation from the core zone area of Faridabad city (67 km^2) considering the LULC character in 1989 and 2022 is given in Table 17.2. It reflects that runoff generation has increased from nearly 16 MCM to about 22 MCM when the quantum of rainfall remains nearly constant during this period. However, this estimation does not consider the increase in the intensity of rainfall due to the reduction of rainy days from nearly 32 days to about 25 days during the same period. It is predicted that the actual generation of runoff must be higher than what has been estimated. The nearly vertical bedding of folded Ajabgarh quartzite of study area has NNE-SSW strike. This produces typical micro fabric for runoff

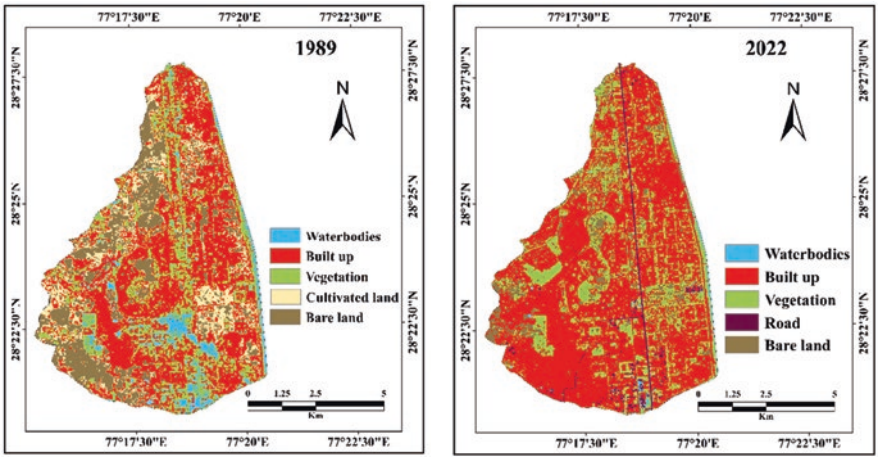

Fig. 17.6 Change in land use land cover from 1989 to 2022 in 67 km^2 Faridabad city area

Table 17.2 Estimation of runoff generation based on LULC between 1989 and 2022 in Faridabad

Class_Name	Coefficient of Runoff (%)	Area 1989 (m^2)	Area 2022 (m^2)	Runoff 1989 (m^3)	Runoff 2022 (m^3)
Waterbodies	0	3,483,000	508,000	0	0
Vegetation	15	11,993,000	13,621,000	1,079,370	1,225,890
Cultivated land	15	8,859,000	0	797,310	0
Buildup area	80	31,034,000	46,195,000	13,034,280	19,401,900
Road	80	0	1,880,000	0	902,400
Bare land	15	12,049,000	5,209,000	1,084,410	468,810
Total (m^3)				15,995,370	21,999,000
Rainfall is taken constant 0.6 m/annum from 1989 to 2022				15.99 MCM	21.99 MCM

generation in this area which gets altered due to the construction of residential colonies, commercial zones, amenities, and infrastructures such as storm water drains, gutters, laying of water supply pipes, cables of electric and telecommunication, construction of roads, etc. (Fig. 17.7).

3.2 Inference from Study of Ponds

One of the major impacts of urbanization can be seen in urban water bodies. Due to urbanization, it has been observed in both the study areas that pond/small water body has been affected. However, the impact of urbanization on the water bodies is dependent on the geographical location and morphological position of such water bodies within the urban area. Based on morphological position and geographical location, the pond may show reduction or enhancement in its water volume apart from total drying

Fig. 17.7 Change in land use between 2004 and 2022 of the Greenfield colony area of Faridabad. (Source: Google Earth)

out due to encroachment and alteration in land use pattern. The ponds in the low-lying area within a higher elevation or ponds of a lower gradient area within the low-lying area have shown an increase in the volume of water, whereas ponds of higher morphological position or on an elevated area have shown a reduction in water volume or even been dried up. In both our study areas, such ponds are available. For example, the IMT pond of Khoh, Manesar (Fig. 17.8), situated in the lower gradient, is showing an increase in water volume; the pond is receiving both drain water and rainwater, whereas the temple pond has gone dry due to urbanization. It has been observed that the increase in the volume of water in IMT ponds is due to the accumulation of grey

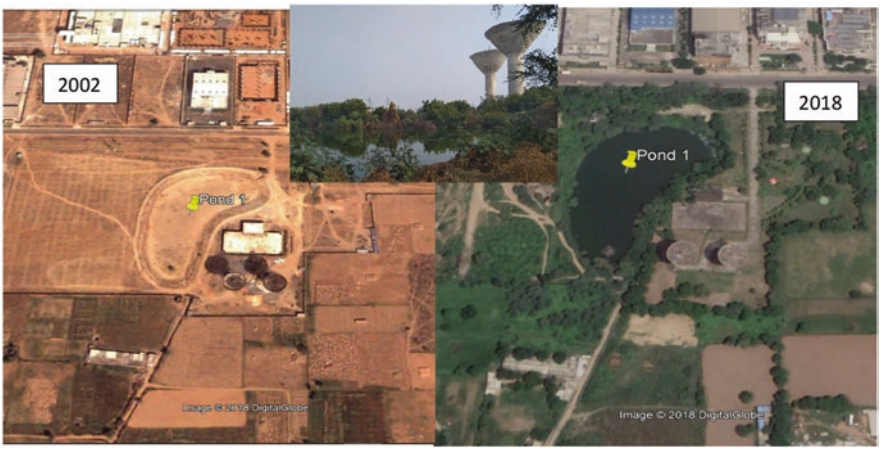

Fig. 17.8 Google image of 2002 and 2018 along with photo of IMT pond Khoh

water, and such cases are plenty in urban areas. The other three ponds have been converted to sewage tanks. On the other hand, change in the land use pattern of the pre-existing water body is very easy and frequent when ponds/water bodies get dry. A unique technique has been developed and named pond hydrograph to assess the pond water level. In this method, with the help of historical images, a particular pond's submergence area is calculated several times. Based on the water-filled area, a time series curve has been plotted to show the fluctuation in water level within a pond. An example of such a pond hydrograph is depicted in Fig. 17.9.

3.3 Disposal of Liquid Waste

Due to urbanization, the local urban bodies are under pressure to provide adequate water to a large part of their population. It has been estimated (CPHEEO, 1999) that 80% of the domestic water supply reappears in the form of household discharge. Therefore, a large quantity of gray water is generated due to urbanization and related population growth. Management of grey water is one of the biggest challenges due to urbanization and industrialization. Presently, no major river in India exists which can provide water of portable quality without treatment. The urban and industrial discharge are largely responsible for such a situation. So, urbanization directly impacts the surface water quality, and many a time, the water quality of canals is driven by such surface water bodies/rivers. At Faridabad, within a stretch of 9.5 km, 7 illegal discharge point has been observed discharging domestic grey water into the canal system. This includes structured channel discharge and non-structured casual discharge. The discharge is also bound to pollute groundwater due to canal seepage, particularly in the relatively shallow groundwater zone. Figure 17.10 depicts points of such discharge in the Gurgaon canal within the Faridabad city area.

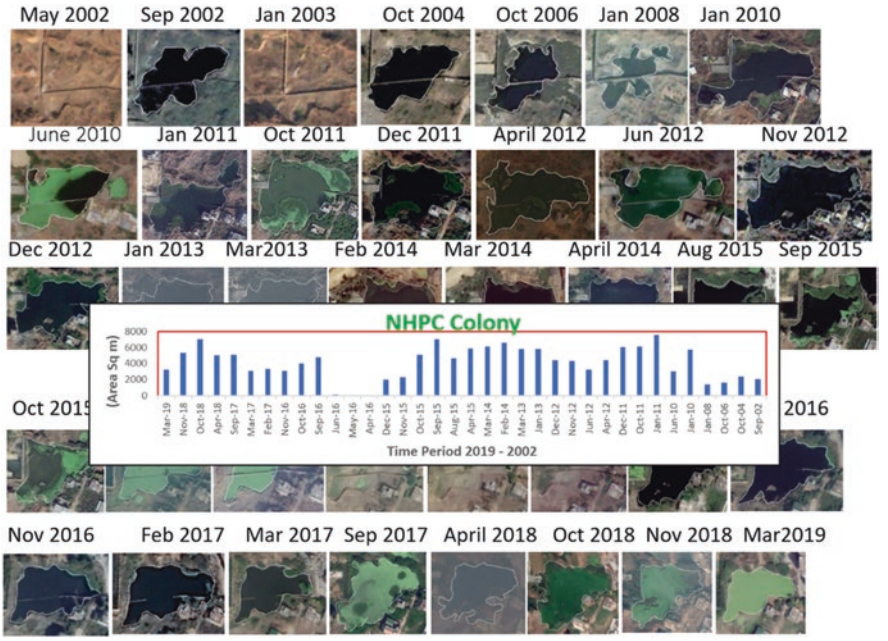

Fig. 17.9 Long-term changes in pond submergence area and pond hydrograph of NHPC pond Faridabad

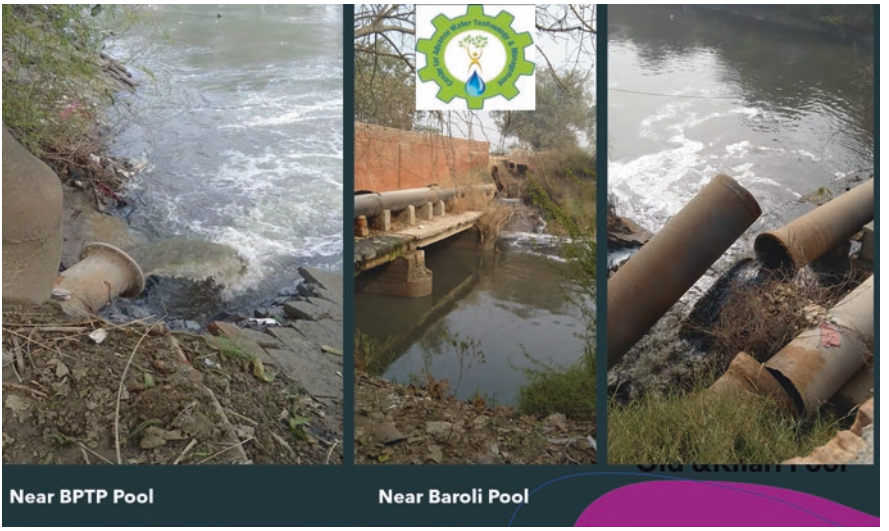

Fig. 17.10 Gray water discharge points along Gurgaon canal in Faridabad city area

3.4 Disposal of Solid Waste

In spite of all efforts, a maximum of 75–80% of solid waste can be collected, segregated, and disposed of properly. Still, 20–25% of solid waste generated every day remains untreated and disposed of in unauthorized way/unscientific ways. Large part of this untreated solid waste obstructs surface run-off/flow from drains carrying grey water and hinders infiltration. Thus, situations often arise when drains overflow or a shallow impervious layer is created due to polyethylene in low-lying urban areas. No scientific data is available on how much impact is created due to the untreated disposal of solid waste material, including plastic materials.

3.5 Groundwater Depletion

Groundwater at present is the only source of water for Khoh Manesar. The population has increased tremendously since 2006. All 5 dug wells, and almost all tube wells (TW) of Khoh in the depth range from 75 to 80 m have gone dry (Fig. 17.11). The numbers of dry TWs in Khoh are a few hundred. The concentration of dry wells is more along the foothill zone where the hard rock aquifer is being tapped. Discharge and sustainability of wells tapping water from 85 to 100 m depth range

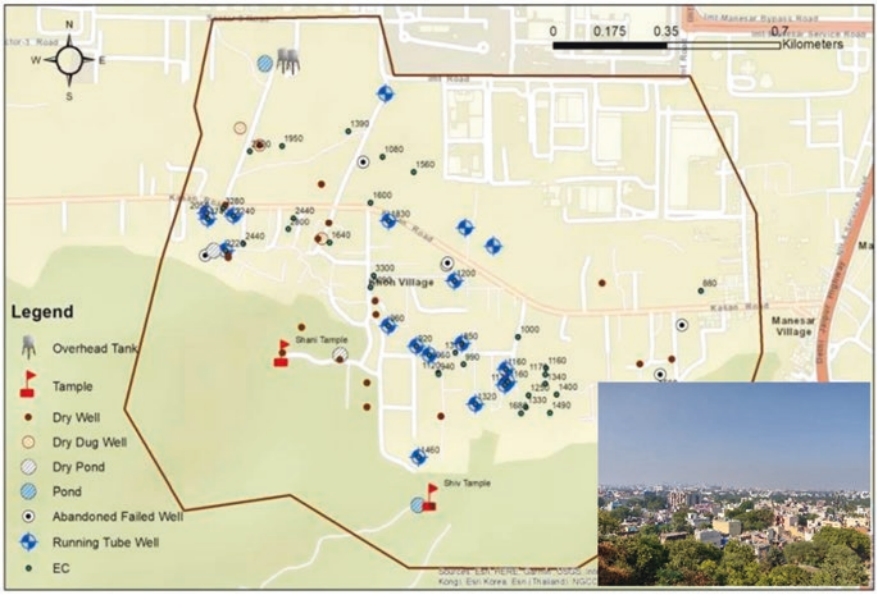

Fig. 17.11 Map of monitored wells and pond in Khoh Manesar along with a photograph showing the intensity of urbanization

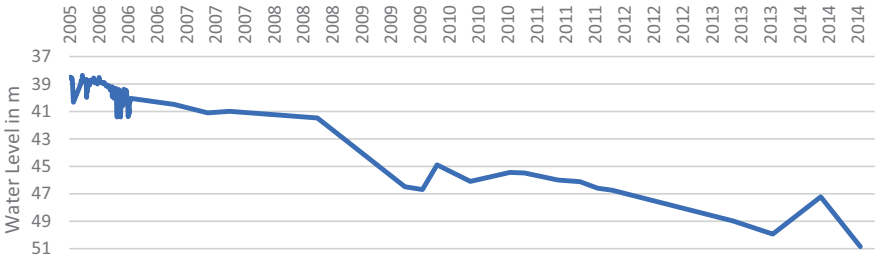

Fig. 17.12 Long-term trend of depleting groundwater of Faridabad

are reducing fast. Earlier, each house had its own TW, but due to well failures and increasing requirements, dependency on supply water is rising daily. The groundwater level in the area varies between 70 and 140 m bgl. Tube well depth ranges from 90 to 225 m bgl. Well discharge is generally low and varies largely from 0.1 to 2.0 lps. The alluvial aquifer has a better discharge than hard rock aquifers. Groundwater quality is found to be fresh to slightly brackish, and EC ranges from 850 to 3300 µs/cm. Due to the sudden and abnormal increase in the population of Khoh, the land use pattern has totally altered. This has reduced natural recharge substantially and increased flash food generated water logging of streets during monsoon. The area has a moderately steep slope, high susceptibility to erosion, moderate overflow, slow permeability, shallow depth, sandy or gravelly soil with low moisture capacity, and low inherent fertility. Though there are few attempts of artificial recharge of groundwater using roof water, no sincere community effort has been taken up in this direction; thus, Khoh area is under water stress condition. The groundwater of the Faridabad urban area has depleted a lot in the last few decades. The depletion rate has been estimated at 0.7 m/year (Fig. 17.12). Faridabad urban area is dependent on groundwater. There exist over 1600 TW and 22 Ranney wells to cater to the needs of the Faridabad area. The area is categorized as over-exploited and hardly able to feed the current requirement of a two million population.

3.6 Groundwater Quality

Long-term assessment of groundwater quality is very important due to its significance in determining suitability for drinking purposes and agricultural, domestic, and industrial uses as well. The groundwater gets contaminated due to a huge amount of hazardous waste from industries, landfills, unabsorbed fertilizers, pesticides, and other statements. Due to extensive urbanization and industrialization, groundwater quality is deteriorating, leading to potential health risks to the citizens. Conductance calculates the flow capability of water that is specifically associated with ion concentration in the water (EPA, 2012). In the present investigation, the data of EC in Faridabad for the last two decades collected from the

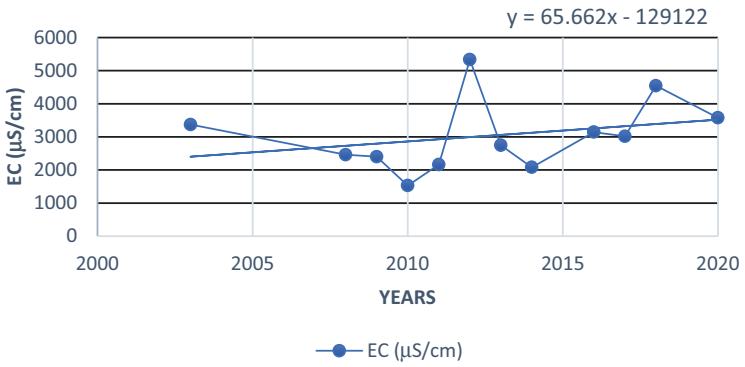

Fig. 17.13 Variation in electrical conductivity during 2002–2022

CGWB groundwater yearbooks has been plotted. The observed values show a range of 1527–4542.5 µs/cm. The groundwater for the entire study area shows an average of 3029 µS/cm of electrical conductivity. The data reveals that there is an increasing trend in EC from 2000 to 2020 from moderate to highly saline (Fig. 17.13). Sewage discharge or agricultural runoff can cause an increase in conductivity due to the presence of anions like nitrate, chloride, and phosphate. Thus, the abrupt rise in conductivity is indicating towards contamination of groundwater. In Khoh village, Gurgaon, the groundwater quality is found to be fresh to slightly brackish, and EC ranges from 850 to 3300 µS/cm.

3.7 Land Subsidence

Land subsidence is considered to be one of the severe geological hazards. According to US Geological Survey (USGS), excessive groundwater extraction is responsible for more than 80% of land subsidence (Garg et al., 2022). The extensive study of land subsidence of Delhi NCR indicates that the extent of subsidence increased continuously with time. Analyzing the land subsidence condition during 2014–2016, the maximum subsidence rate was relatively low, around 2.15 cm/year, and the spatial extent was negligible. However, during subsequent years, the deformation rates increased at a very high rate of 5.3 cm/year by the end of 2018 and 7.83 cm/year for the year 2018–2019 (Garg et al., 2022). This accelerating rate of land subsidence can be correlated with the high rate of groundwater depletion in Faridabad, which acts as reliable evidence of this condition. However, at certain locations, land subsidence and groundwater depletion do not follow a similar trend due to some discrepancies, including aquifer response to groundwater change, seasonal variation of groundwater, and differences in temporal sampling.

4 Conclusions

The impact of urbanization on groundwater conditions has been established in several parts of the country and the world. Further climate change scenario has intensified the adverse impact of urbanization on groundwater conditions. The present study considers two locations of urbanization within the area of the National Capital Region. The study has been able to characterize the key factors that govern the static and dynamic properties of urban areas, which significantly impact the groundwater scenario during changing climatic conditions. The expansion of the city area at the same time enhances the density of paved areas with a growing population has a many-fold impact on recharge discharge phenomena. The current study area largely belongs to alluvial terrain and has shown quality deterioration due to over-extraction of groundwater. Land subsidence has a hazardous impact on a densely populated area. The shrinking area under water bodies and pollution of low-lying surface water bodies are some important findings of this study. The study, however not able to find exact quantification of impact due to expansion and intensive paving and recommend further study on these aspects. The micro-level changes of morpho hydrogeological conditions were found to be significant factors for the flash flood generation.

Acknowledgments The authors thankfully acknowledge the Department of Science and Technology, Government of India, for the grant of Project "Co-solving water logging and groundwater depletion issue in parts of Faridabad Smart City using Underground Taming of Flood Water for Aquifer Storage and Recovery" (DST/TMD/EWO/WTI/2 K19/EWFH/2019/237(G)) to the corresponding author. The authors also thankfully acknowledge the Management of MRIIRS for providing logistic support and allowing authors to publish the paper. Special thanks to Mr. Ritwik Ganguly, Geovale Kolkata, for helping in the preparation of LULC maps. The authors are grateful to the editors of this book for their generous invitation to contribute a chapter in this publication.

References

Census of India. (2011). *Primary census abstract, Haryana, Series 7, Tables – A5-A8*. Directorate of Census Operations.

CGWB. (2015). *Aquifer mapping and formulation of aquifer management plan for the National Capital Region (NCR), Haryana (Volume II)*. Central Ground Water Board Ministry of Water Resources, River Development & Ganga Rejuvenation Government of India North Western Region.

CGWB. (2021). *Ground water year book of Haryana state 2020–2021*. Department of Water Resources, River Development and Ganga Rejuvenation, Ministry of Jal Shakti, Government of India.

Chakraborty, S. D., Kant, Y., Bd, B. (2014, January–February). Study of land surface temperature in Delhi City to manage the thermal effect on urban developments. *International journal of advanced scientific and technical research, 4*(1). ISSN 2249-9954.

Chauhan, A. S., Singh, S., Maurya, R. K. S., Rani, A., & Danodia, A. (2022). Spatio-temporal and trend analysis of rain days having different intensity from, 1901–2020 at regional scale in Haryana, India. https://doi.org/10.1016/j.ringps.2022.100041

CPHEEO. (1999). *Manual on water supply and treatment*. Central Public Health and Environmental Engineering Ministry of Urban Development.

Dandge, K. P., & Patil, S. S. (2021). Spatial distribution of ground water quality index using remote sensing and GIS techniques. *Applied Water Science, 12*(2022), 7. https://doi.org/10.1007/s13201-021-01546-7

Danger, S., Asoka, A., & Mishra, V. (2021). Causes and implications of groundwater depletion in India: A review. *Journal of Hydrology, 596*(2021), 126103.

Dash, S. K., Jenamani, R. K., Kalsi, S. R., & Panda, S. K. (2007). Some evidence of climate change in twentieth-century India. *Climatic Change, 85*(3), 299–321.

Dash, S. K., Kulkarni, M. A., Mohanty, U. C., & Prasad, K. (2009). Changes in the characteristics of rain events in India. *Journal of Geophysical Research – Atmospheres, 114*, D10.

DES. (2014). *Statistical abstract of Delhi*. Directorate of Economics and Statistics.

Dikshit, K. R. (2011). The city and the urban fringe: An introductory note. In J. K. Dikshit (Ed.), *The urban fringe of Indian cities* (p. 1). Rawat Publications.

Duan, H. B., Zhu, L., & Fan, Y. (2014). Review on the integrated assessment model of energy-environment-economy for the global change. *Journal of Systems Engineering, 29*, 852–868. http://cnki.com.cn/Article/CJFDTotal-XTGC201406014.htm

EPA. (2012). *Conductivity in water: Monitoring and assessment*. US Environmental Protection Agency.

Ferreira, F. L. V., Rodrigues, L. N., & da Silva, D. D. (2021). Influence of changes in land use and land cover and rainfall on the streamflow regime of a watershed located in the transitioning region of the Brazilian Biomes Atlantic Forest and Cerrado. *Environmental Monitoring and Assessment, 193*, 16. https://doi.org/10.1007/s10661-020-08782-5

Follman, A., Tups, G., & Dannenberg, P. (2018). Multi-temporal transect analysis of peri-urban developments in Faridabad, India. https://doi.org/10.1080/17445647.2018.1424656

Garg, S., Motagh, M., Indu, J., & Karanam, V. (2022). Tracking hidden crisis in India's capital from space: Implications of unsustainable groundwater use. *Nature Scientific Reports, 12*, 651. https://doi.org/10.1038/s41598-021-04193-9

Goswami, B. N., Venugopal, V., Sengupta, D., Madhusoodanan, M. S., & Xavier, P. K. (2006). Increasing trend of extreme rain events over India in a warming environment. *Science, 314*(5804), 1442–1445. https://doi.org/10.1126/science.1132027

Guhathakurta, P., Narkhede, N., Menon, P., Prasad, A. K., & Sangwan, N. (2020). *Observed rainfall variability and changes over Haryana state* (Met Monograph No.: ESSO/IMD/HS/Rainfall Variability/09(2020)/33). IMD.

IPCC. (2007). Summary for policymakers. In S. D. Solomon et al. (Eds.), *Climate change-the physical science*. Cambridge University Press.

Jain, S. K., & Kumar, V. (2012). Trend analysis of rainfall and temperature data for India. *Current Science (Bangalore), 102*(1), 37–49.

Lal, M. (2003). Global climate change: India's monsoon and its variability. *Journal of Environmental Studies Policy, 6*(1), 1–34.

Mohan, M., Kandya, A., & Battiprolu, A. (2011). Urban heat island effect over National Capital Region of India: A study using the temperature trends. *Journal of Environmental Protection, 2*, 465–472.

National Intelligence Council. (2009). India: The impact of climate change to 2030 a commissioned research report. NIC spacial report no 2009-03D, 54p.

Rahman, T. A., Arpan, S., & Jafri, M. D. A. (2016). Ground water modeling of Faridabad District, Haryana, India. *International Journal of Agriculture Sciences, 8*(47), 1957–1965.

Ranjan, K., Sharma, V., & Ghosh, S. (2021). Assessment of urban growth and variation of aerosol optical depth in Faridabad District, Haryana, India. *Pollution, 8*(2), 447–461. https://doi.org/10.22059/POLL.2021.329185.1163

Saha, D., Marwaha, S., & Mukherjee, A. (2018). Groundwater resources and sustainable management issues in India. In *Clean and sustainable groundwater in India*. Springer. https://doi.org/10.1007/978-981-10-4552-3_1

Saini, H. S., Kaura, L. P. S., Mujtaba, S. A. I., Verma, K., & Pant, N. C. (2017). Assessment of the soils around Faridabad, NCR in the context of changing Landuse, Indian. *Journal of Geosciences, 71*(1), 219–226.

Sati, A. P., & Mohan, M. (2017). The impact of urbanization during half a century on surface meteorology based on WRF model simulations over National Capital Region, India. *Theoretical and Applied Climatology, 134*. https://doi.org/10.1007/s00704-017-2275-6

Sinha, R. K., & Srivastava, A. K. (2000). Is there any change in extreme events like heavy rainfall? *Current Science, 79*(2), 155–158.

Swain, S., Sahoo, S., & Taloor, A. K. (2022). Groundwater quality assessment using geospatial and statistical approaches over Faridabad and Gurgaon districts of National Capital Region, India. *Applied Water Science, 12*, 75. https://doi.org/10.1007/s13201-022-01604-8

Talchabhadel, R., & Karki, R. (2019). Correction to: Assessing climate boundary shifting under climate change scenarios across Nepal. *Environmental Monitoring and Assessment, 191*, 707. https://doi.org/10.1007/s10661-019-7907-0

Teixeira, D. B. D., Veloso, M. F., & Ferreira, F. L. V. (2021). Spectro-temporal analysis of the Paraopeba River water after the tailings dam burst of the C'orrego do Feij˜ao mine, in Brumadinho, Brazil. *Environmental Monitoring and Assessment, 193*, 435. https://doi.org/10.1007/s10661-021-09218-4

Teotia, M. K., & Kumar, R. (2015). *The state of cities in North-Western India: A case of selected JNNURM cities* (Study focus city: Faridabad). CRRID.

United Nations. (2018). *Revision of world urbanization prospects | Multimedia library*. United Nations Department of Economic and Social Affairs. https://www.un.org/development/desa/publications/2018-revision-of-world-urbanizationprospects.html

World Urbanization Prospects. (2018). Published by the Population Division of the United Nations Department of Economic and Social Affairs (UN DESA). https://www.un.org/development/desa/publications/2018-revision-of-world-urbanization-prospects.html

WRIS. (2022). *Water resources information system*. https://indiawris.gov.in/wris/#. Accessed in May 2022.

Index

A
Agriculture, v, 2, 5, 10, 20, 29, 51, 61, 118, 187, 247, 260, 261, 263, 297, 300, 305, 327, 329
Anthropogenic activity, viii, 26, 46, 57, 59–60, 80, 121, 123, 228, 263, 286, 294, 310
Artificial neural network (ANN), ix, 47–49, 81, 204–206, 209–219, 222–224
Artificial Neural Network based Cellular Automata (ANN_CA), 44, 47–49, 51

C
Chalakudy, viii, 81, 82, 84
Change detection, 52–53
Chennai, viii, ix, 28, 30, 31, 33, 54, 58, 60, 134, 274, 275
Chittar catchment, viii, 44, 46–49, 51–53
Climate change, viii, 29, 44, 51, 60, 63, 75, 76, 80, 131, 132, 138, 187, 188, 256, 319, 328–330, 341
Contamination, 30, 32–34, 38, 39, 185, 187, 188, 236–238, 247, 283–286, 294–296, 299, 301, 304, 309–310, 316, 324, 340

D
Database modeling, 204, 206
Dempster-Shafer, viii, 81, 83, 96–99, 106
Drinking, viii, ix, 5, 26, 28–30, 34, 38, 39, 119, 120, 130, 144, 146, 154, 167, 168, 177, 179, 199, 228, 236, 237, 239–249, 251, 252, 294, 299, 339

E
Ennore, ix, 274, 286
Evidential belief function (EBF), viii, 81, 83, 96–101, 106

F
Faridabad-Khoh Manesar, 338
Flood susceptibility zonation (FSZ), viii, 80, 81, 83–85, 96–99, 102–105

G
Ganga River Basins, 113–123
Geochemistry, 195, 197
Geographic Information Systems (GIS), 3, 7, 8, 17, 20, 26, 27, 29, 32, 39, 44, 46, 47, 65–66, 69, 80, 81, 84, 106, 196, 256, 257, 259–261, 324, 332
Geospatial techniques, 3, 21, 29
GIS mapping, 29
Groundwater, v, vii, ix, x, 2–6, 18, 20–22, 26–30, 32–34, 38, 39, 52, 53, 114, 122, 131, 133–139, 144–147, 151, 152, 154, 157, 158, 163, 167–179, 181, 185, 187, 188, 190, 194–199, 204–224, 228–252, 256–263, 265, 268, 274–276, 278–289, 294–310, 314, 316–320, 324–326, 328, 332, 333, 336, 338–341

P. Thambidurai, A. K. Dikshit (eds.), *Impacts of Urbanization on Hydrological Systems in India*, https://doi.org/10.1007/978-3-031-21618-3

Groundwater depletion, 137, 262, 324, 325, 338–341
Groundwater flow model, ix, 175, 190
Groundwater potential, ix, 53, 156, 256–268, 297
Groundwater potential zone (GWPZ), 256, 266
Groundwater recharge, x, 21, 76, 114, 118, 122, 123, 138, 139, 173–175, 228, 256, 258, 262–266, 268, 314–319, 326
Groundwater remediation, ix, 188

H
Hard rock, ix, 5, 33, 144, 147, 153, 154, 156, 157, 161, 256, 260, 262, 268, 297, 304, 309, 328, 338, 339
Himalayas, x, 171, 314, 319

I
Indus River Basin, x, 314
Industrial effluents, 120–122, 247, 286, 294, 295, 299, 301, 306, 309
Industrialization, vii, x, 112, 114, 116, 236, 256, 295, 299, 324, 336, 339
Ion exchange, 26, 197, 198, 284, 286, 298

K
Kappa statistics, 44–45, 48

L
Land subsidence, x, 135, 137, 194, 325, 340, 341
Land Use and Land Cover (LULC), viii, 3, 7, 8, 10, 19, 43–53, 61, 65, 69–71, 73, 76, 91–92, 101, 102, 116, 118, 123, 258, 259, 261, 326, 332–334, 341

M
Multi-criteria decision analysis (MCDA), 3, 4, 7–8, 21

N
Nature-based solutions, viii, 137

P
Pallikaranai, viii, 28, 30–33, 38, 39
Patna, viii, ix, 60–63, 66, 67, 70–76, 115, 121, 167–169, 171–174, 176, 179, 180, 185, 228, 231, 233, 234, 237–244, 246, 248, 250–252
Patna urban area (PUA), ix, 167–171, 173, 174, 177, 180, 181
Population growth, 31, 51, 76, 112, 123, 135, 179, 336

R
Rainfall intensity, x
Rainwater harvesting (RWH), viii, 2–4, 6–11, 14, 17–22, 76, 124, 134, 135, 140, 152, 163, 195
Remote sensing, 6, 22, 27, 47, 65, 80, 84, 106, 141, 196, 256, 259, 260, 267, 332

S
Salinization, 134
Sandbox experiment, 191
Scarcity, ix, 26, 132, 146, 188
SCS Curve Number Method, 7
Snow melt, 319
Spatial variation of groundwater, 14, 27, 204
Support vector machine (SVM), ix, 204, 205, 212, 214, 216, 219–224
Surface water, v, viii, 6, 26, 27, 29, 33, 44, 46, 53, 112, 114–124, 130, 136, 138–140, 144, 187, 195, 196, 198, 199, 204, 236, 260, 268, 294, 299, 326, 336, 341

T
Temporal prediction, ix, 204, 209
Thamirabarani basin, 44, 46

U
Urban floods, viii, 57–60, 76, 77
Urban impact, 60
Urbanization, v, vii–x, 28, 33, 44, 58–60, 69, 73, 76, 80, 112–124, 130, 131, 133, 135–138, 172, 185, 236, 256, 274–289, 294–301, 304, 310, 324–341
Urban water scarcity, 131–135, 137–141

V
Vertical Electrical Sounding (VES), 144–146, 152–156, 160–162, 332

W
Water quality, 26–33, 114, 116, 120–122, 124, 138, 195, 196, 198, 199, 239, 249, 250, 278, 336
Water scarcity, vii, ix, 2, 44, 130, 131, 133, 135, 138, 139, 141, 145–146, 148–163, 230, 329
Weighted linear combination (WLC), ix, 3, 8, 261

Z
Zone prioritization, 4, 20